DIFFERENT COMPUTER MODELS FOR THE SIMULATION OF A TYPICAL TURBOFAN ENGINE ORIGINATING FROM DIFFERENT FAN TREATMENTS AND AIR FLOW DISTRIBUTION

BY PETER J. PETRIDES B.Sc., G.Dip.

THESIS SUBMITTED FOR THE DEGREE OF Ph.D.

DEPARTMENT OF MECHANICAL ENGINEERING
UNIVERSITY OF GLASGOW

OCTOBER 1988

ProQuest LLC.
789 East Eisenhower Parkway
P.O. Box 1346
Ann Arbor, MI 48106 – 1346

TO MY PARENTS JOHN AND EVA PETRIDES

AND

TO ALL MY FRIENDS

ACKNOWLEDGEMENTS

I wish to express my utmost gratitude to my supervisor, Dr. N.R.L. Maccallum, for his valuable guidance and continuous help and interest throughout this project.

I am also indebted to my parents for their financial support which made possible for me to complete this study.

Last but not least i would like to thank my fiancee Sophia for her continuous moral support and encouragement during this study.

LIST OF CONTENTS

SUMMARY

The aim of the research presented in this thesis was to improve the computer modelling for the prediction of the transient performance of the Gas Turbine. The development of computational models to simulate a Gas Turbine had been recognised as valuable tools towards the achievement of better engine designs.

The current investigation concentrated in developing a computer model that would best represent the Fan, and the flow distribution around it, for a typical Turbofan Gas Turbine. The different Fan treatments and flow distributions adopted were modelled and seven computer models deriving from them are presented, Fig.(2A). The earliest model used fixed characteristics for the Inner section of the Fan(which compresses the core air), and for the Outer section of the Fan(which compresses the by-pass air). Subsequent models allowed an interchange of flow between the two sections of the Fan.

Due to the time-consuming nature of the work involved in developing these models, including the "Real engine effects"-see below-, it was decided to compare the predictions of "adiabatic" versions of the models, one with another, and then select the most reasonable looking two or three models. From the comparison, which is described and presented with the appropriate graphs, two programs were selected which both allow for an interchange of flow between the two sections(Inner and Outer) of the Fan.

The first of the two selected programs-AFSREE- incorporates a moving boundary between the two flows(Inner and Outer), at the entry to the Fan, and the interaction between them is achieved by varying the base line(non-dimensional air mass flow rate) of the separate characteristics of the Inner and Outer section of the Fan. The second program-STFREE- uses sets of separate characteristics for each section(Inner and Outer) of the Fan, and each set of a section corresponds to a pressure ratio of the other section of the Fan. Hence the operating point of one of the sections(Inner or Outer) is dictated by the operating point, at that instant, of the other section of the Fan(Outer or Inner), allowing thus an interaction between the two flows by varying the pressure ratio on their characteristics

In order to produce a realistic, accurate and reliable model, it is neccessary to include certain effects, named in this work as "Real engine effects" (e.g. Heat transfer effects, ramped fuel flow etc.), that are present in the real engine and if excluded from the computer model would lead to unrealistic results. Since the final effort of the present work, was to compare the computer models developed with the actual test results of a typical Turbofan engine, these effects had to be incorporated. The importance of the inclusion of these effects was highlighted by comparing the predictions of one of the two final programs (AFSRRE), with and without these effects.

Finally the predictions of the two complete computer models were compared against the test results of a typical Turbofan engine. From the comparison carried out, it was found that the AFSREE program not only predicted more accurately the

behaviour of the Real engine but also used, in general, half the computing running time that the STFREE program needed to simulate the same conditions.

Nevertheless the predictions of both programs showed discrepancies from the Real engine test results for reasons that are explained and discussed in the final chapter.

NOMENCLATURE

A	Flow Area
B	By-pass Ratio
CMF	Continuity of Mass Flow
C.V.	Calorific Value
C_p	Specific Heat Capacity at constant pressure
e	Cooling Effectiveness
F	Thrust
FCSP	Factor of Split
f	Fuel Rate
f	Ratio of the Feat Transfer to the Fluid to the Work Transfer from the Fluid
f	Friction Factor
H.P.	High Pressure
h	Heat Transfer Coefficient
ICV	Inter-component Volume
IGV	Inlet Guide Vanes
I.P.	Intermediate Pressure
i	Angle of Incidence of flow
K.E.	Kinetic Energy
k	Thermal Conductivity
L.P.	Low Pressure
l,L	Length
M	Mach Number
m	Mass flow

m	Index of Expansion
N	Shaft Speed
NDSLP	Non-dimensional Speed of the Low Pressure Compressor
NDSHP	Non-dimensional Speed of the High Pressure Compressor
n	Index of Expansion
P	Pressure
PR	Pressure Ratio
Pr	Prandtl Number
Q	Heat Flux to fluid in Compressor or Turbine
R	Gas Constant
R,r	Radius
T	Temperature
UM	Unfinned Model
u	Velocity
V	Velocity
v	Volume
y	Blade Height

Greek Letters

α	Air Angle
ε	Deflection of Fluid due to Blade
η	Efficiency
μ	Viscocity
ρ	Density
τ	Shear Stress

Subscripts

a	Air
ad	Adiabatic
ave	Average
b	Blade
Con	Contact
c	Cooling Air
cg	Core Gas
e	Thermal
F	Fan
H	High Pressure Shaft
HP	High Pressure
ht	Heat Transfer
j	Jet
L	Low Pressure Shaft
lam	Laminar
m	Mean
N	Net
o	Overall
p	Propulsive
T	Turbine
TR	Transmission
turb	Turbulent

INTRODUCTION

The normal way to use the working fluid in order to extract mechanical power from a thermal source is by the thermodynamic cycle of induction, compression, heating, expansion and exhaust. If all these processes are performed in sequence in the same closed space, the result is a reciprocating engine. If the working fluid flows without an interruption, passing from one single device to the next, then the result is a gas turbine.

The use of gas turbines for aircraft propulsion dates from 1930. Although Hero of Alexandria had the first idea to produce power from the flue gases of a furnace around 150 B.C., only at about 1791, John Barber patented the forerunner of gas turbines. From 1791 to 1930 many designs for gas turbines were developed but all suffered from lack of knowledge of Aerodynamics.

It was the Second World War that forced man to develop the Jet engine, something that 2000 years of human evolution and development had not managed. Since then the gas turbine has become the most important method of aircraft propulsion.

Initially, reciprocating engines were the main method used for aircraft propulsion, but the balancing problems of the reciprocating parts as well as the high reliability needed, together with the possibility of high power to weight ratio from the gas turbine, encouraged the research and development of

what are now highly sophisticated gas turbine engines. Gas turbines were also used in industrial and marine applications, but without any doubt the greatest impact has been in the aircraft propulsion field.

The need for more efficient and quiet engines changed the geometry and the configuration of the gas turbines, creating over a period of several decades, the advanced Turbofan engine from the Jet engine.

It is important to be able to predict the performance of an engine, particularly when the engine is at the design or development stage. During the last decade significant research has been carried out towards improving prediction methods. The simulation procedures should provide both steady-state performance of the engine and also its transient performance, knowledge of the latter being important in order to ensure that satisfactory engine response is to be achieved.

With regard to the prediction of performance during transients, it has been found in recent investigations that allowances for "thermal effects" must be included in the simulation model. As an illustration of "thermal effects", if a gas turbine is rapidly accelerated or decelerated, there is a finite time that elapses following completion of the speed transient before the various components reach their equilibrium temperatures. During that finite time and during the speed transient itself, heat transfer takes place between the various components and the air flowing through the engine. As a result the performance of the engine differs significantly from that predicted from adiabatic assumptions.

It is the purpose of this research to predict the transient performance of a typical modern Turbofan Engine of Medium Bypass Ratio. Emphasis has been given to the use of alternative models for representing the Fan plus Intermediate Compressor sections, originating from different Fan treatments and flow distributions after the Fan. The final development in the research has been the incorporation of all the Heat transfer effects to lead to the most realistic computer model simulating the Turbofan engine.

CHAPTER I

GENERAL INTRODUCTION AND BACKGROUND

1.1 INTRODUCTION

This chapter opens with a general introduction in Gas turbines. It then continues with a discussion on the choice of methods available on Gas turbine transient modelling. A summary on how the Transient performance prediction has been developed is included. The Heat transfer effects are also described together with the research that has been done in the effort to incorporate these effects in computer models simulating the transient as well as the steady running performance of Gas turbines. Finally, since this research is on a modern Turbofan Engine, a more detailed description of this type of gas turbine is also included at the end of the chapter.

As it was mentioned earlier a gas turbine operates using the thermodynamic cycle of induction, compression, heating, expansion and exhaust.

There are two types of gas turbines cycles: Aircraft gas turbine cycles and Shaft power cycles. The second type includes all gas turbines not included on the first type, and could all be included under the name of Industrial Gas Turbines.

There are essentially three main differences between the two types: Firstly the expected life of an Industrial engine without a major overhaul is greater than for an Aircraft engine. Secondly, there are limitations on the size and weight of an Aircraft

engine. Finally, the Aircraft gas turbine makes use of the kinetic energy of the gases leaving the turbine whereas it is wasted in all other types of gas turbines and has to be kept as low as possible.

The Gas turbine cycles could also be distinguished into Open and Closed cycles.

In the Open cycle gas turbine, fresh atmospheric air is drawn into the engine continuously and energy is added by the combustion of fuel in the working fluid (air) itself. The products of combustion are expanded through the turbine(s) and exhausted to the atmosphere. In the Closed cycle gas turbines, the same working fluid is repeatedly circulated through the machine. Clearly the fuel used in this type of engines can be such that it could not be burnt with the working fluid, in order to avoid the erosion of the turbine blades or other detrimental effects of the products of the combustion.

A Turbofan engine is the engine in which the air entering is compressed by a single stage fan and then part of the air by-passes the rest of the engine including the L.P. compressor, and a part flows through the engine.

If the by-pass air emerges separately from the hot gas exhaust of the main engine, then that engine is a Turbofan or bypass Turbojet with Separate exhaust. If the by-pass air is mixed with the hot gases of the main engine, before they are exhausted in the atmosphere, then the engine is a Mixed exhaust gas turbine.

The present work was carried out on a Turbofan Engine with Mixed exhaust.

Now let us consider the mechanics of aircraft propulsion. A diagrammatic representation of a turbojet engine on an aircraft having single exhaust stream is shown in Figure(1).

In order to provide thrust for the aircraft, the engine has to accelerate part of the passing airflow, in otherwords to produce a change in momentum.

Relative to an observer on the aircraft, the air enters the intake to the engine at the design condition with a velocity V_a equal and opposite to the forward speed of the aircraft, and it is accelerated by the engine so that it leaves with the jet relative velocity V_j.

Assuming that the mass flow m is constant, i.e. the fuel flow is negligible and also assuming full expansion, then the net thrust F_N is the rate of change of momentum which is:

F_N = (Momentum flux of flow at plane J behind the engine) - (Momentum flux of flow at plane A infront of engine).

$$F_N = mV_j - mV_a$$

$$F_N = mx(V_j - V_a) \qquad [1]$$

where:

mV_j is called the Gross Momentum Thrust and

mV_a is called the Intake Momentum Drag.

The increase in momentum is imparted using a Heat engine.

All current gas turbines operate on an approximation to the Brayton cycle, Figure(2). The working gas is compressed from point 1 to point 2. Then heat is added, ideally under constant pressure from point 2 to point 3. Then the gas is expanded from point 3 to point 4, ideally the initial pressure.

The compression is done by the compressor configuration. Heat is added by burning fuel in the Combustion Chamber and

the gas is expanded in the Turbine configuration and the Nozzle.

The small departures from to the Brayton cycle is due to the inefficiencies of the various components of the engine. In the same Figure(2) the Real cycle is shown. The pressure and temperature at the inlet of the compressor is not equal to the atmospheric due to the ram compression at the intake of the engine, when the aircraft is moving. Then the fluid is compressed from 1_A to 2' or if the aircraft is stationery, from 1' to 2'. This is a point (1') of lower pressure due to losses at the intake. Then heat is added on the working fluid from 2' to 3', with a loss in pressure due to friction and losses associated with the combustion process. As a result the turbine inlet pressure is slightly lower from the ideal (point 3) compressor delivery pressure. Then the gases are expanded to point 4'. The expansion from 3' to C is the work needed to drive the compressor. This part of the expansion occurs in the turbine(s). The expansion then continues from C to 4' in the nozzle, which produces the useful work output. In the ideal cycle the turbine and compressor work are the same. In the real cycle the turbine work is larger to account for losses, mechanical inefficiencies and power for auxiliaries.

The useful work is in the form of an increase in kinetic energy of the working gas or air.

$$\text{Increase in K.E. per unit time} = 1/2mV_j^2 - 1/2mV_a^2 \qquad \textbf{[2]}.$$

From equation [1] follows that the required thrust can be obtained by designing the engine to produce a high velocity jet of high mass flow.

Thrust power is the product of the net thrust and the aircraft

speed.

$$\text{Thrust Power} = m V_a (V_j - V_a)$$

Now the Propulsive efficiency can be defined as:

$$\text{Propulsive Efficiency} = \frac{\text{Thrust Power}}{\text{Rate of change of K.E. to propulsive system}}$$

$$\eta_p = F V_a / 1/2\, m(V_j^2 - V_a^2) \qquad [3]$$

Thermal efficiency is the efficiency of energy conversion within the power plant itself, or:

$$\text{Thermal Efficiency} = \frac{\text{Rate of useful work output}}{\text{Rate of consumption of thermal energy}}$$

$$\eta_e = [\, 1/2\, m\, (V_j^2 - V_a^2)] / f(\text{C.V.}) \qquad [4]$$

where f is the fuel rate and, and C.V. is the calorific value of the fuel.

The overall efficiency is the ratio of the useful work done in overcoming drag, to the rate of consumption of thermal energy:

$$\eta_o = m V_a (V_j - V_a) / f(\text{C.V.}) \qquad [5]$$

From equations **[3],[4]** & **[5]** it is seen that :

$$\eta_o = \eta_p x \eta_e \qquad [6]$$

The purpose of this analysis has been to make clear that in order to achieve a high overall efficiency it is necessary to maximize both η_e and η_p. The Thermal Efficiency is maximized by increasing the pressure ratio while the Propulsive Efficiency is maximized by decreasing the jet speed. It is then clear that to keep the thrust at the same level higher mass flow rate has to be achieved which imposes that the high speed thrust has to be replaced by the high mass flow rate one. This leads to designs of engines of higher by-pass ratio.

Equation **[6]** applies to all gas turbines for aeroplane

propulsion.

For the turbofan engines with separate exhaust, Bennet Ref.(3), suggests that a third factor should be included. This is the transmission efficiency which expresses how efficiently the power of gas turbine is transferred to the cold propulsive jet in a by-pass engine.

$$\eta_{TR} = \frac{\text{actual K.E. suplied to bypass air}}{\text{ideal K.E. that could be suplied}}$$

or $\eta_{TR} = (1+ Bn_T n_F)/(1+B)$

where B is the by-pass ratio and is defined as:

$$B = \frac{\text{by-pass mass flow rate}}{\text{core gas flow rate}}$$

where η_T & η_F are the Turbine and Fan efficiencies.

In order to produce satisfactory and very efficient by-pass engine designs, the above mentioned efficiencies are the most significant of the many factors that have to be taken into consideration and balanced against one another.

It is not the purpose of this work to go into further details of the various aspects in the design of gas turbines. Such information is given in detail in the References(5&14). It is though worth mentioning that some of the most recent designs of high by-pass ratio Turbofan engines(JT9,CF6, but not the RB-211) incorporate on the same shaft both the Fan and the Intermediate pressure(I.P.) compressor, or otherwise called Booster.

The object of the present study is to investigate the best method of representing the Fan plus I.P. compressor arrangement for predicting the transient as well as the steady

running performance of a Turbofan engine.

1.2 MODELLING OF GAS TURBINES

Research on the transient prediction of Gas turbines has been pursued since comparatively early in the history of the development of the Aircraft engines.

At the early stages of the gas turbine simulation, the prediction of the transient behaviour was based on test bed analysis.

Trying to develop theoretical models to predict the transient performance of gas turbines, it was soon realised that the best way of doing so was by means of the component characteristics.

The unique component characteristics of each engine are available at the very early stage of the design, making possible the construction of a simulator to predict the transient behaviour of the engine over the entire range expected. Hence this accurate reliable and realistic model will be able to show the engine's entire response even as early as at the customer's proposal stage.

The early computer models have assumed adiabatic flow which resulted in unrealistic simulators. During these years of research on transient modelling the gas turbine, two types of prediction procedures have evolved:-

(i)The Inter-Component Volumes (ICV) method; which for the calculation of the engine's pressure changes assumes mismatches of flow occuring at various stations in the engine.

(ii)The Continuity of Mass Flow (CMF) method; which assumes

mass continuity at all times throughout the engine and when the engine operates transiently.

1.2.1 The ICV Method

In the ICV method, volumes are introduced between the various components and all flow imbalances are assumed to occur in these volumes. The size of an intercomponent volume is the volume of the space between any two components plus the half of the volume of each adjacent component.

In this method additional initial guesses of the pressures within the intercomponent volumes must be made, and should be as accurate as possible. Also the mass flow through each individual component is assumed to be constant.

There are different mass flow rates through the engine and the mismatches of these flows are used to evaluate the rate of pressure increase or decrease within the intercomponent volumes, see Figure(4B).

Once all the components have been analysed in this manner, the power delivered or absorbed by the components is evaluated, which then gives the work imbalance on the shaft(s). Hence the new shaft(s) speeds are calculated in order to be used for the next process of evaluation through the components of the engine, at the next time step.

This method is a "once through" calculation for each time step.

The above mentioned procedure is repeated throughout a transient until neither mismatches of flow nor work imbalance along the shaft(s) occurs and thus the transient is completed.

At the early stages of the research in computer simulation of Gas Turbines, H.I.H. Saravanamuttoo, was working on an

analogue computer study of the transient performance of the Orenda 600 HP. Regenerative Gas Turbine, Ref.(36). Seven years later Fawke and Saravanamuttoo published their work, Ref.(37), of the development of a simulation method for the Dynamic performance of a gas turbine .

Their method, which was based on the ICV method, required the characteristics of the engine component and it was necessary to choose a set of engine parameters which permitted the operation of each engine component to be determined. The fuel flow, nozzle area and flight conditions should have also been specified. In this method, it was necessary to calculate the initial engine steady state operating point before being able to calculate a transient.

Fawke and Saravanamutoo used their simulation method to improve the dynamic response of a twin spool turbojet engine, and a year later, 1971, Ref.(38), they verified their method experimentally. The simulator results showed good agreement with the engine test bed results proving the engine simulation an invaluable tool in the development of the gas turbine.

In 1985, T. Shoebeiri and H Haselbacher, Ref.(40), developed a modular computer program which calculates the transient behaviour of individual components as well as of entire gas turbine systems. Their analysis was based on an air storage gas turbine system consisting of a combustion turbine, a generator motor, a compressor train and an underground air storage facility. The transient processes which occur within a component of the system were in general described by the conservation of aero-thermodynamics equations: Continuity equation, Equation

of motion and Mechanical and Thermal energy equations. Due to computer capability limitations they had to consider a one-dimensional approximation. The system simulated by Shobeiri and Haselbacher although it consists of similar components as those used on Aircraft gas turbines, the layout, interaction and way of utilisation of each component is different to those of the aero-engines. Nevertheless, the simulation model developed was compared to the Huntorf compressed air storage plant and results showed a very good agreement.

1.2.2 The CMF Method

In the CMF method the flight conditions and the rotational speed of the compressor are assumed or known.

From these, the inlet conditions to the compressor or fan, are calculated. Guessing a mass flow rate into the engine and interpolating using the known inlet conditions, the outlet thermodynamic variables from the compressor or fan can be calculated. The outlet thermodynamic variables of this component are the inlet conditions for the next one.

For the combustion chamber the outlet temperature is obtained by an energy balance equation using the known fuel flow rate. The outlet pressure is calculated by applying a pressure loss factor to the inlet pressure.

Now the turbine entry conditions are known and using the turbine characteristics and shaft speeds, which are also known, the outlet conditions are evaluated.

This process is carried out for all the components that an engine can incorporate and the mass flows are noted.

The mass flows in general will not satisfy the continuity and hence the initial guessed value has to be revised until convergence is achieved.

During a transient, a work imbalance will exist. The net torque acting on the shaft(s) is calculated using the work imbalance and by knowing the inertia of the shaft, the acceleration or deceleration rate can be calculated. Knowing the incremental time step and the acceleration or deceration time rate, the new rotational speed can be evaluated. This process is continued until no net torque is acting on the shaft.

One of the early models that used the CMF method was the model developed by, Kuhlberg, Sheppard, King and Baker, Ref.(18), which was capable of providing accurate dynamic representation of a gas turbine engine's compressor system. Their first approach, called the Continuity model, utilised the same dynamic coupling techniques used in dynamic engine simulation. Engine simulations generally use a compressor model based on an overall compressor map to provide performance characteristics compatible with those obtained from the simulation of the other components. Dynamic coupling of components was accomplished by using a "lumped" control volume, across which continuity of mass is assumed. Hence this technique consisted of simply maintaining airflow continuity between each of the "lumped" elements. Although their first approach appeared mathematically sound, they used stage pressure rise to enter the stage characteristics in order to determine air flow value. The principal difficulty arose because the stage pressure rise characteristics are double valued and it became impossible to evaluate an output value of the inlet flow

function. Trying to overcome these problems they included the equation of conservation of momentum resulting to their second model of Momentum-Continuity, which permitted the stage characteristic curve to be entered with the inlet flow and thus evaluating a single value of stage pressure rise. This model was proved to be an analytical tool for predicting the dynamic response of a compressor. It must be noted that their analysis was limited to one-dimensional external disturbances.

Since the CMF method is not a "once through" calculation method, it requires a number of iterations until convergence is achieved. Fawke, Ref.(9), had problems of achieving convergence in his model, due to inefficient convergence routine. Durant, Ref.(8), had also problems of convergence when tried to analyse a two-spool by-pass engine, but eventually overcame those problems.

1.2.3 Comparison of Methods

Stoddart, Ref.(41), carried out a comparison between the two methods for a two-spool turbofan engine. During his research he found out that for all components, the steady running points predicted by both methods (ICV and CMF) coincided.

As far as the engine thrust and speed response are concerned, the predictions of the two methods are different. The transient trajectories, relative to time, predicted by the two methods showed the ICV trajectories to lead the CMF one's during all accelerations. At ten seconds into the transient the discrepancy was of the order of 7.4% for the Thrust, 2.9% for the L.P. shaft speed and 1.5% for the H.P. shaft speed. Also the ICV trajectories

were found to lag behind the CMF one's for all decelerations predicted, showing a difference of 13% for the Thrust, 4% for the L.P. shaft speed and 1.6% for the H.P. shaft, all recorded at the 2^{nd} second into the transient

More analytically, when the trajectories are plotted to a base of non-dimensional mass flow rate on the compressor characteristics, the two methods produced identical trajectories for both Inner and Outer fan. For the IP compressor the simulators predicted very similar trajectories with exception of the very first part of the deceleration. This was due to the fact that at the start of a deceleration the CMF method predicts an instantaneous change in the pressure ratio while remaining in the same non-dimensional line. The ICV one predicted a more stable start.

For the HP compressor both methods were in a general agreement. The only difference appearing to be that during both trajectories (acceleration and deceleration) the ICV method predictions are closer to the steady running line than those predicted from the CMF method by a maximum 3.8% during the Deceleration and by 3.1% during the Acceleration. The discrepancies of the two methods were evaluated as a percentage difference in pressure ratio at the non-dimensional speed of 50. Also for both the IP and HP compressor predictions the CMF showed discontinuities purely due to the nature of the logic employed.

As a conclusion it could be noted that the transient predictions of the two methods are in general agreement. The main deficiency of the ICV method is that it requires

approximately more than ten times computing time than the CMF method.

In the above mentioned comparison of the two methods, thermal effects were not included.

Since one of the major tasks of the present research was to incorporate the thermal effects it became obvious that the computing time using the ICV method would become excessive or even impracticable.

Another reason in support of choosing the CMF method in this research was the fact that this method provides a realistic representation of the events occuring in the engine during a transient.

Although the computer used during the first three years of the research was replaced by a new model giving a much faster computer running time, still the ICV method could not be used to incorporate heat transfer effects unless a method of substantially reducing the computing time was developed.

1.2.4 Non-Adiabatic Modelling

The objective of a gas turbine simulation technique is, as mentioned earlier, to predict as accurately as possible the transient performance of an engine. The simulator must also be able to operate over the entire range of the engine's transient running range.

During the last years many programs have been developed to predict the transient performance of gas turbines. Thomson, Ref.(43), quoted the earliest and more simple programs that used equilibrium characteristics for the components and ignored heat transfer effects. The results of his work showed

discrepancies in acceleration times between the predicted and the actual observed results in the order of 20 to 30 per cent for the speed and thrust responses.

One of the most important factors that has to be incorporated in all the computer models, in order to produce realistic results, are the Heat Transfer effects that occur during transients. Neglecting these effects would result in descrepancies between the results of the programs and the actual test bed results of the engine.

In 1969, Maccallum, Ref.(21), started to work on the changes that could be present within a gas turbine during a "thermal soak" transient and would cause the engine's performance to differ from the equilibrium performance. It was found that departures from the equilibrium performance have been accounted to the following transient factors:

a. Heat absorption in the metal of the turbine.

b. Heat absorption in the metal of the compressor.

c. Heat absorption in the jet pipe metal.

d. The turbine nozzle guide vane throat area was lower than the equilibrium.

e Changes in compressor characteristics.

f. Increase in the high pressure cooling air flow due to seal clearance changes.

The effects of the above mentioned factors are now discussed in more detail together with the research undertaken over the years to incorporate them into computer models.

(i) Blade Modelling:-

One of the significant heat transfers that occur in a gas

turbine is with the blading. It is thus necessary to be able to represent the turbomachine blades during temperature transients before modelling of the heat transfer effects can be achieved. Maccallum, Ref.(23), compared several geometric models for the blade and platform arrangement, on accuracy, computing time, simplicity of geometry and suitability for use alongside models for other components of an engine. It was found out that, compared with the more complex multi-element model, an adjusted Finned model was preferable for the prediction of the overall thermal response of the blade. The latter gave an adequate representation of a blade and also proved convenient in terms of computing times and hand calculations

(ii) Non-adiabatic Flow in Turbines and Compressors:-

During the period that the turbine metal is heating, the gas expansion will be non-adiabatic. A simple method of analysing the effect on performance is given below.

In an adiabatic expansion, the polytropic efficiency, η_{pt}, relates elemental changes in temperature and pressure:

$$C_p\, dT = \eta_{pt}\, v\, dP \qquad (1)$$

This leads to the relation between the index of expansion, n, and the isentropic index, γ:

$$\frac{n-1}{n} = \eta_{pt}\,\frac{\gamma-1}{\gamma} \qquad (2)$$

Consider an elemental change in a non-adiabatic expansion in which, f, is the ratio of the heat transfer to the fluid to the work transferred from the fluid. Then equation (1) becomes:

$$C_p\, dT = (1-f)\,\eta_{pt}\, v\, dP \qquad (3)$$

Provided the factor, f, is constant along the turbine, and provided that the fluid properties are uniform over planes through the turbine, then equation (3) can be integrated to give the new index of expansion, m:

$$\frac{m-1}{m} = (1-f)\,\eta_{pt}\,\frac{\gamma-1}{\gamma} \tag{4}$$

The above assumptions are made in this analysis, but it is also assumed that the polytropic efficiency in the non-adiabatic expansion equals the polytropic efficiency in the adiabatic expansion.

The non-adiabatic flow in the compressor can be analysed in a manner similar to that given in the turbine. In this case the index of compression in the transient conditions, m, is related to the isentropic index by:

$$\frac{m-1}{m} = \frac{1-f}{\eta_{pt}}\,\frac{\gamma-1}{\gamma} \tag{5}$$

For the single spool engine, the magnitudes of the heat transfer observed 5 seconds after the conclusion of a rapid acceleration was of the order of 0.03 of the work transfer for the turbine and 0.01 for the compressor. The test has been carried out at sea level.

The heat absorptions in these two components were responsible for much of the observed thrust deficit at that instant (1.7 per cent).

Predictions were also made later, Ref.(22), for accelerations and decelerations of a two-spool engine at altitude. The magnitudes of the transient heat transfer in the various components during the speed transient itself, were found to be

quite considerable rising to 0.3-0.5 of the work transfers in turbines, and 0.15-0.2 of the work transfers in compressors.

(iii) Heat absorbed in the Jet Pipe metal:-

The only case found which this was investigated was Maccallum's study, Ref(21), who found to be small and causing the equivalent of a 0.16 per cent loss of thrust at the end of the acceleration of the single spool engine.

(iv) Throat area of Turbine Nozzle Guide Vanes:-

Heat transfer also affects critical flow areas such as the nozzle guide vane area in the LP and HP turbines. Maccallum, Ref.(22), observed that the steady running line in the HP compressor was found to be affected by changes in the effective capacity(typical maximum 0.2 per cent) of the HP nozzle guide vanes. He then considered the combined effects on the surge line and on the steady running line. The most serious results appeared to arise in the LP compressor during an altitude deceleration, and in the HP compressor when acceleration followed a rapid deceleration.

(v) Changes in Compressor Characteristics:-

The first two factors described earlier are the direct effect of heat being exchanged between the engine metals and the working fluid which also results in changes in compressor characteristics.

An early theoretical investigation on the effects of heat transfer on compressor characteristics and on the working line of the engine was carried out by Maccallum, Ref.(22). This investigation was carried out on a twin spool by-pass engine. Considering, for example, an acceleration, the fluid leaves a blade pair with a reduced temperature. This reduced temperature is the inlet for the next blade pair and the reduction was due to

heat being transfered from the fluid to the material. Hence the fluid will be entering the next stage with properties that differ from the adiabatic ones. This exchange of heat between the fluid and the engine components, alters the fluid's temperature which will therefore change the fluid's density. These changes affect the fluid's axial velocity and also its deflection experienced by the blades. Consequently the characteristics of the component will be altered. Maccallum and Grant, Ref.(29), had found an approximation for the change in deflection due to heat transfer effects in boundary layer changes to be given by:-

$$\Delta\alpha/\epsilon des = (T/1000)x(0.5+0.84x(i-ides))/\epsilon des$$

The heat transfer effects on the LP compressor characteristics were found to be very small while in the HP compressor they are considerable. One effect found was the movement of the effective non-dimensional speed of the HP compressor-typically this could be about 1 per cent. The second effect in the HP compressor is on the surge line and depends on where the stall causing surge occurs.

Further, the change in deflection due to heat transfer effects in blade boundary layers, Grant Ref.(10), could be responsible for the onset of surge in Gas turbines, causing thus changes in the surge margins of the components. It is thus very important to be able to avoid surge in the compressor(s) during transients of aircraft gas turbines. Hence the position of the surge line is very important in order to decide what transient schedule could be allowed. As early as 1965, Robbins and Dugan, Ref.(35), found that one possible approach is to draw the surge line through the peak-pressure ratio points of the performance map. Four years

later, Gray, Ref.(11), indicated that in the surging cycle, stall progresses through all stages and offered another approach. At high rotational speeds the rear stages of the compressor tend to stall first. This can trigger stall to adjacent stages. The triggering advances rapidly through the machine until all stages are stalled and the compressor surges. Thus one criterion used here is that if one of the rear stages of the compressor stalls, then this represents the onset of surge. At low rotational speeds stall first occurs in the early rows of the compressor. Rotating stall cells are established but they exist without causing surge. In the case where the exit flow is sufficiently throttled, the stall cells spread and surge occurs. On Gray's hypothesis, the stall cell zones must have extended along the length of the compressor. Gray also proposed that there are two flow regimes in the annulus. There are stall zones which have zero net throughflow in one section, and in the remainder there is normal unstalled flow. Gray's model was incorporated in Maccallum and Grant's model, Ref(29), by applying the assumption that the flow returns immediately to the normal pattern at the first row at which the average value of incidence is insufficient to cause stall. Hence surge occurs when at least three of the early stages have stall zones or when the overall pressure rise-mass flow characteristic has a positive slope, whichever occurs first. A two-dimensional procedure was adopted by Maccallum and Grant, Ref.(29). The aim of their study was to predict the change in the characteristics of the real three dimensional compressor, due to heat transfer. A reasonable estimate was given by the differences between the two sets of characteristics of the

compressor, as predicted by the two dimensional method with and without heat transfer. Pilidis, Ref.(31), using a choise of methods existing at that time, Ref.(6,7&13), and using also the theory of the onset of surge in gas turbines, see Appendix(1), obtained a simplified correlation to represent the movement of the surge line. This being given by:

$$(PR_{ht}-1)/(PR_{ad}-1) = f(F) \quad \text{and} \quad f(F) = 1+0.541F$$

F being the ratio of the heat transfer to wotk transfer.

Turning now to the effect of heat transfer on the blade boundary layer, a more localised heat transfer effect in a compressor results from changes on the boundary layers which develop on blade surfaces. In general terms, it has been observed, Refs.(10,28&27), that a heat transfer from a surface to a boundary layer increases the rate at which the layer develops due to local density reduction. The presence of an adverse pressure gradient makes the effect more severe. Heat transfer also influences the transition from laminar to turbulent flow in the boundary layer, moving the transition region upstream and reducing its length, Grant, Ref(10). In the case of an axial flow compressor it is probable that the annulus boundary layers will slightly thicken, causing in this way extra losses due to blockage. Similar thickening occurs in the layers on the blading, but this is a more complicated effect due to pressure gradients and is important to look at the pressure surfaces of the blades separately. The pressure surface of the blade is concave and since the boundary layer here is thin, there is a tendency for the hot air near the surface to move towards the edge of the boundary layer. This produces a circulatory effect which is otherwise known as Taylor-Gortler vortices and are present

even during adiabatic conditions, hence heating will strengthen them. Hence this effect prevents the build up of a region of low density air and so the development of these pressure surface boundary layers is not significantly influenced by the heat transfer. On the suction surface, which is convex, the recirculation of hot air is prevented due to the presence of a strong adverse pressure gradient. The wake developed behind each blade thickens appreciably resulting in an increase in losses due to profile drag. There is also a further complication in the angular stream deflection produced by the blades which appear to be reduced. A computer prediction method was employed by Grant, Ref(10), to examine the development of blade boundary layers. In this method, laminar boundary layer growth was predicted by the theory of Luxton and Young, Ref.(20). Normally there is a straight forward transition of the attached boundary layer but in this method an alternative possibility of the development of a separation bubble with subsequent turbulent reattachment was considered. Calculation of turbulent boundary layer development was based on the theory of Head, Ref.(15), as modified for compressible flow from Green, Ref.(12). The modification to the momentum integral equation suggested from Patel, Ref.(30), was used in order to allow for longitudinal surface curvature. The prediction method has been applied to aerofoils and conditions typical of axial flow compressor practice, Ref.(29). It was found that the region of most rapid boundary layer growth was on the suction surface near the trailing edge of each blade, the layer being fully turbulent. In the laminar and transition regions the layers were thin and the predicted effect

of heat transfer was small. Attention was centred on the turbulent boundary layer and in all cases the effect of heat transfer was to increase the displacement thickness of the turbulent boundary layer. The heat transfer in most cases is predicted to cause a small upstream movement of the separation point. The boundary layer on the pressure surface of the blades was found to be largely insensitive to the heat transfer from the blade, and also its thickness and angle of departure from the trailing edge will not change with temperature. However, the more rapid growth of the suction surface boundary layer on a "hot" blade will result in a change on its angle of departure. It was also predicted that at the later stages of the compressor, the effect of the increased air density was to increase the inertia of the flow, reducing boundary layer thickness and delaying separation, but once separation had occured the rate of growth of the displacement thickness was increased. For a given incidence angle, the profile drag is increased if the deflection is reduced, because losses are closely related to the width of the wake which is closely related to the deviation.

Considering the above mentioned effects on the compressor characteristics, it was predicted, Ref.(29), that the reduction in surge margin in a hot acceleration were respectively 25 per cent due to bulk heat transfer effects, and 40 per cent due to boundary layer effects.

(vi) Tip and Seal Clearances:-

The heat being exchanged between the working fluid and the metals of the components of the gas turbine is also responsible for an indirect effect. During transient operation, gas turbines

are subjected to thermal and mechanical loading, which result in changes in dimension of both stationary and rotating parts causing variation in Tip and Seal clearance which results to off design mass flows. Changes in mass flows and efficiency result from variation of Tip clearances, which was earlier mentioned in factor (e). The clearance of a Seal, factor(f), controls the amount of air leaking through it in order to be used to cool hot sections of the engine. If this amount is too much then a performance deterioration will be inevitable. If it is too small, then insufficient cooling will endanger the hot sections of the engine and in particular the turbine discs. These changes that occur in the Tip and Seal clearances due to thermal expansion or contraction, result in changes in the efficiencies and the mass flow in the gas turbine. It is thus very essential to be able to predict the response of the Tip and Seal clearances under any type of transient. Together with the Heat transfer effects there is the Mechanical effect of the centrifugal growth which affects the above mentioned clearances during a transient. In order to produce a very realistic and accurate way to incorporate these changes into the computer model, it is necessary to study separately the Thermal effects and the Mechanical effects responsible for the changes in the Tip and Seal clearances, and then add the two effects together to find out the total change. An investigation was carried out by Maccallum, Ref.(24), in the effort to predict the movements of the critical components of an air seal using simple finite difference models with the appropriate boundary conditions. The gas turbine investigated was a typical two-spool bypass jet engine. The geometry of the seal, which is formed between the tips of four fins attached to

the turbine disc and a stationary ring, was approximately represented by two models. One was for the turbine disc and one for the stationary ring. Appropriate boundary conditions were applied and the two models were used to predict the seal clearances under two testing transients. The acceleration and deceleration between the ground idling and maximum speeds were studied. The predictions of the turbine disc model under steady state were found in reasonable agreement with thermal paint results. For the most severe transient, which was found to be an acceleration from ground idling speed to maximum speed, the predicted seal opening during the speed transient was at least double the equilibrium value.

(vii) Modelling of the above Effects into Prediction Programs:-

In 1979, Maccallum, Ref.(25), produced a method for predicting the transient response of a single spool gas turbine. The changes in the compressor characteristics that occur during transients, excluding surge line changes, have been incorporated in that method. One of the features of this modelling was the choice of correlation for the average heat transfer coefficient on blades. The simple Colburn equation:-

$$hy/k = 0.023(my/A\mu)^{0.8} \times (Pr)^{0.4} \qquad [7]$$

had been used by Saravanamutoo and Fawke, Ref.(39), for flows over compressors and turbine blades. However this assumed that flow was developed and that turbulence had no influence on the heat transfer coefficient. The problem recognised by Maccallum is that the flow over the aerofoil of a blade in a compressor or a turbine is far from developed. Since a new boundary layer has to be started at the leading edge of each

blade, it is more reasonable for the compressor to use the flat plate correlations for developing laminar and turbulent layers. Thus for a laminar layer of length l, the average heat transfer coefficient is given by:-

$$h_{lam} = 0.664k(Pr)^{0.333} \times (m/A\mu l)^{0.5} \qquad [8]$$

and for a turbulent boundary layer:-

$$h_{turb} = 0.037(m/A)xC_p(ml/A\mu)^{-0.2}(Pr)^{-0.667} \qquad [9]$$

It is also possible and reasonable to assume that the boundary layer, in a compressor, on the pressure surface is turbulent throughout its length, while that on the suction surface is initially laminar becoming turbulent downstream. From this assumption an average heat transfer coefficient can be given by:-

$$h_{ave} = 0.25h_{lam} + 0.75h_{turb} \qquad [10]$$

Comparing the results of the equations **[7]** and **[10]** it was found that the value of coefficient given by **[7]** is 30 per cent lower than that given by equation **[10]**. Brown and Burton, Ref.(4), indicated a 60 per cent increase in average heat transfer coefficient for an increase in turbulent intensity from 1.8 to 8.6 per cent, something which is ignored in the above mentioned expressions. Bayley and Milligan, Ref.(2), showed increase of similar nature but depending on the frequency of turbulence fluctuations. The range of increase in coefficients was from 20 to 160 per cent for turbulence intensities varying from 14 to 48 per cent. In order to have more accurate result when calculating for heat transfer coefficients in a compressor, it is reasonable to use the last equation (**[10]**) with the coefficient increased by 60 per cent.

The changes in compressor characteristics result from changes due to heat transfer in the development of the boundary layer and due to the alteration in density of the air, as mentioned earlier.

The changes in the characteristics were approximated, by Maccallum, by using the concept of changes in effective speed, and these changes could be correlated to heat transfer parameters. The method was applied to a single shaft aero gas turbine.

The above analysis was extended to a two-spool by-pass engine with mixed exhaust and overall maximum pressure ratio of 21 by Maccallum, Ref.(26). The pressure ratio of the HP compressor being 7.6 and the by-pass ratio at maximum conditions was 0.58. The changes in effective speed due to boundary layer effects for the LP compressor was given by:-

$$(\Delta N/N)_{\text{boundary layer}} = -0.10 \times Q/(mC_pT_{ave1,2}) \qquad [11]$$

The alteration in effective speed due to density changes as a result of heat transfer was given by:-

$$(\Delta N/N)_{\text{density change}} = -0.10 \times Q/(mC_pT_{ave1,2}) \qquad [12]$$

The corresponding relations for the HP compressor were found to be:-

$$(\Delta N/N)_{\text{boundarylayer}} = -0.15(T_{\text{aerofoil}}-T_{ave1,2})/T_{ave2,3} \qquad [13]$$

where 1,2 = inlet to, outlet from LP compressor

3 = outlet from HP compressor

The effects of heat transfer on the performance of the various components were further studied by Pilidis, Refs.(31,34), who included changes in clearances along with the heat transfer effects already described. In this work, a model was proposed

for the calculation of the tip and seal clearances and a simplified version of that model, treating only with radial clearances, was used in the General Program. Dealing firstly with the thermal effects mentioned earlier, Pilidis used the finite element for transient heat conduction and modified it to analyse the thermal response of the disc component of the rotor. In his work broke the complex shape of the disc into three components; a thick hub portion, a thin diaphragm and an outer section. Different rates of heat transfer result to different paterns of expansion and each part was represented by the appropriate correlations. The model produced was applicable to both compressor and turbine tip movements, using Hall's correlations for all blades. An important feature of all turbine blades is that they are cooled and this was included in the simulation program defining the cooling effectiveness by the equation:-

$$e = (T_{cg} - T_b)/(T_{cg} - T_c)$$

Defining the effectiveness of the cooling flow determines the final metal temperature which in turn produced the transfer of heat. The casing structure was considered as a cylinder in which a smaller cylindrical shape is rotating. The casing exchanges heat with the by-pass air as well as with the internal (core) air. The heat transfer coefficient used, was given by the correlation obtained from the work done by Tachibane and Fukui, Ref.(42). Due to the changing rotational speed during a transient, mechanical effects such as changes of the stresses in the components, result in centrifugal growth. Pilidis used the same subdivision of the rotor and the disc. Distortion in the tangential direction was found to be negligible. The thermal and mechanical

effects were combined ensuring continuity of radial dimensions at the interfaces, thus the overall changes in disc dimension was calculated. The elongation of the blades, which were assumed to be rods of uniform cross sectional area, was calculated by means of integral calculus as a function of the geometry, rotational speed and material properties. The existence of a shroud on the blades was allowed in the calculation of the mechanical effects since its extra weight would have a considerable effect on the cenrifugal growth. All the calculated effects on the dimension of the rotor or compressor, are added together to obtain the resulting change in clearance. It was obvious that would be very excessive to incude each individual blade row of each compressor and turbine into the program, so a single equivalent stage was used which has been proved by Maccallum, Ref.(25), that can give satisfactory results. This single equivalent stage was developed on averaged properties of specific heat, thermal expansion coefficient, Young's modulus and material density, to represent tip clearances and associated efficiency changes. The effect of density changes of the fluid was also considered.

Heat transfer also occurs in the turbines where heat is exchanged between the working fluid and the turbine material. The heat transfer effects on turbine performance characteristics were not included as it was considered that the penalty in accuracy would be very small. The effects of non-design gas angle in the turbine blading result in far smaller effects than those affecting the compressors. The reasons being as follows:-

Any non-design deflection due to modified boundary layers, will have a relatively small effect on the large deflections (much

larger than the compressor) that take place in the turbine blading. Also, no danger of separation, which could result in stall, exists in the turbine, since the flow here experiences favourable pressure gradient and acceleration. Finally the turbines consist of very few stages (e.g. 3) so the effect will not affect many subsequent stages, as happens in the compressor (e.g. onset of surge). The effects of heat transfer in the combustion chamber as well as in the propulsion nozzle were not included in Pilidis's model.

1.3 TYPICAL MODERN TURBOFAN ENGINE

The design of the Turbofan engine was originally conceived to increase the propulsive efficiency by reducing the mean jet velocity and increasing the air mass flow. The reduction in jet velocity had a considerable effect on engine noise. The reduction of jet noise became so critical that new engines went under development for low noise level requirements.

In this type of engine (Turbofan), the by-pass air, a part of the total flow, by-passes the compressor, combustion chamber, turbine and nozzle before being ejected into the atmosphere, in a separate nozzle which is the case of the Separate exhaust engine. It is some times desirable to mix the two exhaust gases.

The Turbofan engines are described in terms of the by-pass ratio. The present investigation is directed towards a typical modern Turbofan engine, of medium by-pass ratio, i.e. by-pass ratio of about 3. An engine of this classification, the Rolls-Royce Tay engine(RB 183-03), has been described by Ashmole, Ref.(1) and as this engine can be regarded as typical, some features of

the Tay engine are given in the current section. These descriptions are based on information contained in Ashmole's paper.

Introducing the TAY engine (RB 183-03), it is essential to mention that it derives its pedigree from the SPEY family of engines. The main factor in the concept of this engine was the reduction in noise.

In order to meet this major requirement, efforts were concentrated on increasing the by-pass ratio and the Low Pressure (L.P.) compressor flow. This was fundamentally achieved by replacing the L.P. compressor of the Spey engine, with a wide chord Fan and an Intermediate Pressure (I.P.) compressor.

Efforts were also directed towards further improvement in fan efficiency which was achieved by using the new technology of the Wide chord Snubberless fan, which has been introduced into the RB 211-535 engine. It can be observed from a typical snubbered fan rotor efficiency profile, Ref.(1), that the presence of the snubber contributes significantly to inefficiency. The best approach to minimize this inefficiency was to delete the snubber from the fan. This removed the fundamental aerodynamic loss, together with the interactive losses on the surrounding aerofoil, hence giving a substantial efficiency gain. The absence of the snubber gives rise to vibration problems which in order to be solved, the new design must have a lower aspect ratio, i.e. wide chord. This resulted in a reduced number of blades, in fact down to 22 from 33 for the RB 211 fan designs. The new design proved to offer many improvements: Satisfactory vibration

characteristics were achieved, improved foreign object damage and also a lighter fan assembly. The latter improved the response of the fan in terms of the centrifugal growth due to the absence of the extra weight of the snubber.

A conical spinner is fitted infront of the fan, made from GRP composite construction to provide optimum flow lines. A soft rubber nose is incorporated on the spinner and the whole assembly is formed at an angle of 56°, the optimum ice shedding angle.

The Tay blade is solid Titanium forging retained in the disc by a curved dovetail root. The blade geometry is conducted by considering robustness of bird strike, weight aerodynamic efficiency and stress and vibration criteria.

The major design objective was to stay with the SPEY Mk 555 core, which had proved very reliable, but also operating at exactly the same conditions as it does in the F28 today. These conditions at the entry of the H.P. compressor are reproduced by mounting a three stage Intermediate Pressure compressor. The increased torque required to drive the Fan and the three stage I.P. compressor was achieved by introducing a three stage, instead of two, L.P. turbine.

CHAPTER II

DIFFERENT COMPUTER MODELS FOR THE SIMULATION OF A TYPICAL TURBOFAN ENGINE ORIGINATING FROM DIFFERENT FAN TREATMENTS AND AIR FLOW DISTRIBUTION.

2.1 INTRODUCTION

This chapter describes the computational models developed to best represent the fan of a typical two-spool turbofan engine as well as the air flow distribution into and after the fan. A tabular summary of the programs using these methods is given in Figure(2A).

The type of turbofan engine considered in this investigation is the two-spool engine in which the compression system on the Low Pressure (L.P.) shaft comprises a Fan, which compresses both the bypass air and the core air, followed by an Intermediate Pressure (I.P.) compressor (or "Booster") for the core air. A typical engine of this type is the Tay engine which was described in section 1.3.

Pilidis and Maccallum, Ref.(33), developed firstly a General program for the prediction of the performance of Gas Turbines, and later a computer model to simulate the Tay engine. Using this program as the basis, the different fan treatments were investigated.

A brief description of the General program, mentioned above, is included, so that the reader can follow easily the required changes for the application of the different fan treatments

2.2 DESCRIPTION OF THE GENERAL PROGRAM FOR THE PREDICTION OF THE TRANSIENT PERFORMANCE OF GAS TURBINES

When the representation of a gas turbine is desired, a model is devised which in this case could either be physical or mathematical. Because of the lengthy calculations required, the mathematical model involves computer programming, in particular for the more complex engines.

In the design stage of a proposed engine, the characteristics of the components have first to be predicted. These are then used by the General program for the calculation of the complete engine's performance. If the design is continued until components are manufactured one then updates the component characteristics using experimental observation of the performance of each component, in order to obtain more accurate and realistic results from the model of the engine.

The characteristics of these components at a particular instant during a transient differ from the characteristics observed in the steady state at the same non-dimensional speed. This difference, as described in Chapter(I) is due to tip clearance changes, seal clearance changes and heat transfer effects, and these have been incorporated in the General program.

Pilidis and Maccallum, Ref.(33), in developing their General program used the method of continuity of mass flow(CMF) which was explained briefly in Chapter I.

The object of the calculation procedure is to determine the acceleration of the engine under different circumstances. The acceleration is primarily a function of parameters such as shaft

speed, fuel flow, inlet temperature and pressure and secondarily a function of several other variables such as component efficiencies, and pressure and temperature ratios. If the external parameters are defined and the rotational speed and fuel flow are known, the compressor's non-dimensional mass flow and isentropic efficiency are obtained. The delivery conditions of the compressor can then be found which are going to be the inlet conditions for the next component. This is repeated for each component until it is necessary to calculate the nozzle area to discharge the flow. If this is different from the actual one available, then, if the turbine is choked, the compressor pressure ratio is modified until the required value of the turbine capacity is obtained. Once this has been achieved the variable to be adjusted to satisfy mass continuity at the final nozzle is the pressure ratio of the choked turbine nearest to this nozzle.

The next step was to evaluate the torque imbalance between the shafts, which determines the instantaneous acceleration for a given time step. This acceleration over the time interval gives the rotational speed of the shaft at the next time step. Having evaluated the acceleration, the rotational speed for the next time interval is found using Euler's simple assumption that the acceleration remains constant for a particular time interval.

Also for by-pass engines with mixed exhaust the principle of momentum conservation must be satisfied by the fraction of core gas and by-pass air to be mixed. In some designs it may be assumed that there is no dissipation in the mixing process.

Before proceeding to a component, all tests on the previous component must be satisfied, if not, then the inlet parameters of the nearest upstream "free component" are modified until a

satisfactory operating point is obtained. "Free component" is one at which the thermodynamic variables for the operation of the component downstream are generated.

This General computer model can also incorporate air bleed systems, re-heat systems and also any form of fuel scheduling can be adopted for control of accelerations and decelerations.

The procedure of the method is illustrated in detail in Reference(33).

2.3 THE AFCSP PROGRAM

As mentioned in the introduction of this chapter, the engine which is the subject of the present study is a medium by-pass two spool turbofan, having mixed exhaust through a single final nozzle. The L.P. shaft compression system comprises of a Fan which compresses the total air flow, followed by a three stage I.P. Compressor which further compresses the core air before it passes to the H.P. compressor.

Two alternative procedures for representing the Fan behaviour have been used in early work to produce transient models for this engine. In the first of these, separate characteristics are used for the Inner portion of the Fan and for the Outer portion, Ref.(33). This implied that changes in the core of the engine, which affect the flow through the Inner fan do not alter the flow through the Outer and vice versa. The procedure and results for this representation (referred to as "Fixed Factor of Split") are described in Section 2.6. However this simplification was thought to be a weakness and an alternative

treatment was adopted using the concept of a "Adjusting Factor of Split". The concept of an adjusting boundary between the Inner and the Outer Fan was introduced to that second computer model of the engine, Ref.(28), resulting in the program labelled AFCSP and now explained more fully. This boundary was introduced in two steps. First step towards achieving an allowance for interchange of flow was achieved by using the Fan characteristics split in the ratio of 1 to 3 between the Inner and the Outer fan, using the separate characteristics mentioned at the beginning of this section. This ratio was based on a frontal area split of 1 to 3 and was quantified in the program by introducing the parameter GEOM. As it can be seen from the following Figure(3), the line representing the GEOM parameter coincides with the boundary of the by-pass duct.

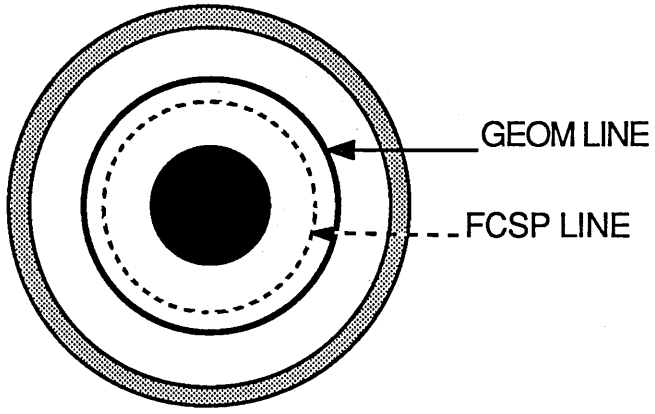

INLET VIEW OF A TYPICAL TURBOFAN ENGINE

Figure (3)

The second step was to allow for another parameter named FCSP (FaCtor of SPlit), so that the fraction of the total annular area that feeds the Inner fan is not always equal to GEOM (1 to 3) but some fraction of it which is the above mentioned FCSP. By allowing the adjustment of the FCSP, the air mass flow rate into the Inner fan is a fraction of the 1 to 3 designed ratio with the

rest of the annular area corresponding to the Outer fan. In the Figure(3) above the FCSP is given for example a value smaller than 1.0, approximately equal to 0.7. The initials AFCSP stand for Adjusting the FaCtor of SPlit and in the method adopted in this program it is assumed that the axial component of velocity of the air into the Fan is constant radially. This utilises the reasonable assumption that the stagnation pressure and the static pressure are both uniform.

In this research it is of interest to investigate and compare the different Fan treatments and flow distributions into and after the Fan, using as basis the AFCSP program.

Since all the changes necessary to adopt the different fan treatments were made on the AFCSP program, the latter is described extensively so that the reader can follow the changes made during this investigation.

Maccallum, Ref.(28), used the method of continuity of mass flow for modelling the performance of a Two Spool Turbojet and Turbofan engines. In this method the calculation procedure at each time step is iterative until continuity of mass flow is achieved at each section. This method requires a number of iteration loops and this number depends on the geometric complexity of the engine.

In this program as well as on all the other computer programs developed, the known starting parameters are the flight conditions and the rotational speeds of the shafts. The flight conditions are the ambient temperature and pressure which determine the altitude, and also the flight Mach number. The engine's stagnation entry temperature and pressure are

calculated using the ambient temperature and pressure as well as the flight Mach number. A pressure recovery factor of 0.995 is used to account for non-isentropic diffusion losses. The mechanics of fluids equations involved are shown in Appendix(B).

Now that the entry conditions to the engine are determined, it is possible to follow the flow diagram of the AFCSP program shown in Figure(4).

Starting from the Inner fan, its characteristics are stored as a table of eight non-dimensional speed lines with eight points (corresponding to eight so called "Beta values") on each line. For each point, the pressure ratio, non-dimensional mass flow rate and isentropic efficiency are tabulated. Together with the eight non-dimensional speeds the corresponding Beta values are tabulated giving eight values for the Inner fan from 1 to 8 inclusive. The tabulation method of the Inner Fan characteristics is shown in Figure(5). All the other components tabulation method is similar to the one used for the Inner Fan. The latter's characteristics are shown in Figure(6).

Knowing the entry conditions described earlier the calculations start by assuming a guessed non-dimensional mass flow rate into the Inner fan and also a guessed Factor of Split, forced initially to be equal to 1.0.

In Appendix (B) the Inner fan calculations are outlined. Using the characteristics of the Inner fan, a linear interpolation is used to calculate the pressure ratio and hence its outlet pressure, isentropic efficiency and exact Beta value. The outlet temperature from the Inner fan is also calculated as shown on

Appendix(B). Now the inlet conditions of the IP compressor are known.

The IP compressor characteristics, are stored as a table of eight constant non-dimensional speed lines with ten points on each line, corresponding to the ten Beta values. For each point the pressure ratio, non-dimensional mass flow rate and isentropic efficiency are tabulated. Using the same interpolation used for the Inner Fan and the characteristics of the IP compressor shown in Fig.(7), the outlet conditions from the IP compressor are calculated. Knowing the mass flow rate and inlet pressure and temperature, the outlet pressure is determined together with the actual Beta value and efficiency of the compressor. At this stage the outlet temperature from the IP compressor can be calculated as shown in Appendix(B). The exit from the IP compressor is now reached and the values of P_{26}, T_{26} and m_{26} have been calculated. These are now the entry conditions to the HP compressor.

The HP compressor characteristics are stored as a table of fifteen non-dimensional speed lines with ten points on each line corresponding to the ten Beta values. For each point the pressure ratio, non-dimensional mass flow rate and isentropic efficiency are tabulated. The characteristics of the H.P. compressor are shown in Figure(8). The known parameters are the non-dimensional mass flow rate and inlet pressure and temperature. During the HP calculations, a guessed HP compressor pressure ratio is used together with the non-dimensional speed, which can be evaluated, in order to determine the non-dimensional mass flow rate and isentropic efficiency. The procedure and the actual calculations are shown in Appendix(B). After the HP calculations,

a comparison is included between the actual and the characteristics obtained non-dimensional mass flow rate. This in turn will trigger either the HP compressor pressure ratio (P_3/P_{26}) under LOGIC(2), or the core non-dimensional mass flow rate under LOGIC(1), to be revised. This can be seen in the flow diagram of the program.

In general LOGIC(1) was used for decelerations and LOGIC(2) for steady running and acceleration.

As it will be seen in the description of the computational models developed in this research, a combination of the two logics was sometimes necessary to be used for steady running and transients.

The triggering of the program, under LOGIC(1), to revise the core non-dimensional mass flow rate implies that all the calculations up to this point have to be performed again from the beginning until convergence is achieved. This will require a number of iterations with cost in computing time.

At the exit of the HP compressor the known parameters are the exit temperature and pressure and the air mass flow rate. These are now used as the inlet conditions for the Combustion Chamber. The fuel mass flow rate is also known either as specified during steady running or as a fuel schedule during transients. The fuel schedule used was a function of the HP compressor pressure ratio. The effective fuel mass flow rate can be calculated by means of a combustion efficiency factor. Another factor is also included in the calculations of the Combustion Chamber, the pressure loss factor, which is a function of the ratio of combustion inlet pressure to the engine

inlet pressure.

Finally a simple energy balance is used to calculate the outlet temperature from the combustion chamber, using the inlet one and the effective fuel mass flow rate.

At this stage (exit from the Combustion Chamber), the actual non-dimensional mass flow rate is compared to the H.P. turbine characteristic's corresponding one and this could revise either the HP compressor pressure ratio under LOGIC(1), or the mass flow rate into the core of the engine under LOGIC(2). This would trigger another series of iterations until convergence is once again achieved.

Following the flow diagram of the program, the calculations of the HP turbine can now be executed. The characteristics of the latter are stored as a table of twenty two non-dimensional speed lines with fifteen points on each line, corresponding to the fifteen "work factor"($C_p \Delta T / T$) values. For each point the work factor, non-dimensional mass flow rate and isentropic efficiency are tabulated. The non-dimensional speed of the HP shaft is calculated using the inlet temperature and shaft speed.

At the beginning of the calculations a guessed work factor is used and the non-dimensional mass flow rate is the one for the previous component. A linear interpolation is used, as shown in Appendix(B), to calculate the non-dimensional mass flow rate and the isentropic efficiency.

The C_p value used in the calculations of the previous component is also initially used in the HP turbine. An actual value of T_5 and the value of γ are calculated in order to evaluate a better C_p value. Then the new C_p value is used to calculate the

isentropic value of T_5 and finally the HP Turbine pressure and temperature at the exit, which includes the cooling flows that exist in this component.

At this point the program compares the actual and the L.P. Turbine characteristic's corresponding non-dimensional mass flow rate. If the two flows are not within the permissible tolerance, then the initially guessed work factor into the HP turbine is revised until convergence is achieved.

As it can be seen from the flow diagram of the program, Fig.(4), the inlet conditions of the LP turbine are now known. The characteristics of the LP turbine are stored as a table of nine non-dimensional speed lines with nineteen points on each line. As for the HP turbine, the work factor, non-dimensional mass flow rate and isentropic efficiency of the LP turbine are tabulated.

The calculations of the LP turbine are identical to the HP turbine ones which were described earlier and are also given in more detail in Appendix(B).

The program now executes the calculations of the Outer fan. The characteristics of the Outer fan are stored similarly to the Inner fan's, with only difference being that the number of Beta values stored for the Outer fan is twelve.

Using the Factor of Split, the actual air mass flow through the Outer fan can be calculated. The calculations for this component are shown in Appendix(B). Apart from the air mass flow, the inlet temperature and pressure are also known since they are the same as the Inner fan inlet ones. Using the Outer fan characteristics, Fig.(9) and the non-dimensional speed, which is also calculated, an interpolation is used to evaluate the pressure

ratio and isentropic efficiency. Hence the pressure and temperature(P_{13},T_{13}) at the exit from the Outer fan can be calculated.

Now the parameters at the inlet to the by-pass duct are known and can be used for the duct calculations. These will enable to find the exact conditions of the air at the inlet to the Mixer, see Figure(4).

Both the by-pass and gas duct at the mixer are assumed to be isentropic. The gas duct's inlet conditions are the exit ones from the LP turbine. Using the equation:

$$m=\frac{PA}{\sqrt{T}}\left[\frac{2\gamma}{(\gamma-1)R}\times\left(\frac{P_s}{P}\right)^{\frac{2}{\gamma}}\left\{1-\left(\frac{P_s}{P}\right)^{\frac{\gamma-1}{\gamma}}\right\}\right]^{\frac{1}{2}}$$

which incorporates the core gas or by-pass air flow areas in conjunction with the ratio of stagnation to static pressure, the two mass flow rates, (gas and air), can be evaluated. The by-pass exit temperature and mass flow rate has already been corrected with the possible addition of bleed flows from the core of the engine. Hence the static pressures of the gas and air after the mixer are calculated and compared. If the difference between them is not lying within the specified permissible tolerance, then the work factor of the LP turbine is revised. This again triggers a series of iterations until convergence is achieved.

Finally the Final Nozzle calculations can now be performed since the inlet parameters, being the outlet from the mixer, are now known.

Previous simulation techniques have proved that an accurate assumption is to treat the core gas and by-pass air separately.

The ratio of ambient to stagnation pressure is calculated in order to determine whether or not the flows are choked. This ratio will be equal or less than unity since supersonic velocities cannot be attained in this engine.

The exit area required for the two flows is then calculated and modified by a coefficient of discharge. The area is calculated using the gas dynamics equation shown below:

$$\frac{m\sqrt{T}}{PA} = M \times \sqrt{\frac{\gamma}{R}} \left(1 + \frac{\gamma-1}{2} M^2\right)^{\frac{\gamma+1}{2(1-\gamma)}}$$

and for choked flow, M=1, which reduces the above equation to :

$$\frac{m\sqrt{T}}{PA} = \sqrt{\frac{\gamma}{R}} \times \left(\frac{1+\gamma}{2}\right)^{\frac{\gamma+1}{2(1-\gamma)}}$$

A test is performed after the Final Nozzle calculations during which the calculated area is compared to the available one and if the two areas do not agree then the Factor of Split is revised at the inlet to the engine, so that a new distribution of air flow is achieved between the Inlet and Outer fan. In this case all the calculations of the program have to be repeated until the values calculated for the two areas agree. The above mentioned test will be called from now on the Final Nozzle test.

2.4 VERIFICATION OF THE FCSP CONCEPT

The AFCSP program was now used to show the significance of the concept of the FaCtor of SPlit (FCSP). The program was used

to predict the steady running and transient results in different flight conditions in order to examine the variation of the FCSP with changes both in Mach number and Altitude.

The following flight conditions were examined:-

a. Sea Level Mach = 0.2

b. 43,000ft. Mach = 0.2

c. 43,000ft. Mach = 0.8

In all conditions the results of the predictions of the program were used to plot the FCSP value against a base line of the Non Dimensional Speed of the Low Pressure compressor ("NDSLP"), and also against the Non Dimensional Speed of the High Pressure compressor ("NDSHP").

The Figures(10,11,12,13,14 and 15) show the variation of the FCSP value during the above mentioned conditions.

For the steady running results, in all conditions, the FCSP has a low value(e.g. 0.7) at low fuel flow and increases in all cases towards the value of 1.0 as the fuel flow and subsequently the shaft speeds increase. This is a result of the characteristics of the compressors selected.

The transient predictions are now discussed. Considering first the decelerations, the results being presented in the form of Factor of Split(FCSP) against non-dimensional speed of the L.P. Compressor(NDSLP), it is seen in all cases that during the deceleration the Factor of Split drops below its corresponding steady running value.

The high pressure system of the engine under investigation was designed to provide high compressive efficiency at the high speed operational conditions (take-off, cruise) and also to be able

to allow the engine to operate at low speeds associated with start-up and ground idling. This is achieved by incorporating variable Inlet Guide Vanes, (IGV's), to the inlet of the HP compressor linked with a seventh stage HP compressor bleed valve. The system is controlled hydraulically using an actuator which responds to the non-dimensional speed of the HP compressor. As the deceleration starts, the HP shaft, following the rapid decrease in fuel flow, starts to decelerate with the LP shaft trying to follow. As the HP shaft speed drops it reaches the non-dimensional speed of 586 where the hydraulic actuator is activated closing the IGV's and open the seventh stage bleed. This results to an even more rapid decrease of the HP compressor mass flow while the inertia of the massive fan assembly keeps the fan running still at high rotational speeds in comparison to the already decelerated HP shaft. This results in an attempt to direct an excessive air flow into the core of the engine, more than the HP components can handle. This behaviour of the engine explains the movement of the FCSP as shown in Figures(10,11 and 12). At the first part of the deceleration the FCSP value decreases by an average of 20 per cent in order to divert more air away from the core and into the by-pass part of the engine, keeping thus the air mass flow rate into the core in agreement with the amount of air flow that the HP components can handle as they decelerate faster than the LP ones.

Both at sea level and altitude, the deceleration starts at H.P. shaft speeds close to the critical speed of the IGV's. The almost immediate response of the IGV's results in a rapid decrease of the value of the FCSP which thus reaches lower values much

sooner than the steady running results predicted. Hence the deceleration results of the FCSP appeared to deviate from the steady running predicted ones from the start and throughout most of the transient.

For the Sea level Mach equal to 0.2 case, the FCSP results for the last part of the deceleration, are very close to the steady running results showing for both an unexpected rapid decrease of the FCSP value at the lower shaft speeds and fuel flows. Since the transient at this stage follows the steady-running line with minimum discrepancies, it is preferable to explain this predicted behaviour of the FCSP by looking at the steady-running results.

The marked downturn of the curve is near the low part of the fan characteristics, starting when the mass flow rate is such that the characteristics move towards the lowest non-dimensional speed line of 93.2. Here the engine is running at very low fuel flow. At that non-dimensional speed the pressure ratio operational range of the Inner Fan is 1.02-1.03-1.02, which is a quite flat curve. At the same speed, the Outer fan's pressure ratio operating range is from 1.02 to approximately 0.97. It can be seen that the Inner fan tries to impose a single point of operation on the Outer fan close to their common pressure ratio of 1.02. However this is an extreme point of operation for the Outer fan as the non-dimensional mass flow rate is very low for both the by-pass duct and the mixer. This explains the behaviour of the FCSP which starts to reduce its value by about 15 per cent in order to push more air to the by-pass duct and the mixer.

For both cases of altitude of 43,000ft. and Mach numbers

equal to 0.8 and to the extreme case of 0.2, the FCSP value appears to decrease at the first part of the transient and moving towards a stabilising point at the end of the transient which coincides with the starting point of the steady-running results. It should be noted that the starting point of the deceleration coincides also with the maximum point of the steady running results.

Turning now to the acceleration results it can be observed from the graphs (Figures 10,11 & 12), that for all conditions, the FCSP versus the NDSLP showed a consistency of results. At the beginning of an acceleration, the FCSP has a very low value similar to the steady running results. This indicates that a small proportion of the total air flow goes into the core part of the engine, see Figure(3) in the previous section of the current chapter.

As the acceleration progresses the H.P. shaft speed reaches the critical speed of the IGV's(552) which this time open, allowing the H.P. compressor air flow to increase rapidly. Also during the acceleration the increase in L.P. shaft speed lags behind that in the H.P. shaft speed, due to the relatively low inertia of the H.P. system and the relatively high inertia of the L.P. system. The sudden increase in air demand for the H.P. compressor when the IGV's begin to open, coupled with the lagging speed of the L.P. shaft, causes the pressure ratio of the I.P. compressor to drop, to deliver a larger air mass flow, and the Factor of Split to increase.

This appears in the Sea level, Mach=0.2 results as a deviation from the steady running results towards higher FCSP values

during a range of NDSLP between 200 and 440. As the acceleration continues the FCSP moves towards the design operating point of 1.0 in order to allow increasingly more air to go through the Inner Fan and the core part of the engine.

In the extreme case of altitude of 43,000ft. and low Mach number equal to 0.2, Figure(11), the results are very close to the previous described case. Again the FCSP shows an increase from 0.825 to 0.875 during a change of NDSLP between 310 and 320, showing thus a very rapid increase. Then the rate of increase decreases as the value of FCSP moves towards the design point.

For the case of Mach number of 0.8 at 43,000ft., a more reasonable response of the FCSP is shown in Figure(12), appearing to increase rapidly at the beginning of the transient, as it would be expected, and continuing to increase normally towards the value of 1.0 for the rest of the transient.

In general it could be concluded from the above comparison, that the acceleration results, when plotted against the NDSLP compressor, show a consistency in all flight conditions. The FCSP values always lying higher than the steady running ones and all showing a rapid increase during the first part of the acceleration and then a normal increase towards the design point of 1.0 as the transient progresses to the highest fuel flows and shaft speeds.

The effect of changing the altitude at constant Mach number, is to cause a difference in the range of the FCSP values. At sea level there is a range of around 35 per cent while this is reduced to below 20 per cent as the altitude is increased to 43,000ft..

The change in Mach number keeping the same altitude of 43,000ft., also shows a change of the range of the FCSP values

breifly from just below 20 per cent in the case of Mach equal to 0.2, to around 40 per cent at Mach number equal to 0.8.

The variation of the Factor of Split(FCSP) is also illustrated in Figures(13,14 & 15), as a function of the non-dimensional speed of the H.P. compressor(NDSHP). The range in the values of the FCSP is of course the same as in the previous plots (versus NDSLP) but the relationship with NDSHP is not obvious, apart from the known result that the FCSP rises as the engine moves from idling to maximum speed. The apparent distortions in the plots arise from the complex interactions of the shaft speeds, which are discussed in the next chapter.

2.5 COMPARISON OF THE AFCSP AND AFSPSH PROGRAMS

2.5.1 The AFSPSH Program

A knowledge of flow distribution problems and the necessity of being able to analyse quantitatively problems involving flow distribution has become increasingly important in modern fluid flow and heat transfer systems.

Flow distribution non-uniformity occurs in almost every real flow system. The maldistribution of fluid flow can be caused by several factors such as viscosity effects, flow geometry, or a flow control device (blockage, flow injection, local heating, e.t.c). The most important and obvious consequence of flow maldistribution is on the pressure.

These effects were studied and represented as a new model for simulating the Typical Turbofan engine incorporating allowance for the flow redistribution after the fan.

The program AFCSP, as mentioned earlier, allows the flow distribution into the core and by-pass regions to vary by a factor named Factor of Split (FCSP). Consider now the Figure(16), which shows the region between the fan and the by-pass splitter of the engine.

Assume that at a particular instant the FCSP has the value of 1.0. In this case A_{13} is the area corresponding to the by-pass flow which is going to be equal to A_{14} (FCSP = 1.0) which is the area at the entrance of the by-pass duct of the engine. Similarly the area A_{24} is the area corresponding to the core flow just after the fan and A_{25} is the area at the entrance of the core region just after the by-pass splitter. The two areas have a very small difference.

In the case that the FCSP is not equal to 1.0-for illustration a value less than 1.0 is assumed, then A_{24} is going to be smaller and A_{13} is going to be larger as it shown in the Figure (17).

Then:

$$L'_{24}=FCSP \times L_{24} \qquad \text{where} \qquad L_{24}=124mm$$

$$L_{25}=120mm,$$

$$L_{14}=204mm,$$

$$L_{13}=204mm,$$

$$L_{b_{24}}=212mm,$$

$$L_{b_{25}}=220mm,$$

$$A'_{24}=\pi(L_{b_{24}}+L'_{24})^2-\pi(L_{b_{24}})^2$$

$$A'_{13}=\pi(L'_{13}+L'_{24}+L'_{b_{24}})^2-\pi(L'_{24}+L'_{b_{24}})^2$$

$$L'_{13}=L_{13}+L_A$$

$$L_A = L_{24} - (FCSP \times L_{24})$$

This means that the flow intended to by-pass the engine, emerges behind the Fan in the area A'_{13} which is larger than the actual by-pass area A_{14}. The inverse is the case with the core flow where the area A'_{24} is now smaller than the A_{25}

At this point is evident that a maldistribution of flow occurs. The control volume shows, in Figure (17), that the by-pass flow converges into a nozzle of inlet area A'_{13} and outlet A_{14} where $A'_{13} > A_{14}$ and having one wall as the outer casing of the engine and the other "wall" being the core flow. Since the outer flow is forced to a smaller area from a larger one, this will give rise to an increase in the flow's velocity and a decrease in its pressure.

The inverse occurs for the inner flow which is decelerated as it flows through a divergent nozzle after the fan and into the core region of the engine, as it can also be seen in the Figure (17). Hence both flows have a common boundary which effectively is the common wall of the convergent nozzle of the by-pass flow and of the divergent nozzle of the core flow.

At that interface, the by-pass flow moving relatively faster than the core one, tends to accelerate the latter while the core flow tends to decelerate the by-pass one. It is obvious that both flows do not experience a sudden change in velocity but this happens gradually over an area which is named as the Area of Contact between the two flows which is the area of the common boundary of the two flows.

At the interface, molecules from each region, can move freely into the other region, thus giving or taking up velocity depending from which flow the molecules originated. This gives rise to a momentum transfer across the Area of Contact, (A_{Con}).

This change in momentum is the one that tends to accelerate the core flow or decelerate the by-pass flow, resulting in a shear stress at the interface (Area of Contact) of the two regions.

The existence of the difference in velocities of the two flows and hence of the shear stress, will result in different pressures of the flows at their entrance to the by-pass and core region respectively. Until now the pressures of the flows just after the fan, were the ones considered as the inlet pressures for the next components (the IP compressor and the by-pass duct). The possibility of the existence of this difference was investigated and the theory was used to form, first a mathematical model and then a computer model named AFSPSH (Adjusting the Factor of SPlit considering also the SHear stress between the flows just after the fan).

The magnitude of the Area of Contact depends on the actual FCSP value and on the distance from the engine's splitter, where the two flows start to separate moving towards their final destination, the by-pass or core region.

Unfortunately at the time when the present investigation was carried out, there were not enough informations on predicting the separation of two jets of flow upstream of a splitter, and was decided to start the modelling considering that the separation point was immediately after the Fan. In this way the Area of Contact was maximised so that the results of the investigation would be under the extreme conditions, helping in this way to decide if the above mentioned effects are worth of consideration.

From the work of Ellingsworth, Shu and Kuo, Ref.(*Journal of Engineering for Gas Turbine Power, Vol.106, Year 1984*) and

from the Ref.(*Handbook of Fluid Mechanics*), it was decided to use a friction factor of 0.094.

By applying a momentum balance on the control volume shown in Figure (17) the following expressions are obtained:

Momentum equation for the Outer flow:

$$(P_{13} \times A_{13}) - (P_{14} \times A_{14}) - \left(\frac{P_{13}+P_{14}}{2}\right) \times (A_{13}-A_{14}) - \tau \times A_{Contact} =$$

$$= m_{outer} u_{14} - m_{outer} u_{13}$$

but $m = \rho A u$ (Continuity)

Hence $m = \rho_{14} A_{14} u_{14}^2 - \rho_{13} A_{13} u_{13}^2$

From $PV = mRT$ and $m/V = \rho$ we get that $\rho = P/RT$

Also $u = M\sqrt{\gamma RT}$

Hence the momentum equation can be reformed to:

$$P_{13}A_{13}(1+\gamma M_{13}^2) - P_{14}A_{14}(1+\gamma M_{14}^2) - \frac{(P_{13}+P_{14})}{2} \times (A_{13}-A_{14})$$

$$-\tau \times A_{CON} = 0 \quad \text{...[I]}$$

where

$$P_{13}A_{13}(1+\gamma M_{13}^2) \text{ and } P_{14}A_{14}(1+\gamma M_{14}^2)$$

are the Impulse Functions and by definition the shear stress τ is given from the equation:

$$\tau = f \times \left(\frac{\rho u^2}{2}\right)$$

In equation [I], since the term $(P_{13} + P_{14})/2 \times (A_{13}-A_{14})$ is an approximation, it is essential at this stage to justify how successful is. In order to justify it, the case where $\tau = 0$ is considered and then equation [I] becomes:

$$P_{13}A_{13}(1+\gamma M_{13}^2) - P_{14}A_{14}(1+\gamma M_{14}^2) - \left(\frac{P_{13}+P_{14}}{2}\right)(A_{13} - A_{14}) = 0$$

also

$$P_{013}=P_{014} \text{ or } P_{13}\left(1+\frac{\gamma-1}{2}M_{13}^2\right)^{\frac{\gamma}{\gamma-1}} = P_{14}\left(1+\frac{\gamma-1}{2}M_{14}^2\right)^{\frac{\gamma}{\gamma-1}} \quad \text{...[II]}$$

Now by using as typical values $P_{13}=110{,}000\ N/m^2$ and $M_{13}=0.3$ and $M_{14}=0.333$ the equation [II] gives:

$$\frac{P_{14}}{P_{13}} = \left(\frac{1+\frac{\gamma-1}{2}M_{13}^2}{1+\frac{\gamma-1}{2}M_{14}^2}\right)^{\frac{\gamma}{\gamma-1}} = \left(\frac{1.0180}{1.02178}\right)^{3.5} = 0.987112 \quad \text{...(1)}$$

From Continuity it can be obtained that $A_{13}u_{13}\rho_{13}=A_{14}u_{14}\rho_{14}$ which can also been written as:

$$A_{13}M_{13}\sqrt{\gamma RT}\frac{P_{13}}{RT_{13}} = A_{14}M_{14}\sqrt{\gamma RT}\frac{P_{14}}{RT_{14}} \quad \text{...(2)}$$

But it is also known that:

$$T_{13}\left(1+\frac{\gamma-1}{2}M_{13}^2\right) = T_{14}\left(1+\frac{\gamma-1}{2}M_{14}^2\right) \quad \text{...(3)}$$

By substituting equation (3) into (2) we get :

$$A_{13}M_{13}P_{13}\sqrt{1+\frac{\gamma-1}{2}M_{13}^2} = A_{14}M_{14}P_{14}\sqrt{1+\frac{\gamma-1}{2}M_{14}^2} \quad \text{...[III]}$$

Substituting the results obtained from (1) to equation [III] the following result is obtained:

$$A_{14}=A_{13} \times 0.919255 \qquad \text{...(4)}$$

By substituting the results of **(4)** to equation **[I]** together with the rest of the known parameters, then the equation **[I]** reduces to an equality $0.000024=0$, which is correct within a 0.03% error. Hence it is justified that the approximation of equation **[I]** is correct within the above mentioned error.

Equation **[I]** as it stands, is very complicated to be incorporated into a computer program and it was thought, at this stage, to attempt to simplify it.

Consider now the case where the control volume representing the air flow after the Fan, Fig.(18), is divided into two parts. The first part of the flow is isentropic and the second is considered with friction. For the first part a difference in area is also allowed to occur as it is shown in the Figure (18) below:

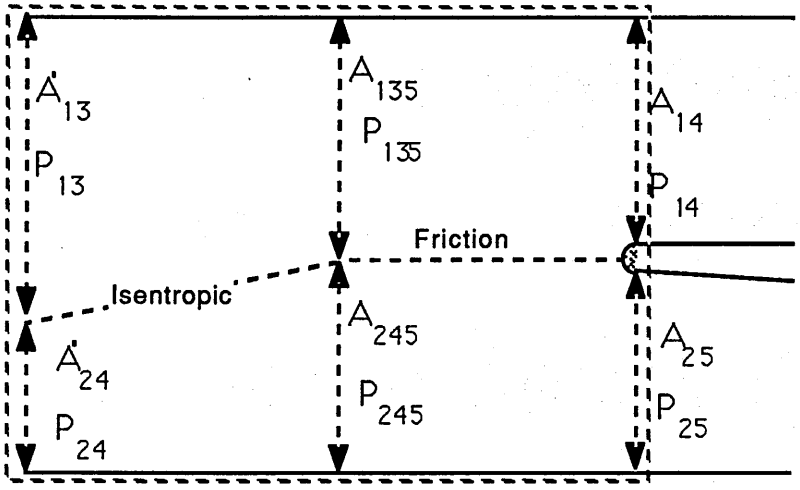

Figure (18)

The second part, where friction is allowed, there is no change in area.

In this particular case described above a simpler version of equation **[I]** will be tested for its adequacy to describe the flow.

$$P_{013} \times A_{14} - P_{014} \times A_{14} = \tau \times A_{CONTACT} \qquad \text{...[IV]}$$

It is now necessary to justify how accurate is the above simplified version of equation **[I]**.

Consider $M_{13}=0.30$ $M_{135}=0.33$ $M_{14}=0.35$

$P_{013}=P_{0135}$ and $P_{013}=110,000 N/m^2$

For the flow between the station 135 and 14 it is possible to use the equation **[III]**, which will become:

$$A_{135}M_{135}P_{135}\sqrt{1+\frac{\gamma-1}{2}M_{135}^2} = A_{14}M_{14}P_{14}\sqrt{1+\frac{\gamma-1}{2}M_{14}^2}$$

but $A_{135}=A_{14}$ and also P_{135} and P_{14} are static pressures and have to be converted to stagnation ones. Hence the above equation is transformed to:

$$\frac{P_{0135}}{\left(1+\frac{\gamma-1}{2}M_{135}^2\right)^{\frac{\gamma}{\gamma-1}}}\times\sqrt{1+\frac{\gamma-1}{2}M_{135}^2}\times M_{135}=\frac{P_{014}}{\left(1+\frac{\gamma-1}{2}M_{14}^2\right)^{\frac{\gamma+1}{2(\gamma-1)}}}M_{14}$$

By substituting all the known values to the above equation and solving for P_{014} the result is $P_{014}=104,544.76$ Hence P_{14} and P_{13} can be calculated and are found to be :

$$P_{14}=96,052.879 \quad \text{and} \quad P_{13}=103,341.67$$

Now the above found values can be substituted to equation **[III]**, which results in:.

$$A_{13}\times 31280.279 = A_{14}\times 34027.842$$

or

$$A_{14} = 0.919255 \times A_{13}$$

By using the above results found from equation **[III]**, to the equation **[IV]** and also to equation **[I]**, it is then possible to compare the results between **[I]** and **[IV]** and decide whether or not their discrepancy is acceptable.

From **[IV]** it is found:

$$A_{13} \times (101,118.05-96,103.293) = \tau\ (A_{Con}) \text{ or}$$

$$(\tau \times A_{Con}) = 5014.757 \times A_{13}$$

From **[I]** it is found:

$$(\tau \times A_{Con}) = 4872.6236 \times A_{13}$$

The results of the two equations show a discrepancy of 2.8% which is within the reasonable limits of error acceptance and hence equation **[IV]** can be used reliably as a simplified form of the equation **[I]**.

As mentioned earlier the Area of Contact depends on the value of the FCSP. In order to be able to continue this investigation the Area of contact has to be evaluated. The Figure(17) shows the dimensions in the control volume, obtained from the General Arrangement Drawing of a typical turbofan engine of scale 0.5:1. Knowing all the dimensions required then the Area of Contact ($A_{Con.}$) is equal to the area of a surface of revolution, as shown in the Figure(19) below:

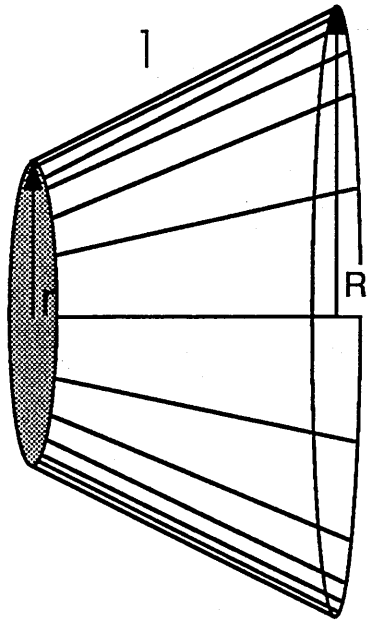

Figure(19)

The corresponding dimensions to the above Figure are:

$r = L_{24} \times FCSP = L'_{24}$ where $L_{24} = 124$ mm

$R = L_{25} = 120$ mm and $L_G = 60$ mm

$L_A = L_{24} - L_{24} \times FCSP = L_{24}(1 - FCSP)$

$$L_F = \sqrt{L_G^2 + L_A^2}$$

Also $A_{14} = \pi (L_{14} + L_{25})^2$ where $L_{14} = 204$ mm

By substituting the above mentioned known values then $A_{14} = 0.566542$ m^2, and equation **[IV]** can be written as:

$$P_{013} - P_{014} = \frac{\tau \times A_{Con.}}{A_{14}}$$

Consider now the case where the conditions in stations 14 and 25 are the same with the conditions in stations 13 and 24. Then the velocity at 14 can be represented as a function of P_{013}, T_{013}, $m_{by-pass}$ and A_{14}.

Using the Continuity equation the following formula can be obtained:

$$m_{bp} = \frac{P_{013} \times A_{14}}{\sqrt{T_{013}}} \times \sqrt{\frac{\gamma}{R}} \times \frac{M_{14}}{\left(1 + \frac{\gamma - 1}{2} M_{14}^2\right)^{\frac{\gamma+1}{2(\gamma-1)}}}$$

It is important to be able to calculate the velocity of each flow (core or by-pass) at the exit from the control volume shown in Fig.(17 and 18). This will enable to calculate the relative velocity between the two flows which can then be used to evaluate the shear force at the contact of the two air streams. The pressures of the two flows can then be calculated at the inlet of the core and by-pass regions.

Parameters obtained from the steady state results predicted from the AFCSP program at Sea level and Mach equal to 0.2, were substituted in the above mentioned equation. These parameters were: T_{013}=295.94, P_{013}=109.46, and also the by-pass non-dimensional mass flow rate. The above equation can then be re-written in the simplified form shown below:

$$\frac{M_{14}}{(1+0.2M_{14}^2)^3}=0.2210355$$

The calculations involved are shown in Appendix (C).

In order to calculate M_{14} from the above simplified equation a NAG subroutine (E04ABF), was used in the main program, which calculates the least values of the the above equation written in the form:

$$\left[\frac{M_{14}}{(1+0.2M_{14}^2)^3} - 0.2210355\right]^2 = 0$$

The whole equation was raised to the power of 2 in order to secure positive results.

Hence M_{14} is evaluated and then U_{14} is given by :

$$U_{14}=M_{14}\sqrt{\gamma RT_{013}}$$

The same procedure is repeated for the core flow and similarly U_{25} is calculated.

The mathematical justification and procedure of calculations is shown in Appendix(C).

Once U_{14} and U_{25} are known, then their difference is used to evaluate τ from the formula:

$\tau = 1/2\ f \rho U^2$ where f is equal to 0.094 and ρ is

calculated from:

$$\rho=\frac{P}{RT}=\frac{\frac{P_{025}+P_{014}}{2}}{R\left(\frac{T_{025}+T_{014}}{2}\right)}=\frac{\frac{P_{024}+P_{013}}{2}}{R\left(\frac{T_{024}+T_{013}}{2}\right)}$$

Both τ and $A_{Con.}$ are substituted into equation **[IV]** to calculate the new pressures at the inlet of the by-pass and core parts of the engine. These new values are the ones used for the calculations of the next components.

The calculations involved are also shown in Appendix(C). More hand calculations were done using other input parameters from the AFCSP program in order to compare and justify the predictions of the program AFSPSH.

2.5.2 Comparison Of Predictions

The new program was used to predict the Steady State results of the typical Turbofan engine in two different flight conditions:

Sea Level and Mach = 0.2 and

Altitude = 47,000ft., Mach = 0.92

Figures(20 to 24) show the comparison of the AFSPSH results to those obtained from the AFCSP program, which was run under the same flight conditions.

Figures(20 and 21) show the LP and HP shaft speeds against the Fuel flow predictions for both programs. Their results show no divergencies. The predictions are also identical for the Thrust versus the Fuel flow, as shown in Figure (22).

Finally for the Sea Level condition, the two new pressure ratios of the AFSPSH program (P_{14}/P_1 and P_{25}/P_1) were plotted

against the Outer and Inner Fan non-dimensional mass flow rates. The corresponding pressure ratios of the AFCSP program were superimposed in the same graphs in order to outline any significant difference. Figures(23 and 24) show that the two programs give identical predictions.

Similarly for the Altitude=47,000ft. predictions, the two programs were used to plot the LP and HP shaft speeds against the fuel flow.

While the LP versus the Fuel flow results show no discrepancy, Fig.(26), the HP shaft speed showed a difference at the middle of the HP shaft speed range. This difference between the two programs is of the order of 0.47% as it can be seen in Figure(27).

The same appears to exist when the LP shaft speed was plotted against the HP one, see Fig.(25). The discrepancy was again at the middle of the speed range and of the order of 0.47%.

The predictions of the two programs were also used to plot the two new, shear force including, pressure ratios and the ones obtained from the AFCSP program against the non-dimensional air mass flow rate. Figure(29) shows the P_{13}/P_1 (AFCSP prediction) and P_{14}/P_1 (AFSPSH predictions) plotted against the Outer Fan air mass flow rate. Figure(30) shows the corresponding parameters plotted for the Inner Fan. Both Figures show that there is no significant discrepancy between the predictions of the two programs.

From the results of the AFSPSH program and their comparison to the AFCSP ones, it is noted that the effects that were modelled in the AFSPSH program, although it was proved that they exist and cause some changes, there is not any significant departure

from the AFCSP predictions. Since shear force effects due to maldistribution of flow will exist in other parts of the engine also, (e.g. in front of the Fan), the current investigation proved that these effects are negligible and can be ignored. The AFSPSH program executes significantly more calculations and iterations under the expense of computing running time, something to become very essential when incorporation of other effects will take place, such as Heat Transfer effects.

For the above mentioned reasons as well as for the fact that the AFSPSH predictions were identical to the AFCSP ones, it was decided to drop the AFSPSH program from the subsequent investigation.

2.6 THE FFCSP AND FFSCCH PROGRAMS

2.6.1 The FFCSP Program

In this program a different air flow representation into the Fan is considered. This model does not allow any redistribution or interchange of flow between the Inner and the Outer sections of the Fan. This was achieved by using the AFCSP program as it is, but forcing the Factor of Split (FCSP) to be fixed at all times and equal to 1.0. Hence the program derives its name from the Fixed FaCtor of SPlit (FFCSP) concept.

The link which had existed between the Inner and Outer Fan on the AFCSP program, see Figure(4), has now been removed. The final problem to be solved before the program could simulate a typical Turbofan engine, was the adjustment of the test between the required and available nozzle area. In AFCSP

program, once the calculation procedure had reached the Final Nozzle Test, then if no agreement existed between the two areas, the FCSP was revised at the entrance to the Inner Fan and all calculations were repeated until convergence was achieved. In the FFCSP program, since the Factor of Split is always equal to 1.0, the total air mass flow rate into the engine is revised, once the test of the two areas is reached, and the calculations are repeated until convergence is once again achieved.

2.6.2 The FFSCCH Program

Since in practice it is not possible to measure the conditions in between the Inner Fan and the Intermediate Pressure compressor (IP or Booster), it was considered that the two components could be combined and represented as one section.

The programs AFCSP and FFCSP at the appropriate stage read the values of the characteristics of the Inner Fan, IP compressor and Outer Fan, in the sequence just mentioned. The new program developed, by-passes the characteristics of the IP compressor and instead of reading the Inner Fan's characteristics, these are replaced with the characteristics of the Combined Inner Fan and IP compressor section, produced from the program CH INFCIPC.

This program, (CH INFCIPC), has been developed to produce the characteristics of the new section consisting of the combined Inner Fan and IP compressor. It used the separate characteristics of the two components and with certain interpolations produced the new combined characteristics. These shown in Figure B in the separate report which is included in Appendix(D).The program (CH INFCIPC) gives the combined :

Pressure Ratio=RCMPC

Non-dimensional air mass flow rate=AI1ERR

Beta values=BETAC

In order for the program to by-pass the characteristics of the IP compressor, a new parameter was introduced, named NDELI.

If this parameter is given the value of 1, then the program uses the combined characteristics instead of the Inner Fan's, by-passes the IP compressor's ones and then reads the Outer Fan's.

This program, like the FFCSP, keeps the Factor of Split fixed and revises the air mass flow into the engine until equality is achieved between the required and available nozzle area. This new program is thus labelled as FFSCCH (Fixed Factor of Split considering Inner Fan and IP Compressor Combined CHaracteristics).

The results presented in this research showed that the two programs gave as expected, virtually the same predictions.

2.6.3 Comparison of the FFCSP and FFSCCH Programs

The two programs were used to predict the steady state results under two flight conditions:

Sea Level, Mach=0.2

and: Altitude=47,000ft., Mach=0.92

Figures (31 to 35) show the results for the Sea level condition. To compare the two programs several parameters were plotted in the above mentioned graphs. Figure (31) shows the HP shaft speed plotted against the the LP shaft speed. The results of the two programs show no significant differences. At the top range of the shaft speeds there is a very slight discrepancy which can be considered as negligible.

In Figure (32), P_{26}/P_1 is plotted against the non-dimensional speed of the LP shaft. The predictions of the two programs are again identical, as is the case when the LP and HP shaft speeds were plotted against the Fuel Flow, as shown in Figures (33 and 34). Only in the top speed range is there a slight discrepancy which can also be considered as negligible. The results are once again identical when the Thrust was plotted against the Fuel Flow, see Figure(35).

The same parameters and graphs, Figures(36,37,38,39 and 40), were used to compare the predictions of the two programs at Altitude of 47,000ft. and Mach=0.92. Again there were no significant differences between the two programs.

Because of the exact agreement of the predictions of the two programs it was decided to use in the subsequent study only the FFCSP and discontinue the investigation of program FFSCCH.

2.7 THE AFSPOF PROGRAM

Initially this new computer model was devised to allow for a variation of the Factor of Split(FCSP) but applied only to the Outer Fan.

A guessed core air mass flow rate was used at the start of the program and during the first calculation through the Outer Fan, the by-pass air mass flow rate was simply regarded as being three times the core one(3 to 1 by-pass ratio). When the Final Nozzle test is reached then the Total air mass flow rate was revised and also a new Factor of Split(initially equal to 1.0) was calculated according to the values of the Total(revised) and the

core air mass flow at that instant. Then the new values of Total air flow and Factor of Split were now fed into the calculations of the Outer Fan in order to evaluate a new by-pass air mass flow rate. The same process was repeated until convergence was achieved in the Final Nozzle Test. In this way the variation of the FCSP did not re-evaluate directly the core flow.

Although a movement of the FCSP imposes that a part of one of the two flows (core or by-pass) is fed into the other one, in this program, the non re-evaluation of the core flow by the FCSP, leads to the thought that a part of the Total air mass flow rate into the engine is used twice. For example, if the FCSP at an instant is less than 1.0, say 0.8, then the part of the core flow that is fed into the by-pass duct would be equal to:

$$(1\text{-}0.8) \times (\text{CORE FLOW})$$

Before the Final Nozzle test is reached, the core flow is readjusted to meet the flow capacities of the subsequent components, particularly the H.P. compressor. Hence it seems that the part of the core flow that is supposed to be fed into the by-pass duct;

$$(1\text{-}0.8) \times (\text{CORE FLOW})$$

$$\text{or } (1\text{-}0.8) \times (0.25) \times (\text{TOTAL FLOW})$$

is used once in the by-pass and once in the core flow calculations plus or minus the revised amount of core flow necessary to meet the demand of the subsequent components. In order to account for this potential error it was decided, once the Final Nozzle Test was reached, not to use the FCSP to readjust the by-pass air mass flow. Instead, the revised Total air mass flow rate was fed back into the Outer Fan calculations and a new by-pass air mass

flow rate was evaluated by subtracting from the (revised) Total air mass flow, the core one at that instant. It was thus possible to allow for an interchange of flow by readjusting directly only the by-pass air mass flow rate. Since this new computer model derived from the initial concept of Adjusting the Factor of SPlit for the Outer Fan only, it was labelled AFSPOF and a block diagram of its logic is shown in Figure(4A).

This program, similarly to the FFSCCH one, considers the Inner Fan and I.P. compressor characteristics combined. The same method that was used in the FFSCCH program to combine read and use the combined characteristics, was also employed in this new model.

A new problem appeared in the use of this new program when transients were performed at the highest rotational shaft speeds. As it can be seen from the Outer Fan characteristics, see Figure(9), at the higher non-dimensional speeds, a large range of the constant speed lines is vertical. In the interpolation used during the Outer Fan calculations, the non-dimensional air mass flow rate is used as an input in order to calculate the pressure ratio, knowing the non-dimensional speed. Since the characteristic lines are vertical, or almost vertical, at that particular region mentioned earlier, the computer could not perform the interpolation for obvious reasons. Hence an "Alternative Logic" was employed to overcome this difficulty.

In case of the L.P. shaft's non-dimensional speed being at the highest range attainable, then the program is forced to execute a linear interpolation that uses the pressure ratio of the Outer Fan as an input and calculates a value for the non-dimensional air mass flow rate. In the event of the program having to use the

Alternative Logic during its very first calculation (i.e. starting a deceleration from the higher attainable rotational shaft speeds), then a guessed value for the Outer Fan pressure ratio is used. This first guessed value is later revised according to the Final Nozzle test. At the latter, the Alternative Logic revises the pressure ratio of the Outer Fan (either guessed or already calculated). Also calculates the new Total air mass flow rate according to the by-pass air mass flow rate used in the previous cycle of calculations. The new Outer Fan pressure ratio and Total air mass flow rate are fed in the Outer Fan calculations. The process is repeated until convergence is achieved in the Final Nozzle test.

This Alternative Logic was found to be necessary in all the other programs, except the AFCSP program, and was therefore incorporated.

The new modelling of the Fan gave results which were very close to the results of the other programs developed in this research. The results of all the programs are compared in the next chapter.

2.8 THE STACK FAN PROGRAMS

The allowance of flow interchange between the Inner and Outer Fan was achieved, until now, by directly altering the air mass flow rate of both or one of the two sections of the Fan(Inner or Outer).

As a first step, this was achieved by using divided characteristics for the Inner and Outer Fan sections. Further the

Factor of Split was introduced to allow for air flow interchange between the two sections.

The new Fan treatment employed in this model, uses again separate characteristics but there is no "direct" allowance for air flow interchange such as the one imposed by the use of the Factor of Split concept.

In this new approach the characteristics of each of the two sections are subdivided into the equivalent characteristics corresponding to a range of pressure ratios (expressed as Beta values) of the other Fan section. There is therefore an "indirect" allowance for flow interchange.

In all the previous computer models described, the characteristics of the Inner and Outer Fan included the non-dimensional mass flow rate and speed as well as the isentropic Efficiency and Beta values, see Figure(5). Now the characteristics are tabulated as follows.

For the Inner Fan there are thirteen non-dimensional speed lines with fourteen points on each line corresponding to the fourteen Beta values. For each point the non-dimensional mass flow rate and pressure ratio as well as the temperature difference ratio, instead of the isentropic efficiency, is also tabulated. This set of values corresponds to one particular Beta value of the Outer Fan. The Inner Fan characteristics include five different sets of characteristics which correspond to five from the thirteen Outer Fan Beta values.

The Outer Fan characteristics are tabulated in a similar manner, the only difference being that there are thirteen Outer Fan Beta values and also there are only four sets of

characteristics corresponding to four from the fourteen Inner Fan Beta values.

In order to show the different set up of Fan characteristics representation, the two different tabulation methods are shown in two schematic diagrams in Figures (5 & 41). Figure(41) shows the Inner Fan characteristics tabulation for three of the five Outer Fan Beta values. These are b=13,9,6. For the remaining two the tabulation method is exactly the same.

The characteristics of the Inner and Outer Fan, as used in the new computer models, are shown in Figures (42.and 43). Each of the figures shows the characteristics corresponding to one only Beta value of the other section of the Fan, since little visual difference existed for the corresponding characteristics of the other Beta values for both sections of the Fan.

For all the previously described programs, (AFCSP, FFCSP, AFSPOF), the procedure of Inner Fan calculations, used the non-dimensional air mass flow rate and speed as well as the characteristics to evaluate the pressure ratio correct Beta value and isentropic Efficiency and hence the outlet temperature T_{24}.

In the new model the procedure uses as inputs, either known or guessed, the non-dimensional mass flow rate and speed as well as a Beta value of the Outer Fan. This will enable as to which of the five sets of characteristics of the Inner Fan to be used. Using a three dimensional interpolation on the characteristics, the Pressure ratio, Inner Fan Beta value and the Temperature difference ratio are evaluated. The same procedure is followed for the Outer Fan calculations.

In this new Fan treatment an interchange of flow between the two sections of the Fan is allowed by using different set of

characteristics and hence different air mass flow rate depending on the operating conditions of the other section, i.e. the Beta value of the Outer Fan will impose at any time the operating point of the Inner and vice versa.

The Block diagram of the new computer model is shown in Figure(44). The procedure can now be followed.

The known parameters at the beginning of the program are the shaft speeds and the flight conditions, which, as explained earlier, allow for the calculations of :

$$\frac{N_L}{\sqrt{T_1}}, \; T_1, \; P_1$$

An initially guessed core air mass flow rate together with the known parameters enables to calculate the non-dimensional air mass flow rate. Also a guessed Outer Fan Beta value is assumed at this stage to be equal to 5.0 and in addition a guessed Outer Fan pressure ratio equal to 1.5.

These parameters, known and guessed, together with the new form of Inner Fan characteristics are adequate to complete this section's calculations and determine the outlet parameters which are the inlet for the next component. The rest of the core engine components calculations remain unchanged, as explained in detail in Appendix(B).

The new method now involves changes in the Outer Fan calculations. The air mass flow rate into the Outer fan is initially set to be three times the core mass flow rate. The Beta value of the Inner Fan, which was evaluated during the latter's calculations, is now used to impose the exact set of Outer fan

characteristics to be used in the three dimensional interpolation. From the interpolation, the Pressure ratio, exact Outer Fan Beta value and Temperature difference ratio are evaluated and hence the outlet temperature from this component is calculated.

The new Fan treatment involves changes in the actual mechanism of making the computer model to converge. The results of the calculation of the core and of the by-pass sections of the engine enter the Mixer, as can be seen in the Block diagram of the program in Figure(44). If the test just after the Mixer, between the air and gas pressures, is passed, then the Final nozzle test has to be performed. If the requirements of the latter do not meet then the air mass flow rate into the Outer Fan is revised and the whole procedure is repeated until convergence is achieved at the Final Nozzle test. This was the final part of all the previous computer models.

Once the Final nozzle test has passed then, at this stage, all the conditions are met except that the Beta value that emerged from the last calculations of the Outer Fan differs from the one that was initially used as input into the Inner Fan calculations. Hence a new test had to be added after the Final Nozzle one in order to revise the Outer Fan's Beta value until there is an agreement between the value used as input into the Inner Fan and the one that emerged from the Outer Fan calculations. It is evident that once the Outer Fan Beta value has been changed accordingly and fed into the Inner Fan, a new Beta value for the Inner Fan will emerge from the latter's calculations, which in turn is fed as an input into the Outer Fan. This forces the program to execute all the components calculations several times until convergence is achieved which obviously affects the computer running time of

the program, a problem which is discussed later.

This computer model was named STKFAN from the STacKing of the FAN concept. It was now thought to use this new concept of representing the Fan, to devise another computer model that would not allow any interchange of flow between the two sections of the Fan but would still use the same Fan characteristics representation. This was easily achieved by not allowing the Beta value of the Inner Fan to alter the characteristics of the Outer. The Inner Fan Beta value that was fed into the Outer Fan calculations was always kept constant and equal to 5.0. The same implied for the Inner Fan calculations. This new model had the same effect as of the Fixed Factor of Split (FFCSP) program. The name that was given to this computer model was STFFIX.

The Alternative Logic that was firstly introduced into the AFSPOF program was also used in both the new programs. Another three dimensional interpolation had to be devised in order to be able to use as inputs the non-dimensional speed and the Pressure ratio of the Outer Fan and give as outputs the non-dimensional air mass flow rate, exact Beta value of the component as well as the temperature difference ratio.

Both programs were tested for reliability and accuracy of results and their predictions are used in Chapter **III.**

CHAPTER III

COMPARISON BETWEEN THE COMPUTER MODELS

3.1 INTRODUCTION

In the previous chapter, the different Fan treatments and flow distributions before and after the Fan of a typical Turbofan engine, were outlined together with the computational models that originated from them.

In order for a simulation model to be successful it must predict results that, within an acceptable error, are very close to the behaviour of the real engine.

In order for this to be achieved, certain real engine effects have to be incorporated into the computational model. These real engine effects are:-

(i) specific heat capacity of air/gas as a function of temperature

(ii) specific heat capacity of air/gas as a function of temperature and fuel to air ratio

(iii) heat transfer effects(see Chapter I)

(iv) lag during transients in the response of the fuel system.

In the previous chapter seven computational models were described, each using a different Fan representation.

Since it is of interest in the present research to develop the computational model that would best simulate a typical Turbofan engine, the above mentioned effects have to be

included in the computational models and then they have to be compared against the test results of a typical Turbofan engine. Each of the programs. if it included all the real engine effects mentioned above, would require considerable computing time. It was therefore decided to make the initial comparison among these seven Fan procedure programs by using simpler versions which incorporate only one of the real engine effects- effect(i) above, i.e specific heat of air/gas as a function of temperature but independent of composition. The first of these comparisons have already been described in the previous chapter. The programs contrasted were the AFCSP(Adjusting the Factor of Split-section 2.3) against AFSPSH(Adjusting the Factor of Split allowing for Shear forces effect-section 2.5.1), and the FFCSP(Fixed Factor of Split-section 2.6.1) against the FFSCCH(Fixed Factor of Split considering also combined characteristics of Inner Fan and I.P. compressor-section 2.6.2).

In this chapter the remaining computational models were used to predict both the Steady running and the Transient results under two flight conditions:

(i). Sea Level, Mach=0.2

(ii). Altitude of 43,000ft., Mach=0.8

The programs used are the:

1. AFCSP=Adjusting the FaCtor of SPlit
2. FFCSP=Fixed FaCtor of SPlit
3. AFSPOF=Adjusting the Factor of SPlit for the Outer Fan only
4. STFFIX=STack Fan concept with the effect of the FIXed Factor of Split

5.STKFAN=STacK FAN concept

From the predicted results, several parameters were used to plot the Working lines and the Trajectories as well as several other parameters in order to outline any significant discrepancies between the computational models.

The computing running time, that each computational model needed to execute and produce the relevant results, was also recorded and used in the current comparison. The results of the comparison of the different computing running times are given in section 3.6 of this chapter together with information about the computer used during the current research(section 3.6.1).

The numbering and labelling of the programs given above is also used in all the graphs that present the results of the comparison. In these graphs, all five programs are always represented with the same marks.

Note on Units used: In many of the graphs the pressure ratio of the component under investigation was plotted against a base line of the non-dimensional mass flow rate of the particular component. The units used are

$$\frac{lb/sec\sqrt{K}}{lbf/in^2}$$

3.2 INNER FAN PLUS I.P. COMPRESSOR

From the predictions obtained, the pressure ratio P_{26}/P_1 was plotted against the non-dimensional mass flow rate through the Core of the engine. It was thought to consider in the comparison, the Inner Fan combined with the I.P. compressor because the

program AFSPOF does not predict separate results for the above mentioned sections of the engine(See section 2.7).

In Figure(45) the Sea level steady-running working lines are shown for all five computational models. The four programs; AFCSP, AFSPOF, STFFIX, STKFAN, predicted Inner Fan working lines that almost coincide. The FFCSP program shows a steady-running line that is slightly lifted towards the surge line. The difference is of the order of 0.03%.

In Figure(46) the Sea level acceleration trajectories show no difference between the predictions of the programs. There is also no significant difference between the acceleration trajectories and the steady-running lines for all five programs. The steady-running lines of all the computational models were represented by the working line predicted by the AFCSP program, because no significant discrepancy existed between them.

Differences appeared at the start of the Sea level deceleration. In Figures(47&47A), the deceleration trajectories of all five programs are shown together with the steady-running line represented by the AFCSP program's one. Figure(47A) is the enlargement of the "window" shown in Figure(47). This was frequently used in the current comparison to assist in the observation and calculation of the differences between the predictions of the different models. At the value 110 of the non-dimensional air mass flow rate, all five programs were compared for different pressure ratio values between the deceleration and steady-running results of each program, as well as for the percentage difference between them.

The following Table shows the differences between the programs during the start of the Sea level deceleration at

Mach=0.2.

$\left(\frac{\dot{m}\sqrt{T}}{P}\right)_{COFE}=110$	Steady Running P_{26}/P_1	Deceleration P_{26}/P_1	Difference	% Difference
1. AFCSP	2.22	2.51	0.29	13.06%
2.FFCSP	2.25	2.54	0.32	14.2%
3.AFSPOF	2.22	2.57	0.35	15.76%
4.STFFIX	2.22	2.50	0.28	12.6%
5.STKFAN	2.22	2.48	0.25	11.7%

Table (3.2.1)

The table above shows that the differences of the programs are not significant. Programs 4 and 5(Stack Fan concept) give virtually the same predictions and the least departure from the Steady running line. AFCSP program shows a large decrease, (32%), in non-dimensional air mass flow rate at the very first part of the deceleration, against a 10% decrease in the pressure ratio. The movement of its trajectory towards the surge line is of the order of 13%, which is slightly higher than the Stack Fan programs but less than programs 2 and 3. These two appear to have a shifted deceleration trajectory by 14.2% and 15.8% respectively.

At this stage of the comparison, it is very early to draw any conclusions, and the discussion carried out is purely observational. Final conclusions will be decided later after the discussion of all the results predicted from the five programs.

The Altitude predictions of the Inner Fan did not show any significant differences and hence no effort was made to plot these results.

3.3 OUTER FAN

The pressure ratio P_{13}/P_1 of the Outer Fan was plotted against the non-dimensional air mass flow rate through the Outer Fan in order to create the working lines and trajectories of this component of the engine.

For the Outer Fan both the Sea Level and the Altitude results showed differences among the predictions of the five models and were used to plot several graphs that are described in this paragraph.

The predicted working lines at Sea Level and Mach=0.2, are shown in Figure(48). The results of all five programs show no descrepancies and hence the FFCSP program's steady-running line was used to represent the working lines of all the other models in Figures(49,50&50A).

The acceleration trajectories at Sea Level and Mach=0.2, are shown in Figure(49) for all the models and also a steady-running line is also included and represented by the FFCSP program's one, as mentioned above.

The results show no significant discrepancies existing among the predictions of the programs and also a consistency in deviation from the steady-running line.

The Altitude acceleration predictions showed similar results to the Sea level ones and hence there was no need to be graphically represented.

Significant discrepancies appear during the first second of the Sea Level deceleration predictions of the five programs, shown in Figure(50) The differences that occur at the beginning of the

transient are highlighted in the "window" appearing in Figure(50), which is enlarged and shown in Figure(50A). Programs 1 and 3, which allow for an interchange of flow between the two sections of the Fan, showed similar results. Although it is a deceleration, both programs (1 and 3), show, for the very first part of the transient, an increasing Outer Fan non-dimensional air mass flow rate with decreasing pressure ratio. This is a direct effect of the Factor of Split concept which has been explained in more detail in section 2.4.

At the start of the deceleration the FCSP decreases rapidly in order to reduce the amount of air flow through the core of the engine. Hence a large amount of air is diverted towards the Outer Fan which explains why at the start of the transient the air mass flow rate through the Outer Fan is predicted to increase instead of decreasing.

An entirely opposite prediction, as shown in Figures(50 and 50A), is the deceleration trajectory predicted from the FFCSP program (which does not allow for interchange of flow between the Inner and Outer sections of the Fan). The deceleration trajectory of the FFCSP model shows a smooth rate of decrease of the pressure ratio with the non-dimensional air mass flow rate.

Programs 4 and 5 (Stack Fan concept), show results that lie in between the two extreme cases of the FFCSP and of the AFCSP. The STFFIX program, following a Fixed Factor of Split concept, predicts results that are closer to the FFCSP ones, while the STKFAN program shows results that are closer to the AFCSP and AFSPOF ones.

Their differences are shown more clearly in the Table (3.3.1) below:

$\frac{P_{13}}{P_1}=1.6$	Steady Running $\left(\frac{\dot{m}\sqrt{T}}{P}\right)_{OUTER}$	Deceleration $\left(\frac{\dot{m}\sqrt{T}}{P}\right)_{OUTER}$	Difference	% Difference
1. AFCSP	356.9	378.1	21.2	5.94%
2. FFCSP	356.9	365.9	9.0	2.52%
3. AFSPOF	356.9	378.0	21.1	5.91%
4. STFFIX	356.9	364.2	7.3	2.04%
5. STKFAN	356.9	367.7	10.8	3.02%

Table(3.3.1)

At P_{13}/P_1 equal to 1.6, the corresponding non-dimensional air mass flow rate value for the steady-running results is 356.9 for all five programs.

During the first part of the deceleration, programs 1 and 3 show a deviation of their predicted trajectory from the steady-running line of approximately 6%, against a 2.5% of the FFCSP, a 2% of the STFFIX and a 3% of the STKFAN program.

It appears that both AFCSP and AFSPOF models over accounted the allowance of flow interchange between the Inner and Outer sections of the Fan, resulting thus in the increase, instead of decrease, of the non-dimensional air mass flow rate through the Outer Fan during the very first part of the deceleration.

In between the two extreme cases lie the results of the Stack Fan concept programs. STFFIX program shows a more realistic trajectory but appearing to lie very close to the steady-running at the start of the deceleration. It then shows a rapid decrease to lower values than the ones predicted by the FFCSP program and finally converges towards the trajectories of all the other computer programs.

The deceleration trajectory predicted by the STKFAN program appears to be the more realistic one, showing the rapid decrease in pressure ratio with a small decrease in air mass flow rate that would be expected during that first part of the deceleration. This is a direct effect of the allowance of air flow interchange between the two sections of the Fan but with no over accounting of the latter effect. After the first part of the deceleration the air mass flow rate starts to decrease in a similar rate as the pressure ratio, resulting in the trajectory shown in Figures(50 and 50A), which later in the transient it coincides with the trajectories of the other computational models. Hence it appears that the STKFAN program predicted realistic results by allowing flow interchange between the Inner and the Outer Fan but avoiding over prediction problems such as those encountered by the AFCSP and AFSPOF programs.

The working lines and deceleration trajectories were also plotted for the Altitude flight condition in order to observe how the higher altitude and flight Mach number will affect the differences that were observed in Figures(50 and 50A).

As it can be seen from Figure(51), the first effect on the increase of Altitude and flight Mach number is that the working lines of all five programs are moved away from the Sea level ones in a direction opposite to the surge line(lower pressure ratio) by an average of 6.7%.

The predicted steady-running line of the FFCSP program has the least deviation from the Sea level one. All the other computational models predicted working lines that are very close to each other apart from the region of the higher fuel flow

rates where significant discrepancies occur between all the programs. This region is outlined in the "window" shown in Figure(51) which is also enlarged and shown in Figure(51A). Once again the AFCSP and AFSPOF predictions are very close and also the most deviated away from the Sea level ones. The STFFIX program shows a critical deviation of its steady-running line at the highest fuel flow rates, which crosses the FFCSP working line predicting thus results that are even closer to the Sea level ones. Apart from that particular region, the predicted working line by the STFFIX program, lies very close to the ones predicted from the programs AFCSP, AFSPOF and STKFAN.

As a result of the deviations of the steady-running lines, the Altitude deceleration trajectories of all five programs showed similar deviations, Figure(58). The results of the transient are consistent with the Sea level ones with only exception the cross over of the STFFIX program's trajectory towards the steady-running line at the start of the deceleration. This was expected because of the similar prediction of its Altitude steady-running line.

The differences between the steady-running and transient predictions of all the five programs are given in the Table(3.3.2) below where for the pressure ratio equal to 1.5 the different non-dimensional air mass flow rates are noted together with their percentage difference.

Altitude Results

P_{13}/P_1=1.5	Steady Running $\left(\frac{\dot{m}\sqrt{T}}{P}\right)_{OUTER}$	Deceleration $\left(\frac{\dot{m}\sqrt{T}}{P}\right)_{OUTER}$	Difference	% Difference
1. AFCSP	365.8	379.0	13.2	3.6%
2. FFCSP	359.6	366.5	6.9	1.92%
3. AFSPOF	364.9	380.0	15.1	4.14%
4. STFFIX	360.7	364.0	3.3	0.91%
5. STKFAN	363.5	368.0	4.5	1.24%

Table(3.3.2)

The least transient trajectory deviation from the steady-running line was predicted by the STFFIX program following the movement of its working line towards the sea level results. At the start of the deceleration, the results of this program could be regarded as unrealistic, firstly due to the above mentioned reason and secondly because the deceleration trajectory appears to be very close to the steady-running line both at the Sea level and at the Altitude flight conditions but only for the very first part of the transient. Later in the transient, the trajectory predicted, converges towards the ones predicted by the programs AFCSP, AFSPOF and STKFAN. As it would be expected the FFCSP program predicted results that are closer to the STFFIX ones than to any of the others computational models.

The Altitude working line shows though the opposite effect from the one predicted by the STFFIX program. At the higher fuel flow rates the predictions of the program are closer to the STKFAN ones, as it can be seen in Figures(51 and 51A), but the rest of the working line is alleviated towards the Sea level one. As a result the deceleration trajectory followed a similar path

showing a difference of approximately 1.92% from its working line.

It could be concluded from the already obtained results that both FFCSP and STFFIX programs show results that cannot be considered realistic enough due to the above mentioned predicted behaviour of their Altitude working lines as well as because of the predicted deceleration trajectories, both at Sea level and Altitude.

On the other hand the opposite exists with the predictions obtained from the AFCSP and AFSPOF computational models, which due to the over accounting of the flow interchange allowance, show an increasing non-dimensional air mass flow rate during the very first part of the deceleration during both the Sea level and Altitude flight conditions. Apart from the above mentioned unrealistic part, which can be observed in more detail in Figure(51A), both programs show results that are very close to the rest of the computational models.

Finally, from the investigation that was carried out so far, the STKFAN program shows results that one would expect to lie closer to the results of a real Turbofan engine during both flight conditions, but this is still to be proved in the process of the current investigation.

So far the most important results were obtained from the deceleration trajectories of the Outer fan where the plotting of the P_{13}/P_1 versus the non-dimensional mass flow rate showed significant discrepancies among the predictions of the different computational models both at Sea level and Altitude.

Some test data, including values of pressures at stations 1 and

13(see Figure4) became available on the transient behaviour of a real Turbofan engine. However, the data did not include values of air flows due to understandable experimental difficulties. The results did include values of shaft speeds and therefore it was anticipated that plotting the Outer Fan pressure ratio(P_{13}/P_1) against the non-dimensional speed of the L.P. shaft could be a valuable test of the validity of the alternative Fan models. Hence the predictions of the Outer Fan pressure ratio, illustrated above, have also been plotted to a base of the L.P. shaft non-dimensional speed.

The Sea level steady-running predictions are shown in Figures(52 &52A). No significant discrepancy exists among the predictions of all five programs with exception the steady-running results obtained from the FFCSP program which show lower pressure ratio operating points, the difference from the other computational models being of the order of 1.3%. The above mentioned difference can be seen in Figure(52A) which is an enlargement of the "window" shown in Figure(52).

The Sea level deceleration results are plotted and shown in Figures(53&53A). Since the steady-running results of all five programs are very close, they were represented in the deceleration comparison by the results of the AFCSP program. The predictions of the programs show significant discrepancies for the very first part of the deceleration (first second). The "window" of Figure(53) includes the predictions of the first part of the deceleration and its enlargement is shown in Figure(53A). The different Outer Fan pressure ratios predicted by all programs at steady-running and deceleration are compared at the same L.P. shaft non-dimensional speed of 420. The results

and their comparison are outlined in the following Table(3.3.3):

SEA LEVEL

$\frac{N_L}{\sqrt{T_1}}=420$	Steady Running P_{13}/P_1	Deceleration P_{13}/P_1	Difference	% Difference
1. AFCSP	1.555	1.536	0.019	1.2%
2.FFCSP	1.534	1.488	0.046	3.0%
3.AFSPOF	1.555	1.536	0.019	1.2%
4.STFFIX	1.560	1.506	0.054	3.5%
5.STKFAN	1.560	1.520	0.04	2.5%

TABLE(3.3.3)

The predictions of the AFCSP and AFSPOF show once again similar results having the least deviation from the steady-running ones by 1.2%, as shown in the Table(3.3.3) above. The FFCSP transient prediction, following the steady-running deviation of 1.3%, lie the most away from the steady-running line(represented in Figure53A), but having an actual difference of the order of 3.0%. The STFFIX and STKFAN predictions are, as expected, in between the predictions of the other programs. The STFFIX results showed the biggest deviation of 3.5% and are closer to the deceleration results of the FFCSP program, while the STKFAN transient prediction showed a deviation of 2.5% and are closer to the AFCSP program's results. As it can be seen from Figure(53A), the FFCSP program shows a comparatively rapid drop in pressure ratio at the start of the deceleration, which is due to the equally rapid decrease of the air mass flow rate and of the shaft speed. On the other hand the predictions of the programs AFCSP and AFSPOF show the opposite effect. This was once again a direct effect of the allowance of flow interchange

between the two sections of the Fan. A more linear and steady pressure ratio drop was predicted by the STFFIX and STKFAN models. Apart from the first part of the deceleration, the predictions of all five programs converge to a common line which is also very close to the steady-running results.

The Altitude predictions were also used to plot the same graphs as before for both the steady-running and deceleration results for all five programs. Figure(54) shows the steady-running results predicted by the computational models at 43,000ft. and Mach=0.8. All the steady-running results are shifted away from the sea level ones in a direction of a lower pressure ratio. At the same non-dimensional speed of 420, which was also used for the Sea level comparison, the Altitude steady-running results show an average deviation of the order of 6%. The following table shows the effect of Altitude change in the steady-running results as a percentage difference between the Sea level and Altitude steady-running predictions.

Steady Running

$\frac{N_L}{\sqrt{T_1}}=420$	Sea Level P_{13}/P_1	43,000ft. P_{13}/P_1	Difference	% Difference
1. AFCSP	1.555	1.494	0.061	3.9%
2.FFCSP	1.534	1.420	0.114	7.4%
3.AFSPOF	1.555	1.494	0.061	3.9%
4.STFFIX	1.560	1.445	0.115	7.4%
5.STKFAN	1.560	1.460	0.1	6.4%

Table(3.3.4)

As it can be seen from Table(3.3.4), the steady-running results of the AFCSP and AFSPOF show the least deviation for the

two flight conditions, while the FFCSP and STFFIX programs, which use an opposite Fan treatment, show the biggest deviation in steady-running results. The STKFAN program showed a deviation of 6.4% predicting thus results that lie in between those predicted by the two opposite Fan treatments but being slightly closer to the FFCSP and STFFIX programs results.

The steady-running results were now used to compare the actual deviation predicted during a deceleration at 43,000ft. and Mach=0.8. The transient results predicted from the five programs are shown in Figure(55), where the Outer Fan pressure ratio is plotted against the non-dimensional L.P. shaft speed.

The Altitude deceleration results show large differences from the Sea level ones. Once again the two programs, AFCSP and AFSPOF, show similar results. For the first part of the transient the STFFIX predictions are closer to the FFCSP ones but later in the process of the transient the results converge towards those predicted by the STKFAN program. It is again the case of the two opposite Fan treatments of the AFCSP,AFSPOF and FFCSP that predict the extreme results and the Stack Fan concept programs which give results that lie in between the above mentioned programs. The exact deviation of the deceleration results from the steady-running ones is shown in the Table(3.3.5) below. The results that are shown in the table confirm the above mentioned comparison. It can also be seen from Figures(54 and 55) that the transient results of all five computational models follow the paths and deviations imposed by their steady-running results.

43,000ft.

$\frac{N_L}{\sqrt{T_1}}=420$	Steady Running P_{13}/P_1	Deceleration P_{13}/P_1	Difference	% Difference
1. AFCSP	1.494	1.460	0.034	2.27%
2.FFCSP	1.420	1.360	0.060	4.2%
3.AFSPOF	1.494	1.460	0.034	2.27%
4.STFFIX	1.445	1.389	0.056	3.9%
5.STKFAN	1.460	1.416	0.044	3.0%

Table(3.3.5)

The same parameters of the Outer fan were used to compare the acceleration predictions of the five computational models.

The acceleration predictions of all five programs, for the Sea level flight condition, did not show any significant discrepancies. This was expected since the corresponding acceleration trajectories(of pressure ratio versus the non-dimensional air mass flow rate) had not show any important deviations between the predictions of the programs. The Sea level acceleration results are shown in Figures(56&56A). For this transient, all programs predicted similar results that are very close to the steady-running ones.

As it was shown earlier, the programs predicted different steady-running results for the Altitude flight condition. As a result the Altitude acceleration results of all five programs showed consistent deviations with their Altitude steady-running ones. Hence the deviations that appear in Figures(57&57A) are a direct effect of the individual steady-running prediction and not of any significance.

Due to the important discrepancies that had been observed in the Outer Fan deceleration trajectories, shown in Figures (58,50 and 50A), it was decided to investigate also the change of the Outer Fan's air mass flow rate and pressure ratio with Time during the Altitude deceleration.

The Outer Fan's non-dimensional air mass flow rate was plotted against the Time for the 43,000ft., Mach=0.8, deceleration. It is possible in this graph, Figure(59), to observe the direct effect of the different Fan treatments on the Outer Fan's change in air mass flow rate. The two programs AFCSP and AFSPOF show the increase of air flow through the Outer Fan during the first part of the transient. This was discussed extensively earlier in this chapter. The FFCSP program shows a constant drop of air mass flow rate from the beginning of the transient but it predicts a much lower operating air mass flow rate than all the other programs by approximately 3%. The start of the deceleration predicted by the STKFAN program appears the most reasonable one, showing a very small decrease at the beginning of the transient, due to the interchange of flow, and once the LP shaft is able to decelerate, the air mass flow rate starts to decrease rapidly. The STFFIX program shows also very reasonable results which for the very first part of the transient could be classified as the intermediate predictions between the STKFAN and FFCSP programs. Later in the transient the predictions of the STFFIX program deviate away from the FFCSP ones and converge towards the predictions of the rest of the computational models.

It was expected that during a deceleration at the same flight conditions, the Outer Fan's pressure ratio rate of decrease would

show differences between the predictions of the computational models, but only for the very first part of the transient. Figure(60) shows the predictions of the Outer Fan's pressure ratio drop with Time for the first second of the 43,000ft., Mach=0.8 deceleration. As it can be seen from the graph, the deviations between the predictions of the programs are of the same magnitude as those of the non-dimensional air mass flow rate. The maximum discrepancy exists, as expected, between the AFCSP and FFCSP programs,which is of the order of 3.5% for both cases. The graphs in Figures(60&61), outline the different predictions obtained by the different fan treatments, showing as extreme cases the results obtained from the programs allowing an interchange of flow using the Factor of Split concept and the FFCSP program that does not allow any interchange of flow between the two sections of the Fan. Both Stack Fan programs, although the STKFAN allows an interchange of flow and the STFFIX adopts a concept similar to the FFCSP one, predicted results that are, in most cases, in between the two extreme cases mentioned above. This was the reason that the STFFIX program's results were in most cases closer to the FFCSP ones and on the other hand the STKFAN predictions were closer to the AFCSP and AFSPOF ones.

3.4 H.P. COMPRESSOR

So far the comparison of the different computational models has been concentrated in the Outer fan deceleration results for both flight conditions. From the comparison of the Sea level

working lines and trajectories it was observed that the most significant discrepancies between the different fan treatments became more evident when the Outer Fan deceleration predictions were analysed. This is due to the fact that since all the computational models developed in the present research are based on different ways of representing the Fan, any change in the interpretation of the Fan itself will have greater impact on the predicted behaviour of the Outer Fan, since it copes with larger amounts of air mass flows.

The prediction programs, with their various Fan representations, have also been used to predict the H.P. compressor behaviour. The results predicted by the different models for the HP compressor are shown in Figures(62&63). The programs were used to predict the Sea level working lines as well as the acceleration and deceleration trajectories.

The steady-running lines predicted by all five programs show no discrepancies, as also is the case with the acceleration and deceleration trajectories. Figure(62) shows the working lines of all five programs which coincide, and Figure(63) shows the transient trajectories of all five programs together with one steady-running line represented by the working line of the AFCSP program. The predictions of the models do not show any discrepancies.

3.5 THRUST RESPONSE

As it was proved from the comparison of the predicted results of the HP compressor, the five computational models show

differences only with regard to the Fan of the engine. This was expected since the computational models were developed on a basis of different Fan treatments. As a results their main differences would appear in predictions relevant to the Fan of the engine.

In addition, changes in the way that the Fan of a Turbofan engine is represented, might create changes in the predicted thrust response of the engine.

In view of the above mentioned possible discrepancies between the predictions of the five programs, the results of the computational models were used to plot the Thrust response during Sea level and Altitude transients.

Figure(64) shows the Thrust response with time, for all five programs, during the Sea level deceleration. All programs predicted the same response. The only slight difference appears after the thrust has dropped lower than the 3000lb. where the two programs STFFIX and STKFAN appear to converge slightly slower to the minimum thrust that is attained at the end of the transient. Their discrepancy with the rest of the computational models can be regarded as negligible, as can be ascertained from Figure(64).

Very interesting results have been predicted during the Sea level, Mach=0.2 acceleration. The Thrust response, Figure(65), shows significant discrepancies between the predictions of all programs. The two Stack fan programs were the only ones that showed similar predictions. All programs show a consistency of results for the first 3-4 seconds of the transient. The "real" acceleration occurs just before the 6^{th} second. In a matter of a further two seconds all programs predicted the engine reaching

90% of its maximum thrust. The more significant discrepancies occur during that crucial time interval between the 6^{th} and 8^{th} second where most of the acceleration takes place. For this reason the predictions of all programs for the above mentioned two seconds have been enlarged and shown in Figure(65A). In this graph, the similarity of predictions of the two Stack fan programs that was mentioned earlier, becomes more clear. The slowest response is predicted by the AFCSP program and the fastest one by the Stack Fan programs(STFFIX and STKFAN). The AFCSP program predicts a thrust of 6,000lb.(middle of the range) in 7.74 seconds while the AFSPOF predicts the same thrust in 7.65 seconds. That is a 1.2 per cent faster response than is predicted by the AFCSP computational model. The FFCSP program predicts the same thrust of 6,000lb. in 7.42 second which is an even faster response by 4.1 per cent. By far the fastest response was predicted, as mentioned above, by the STFFIX and STKFAN programs which showed a difference of the order of 8.3 per cent.

The two programs STKFAN and STFFIX, that show a much faster response, predicted also higher component efficiencies. The Inner and Outer Fan efficiencies predicted by the two programs mentioned above were 0.944 and 0.877 respectively, while those predicted by the AFCSP program at the same instant in the transient(7th second), were 0.762 and 0.812 respectively. This is a difference of the order of 14% between the efficiencies used by the two computational models. This is due to the fact that the characteristics provided for the Stack Fan programs representation of the Fan(Inner and Outer), were considerably

different from the ones used in the AFCSP program and hence the engine with the more efficient Fan accelerates more rapidly.

Although the characteristics used in the AFCSP, AFSPOF and FFCSP programs were all the same, still these models predicted different thrust responses. The FFCSP program, as it was mentioned earlier, shows a faster thrust response by 4.1 per cent. The explanation for this discrepancy lies with the difference in Fan treatments employed by the two programs. Figure(65B) shows the variation of the Factor of Split(FCSP) for the AFCSP model during the same time interval between the 6^{th} and 8^{th} second of the Sea level acceleration. At the beginning of the 6^{th} second, the FCSP has a value of 0.82 while for the FFCSP program is always kept constant and equal to 1.0. This implies that at that particular instant, the core of the engine for the AFCSP program's prediction, receives approximately 20% less air. However the effect of, the lagging of the LP shaft behind the HP one(see chapter II) during the start of the "real" acceleration at the 6^{th} second, is less existing in the FFCSP program since the Fan treatment employed here allows for a 20% more air into the core of the engine than that allowed by the AFCSP Fan treatment.

As it can be seen from Figure(65B), the Factor of Split is then forced to a rapid increase in order to allow more air through the core of the engine, so that the demand of air at the start of the "real" Acceleration can be satisfied. Nevertheless this procedure of events takes a certain amount of time and the effect of it can be clearly shown as a discrepancy in the predictions of the thrust response of the two programs.The AFSPOF program shows

a slightly faster response than the AFCSP one and once again the explanation lies within the concept of the variable Factor of Split.

3.6 COMPARISON OF COMPUTING TIME

3.6.1 Type Of Computer Used

The computer simulation of highly complex engines can be carried out by using either an analogue or a digital computer. The main advantage of the analogue computer is that it can offer "real time" simulation, irrespective of the engine's complexity, by enabling simultaneous evaluation of the different component parameters. The term "real time" denotes the capability of the computer to carry out the simulation at the same time that the real engine would need to perform the same action. It is thus the analogue computer which is ideal for the design and test of actual control systems. Saravanamuttoo and Fawke Ref.(37) described in detail such analogue systems.

The above mentioned advantages of the analogue computer come as the expense of the time needed to set up the large number of function generators. These are the electrical circuits that would represent the parameters and their performance characteristics. The results of the simulation are in voltages which represent the thermodynamic variables.

Although reliability and repeatability is not a major problem for the analogue computer, on the other hand the digital computer can guarantee them once the program is running. It should be mentioned that the user would need much more expertise to set up the analogue circuits than to program the

digital computer. The latter performs calculations in an order predetermined by the program, so that the results would simulate the real engine. Depending on the complexity of the engine, in most cases the calculation procedure has to be repeated several times which result in slow computing time. Hence "real time" simulation cannot be achieved with the digital computer unless the engine is of a very simple form. Another advantage of the digital computer is that it gives the opportunity, once the program has been set up, to test different configurations, components or component characteristics by making simple changes in the actual program or changing the data files that are being used.

The current research used the main frame digital computer of the University of Glasgow for the necessary changes and compilations needed to form and develop the different computational models presented.

From September 1984, when the current research started, until the September of 1987, the main frame of the University of Glasgow used the ICL 2988 computer. During late September-early October 1987 that machine was gradually replaced by the ICL series 39 Level 80 machine which was abbreviated as 3980. The new machine offered the same VME service as the 2988 but some minor changes were inevitable, such as the end of using the FORTRAN IV and at that time all programs had to be transformed into FORTRAN 77.

The new Level 80 system is the most powerful single 'node' system that ICL currently offers. Ofcourse multinodal systems were also available which were composed by linking single

'node' systems, all running one copy of VME.

This single 'node' system consists of:

1. An **instruction processor** which included also a scientific unit to enhance the execution of mathematical and array handling
2. The **mainstore**
3. A **node-support computer** being a separate processor responsible for overseeing the basic functioning of the node complex
4. Two **input/output devices** responsible for connecting fast and slow peripheral devices into the node complex.

The new machine is significantly different from the 2988 and in some respect significantly different from the more usual technology provided by other mainframe suppliers.

Although the design and construction of the node itself is different from the early 2900 systems, developments of the new system are found in parallel in the equipment of other mainframe suppliers, particularly where these are based in Fujitsu originated technology.

The most important effect that the new system had in the current research was that the data processing times were now faster by 4 to 5 times than those that the 2988 machine could achieve.

It is the computing time needed for a program to be executed, that is of interest in this section and it is going to be used as a means of comparison between the different computational models developed in the current research.

3.6.2 Comparison Of Computing Time

The computing time needed by the computer to process all the data, compile the program and produce the relevant results is called OCP time. To simplify the way that the comparison is going to be conducted, the OCP times for acceleration and deceleration at only the Altitude case of 43,000ft. and Mach=0.8, are tabulated in the Table(3.6). shown below.

An average OCP time between the acceleration and deceleration for each program was also calculated so that the relative average difference between the computational models could be obtained.

43,000ft., Mach=0.8

	Acceleration OCP Time	Deceleration OCP Time	Average OCP Time
AFCSP	36.3	24.5	30.45
FFCSP	23.5	73.3	49.9
AFSPOF	32.4	25.7	29.05
STFFIX	69.6	66.5	68.0
STKFAN	86.7	92.4	89.5

Table(3.6)

It is once again the case of the two programs AFCSP and AFSPOF showing a consistency of results since they need virtually the same OCP time. As it can be seen from the Table(3.6) above, these are the fastest programs. The Stack fan programs, due to the different representation of the Fan characteristics, need more iterations until convergence is achieved, which results in excessive computing time. The STKFAN program which is the slowest one needs approximately 66% more computing time than the AFCSP and AFSPOF ones. It is

also slower than the FFCSP program by 44% and the STFFIX one appears to be faster than the STKFAN by 24%.

It should be emphasized that the results under comparison are of the Altitude flight condition which need half the OCP time compared to the corresponding Sea level cases. For example the STKFAN program was found to need 153.1 sec. OCP time to run the Sea level deceleration which is nearly double the time needed for the Altitude one.

3.7 CONCLUSION OF COMPARISON

It is a very difficult task to try to compare and judge which program is the best, since no comparison takes place between the computational models and the real engine. At this stage, speculation on which program predicts the more reasonable results could be our only means of comparison. An analysis on why its model predicts the results that were obtained under the various flight conditions could also help the comparison.

As it was mentioned earlier, it was not possible mainly for computing time reasons, to compare all the computational models developed in this research, with the real engine test results.

The scope of this comparison was to try to investigate the potential advantages and disadvantages of the programs in order to choose those on which the real engine effects would be incorporated. In order to be able to best represent a typical turbofan engine, these effects have to be included otherwise the result of the simulation would be unrealistic and the simulator

would not serve its purpose.

All the results used in the comparison of the computational models showed in general a consistency in the predictions of the programs. From the investigation carried out, it can be recognized that the AFCSP and AFSPOF constitute one extreme case and the Fixed Factor of Split concept of the FFCSP program can be regarded as the other extreme. The Stack Fan programs were in general predicting results that could be accepted as the average case between the two extreme ones.

The AFSPOF program adopts a Fan treatment which simulates a situation that could not exist in a real engine. Nevertheless its concept was worth investigating for the merit of research but the results of the comparison showed the program's predictions to lie very close to the AFCSP ones. Since the latter's Fan treatment is closer to the real engine it was thus decided not to consider the AFSPOF program for the further investigation that is discussed in the following chapters.

The whole comparison is now virtually concentrated between the two concepts of allowing or not an interchange of flow between the two sections of the Fan. The comparison showed the FFCSP program predicting results that probably would not in general agree with the real engine expected behaviour. The STFFIX program, although in general agreed with the FFCSP program's predictions, there were isolated cases that appear unrealistic. As an example of this we could be referred to the Sea level deceleration trajectory of the Outer Fan where the predicted by the STFFIX program trajectory lies too close to the steady-running line for the first part of the deceleration. For the

reasons mentioned above and also during the process of the comparison, the two programs, FFCSP and STFFIX were discarded from the incorporation of the Real engine effects and hence from the investigation followed.

Since the STKFAN program was the only one predicting consistently realistic results, it was thought that the allowance of interchange of flow concept would allow for a more realistic simulation. The other program(AFCSP) adopting the same concept showed also consistently realistic results with the exception of the over-accounting of interchange of flow in the deceleration cases.

An other very important factor that has to come under consideration at this point is the computing time that each program needs, which appears also to be the main disadvantage of the STKFAN program. As it was seen earlier the STKFAN program needs double the computing time of the fastest AFCSP program.

The computing time is increased dramatically when the Heat transfer effects are included in the models(see chapter IV). Hence it was decided to use the AFCSP program, which is the fastest one, and the STKFAN, which is the slowest one, in the incorporation of the real engine effects. It will thus be possible to judge if the perfection and realism are worth the penalty of the excessive computing time. The two programs, AFCSP and STKFAN, are used for the incorporation of the real engine effects mentioned at the beginning of the current chapter.

CHAPTER IV

COMPARISON OF PROGRAMS "AFSREE" AND "STFREE" WITH THE REAL ENGINE TEST RESULTS

4.1 INTRODUCTION

The computer simulation method, in order to be accurate, must include several effects to account for component losses and also for any deviation from the theoretically evaluated values of certain parameters.

The heat transfer effects have long been the subject of investigation since their existence is of the outmost importance in the performance of the gas turbine. Inclusion of these effects in any simulator is necessary in order to be able to predict realistic and accurate results.

Prediction methods for the heat transfer effects have already been used successfully by Pilidis, Ref.(31). These methods, with necessary improvements, have been incorporated in the current investigation in order to best simulate the transient performance of a typical Turbofan engine.

Changes in temperature and pressure occur throughout the engine. These changes affect the values of Specific Heat Capacity and also of γ.The variations of C_p and γ, for both air and gases, were included into the computer models (AFCSP, STKFAN) in order to achieve a better accuracy in the predictions.

As a final "real engine effect", i.e. effect which if included will allow the simulator to give predictions closer to the real engine,

was the inclusion of the initially ramped fuel schedule during a transient. In the previous predictions it was assumed that the fuel flow changed instantaneously from the steady running value to the value dictated by the fuel schedule. Real engine tests indicated that this was unrealistic, since the above mentioned change of fuel flow occurs over a period of 0.4 to 0.5 seconds. This was incorporated in the two programs.

As discussed in this chapter, these effects have been included into both AFCSP and STKFAN programs and their predictions had been compared with actual test results of a typical Turbofan Engine. The two programs, AFCSP and STKFAN, after the inclusion of the "real engine effects", have been renamed as AFSREE and STFREE respectively. The AFSREE name stands for Adjusting the Factor of Split including also the Real Engine Effects and similarly for the STFREE program.

4.2 VARIATION OF THE SPECIFIC HEAT CAPACITY C_P

As it was mentioned earlier, the values of C_P and γ of the working fluid vary due to changes that occur in temperature and pressure throughout the gas turbine. Changes in chemical composition in internal combustion can also lead to changes of the specific heat capacity.

The values of C_P and γ are very important in the evaluation of the performance of a component or a cycle.

It is well known that:

$$\frac{C_P}{C_v}=\gamma \qquad \text{and}$$

$C_P - C_v = R$ where R is the Gas constant and the specific heat capacity can be expressed as:

$$C_P = \frac{\gamma R}{\gamma - 1}$$

The ratio of Specific heats, γ, is used in the calculation of various parameters through the gas turbine cycle. Hence any variation of the C_P value will affect γ and hence the performance of the engine's individual component as well as of the whole cycle.

The variation of the C_P and γ can be seen in the Figure below:

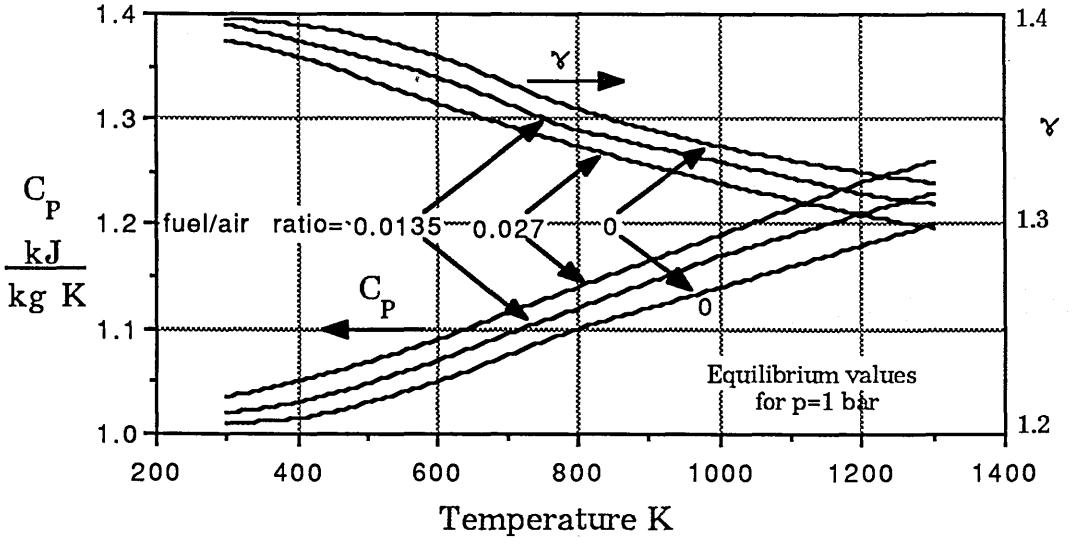

Figure(66)

The Figure(66) above shows a variation in temperature from 200 to 1200K. For the compressor only the left hand portion is of interest since a high pressure compressor(e.g. pressure ratio as high as 14) will show a temperature rise of no more than 400K.

At high temperatures as those at the inlet to the turbine, the mixture of air and the products of combustion are subjected to an additional phenomenon of the dissociation. Since dissociation is closely affected by pressure then the specific heat capacity

would also be affected by the pressure. Both C_p and γ are significantly affected by dissociation at temperatures of 1500K and over. For temperatures higher than 1500K the variation of C_p and γ with increase of the fuel to air ratio is applicable only to a pressure of 1 bar. For example, if at 1800K the pressure is reduced to 0.01 bar, Cp increases by 3-4 per cent, while an increase of pressure to 100 bar decreases Cp by only 1 per cent. Since a typical turbine inlet temperature is around 1300-1400K it was decided to ignore any effect of pressure changes on the specific heat capacity.

Initially the programs AFCSP and STKFAN, allowed for a variation of Specific Heat capacity as a function of temperature. This was now improved by allowing a variation of C_p as a function of both the temperature and the air to fuel ratio. The changes in C_P were included in the calculations of the combustion chamber and HP and LP turbines. A C_P value estimated from the previous components was used as the initial value. This initial C_P value was used to calculate the temperature difference and consequently the new value of C_P, (once through calculation method). The improved C_P value was used once again through the same calculations to estimate a more accurate one, (successive approximations method).

The AFCSP program was used to show the significance of the incorporation of the variation with composition of the specific heat capacity. Three versions of the program were run at Sea level, Mach=0.2, for steady running predictions only. The first version did not allow for any variation of C_P, the second allowed variation but used the once through calculation method and the third version used the successive approximations method.

The predictions of the program were used to plot the H.P. and L.P. shaft speed as well as the Specific Fuel Consumption(SFC) against a base line of Thrust, for a variation of Fuel flow from 24 to 100 per cent of the maximum, Figures(67,68&69).

The allowance for variation of the C_P value did not have any affect on the HP and LP shaft speed relationship, Figures (67&68). The discrepancies between the three versions could be regarded as negligible.

The Specific Fuel Consumption(SFC) plotted against the Thrust is shown in Figure(69). From the graph it can be seen that the variation of C_P affected the predicted SFC over a wide range of Thrust. No variation of C_P predicted generally a higher SFC by 1.5 per cent from the once through calculation version and a 2.1 per cent from the successive approximations method.

In the effort to develop a computational model which is as accurate as possible, the second approximation method was now incorporated in both the AFCSP and the STKFAN programs once its penalty in computing time could be regarded as negligible and the advantage in accuracy was proven to be of the order of 2 per cent.

4.3 HEAT TRANSFER EFFECTS

In the first chapter of the current investigation, an extensive survey was reported on the research that had been carried out on the heat transfer effects and their representation in computer models.

The representation methods of all the effects that had been

adopted by Pilidis, Ref.(31), and Pilidis & Maccallum, Ref.(32,34), were also used in the present research with modifications necessary to improve the accuracy and realism of the predictions.

However these procedures did not include any allowance for heat transfer effects in the combustion chamber. A crude model for representing the heat transfer effects in the combustion chamber was developed and incorporated in both AFSREE and STFREE programs together with the heat transfer effects for the rest of the engine's components.

These models which have been used in the present work were at the state to which they had been developed in June 1988. Further development has been carried out, Ref(45), which leads to significantly different predictions. These improvements, and their impact on the predictions which account for thermal effects, are discussed later, in Chapter V. However for the present investigation of representation of Fans, it had been necessary to use the "thermal effects" prediction program at its earlier stage of development of June 1988.

To highlight the significance of the incorporation of these effects in a gas turbine simulation model, the AFSREE program, was used to predict the steady-running, acceleration and deceleration results at Sea level, Mach=0.2, with and without the incorporation of the Heat transfer effects. The results of the predictions were used to plot the working lines as well as the transient trajectories of the combined Inner Fan and I.P compressor as well as of the H.P. compressor. These results are now discussed.

4.3.1 Combined Inner Fan and I.P. compressor results

The AFSREE program was used to predict both the adiabatic and non-adiabatic working lines of the combined Inner Fan and I.P. compressor at Sea level, Mach=0.2. The steady running lines of both cases (adiabatic and non-adiabatic) showed no divergencies, as can be seen in Figure(70).

The predicted deceleration and acceleration trajectories together with the combined characteristics are shown in Figure(71). The significance of the Heat transfer effects are shown in both transients but by far the most important discrepancy appears during the deceleration.

During the cold acceleration the predicted trajectory appears lower than the adiabatic one, mainly due to changes in compressor characteristics. The deviation from the adiabatic prediction is of the order of 4 per cent in terms of pressure ratio.

Turning to the deceleration results, the predicted non-adiabatic trajectory is raised significantly towards the surge line by approximately 9 per cent in terms of pressure ratio at a mass flow. As it can be seen from Figure(71), the inclusion of the thermal effects had reduced considerably the surge margin of the combined Inner Fan and I.P. compressor.

4.3.2 H.P. Compressor Results

The inclusion of the heat transfer effects altered the behaviour of the H.P. compressor in both transients that the AFSREE program predicted.

The cold acceleration prediction shows the non-adiabatic trajectory lowered from the adiabatic one by approximately 7 per cent towards the steady running line. Hence, as it can be

seen from Figure(72), the surge margin during a cold acceleration is considerably greater than is predicted adiabatically.

The predicted deviation from the adiabatic one is due to compressor characteristics changes as well as due to losses of H.P. cooling air through the seals. There are also altered tip clearances during a cold acceleration which would affect the behaviour of the compressor.

The deceleration trajectories are shown in Figure(73). The inclusion of the thermal effects has caused the trajectory to be lifted towards the steady running line. The discrepancy observed in comparison to the adiabatic prediction is small with the exception of a "kink" in the trajectory that appears at a non dimensional air mass flow rate between 37 and 43. The engine reaches that range after 0.87 seconds into the transient. When the L.P. shaft's non-dimensional speed is close to the value of 560, the deviation from the adiabatic prediction has risen to 14 per cent. This significant deviation lasts for 0.5 seconds and then the trajectory returns to its normal path.

This behaviour of the H.P. compressor had to be investigated further in order to identify the cause of the deviation. From the first results obtained it was observed that during that 0.5 seconds, when most of the deviation occurs, several parameters of the engine showed important changes. Firstly, higher heat transfer rates were predicted for the H.P. compressor, H.P. turbine and L.P. turbine, being 890 KW, 580KW and 560KW respectively. The H.P. turbine's blades showed significantly higher temperatures than the stabilised ones and also than

would be expected during that range of the transient. The efficiency of the H.P. turbine had also fallen by 1.7 per cent against a 0.3 per cent of the H.P. compressor. As a result of the higher temperatures in the H.P. turbine the Factor of Split was lowered by 4 per cent from the adiabatically predicted one. In order to identify in which component the problem had initiated, the AFSREE program was now used to predict the same transient but this time was run several times and each time one only of the heat transfer effects was incorporated successively into one of the components until all the effects were added on all the components. The results of the investigation showed that the behaviour of the H.P. compressor had been affected by changes in density and the boundary layer, due to heat transfer, which in turn affect the compressor characteristics. These changes were shown in Figure(73), as a rapid reduction of non-dimensional air mass flow rate with a small decrease in pressure ratio. The decrease in air mass flow rate had as a result the increase of the operating temperature of the H.P. turbine blades which led to a reduction in efficiency of the H.P. turbine of 1.7 per cent. It should be mentioned that further investigation could be essential as to determine the exact cause and location of initiation of the problem. As the transient progresses the discrepancy between the two predictions deteriorates. This is due to the fact that at the end of the deceleration had elapsed sufficient time to allow for most of the heat transfer to take place.

In both transients, the steady running line was represented by the adiabatically predicted one since no discrepancies

appeared between the steady running lines predicted with and without the inclusion of the heat transfer effects.

The beneficial results of the inclusion of the above mentioned effects, can be observed in the acceleration case where the surge margin of the H.P. compressor, in some regions of the trajectory, is doubled.

4.3.3 Thrust Response

From the same results obtained for the Sea level, Mach=0.2, acceleration and deceleration, the Thrust response with Time was also studied for the adiabatic and non-adiabatic predictions. [Note on Units Used: Thrust values are quoted in units of pound force, lbf, since these are the units used by the engine manufacturers.]

The thrust response during the acceleration, Figure(74), shows discrepancies between the two predictions at the start of the "real" acceleration, i.e. after the 5^{th} second, and also at the end of the transient. The adiabatic acceleration appears to be slower than the non-adiabatic one by approximately 3.5 per cent. The difference gradually reduces as the transient progresses, but still at the end of the thirteen seconds, the inclusion of the heat transfer effects predicted a trajectory which stabilized at a lower thrust from the adiabatic one, although the maximum attainable fuel flow was the same for both cases. The difference of thrust at time thirteen seconds is about 3 per cent.

Similarly, Figure(75), shows the deceleration thrust response for both cases studied in this section. When the heat transfer effects are included, the thrust response is slower in particular towards the end of the transient. Since the Figure(75) shows the

transient during the full time allowed for the speed to stabilize, i.e. thirteen seconds, the existing discrepancies between the predictions of the two cases are not clearly observed. For this reason the first and last part of the deceleration trajectories have been enlarged and shown in two different figures. Figure(76), shows the thrust response for the first two seconds in the transient. The inclusion of the thermal effects show discrepancies with the predicted adiabatic results only after the first second where the thrust of the engine had dropped by approximately 64 per cent. At the end of the 2^{nd} second, the adiabatic trajectory predicts a faster deceleration from the non-adiabatic one. The difference is approximately 14.3 per cent in time at a thrust of 2000 lbf.

At the last part of the transient, as shown in Figure(77), the discrepancy that first existed after the 2^{nd} second, is growing to a significant difference of approximately 35 per cent, higher predicted thrust of the non-adiabatic case at time thirteen seconds.

The reader is however reminded that the thermal models on which the predictions were based have been improved-see section 4.3 and Chapter V.

4.4 COMPARISON OF THE SIMULATION PREDICTIONS WITH THE REAL ENGINE RESULTS

4.4.1 Acceleration and Deceleration at 43,000ft., Mach=0.8

The Real engine test results available did not include measurements of the mass flow rate and hence all the

comparison was based on the shaft speeds, pressures and temperatures recorded at various stations in the engine. In most of the graphs the non-dimensional speed was used as the base line.

The two programs, AFSREE and STFREE, used exactly the same ambient conditions that were achieved during the test results of the Real engine. The comparison was carried out for a "cold" Acceleration, a Deceleration and a "Bodie" or Hot re-acceleration, all at 43,000ft. and Mach=0.8, which were the only Real engine test data available.

The two computer models were run firstly at steady running at the above mentioned ambient conditions in order to establish the maximum range of shaft speeds and fuel flow. The AFSREE program predicted a higher maximum attainable point of operation than the STFREE program, for the same maximum fuel flow rate. These maximum points of operation, in terms of shafts speeds and fuel flow rates, are the ones normally used as the starting points for the deceleration. It was decided to use for both programs the deceleration starting point predicted by the STFREE program in order for the shafts to have the same kinetic energy at the beginning of the transient since these speeds were also closer to the starting speeds of the Real engine.

Figure(78) shows the L.P. shaft speed response with time during the cold Acceleration. Both programs predict a considerably faster L.P. shaft acceleration by an average of 60 per cent. Considering the stabilising L.P. shaft speed, it is seen that the Real engine and the AFSREE program showed about the same speed, while the STFREE program predicted a lower speed.

The difference between the predictions of the two computational models is about 2.5 per cent.

The corresponding H.P. shaft speed response comparison is shown in Figure(79). Both programs predicted a considerably faster Acceleration by approximately 66 per cent, showing thus a discrepancy of the order of 10 per cent from the test results in terms of thrust at a particular instant. Program AFSREE predicted a lower stabilizing H.P. shaft speed than the real engine achieved by 4.3 per cent, while the STFREE program predicted a speed lower by 3.0 per cent.

As an overall comparison of the shafts speeds responses, it was decided to plot the H.P. shaft speed against the L.P. shaft speed, the results being shown in Figure(80). The highest discrepancies from the Real engine are approximately 4 per cent for the STFREE program and 5 per cent for the AFSREE program. From the comparison of the shaft speed responses so far it can be concluded that for the cold Acceleration the AFSREE program predicts a better L.P. shaft speed response than the STFREE one while the latter predicts a better H.P. shaft speed response.

In order to compare the Outer Fan behaviour during the cold Acceleration, the Outer Fan pressure ratio,(P_{13}/P_1), was plotted against the non-dimensional speed of the L.P. shaft as shown in Figure(81). At the non-dimensional speed of 420, the Real engine had a pressure ratio of 1.6, while the predicted one by both programs, (predictions coincide at that instant), is 1.514, which shows a difference of 14 per cent in terms of pressure rise. At the non-dimensional speed of 470 the pressure ratio recorded for the Real engine is 1.7, while the programs predicted an Outer Fan pressure ratio of 1.61 showing thus a difference again of the

order of 13 per cent in pressure rise.

It should be noted at this point that at the same non-dimensional speeds, the Outer Fan pressure ratios obtained by the Real engine are higher than those predicted by the two computer models which in effect implies that the Outer Fan mass flow rate of the Real engine will be slightly less than the predicted one. Although the shapes of the transient lines predicted by the two computational models are in general agreement with the shape of the transient line of the engine, an important difference exists at the top end of the curves(last part of the transient). The Real engine curve appears to flatten out at the range of dimensionless speeds higher than 430. This is correctly predicted by the AFSREE program, while the STFREE one not only failed to predict this behaviour of the engine (increase of non-dimensional speed with small or none increase in pressure ratio), but also failed to reach the maximum non-dimensional speed that the engine attained and also the AFSREE program predicted. That discrepancy in non-dimensional speed between the two models is of the order of 4 per cent. The results of the comparison of the Outer Fan behaviour during the cold Acceleration are used later in conjunction with the Deceleration results.

During the Real engine tests, the conditions between the Inner Fan and the I.P. compressor were impossible to be measured and hence the pressure(P_{26}) recorded after the I.P. compressor was used to evaluate the combined Inner Fan and I.P. compressor pressure ratio (P_{26}/P_1), which was plotted against the non-dimensional speed of the L.P. shaft, Figure(82). Both programs

are able to predict both the individual and the combined pressure ratio of the two components mentioned above. The predictions of both computer models during the Acceleration, show generally good agreement with the real engine test results. The maximum discrepancy in pressure rise at a non-dimensional speed is about 6 per cent. The STFREE program shows a better prediction than the AFSREE one, for the very first part of the transient, by 5 per cent (in terms of difference in pressure rise at a particular non-dimensional speed). As in the case of the Outer Fan, at the last part of the Acceleration, the STFREE program predicts a lower maximum non-dimensional speed and pressure ratio than the Real engine achieved and AFSREE program predicted. The discrepancy between the predictions of the two computer models is approximately 3.5 per cent in non-dimensional speed.

Continuing the comparison, the H.P. compressor results and predictions are shown in Figure(83). The predictions of the two programs coincide but have considerable discrepancies from the Real engine test results. The largest difference is about 12 per cent in pressure rise at the non-dimensional speed of 590. Another important feature is that the Real engine shows both the pressure ratio and non-dimensional speed increasing to a maximum and then stabilising to a lower point of operation at the maximum fuel flow rate. As it has been already mentioned the H.P. shaft starts the acceleration sooner and faster than the L.P. shaft. As a results of this the non-dimensional speed of the H.P. compressor reaches a maximum value while the L.P. shaft still accelerates and hence delivering higher temperature (T_{26}).

Since the H.P. shaft has already reached its maximum speed the increase of T_{26} results in decease of the non-dimensional speed of the H.P. compressor. This explains the behaviour of the H.P. compressor shown in Figure(83). The two programs had successfully predicted this behaviour of the H.P. system but both predicted a much lower stabilizing point. The stabilizing point predicted by the STFREE program is closer to the Real engine one than the stabilising point predicted by the AFSREE program. The difference of the two predictions in that aspect was calculated to be of the order of 5 per cent in terms of an average discrepancy in both the pressure rise and non-dimensional speed.

As mentioned earlier, the test results of the engine did not include any mass flow rate measurements, nor were any thrust measurements available. It was thus decided to plot:

$$\frac{P_6}{P_{01}} \text{ vs } \frac{N_L}{\sqrt{T_{o1}}}$$

where P_{01} and T_{01} are the ambient stagnation pressure and temperature and P_6 is the pressure at the exit from the L.P. turbine, in order to have an indication of what would be the thrust response. The comparison of the engine's test data and the predictions of the models for the Acceleration are shown in Figure(84). The results of the programs are in general agreement with the real engine apart from the last part of the transient where the engine stabilizes at a higher operating point. The difference is of the order of 8 per cent. This was due to the fact that the engine reached higher fuel flow rates than the programs could predict. The results of the predictions for the cold Acceleration were in general agreement with the real engine

results with a mean average discrepancy of 5.6 per cent.

The deviations between the acceleration predictions of the two models, discussed above, will later be used in conjunction with the rest of the results discussed in this chapter in order to conclude which program could better simulate a typical turbofan engine.

Next the Deceleration results are discussed. The results are shown in Figures(85 to 91).

The L.P. shaft speed response with time is shown in Figure(85). For the crucial first two seconds of the transient, where most of the deceleration occurs, both programs succeeded in predicting results close to the Real engine ones. As the transient progresses the STFREE program predicts a much slower deceleration by approximately 22 per cent (in time) while the AFSREE program by only 10 per cent. Both programs predicted also higher final stabilizing speeds than the Real engine achieved, the STFREE program by 8 per cent while the AFSREE by 4 per cent. Hence, the AFSREE program predicted a better L.P. shaft speed response than the STFREE did by an average of the order 7 per cent.

Although the starting shaft speeds of the Deceleration used by the two computer models were lower than those of the engine, both programs predicted an H.P. shaft speed response which is very close to the Real engine one, as it can be seen in Figure(86). The two models predicted at the third second a higher H.P. shaft speed of the order of 1.5 per cent, which was the maximum discrepancy, and also a higher final stabilizing speed by 0.9 per cent. Both shaft speed responses predicted by the two computer

models are in good agreement with the test results showing a mean discrepancy of about 1 per cent. This can also be verified by the H.P. versus the L.P. shaft speed graph which is shown in Figure(87).

By far the most interesting results are shown in Figure(88), where the Outer Fan test results and predictions are compared. The Real engine behaviour during the Deceleration shows a very noticeable increase in pressure ratio, after the initial rapid drop at the beginning of the transient, and holds at this higher pressure ratio for a range of non-dimensional speed between 490 and 450 before starting the rapid drop again. The transient line predicted by the STFREE program showed a continuous decline throughout the transient, while the AFSREE program succeeded to predict a transient line closer to the Real engine one.

It would now be very helpful to consider also the Outer Fan results and predictions obtained during the Acceleration, in order to conceive a more complete picture of the comparison and cause of discrepancy between the programs and the Real engine. The table below includes the pressure ratios of the Outer Fan during the Acceleration and Deceleration for the non-dimensional speeds of 420 and 470 for the Real engine and the STFREE and AFSREE programs.

		$N_L/\sqrt{T_1}=420$			$N_L/\sqrt{T_1}=470$		
		ENGINE	STFREE	AFSREE	ENGINE	STFREE	AFSREE
$\frac{P_{13}}{P_1}$	**Accel.**	1.60	1.517	1.517	1.7	1.614	1.597
	Decel.	1.6575	1.4275	1.4795	1.7325	1.56	1.5715

Table(4.4.1)

From the table above, it is clear that the Real engine's Outer Fan Pressure ratio at both 420 and 470 non-dimensional speeds, is higher during the Deceleration than in the Acceleration. The opposite is the case of the predictions of the two computer models. As it was mentioned earlier, the Real engine shows during the Deceleration an increase in pressure ratio after the initial rapid drop. This indicates that an increase in mass flow rate through the by-pass duct could be responsible. It is important to note at this point that the STFREE program predicted a steep fall in pressure ratio from the beginning and throughout the transient, while the AFSREE program predicted the same initial steep drop but it became less rapid at the same non-dimensional speed region that the engine shows the increase of the pressure ratio. It should also be noted that the Outer Fan pressure ratio predicted by the STFREE program during the deceleration is much lower than that predicted by the AFSREE program-see Table(4.4.1) above. In general it could be concluded at this point that the shape of transient line predicted by the AFSREE program for the Deceleration is closer to the real

engine behaviour than that predicted by the STFREE program.

At the time when the present work was carried out, the data available from the manufacturers of the engine under investigation did not include any information as to the existence of an I.P. loss of air. Supposing an I.P. compressor bleed or "leak" existed, then the pressure ratio across the bleed "orifice" at the non-dimensional speed of 470 can be evaluated and is shown in the following table:-

	$\frac{P_{26}}{P_1}$	$\frac{P_{13}}{P_1}$	$\frac{P_{26}}{P_{13}}$
Accel.	2.45	1.7	1.44
Decel.	2.54	1.7325	1.46

Table(4.4.2)

Hence during the Deceleration the bleed "orifice" would become more effective since the pressure in the core of the engine is higher than at the by-pass part. An escape of air from the core to the by-pass would probably affect the response of the Outer Fan but also of the L.P. shaft. It was thought at this stage to use the two programs to simulate the same conditions as before but with the incorporation of a 5 per cent I.P. compressor bleed. The influence of the inclusion of a 5 per cent I.P. bleed in the predictions of the two programs is discussed in section (4.4.2) of the current chapter.

The behaviour of the combined Inner Fan and I.P. compressor during the Deceleration is shown in Figure(89). Both programs predicted an initial increase in pressure ratio. This was explained earlier as the result of the Fan, which, during the start of the

transient, fails to decelerate immediately due to its inertia. It hence delivers to the core of the engine more air than the H.P. system can possibly handle and it is at this point that the concept of the adjustable boundary between the Inner and Outer flows comes into effect and diverts air mass flow from the core to the by-pass part of the engine. This results in a decreased mass flow rate through the core, which is shown in Figure(89) as an increase (temporary) in pressure ratio. Although this was how the Real engine's Inner Fan plus I.P. compressor was expected to behave, instead it showed a steep decrease in pressure ratio from the start and throughout the transient, appearing thus to be able to cope with larger amounts of air through the H.P. compressor without surge being created. The above mentioned difference between predictions and Real engine behaviour was considered as an additional reason in support of the existence of an I.P bleed or even "leak" which was later incorporated in the computer models.

The H.P. compressor results show, as in the case of the Acceleration, considerable discrepancies between the simulation and the test results of the engine. It can be seen from Figure(90) that between the two models, the STFREE program predicted a characteristic whose shape is, in general, closer to the Real engine one.

In Figure(91), an indication of what could have been a comparison of the thrust response is shown. The characteristic line predicted by the AFSREE program, in comparison with the line predicted by the STFREE program, is in better agreement with the Real engine's one. Both programs show a discrepancy from the real engine results of the order of 5.5 per cent.

4.4.2 Acceleration and Deceleration at 43,000ft., Mach=0.8, Including 5% I.P. Compressor Bleed

The results tabulated in Table(4.4.2) showed that the P_{26}/P_{13} value is higher in the case of the Deceleration than during the Acceleration. This indicates that an uncontrolled leak of air would have more effect during the Deceleration. Nevertheless both programs were used to include a 5 per cent bleed for both cases of Acceleration and Deceleration. The fact that the leak would be less effective or not existing at all during the Acceleration, would affect significantly the outcome of the comparison of the predictions of the programs with the Real engine results. In fact this was confirmed in the presentation of the results of the Acceleration comparison which are shown in Figures(92 to 97) and also in Figure(104). In all graphs it can be seen that the discrepancies between the predicted and actual test engine results had increased. That having been noted, these results are not discussed further.

The Deceleration results are now considered. Figure(98) shows the L.P. shaft response with time. The results of the programs without the 5 per cent I.P. bleed, shown in Figure(85), predicted a discrepancy of 10 per cent, for the AFSREE, and 22 per cent, for the STFREE program, from the engine's test results. The incorporation of the I.P. bleed improved both program predictions which, as shown in Figure(98), decreased the discrepancy from the Real engine to 4 per cent for the AFSREE program and to 10 per cent for the STFREE one. Hence the existence of a 5 per cent bleed improved the agreement of the AFSREE L.P. shaft speed response by 60 per cent and by 54 per

cent for the STFREE program. The comparison was carried out with regard to the time that the two programs and the engine needed to reduce the L.P. shaft speed down to 6500 rev./min..

Similarly for the H.P. shaft speed response, at the same instant, i.e. third second into the transient, the results of the engine and of the programs including the 5 per cent bleed, shown in Figure(99), are compared with the ones without the incorporation of the bleed which were described in Figure(86). Again the predictions of both programs had improved and the discrepancy between the predictions and the actual engine test results can be regarded as negligible. This is also confirmed from the results of the H.P. versus the L.P. shaft speed, shown in Figure(100).

Although the incorporation of the bleed resulted in considerable improvements in the predictions of the shaft responses, no significant change appeared in the Outer Fan results, which are shown in Figure(101). It is again the case of the AFSREE program predicting a characteristic which is closer to the behaviour of the Real engine than the STFREE program predicted. The latter predicted a steeper drop of pressure ratio during the first part of the transient, which is opposite to what the engine test results showed.

The combined Inner Fan plus I.P. compressor predictions were, in general, very close to the engine test results, without (Figure89) and with the incorporation of the 5 per cent bleed shown in Figure(102). Attention should be focussed now on the shape of the characteristic predicted by the STFREE program during the very first part of the Deceleration. The inclusion of

the I.P. bleed had as an effect the initial drop, instead of increase(without the 5% bleed), of the pressure ratio, which lines up with the behaviour of the Real engine but at a lower pressure ratio.

The incorporation of the I.P. bleed improved also the H.P. compressor predictions, Figure(103). In Figure(90), i.e. no I.P. bleed, the programs, in general, predict the same behaviour of the H.P. compressor as that of the engine but have significant discrepancies both at the start and at the last part of the transient. At the beginning of the transient and at a pressure ratio of 6.5 the STFREE program, which lies closer to the Real engine results, shows a discrepancy of 1.7 per cent in terms of non-dimensional speed. At the same pressure ratio, the AFSREE program has a discrepancy of 2.1 per cent. The incorporation of the I.P. bleed improved both program predictions by an average of 40 per cent. The STFREE program has decreased its discrepancy to 0.78 per cent and the AFSREE to 1.5 per cent.

It should be noted that the above investigation has used a fixed I.P. compressor bleed of 5 per cent. It would be more realistic to use a variable bleed which is a function of the pressure ratio across the bleed "orifice"- see Table(4.4.2).

4.4.3 "Bodie" at 43,000ft., Mach=0.8

The investigation was further extended in the comparison of the "Bodie" results, (Hot re-acceleration), at 43,000ft. and Mach number equal to 0.8. The "Bodie" consists of a deceleration which is followed immediately by an acceleration to the maximum attainable fuel flow.

Unfortunately the starting conditions (shafts speeds and fuel

flow rate) and all the relevant information for the first two seconds of the deceleration(where most of the transient takes place) of the Real engine were not available. It was thus decided for the two programs to start the deceleration from the highest operating point that had been achieved under steady running at the maximum fuel flow rate. The finishing fuel flow rate was the steady running minimum one. Eight seconds were allowed for the deceleration and another eight for the acceleration

Figure(106) shows the comparison of the L.P. shaft speed response with time. From the plot of the Real engine results it can be seen that the engine probably started the deceleration from a lower shaft speed. Nevertheless the prediction of the AFSREE program is very satisfactory since it produced the same shaft speed response with the Real engine regarding the last part of the deceleration and the acceleration. The prediction appeared shifted towards higher operating shaft speeds due to the higher initial starting speed. During the hot acceleration the AFSREE program predicted a faster response by 19 per cent maximum. Taking into account the fact that the starting point of the hot acceleration was higher than the Real engine one by 5.4 per cent, it can be concluded that this program(AFSREE) could predict an L.P. shaft speed response within acceptable discrepancy from the Real engine given that both simulator and engine will have the same starting conditions. On the other hand the STFREE program, although it used lower starting shaft speeds for the deceleration than the AFSREE program did, the predicted starting shaft speed of the hot acceleration is much higher from the Real engine one and from the AFSREE predicted one. The discrepancy between

the two programs at the eighth second is of the order of 2.7 per cent in terms of difference in shaft speed. The STFREE program also predicted a final stabilizing speed at the end of the hot acceleration very close to the one reached by the Real engine. In conjunction with the cold acceleration predictions of the STFREE program,(Figures 78&92), it can be seen that if the latter used the same deceleration starting speeds as of the Real engine, it would predict a faster acceleration.

The H.P. shaft speed response comparison, which is represented in Figure(107), did not show any difference from the cold acceleration one. Both programs predicted the same shaft speed response and degree of discrepancy as with the normal cold acceleration.

Turning now to the Outer Fan performance, this is shown in Figures(108, 108A and 108B). Because it was difficult to account from the same graph for the individual predictions of each program, the predictions of AFSREE and of STFREE were plotted individually with the Real engine results and are shown in separate Figures(A&B). The hot acceleration resulted in slightly different predictions for both programs. Referring to a non-dimensional speed of 420, which was also used in the cold acceleration comparison, both programs had shown a discrepancy with the Real engine of about 5.4 per cent, which has now dropped to 5 per cent for the AFSREE program and increased to 5.6 percent for the STFREE one. At the last part of the acceleration the Real engine shows a very small increase of pressure ratio while the non-dimensional speed continues to increase. This is successfully predicted by the AFSREE and the

STFREE programs.

The hot acceleration comparison for the combined Inner Fan plus I.P. compressor did not show any significant differences from the results and predictions of the cold acceleration. Both programs predicted the same, in general, response as it can be seen in Figure(109). The differences between the predictions of the two programs and the results of the engine are more clearly shown in the individual graphs, Figures(109A and 109B) for the AFSREE and STFREE program respectively. The maximum discrepancy for both models occurs during the first part of the transient and is of the same order as the one recorded during the cold acceleration, i.e. approximately 6 per cent, in terms of pressure rise difference at the non-dimensional speed of 400. The AFSREE program predicted higher operating points since it started also from higher ones. The same is also the case for the STFREE model. A difference that did not exist in the cold acceleration results, is during the very first part of the transient (hot acceleration), where the AFSREE program predictions are much closer to the Real engine than the STFREE program predictions. This can be seen in Figures 109A and 109B in the region of non-dimensional speed between 360 and 400.

Finally the H.P. compressor engine test results and predictions of the two computer models are shown in Figures(110, 110A and 110B). The big discrepancy that existed between the programs and the engine results during the cold acceleration in the region of non-dimensional speed of 590, also existed in the hot acceleration. As in the case of the cold acceleration the Real engine reached a maximum pressure ratio and non-dimensional speed and then dropped to lower final stabilizing operating

point. The AFSREE program, although predicted a maximum operating point closer to the engine one than the STFREE program managed to predict, it failed to stabilize at an operating point close to the Real engine one. On the other hand, the STFREE model stabilized at an operating point in between the one predicted by the AFSREE program and the one reached by the engine. Hence the hot acceleration comparison did not show any significant differences from the cold acceleration one.

4.4.4 Conclusions of comparison

Although, in general, the predictions of the two computer models developed in the current research, were in satisfactory agreement, there were isolated cases of discrepancies between the simulators and the engine test results.

There were reasons, that are discussed in the following chapter, for expecting discrepancies between the programs predictions and the actual test results of the Real engine. Hence the comparison was mostly concentrated on assessment of which program would predict an engine behaviour similar or acceptably close to the behaviour of the engine.

Both programs predicted faster L.P. and H.P. shaft accelerations by an average of 15 per cent. The AFSREE program predicted an L.P. shaft final stabilizing speed very close to the Real engine one. The opposite is the case for the H.P. shaft speed, where the STFREE program predicted a stabilizing speed closer to the engine than the AFSREE predicted, by 2.5 per cent. For the deceleration with and without the 5 per cent I.P. compressor bleed, the AFSREE program predicted a more accurate shaft

response than the STFREE did by an average of 5 per cent. The STFREE program predicted not only a slower L.P. shaft speed response but also a higher final stabilizing speed. The H.P. shaft speed response did not show any significant difference between the two computer models.

The Outer Fan behaviour, during all transients examined, was without any doubt better predicted by the AFSREE program, as was clearly shown in the relevant Figures during the comparison.

The Inner Fan and I.P. compressor predictions of both programs were in good agreement with the engine. The STFREE program predicted a slightly better response than the AFSREE did during the very first part of the Acceleration by 2.7 per cent in terms of difference in pressure ratio at a particular non-dimensional speed, but on the other hand predicted a lower maximum point of operation than the AFSREE predicted and the Real engine achieved. The difference is of the order of 5 per cent in terms of an average deviation in both pressure ratio and non dimensional speed. Significant difference between the two predictions exists also during the very first part of the deceleration(first second) but it should be noted, for the STFREE program, that the inclusion of the 5 per cent I.P. bleed improved the agreement with the Real engine behaviour of the combined Inner Fan and I.P. compressor.

The inclusion of the I.P. bleed improved also the H.P. compressor predictions of both programs but in general the behaviour predicted by the STFREE program was closer to the Real engine one.

From the comparison that was carried out in the present chapter it can be concluded that the AFSREE program gave a better representation of the actual engine's behaviour and especially for the "L.P. system", (L.P. shaft, Outer Fan, Combined Inner Fan and I.P. compressor), which was also confirmed by the results of the "Bodie" comparison. The STFREE program predicted a more realistic "H.P. system", (H.P. shaft and H.P. compressor), for the acceleration and the deceleration but not for the "Bodie" transient.

At this stage, as the final part of the comparison of the two computer models, it is very important to examine the computing running time required by the two programs for each of the transients. The table below shows the OCP time(in seconds) used by the two computer models for all the transients simulated in the current comparison.

	OCP TIME				
Program	Accel	Decel	Bodie	Accel./Bleed	Dec./Bleed
AFSREE	97.56	68.60	86.63	75.65	91.21
STFREE	142.97	122.80	193.85	133.07	184.5

Table(4.4.4)

From the computing times tabulated above, it can be seen that the AFSREE program is significantly faster than the STFREE one during all transients by an average of 45 per cent. For the simulation of the "Bodie", the latter required an excessive 193.8 seconds, while the AFSREE required just 86.6 seconds showing thus a faster simulation by 55 per cent.

In view of the results obtained from the comparison of the two computer models and also their computing running times it

can be concluded that the AFSREE program, and the modelling of the Fan on which it is based, gives a satisfactory and economic representation of a typical Turbofan engine. It will thus be satisfactory for use in further investigation necessary to improve the modelling of Turbofan engines.

CHAPTER V

CONCLUSIONS AND FURTHER INVESTIGATION

The different Fan treatments considered during the current investigation were successfully represented in computational models. The programs developed were based on the General computer model for the prediction of the transient performance of Gas turbines, developed by Pilidis and Maccallum, Ref.(33).

A major problem encountered during the research, was the difficulty in achieving convergence of each new program developed. The development of a computer model proved to be a very time consuming research not only for the reason mentioned above but also due to the fact that each program required considerable computing running time mainly because of the complexity of the engine and the large number of iterations required until convergence is achieved. Depending on the complexity of the Fan treatment there was a penalty in computing running time.

After the computer models were developed the next step was to incorporate the "Real Engine Effects" which were discussed extensively in the current thesis. The incorporation of these effects and particularly of the Heat transfer effects, increase significantly the computing running time of the programs. It was thus decided to compare the programs one with another in their simpler adiabatic forms. Such comparison was done in the second chapter which reduced the number of programs, from

seven initially, down to five. The programs excluded at that stage were the AFSPSH (Adjusting the Factor of SPlit considering also the SHear stress between the flows just after the Fan) which predicted results similar to the AFCSP (Adjusting the FaCtor of SPlit) but was significantly more complex, and also the FFSCCH (Fixed Factor of Split considering Combined Inner Fan and I.P. compressor CHaracteristics) which predicted results similar to the FFCSP (Fixed FaCtor of SPlit).

Next, for the remaining five programs, a comparison was carried out among them on a basis of examination as to which program or programs would predict the more reasonable results. From the comparison carried out two programs were selected to incorporate the "Real Engine Effects". Both programs-initially labelled AFCSP and STKFAN (STacKing of the FAN concept)-use different methods to allow for an interaction of the flow between the Inner and the Outer sections of the Fan.

The AFCSP program (re-named AFSREE after the inclusion of the Real Engine Effects) was used to show the significance of the incorporation of the variation of the Specific Heat Capacity(C_p). All the computational models initially incorporated a varying specific heat capacity as a function of temperature only. This was improved and the specific heat capacity was considered as a function of temperature and fuel to air ratio. The AFCSP program was used to predict the Sea level, Mach=0.2, steady running as well as transient performance firstly with no variation in Specific Heat capacity(C_p). Secondly, the C_p was allowed to vary as a function of temperature and fuel to air ratio but using the so called "once through calculation method". As final improvement,

the C_p was allowed to vary in the same way as described above but now the method of "successive approximations" was used to calculate an even better C_p value. The comparison of the different methods showed that if no variation of the C_p is allowed then the program predicted a higher Specific Fuel Consumption(SFC) by 2 per cent than the one predicted by the more accurate "successive approximations" method. The method of successive approximations was used thereafter in the study.

The program AFSREE was also used to show the significance of the incorporation of the Heat Transfer effects. The models for these Heat Transfer Effects which were included in the transient program were those that had been developed by June 1988. Subsequent and future developments of these thermal models are discussed under the proposals for future research in the current Chapter. The program was used to predict the steady running, acceleration and deceleration performance at Sea level, Mach=0.2, with and without the heat transfer effects. The most significant discrepancies between the adiabatic and non-adiabatic predictions were shown during the deceleration. The adiabatic trajectory of the combined Inner Fan and I.P. compressor was raised towards the surge line(higher pressure ratios) by approximately 9 per cent. For the H.P. compressor the non-adiabatic cold acceleration trajectory prediction showed a greater surge margin, than the adiabatic one, of the order of 7 per cent. Significant discrepancies were also predicted in the thrust response. The adiabatic thrust response during the acceleration appeared slower than the non-adiabatic one by a maximum of 3.5 per cent. In the case of the deceleration, the adiabatic thrust response was faster than the the non-adiabatic

one in the order of 14 per cent.

The above mentioned comparisons confirmed the significance of the incorporation of the "Real Engine effects" in any computer model.

Finally, after the inclusion of the above mentioned effects, the two programs AFCSP and STKFAN (renamed as AFSREE and STFREE) were used to predict both the acceleration and deceleration as well as "Bodie" results at an altitude of 43,000ft. and Mach equal to 0.8. These were also the conditions under which a Real engine has been tested.

There were certain reasons for which the two programs could not predict exactly the same results as the real engine and hence the comparison had to be based on which of the two computational models would generally predict more accurately the behaviour of the Real engine. The degree of accuracy of results was taken into account only in the cases where there was a good agreement between the Real engine test data and the predictions of the models.

The programs predicted first the acceleration and deceleration results at the above mentioned conditions. From the comparison of the results, especially those of the deceleration, there were reasons, which were explained in the previous Chapter-(section 4.4.2), that indicated the possible existence of an I.P. compressor leak of air to the by-pass duct. Since no information was available from the manufacturers of the Real engine about the existence of an I.P. bleed, it was thus decided to include a 5 per cent bleed in both programs. The above mentioned transients were performed again for the same flight

conditions. This decision tested the reliability of the simulators even further than just predicting the behaviour of the Real engine. If the assumption was correct then the predictions of the programs, in comparison to the Real engine results, should improve. From the investigation carried out(see section 4.4, Table 4.4.2) it was evident that the "leak" would become more effective during the deceleration than during the acceleration. The simulators were proved successful since the incorporation of the 5 per cent I.P. compressor bleed improved significantly their deceleration predictions and especially those of the AFSREE program. Hence the programs developed, not only successfully predicted the behaviour of the Real engine but also predicted a fault or a feature that was not included during the construction of the programs.

The AFSREE program, in general, predicted more accurately the behaviour of the Real engine with and without the 5 per cent I.P. compressor bleed, and the same was the case for the "Bodie" transients.

The predictions of the two selected programs and their comparisons with the Real engine behaviour are now summarised. For the acceleration, both programs predicted significantly faster L.P. and H.P. shaft speed responses by approximately 60 per cent. The deceleration shaft response predictions of the AFSREE program could be regarded as successful since the discrepancy(slower prediction) here was of the order of 10 per cent. The STFREE program, for the deceleration, was even slower than the AFSREE model and predicted also a higher final stabilising speed.

Turning now to the Outer Fan comparison, although there were significant discrepancies between the simulators and the Real engine test results, the AFSREE program predicted more accurately the unexpected behaviour of the Real engine during the first part of the deceleration (see Chapter IV).

For the combined Inner Fan and I.P. compressor, both programs predicted results in very good agreement with the Real engine's test results. The STFREE program predicted slightly more accurate results during the first part of the transient(by 2.7 per cent in pressure ratio difference). On the other hand it predicted a lower maximum stabilising speed than the AFSREE program predicted and the Real engine achieved, by approximately 5 per cent.

Discrepancies between simulators and Real engine also appeared in the H.P. compressor comparison, but the inclusion of the 5 per cent I.P. compressor bleed improved the predictions of both programs. Again the STFREE program was slightly more accurate by 0.7 per cent. The "Bodie" predictions of the AFSREE program were much closer to the behaviour of the Real engine.

Proposals for Further Research:

The decision in selecting the best computational model could not be based on how accurately the models predicted the Real engine results, but on a more general observation on which one successfully predicted the behaviour of the engine. The reasons for this limitation in the comparison was the existence of significant discrepancies between the simulators and the Real engine results, mainly in the H.P. system and the shafts speed responses (acceleration).

Several factors contributed in the existence of these

discrepancies:-

(i) Firstly it should be noted that the H.P. compressor characteristics provided for the development of the computational models in the current research, were the characteristics of a Turbofan engine still under development. Later, when the first test data of the same engine became available, it was found that the H.P. compressor characteristics used in the computational models differed significantly from the Real engine's ones. This was discussed in the separate report(unpublished) included in Appendix D and the differences in the characteristics were shown in Figure C in the same Appendix. Investigation is thus necessary to line up the characteristics used in the computational models with the characteristics of the Real engine.

(ii) A second reason for the above mentioned discrepancies is the fact that both programs used as a base for the calculation of the clearances(see Heat transfer effects) the stabilised clearance at the instantaneous gas temperature. This concept created inaccuracies depending on the transient under simulation (acceleration or deceleration). A better method was adopted in August 1988, Ref(44), which calculated the clearances based on their steady running value at the particular shaft speed(but not the non-dimensional speed). Unfortunately time did not permit to include this new method into the two programs selected to incorporate the Real engine effects, as those had already been incorporated and the comparison to the Real engine results had been carried out. This development should be included in future work.

(iii) A third reason-problem was observed during the operation of the program at the start of each transient in both programs. Prior to Time=0.0, when the transient starts, each program allows for a finite time(Time=-0.2 to Time=0.0) in order to initialise the metal temperatures of the components that are included in the Heat transfer effects. During that "initializing" time it was observed that the starting shafts speeds (L.P. and H.P.) had drifted away from their initial values. Hence the shafts at the start of the transient under investigation had different kinetic energies from the shafts of the Real engine at the same instant. It is thus necessary for future work to ensure same shaft speeds at Time equal to 0.0.

(iv) Finally another source for inaccuracy in the predictions of the computational models, was the modelling of the heat transfer effects in the combustion chamber. As it was mentioned earlier(Chapter IV), both programs incorporated a crude method for the incorporation of the heat transfer effects in the combustion chamber which was far from accurate. In parallel with the current investigation, research has been carried out in the University of Glasgow to improve the modelling of the combustion chamber. This model, when complete, should be included in the program.

All the above mentioned sources of inaccuracies in the predictions of the models are in need of further investigation until perfection is achieved. Then the computational model which will include these improvements has to be tested against the performance of a Real Turbofan engine.

In view of all the reasons which existed for discrepancies

between the programs predictions and the Real engine results, it could be concluded that the AFSREE program successfully predicted the behaviour of the Real engine within acceptable accuracy. It used about half the computing running time that the STFREE program needed to simulate the same conditions.

As an epilogue to the investigation carried out, it could be mentioned that the AFSREE computational model can be regarded as the appropriate program to be used for the further investigation needed to tackle the above mentioned causes of inaccuracy. Once these problems are solved, it will lead to the Ideal Model which is able to predict accurately and reliably the transient performance not only of the Turbofan engine but also of any Gas turbine.

REFERENCES

1. Ahsmole P.J.,

   "Introducing the Rolls-Royce Tay."

   Rolls-Royce Limited, East Kilbride,

   AIAA/SAE/ASME, 19th Joint Propulsion Conference, June 27-29, 1983.

2. Bayley F.J., Milligan R.W.,

   "The Effect of Free-stream Turbulence upon Heat Transfer to Turbine Blading."

   AGARD, Propulsion and Energetics Panel Meeting, Ankara, Sept. 1977.

3. Bennet, H.W.,

   "Aero Engine Development of the Future".

   Proc. I. Mech. Eng., Vol. 197,1983

4. Brown A., Burton R.C.,

   "The Effects of Free-stream Turbulence Intensity and Velocity Distribution on Heat Transfer to Curved Surfaces."

   ASME Paper 77-GT-48.

5. Cohen H., Rogers G.F.C., Saravanamuttoo H.I.H.,

   "GAS TYRBINE THEORY"

   Second Edition, Longman.

6. Cumpsty N.A., Greitzer E.M.,

   "A Simple Model for Compressor Stall Cell Propagation."

   ASME Paper 81-GT-73, 1981.

7. Day I.J., Greitzer E.M.,Cumpsty N.A.,
"Prediction of Compressor Performance in Rotating Stall."
ASME Paper 77-GT-10, 1977.

8. Durand, H.P.,
"Simulation of Engine Transient Performance"
ASME Journal of Engineering for Power, July 1977

9. Fawke, A.J.,
"Digital Computer Simulation of Gas Turbine Dynamic Behaviour."
Ph.D. Thesis, University of Bristol, 1970

10. Grant. A.D.,
"The Effect of Heat Transfer on Boundary Layer Stability in Axial Flow Compressors."
ibid 252-258

11. Gray S.,
"Stage Matching, Stall, and Surge in Multistage Axial Flow Compressors."
Proc. Inst. Mech. Eng. 1969-1970, 134, 49-56.

12. Green J.E.,
"The Prediction of the Turbulent Boundary Layer Development in Compressible Flow."
J. Fluid Mech. 1968, 31, 753-778.

13. Greitzer E.M.,
"Surge and Rotating Stall in Axial Flow Compressors."
ASME Journal for Engineering Power, April 1976.

14. Harman T. Richard,
"Gas Turbine Engineering"

The Macmillan Press. 1981.

15. Head M.R.,

"Entailment in the Turbulent Boundary Layer."

ibid, 3152,1960.

16. Howell A.R,

"The Present Basis of Axial Flow Compressor Design."

Part I, Cascade Theory and Performance.

A.R.C. R&M 2095, 1942.

17. Howell A.R. and Bonham R.P.,

"Overall and Stage Characteristics of Axial Flow Compressors."

Proc. Inst. Mech. Eng., 10950, 163, 235-248.

18. Kuhlberg J.F., Shepard D.E., King E.O., Baker J.R.,

"The Dynamic Simulation of Turbine Engine Compressors".

Pratt & Whitney Aircraft Engineering Department, East Hartford, Connecticut, 06108.

19. Larjola J.,

"Transient Simulation of Gas Turbines Including the Effects of Heat Capacity of the Solid Parts."

Ph.D. Thesis, Helsinki University of Technology, 1982.

20. Luxton R.E., Young A.D.,

"A Generalised Method for the Calculation of the Laminar Compressible Boundary Layer with Heat Transfer and Non-uniform Pressure Distribution."

Aeronautical Proc. Coun. Rep. Memo 3233, 1960.

21. Maccallum N.R.L.,

"The Performance of Turbojet Engines During Thermal Soak Transient."

Proc. Inst. Mech. Eng., 1969-70, 184(Part 3 GII).

22. Maccallum N.R.L.,
"Effect of Bulk Heat Transfer in Aircraft Gas Turbines on Compressor Surge Margins."
Inst. Mech. Eng., 1974

23.Maccallum N.R.L.,
"Models for the Representation of Turbomachine Blades During Temperature Transients."
ASME Paper, 76-GT-23.

24.Maccallum N.R.L.,
"Transient Expansion of the Component of an Air Seal on a Gas Turbine Disc."
Aerospace Meeting, SAE Paper 770974, 14/11/1977

25. Maccallum N.R.L.,
"Thermal Influences in Gas Turbine Transients-Effects of Changes in Compressor Characteristics."
ASME Paper 79-GT-143.

26. Maccallum N.R.L.,
"Further Studies of the Influence of Thermal Effects on the Predicted Acceleration of Gas Turbines."
ASME Paper, 81-GT-21.

27. Maccallum N.R.L.,
"Axial Flow Compressor Characteristics During Transients."
AGARD CP 324, 1982.

28. Maccallum N.R.L.,
"Prediction of Performance of Two Spool Bypass and Turbofan Engines."

Glasgow University, Mechanical Engineering
Departmental Report, August 1984.

*Maccallum N.R.L., see also 44

29. Maccallum N.R.L., Grant A.D.,
"The Effect of Boundary Layer Changes due to Transient Heat Transfer on the Performance of an Axial Flow Air Compressor."
SAE Paper 770284, 1977.

30. Patel V.C.,
"The Effects of Curvature on the Turbulent Boundary Layer."
Aeron. Res. Coun. Rep. Memo 3599, 1969.

31. Pilidis P.,
"Digital Simulation of Gas Turbine Performance"
Ph.D. Thesis, University of Glasgow, November 1983.

32. Pilidis P., Maccallum N.R.L.,
"A Study of the Predictions of Tip and Seal Clearances and their Effects in Gas Turbine Transients."
ASME Paper 84-GT-245.
International Gas Turbine Conference, 1984.

33. Pilidis P., Maccallum N.R.L.,
"A General Program for the Prediction of the Transient Performance of Gas Turbines."
ASME Paper 85-GT-209, 1985

34. Pilidis P., Maccallum N.R.L.,
"The Effects of Heat TRansfer on Gas Turbine Transient."
ASME Paper 85-GT-275, International Gas Turbine

Conference, 1985.

35. Robbins W.H. and Dugan Jr. J.F.,
"Prediction on Off-design Performance of Multistage Compressors."
Ch.X. Aerodynamic design of Axial flow compressors, N.A.S.A.-S.P. 36, 1965

36. Saravanamuttoo H.I.H.,
"Analogue Computer Study of the Transient Performance of the Orenta 600HP Regenerative Gas Turbine."
ASME Paper 63-AHGT-38, presented at ASME Gas Turbines Conferences in Los Angeles, March1963.

37.Saravanamuttoo H.I.H., Fawke A.J.,
"Simulation of Gas Turbine Dynamic Performance"
ASME Paper 70-GT-23

38. Saravanamuttoo H.I.H., Fawke A.J.,
"Experimental Investigation of Methods for Improving the Dynamic Response of a Twin-Spool Turbojet Engine"
ASME Paper, 71-GT-14.

39. Saravanamuttoo H.I.H., Fawke A.J.,
"Digital Computer Simulation of the Dynamic Response of a Twin-spool Turbofan with Mixed Exhaust."
Aeronautical Journal, Vol. 77, Sept. 1973, pp. 471-478.

40.Schobeiri T., Haselbacher H., BBC Brown, Boveri&Company, Ltd, Baden Switzerland.
"Transient Analysis of Gas Turbine Power Plants, Using the Huntorf Compressed Air Storage Plant as an Example."

ASME Paper 85-GT-197

41. Stoddart R.,

"Prediction of the Transient Performance of the Rolls-Royce Tay Engine Using the Method of Intercomponent Volumes."

Final Year Project, University of Glasgow, May 1987.

42. Tachibana F., Fukui S.,

"Convective Heat Transfer of the Rotational and Axial Flow Between Concentric Cylinders."

Bull. of Japanese Soc. of Mech. Eng.,Vol 7, 1964.

43. Thomson B.,

"Basic Transient Effects of Aero Gas Turbines."

AGARD conference Proc.151, February 1975.

*45.Maccallum N.R.L.,

"Initial Study of the Influence of the Inclusion of Thermal Effects in a Transient Prediction Procedure for the Rolls-Royce Tay Engine."

University of Glasgow Report, October 1988.

FIGURES

Note on Units Used

In all the Figures, the units of the parameters used in the graphs are as follows:

(i) Non -dimensional mass flow rate

$$\frac{\dot{m}\sqrt{T}}{P} = \frac{\text{lb/sec}\sqrt{K}}{\text{lbf/in}^2}$$

(ii) Thrust in pounds force=lbf.

(iii) Fuel Flow in kilograms per second=kg./sec.

(iv) Shaft speeds in revolutions per second=rev./sec.

(v) Time in seconds=sec.

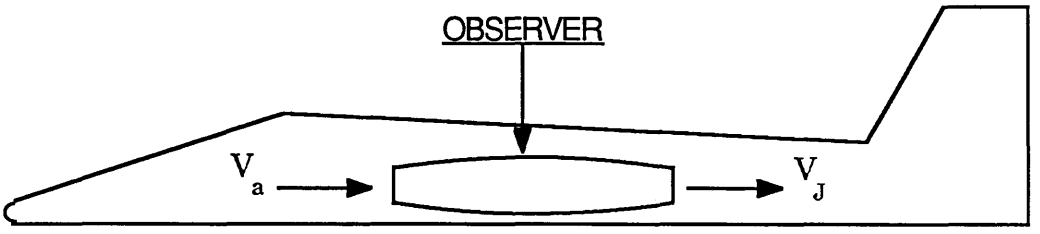

FIGURE (1)

BRAYTON AND REAL CYCLE

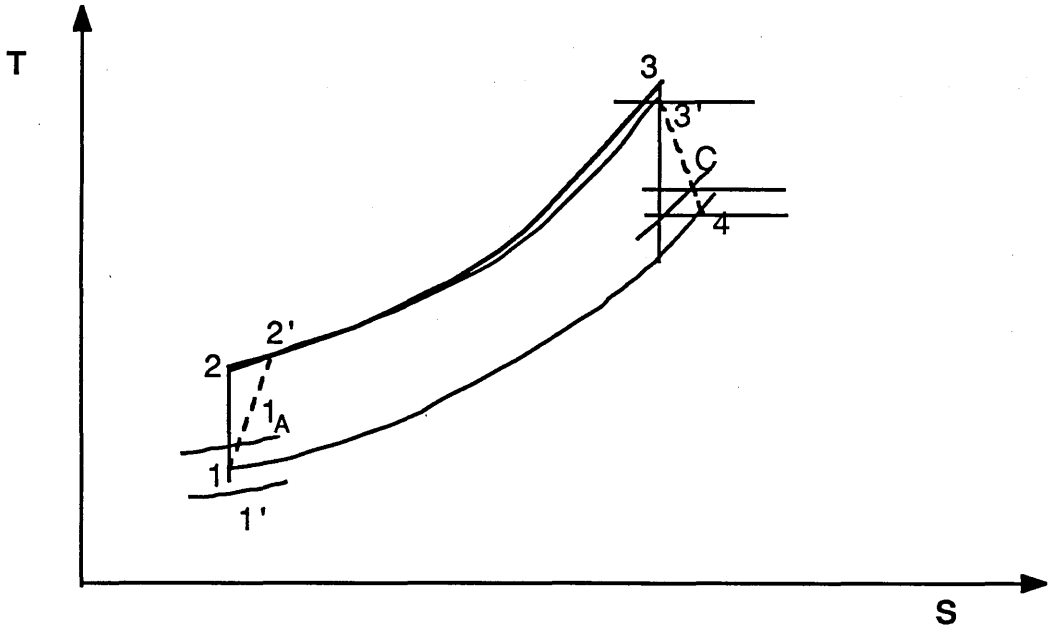

FIGURE (2)

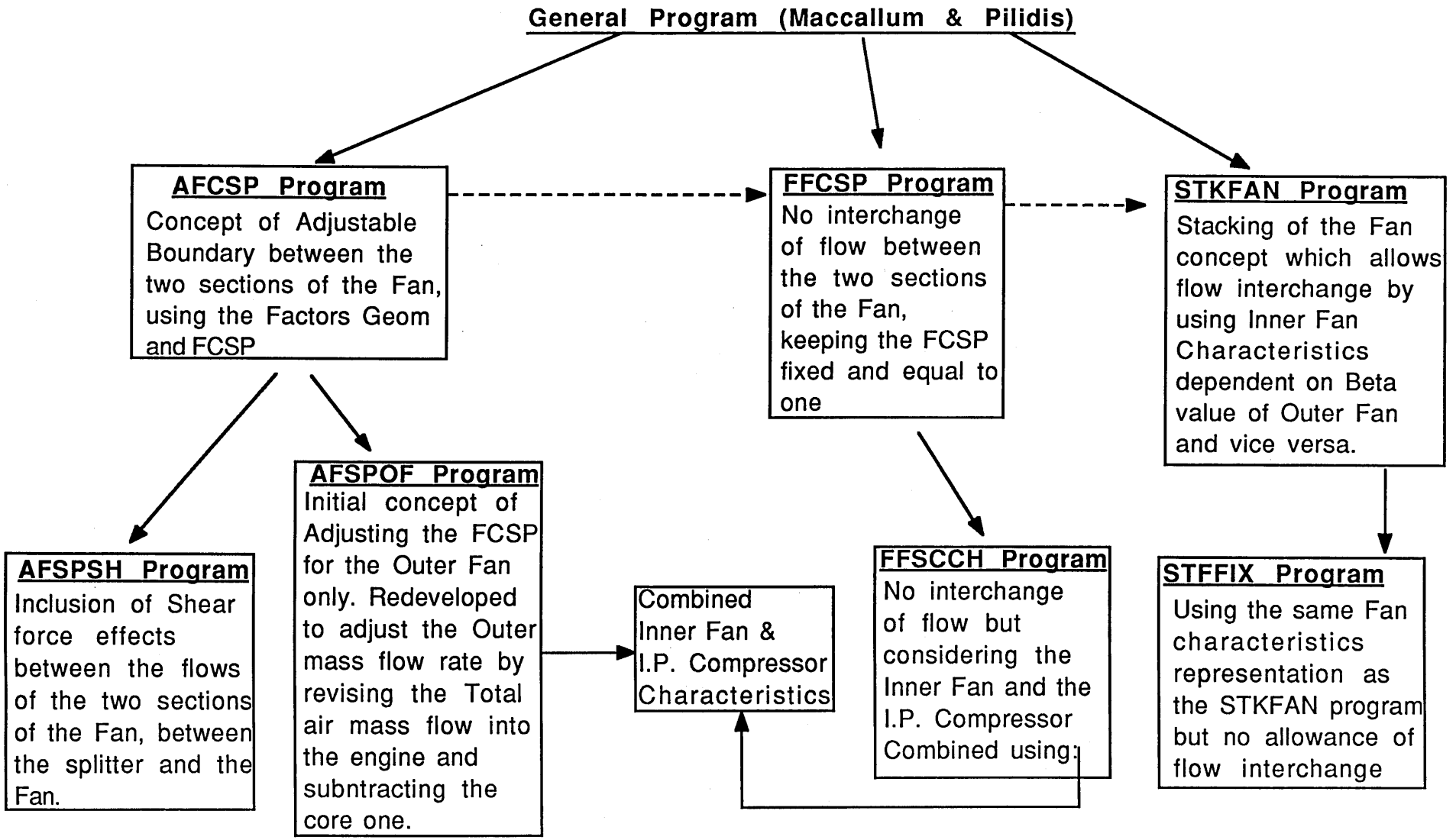
General Program (Maccallum & Pilidis)
AFCSP Program
Concept of Adjustable Boundary between the two sections of the Fan, using the Factors Geom and FCSP
FFCSP Program
No interchange of flow between the two sections of the Fan, keeping the FCSP fixed and equal to one
STKFAN Program
Stacking of the Fan concept which allows flow interchange by using Inner Fan Characteristics dependent on Beta value of Outer Fan and vice versa.
AFSPSH Program
Inclusion of Shear force effects between the flows of the two sections of the Fan, between the splitter and the Fan.
AFSPOF Program
Initial concept of Adjusting the FCSP for the Outer Fan only. Redeveloped to adjust the Outer mass flow rate by revising the Total air mass flow into the engine and subntracting the core one.
Combined Inner Fan & I.P. Compressor Characteristics
FFSCCH Program
No interchange of flow but considering the Inner Fan and the I.P. Compressor Combined using:
STFFIX Program
Using the same Fan characteristics representation as the STKFAN program but no allowance of flow interchange

FIGURE (2A)

PROGRAM AFCSP-BLOCK DIAGRAM

FIGURE(4)

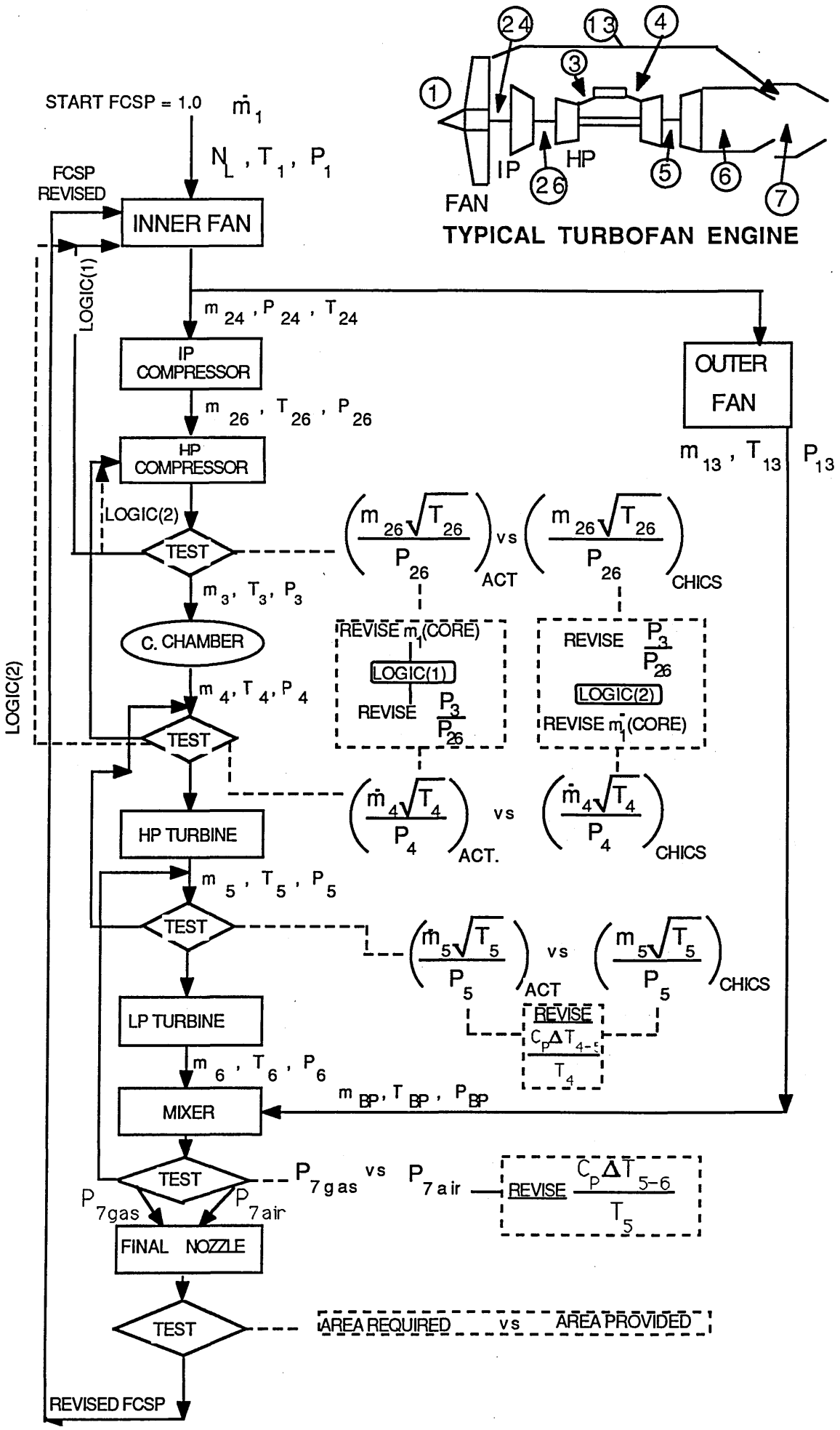

PROGRAM AFSPOF-BLOCK DIAGRAM

FIGURE(4A)

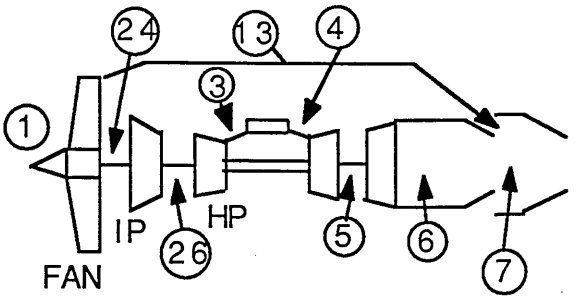

TYPICAL TURBOFAN ENGINE

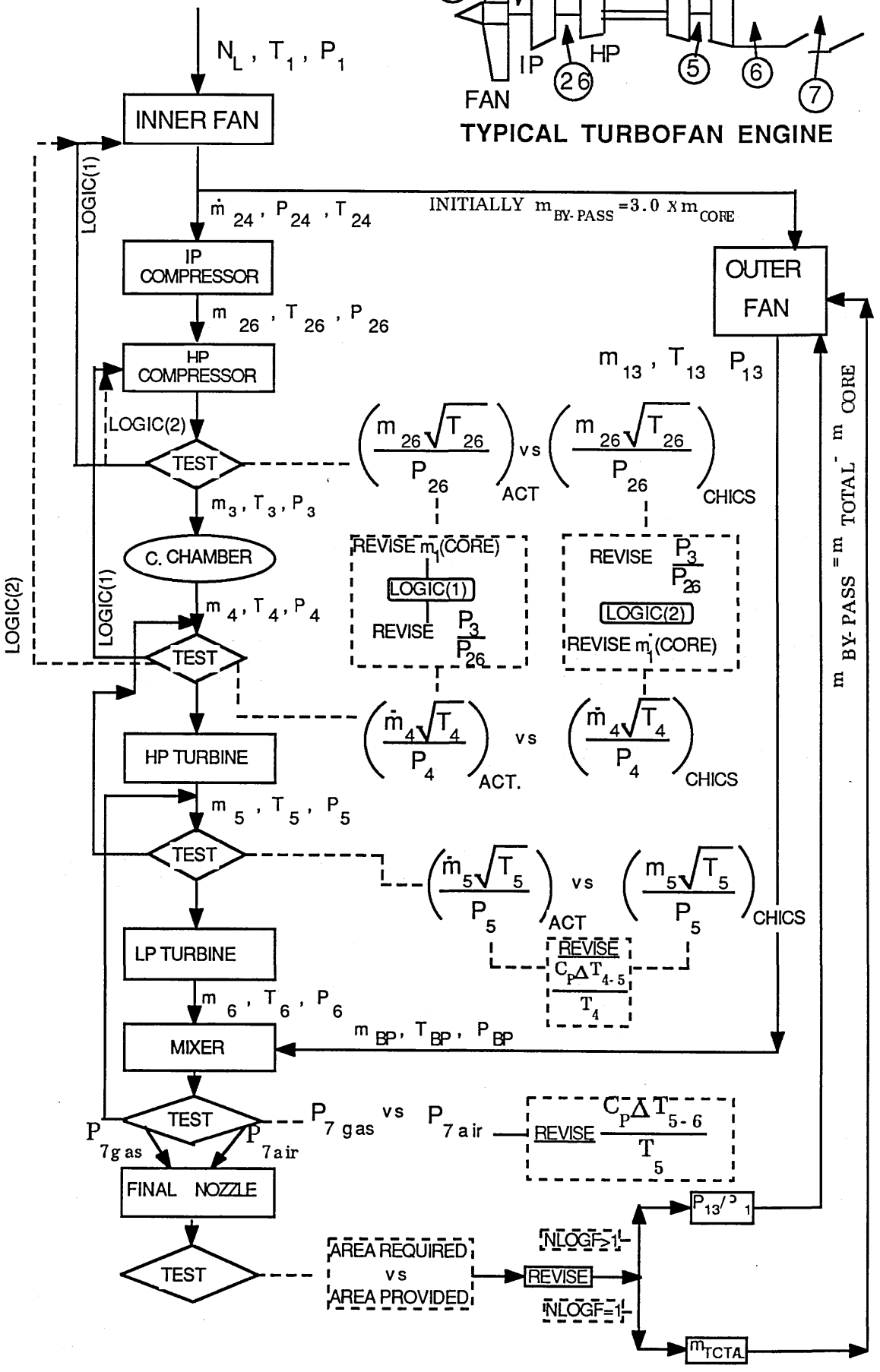

FIGURE (4B)

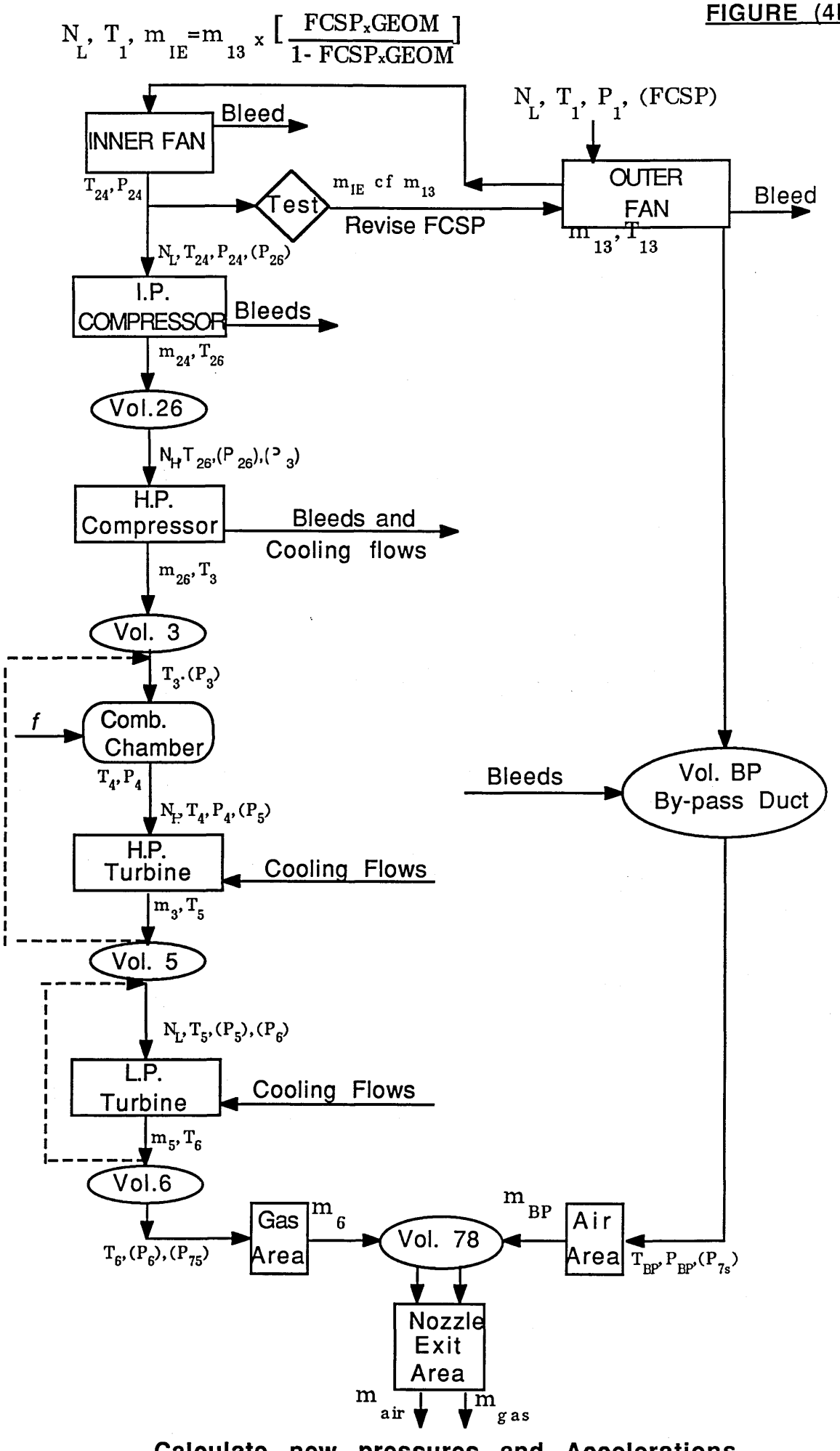

Calculate new pressures and Accelerations

FIGURE (5)

INNER FAN CHARACTERISTICS TABULATION

AS USED IN PROGRAMS : AFCSP, AFSPSH, FFCSP,FFSCCH & AFSPOF

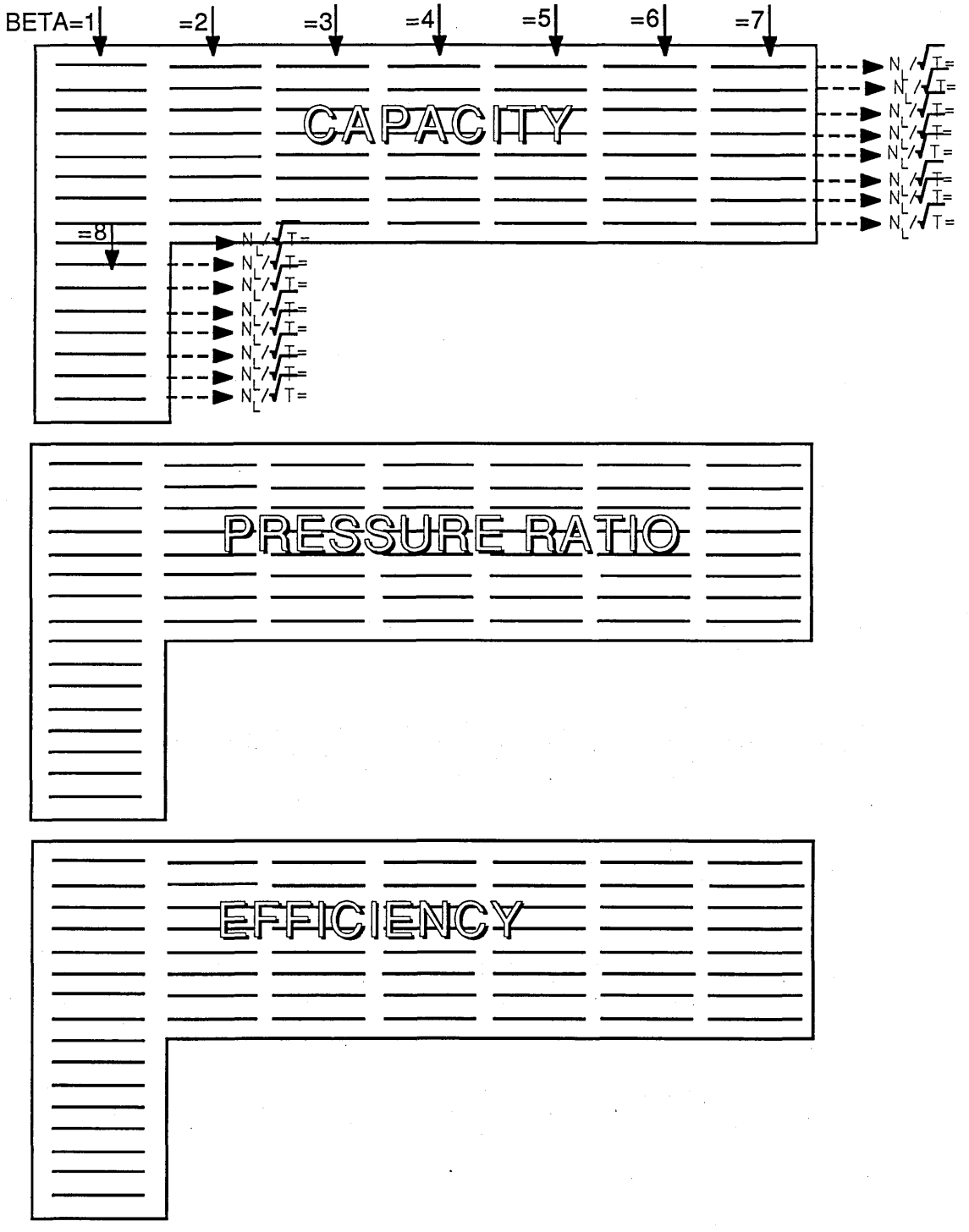

93.2 186.4 279.6 326.1 372.7 419.3 465.9 → $N_L/\sqrt{T}$

512.5

1 2 3 4 5 6 7 → BETA VALUES

8

TYPICAL TURBOFAN ENGINE

INNER FAN CHARACTERISTICS

Data from "TABLE 16"

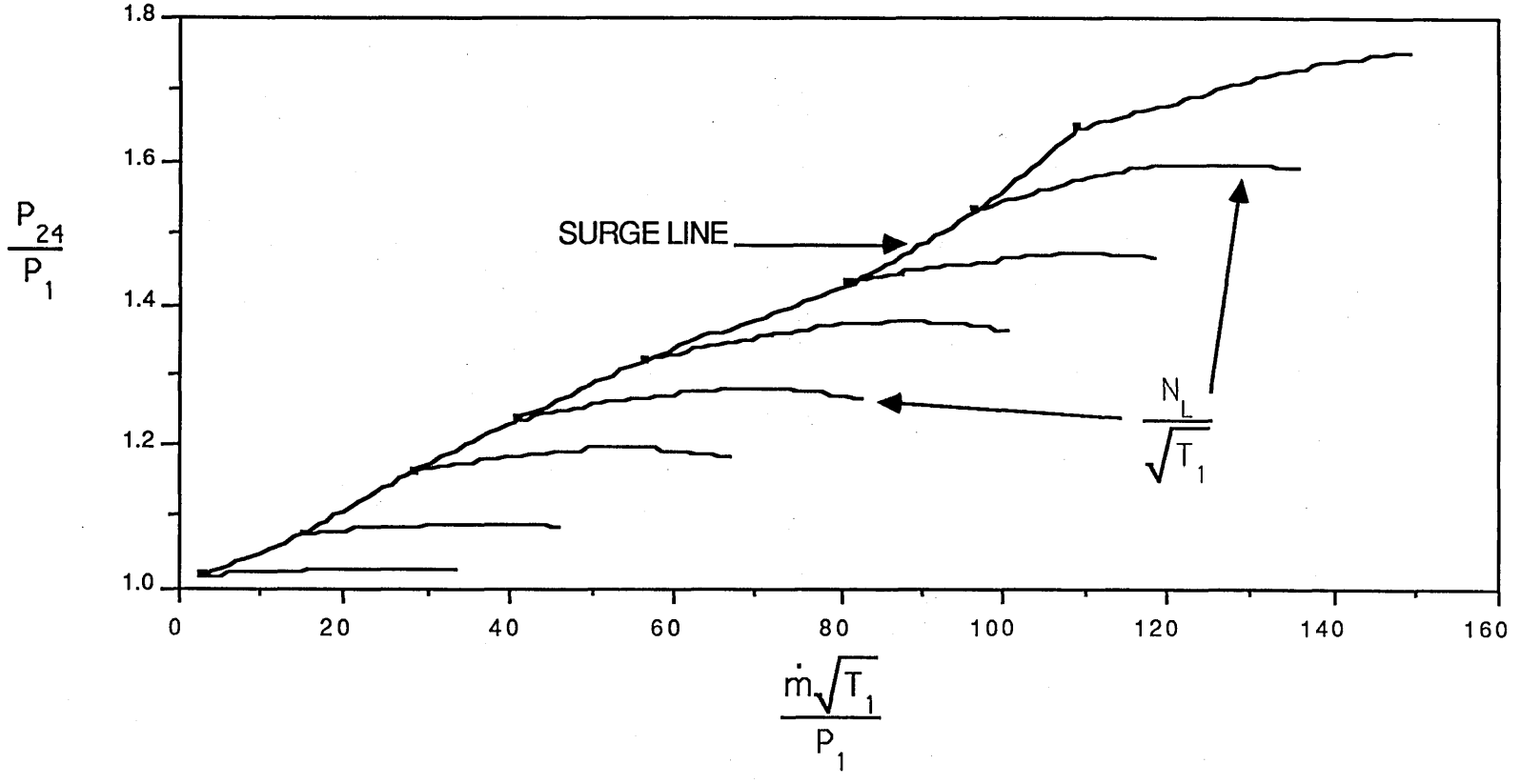

FIGURE (6)

TYPICAL TURBOFAN ENGINE

INTERMEDIATE PRESSURE COMPRESSOR (I.P.) CHARACTERISTICS

Data from "TABLE 17"

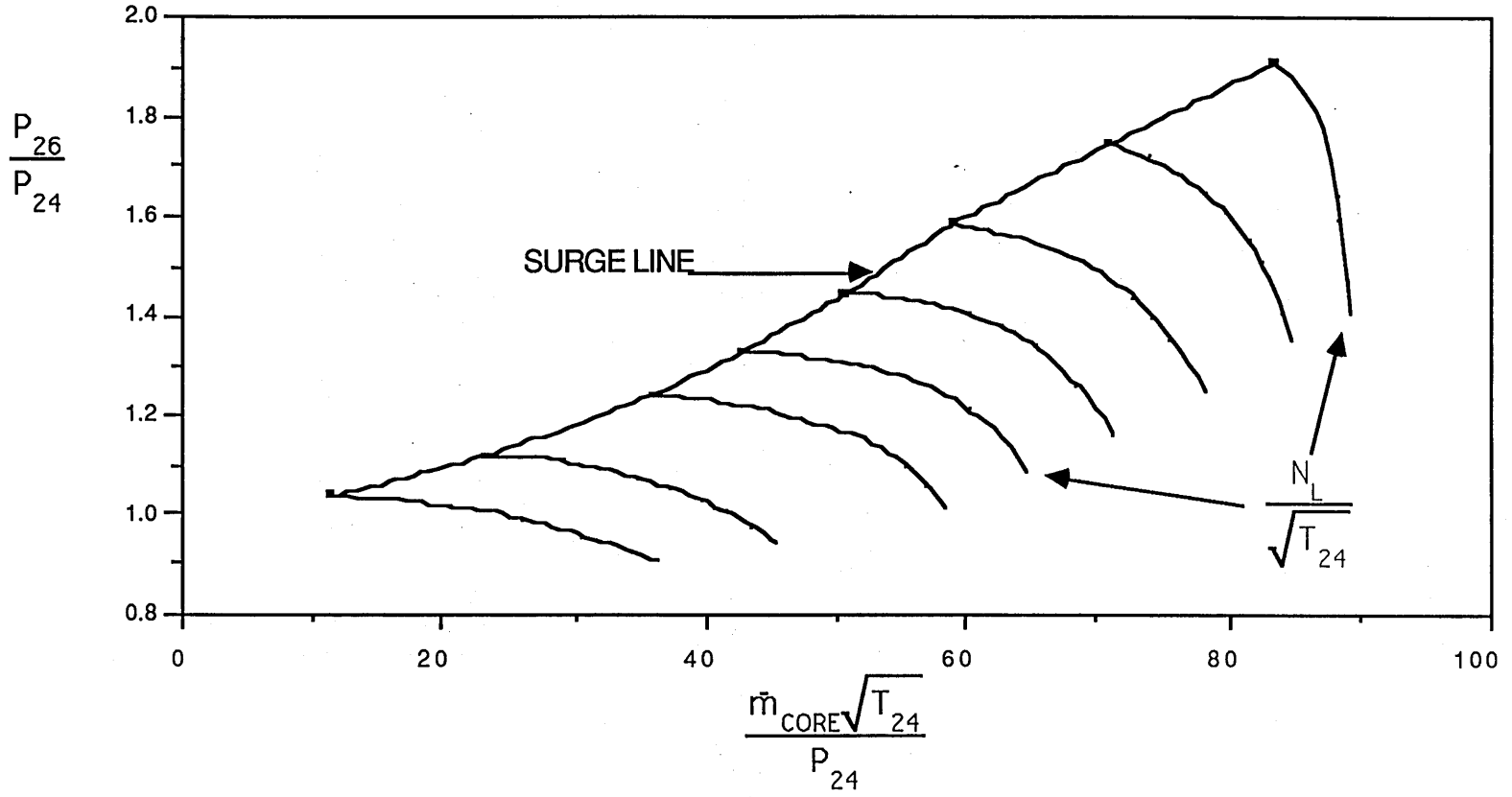

FIGURE (7)

FIGURE (8)

TYPICAL TURBOFAN ENGINE

HIGH PRESSURE COMPRESSOR (H.P.) CHARACTERISTICS

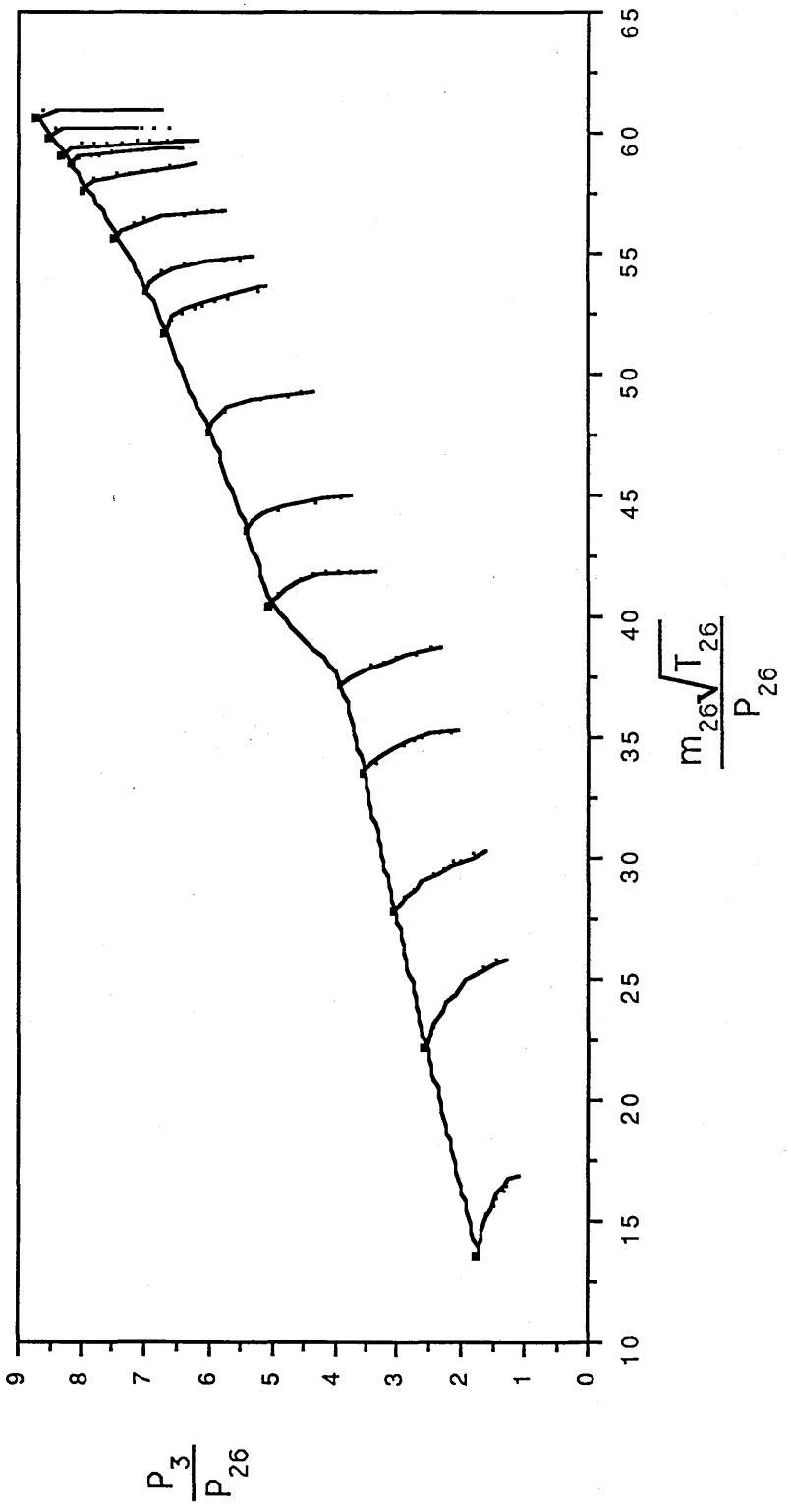

FIGURE (9)

TYPICAL TURBOFAN ENGINE

OUTER FAN CHARACTERISTICS

Data from "TABLE 19"

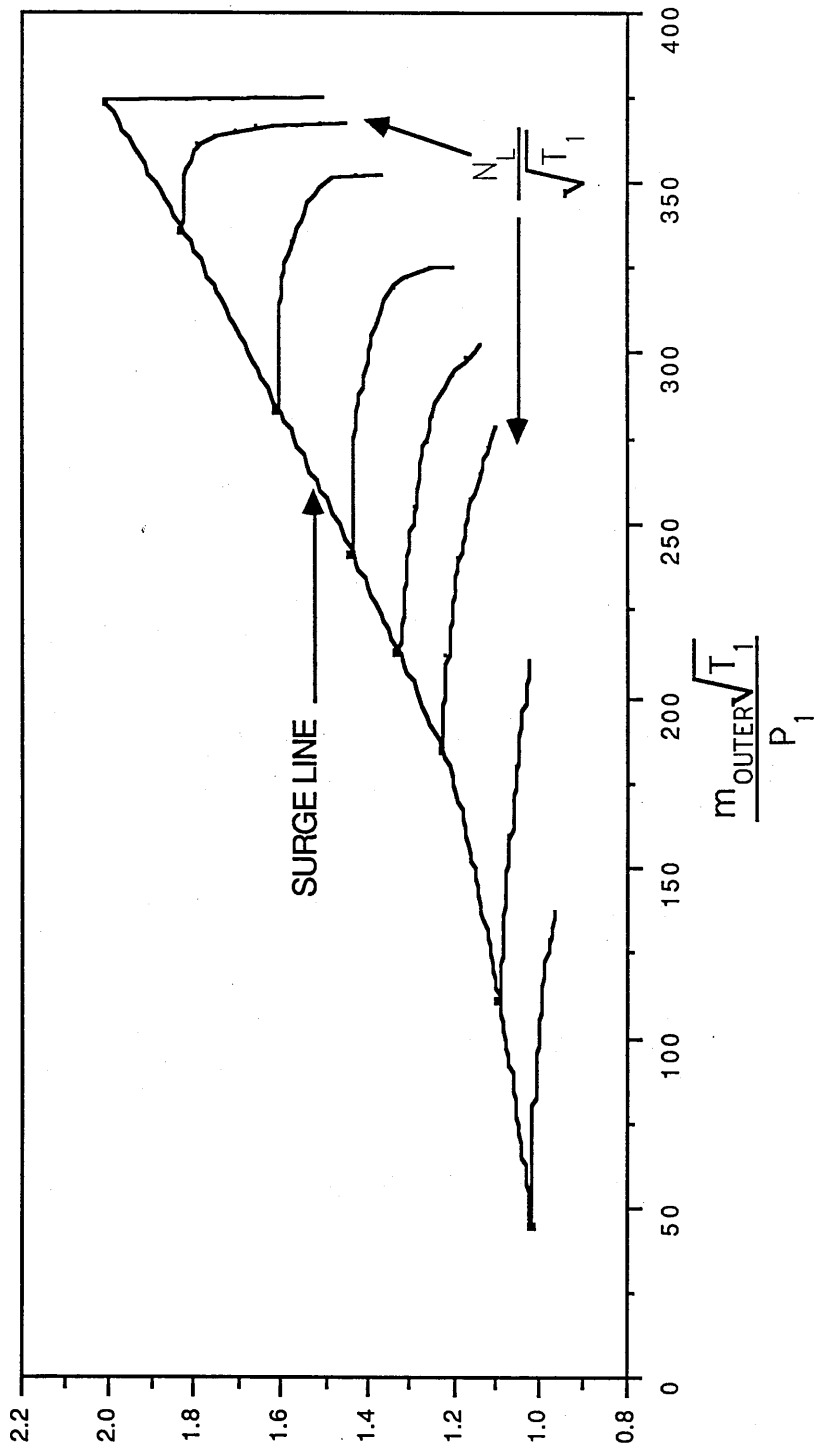

FIGURE (10)

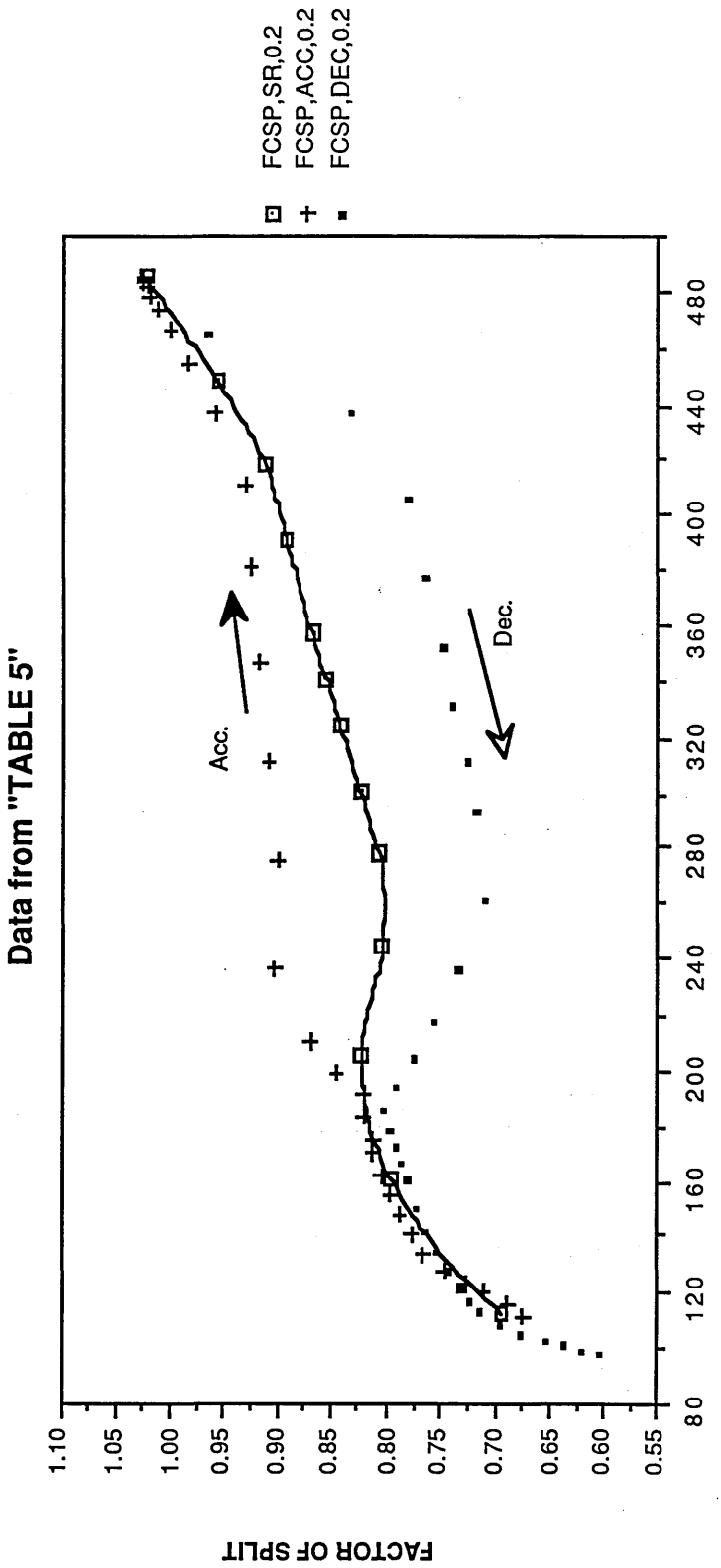

FCSP,SR,0.2 = STEADY RUNNING RESULTS AT: SEA LEVEL, MACH = 0.2

FCSP,ACC,0.2 = ACCELERATION RESULTS AT: SEA LEVEL, MACH = 0.2

FCSP,DEC,0.2 = DECELERATION RESULTS AT: SEA LEVEL, MACH = 0.2

FIGURE (11)

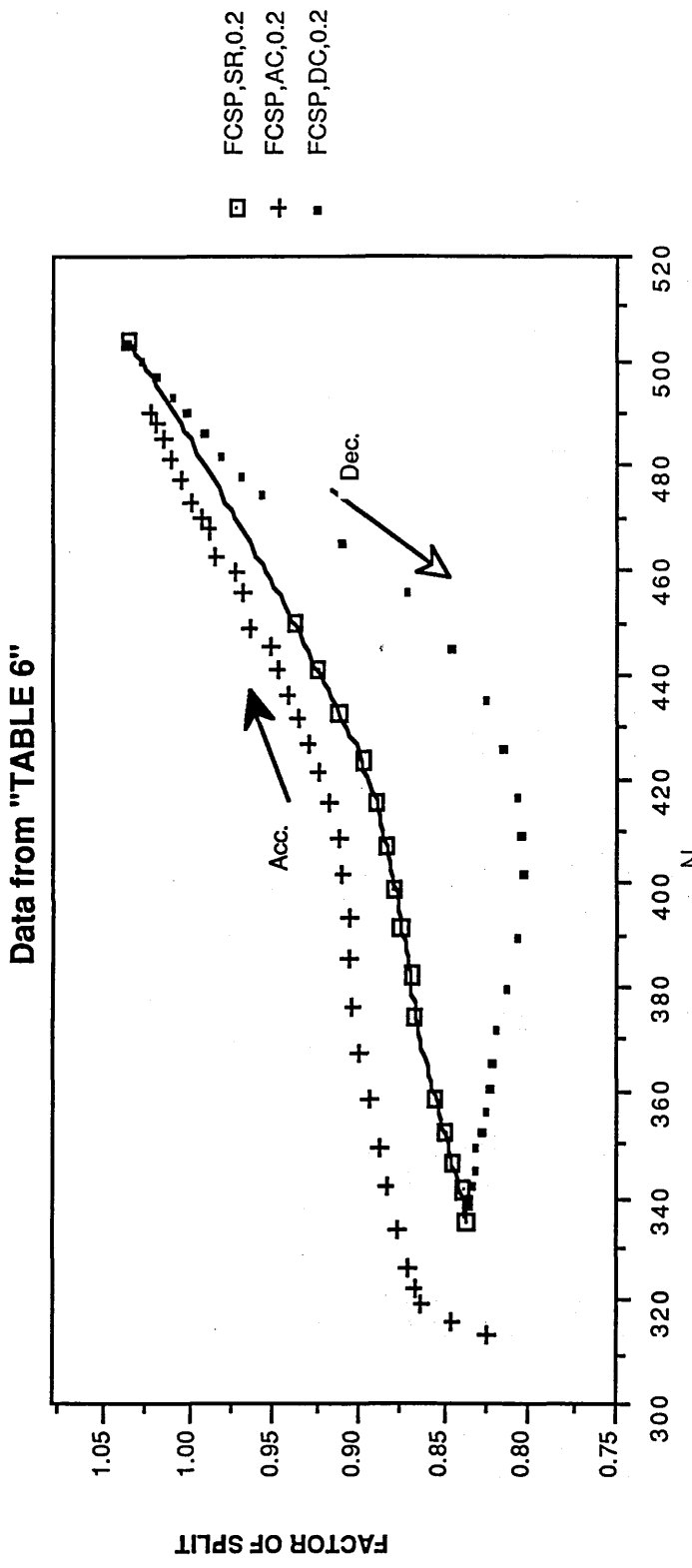

FCSP,SR,0.2 = STEADY RUNNING RESULTS AT : 43000ft., MACH = 0.2

FCSP,AC,O.2 = ACCELERATION RESULTS AT : 43000 ft., MACH = 0.2

FCSP,DC,0.2 = DECELERATION RESULTS AT : 43000 ft., MACH = 0.2

FIGURE (12)

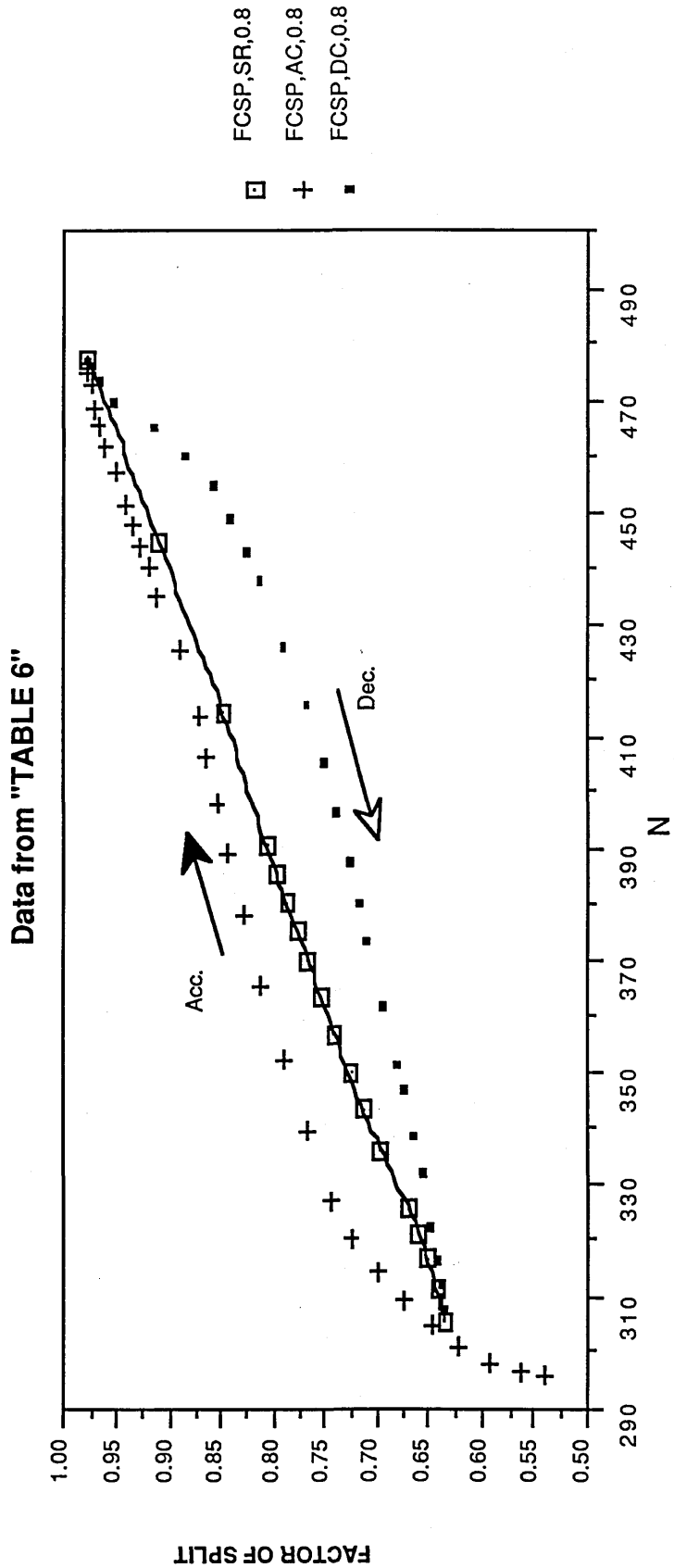

FCSP,SR,0.8 = STEADY RUNNING RESULTS AT: ALTITUDE = 43000 ft., MACH = 0.8

FCSP,AC,0.8 = ACCELERATON RESULTS AT: ALTITUDE = 43000 ft., MACH = 0.8

FCSP,DC,0.8 = DECELERATION RESULTS AT: ALTITUDE = 43000 ft., MACH = 0.8

FIGURE (13)

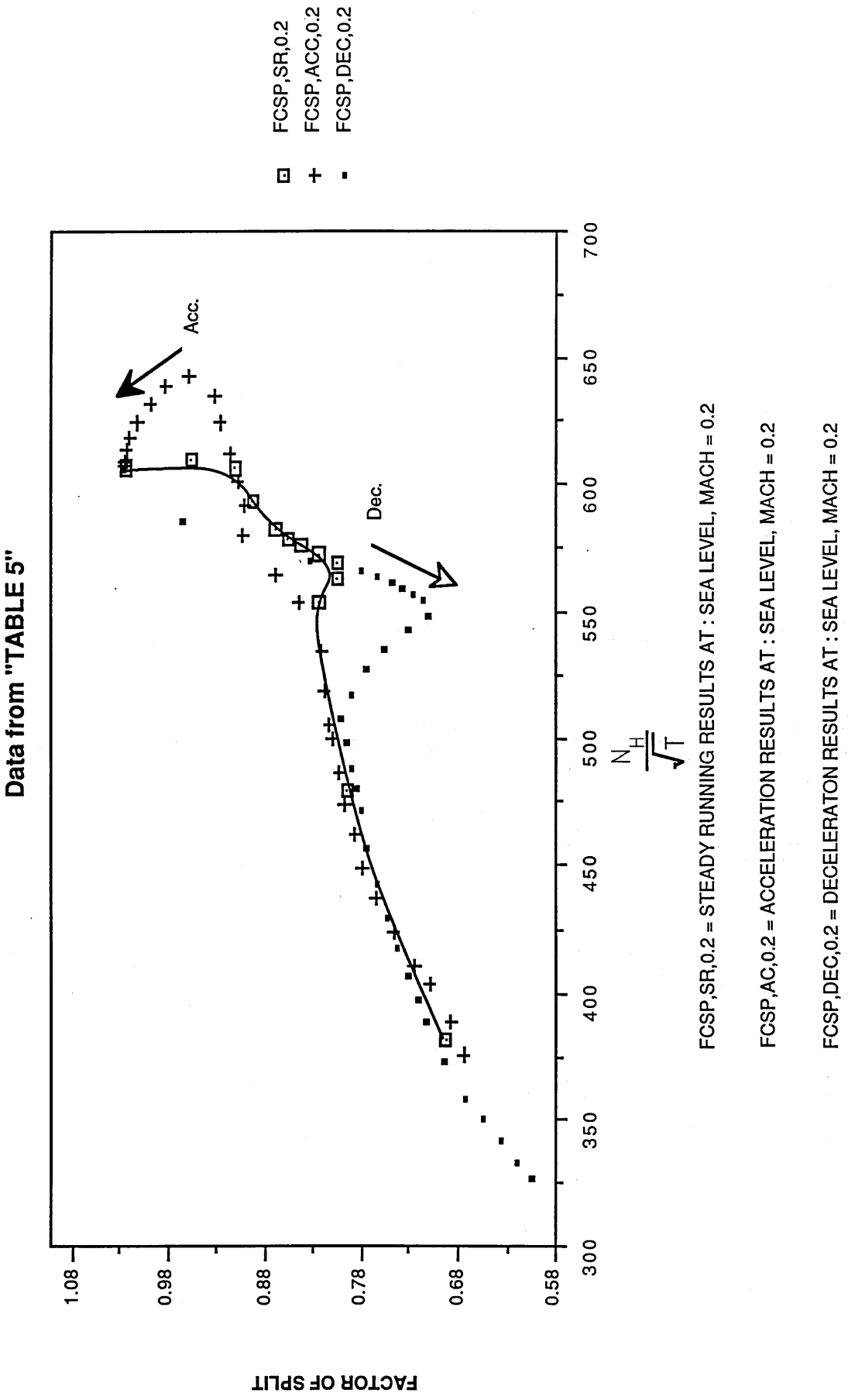

FCSP,SR,0.2 = STEADY RUNNING RESULTS AT : SEA LEVEL, MACH = 0.2

FCSP,AC,0.2 = ACCELERATION RESULTS AT : SEA LEVEL, MACH = 0.2

FCSP,DEC,0.2 = DECELERATON RESULTS AT : SEA LEVEL, MACH = 0.2

FIGURE (14)

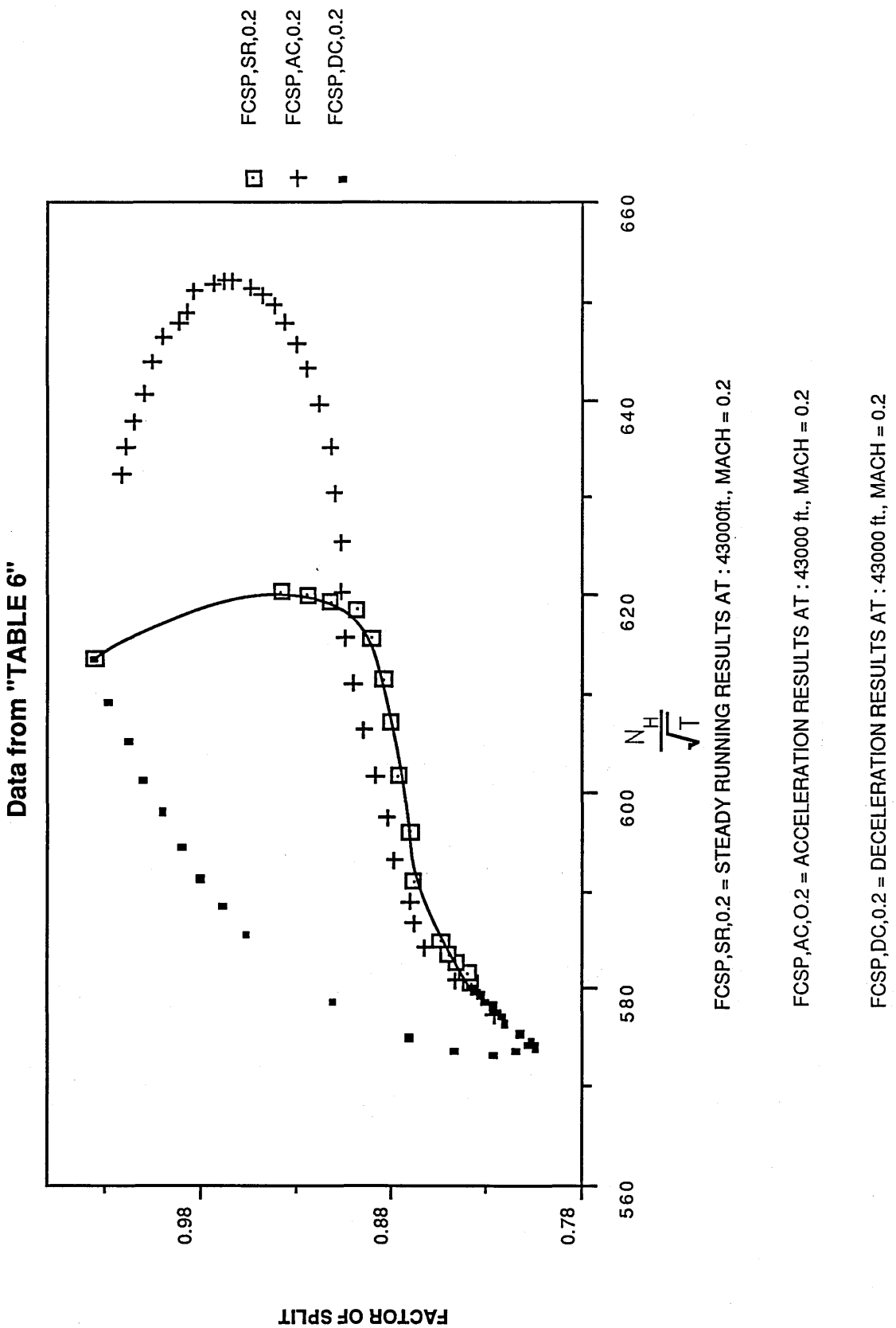

FCSP,SR,0.2 = STEADY RUNNING RESULTS AT : 43000ft., MACH = 0.2

FCSP,AC,O.2 = ACCELERATION RESULTS AT : 43000 ft., MACH = 0.2

FCSP,DC,0.2 = DECELERATION RESULTS AT : 43000 ft., MACH = 0.2

FIGURE (15)

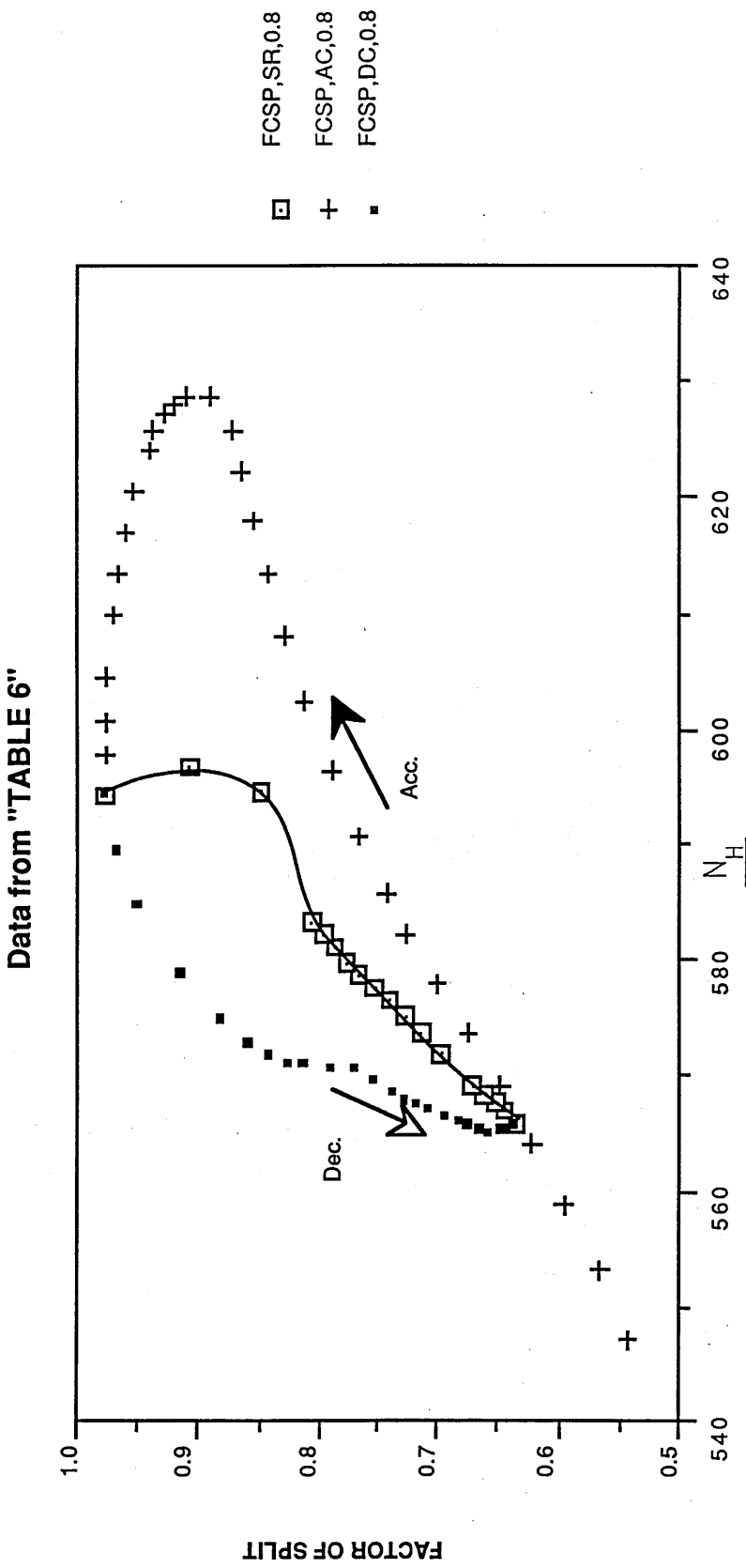

FCSP,SR,0.8 = STAEDY RUNNING RESULTS AT: 43000 ft., MACH = 0.8

FCSP,AC,0.8 = ACCELERATION RESULTS AT: 43000 ft., MACH = 0.8

FCSP,DC,0.8 = DECELERATION RESULTS AT: 43000 ft., MACH = 0.8

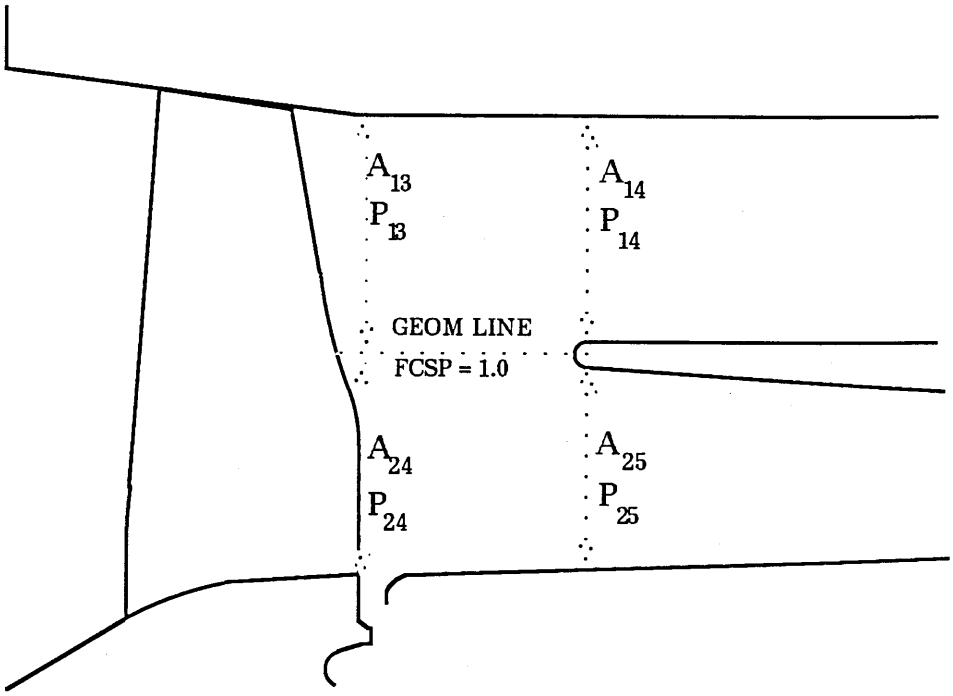

FIGURE 16

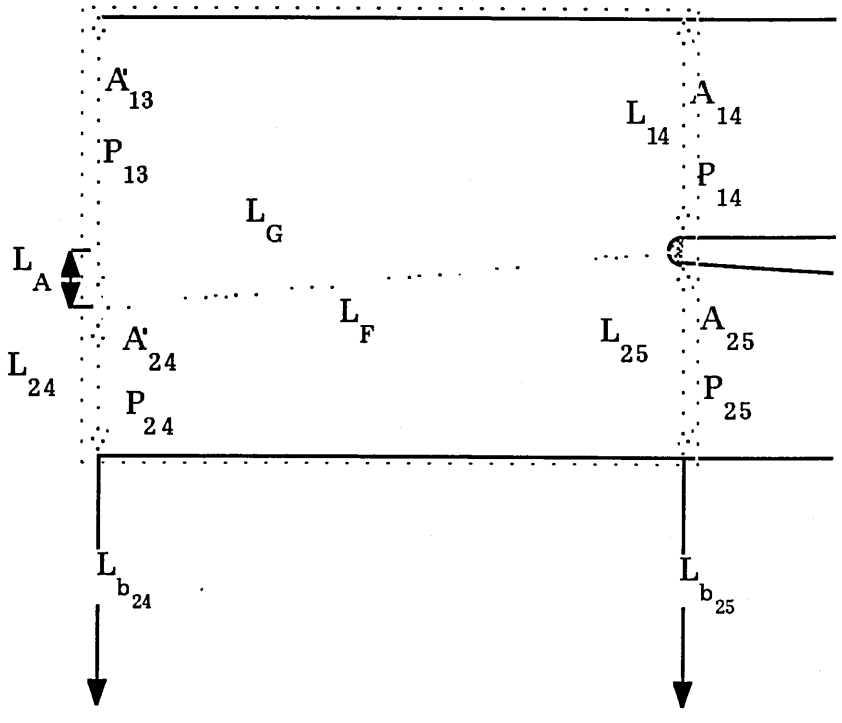

Distances to the centre line of the engine

FIGURE 17

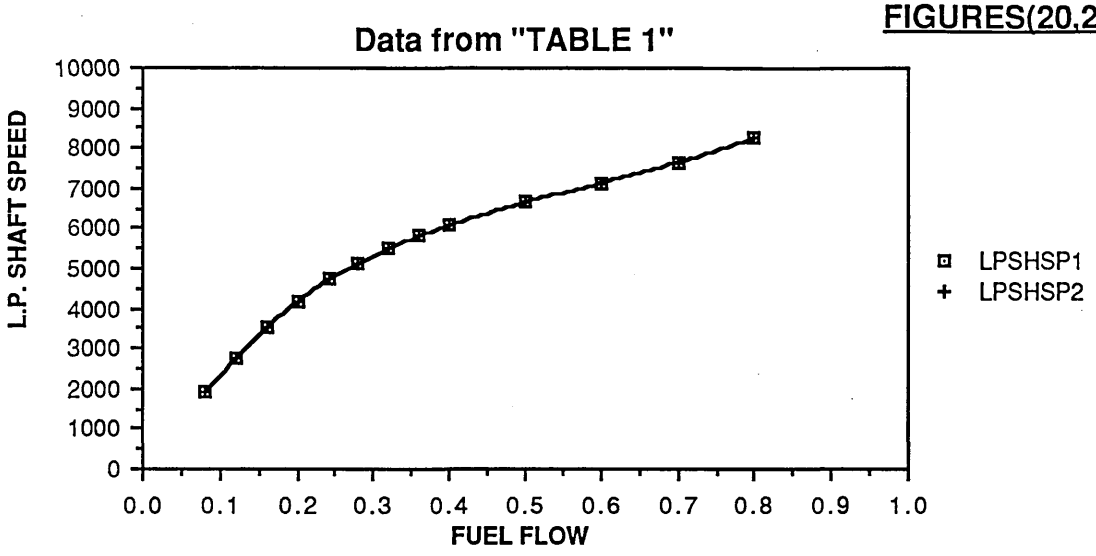

LPSHSP1 = AFCSP PROGRAM L.P. SHAFT SPEED
LPSHSP2 = AFSPSH PROGRAM L.P. SHAFT SPEED

FIGURE (20)

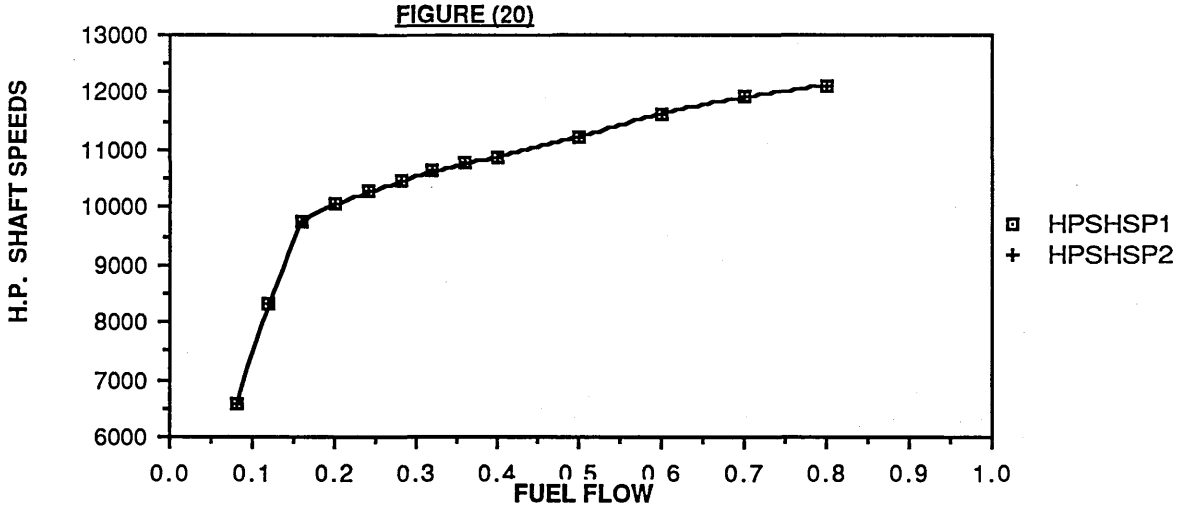

HPSHSP1 = AFCSP PROGRAM H.P. SHAFT SPEED
HPSHSP2 = AFSPSH PROGRAM H.P. SHAFT SPEED

FIGURE (21)

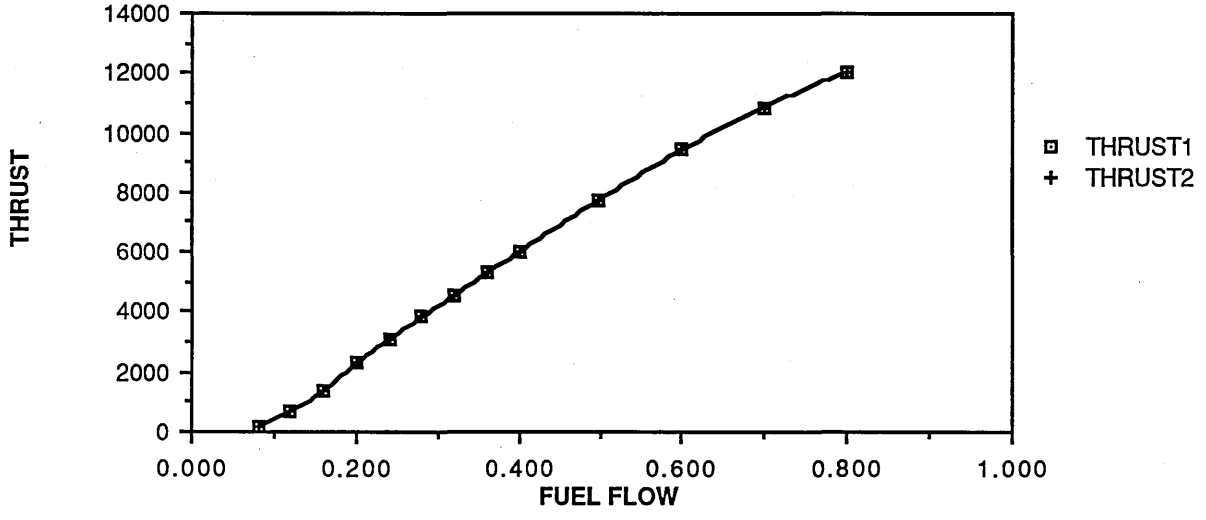

THRUST 1= AFCSP PROGRAM RESULTS
THRUST 2 = AFSPSH PROGRAM RESULTS

FIGURE (22)

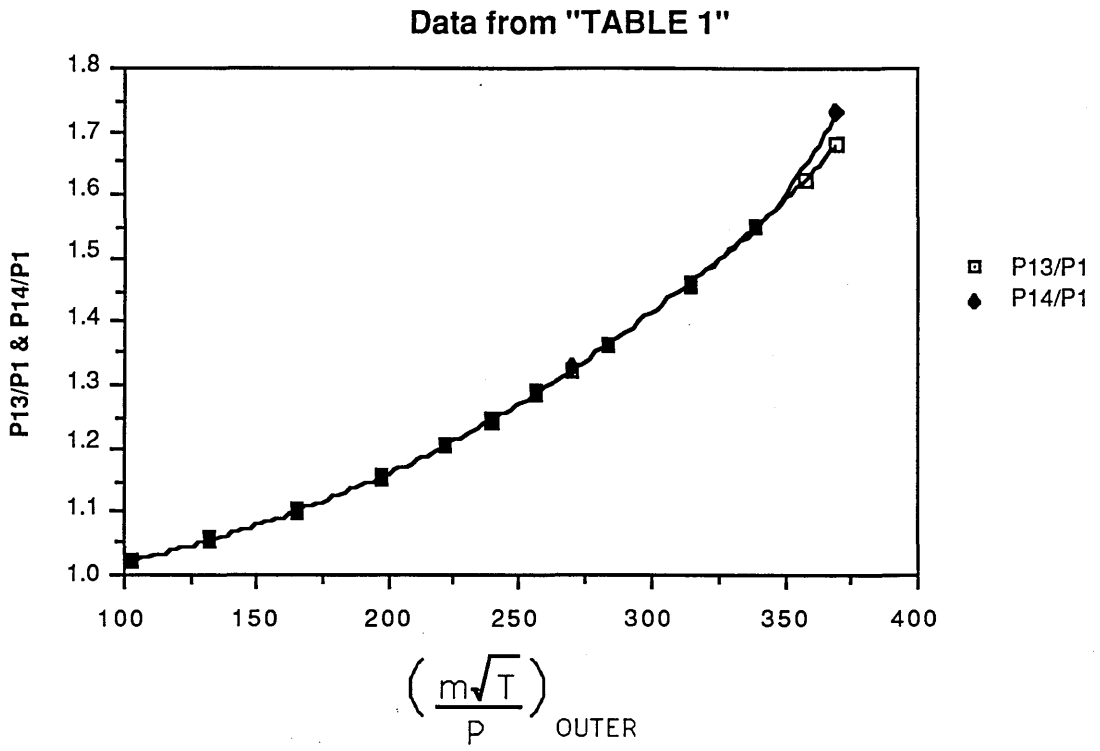

P13/P1 = AFCSP PROGRAM RESULTS

P14/P1 = AFSPSH PROGRAM RESULTS

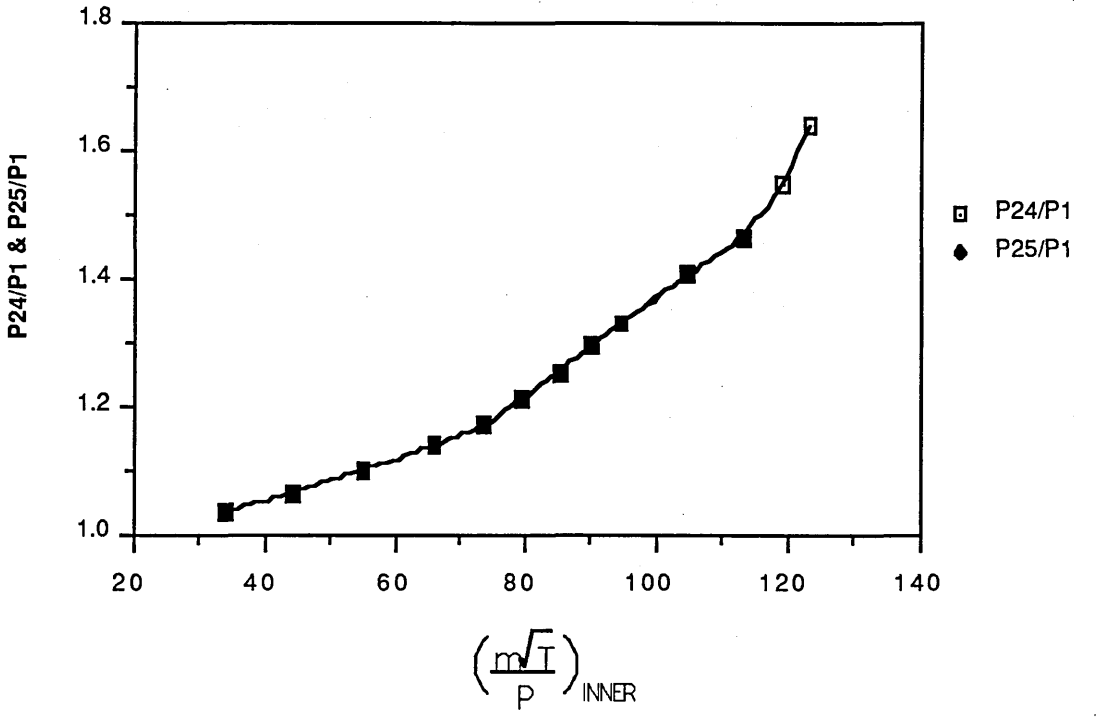

P24/P1 = PROGRAM AFCSP RESULTS

P25/P1 = AFSPSH PROGRAM RESULTS

STEADY STATE RESULTS AT : SEA LEVEL, MACH = 0.2

FIGURE (25)

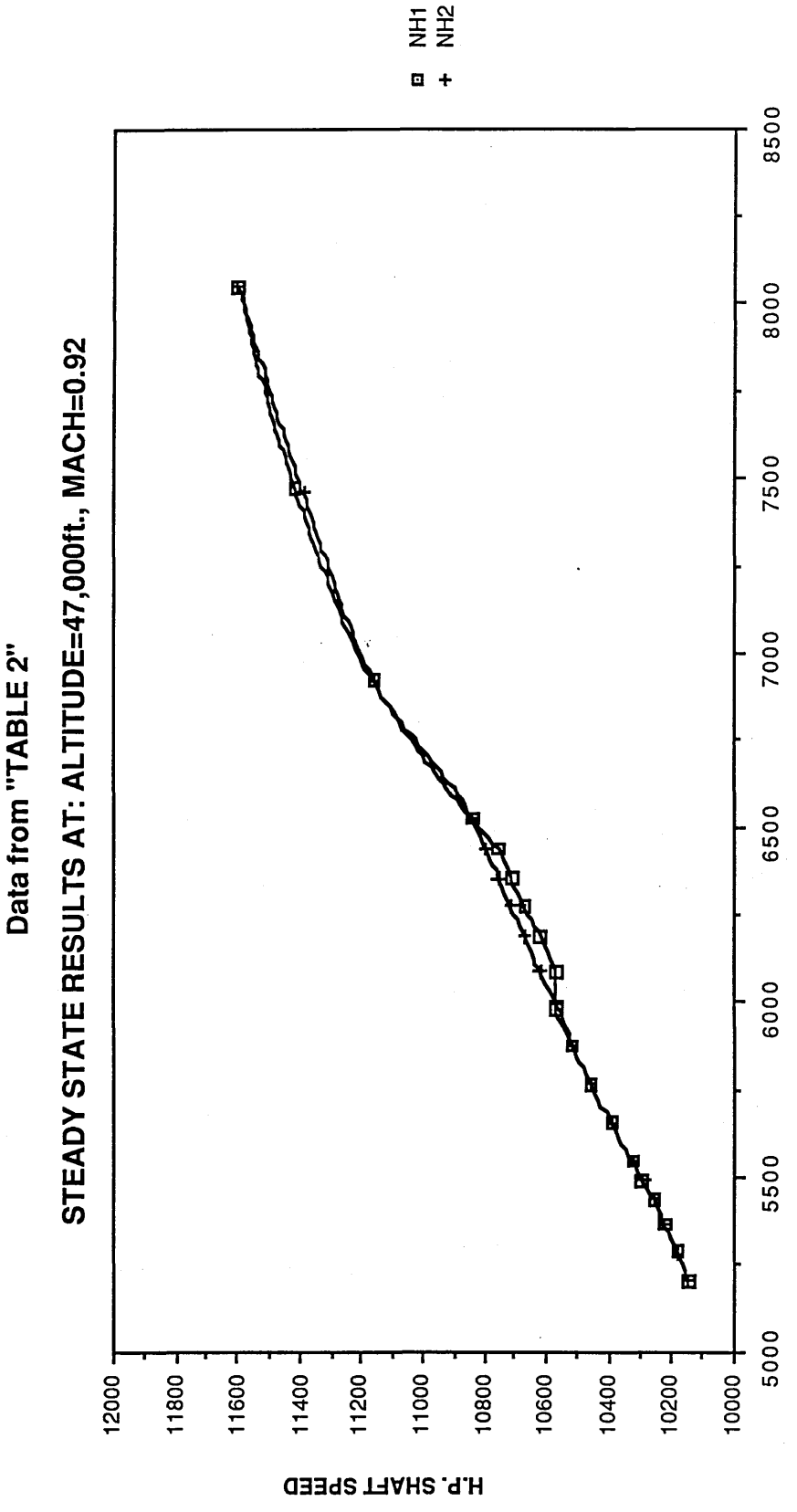

NH1 = AFCSP PROGRAM RESULTS

NH2 = AFSPSH PROGRAM RESULTS

FIGURES (26,27 & 28)

Data from "TABLE 2"

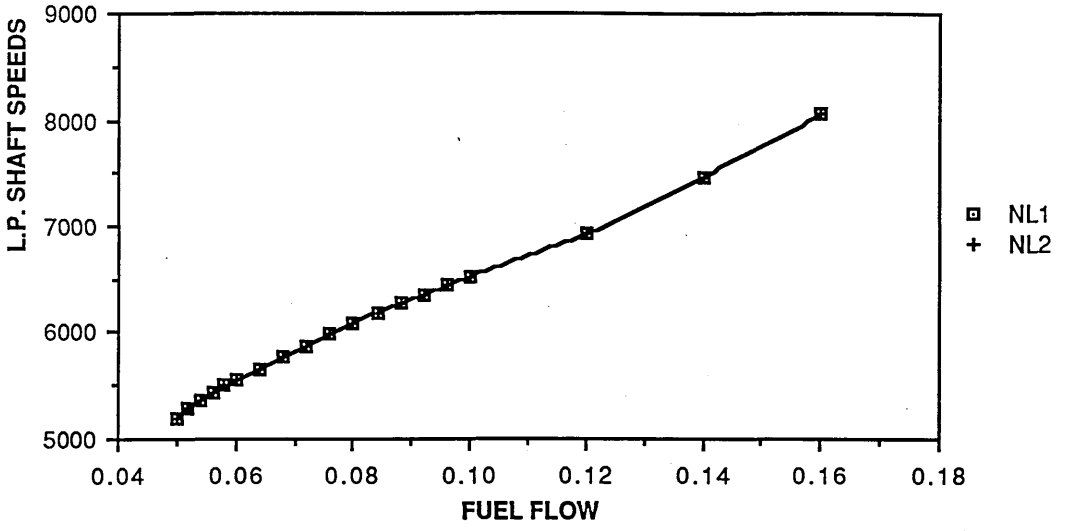

NL1 = AFCSP PROGRAM RESULTS
NL2 = AFSHSP PROGRAM RESULTS

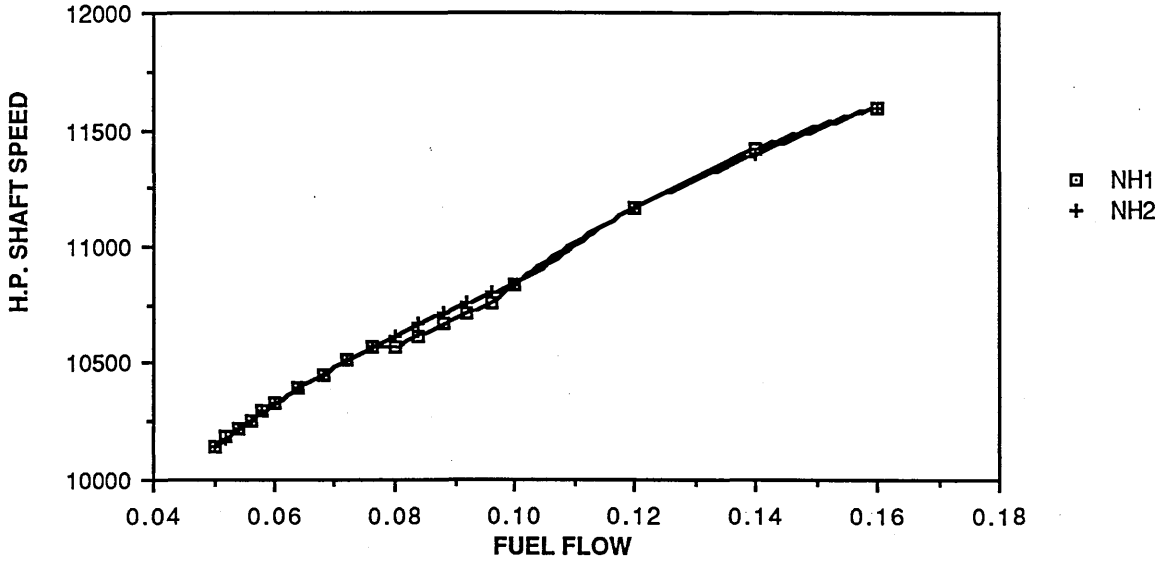

NH1 = AFCSP PROGRAM RESULTS
NH2 = AFSHSP PROGRAM RESULTS

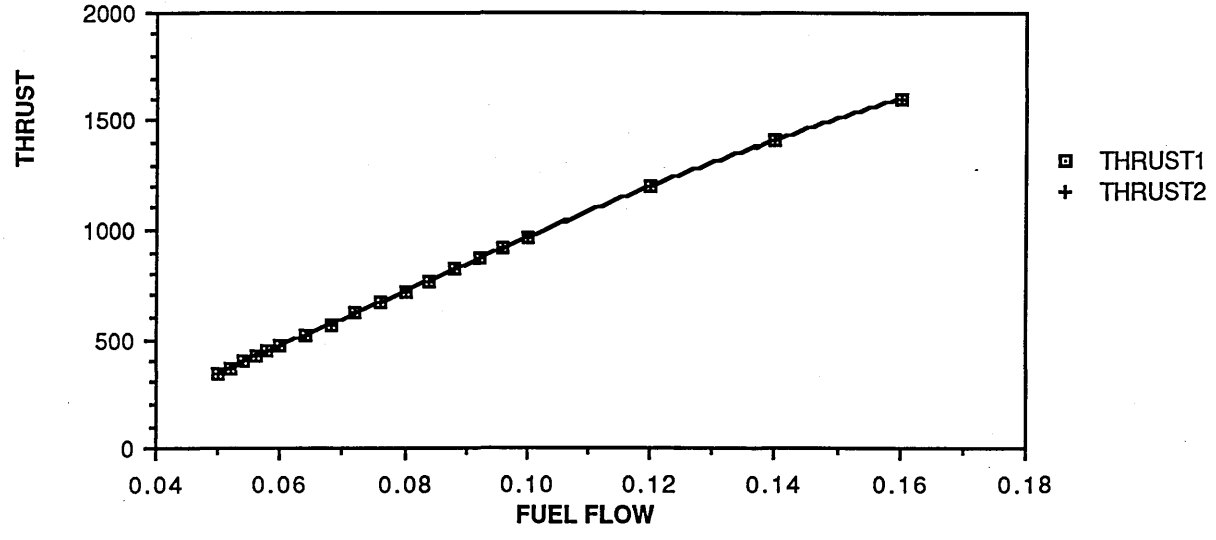

THRUST1 = AFCSP PROGRAM RESULTS
THRUST2 = AFSPSH PROGRAM RESULTS

STEADY STATE RESULTS AT: ALTITUDE=47,000ft., MACH=0.92

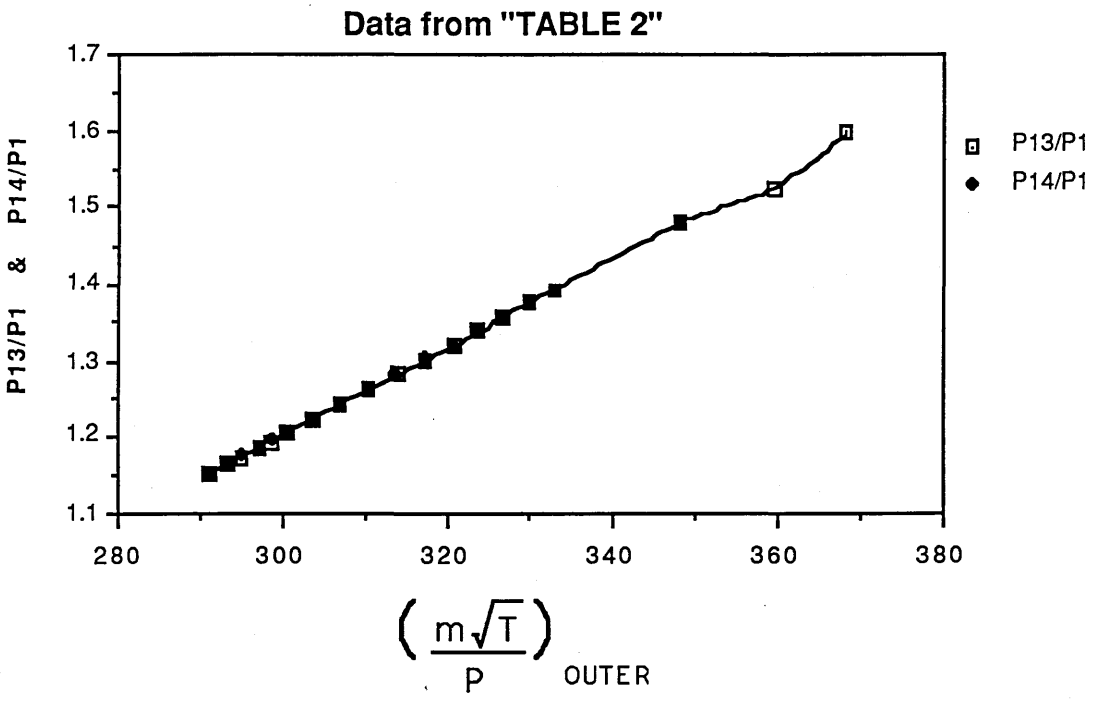

P13/P1=AFCSP PROGRAM RESULTS

P14/P1=AFSPSH PROGRAM RESULTS

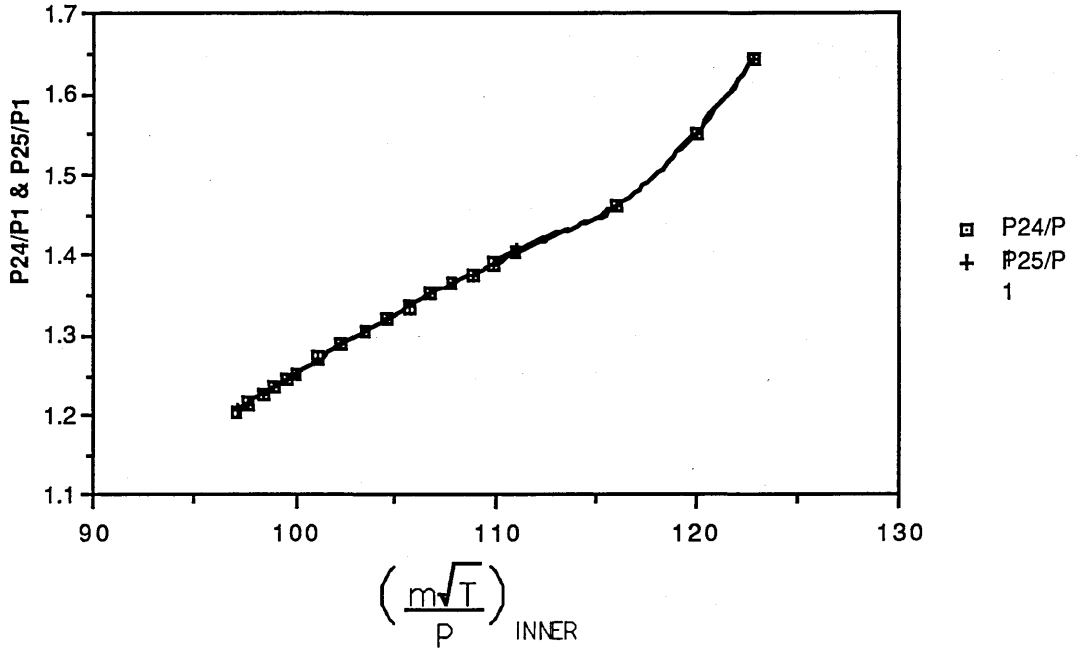

P24/P1 = AFCSP PROGRAM RESULTS

P25/P1 = AFSPSH PROGRAM RESULTS

STEADY STATE RESULTS AT:
ALTITUDE=47,000ft., MACH=0.92

STEADY STATE RESULTS AT : SEA LEVEL, MACH=0.2

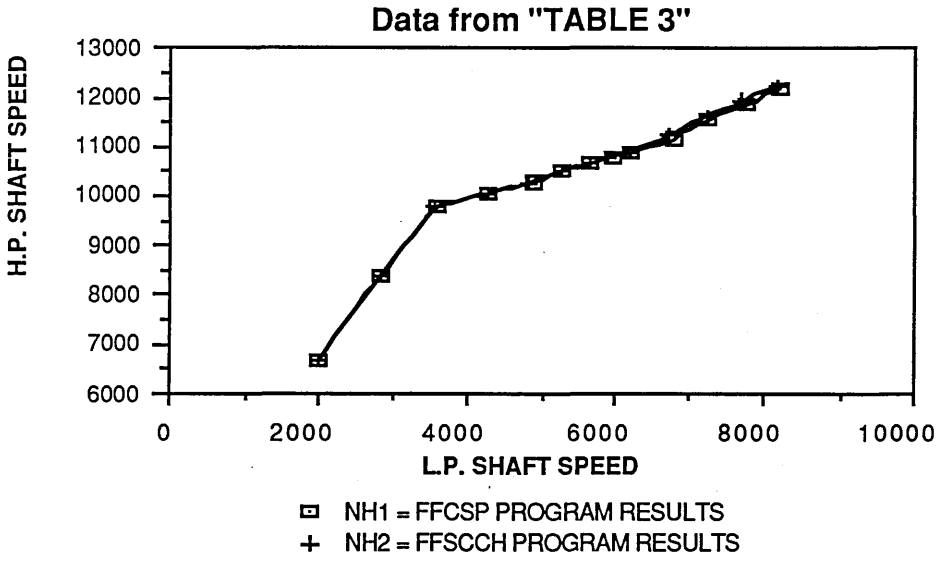

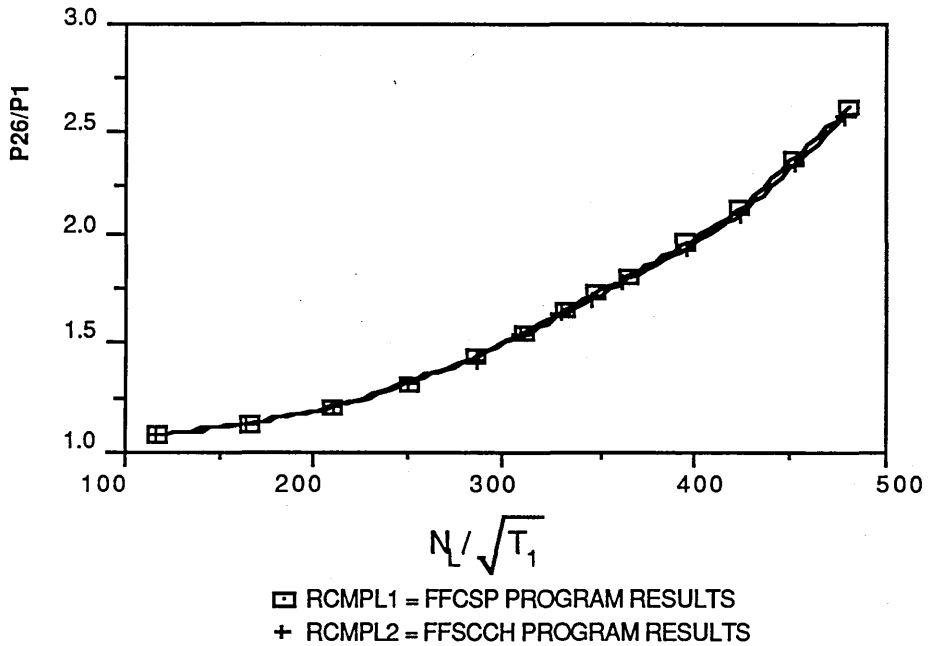

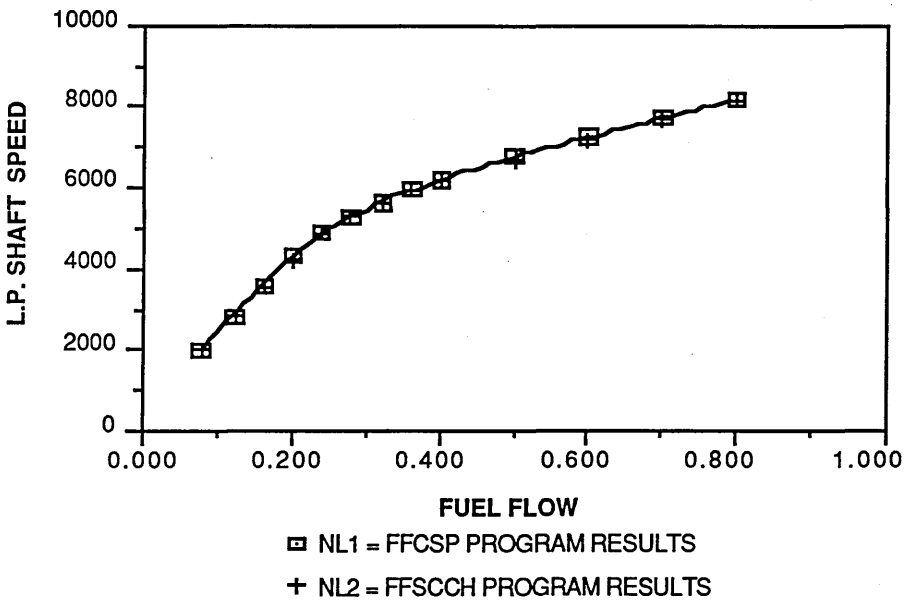

STEADY STATE RESULTS AT: SEA LEVEL, MACH=0.2

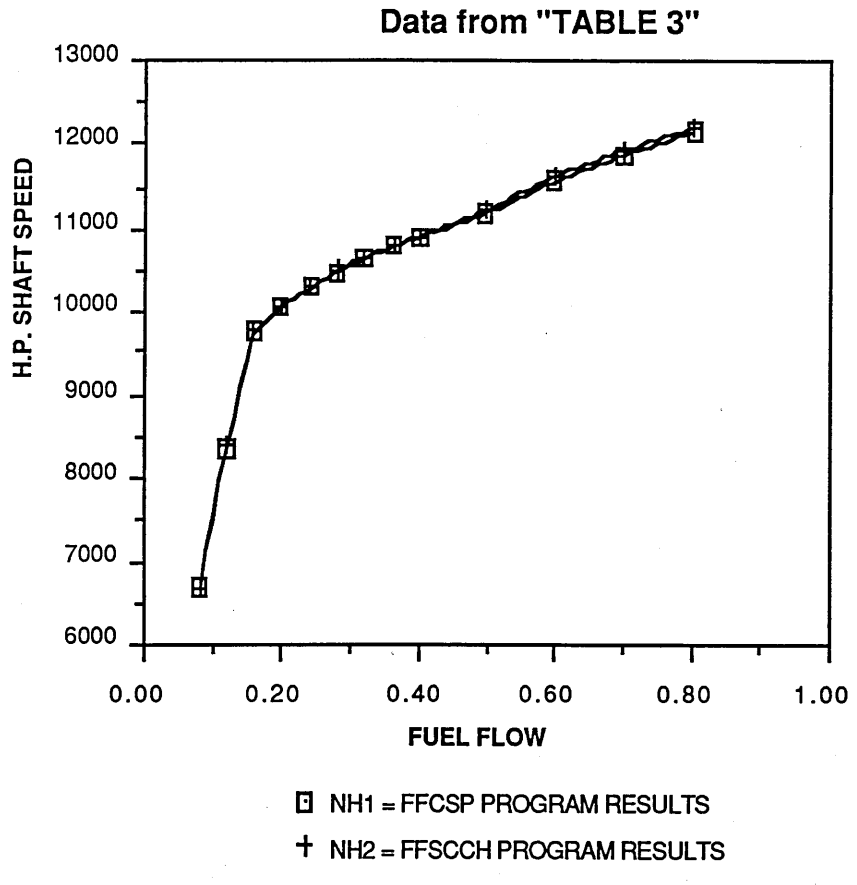

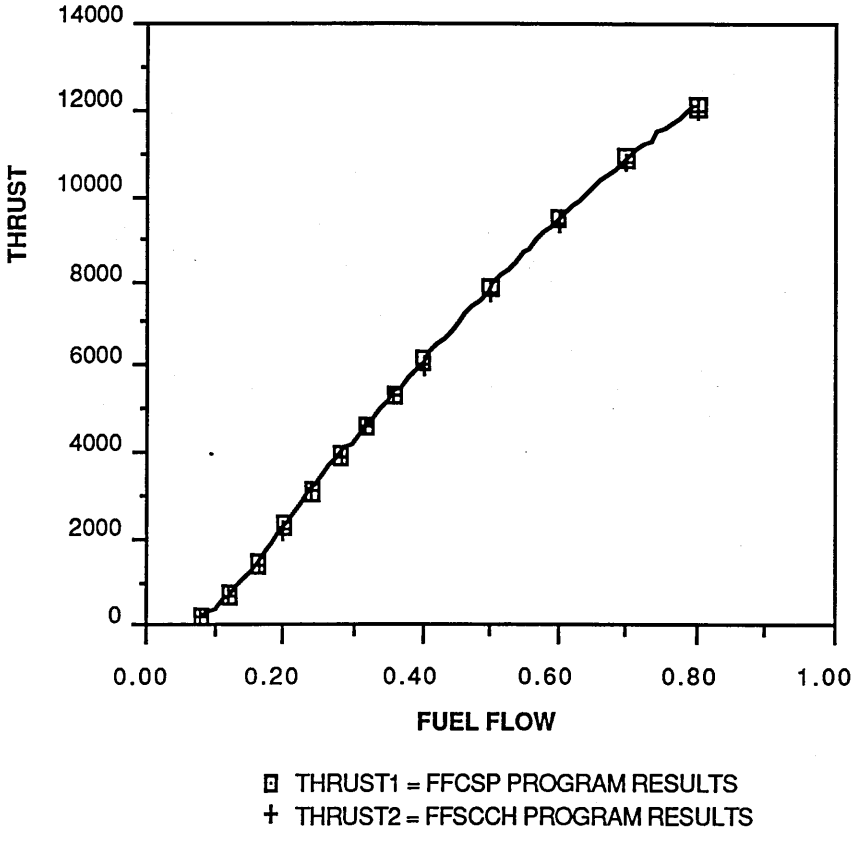

STEADY STATE RESULTS AT:
ALTITUDE=47,000ft., MACH=0.92

Data from "TABLE4"

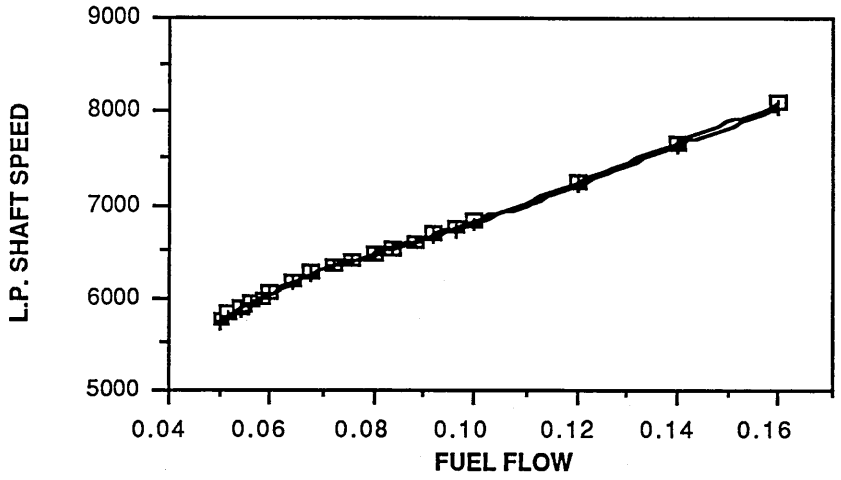

NL1 = FFCSP PROGRAM RESULTS

NL2 = FFSCCH PROGRAM RESULTS

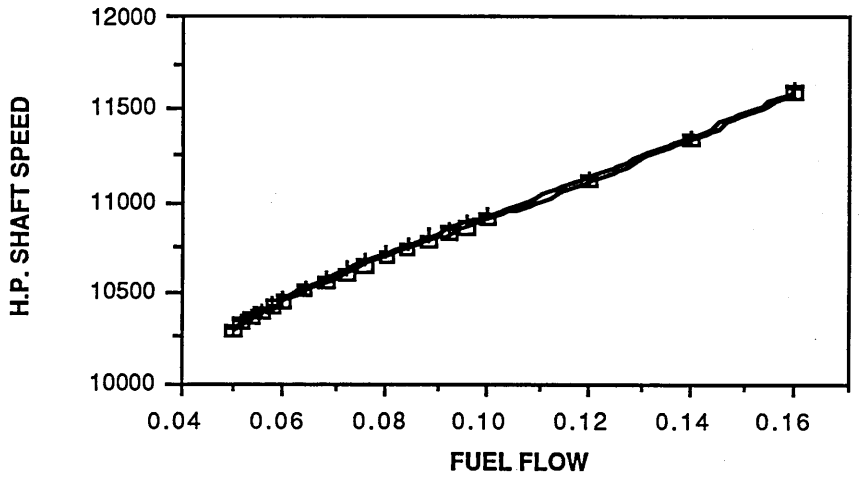

NH1 = FFCSP PROGRAM RESULTS

NH2 = FFSCCH PROGRAM RESULTS

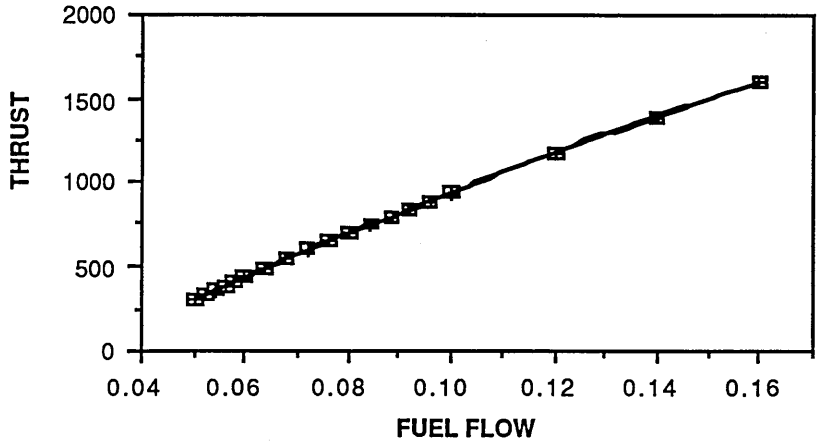

THRUST1 = FFCSP PROGRAM RESULTS

THRUST2 = FFSCCH PROGRAM RESULTS

STEADY STATE RESULTS AT:
ALTITUDE=47,000ft., MACH=0.92

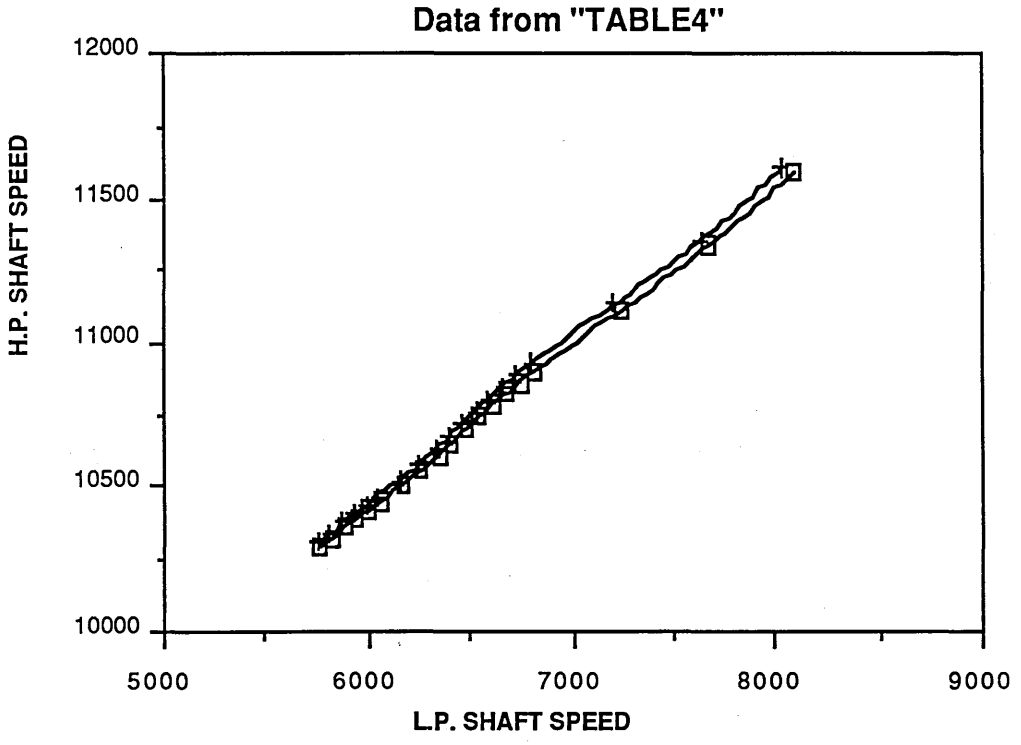

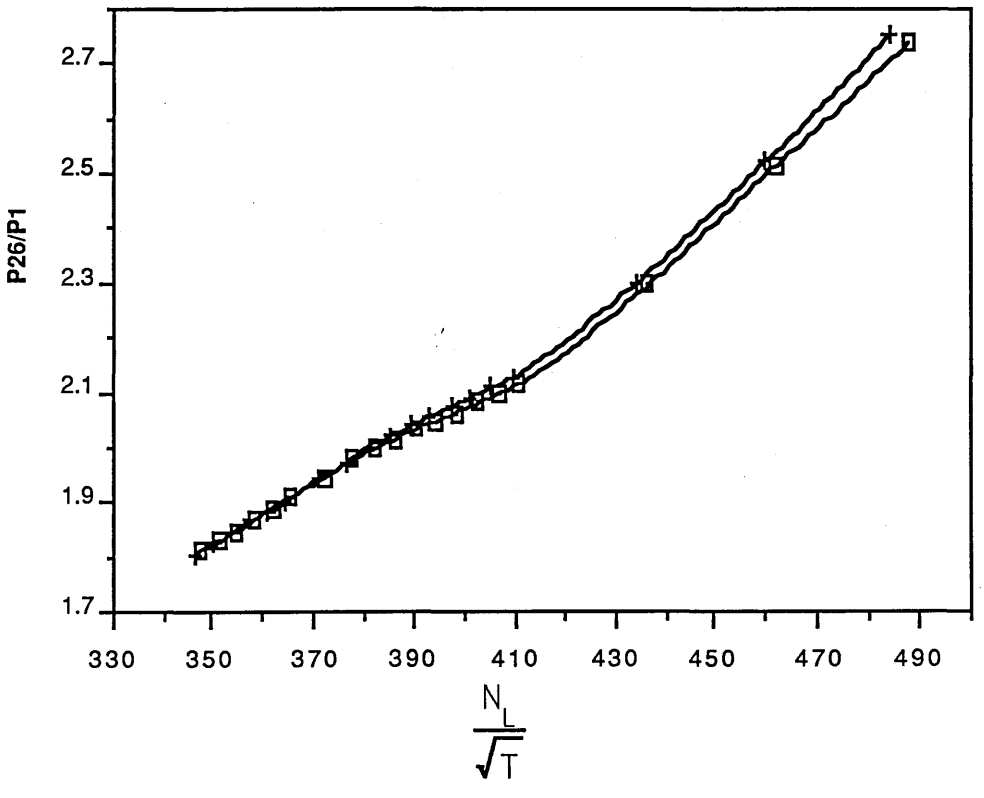

INNER FAN CHARACTERISTICS TABULATION AS USED IN PROGRAMS STFFIX AND STKFAN

FIGURE (41)

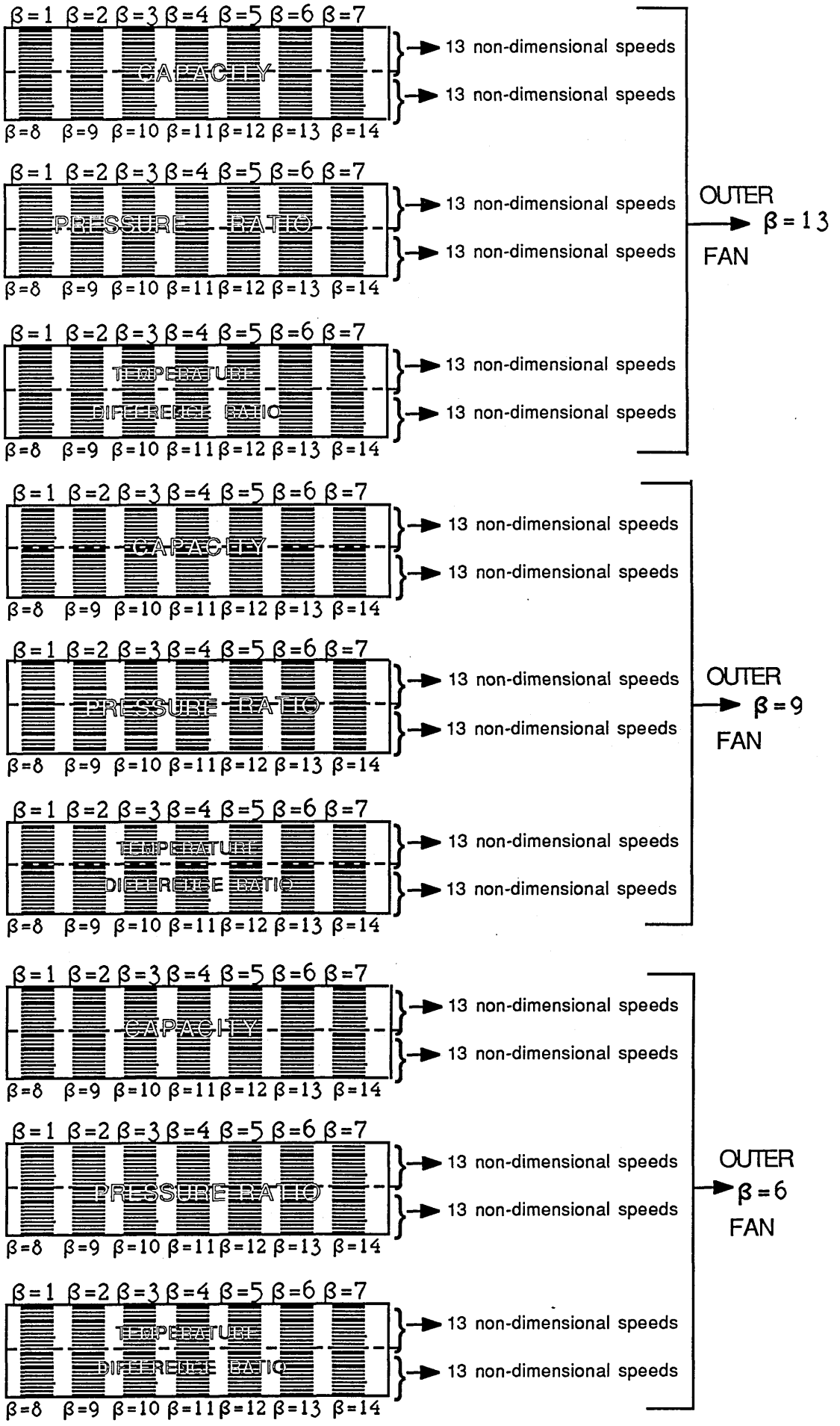

INNER FAN CHARACTERISTICS AS USED IN STKFAN AND STFFIX PROGRAMS

CORRESPONDING TO OUTER FAN BETA VALUE=13

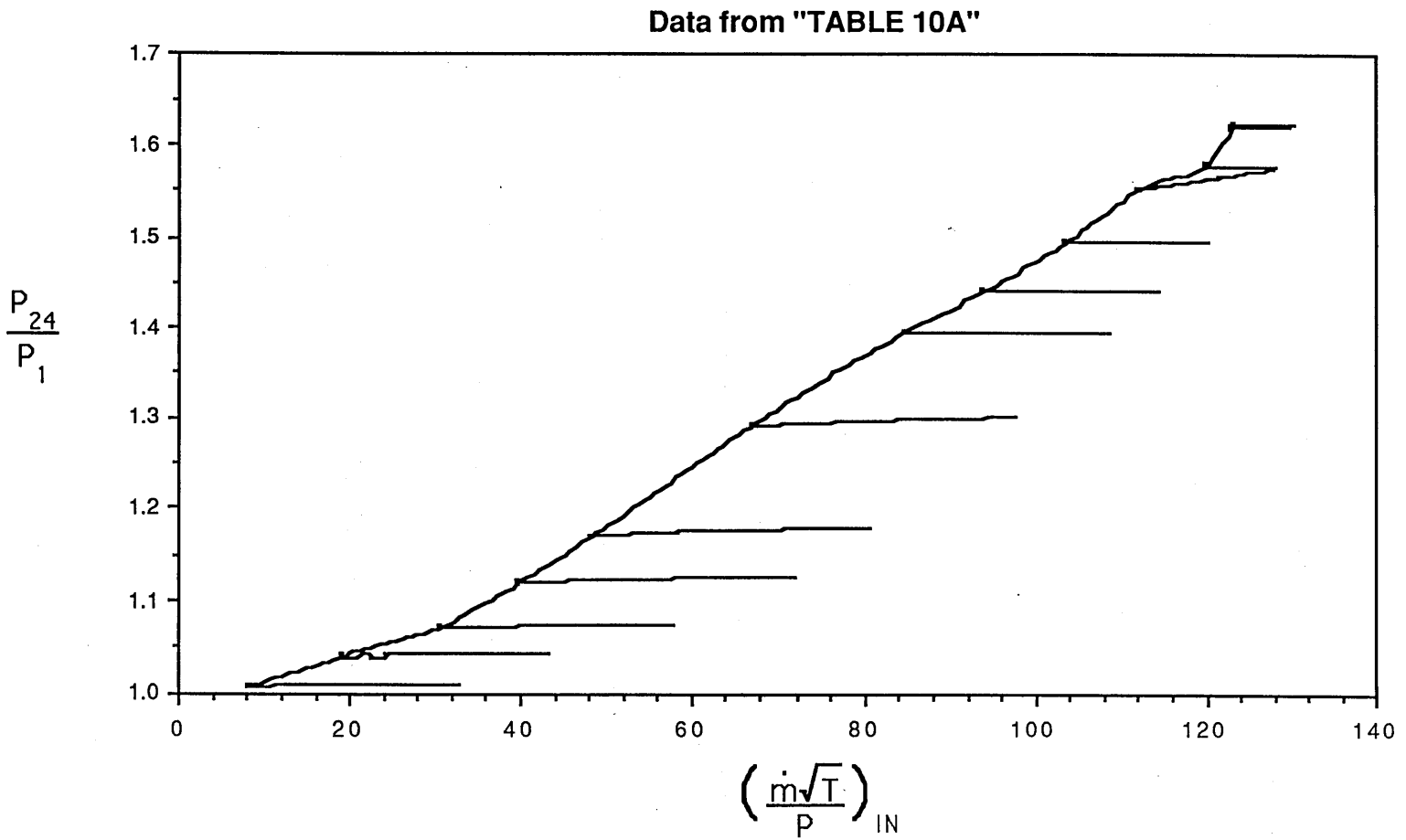

FIGURE (42)

OUTER FAN CHARACTERISTICS AS USED IN PROGRAMS STKFAN AND STFFIX

CORRESPONDING TO INNER FAN BETA VALUE=14

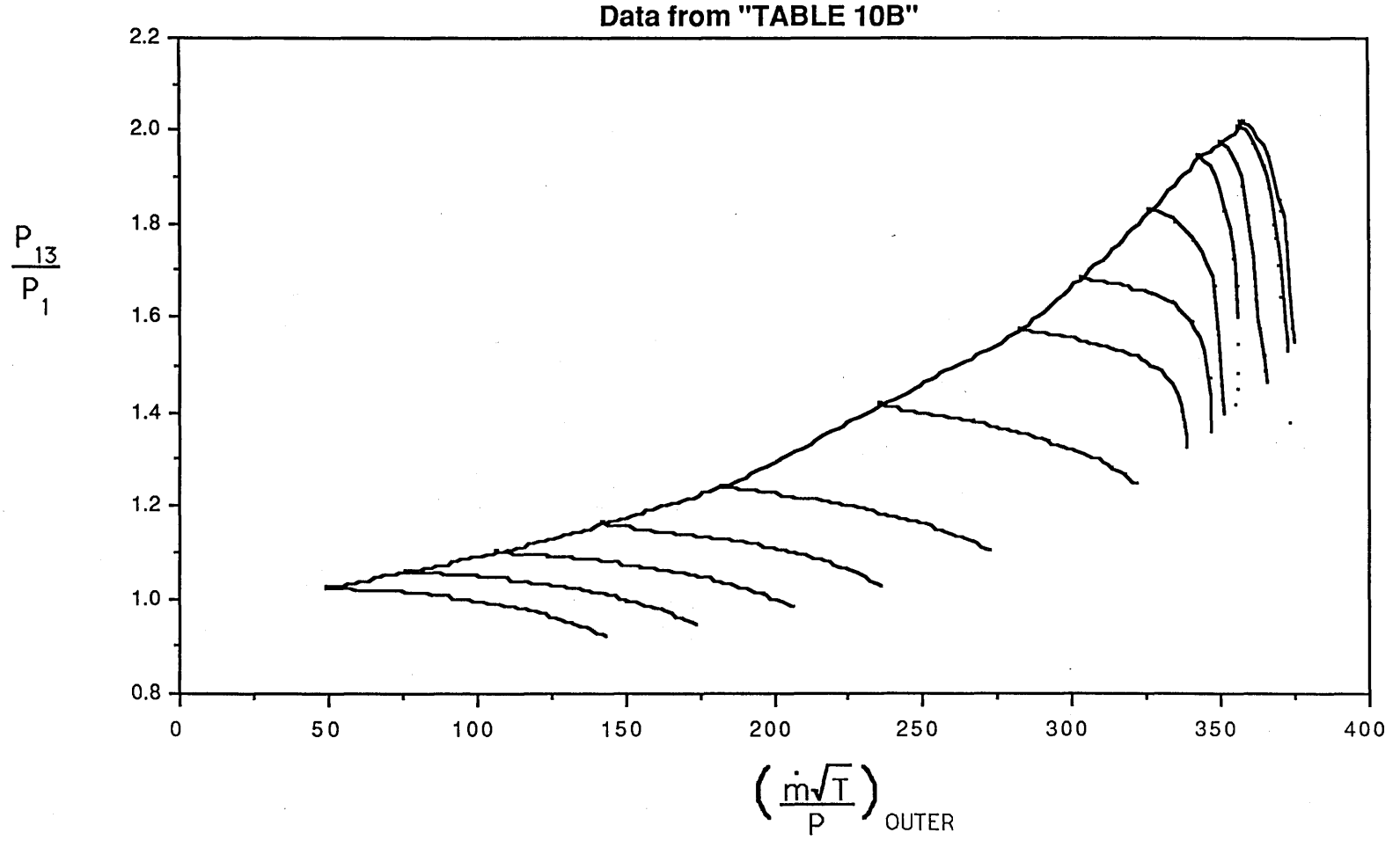

FIGURE (43)

FIGURE (44)

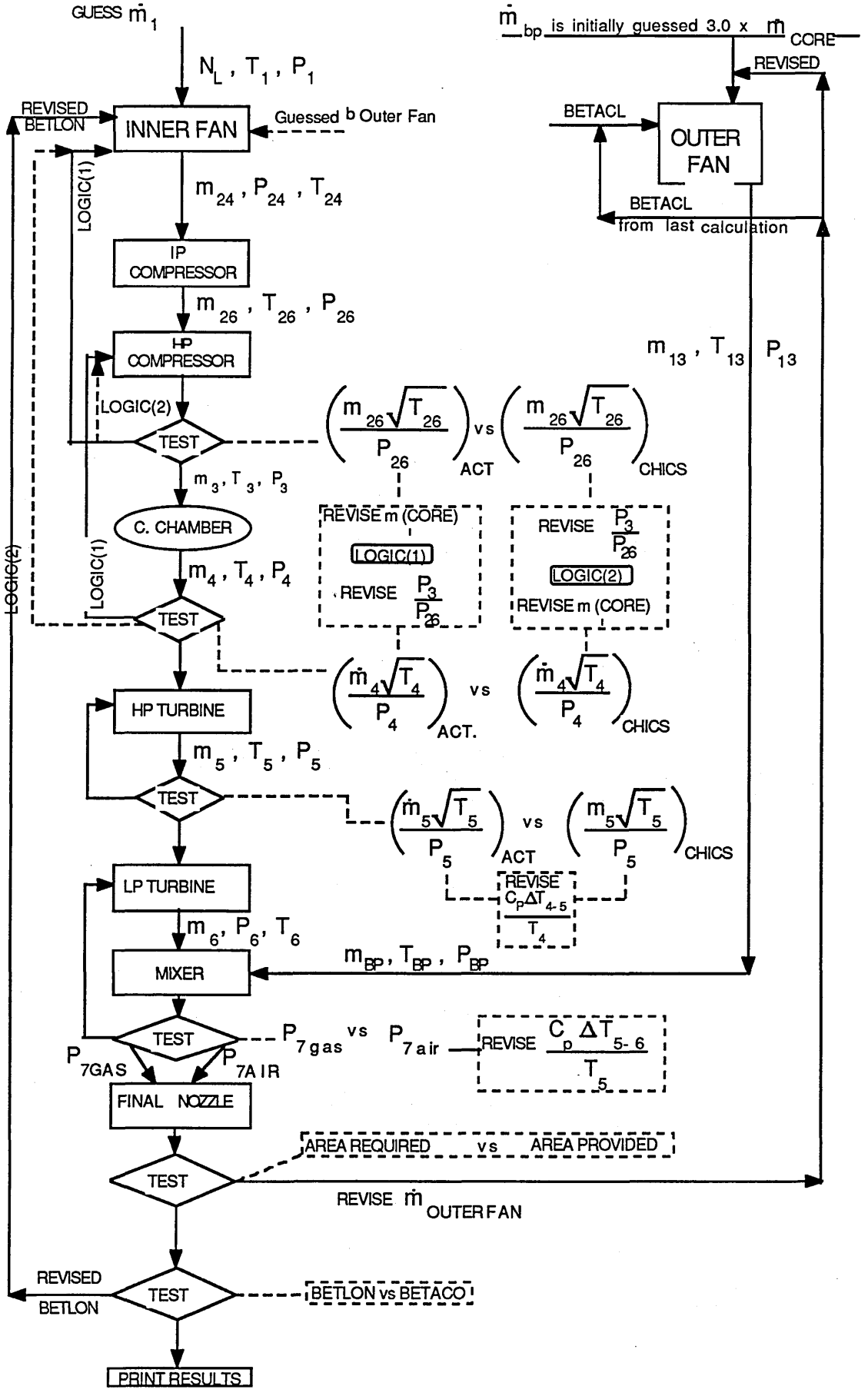
GUESS $\dot{m}_1$
N_L , T_1 , P_1
REVISED BETLON
INNER FAN
Guessed b Outer Fan
LOGIC(1)
m_{24} , P_{24} , T_{24}
IP COMPRESSOR
m_{26} , T_{26} , P_{26}
HP COMPRESSOR
LOGIC(2)
TEST
$\left(\frac{m_{26}\sqrt{T_{26}}}{P_{26}}\right)_{ACT}$ vs $\left(\frac{m_{26}\sqrt{T_{26}}}{P_{26}}\right)_{CHICS}$
m_3, T_3, P_3
C. CHAMBER
m_4 , T_4 , P_4
REVISE m (CORE)
LOGIC(1)
REVISE $\frac{P_3}{P_{26}}$
REVISE $\frac{P_3}{P_{26}}$
LOGIC(2)
REVISE m (CORE)
LOGIC(2)
LOGIC(1)
TEST
$\left(\frac{\dot{m}_4\sqrt{T_4}}{P_4}\right)_{ACT.}$ vs $\left(\frac{\dot{m}_4\sqrt{T_4}}{P_4}\right)_{CHICS}$
HP TURBINE
m_5 , T_5 , P_5
TEST
$\left(\frac{\dot{m}_5\sqrt{T_5}}{P_5}\right)_{ACT}$ vs $\left(\frac{m_5\sqrt{T_5}}{P_5}\right)_{CHICS}$
LP TURBINE
REVISE $\frac{C_p\Delta T_{4-5}}{T_4}$
m_6, P_6, T_6
MIXER
m_{BP}, T_{BP} , P_{BP}
$\dot{m}_{bp}$ is initially guessed 3.0 x $\dot{m}_{CORE}$
REVISED
BETACL
OUTER FAN
BETACL
from last calculation
m_{13} , T_{13} P_{13}
TEST
P_{7gas} vs P_{7air}
REVISE $\frac{C_p\Delta T_{5-6}}{T_5}$
P_{7GAS}
P_{7AIR}
FINAL NOZZLE
AREA REQUIRED vs AREA PROVIDED
TEST
REVISE $\dot{m}_{OUTER\ FAN}$
REVISED BETLON
TEST
BETLON vs BETACO
PRINT RESULTS

FIGURE 45

TYPICAL TURBOFAN ENGINE

COMBINED INNER FAN AND I.P. COMPRESSOR
WORKING LINES
AT: SEA LEVEL, MACH=0.2

COMPARISON OF RESULTS OF ALL FIVE PROGRAMS

Data from "TABLE 9"

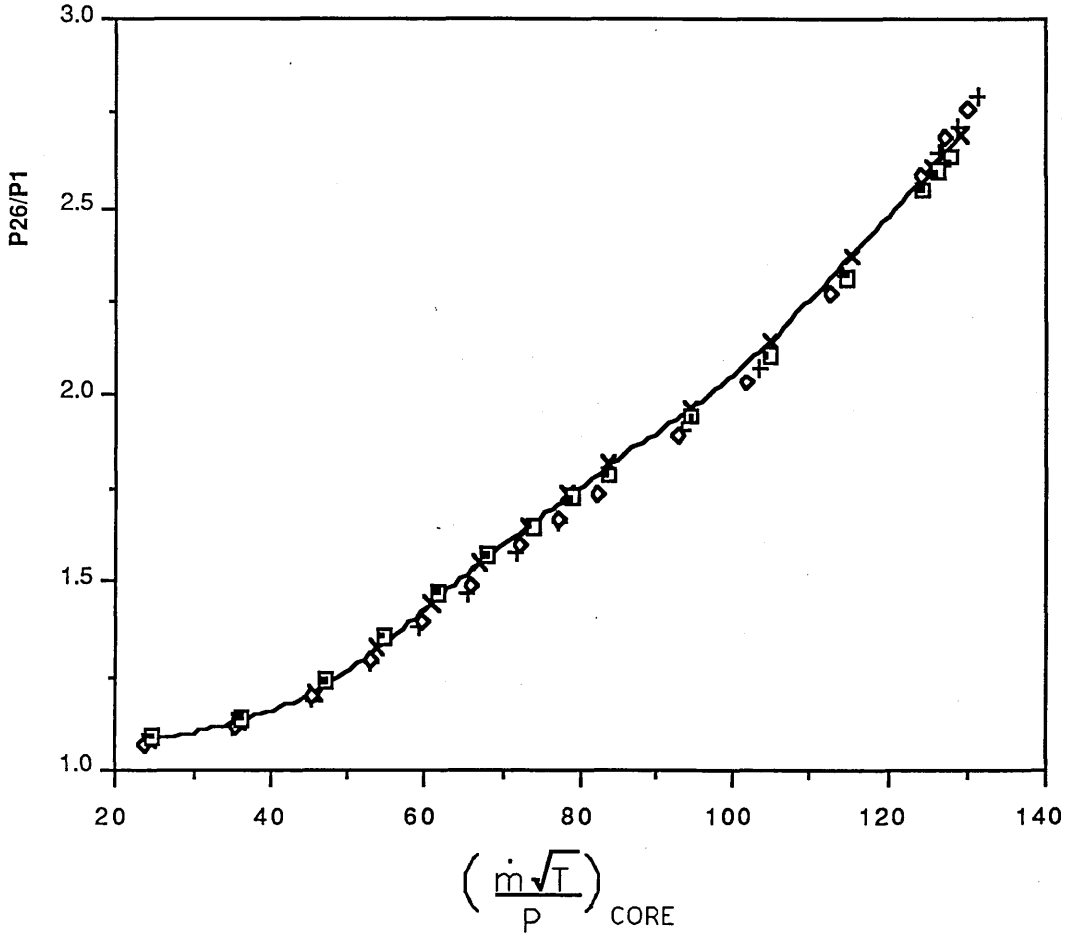

+ 1.(P26/P1)SR =AFCSP PROGRAM ,STEADY RUNNING

× 2.(P26/P1)SR = PROGRAM FFCSP STEADY RUNNING

• 3.(P26/P1)SR =AFSPOF PRGRAM, STEADY RUNNING

▪ 4.(P26/P1)SR =STFFIX PROGRAM, STEADY RUNNING

□ 5.(P26/P1)SR =STKFAN PROGRAM, STEADY RUNNING

FIGURE 46

TYPICAL TURBOFAN ENGINE

COMBINED INNER FAN AND I.P. COMPRESSOR
ACCELERATION TRAJECTORIES
AT SEA LEVEL, MACH = 0.2

COMPARISON OF RESULTS ALL FIVE PROGRAMS

Data from "TABLES 9 & 9A"

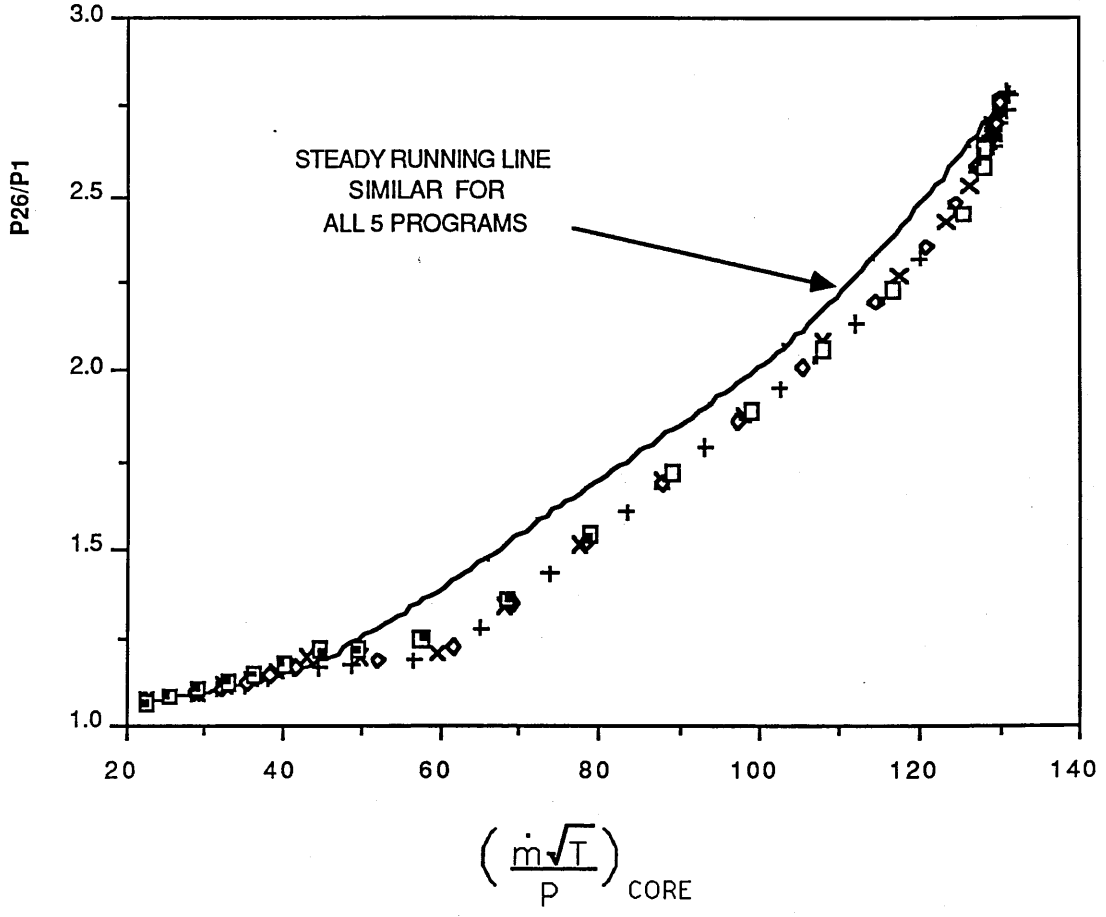

⁄	1.(P26/P1)SR	=AFCSP PROGRAM, STEADY RUNNING LINE
+	1.(P26/P1)Ac	=AFCSP PROGRAM, ACCELERATION RESULTS
×	2.(P26/P1)Ac	=FFCSP PROGRAM, ACCELERATION RESULTS
◇	3.(P26/P1)Ac	=AFSPOF PROGRAM, ACCELERATION RESULTS
·	4.(P26/P1)Ac	=STFFIX PROGRAM, ACCELERATION RESULTS
□	5.(P26/P1)Ac	=STKFAN PROGRAM, ACCELERATION RESULTS

TYPICAL TURBOFAN ENGINE

COMBINED INNER FAN AND I.P. COMPRESSOR
DECELERATION TRAJECTORIES
AT: SEA LEVEL, MACH = 0.2

COMPARISON OF RESULTS OF ALL FIVE PROGRAMS

Data from "TABLES 9 & 9A"

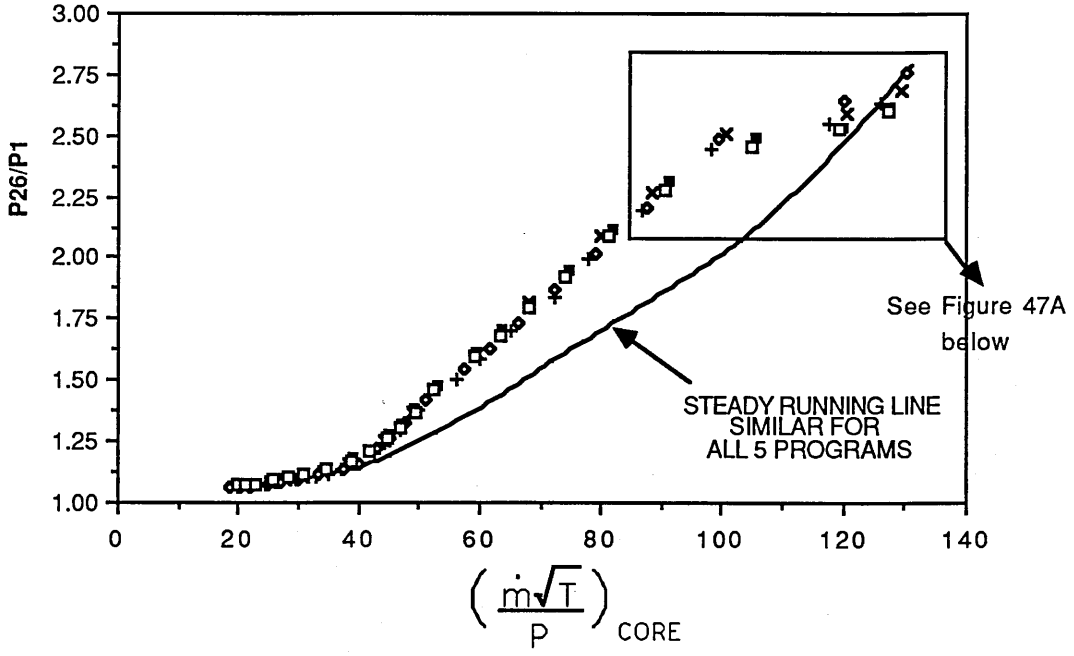

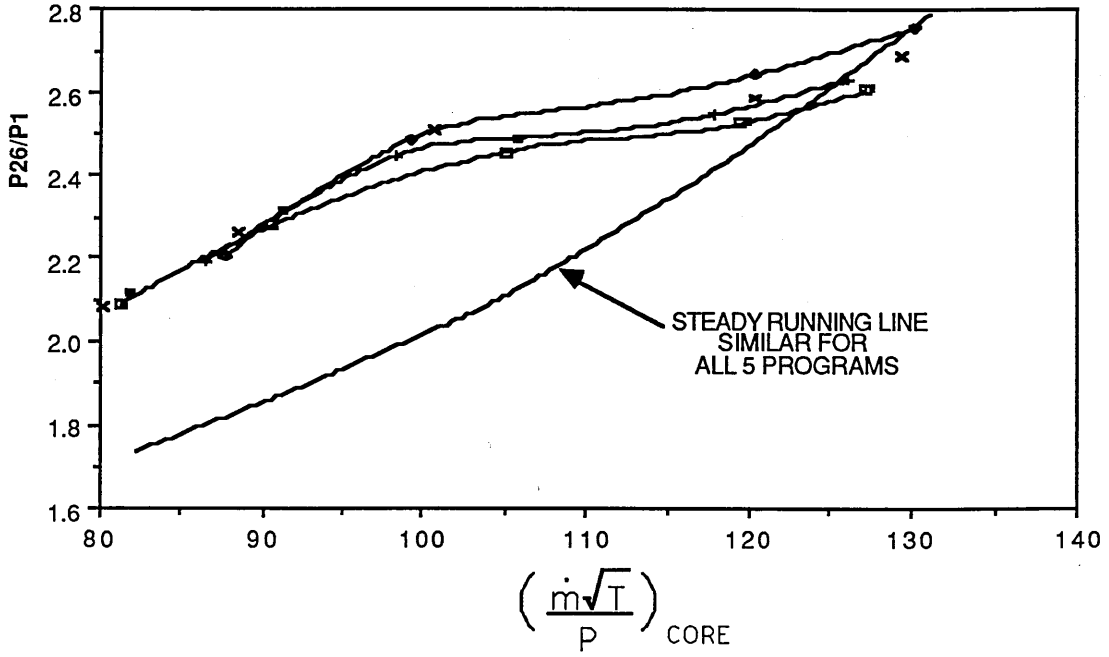

·	1.(p26/p1)SR	= AFCSP PROGRAM, STEADY RUNNING LINE
+	1.(p26/p1)Dc	=AFCSP PROGRAM, DECELERATION RESULTS
×	2.(p26/p1)Dc	=FFCSP PROGRAM, DECELERATION RESULTS
◆	3.(p26/p1)Dc	=AFSPOF PROGRAM, DECELERATION RESULTS
■	4.(p26/p2)Dc	=STFFIX PROGRAM, DECELERATION RESULTS
□	5.(p26/p1)Dc	=STKFAN PROGRAM, DECELERATION RESULTS

FIGURE 48

TYPICAL TURBOFAN ENGINE

COMPARISON OF OUTER FAN WORKING LINES
OF ALL FIVE PROGRAMS
AT SEA LEVEL. MACH = 0.2

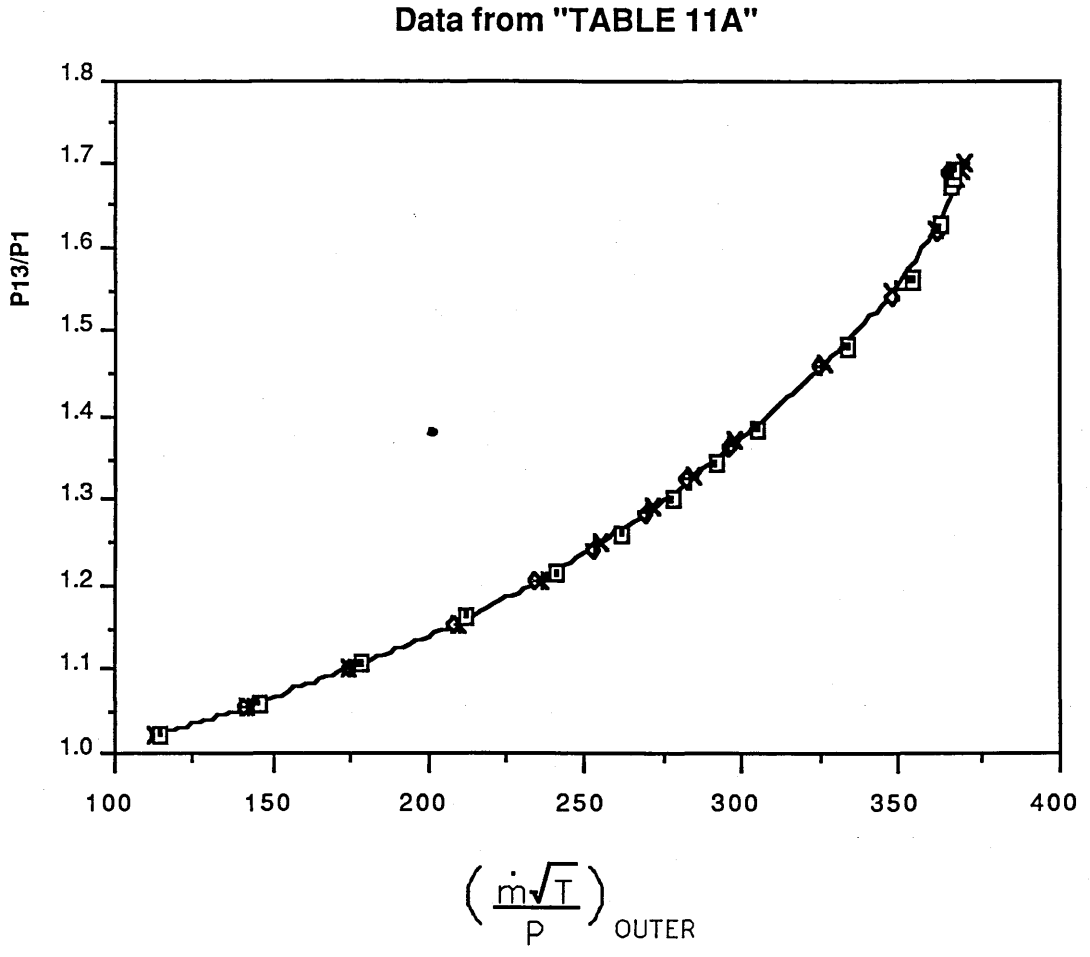

FIGURE 49

TYPICAL TURBOFAN ENGINE

COMPARISON OF OUTER FAN ACCELERATION TRAJECTORIES

AT SEA LEVEL, MACH = 0.2

FOR ALL 5 PROGRAMS

Data from "TABLE 11A"

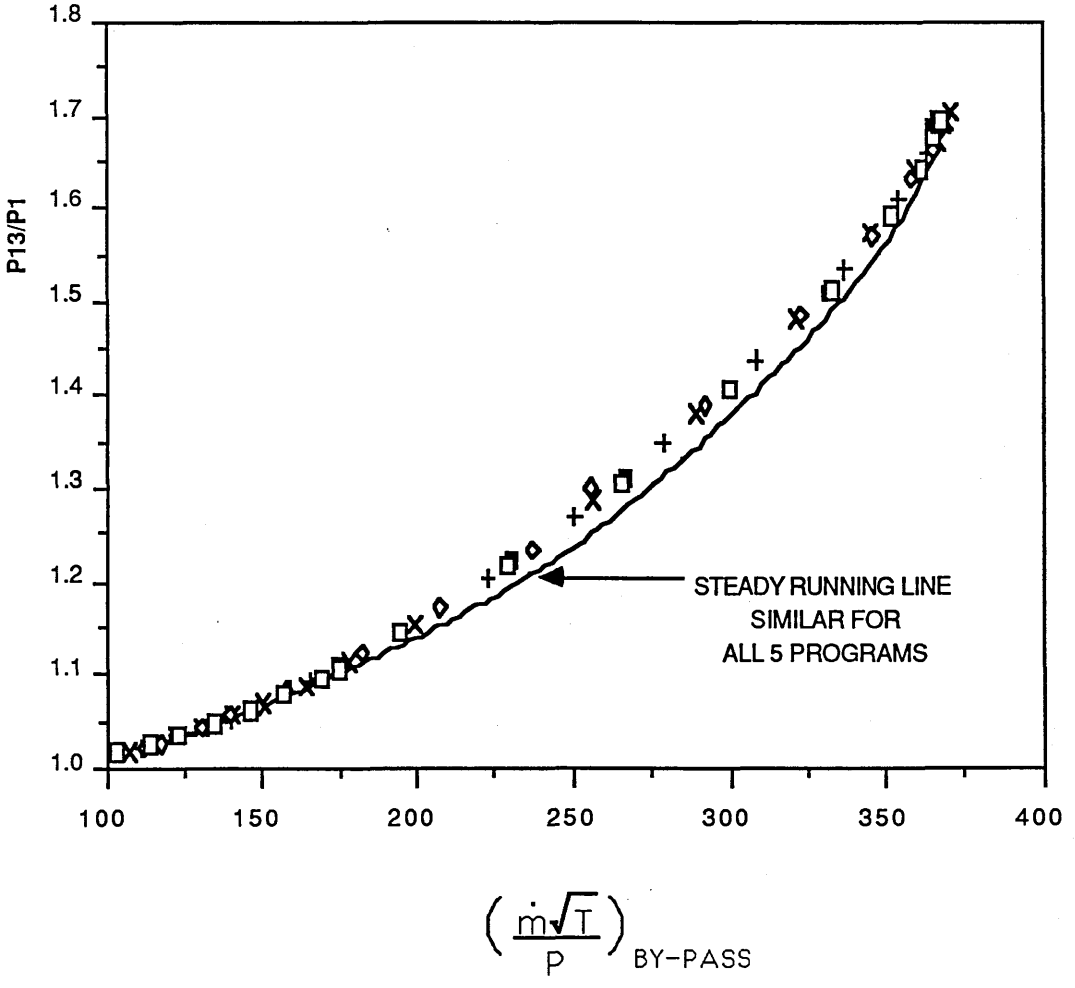

2.(P13/P1)SR =FFCSP PROGRAM, STEADY RUNNING LINE

\+ 1.(P13/P1)Ac =AFCSP PROGRAM, ACCELERATION RESULTS

× 2.(P13/P1)Ac =FFCSP PROGRAM, ACCELERATION RESULTS

◇ 3.(P13/P1)Ac =AFSPOF PROGRAM, ACCELERATION RESULTS

■ 4.(P13/P1)Ac =STFFIX PROGRAM, ACCELERATION RESULTS

□ 5.(P13/P1)Ac =STKFAN PROGRAM, ACCELERATION RESULTS

FIGURES 50 & 50A

TYPICAL TURBOFAN ENGINE

COMPARISON OF OUTER FAN DECELERATION TRAJECTORIES
AT SEA LEVEL, MACH = 0.2
FOR ALL 5 PROGRAMS

Data from "TABLE 11A"

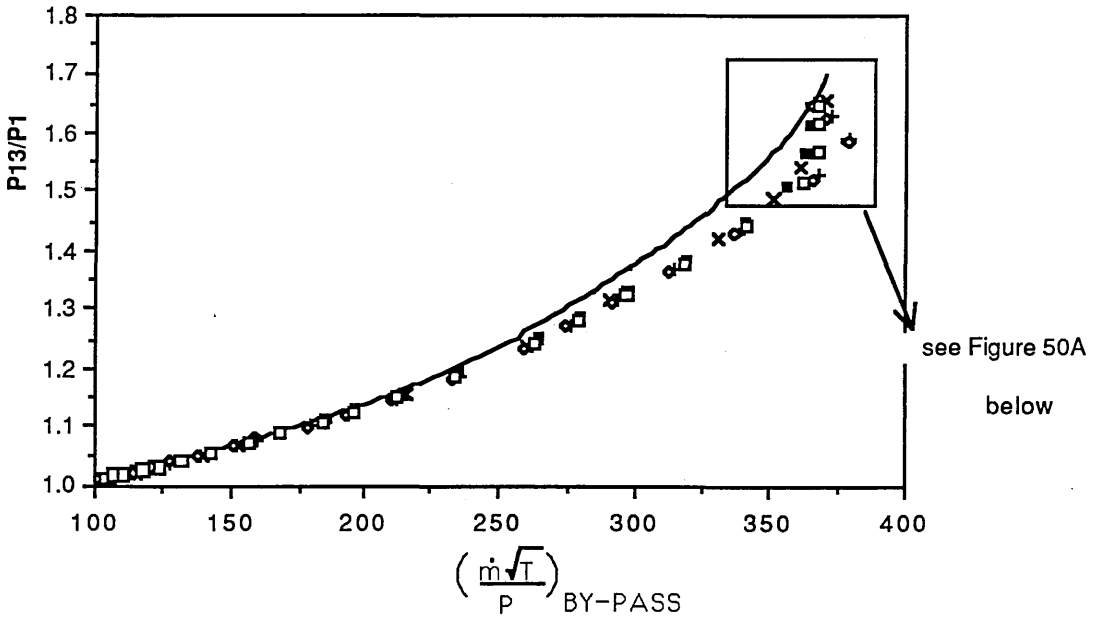

Data from "TABLE 11D"

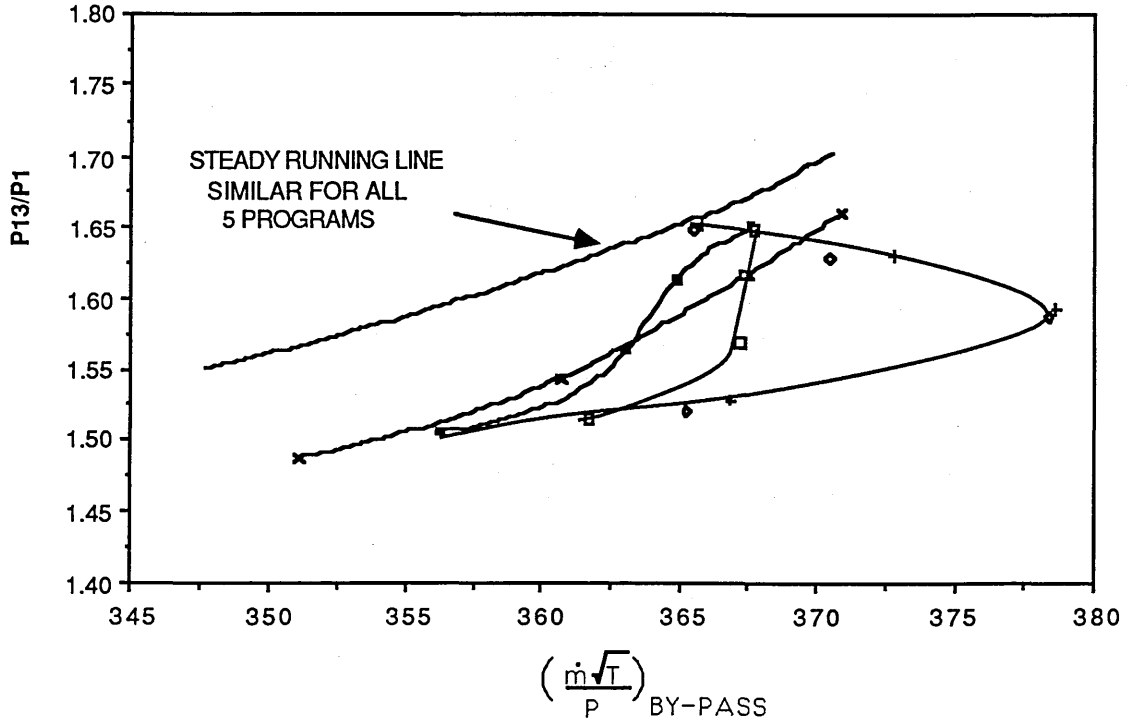

·	2.(P13/P1)SR	=FFCSP PROGRAM, STEADY RUNNING RESULTS
+	1.(P13/P1)Dc	=AFCSP PROGRAM, DECELERATION RESULTS
×	2.(P13/P1)Dc	=FFCSP PROGRAM, DECELERATION RESULTS
◇	3.(P13/P1)Dc	=AFSPOF PROGRAM, DECELERATION RESULTS
■	4.(P13/P1)Dc	=STFFIX PROGRAM, DECELERATION RESULTS
□	5.(P13/P1)Dc	=STKFAN PROGRAM, DECELERATION RESULTS

FIGURE 51

TYPICAL TURBOFAN ENGINE

COMPARISON OF OUTER FAN WORKING LINES
OF ALL FIVE PROGRAMS
AT : 43,000ft, MACH=0.8

Data from "TABLES 14 & 14A"

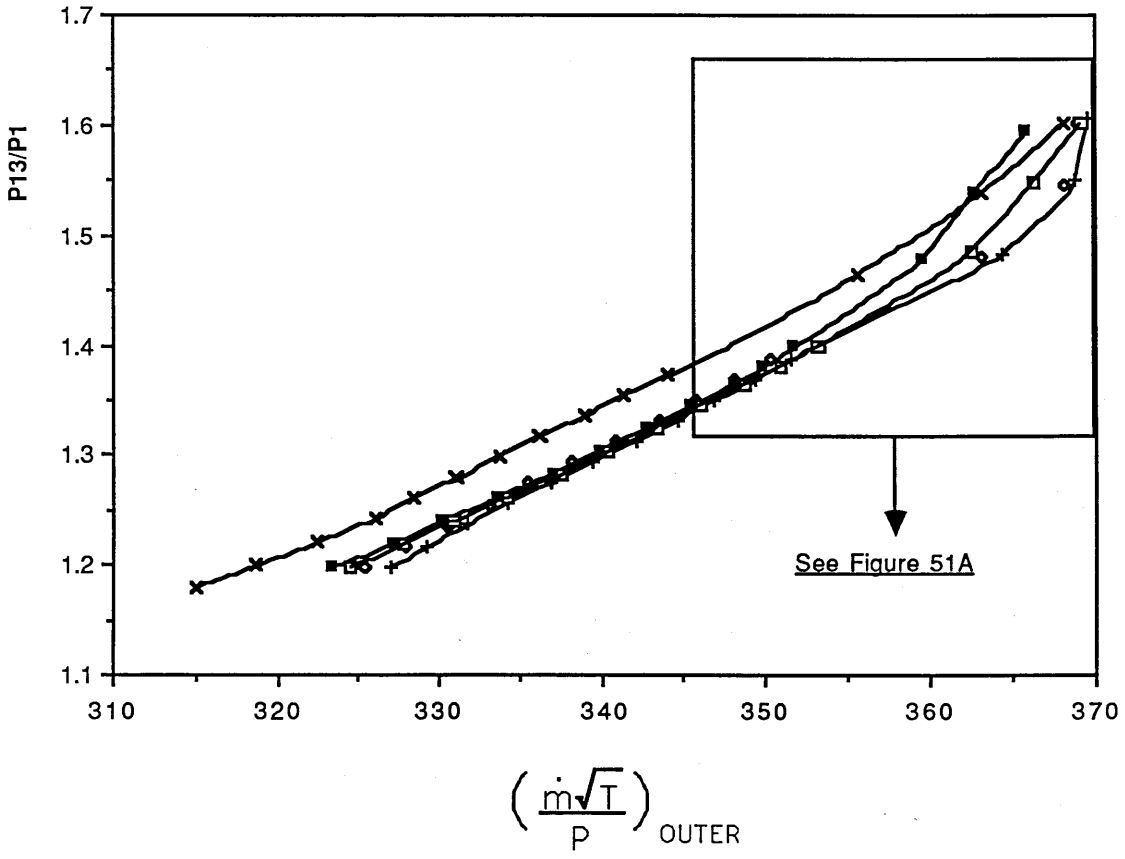

+ 1.(P13/P1)SR =AFCSP PROGRAM
× 2.(P13/P1)SR =FFCSP PROGRAM
◇ 3.(P13/P1)SR =AFSPOF PROGRAM
■ 4.(P13/P1)SR =STFFIX PROGRAM
□ 5.(P13/P1)SR =STKFAN PROGRAM

→ STEADY RUNNING RESULTS

FIGURE 51A

TYPICAL TURBOFAN ENGINE

COMPARISON OF OUTER FAN WORKING LINES

OF ALL FIVE PROGRAMS

AT : 43,000ft, MACH=0.8

Data from "TABLE 14B"

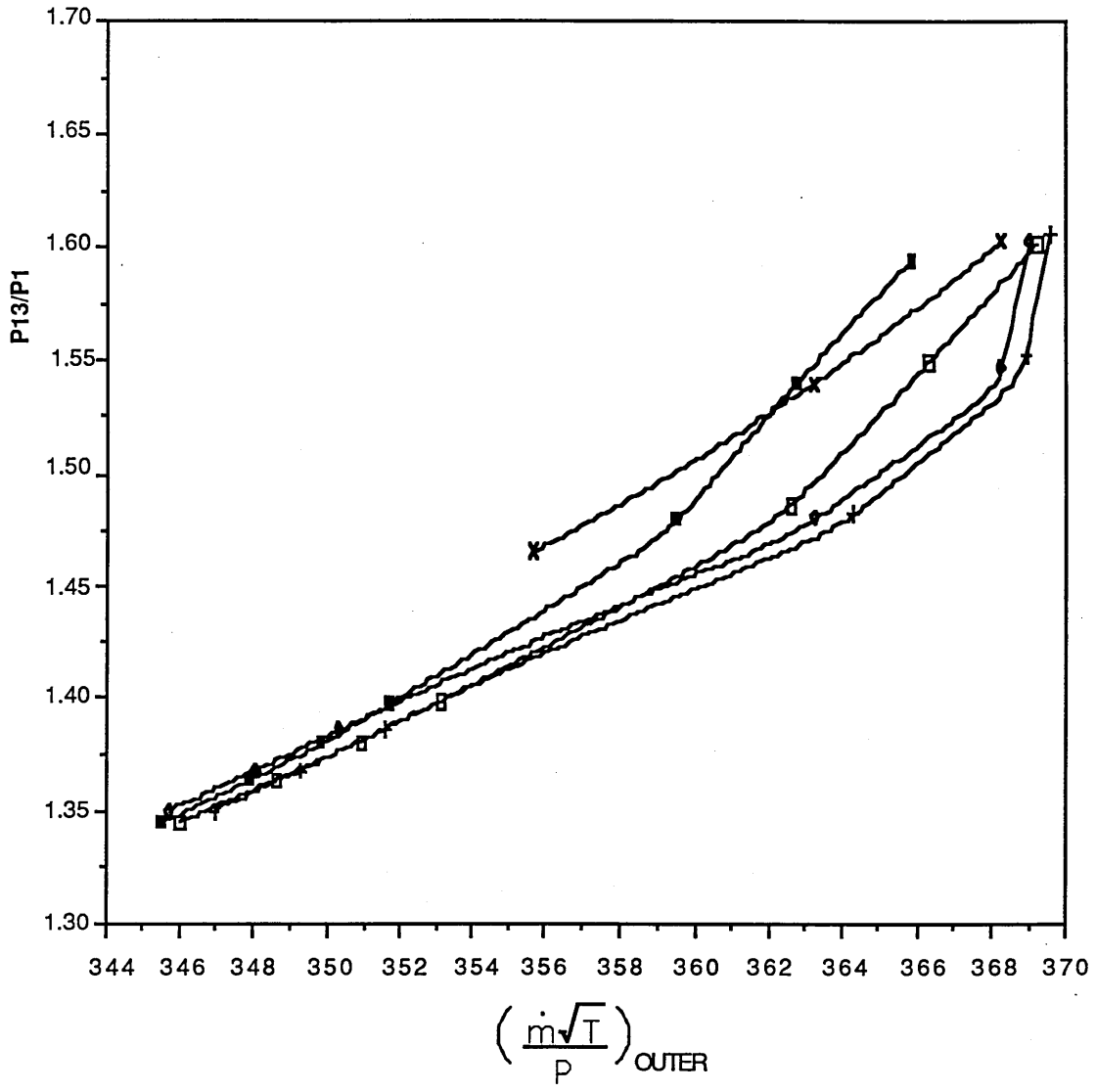

+ 1.(P13/P1)SR =AFCSP PROGRAM
× 2.(P13/P1)SR =FFCSP PROGRAM
◇ 3.(P13/P1)SR =AFSPOF PROGRAM
■ 4.(P13/P1)SR =STFFIX PROGRAM
□ 5.(P13/P1)SR =STKFAN PROGRAM

→ STEADY RUNNING RESULTS

FIGURE 52

TYPICAL TURBOFAN ENGINE

COMPARISON OF STEADY RUNNING RESULTS

AT SEA LEVEL, MACH = 0.2

FOR ALL 5 PROGRAMS

Data from "TABLE 11B"

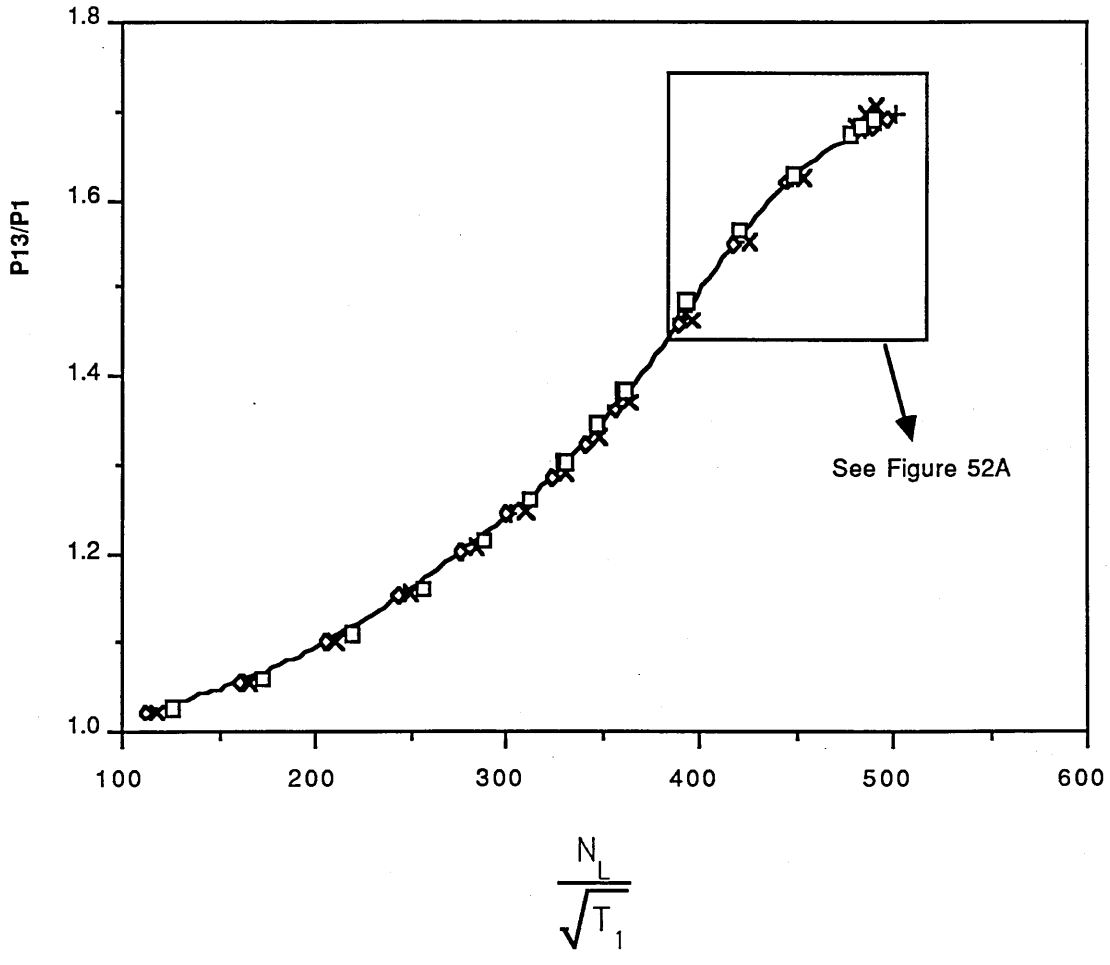

+ 1.(P13/P1)SR =AFCSP PROGRAM, STEADY RUNNING RESULTS
× 2.(P13/P1)SR =FFCSP PROGRAM, STEADY RUNNING RESULTS
◆ 3.(P13/P1)SR =AFSPOF PROGRAM, STEADY RUNNING RESULTS
■ 4.(P13/P1)SR =STFFIX PROGRAM, STEADY RUNNING RESULTS
□ 5.(P13/P1)SR =STKFAN PROGRAM, STEADY RUNNING RESULTS

FIGURE 52A

TYPICAL TURBOFAN ENGINE

COMPARISON OF STEADY RUNNING RESULTS
AT SEA LEVEL, MACH = 0.2

FOR ALL 5 PROGRAMS

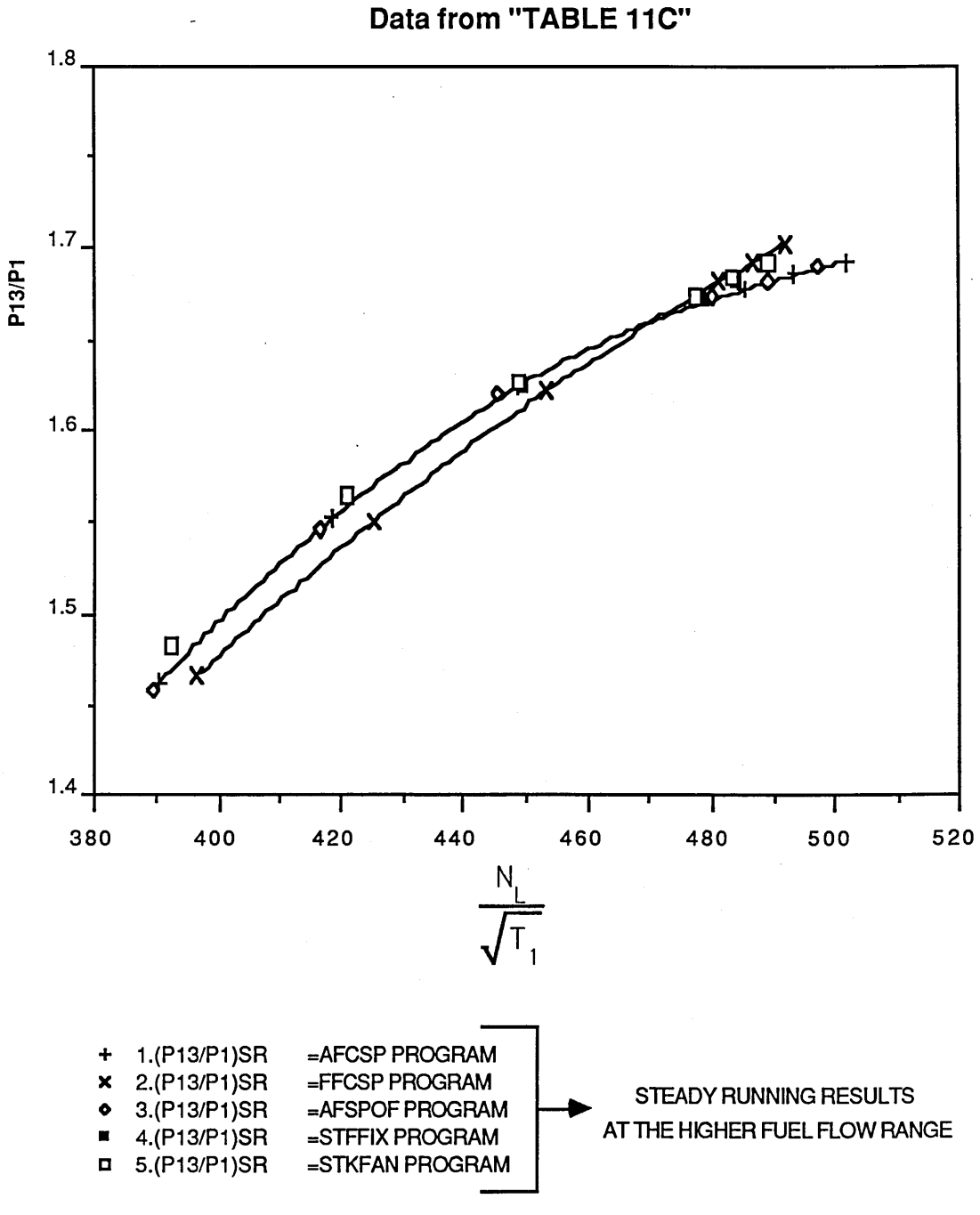

TYPICAL TURBOFAN ENGINE

COMPARISON OF DECELERATION RESULTS
AT SEA LEVEL, MACH = 0.2

FOR ALL 5 PROGRAMS
Data from "TABLES 11B & 11C"

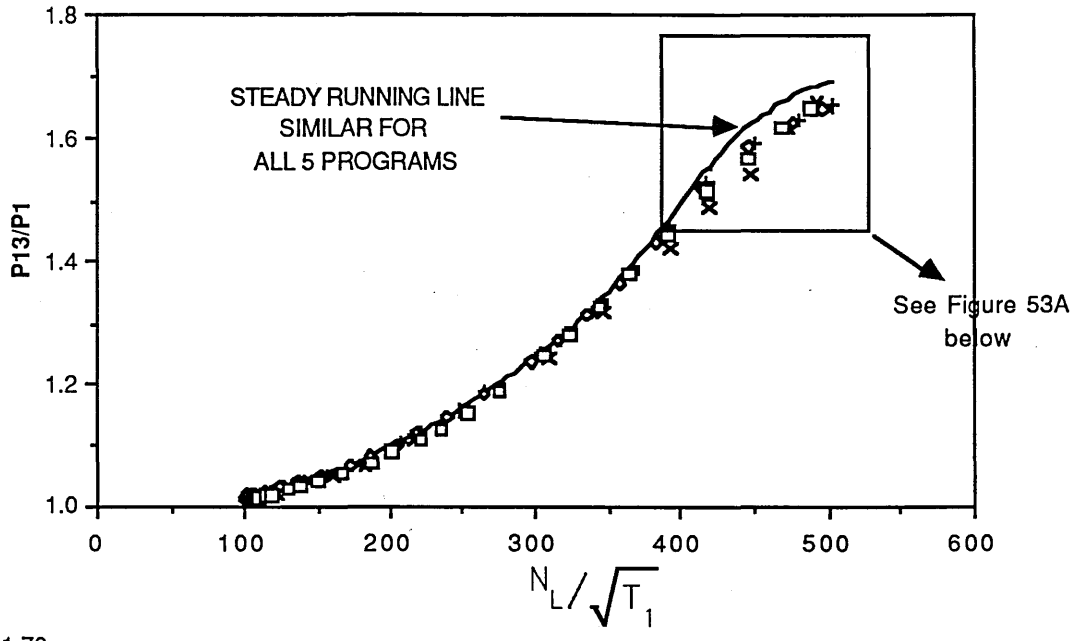

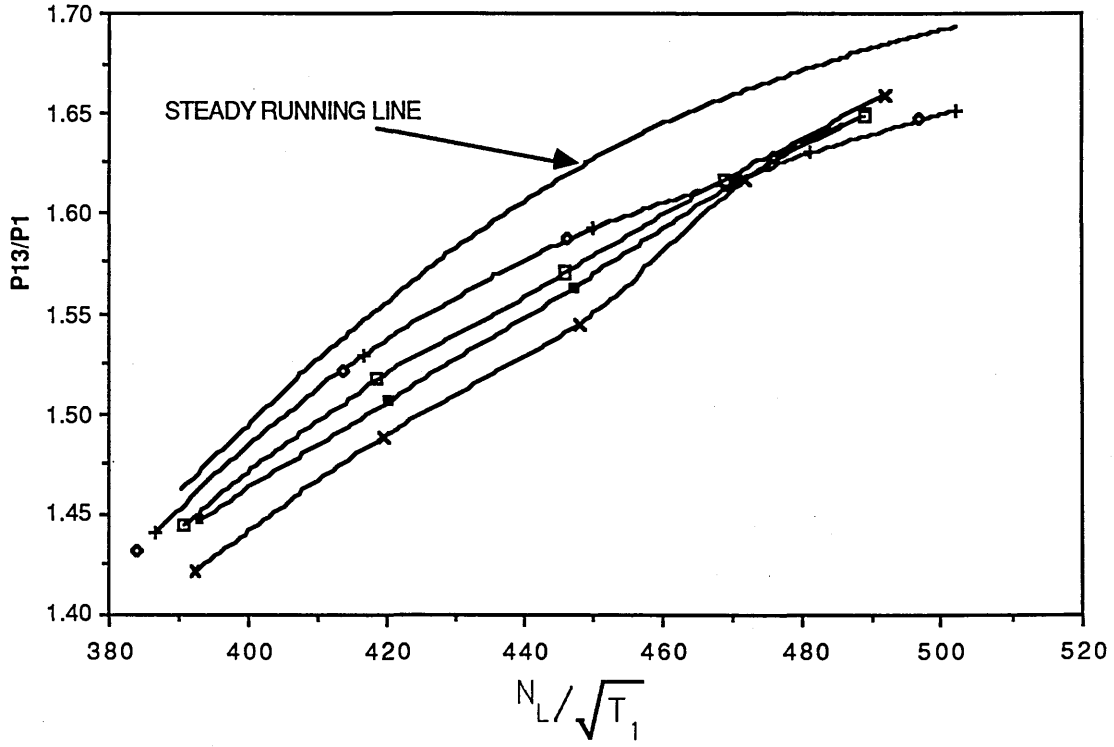

·	1.(P13/P1)SR	=AFCSP PROGRAM, STEADY RUNNING LINE
+	1.(P13/P1)Dc	=AFCSP PROGRAM, DECELERATION RESULTS
×	2.(P13/P1)Dc	=FFCSP PROGRAM, DECELERATION RESULTS
◇	3.(P13/P1)Dc	=AFSPOF PROGRAM, DECELERATION RESULTS
■	4.(P13/P1)Dc	=STFFIX PROGRAM, DECELERATION RESULTS
□	5.(P13/P1)Dc	=STKFAN PROGRAM, DECELERATION RESULTS

FIGURE 54

TYPICAL TURBOFAN ENGINE

COMPARISON OF STEADY RUNNING RESULTS
FOR ALL FIVE PROGRAMS
AT: 43,000ft., MACH = 0.8

Data from "TABLE 14 & 14A"

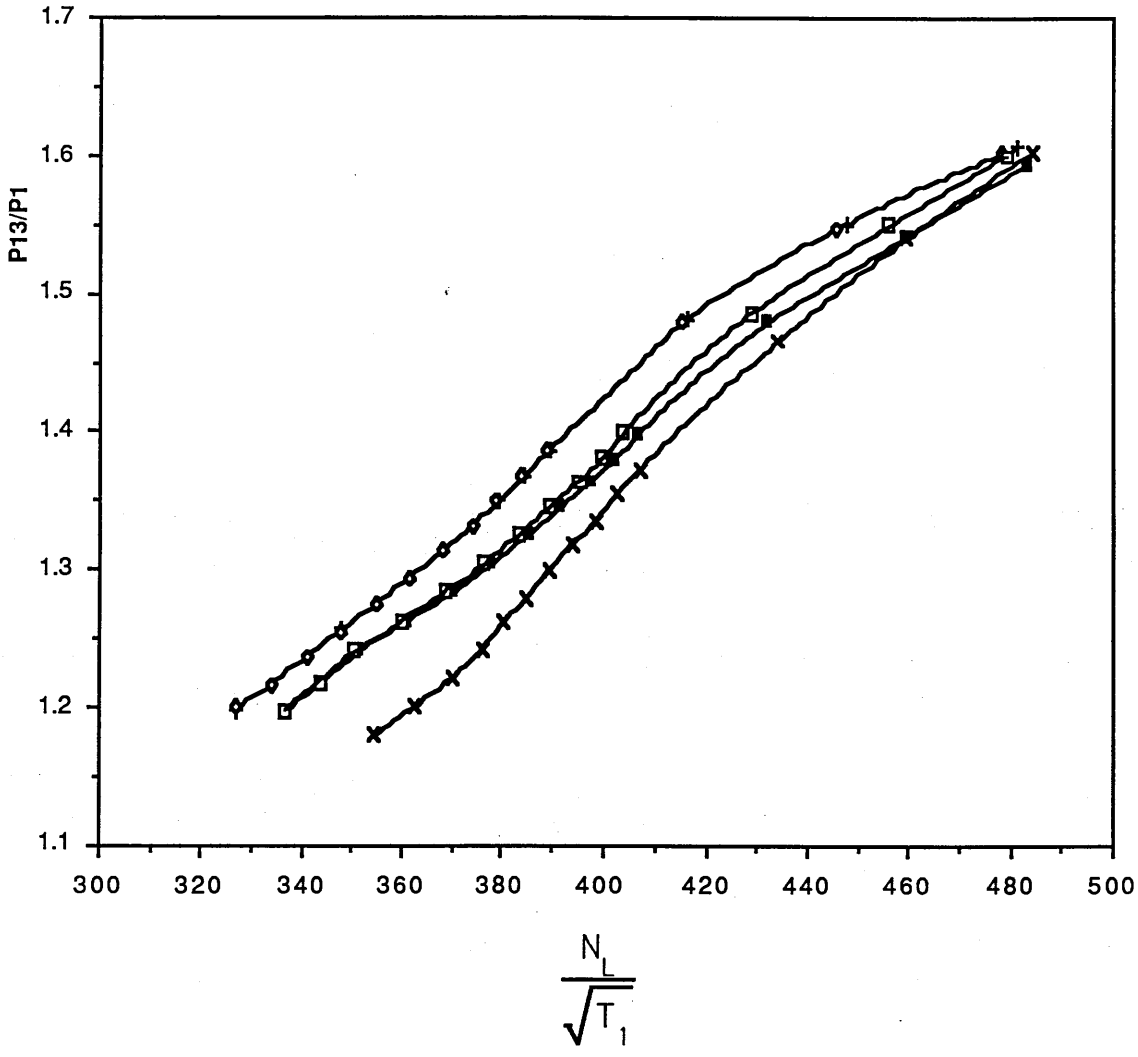

+ 1.(P13/P1)SR =AFCSP PROGRAM
× 2.(P13/P1)SR =FFCSP PROGRAM
◇ 3.(P13/P1)SR =AFSPOF PROGRAM
■ 4.(P13/P1)SR =STFFIX PROGRAM
□ 5.(P13/P1)SR =STKFAN PROGRAM

→ STEADY RUNNING RESULTS

FIGURE 55

TYPICAL TURBOFAN ENGINE

COMPARISON OF DECELERATION RESULTS
OF ALL FIVE PROGRAMS
AT : 43,000ft., MACH = 0.8

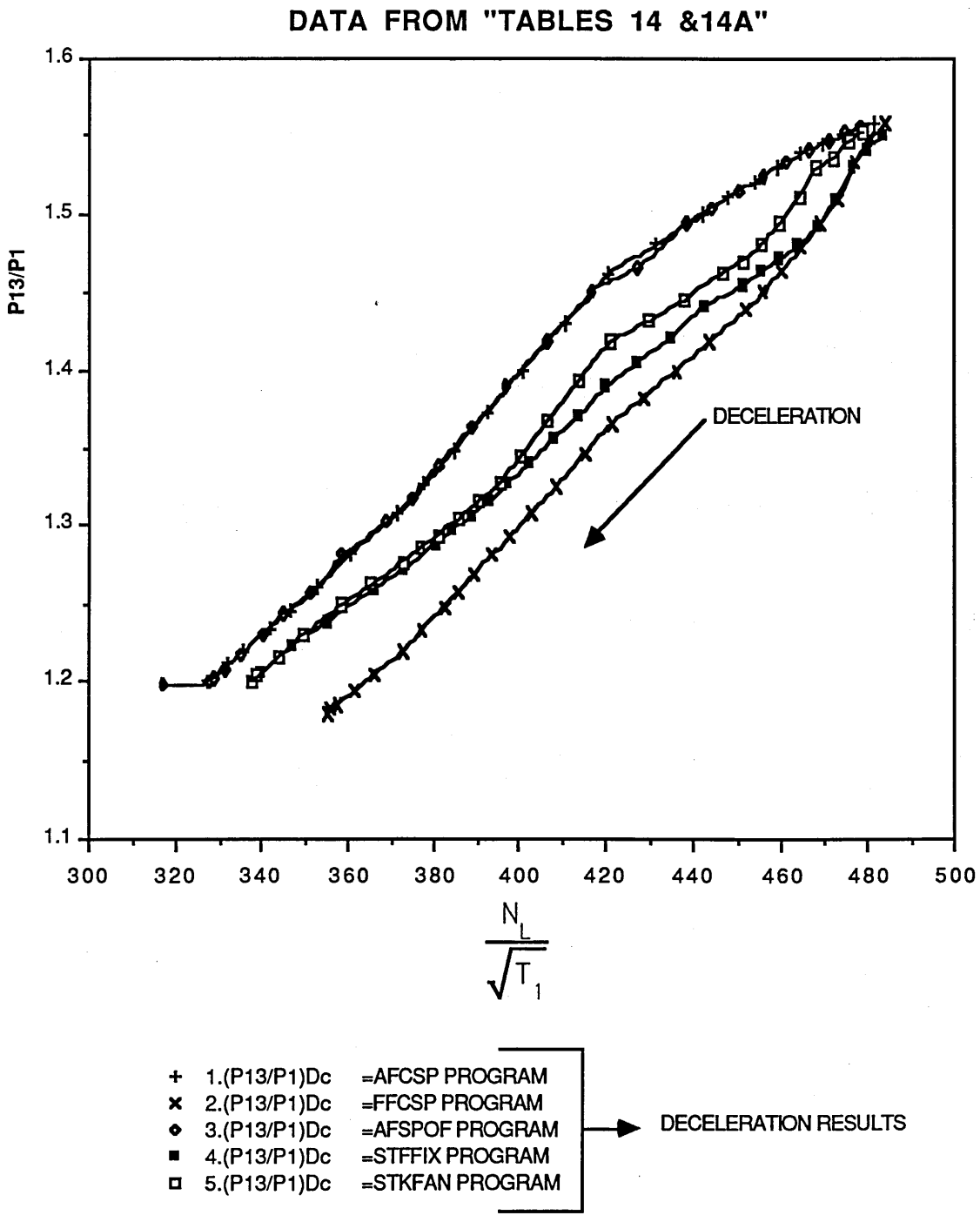

TYPICAL TURBOFAN ENGINE

COMPARISON OF ACCELERATION RESULTS AT SEA LEVEL, MACH = 0.2 FOR ALL 5 PROGRAMS

Data from "TABLES 11B & 11C"

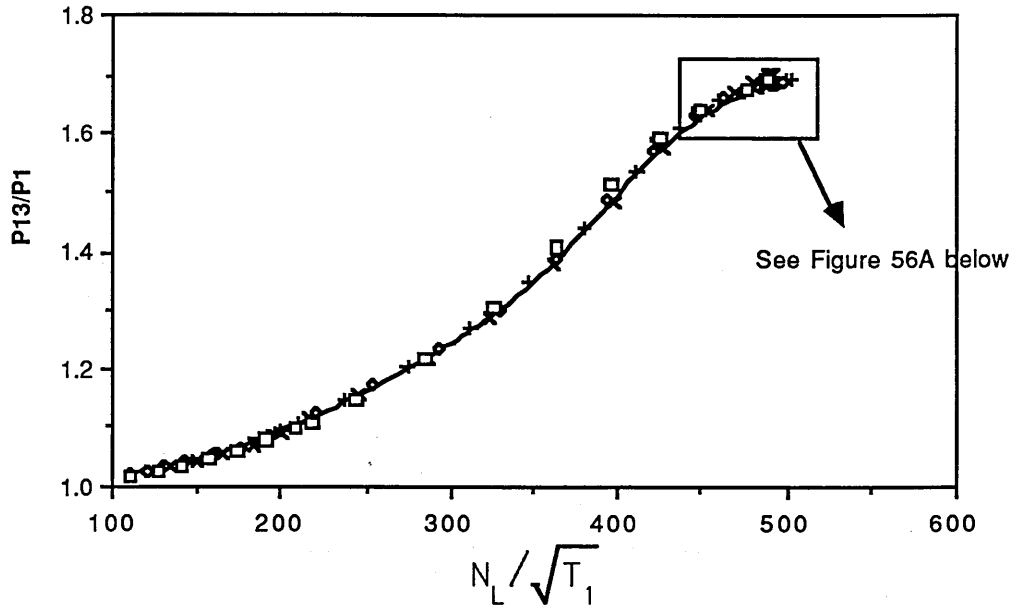

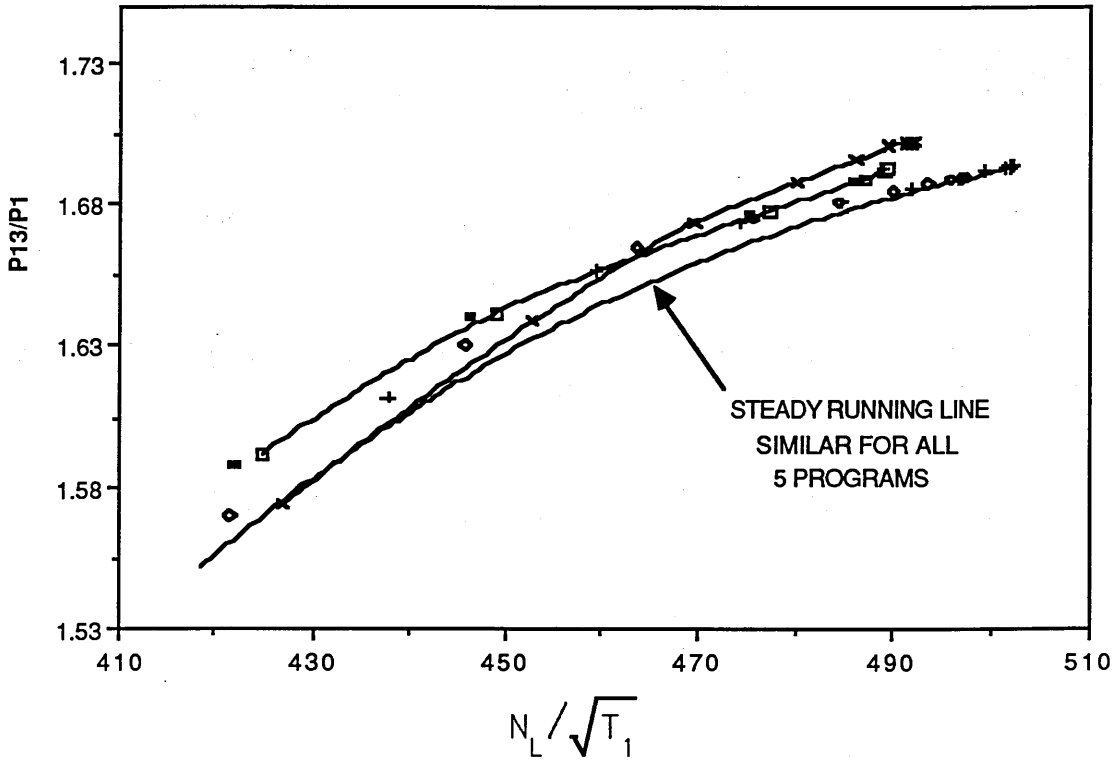

·	1.(P13/P1)SR	=AFCSP PROGRAM, STEADY RUNNING RESULTS
+	1.(P13/P1)Ac	=AFCSP PROGRAM, ACCELERATION RESULTS
×	2.(P13/P1)Ac	=FFCSP PROGRAM, ACCELERATION RESULTS
◇	3.(P13/P1)Ac	=AFSPOF PROGRAM, ACCELERATION RESULTS
■	4.P13/P1)Ac	=STFFIX PROGRAM, ACCELERATION RESULTS
□	5.(P13/P1)Ac	=STKFAN PROGRAM, ACCELERATION RESULTS

FIGURE 57

TYPICAL TURBOFAN ENGINE

COMPARISON OF ACCELERATION RESULTS

FOR ALL FIVE PROGRAMS

AT : 43,000ft., MACH = 0.8

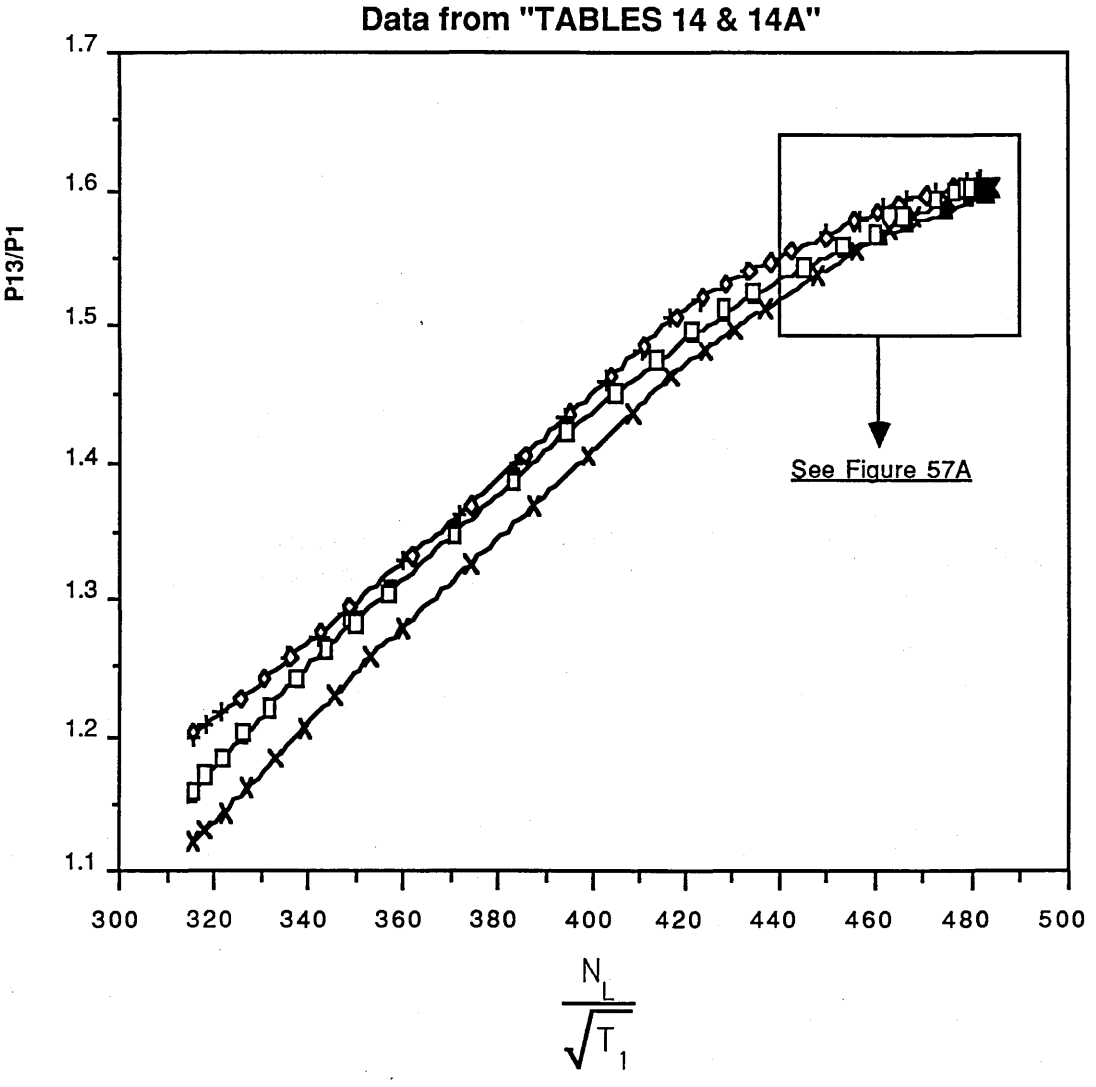

+ 1.(P13/P1)Ac =AFCSP PROGRAM, ACCELERATION RESULTS
× 2.(P13/P1)Ac =FFCSP PROGRAM, ACCELERATION RESULTS
◇ 3.(P13/P1)Ac =AFSPOF PROGRAM, ACCELERATION RESULTS
■ 4.(P13/P1)Ac =STFFIX PROGRAM, ACCELERATION RESULTS
□ 5.(P13/P1)Ac =STKFAN PROGRAM, ACCELERATION RESULTS

FIGURE 57A

ENLARGED SECTION OF FIGURE 57

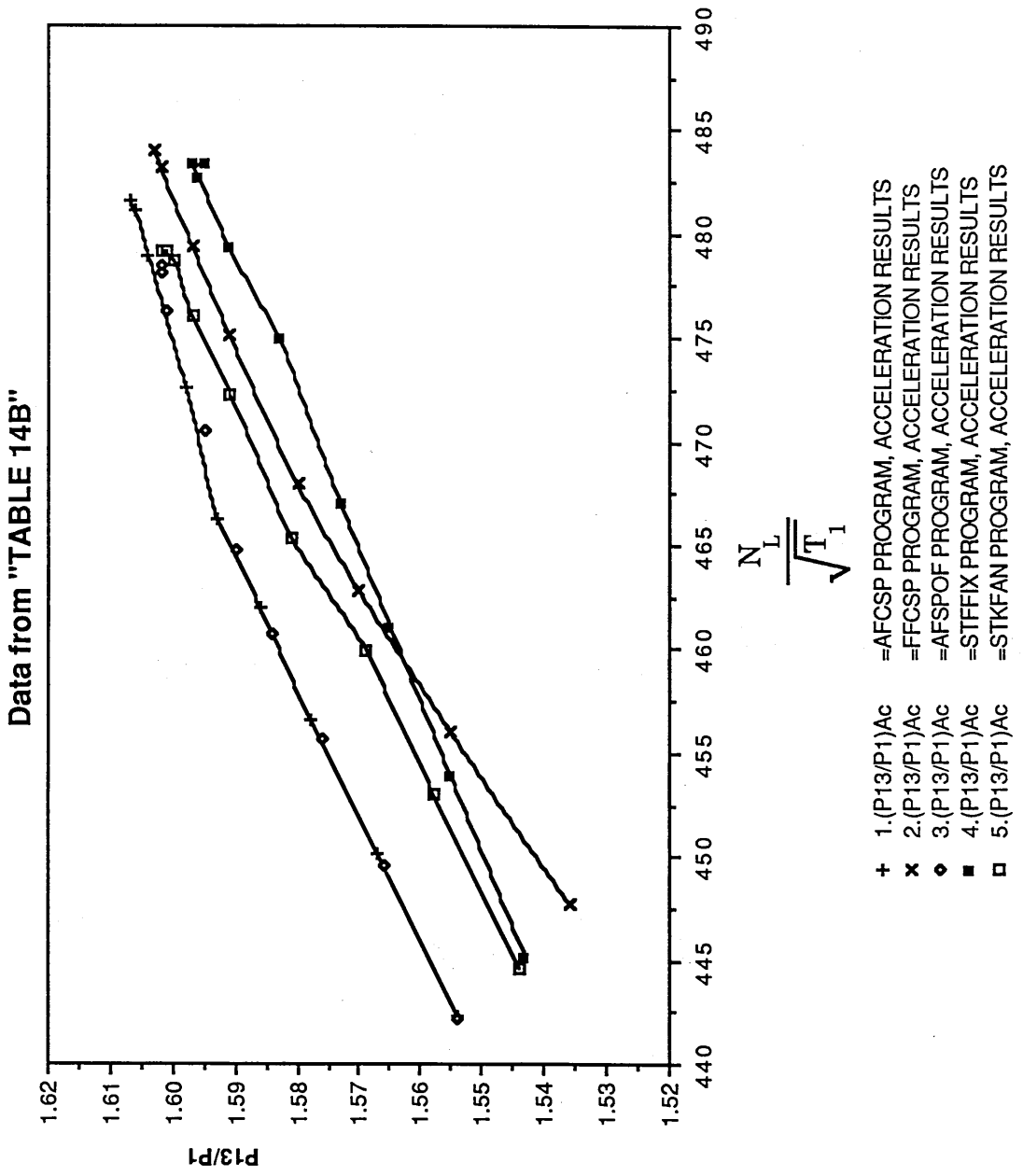

FIGURE 58

TYPICAL TURBOFAN ENGINE

COMPARISON OF DECELERATION TRAJECTORIES
FOR ALL FIVE PROJECTS
AT: 43,000ft., MACH = 0.8

Data from "TABLES 14 & 14A"

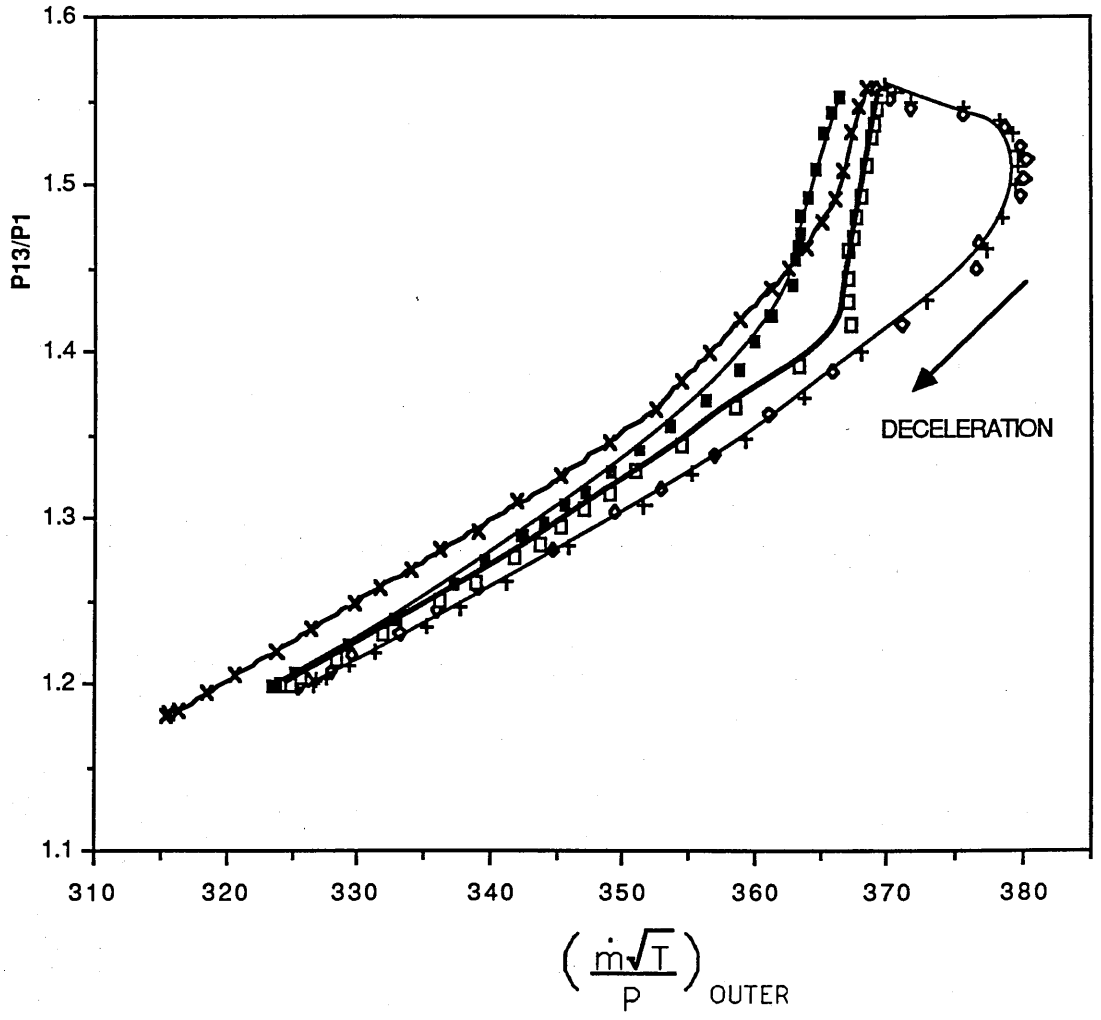

+	1.(P13/P1)Dc	=AFCSP PROGRAM DECELERATION RESULTS
×	2.(P13/P1)Dc	=FFCSP PROGRAM DECELERATION RESULTS
◇	3.(P13/P1)Dc	=AFSPOF PROGRAM DECELERATION RESULTS
■	4.(P13/P1)Dc	=STFFIX PROGRAM DECELERATION RESULTS
□	5.(P13/P1)Dc	=STKFAN PROGRAM DECELERATION RESULTS

TYPICAL TURBOFAN ENGINE

COMPARISON OF DECELERATION RESULTS FOR ALL FIVE PROGRAMS

AT : 43,000ft., MACH = 0.8

Data from "TABLE 14"

$\left(\frac{\dot{m}\sqrt{T}}{P}\right)_{OUTER}$

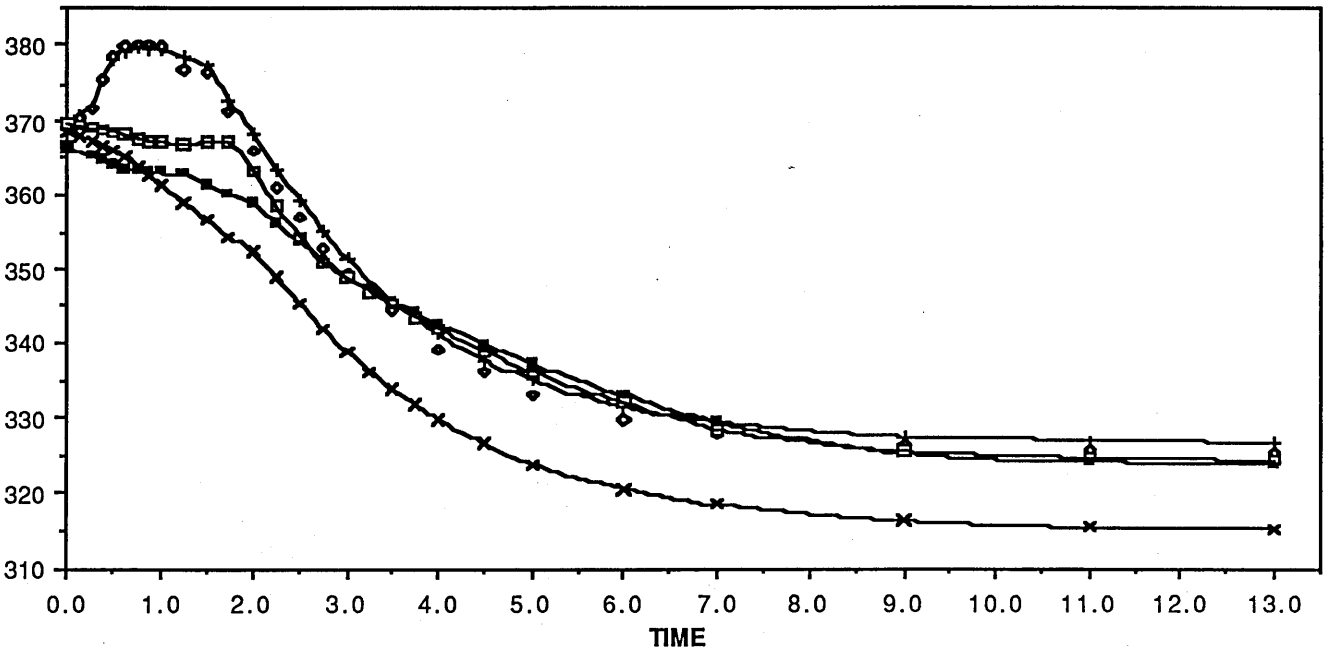

+ 1.(P13/P1)Dc =AFCSP PROGRAM
× 2.(P13/P1)Dc =FFCSP PROGRAM
◇ 3.(P13/P1)Dc =AFSPOF PROGRAM
■ 4.(P13/P1)Dc =STFFIX PROGRAM
□ 5.(P13/P1)Dc =STKFAN PROGRAM

→ DECELERATION RESULTS

FIGURE 59

TYPICAL TURBOFAN ENGINE

COMPARISON OF THE OUTER FAN PRESSURE RATIO DROP WITH TIME

DURING THE FIRST SECOND OF THE DECELERATION

Data from "Table 13A"

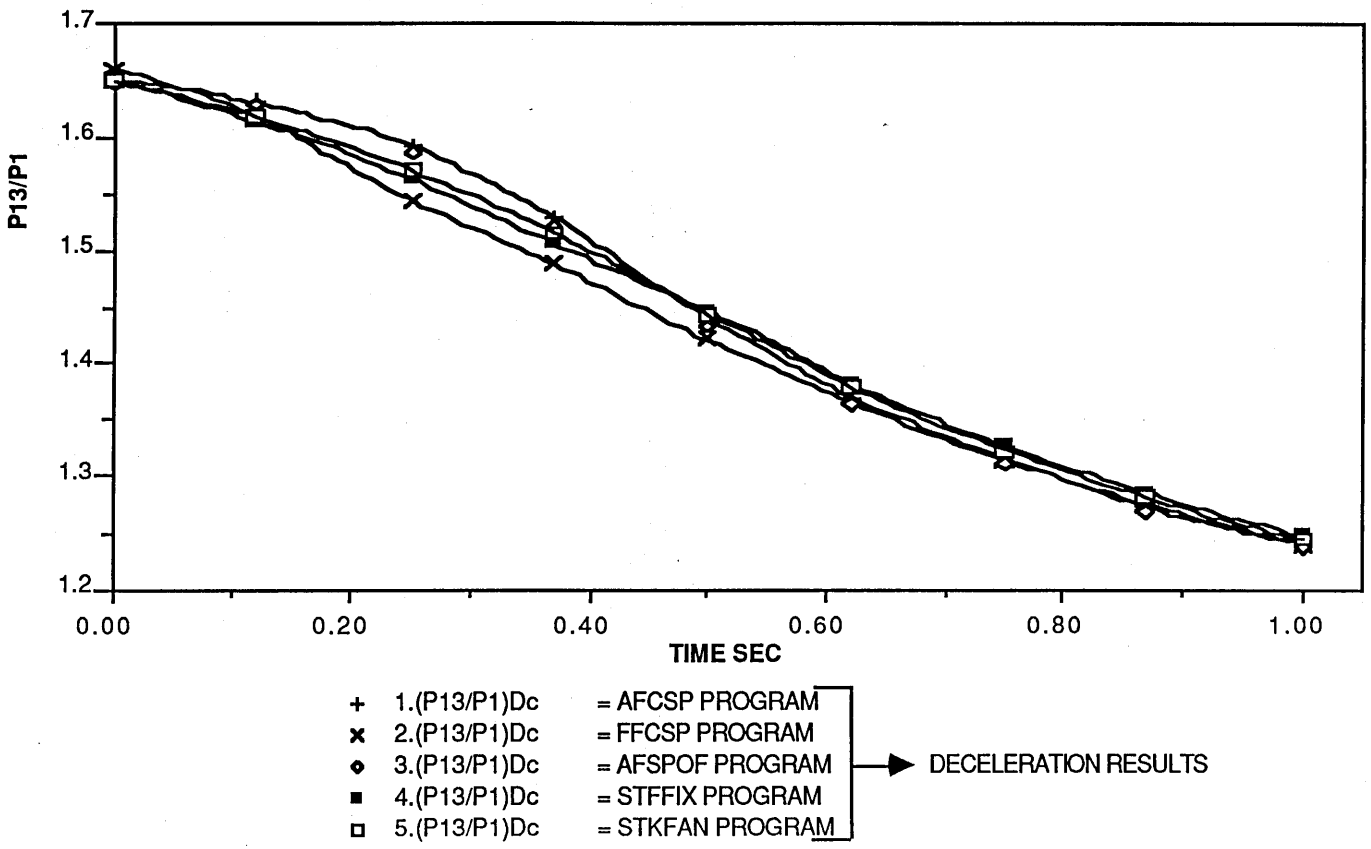

FIGURE 60

FIGURE 61

TYPICAL TURBOFAN ENGINE

COMPARISON OF THRUST RESPONSE WITH TIME
FOR ALL FIVE PROGRAMS
DURING AN ACCELERATION AT : 43,000ft., MACH = 0.8

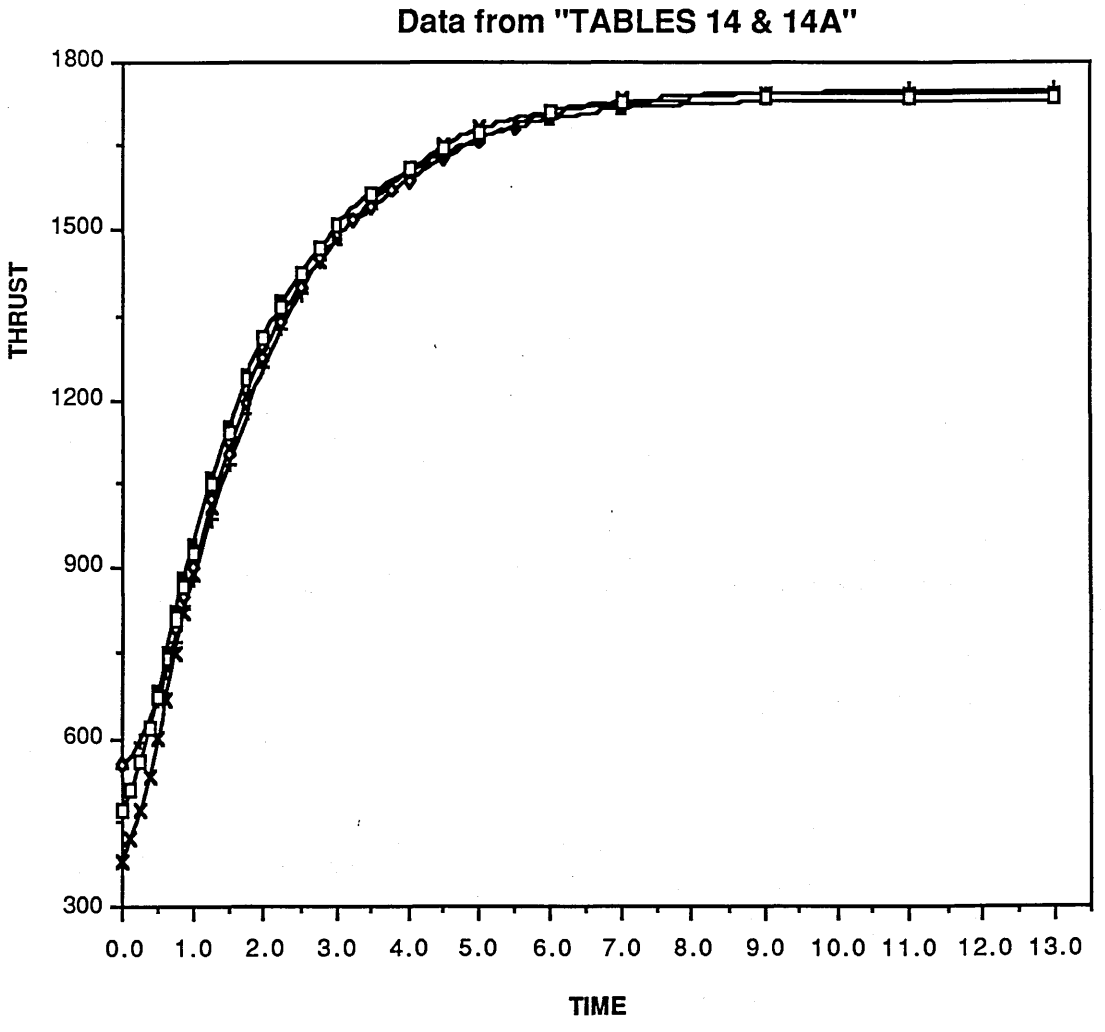

+ 1.(THRUST)Ac = AFCSP PROGRAM, ACCELERATION RESULTS
× 2.(THRUST)Ac = FFCSP PROGRAM, ACCELERATION RESULTS
◇ 3.(THRUST)Ac = AFSPOF PROGRAM, ACCELERATION RESULTS
■ 4.(THRUST)Ac = STFFIX PROGRAM, ACCELERATION RESULTS
□ 5.(THRUST)Ac = STKFAN PROGRAM, ACCELERATION RESULTS

FIGURE 62

TYPICAL TURBOFAN ENGINE

COMPARISON OF H.P. COMPRESSOR WORKING LINES

AT : SEA LEVEL, MACH = 0.2

FOR ALL 5 PROGRAMS

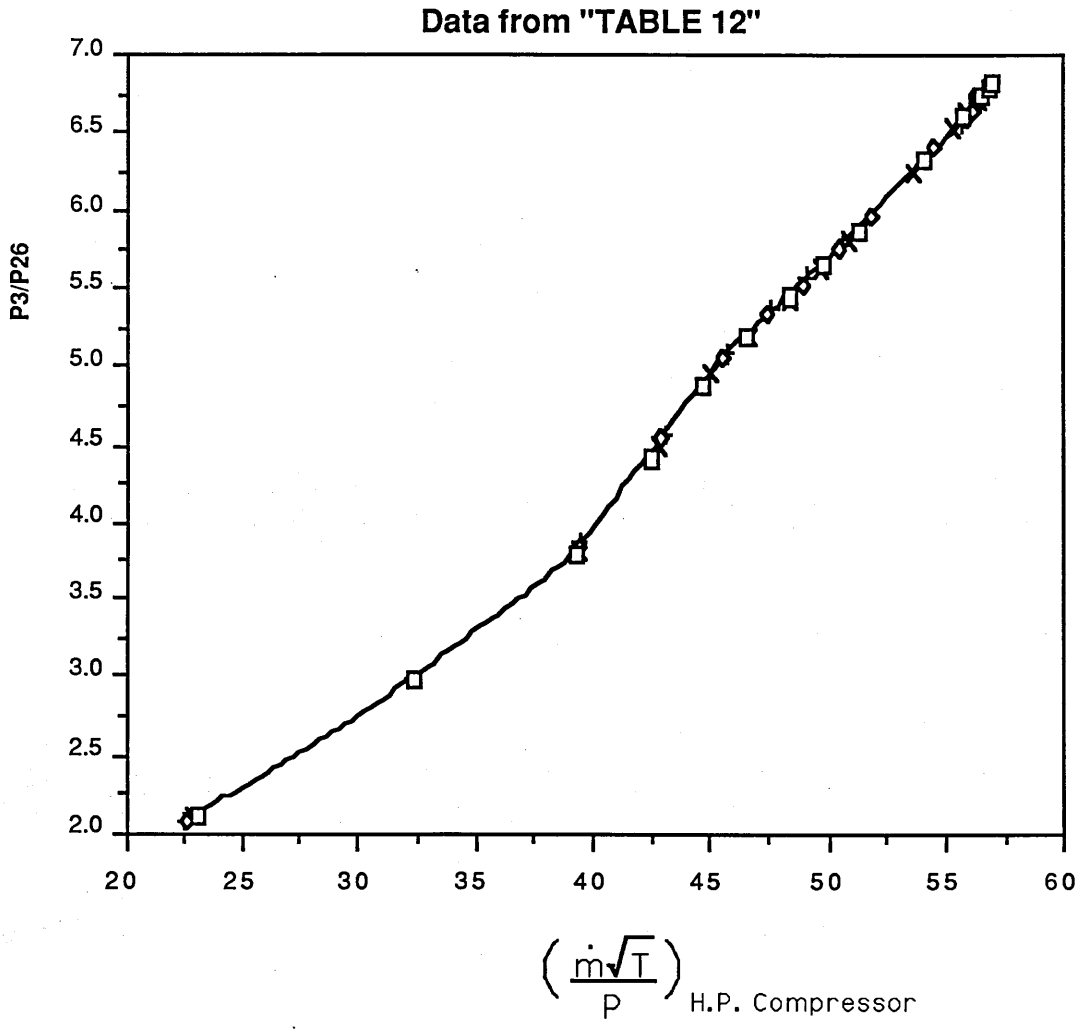

FIGURE 63

TYPICAL TURBOFAN ENGINE

COMPARISON OF H.P. COMPRESSOR TRANSIENT TRAJECTORIES

AT SEA LEVEL, MACH = 0.2

FOR ALL 5 PROGRAMS

Data from "TABLE 12"

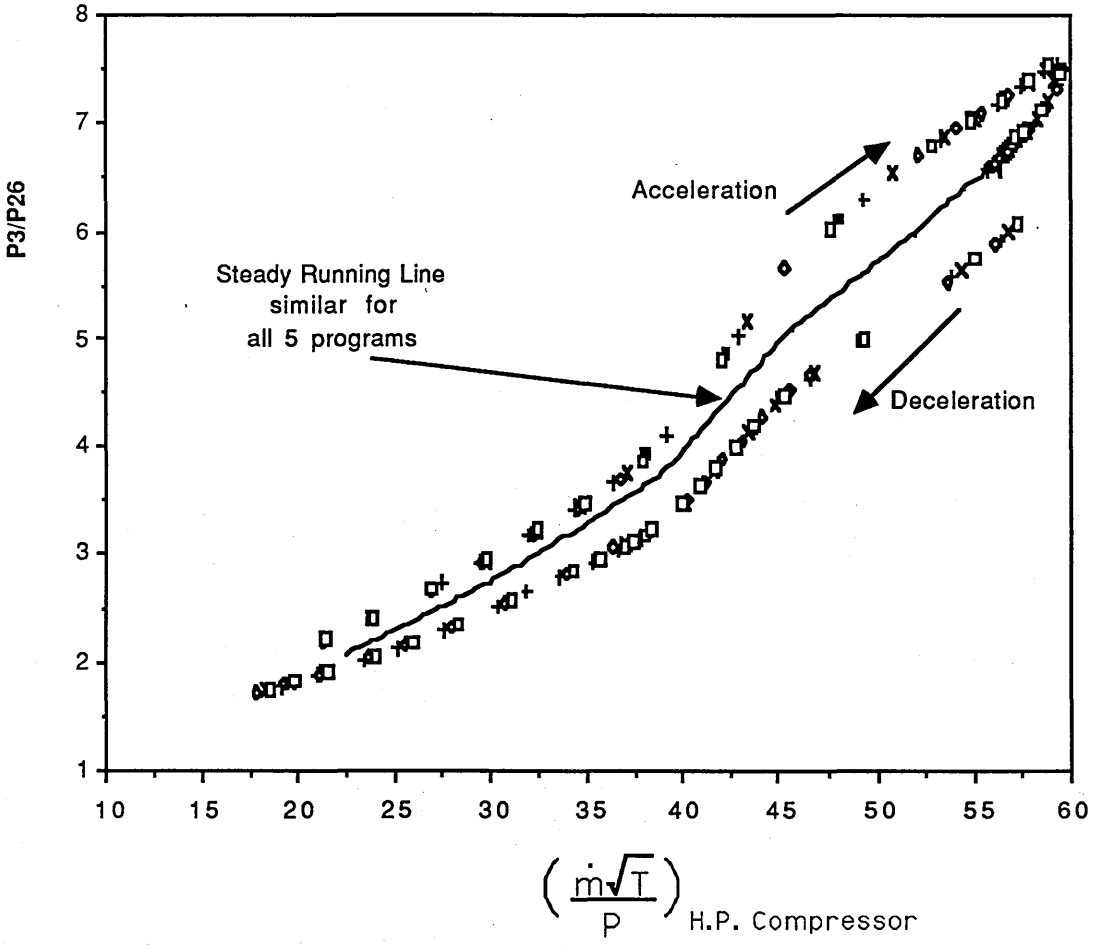

·	1.(P3/P26)SR	=AFCSP PROGRAM, STEADY RUNNING LINE
+	1.(P3/P26)Ac	=AFCSP PROGRAM, ACCELERATION AND DECELERATION RESULTS
×	2.(P3/P26)Ac	=FFCSP PROGRAM, ACCELERATION AND DECELERATION RESULTS
◆	3.(P3/P26)Ac	=AFSPOF PROGRAM, ACCELERATION AND DECELERATION RESULTS
■	4.(P3/P26)Ac	=STFFIX PROGRAM, ACCELERATION AND DECELERATION RESULTS
□	5.(P3/P26)Ac	=STKFAN PROGRAM, ACCELERATION AND DECELERATION RESULTS

FIGURE 64

TYPICAL TURBOFAN ENGINE

COMPARISON OF CHANGE OF THRUST WITH TIME DURING A DECELERATION AT : SEA LEVEL, MACH = 0.2

FOR ALL 5 PROGRAMS

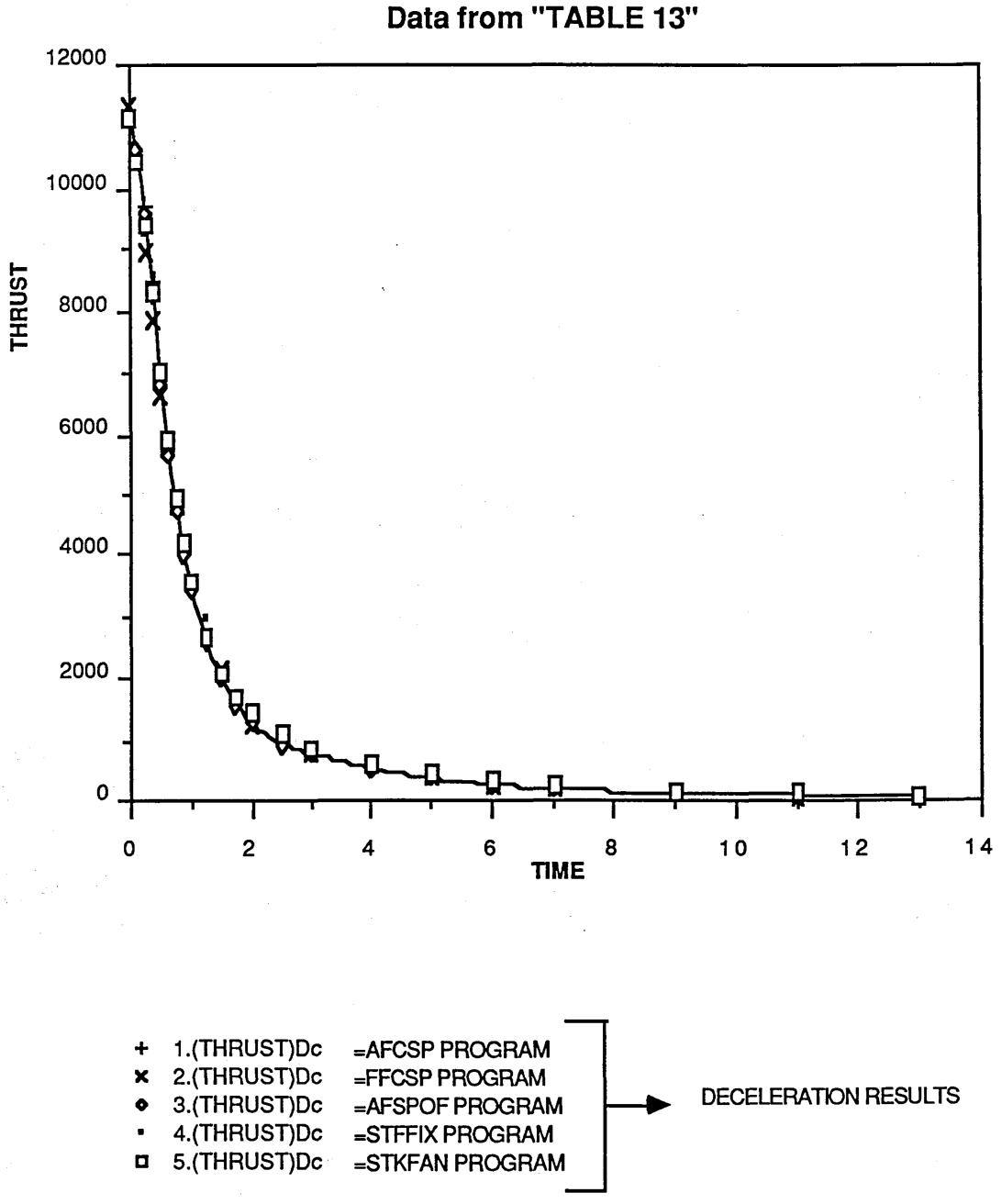

FIGURE 65

TYPICAL TURBOFAN ENGINE

COMPARISON OF CHANGE OF THRUST WITH TIME DURING ACCELERATION AT: SEA LEVEL, MACH=0.2 FOR ALL FIVE PROGRAMS

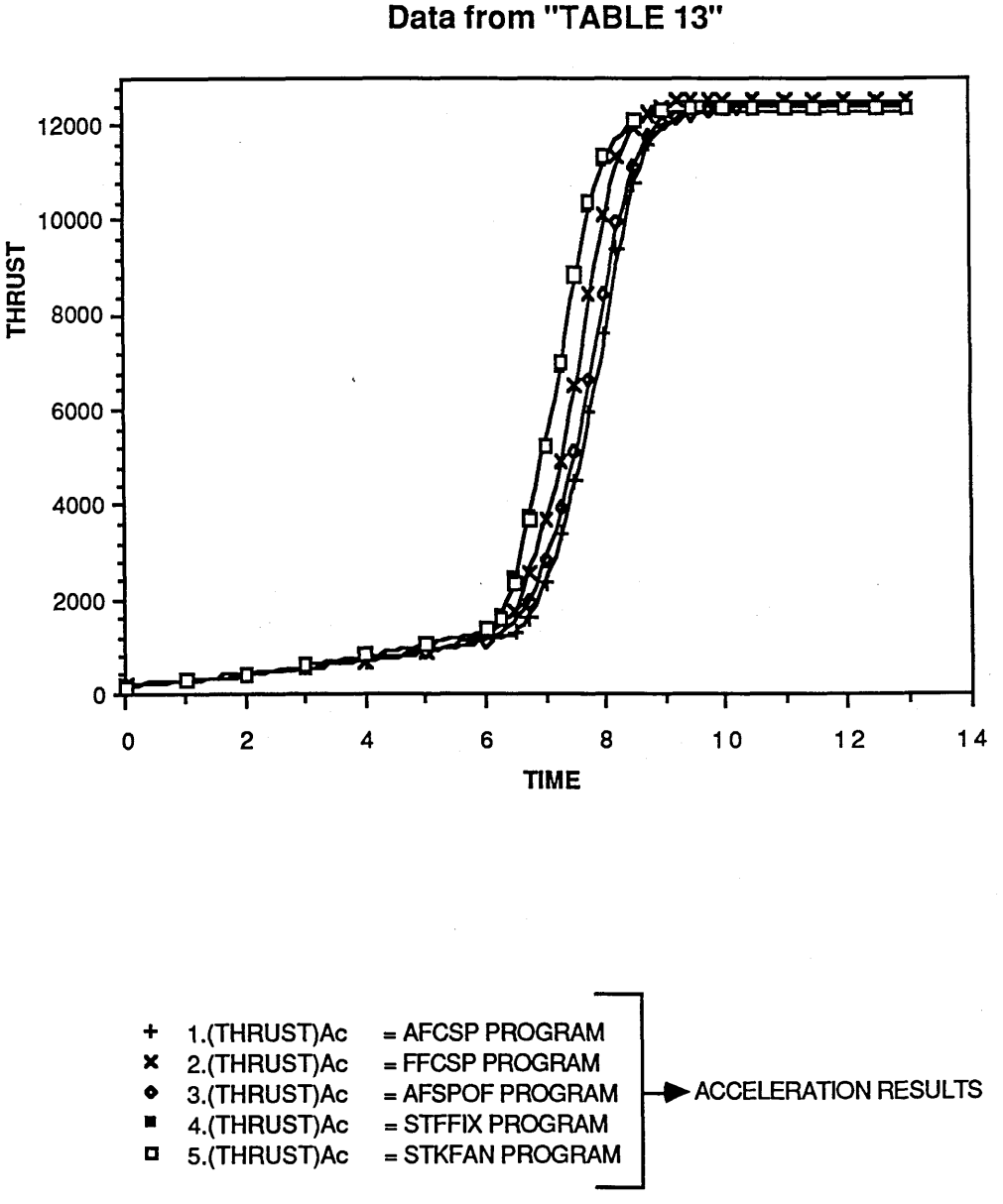

FIGURE 65A

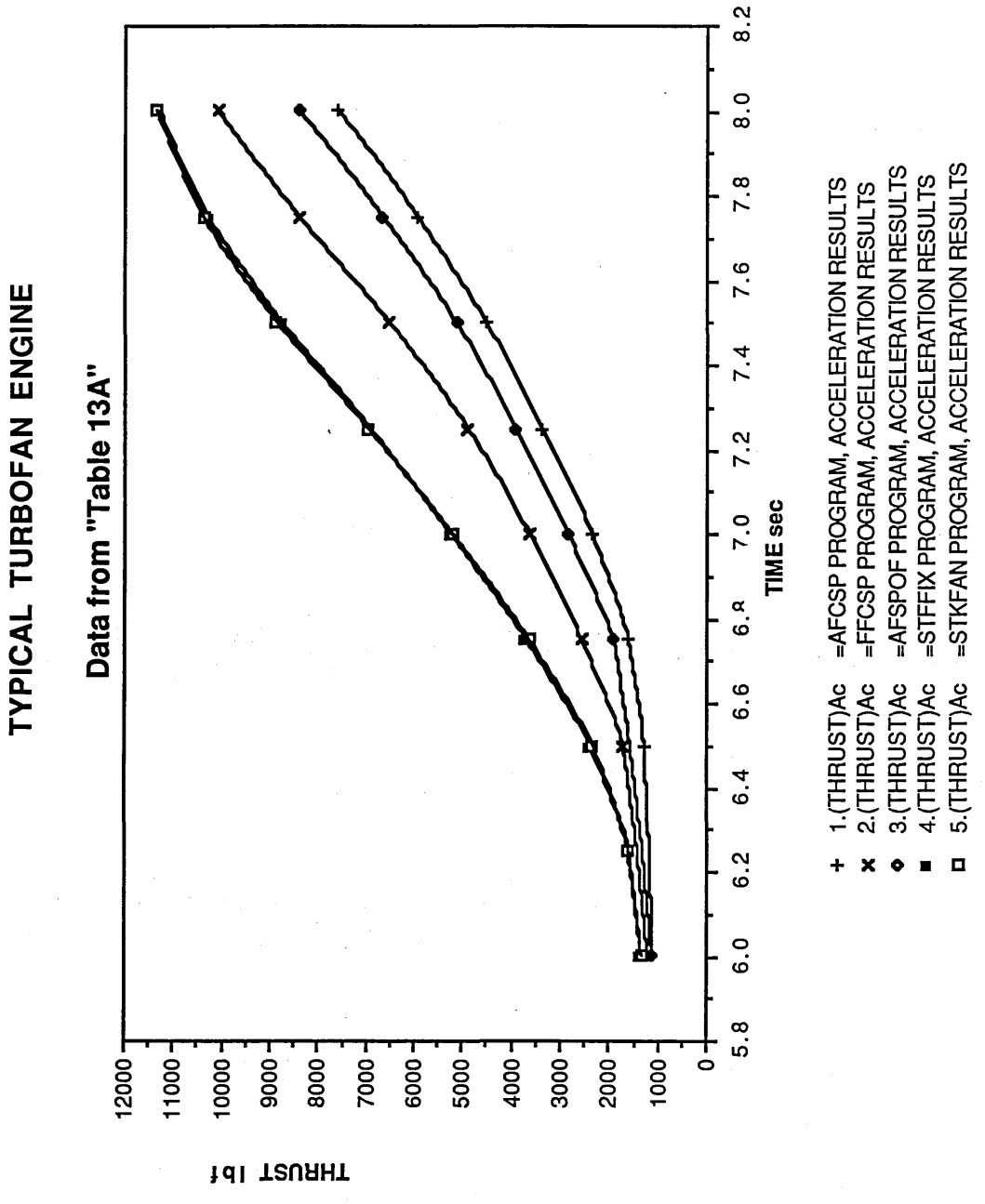
TYPICAL TURBOFAN ENGINE
Data from "Table 13A"
THRUST lbf
12000
11000
10000
9000
8000
7000
6000
5000
4000
3000
2000
1000
0
5.8
6.0
6.2
6.4
6.6
6.8
7.0
7.2
7.4
7.6
7.8
8.0
8.2
TIME sec
+ 1.(THRUST)Ac =AFCSP PROGRAM, ACCELERATION RESULTS
× 2.(THRUST)Ac =FFCSP PROGRAM, ACCELERATION RESULTS
◆ 3.(THRUST)Ac =AFSPOF PROGRAM, ACCELERATION RESULTS
■ 4.(THRUST)Ac =STFFIX PROGRAM, ACCELERATION RESULTS
□ 5.(THRUST)Ac =STKFAN PROGRAM, ACCELERATION RESULTS

TYPICAL TURBOFAN ENGINE

FACTOR OF SPLIT VARIATION WITH TIME DURING A SEA LEVEL, MACH=0.2 DECELERATION

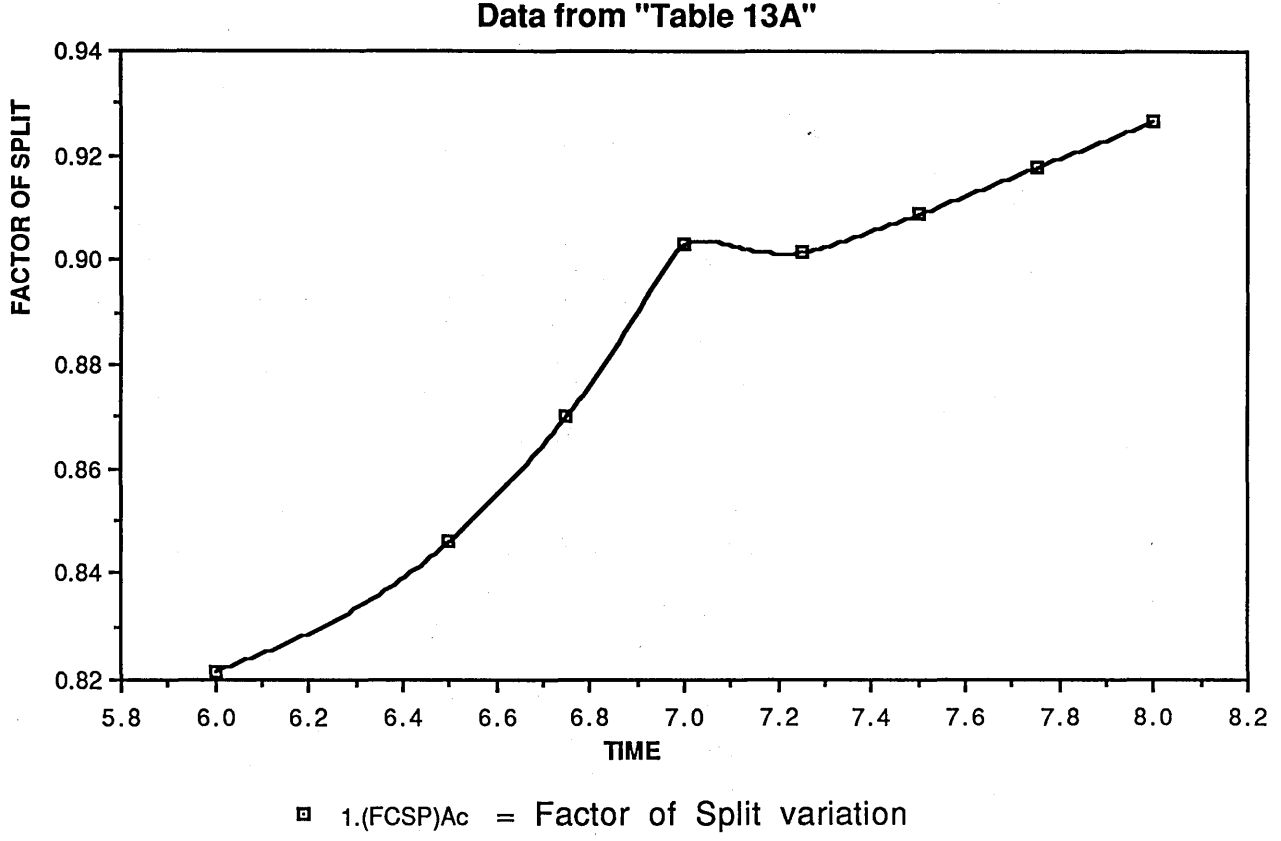

FIGURE 65B

TYPICAL TURBOFAN ENGINE

COMPARISON OF CHANGE OF L.P. AND H.P. SHAFT SPEEDS WITH THRUST DURING STEADY RUNNING AT SEA LEVEL, MACH=0.2 FOR DIFFERENT Cp EVALUATION METHODS

Data from "TABLE 15"

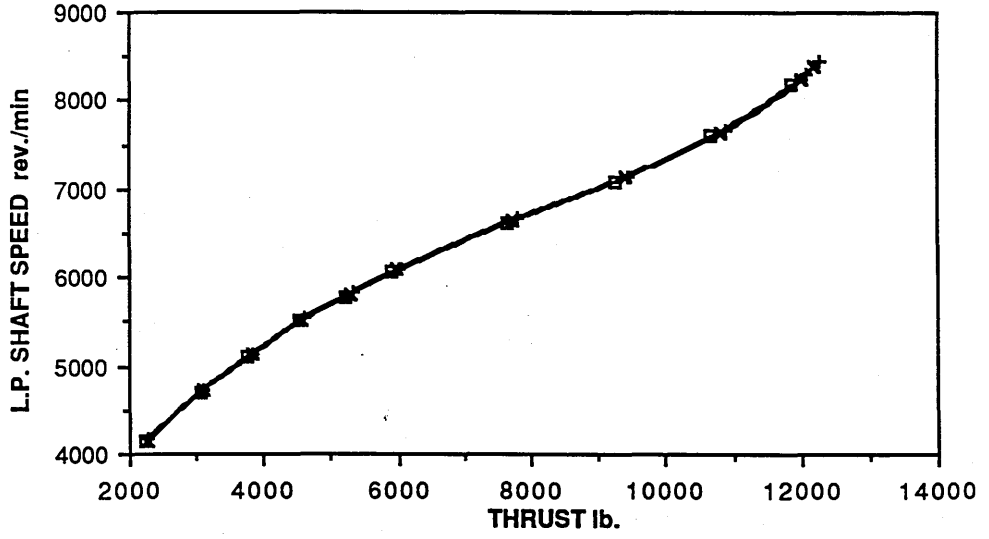

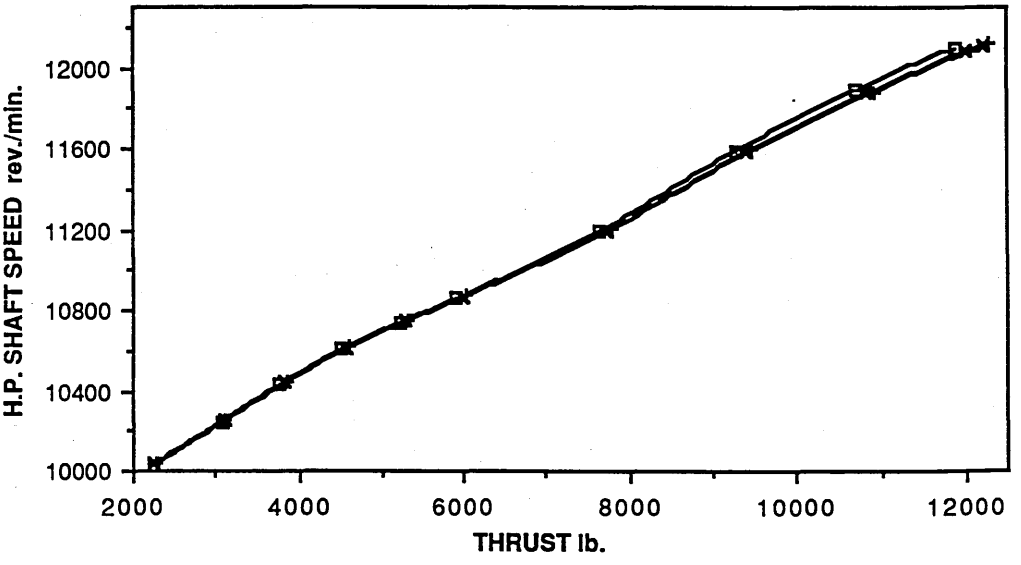

- ▫ NL.NC = No variation of Cp
- × NL.R = Once through calculation method of Cp
- \+ NL.IC = Successive approximations method

TYPICAL TURBOFAN ENGINE

COMPARISON OF CHANGE OF S.F.C. WITH THRUST DURING STEADY RUNNING
AT: SEA LEVEL, MACH=0.2
FOR DIFFERENT Cp EVALUATION METHODS

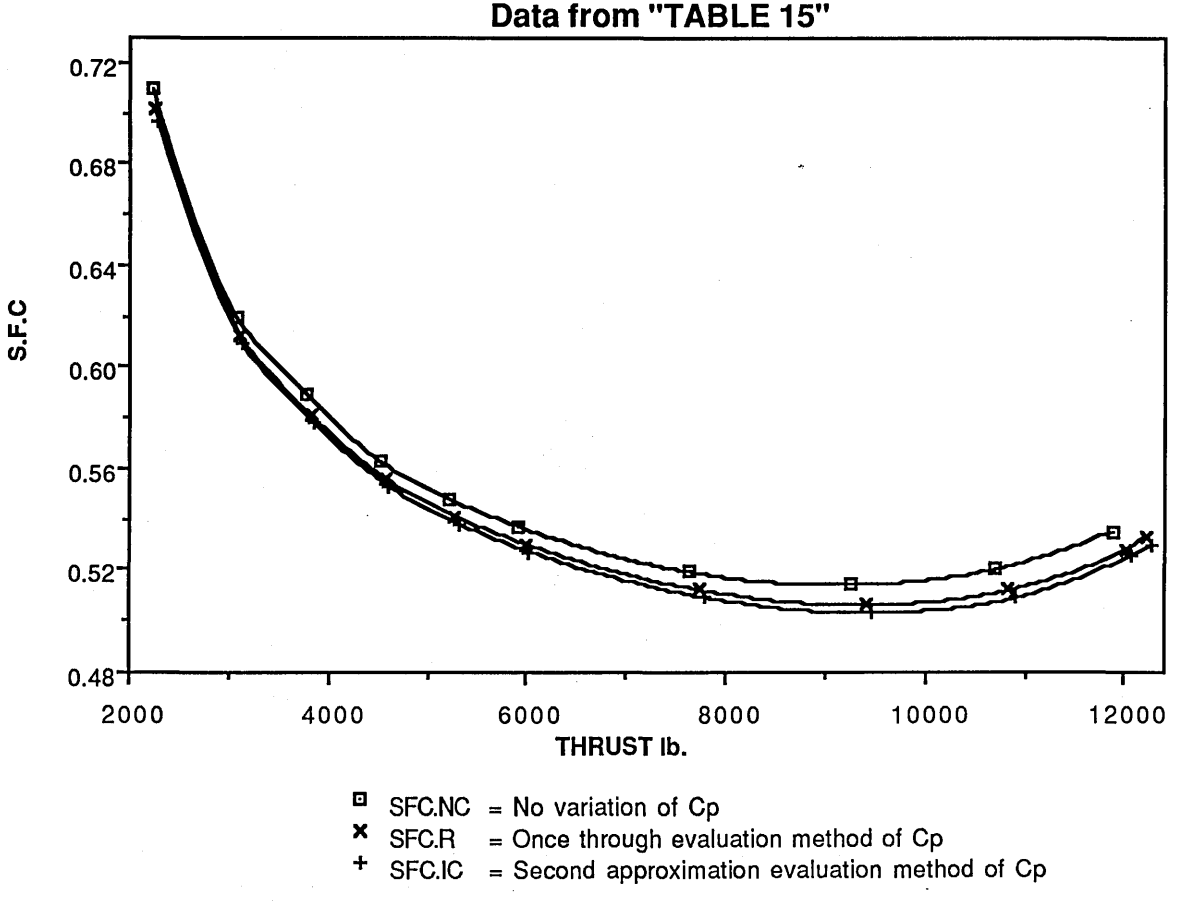

FIGURE 69

FIGURE 70

TYPICAL TURBOFAN ENGINE

COMBINED INNER FAN AND I.P. COMPRESSOR
COMPARISON OF STEADY RUNNING LINES BETWEEN
ADIABATIC AND NON-ADIABATIC PREDICTIONS OF
PROGRAM AFSREE
AT: SEA LEVEL, MACH=0.2

Data from "TABLE 18"

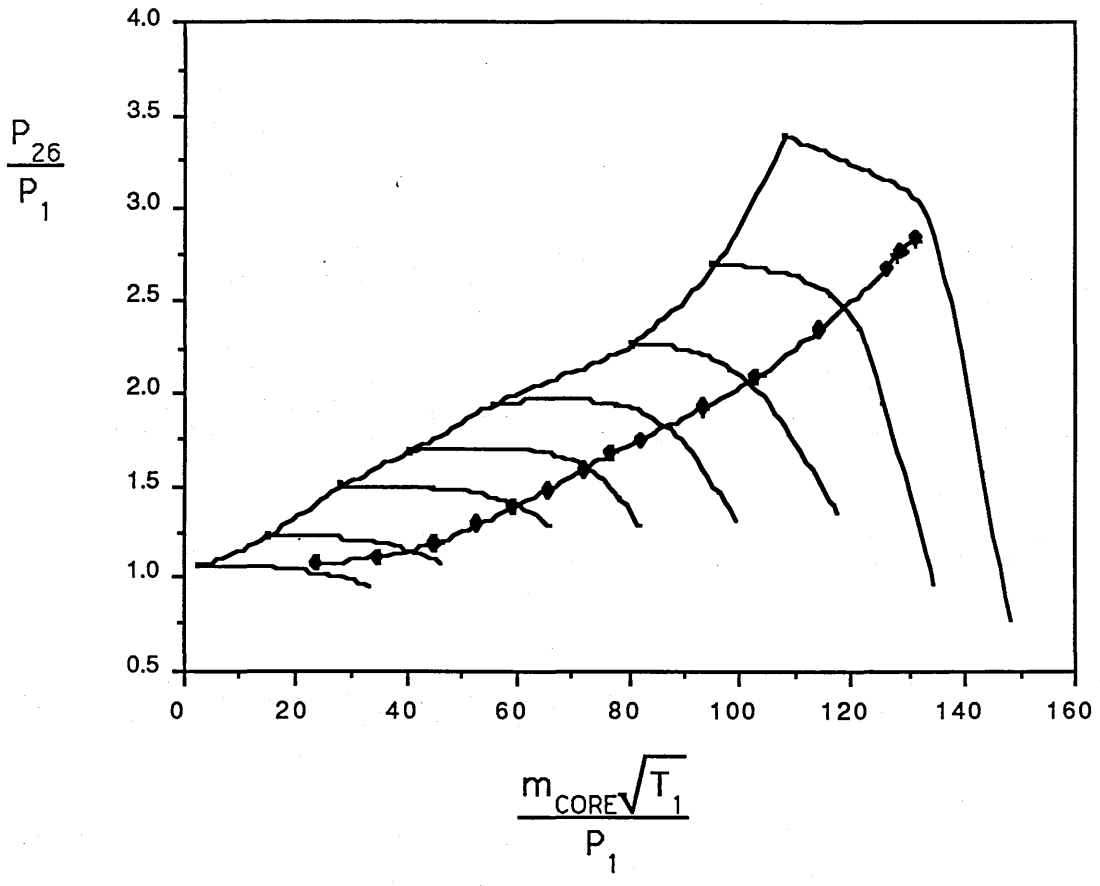

+ SR.PR-AD = ADIABATIC PREDICTIONS

◆ SR.PR-HT = PREDICTIONS INCLUDING HEAT TRANSFER EFFECTS

TYPICAL TURBOFAN ENGINE

COMBINED INNER FAN AND I.P. COMPRESSOR PREDICTIONS
AT SEA LEVEL, MACH=0.2

Data from "TABLES 18 & 21"

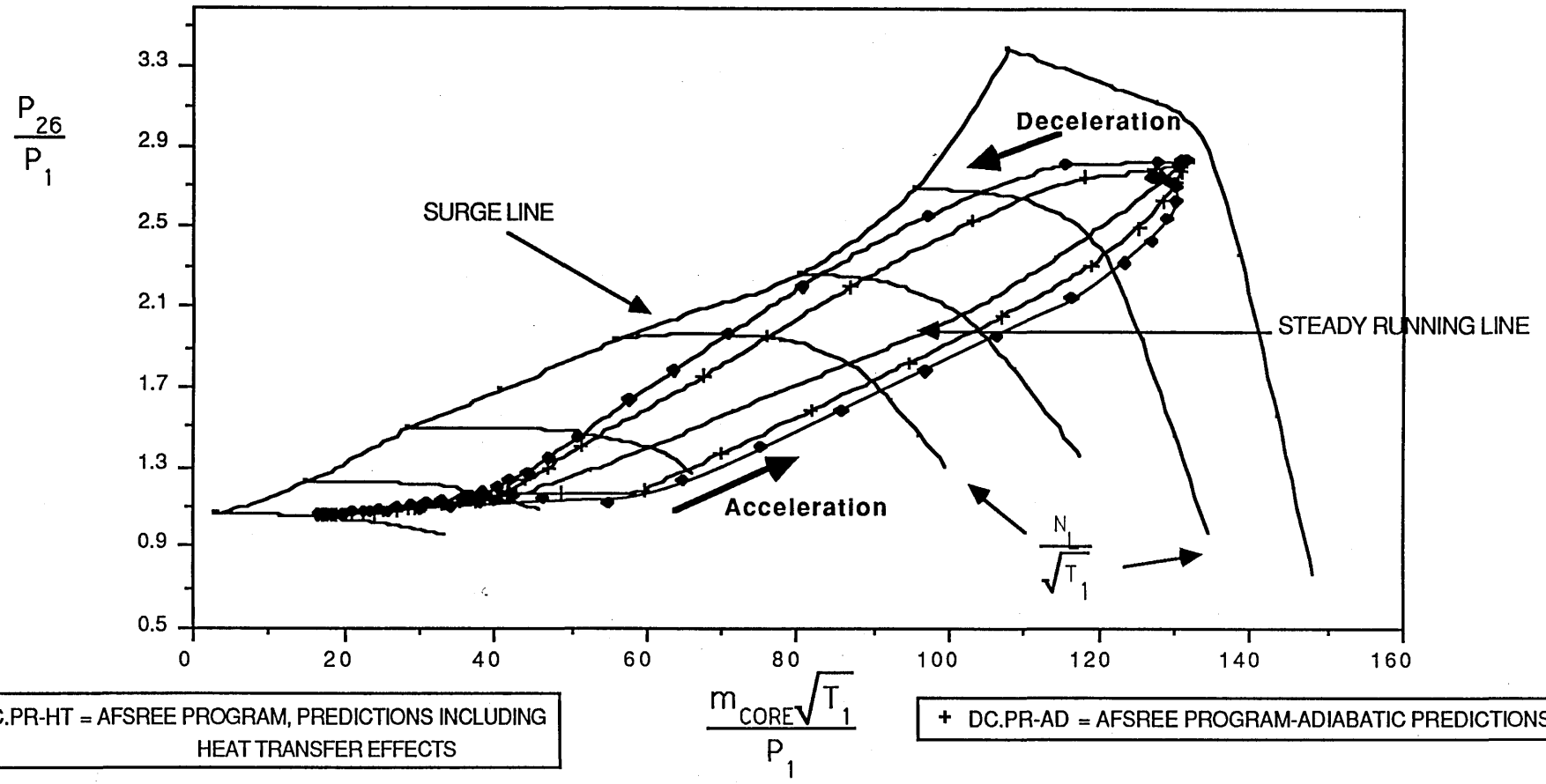

◆ DC.PR-HT = AFSREE PROGRAM, PREDICTIONS INCLUDING HEAT TRANSFER EFFECTS

\+ DC.PR-AD = AFSREE PROGRAM-ADIABATIC PREDICTIONS

FIGURE 71

TYPICAL TURBOFAN ENGINE

HIGH PRESSURE COMPRESSOR (H.P.) STEADY RUNNING LINE AND ACCELERATION TRAJECTRIES

AT: SEA LEVEL, MACH=0.2

Data from "TABLE 20"

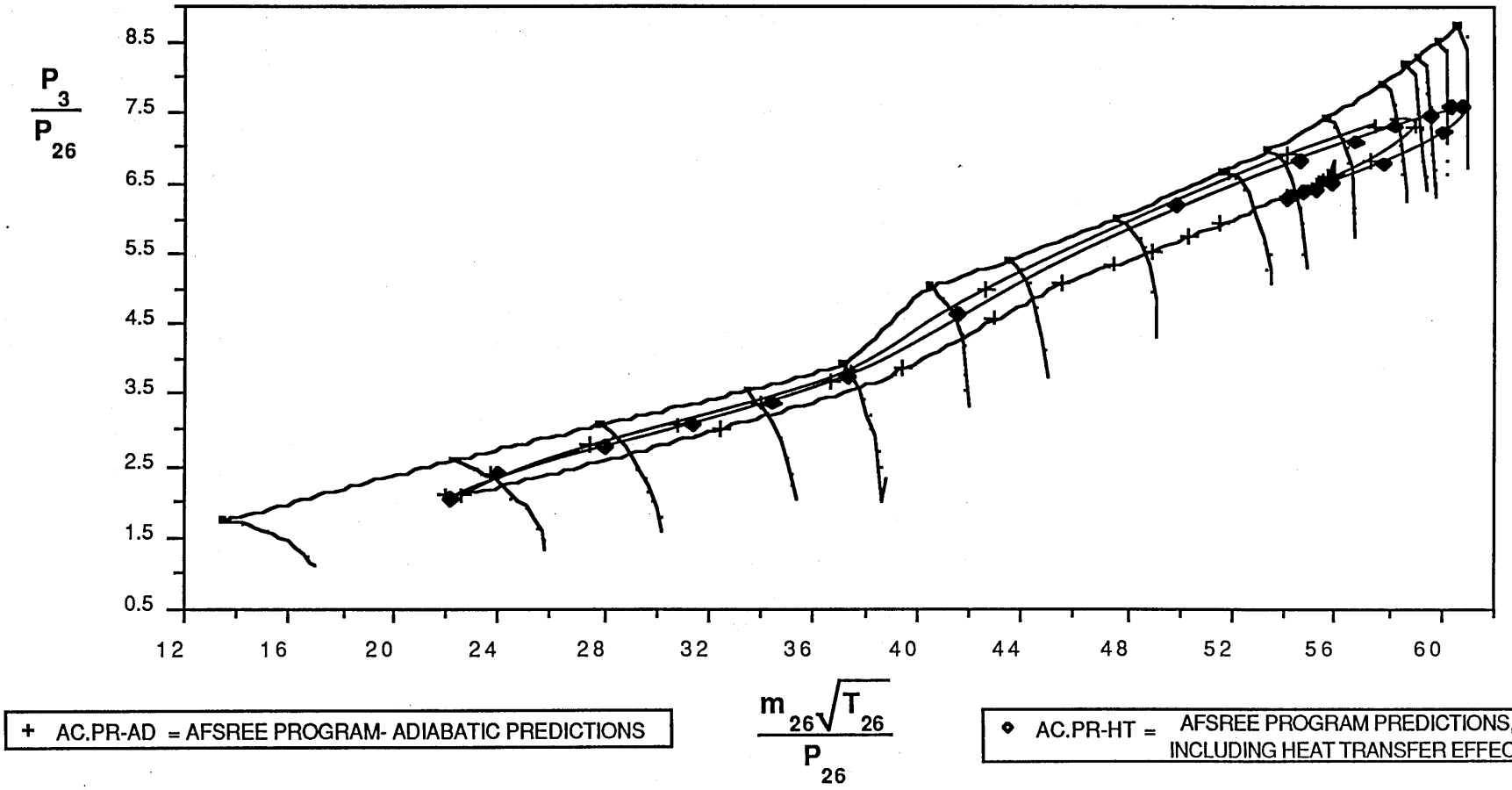

+ AC.PR-AD = AFSREE PROGRAM- ADIABATIC PREDICTIONS

◇ AC.PR-HT = AFSREE PROGRAM PREDICTIONS, INCLUDING HEAT TRANSFER EFFECTS

FIGURE 72

TYPICAL TURBOFAN ENGINE

HIGH PRESSURE COMPRESSOR (H.P.) WORKING LINE AND DECELERATION TRAJECTORIES

Data from "TABLE 20"

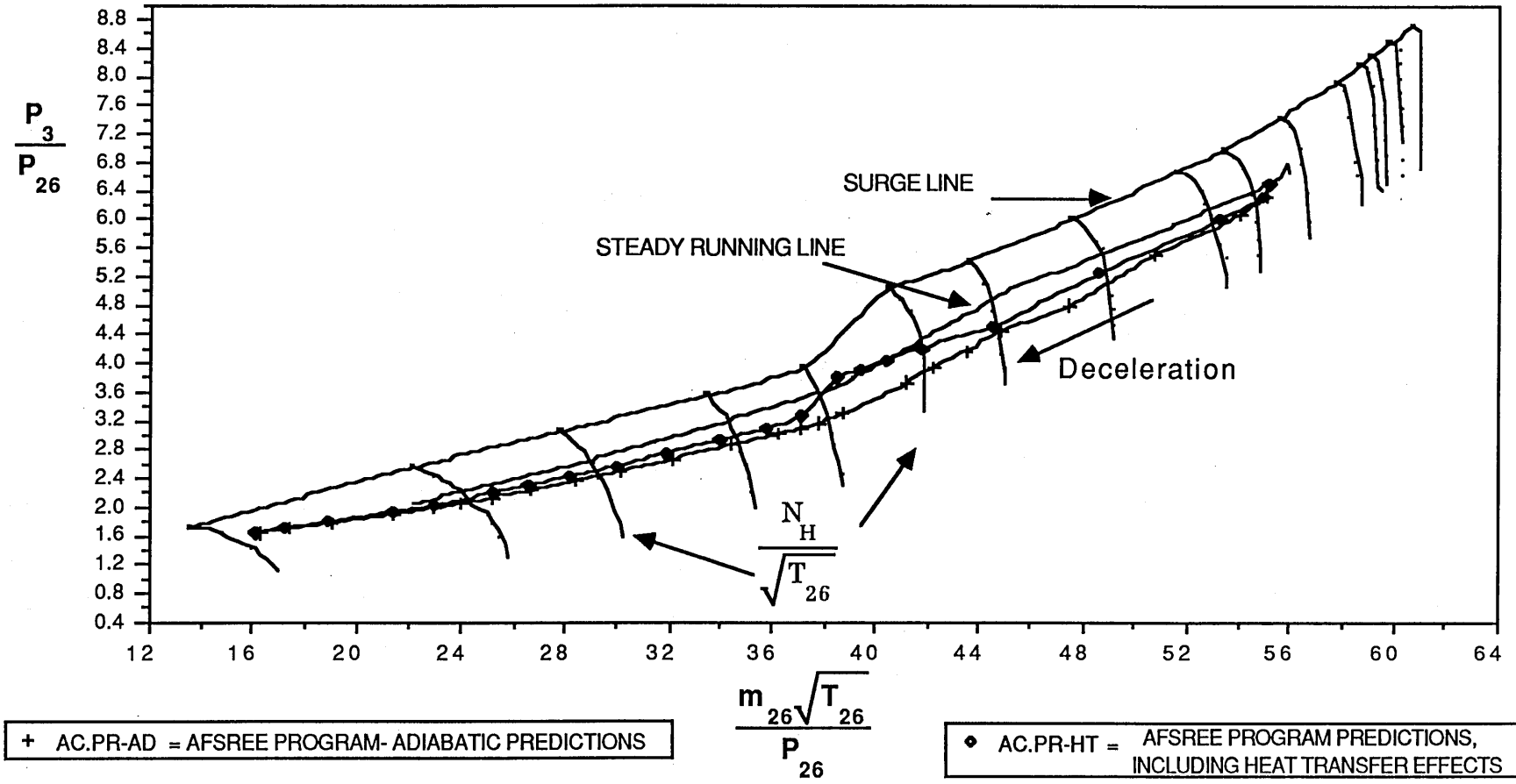

+ AC.PR-AD = AFSREE PROGRAM- ADIABATIC PREDICTIONS

◆ AC.PR-HT = AFSREE PROGRAM PREDICTIONS, INCLUDING HEAT TRANSFER EFFECTS

FIGURE 73

TYPICAL TURBOFAN ENGINE

PREDICTION OF THRUST RESPONSE WITH TIME

DURING A "COLD" ACCELERATION AT SEA LEVEL, MACH=0.2

Data from "TABLE 21"

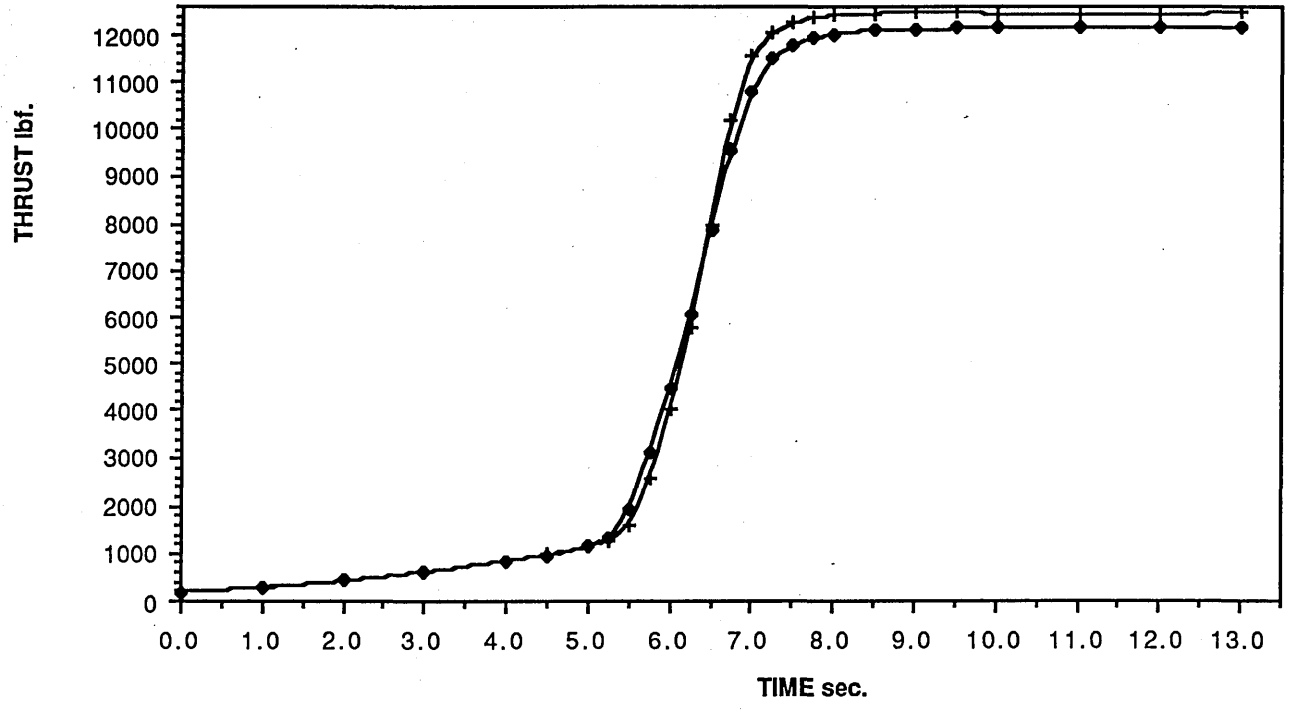

◆ THR.AC-HT = AFSREE PROGRAM PREDICTION INCLUDING HEAT TRANSFER EFFECTS

\+ THR.AC-AD = AFSREE PROGRAM ADIABATIC PREDICTIONS

FIGURE 74

TYPICAL TURBOFAN ENGINE

COMPARISON OF THRUST RESPONSE WITH TIME

DURING A DECELERATION

AT SEA LEVEL, MACH=0.2

Data from "TABLE 21"

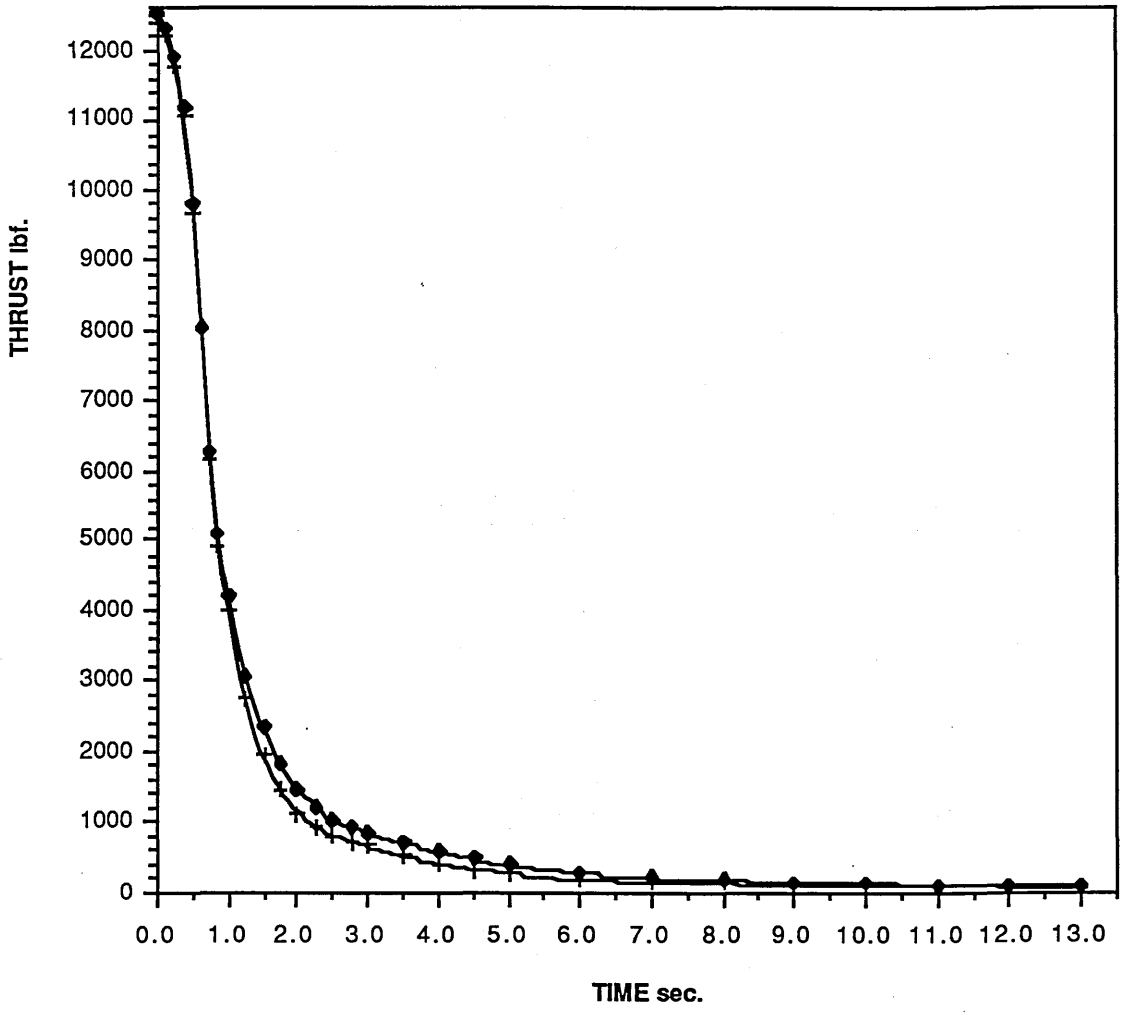

◆ THR.DC-HT = AFSREE PROGRAM PREDICTIONS-NON ADIABATIC

\+ THR.DC-AD = AFSREE PROGRAM-ADIABATIC PREDICTIONS

FIGURES 76 & 77

TYPICAL TURBOFAN ENGINE

COMPARISON OF THRUST RESPONSE WITH TIME

DURING A DECELERATION

AT SEA LEVEL, MACH=0.2

Data from "TABLE 21"

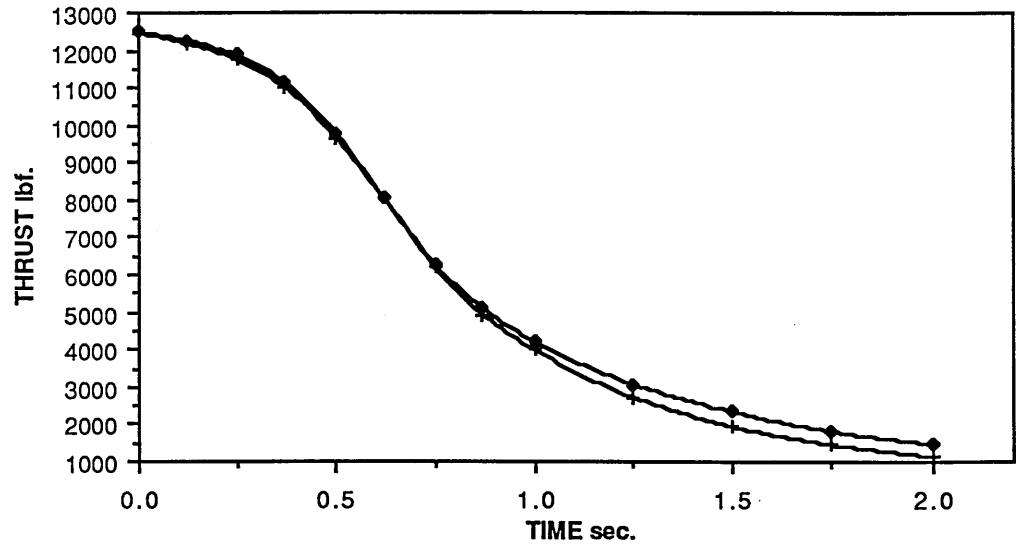

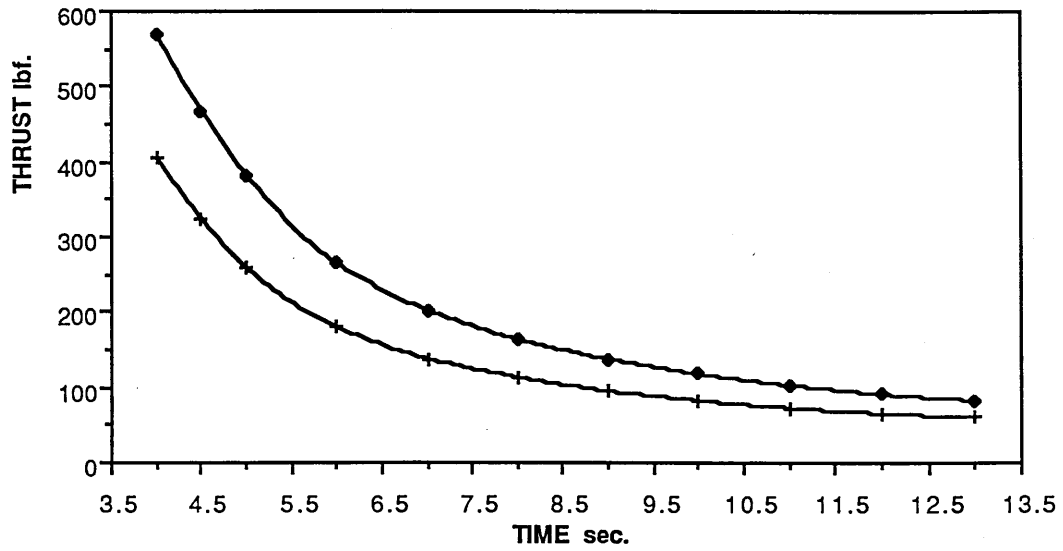

◆ TH.DC.HT.L = AFSREE PROGRAM PREDICTIONS-NON ADIABATIC

\+ TH.DC.AD.L = AFSREE PROGRAM-ADIABATIC PREDICTIONS

FIGURE 78

COMPARISON OF CHANGE OF L.P. SHAFT SPEED WITH TIME

DURING A "COLD" ACCELERATION AT 43,000ft.

MACH=0.8

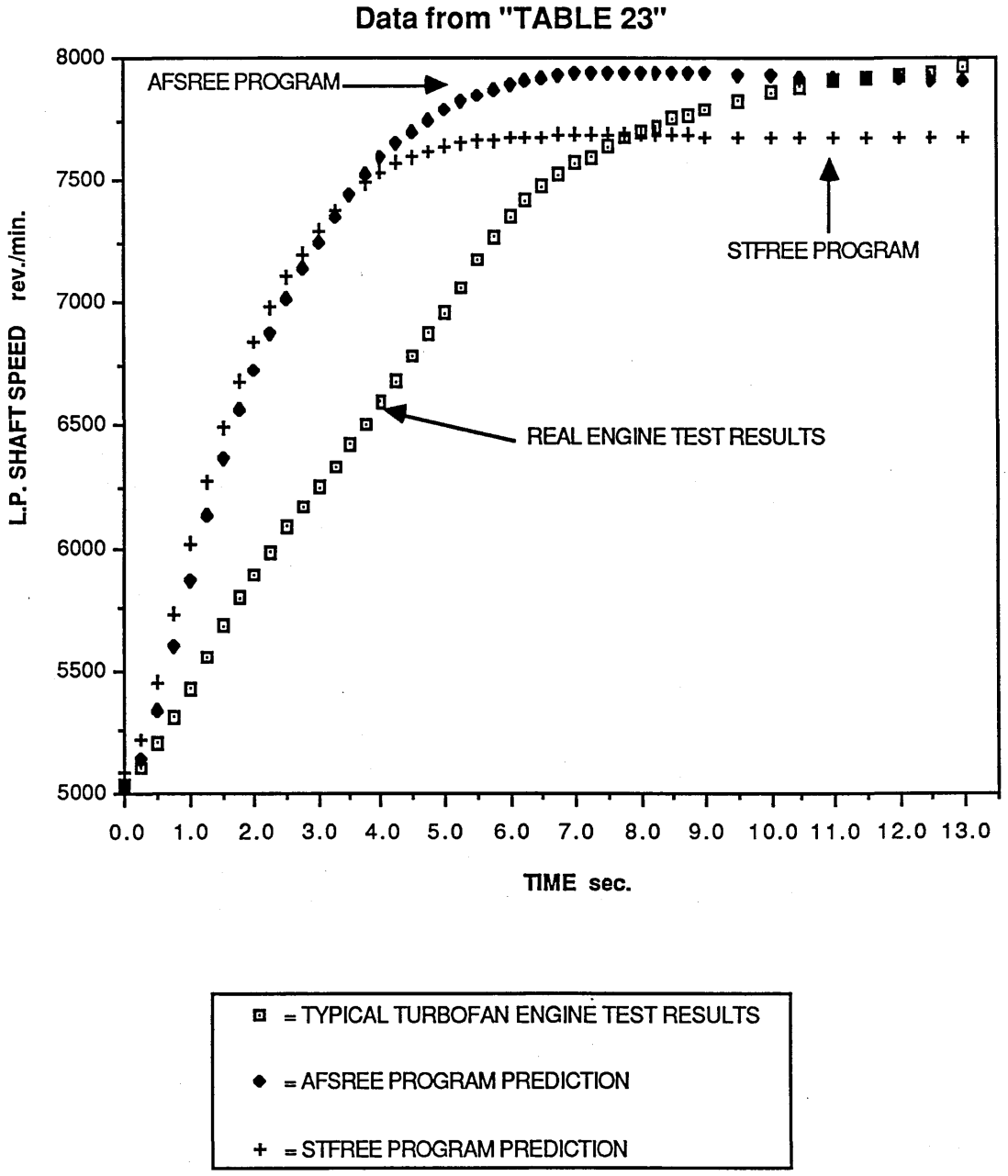

FIGURE 79

COMPARISON OF CHANGE OF H.P. SHAFT SPEED WITH TIME

DURING A "COLD" ACCELERATION AT 43,000ft.

MACH=0.8

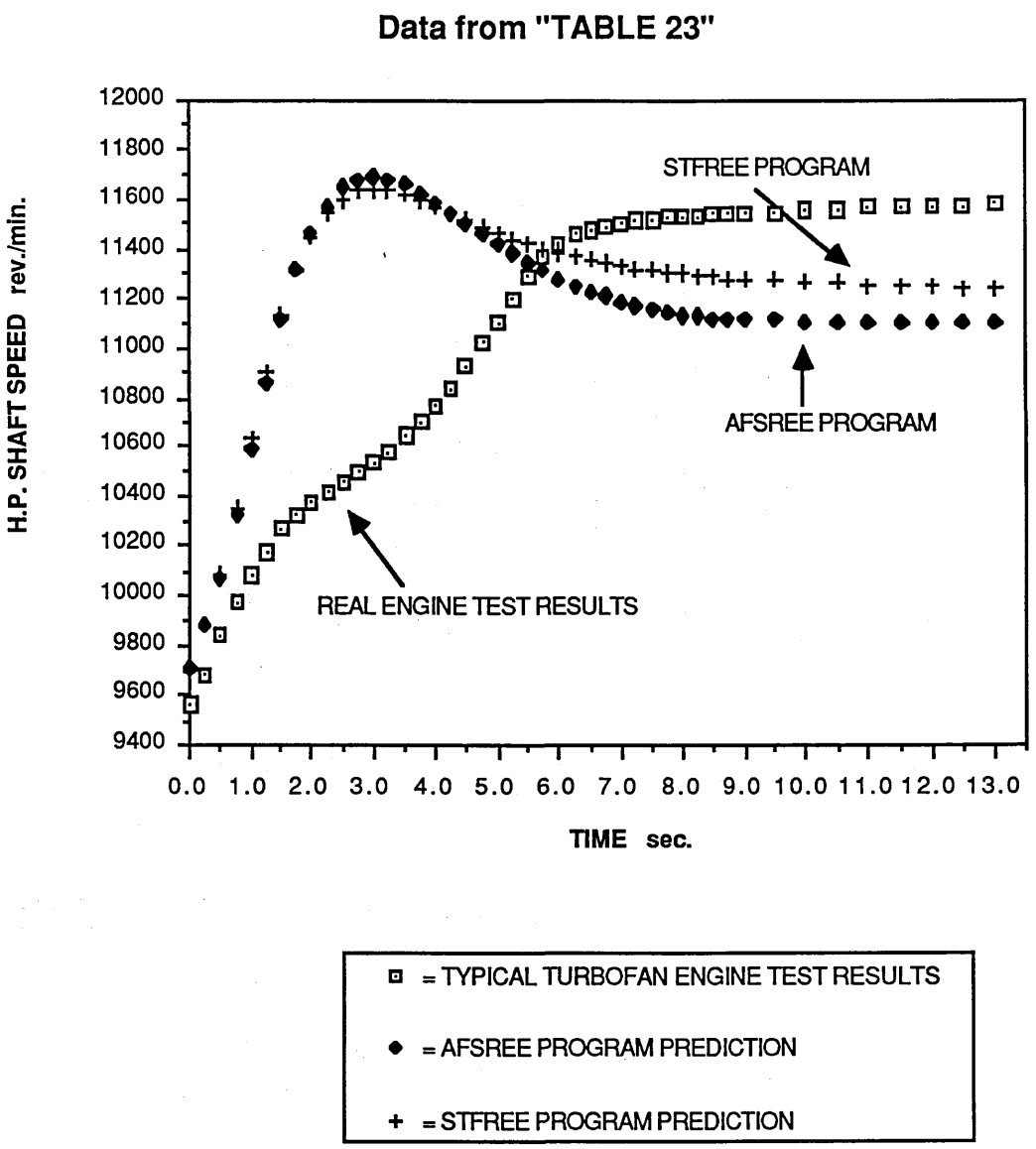

FIGURE 80

COMPARISON OF L.P. vs. H.P. SHAFT SPEED RESPONSE

DURING A "COLD" ACCELERATION AT 43,000ft.

MACH=0.8

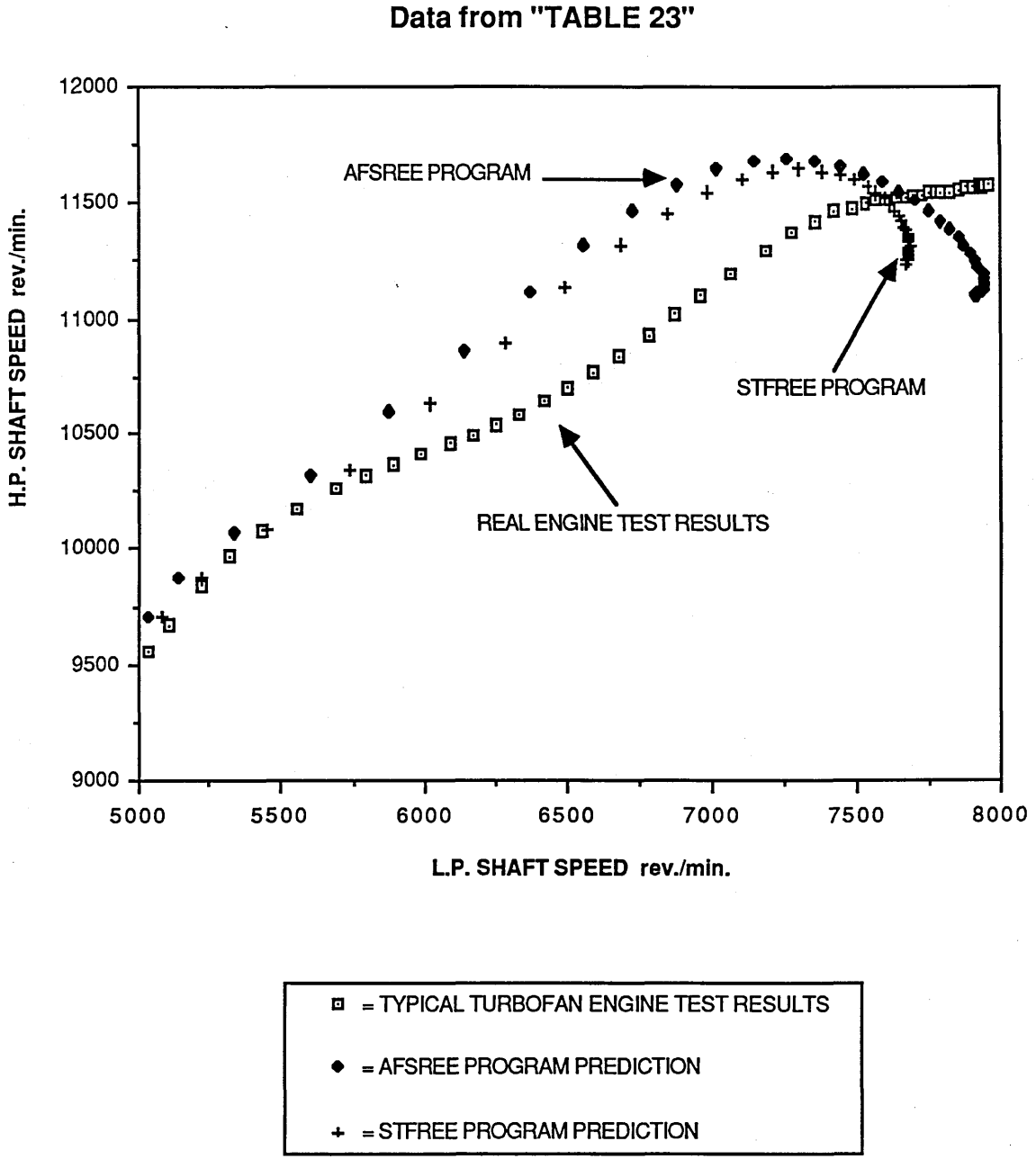

FIGURE 81

COMPARISON OF OUTER FAN PERFORMANCE

BETWEEN PREDICTED AND ACTUAL TEST RESULTS

DURING A "COLD" ACCELERATION AT 43,000ft.

MACH=0.8

Data from "TABLE 23"

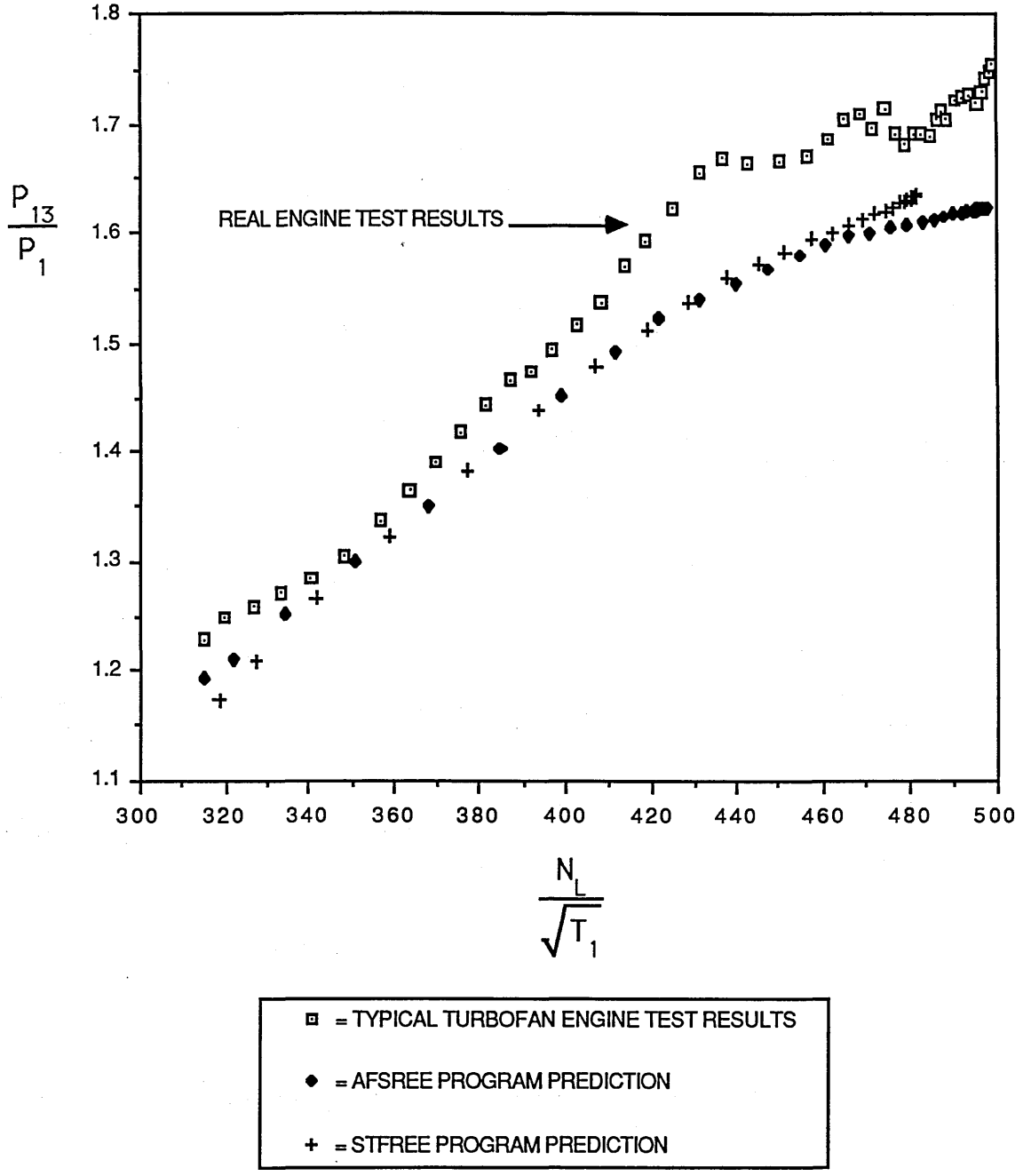

FIGURE 82

COMPARISON OF COMBINED INNER FAN AND I.P. COMPRESSOR PERFORMANCE

BETWEEN PREDICTED AND ACTUAL TEST RESULTS

DURING A "COLD" ACCELERATION AT 43,000ft.

MACH=0.8

Data from "TABLE 23"

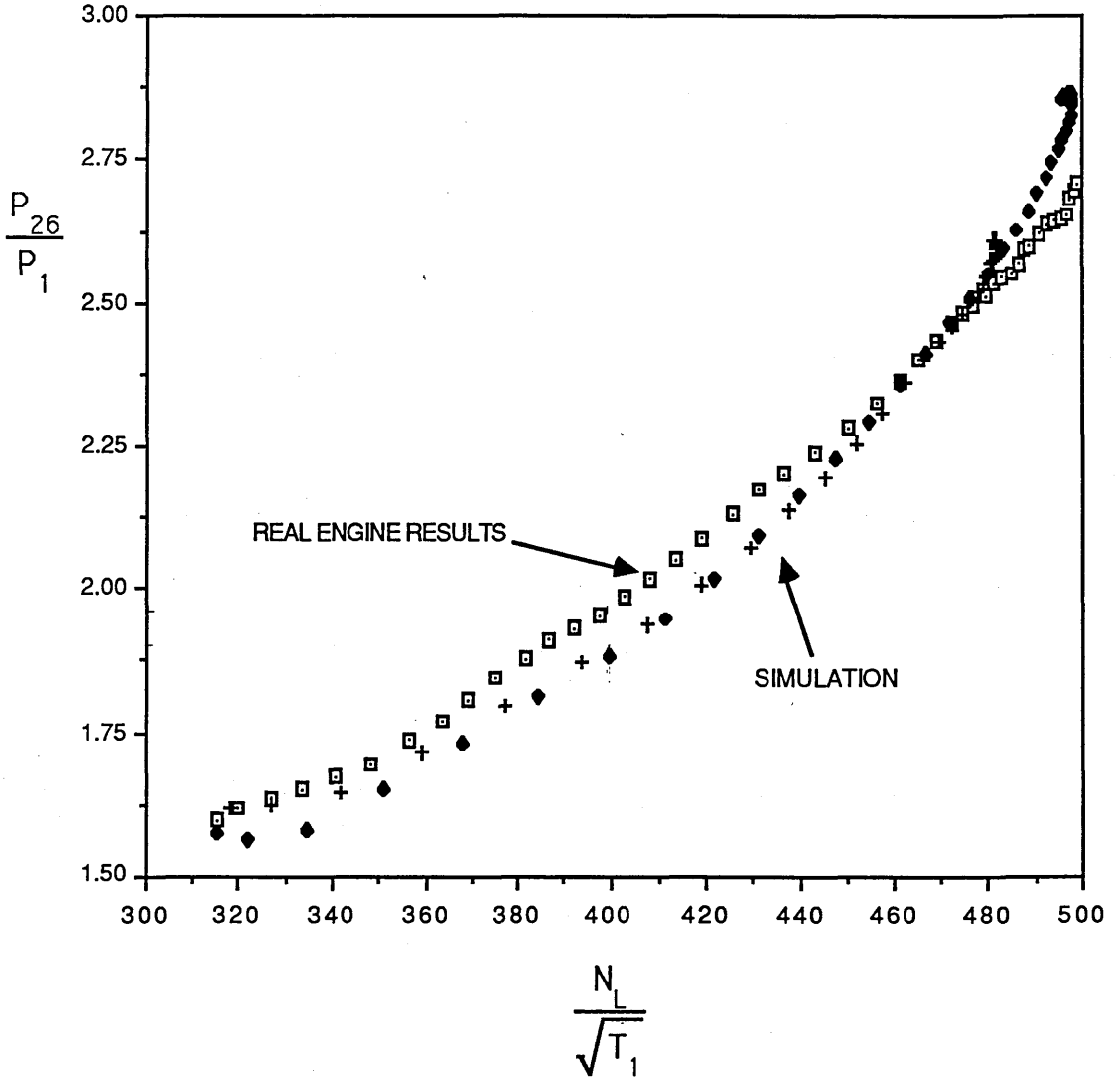

FIGURE 83

COMPARISON OF H.P. COMPRESSOR PERFORMANCE

BETWEEN PREDICTED AND ACTUAL TEST RESULTS

DURING A "COLD" ACCELERATION AT 43,000ft.

MACH=0.8

Data from "TABLE 23"

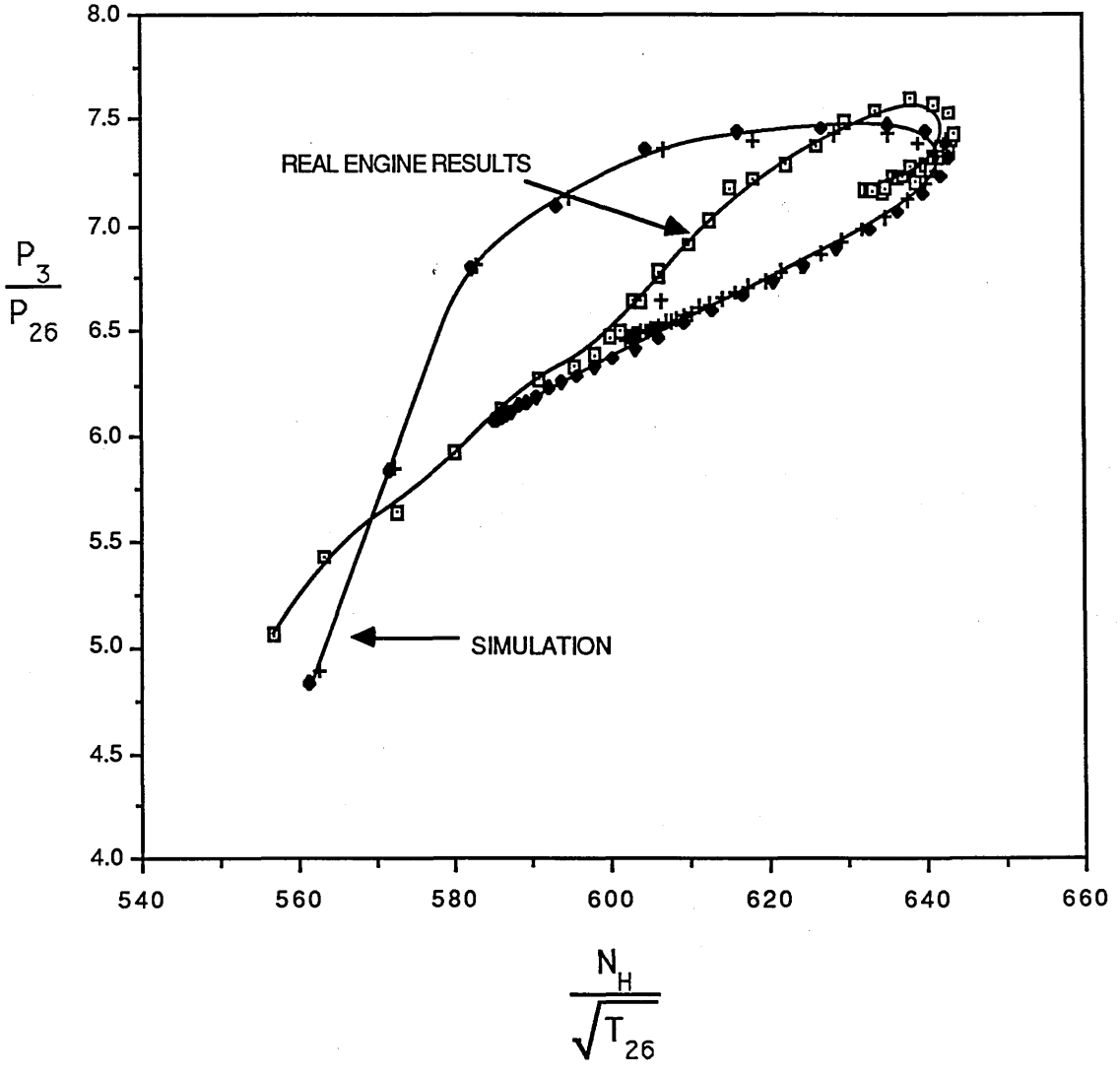

FIGURE 84

COMPARISON BETWEEN PREDICTED AND ACTUAL TEST RESULTS

DURING A "COLD" ACCELERATION AT 43,000ft.

MACH=0.8

Data from "TABLE 23"

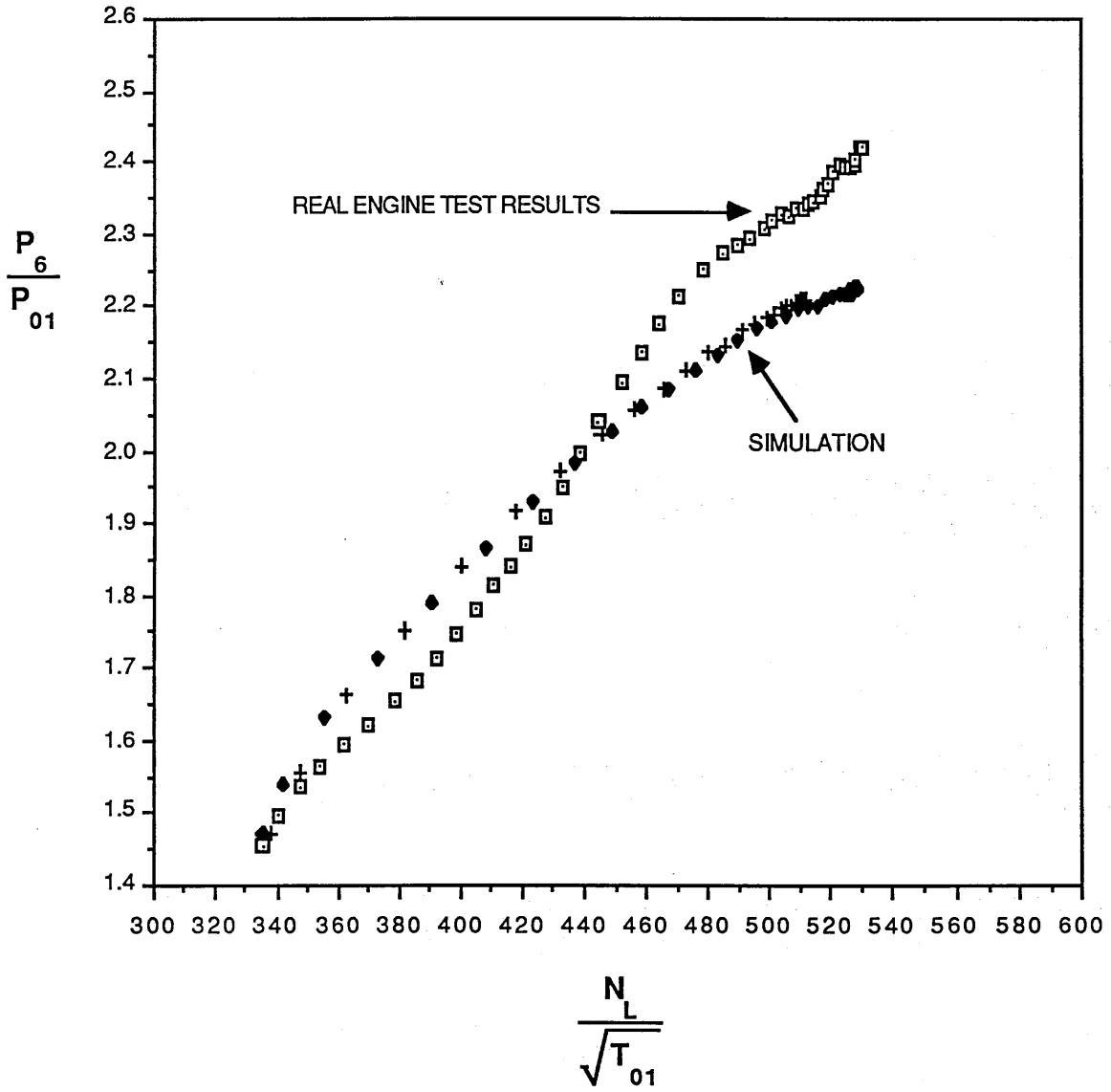

□ = TYPICAL TURBOFAN ENGINE TEST RESULTS

◆ = AFSREE PROGRAM PREDICTION

\+ = STFREE PROGRAM PREDICTION

FIGURE 85

COMPARISON OF CHANGE OF L.P. SHAFT SPEED WITH TIME

DURING A DECELERATION AT 43,000ft.

MACH=0.8

Data from "TABLE 24"

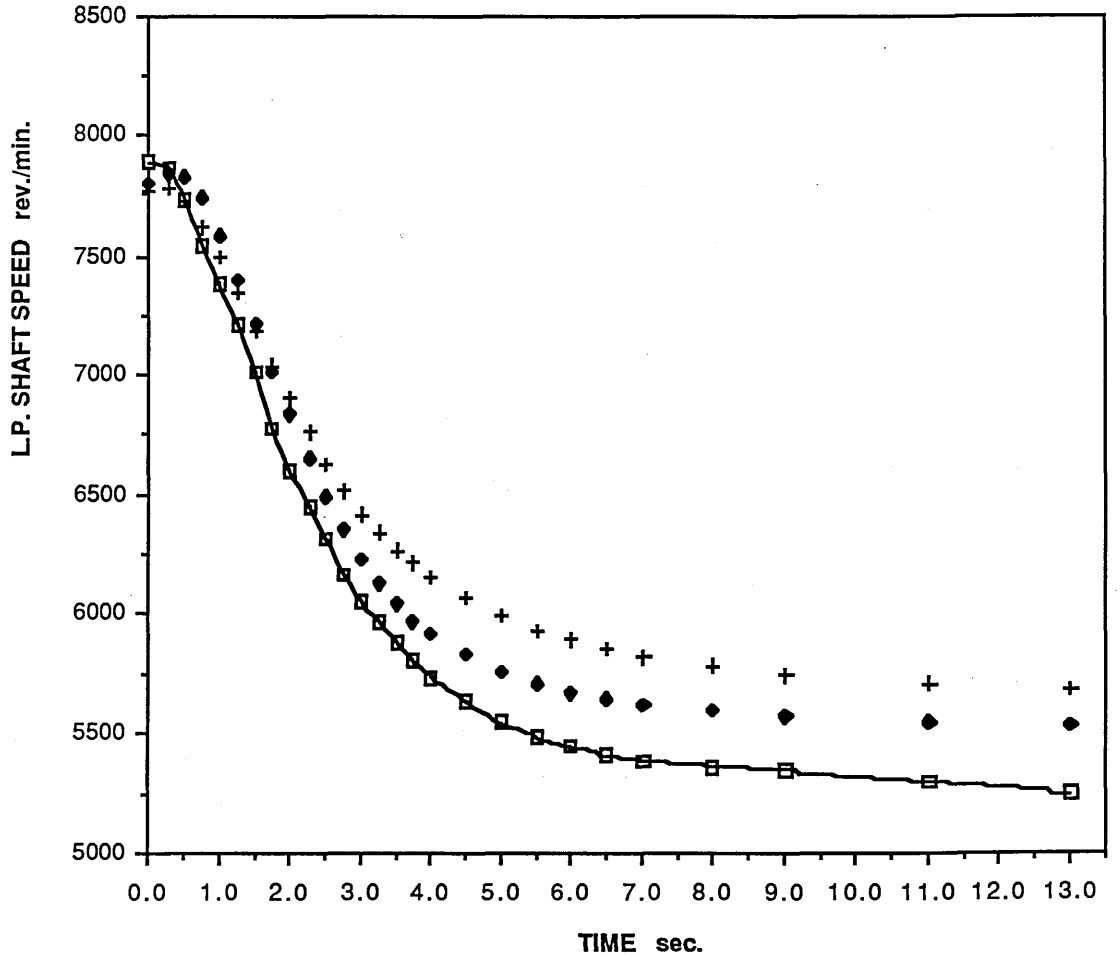

□ = TYPICAL TURBOFAN ENGINE TEST RESULTS

◆ = AFSREE PROGRAM PREDICTION

\+ = STFREE PROGRAM PREDICTION

FIGURE 86

COMPARISON OF CHANGE OF H.P. SHAFT SPEED WITH TIME

DURING A DECELERATION AT 43,000ft.

MACH=0.8

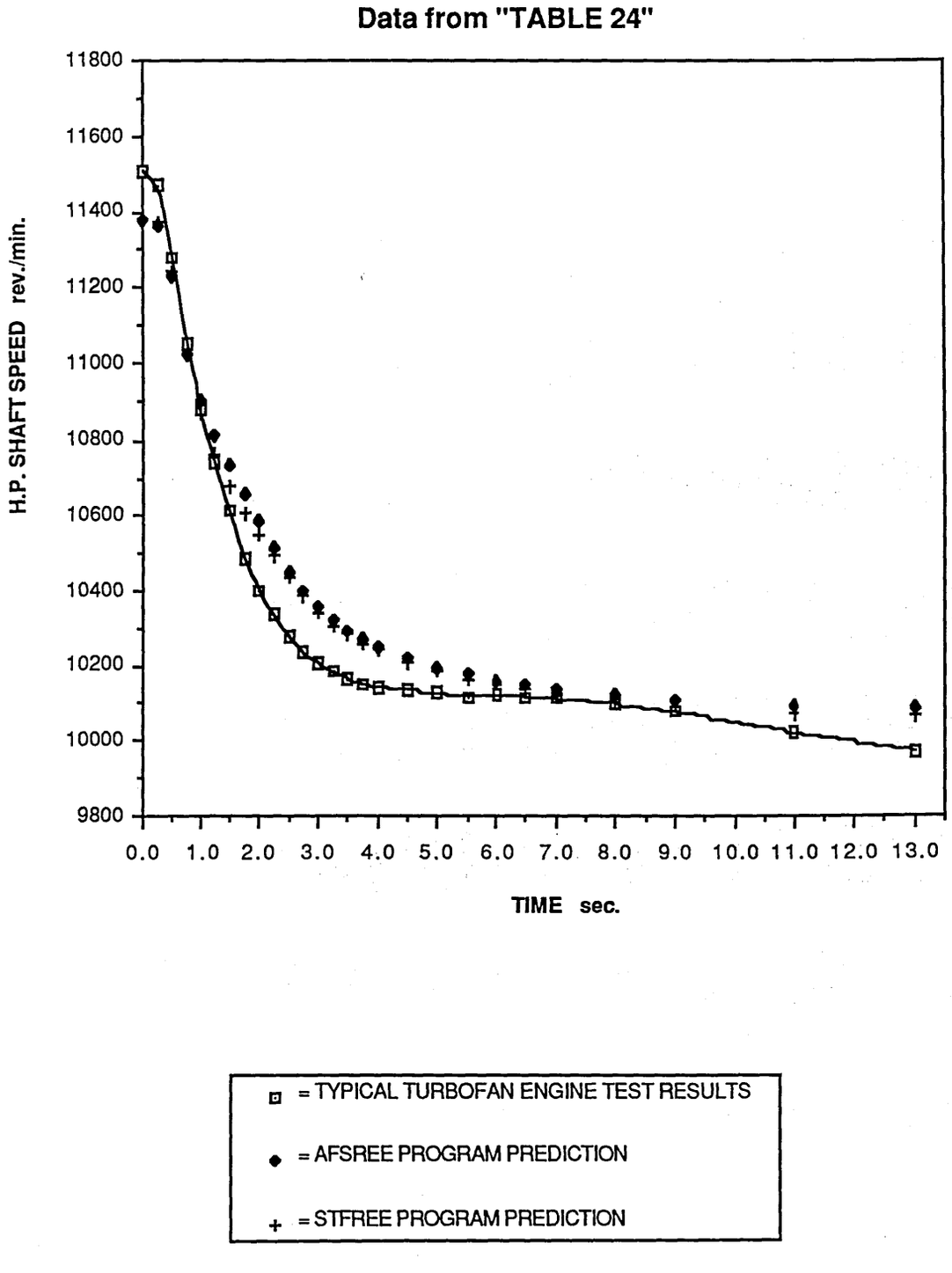

FIGURE 87

COMPARISON OF L.P. vs. H.P. SHAFT SPEED RESPONSE

DURING A DECELERATION AT 43,000ft.

MACH=0.8

Data from "TABLE 24"

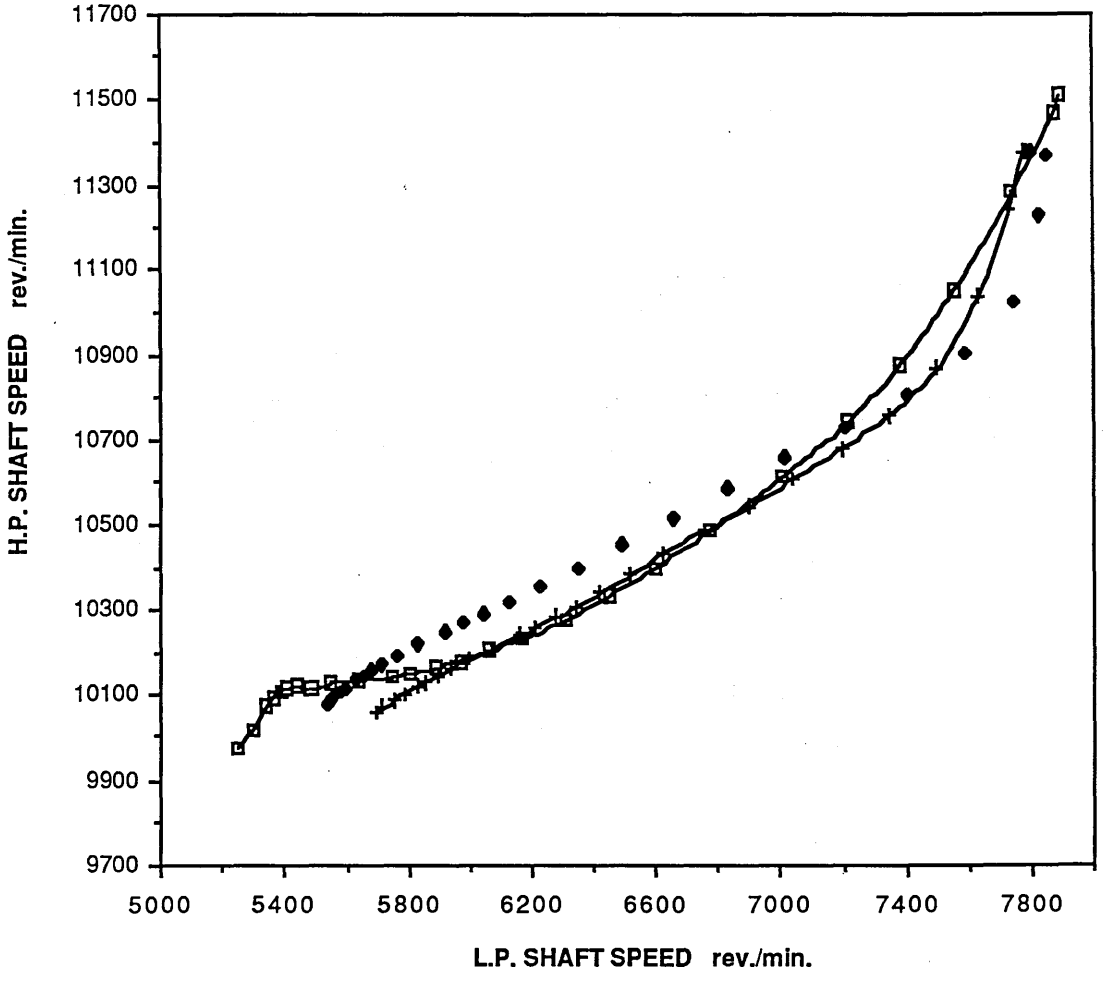

□ = TYPICAL TURBOFAN ENGINE TEST RESULTS

◆ = AFSREE PROGRAM PREDICTION

\+ = STFREE PROGRAM PREDICTION

FIGURE 88

COMPARISON OF OUTER FAN PERFORMANCE

BETWEEN PREDICTED AND ACTUAL TEST RESULTS

DURING A DECELERATION AT 43,000ft.

MACH=0.8

Data from "TABLE 24"

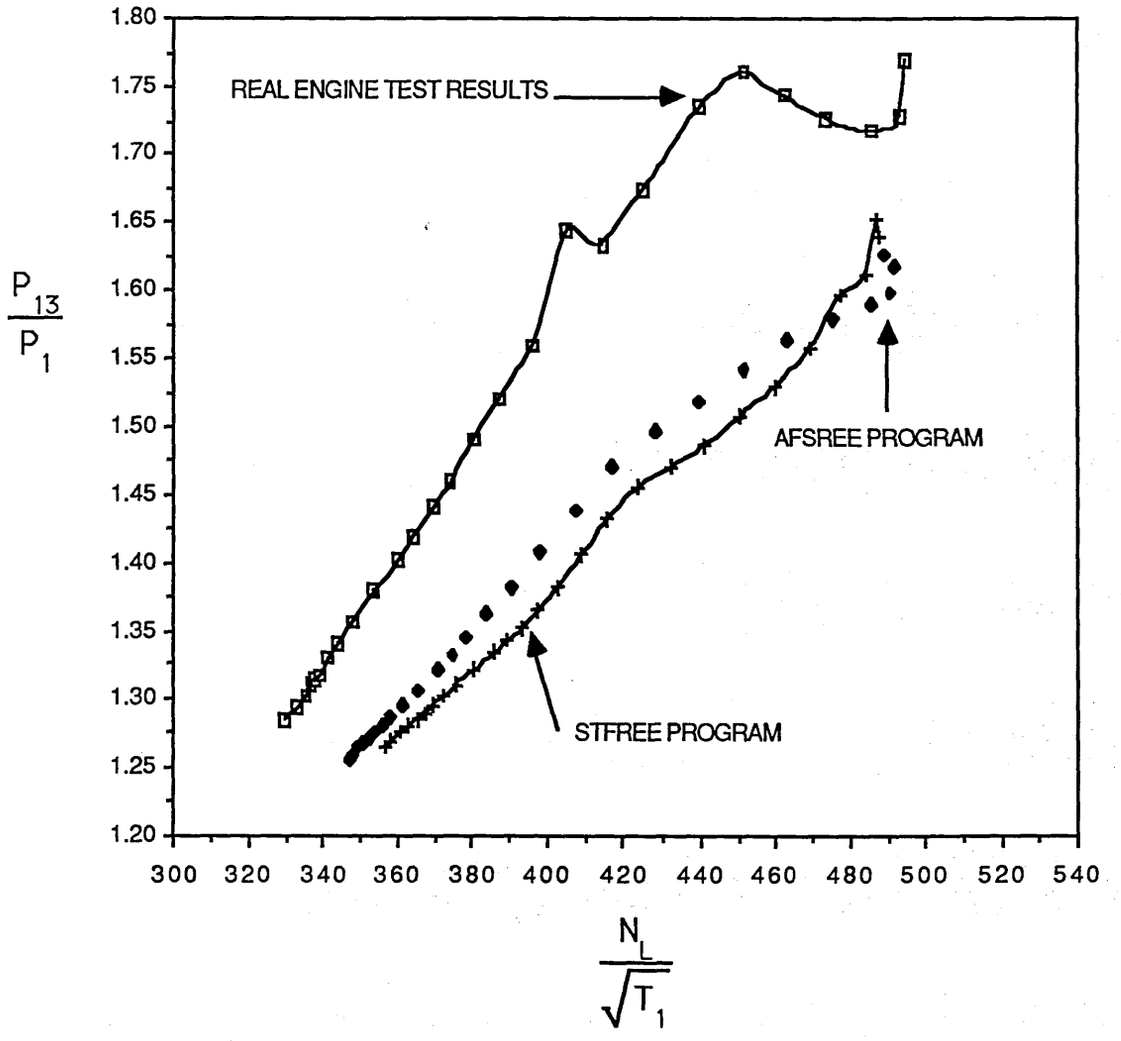

FIGURE 89

COMPARISON OF COMBINED INNER FAN AND I.P. COMPRESSOR PERFORMANCE

BETWEEN PREDICTED AND ACTUAL TEST RESULTS

DURING A DECELERATION AT 43,000ft.

MACH=0.8

Data from "TABLE 24"

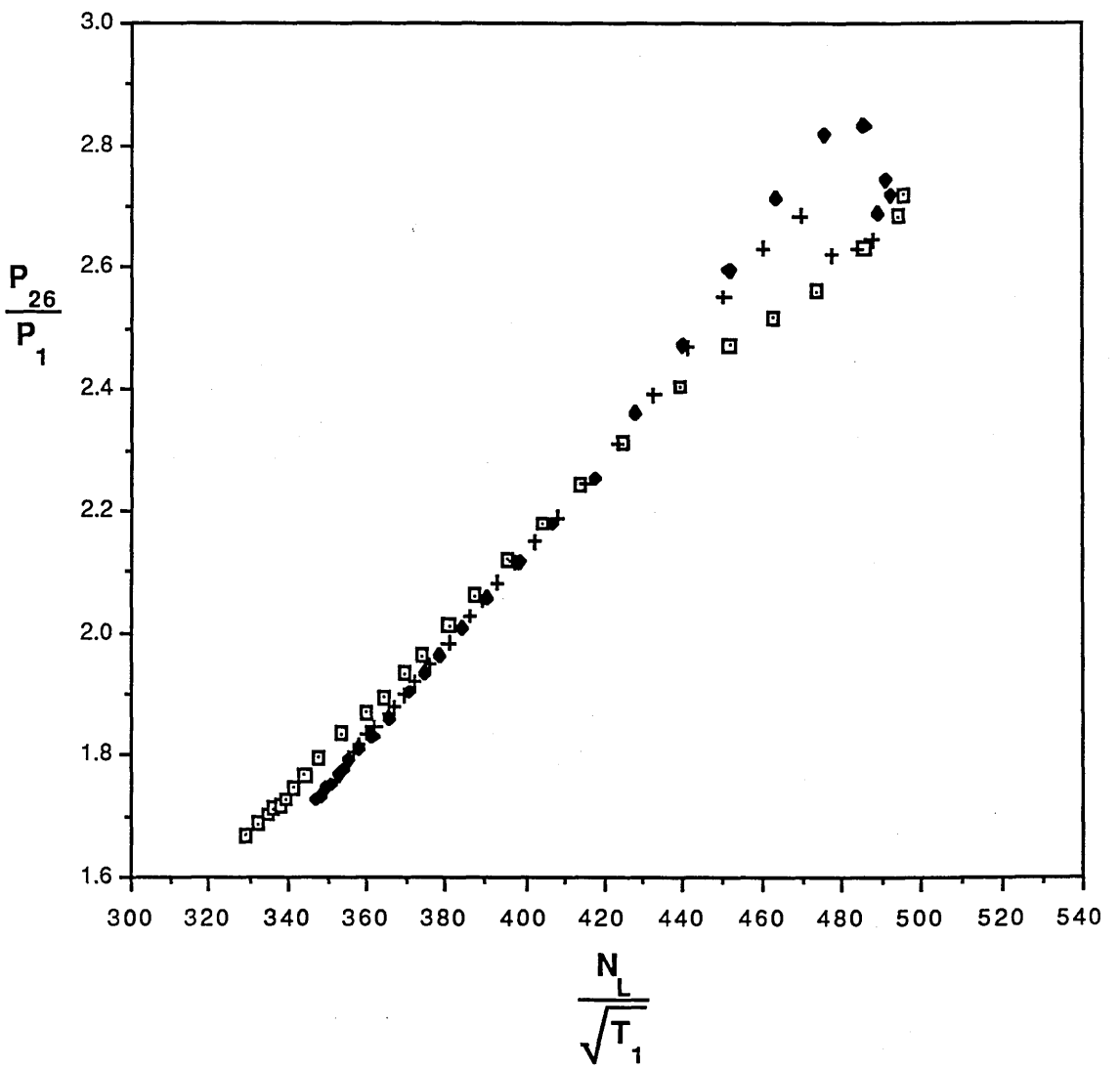

FIGURE 90

COMPARISON OF H.P. COMPRESSOR PERFORMANCE

BETWEEN PREDICTED AND ACTUAL TEST RESULTS

DURING A DECELERATION AT 43,000ft.

MACH=0.8

Data from "TABLE 24"

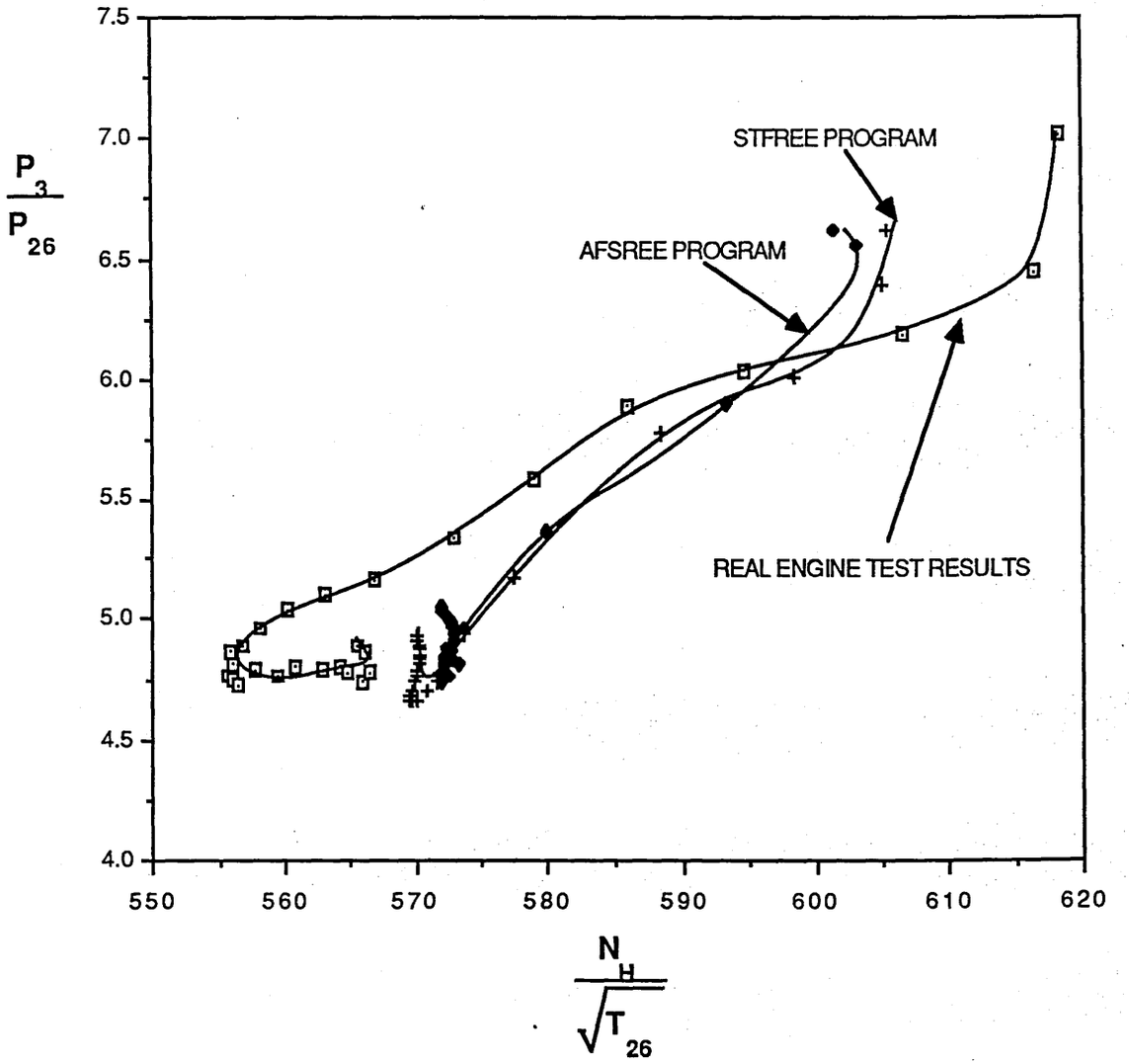

□ = TYPICAL TURBOFAN ENGINE TEST RESULTS

◆ = AFSREE PROGRAM PREDICTION

\+ = STFREE PROGRAM PREDICTION

FIGURE 91

COMPARISON BETWEEN PREDICTED AND ACTUAL TEST RESULTS

DURING A DECELERATION AT 43,000ft.

MACH=0.8

Data from "TABLE 24"

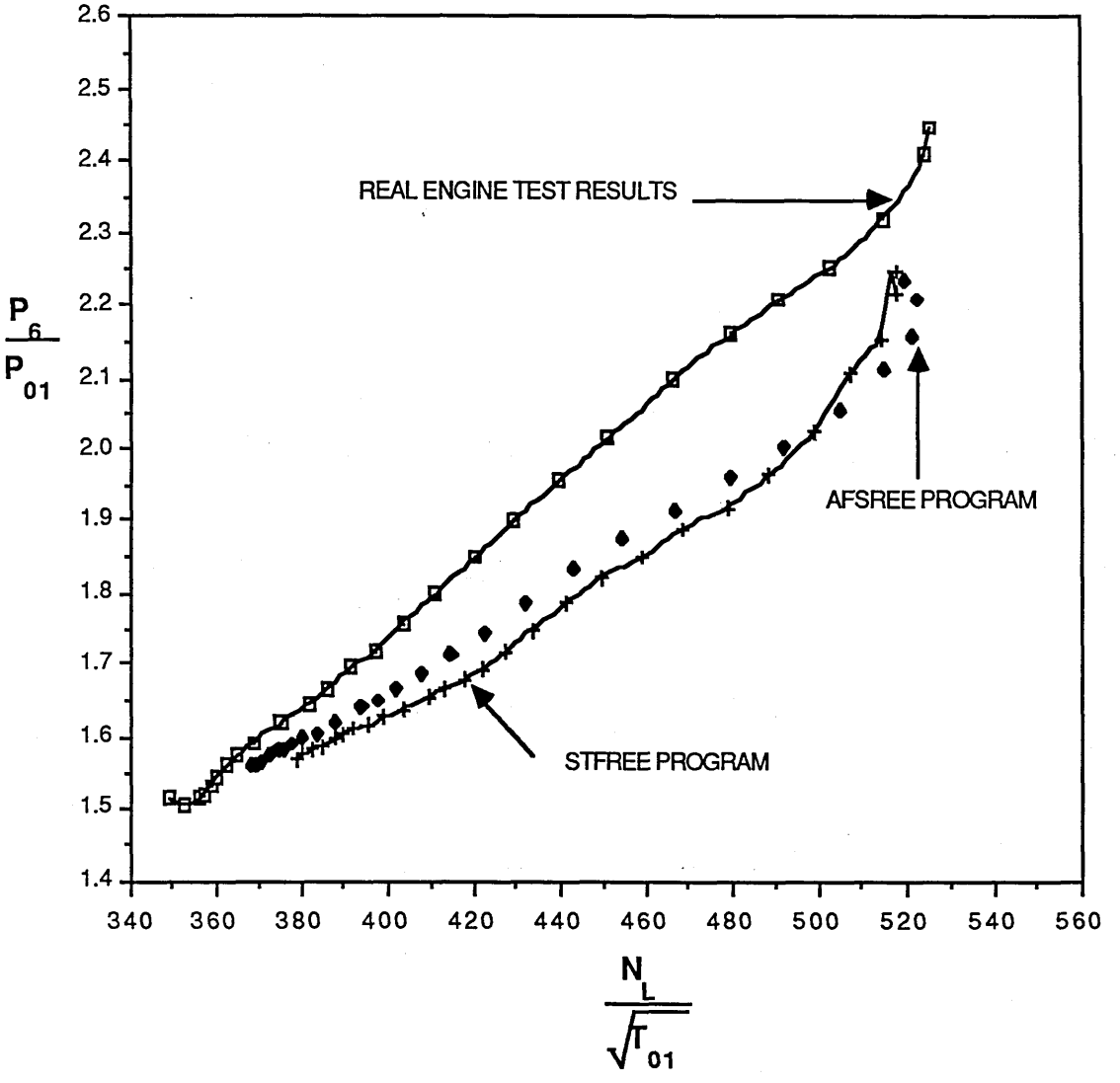

FIGURE 92

COMPARISON OF CHANGE OF L.P. SHAFT SPEED WITH TIME

DURING A "COLD" ACCELERATION AT 43,000ft.

MACH=0.8

WITH 5% I.P. COMPRESSOR BLEED

Data from "TABLE 25"

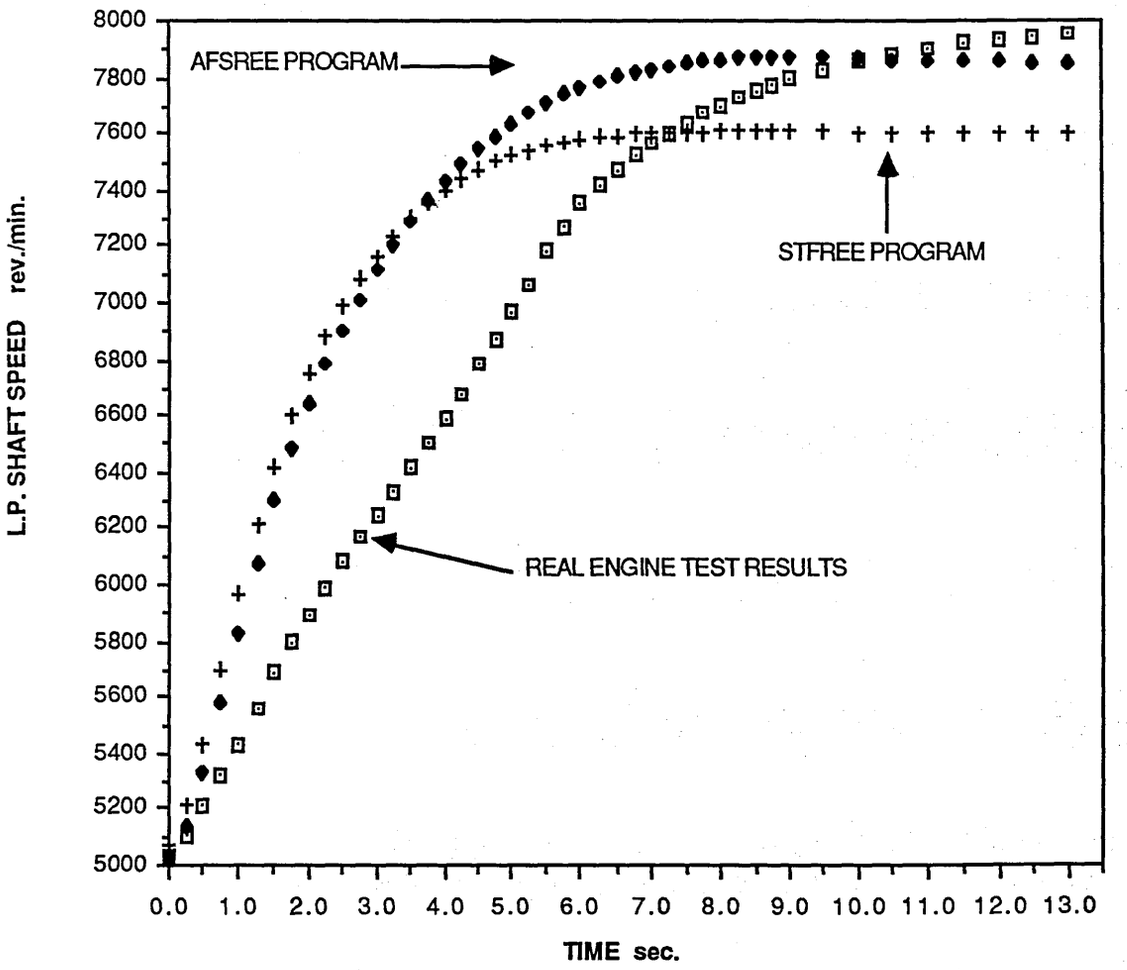

□ = TYPICAL TURBOFAN ENGINE TEST RESULTS

◆ = AFSREE PROGRAM PREDICTION

\+ = STFREE PROGRAM PREDICTION

FIGURE 93

COMPARISON OF CHANGE OF H.P. SHAFT SPEED WITH TIME

DURING A "COLD" ACCELERATION AT 43,000ft.

MACH=0.8

WITH 5% I.P. COMPRESSOR BLEED

Data from "TABLE 23"

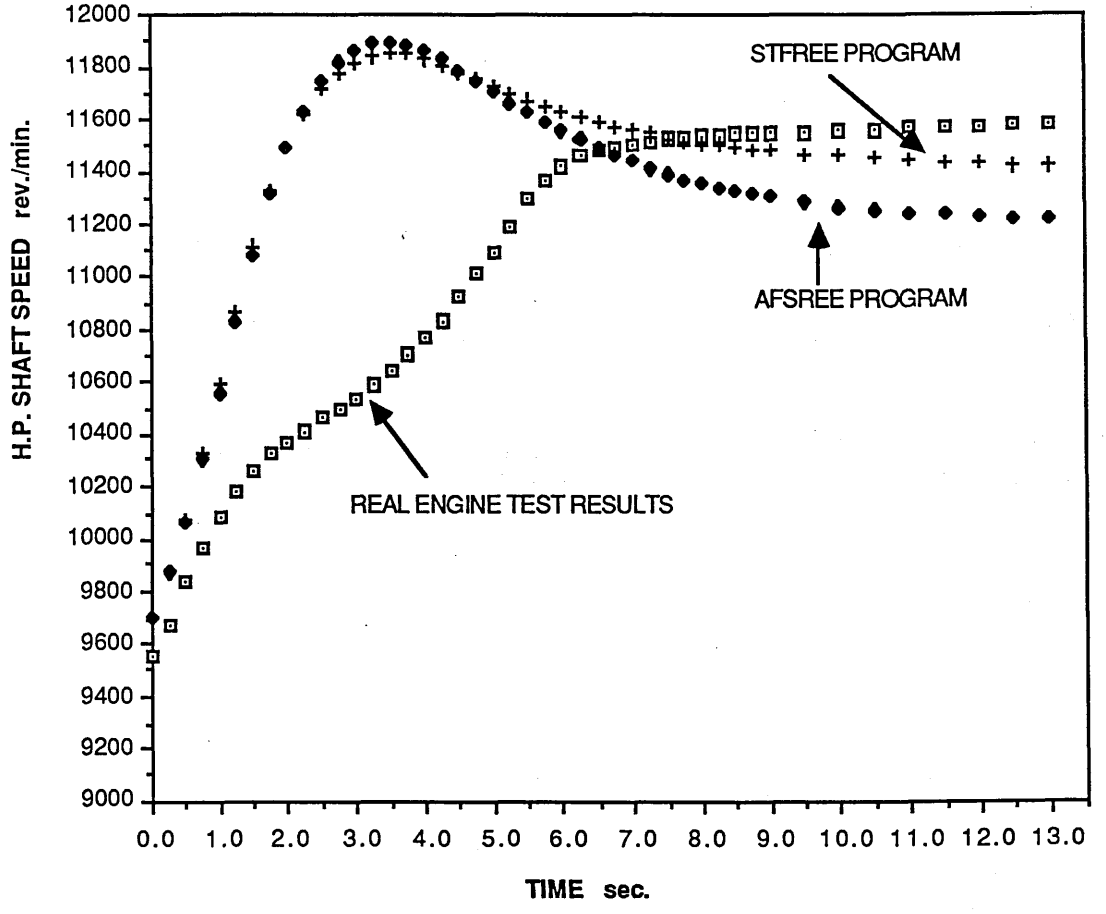

□ = TYPICAL TURBOFAN ENGINE TEST RESULTS

◆ = AFSREE PROGRAM PREDICTION

\+ = STFREE PROGRAM PREDICTION

FIGURE 94

COMPARISON OF L.P. vs. H.P. SHAFT SPEED RESPONSE

DURING A "COLD" ACCELERATION AT 43,000ft.

MACH=0.8

WITH 5% I.P. COMPRESSOR BLEED

Data from "TABLE 25"

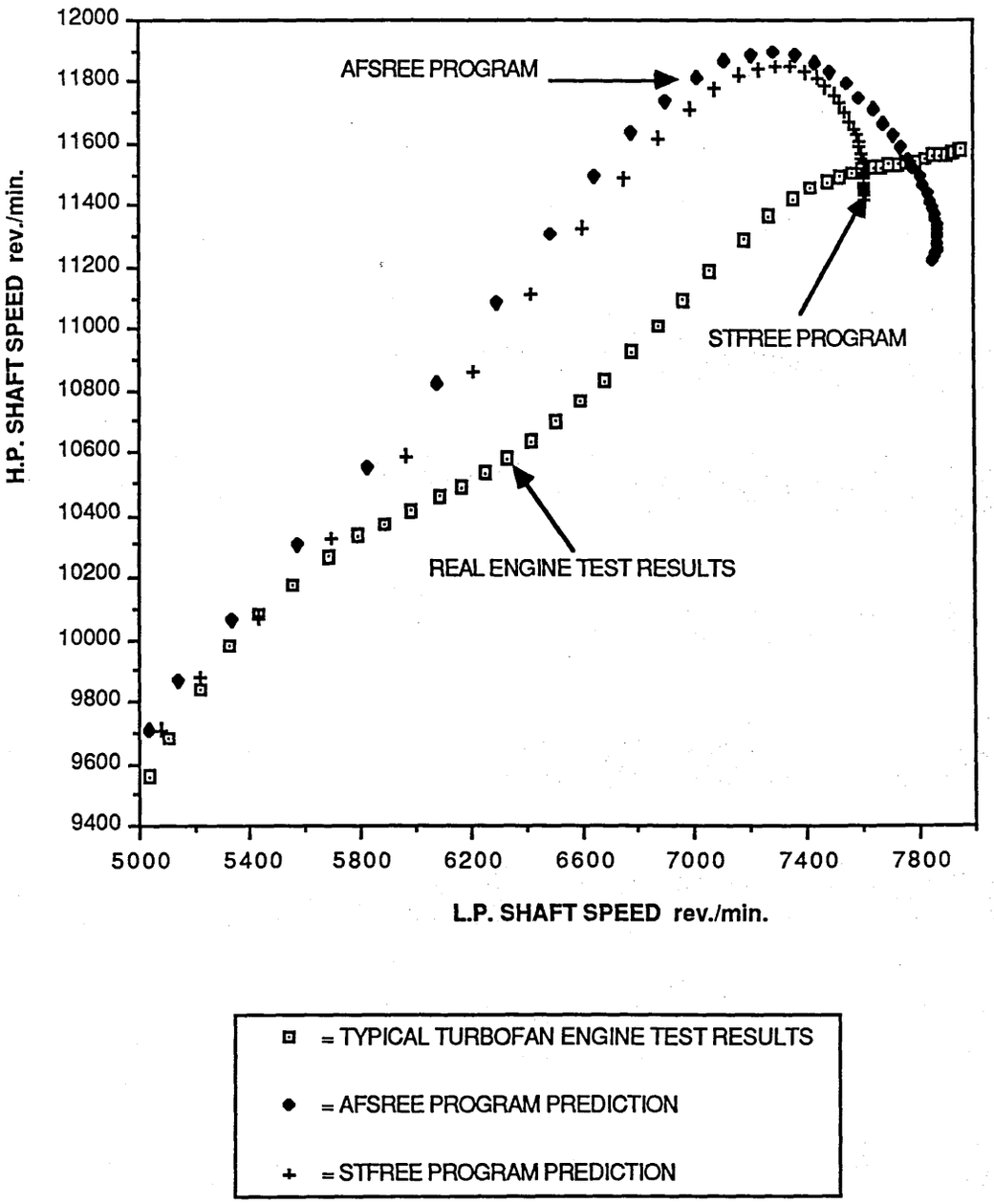

FIGURE 95

COMPARISON OF OUTER FAN PERFORMANCE

BETWEEN PREDICTED AND ACTUAL TEST RESULTS

DURING A "COLD" ACCELERATION AT 43,000ft.

MACH=0.8

WITH 5% I.P. COMPRESSOR BLEED

Data from "TABLE 25"

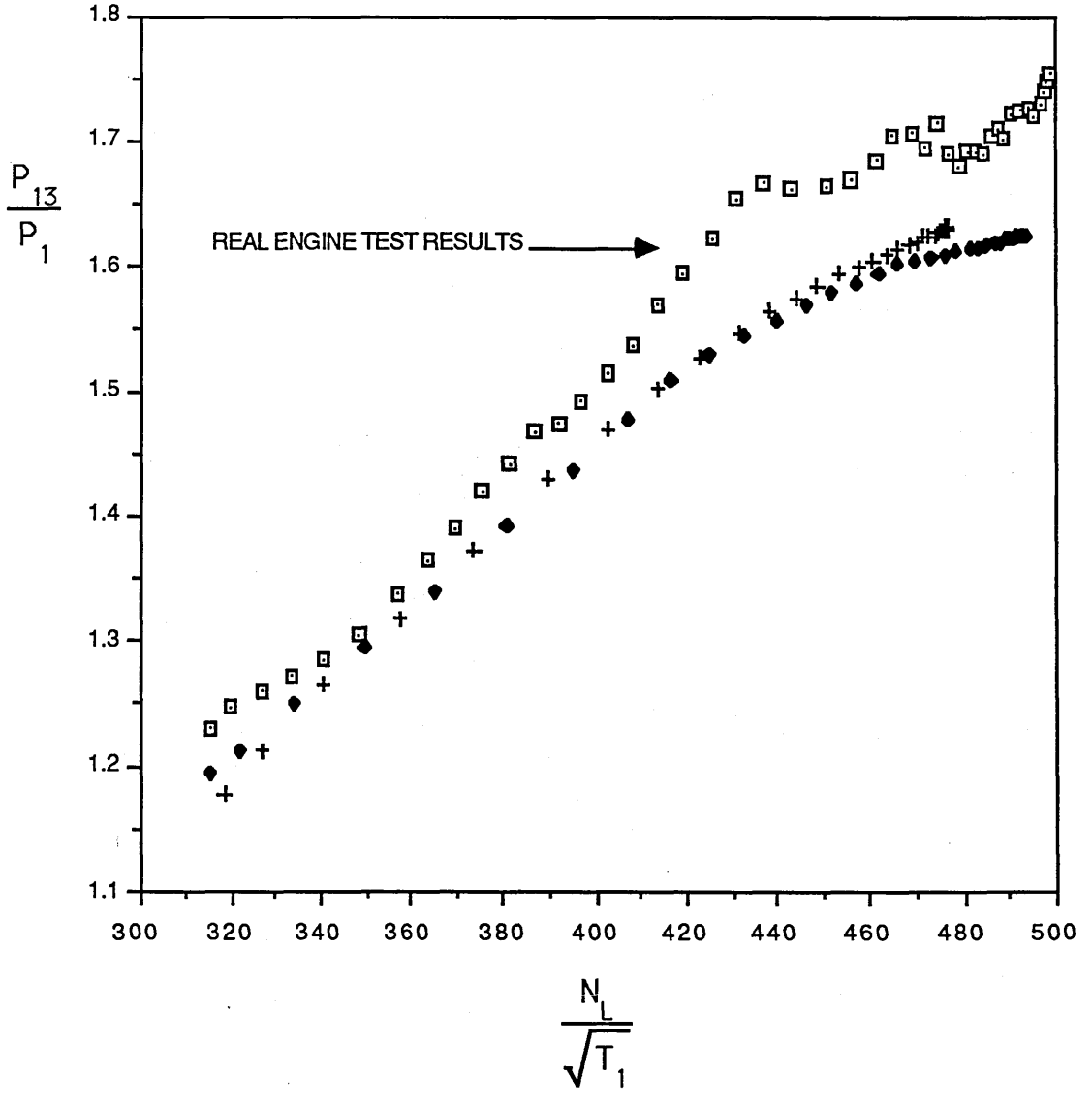

FIGURE 96

COMPARISON OF COMBINED INNER FAN AND I.P. COMPRESSOR PERFORMANCE

BETWEEN PREDICTED AND ACTUAL TEST RESULTS

DURING A "COLD" ACCELERATION AT 43,000ft.

MACH=0.8

WITH 5% I.P. COMPRESSOR BLEED

Data from "TABLE 25"

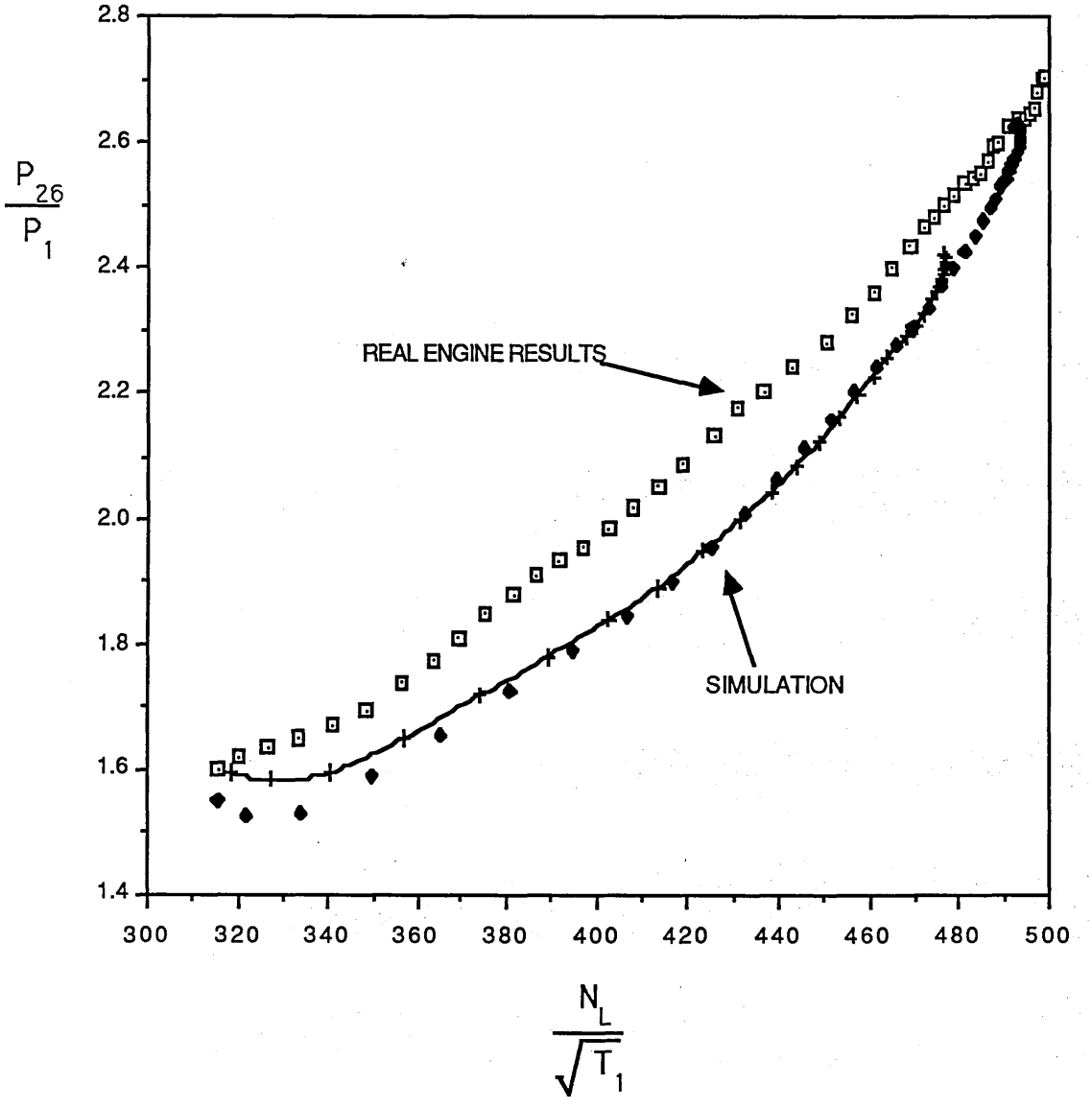

FIGURE 97

COMPARISON OF H.P. COMPRESSOR PERFORMANCE

BETWEEN PREDICTED AND ACTUAL TEST RESULTS

DURING A "COLD" ACCELERATION AT 43,000ft.

MACH=0.8

WITH 5% I.P. COMPRESSOR BLEED

Data from "TABLE 25"

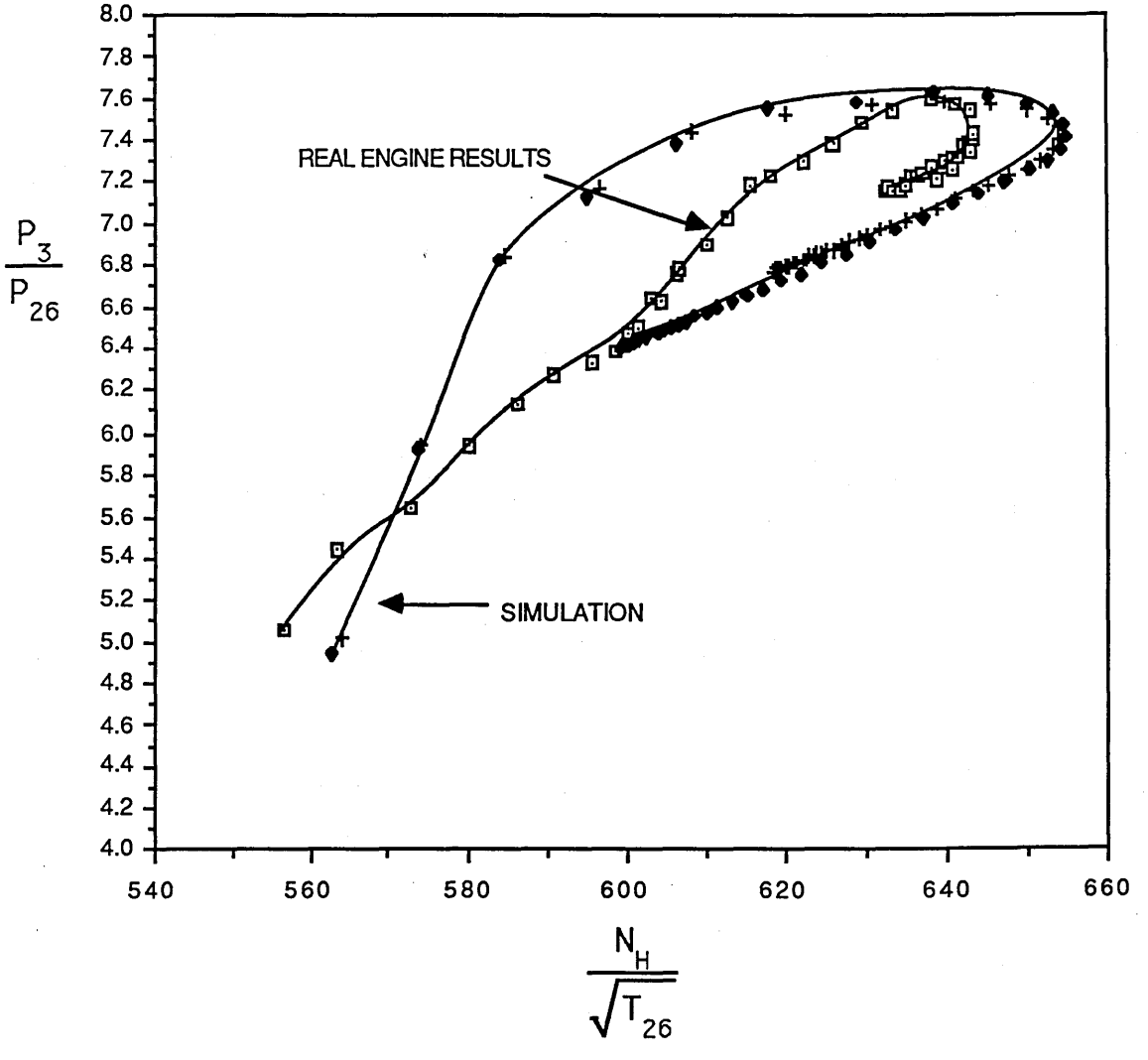

□ = TYPICAL TURBOFAN ENGINE TEST RESULTS

◆ = AFSREE PROGRAM PREDICTION

\+ = STFREE PROGRAM PREDICTION

FIGURE 98

COMPARISON OF CHANGE OF L.P. SHAFT SPEED WITH TIME

DURING A DECELERATION AT 43,000ft.

MACH=0.8

WITH 5% I.P. COMPRESSOR BLEED

Data from "TABLE 26"

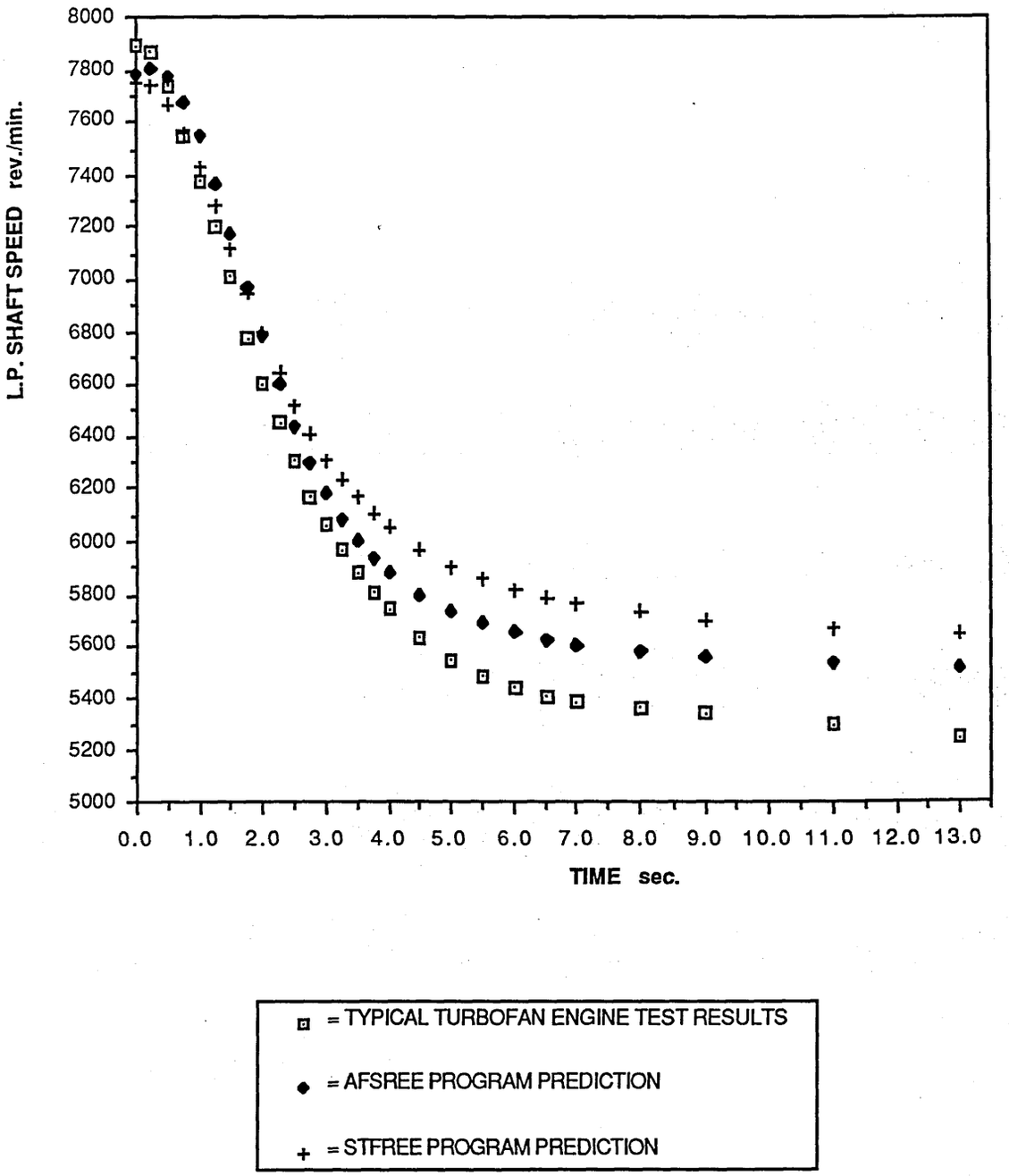

FIGURE 99

COMPARISON OF CHANGE OF H.P. SHAFT SPEED WITH TIME

DURING A DECELERATION AT 43,000ft.

MACH=0.8

WITH 5% I.P. COMPRESSOR BLEED

Data from "TABLE 26"

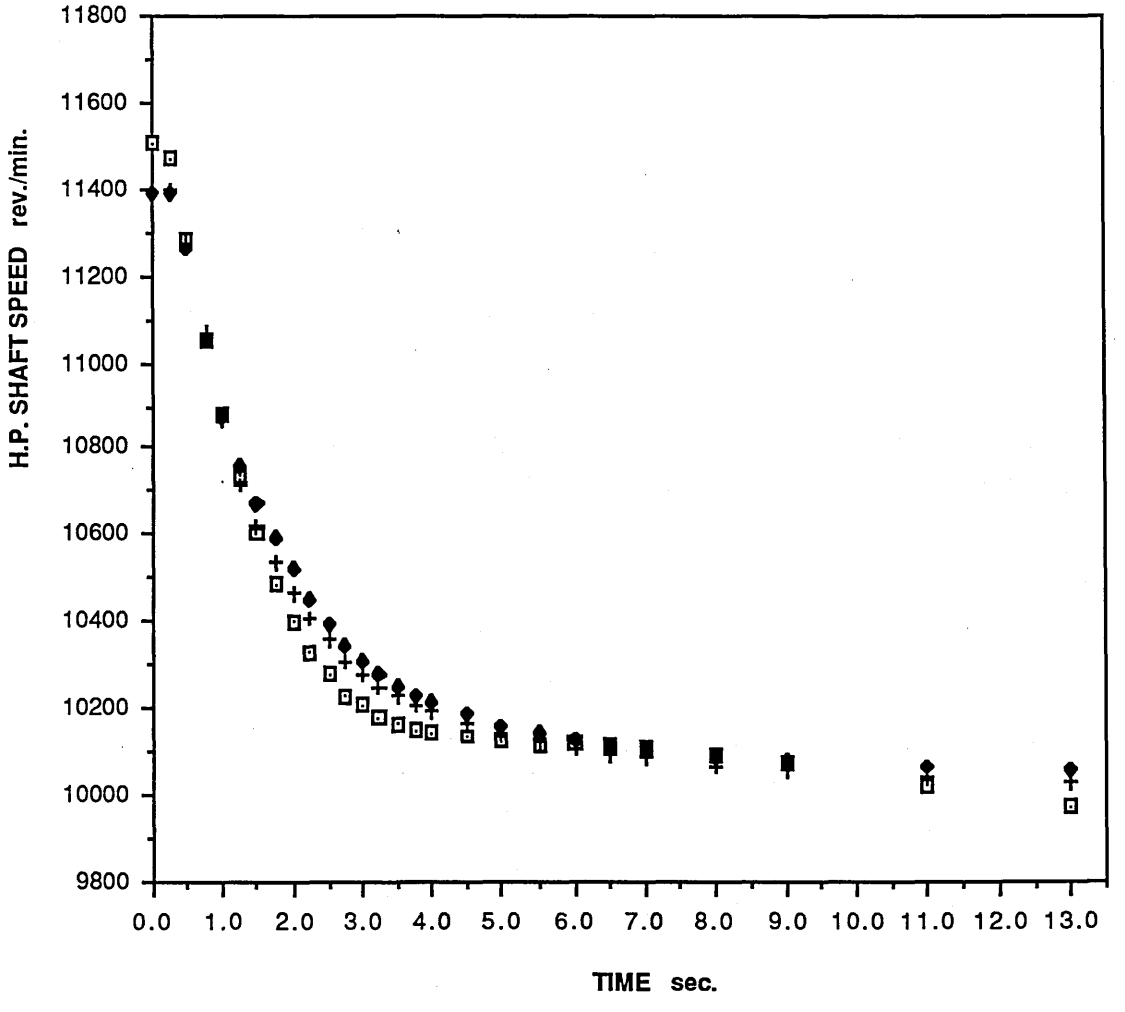

□ = TYPICAL TURBOFAN ENGINE TEST RESULTS

◆ = AFSREE PROGRAM PREDICTION

\+ = STFREE PROGRAM PREDICTION

FIGURE 100

COMPARISON OF L.P. vs. H.P. SHAFT SPEED RESPONSE

DURING A DECELERATION AT 43,000ft.

MACH=0.8

WITH 5% I.P. COMPRESSOR BLEED

Data from "TABLE 26"

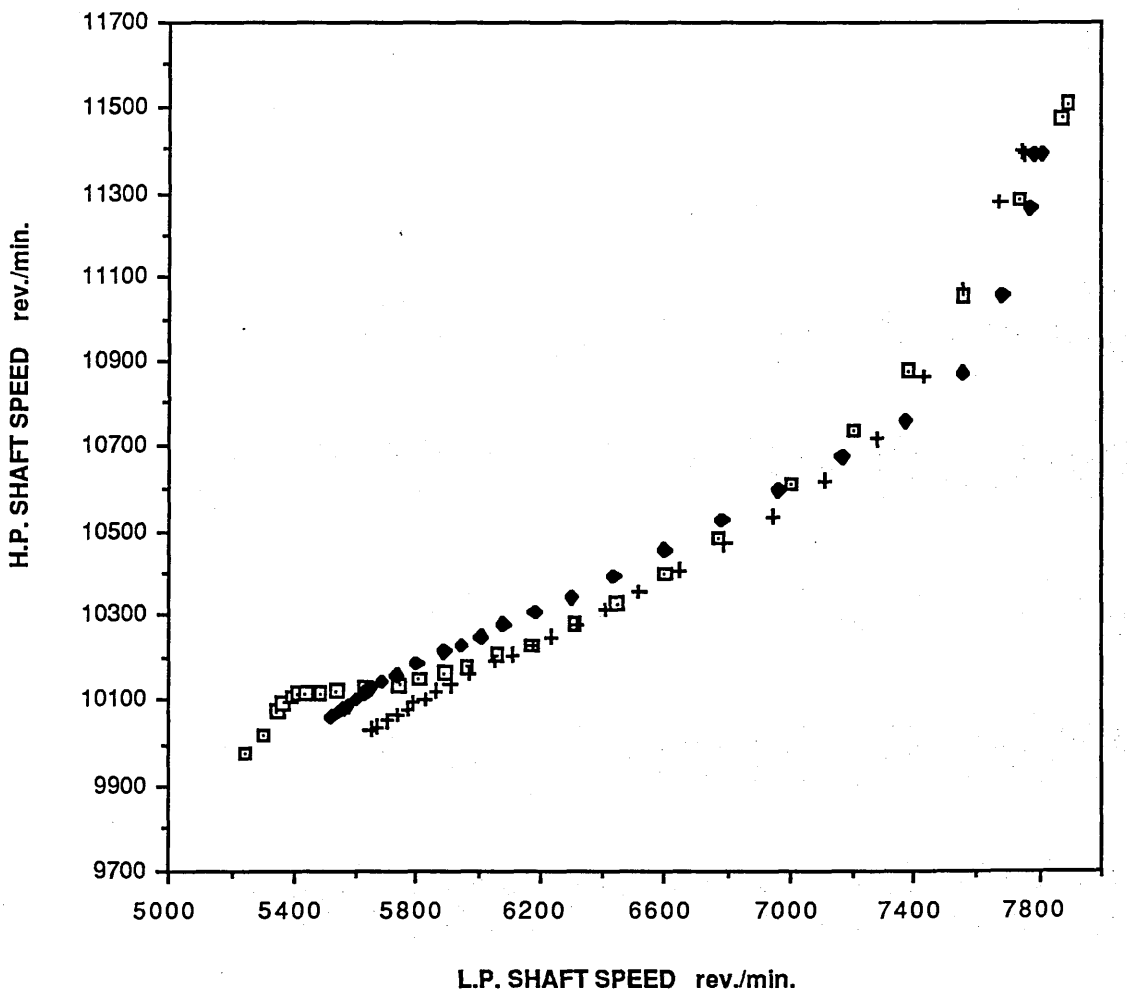

□ = TYPICAL TURBOFAN ENGINE TEST RESULTS

◆ = AFSREE PROGRAM PREDICTION

\+ = STFREE PROGRAM PREDICTION

FIGURE 101

COMPARISON OF OUTER FAN PERFORMANCE

BETWEEN PREDICTED AND ACTUAL TEST RESULTS

DURING A DECELERATION AT 43,000ft.

MACH=0.8

WITH 5% I.P. COMPRESSOR BLEED

Data from "TABLE 26"

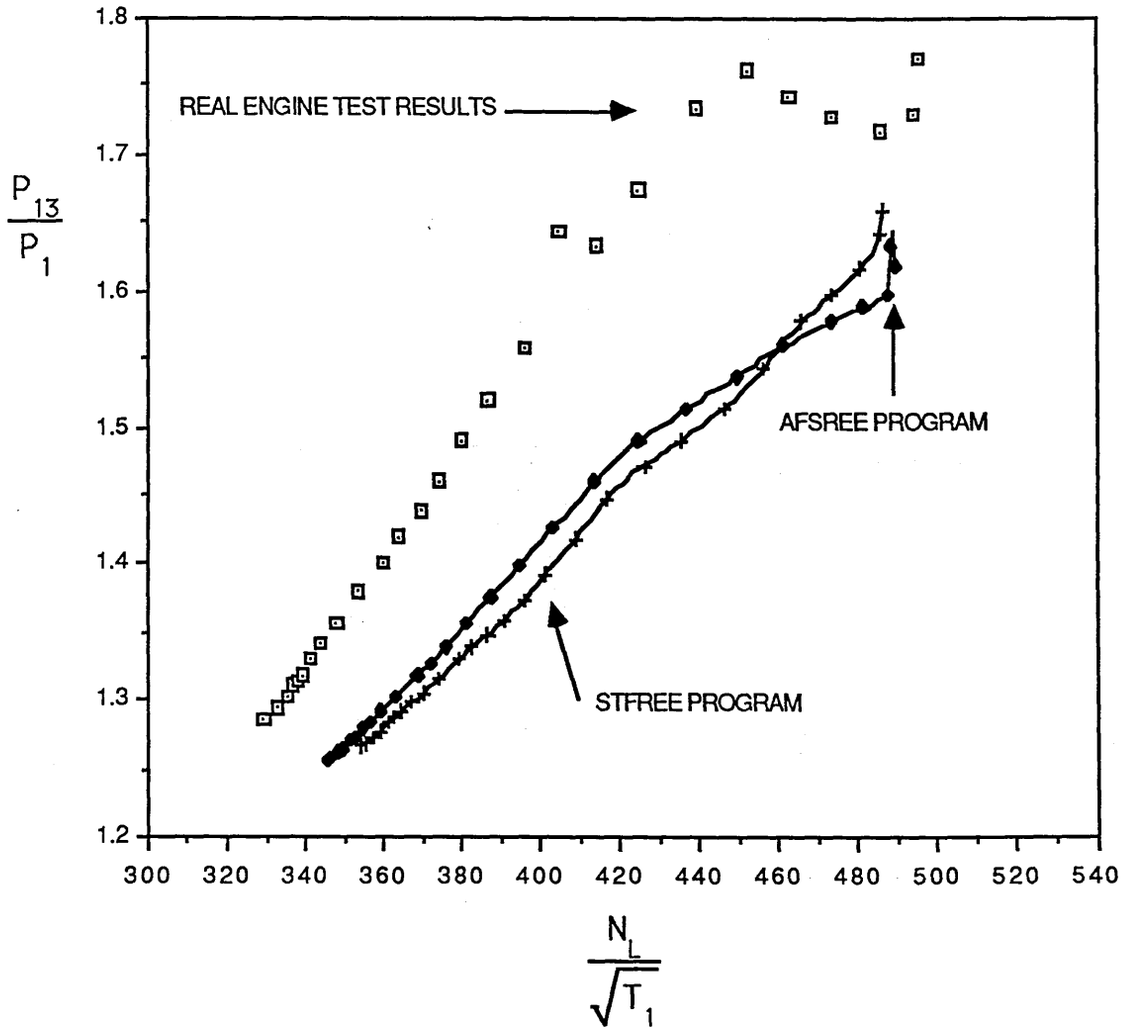

□ = TYPICAL TURBOFAN ENGINE TEST RESULTS

◆ = AFSREE PROGRAM PREDICTION

\+ = STFREE PROGRAM PREDICTION

FIGURE 102

COMPARISON OF COMBINED INNER FAN AND I.P. COMPRESSOR PERFORMANCE

BETWEEN PREDICTED AND ACTUAL TEST RESULTS

DURING A DECELERATION AT 43,000ft.

MACH=0.8

WITH 5% I.P. COMPRESSOR BLEED

Data from "TABLE 26"

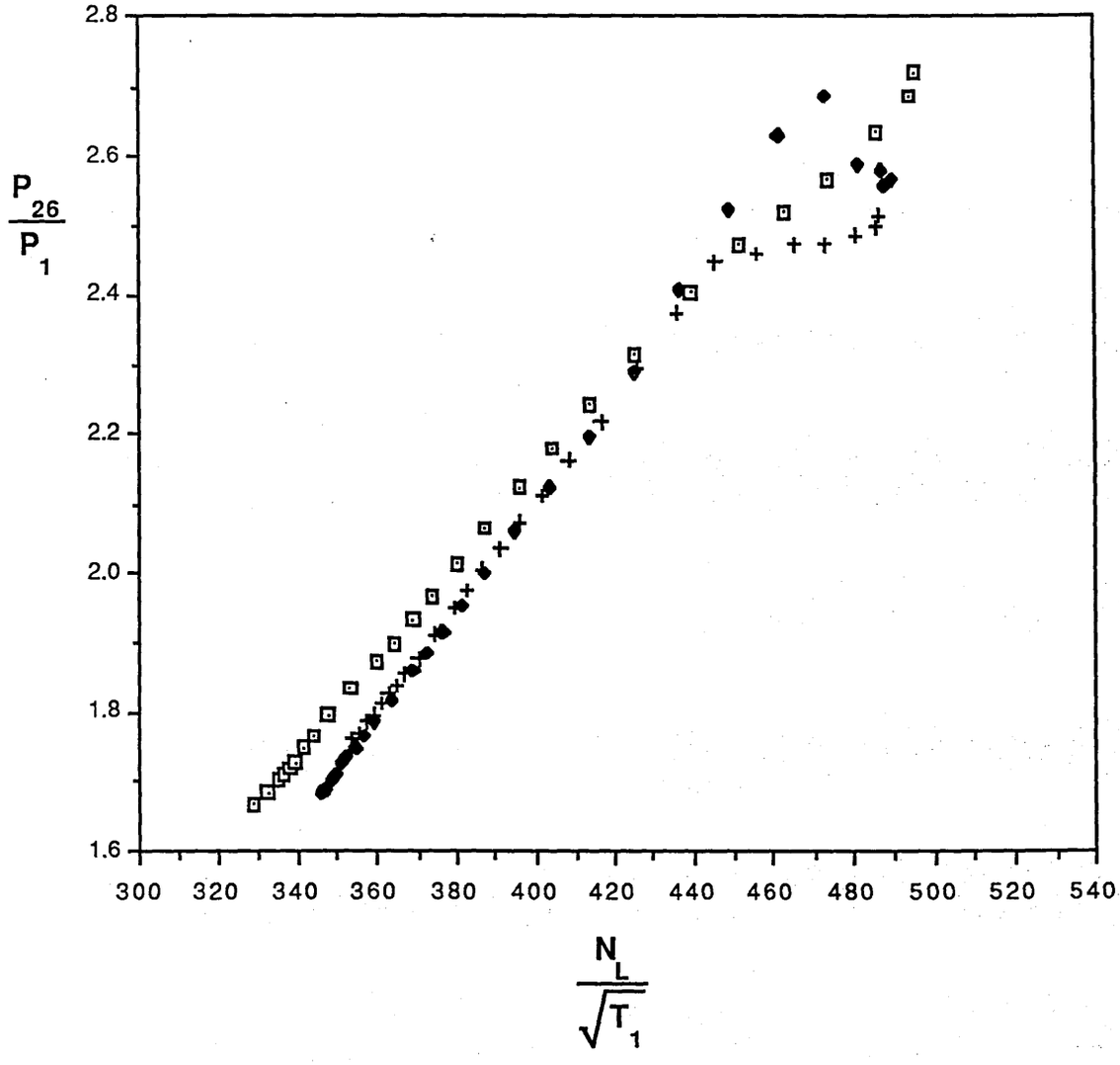

FIGURE 103

COMPARISON OF H.P. COMPRESSOR PERFORMANCE

BETWEEN PREDICTED AND ACTUAL TEST RESULTS

DURING A DECELERATION AT 43,000ft.

MACH=0.8

WITH 5% I.P. COMPRESSOR BLEED

Data from "TABLE 26"

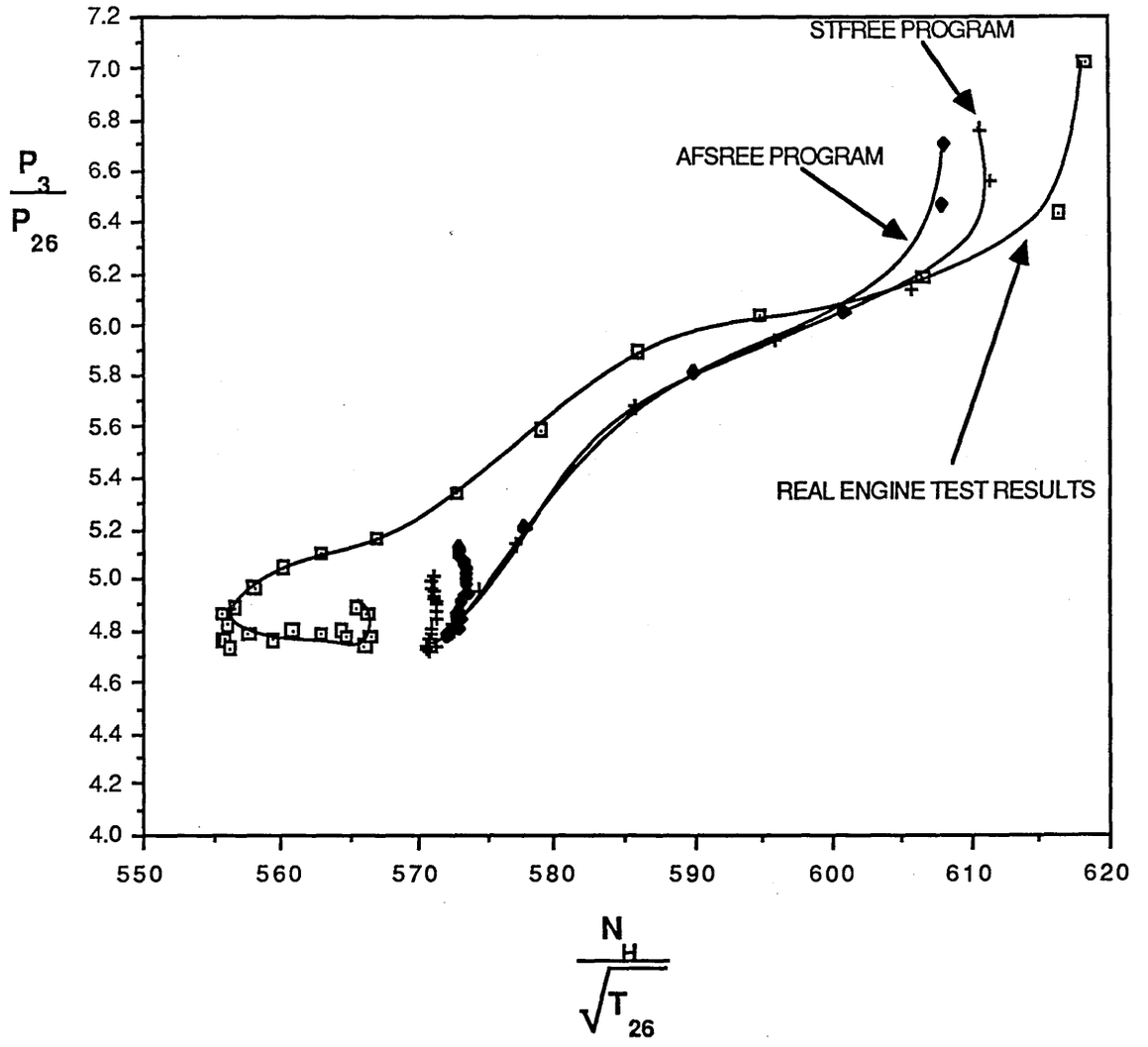

= TYPICAL TURBOFAN ENGINE TEST RESULTS

◆ = AFSREE PROGRAM PREDICTION

\+ = STFREE PROGRAM PREDICTION

FIGURE 104

COMPARISON BETWEEN PREDICTED AND ACTUAL TEST RESULTS

DURING A "COLD" ACCELERATION AT 43,000ft.

MACH=0.8

WITH 5% I.P. COMPRESSOR BLEED

Data from "TABLE 25"

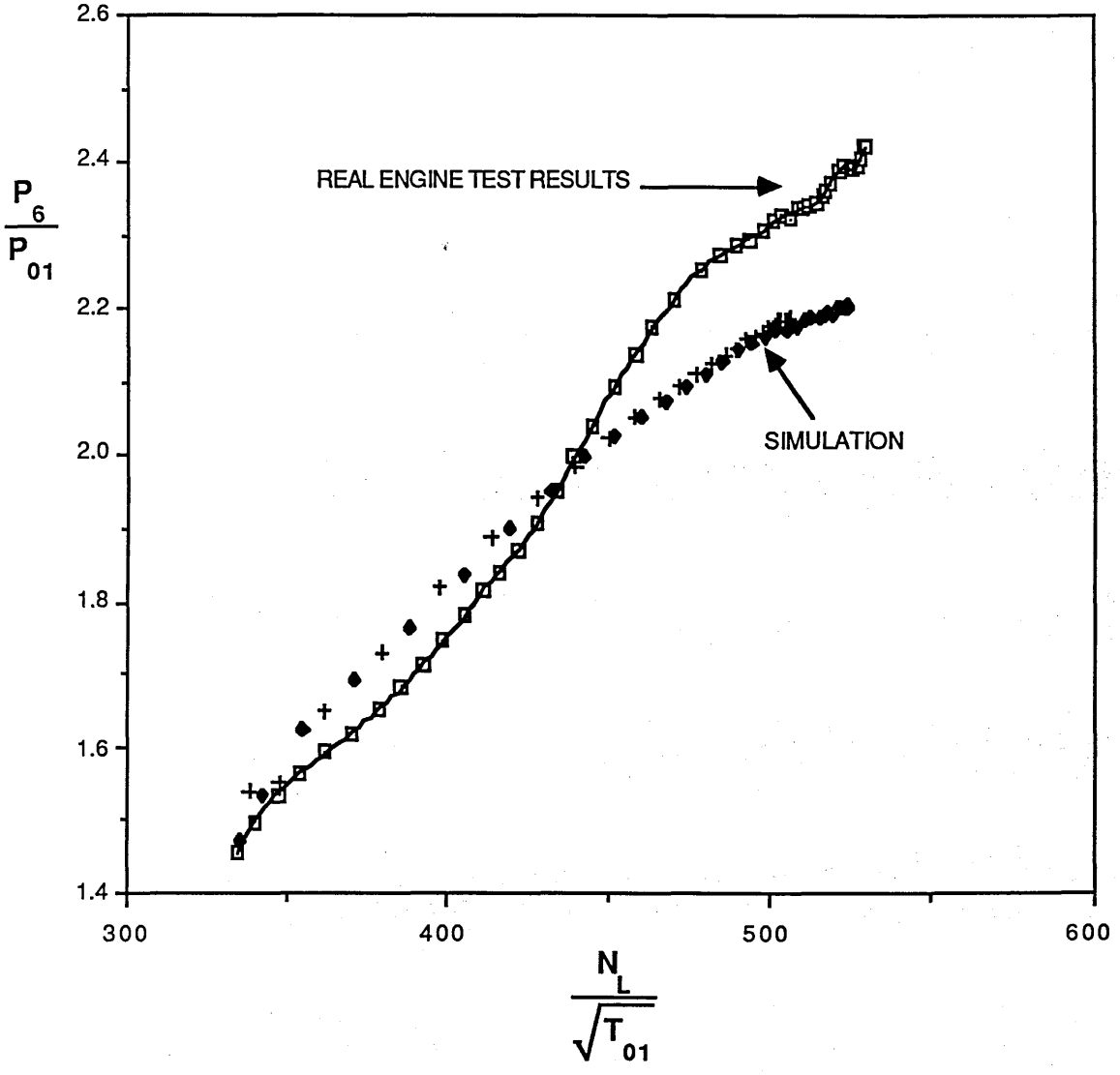

□ = TYPICAL TURBOFAN ENGINE TEST RESULTS

◆ = AFSREE PROGRAM PREDICTION

\+ = STFREE PROGRAM PREDICTION

FIGURE 105

COMPARISON BETWEEN PREDICTED AND ACTUAL TEST RESULTS

DURING A DECELERATION AT 43,000ft.

MACH=0.8

WITH 5% I.P. COMPRESSOR BLEED

Data from "TABLE 26"

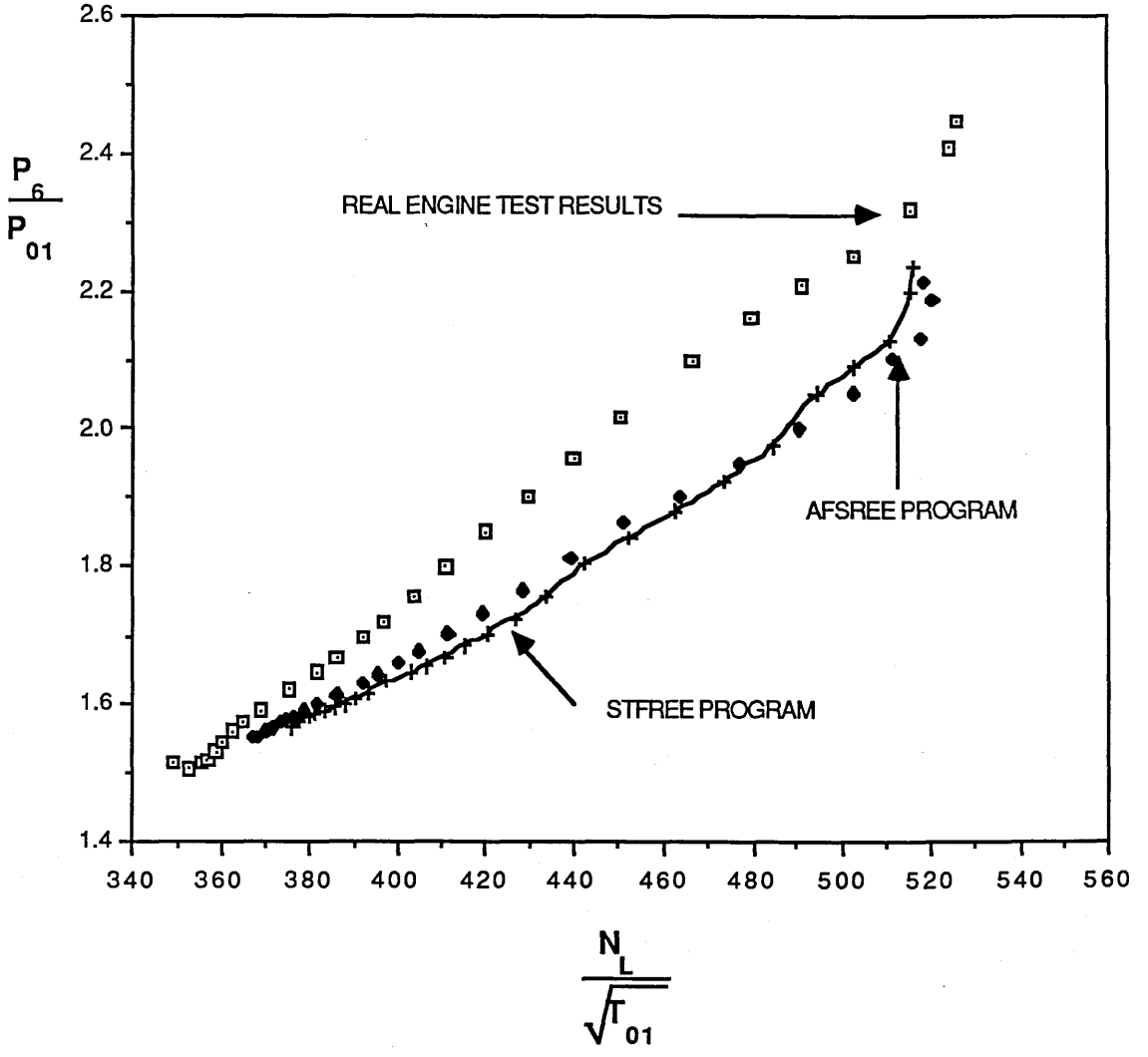

□ = TYPICAL TURBOFAN ENGINE TEST RESULTS

◆ = AFSREE PROGRAM PREDICTION

\+ = STFREE PROGRAM PREDICTION

FIGURE 106

COMPARISON OF CHANGE OF L.P. SHAFT SPEED WITH TIME

DURING A "BODIE" AT 43,000ft.

MACH=0.8

Data from "TABLE 27"

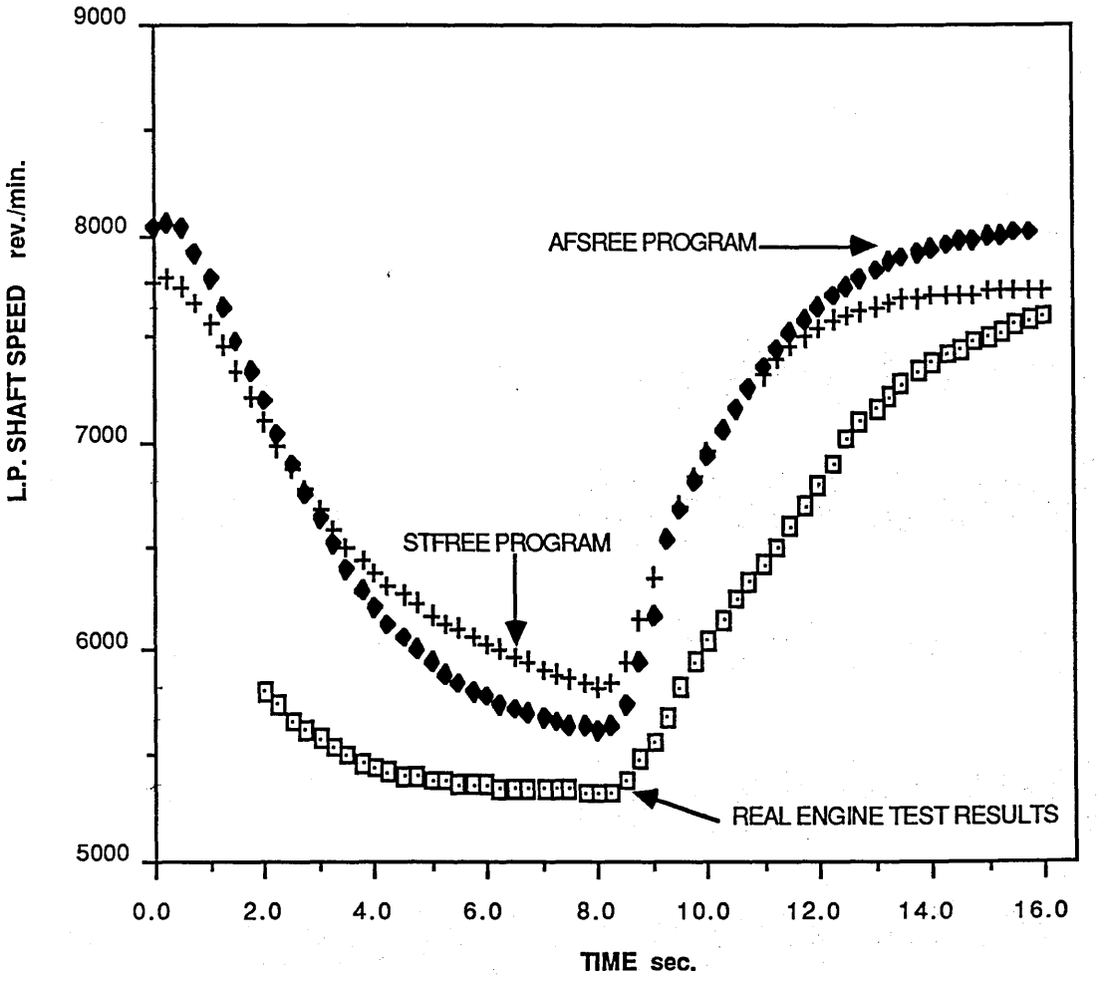

▫ = TYPICAL TURBOFAN ENGINE TEST RESULTS

◆ = AFSREE PROGRAM PREDICTION

\+ = STFREE PROGRAM PREDICTION

FIGURE 107

COMPARISON OF CHANGE OF H.P. SHAFT SPEED WITH TIME

DURING A "BODIE" AT 43,000ft.

MACH=0.8

Data from "TABLE 27"

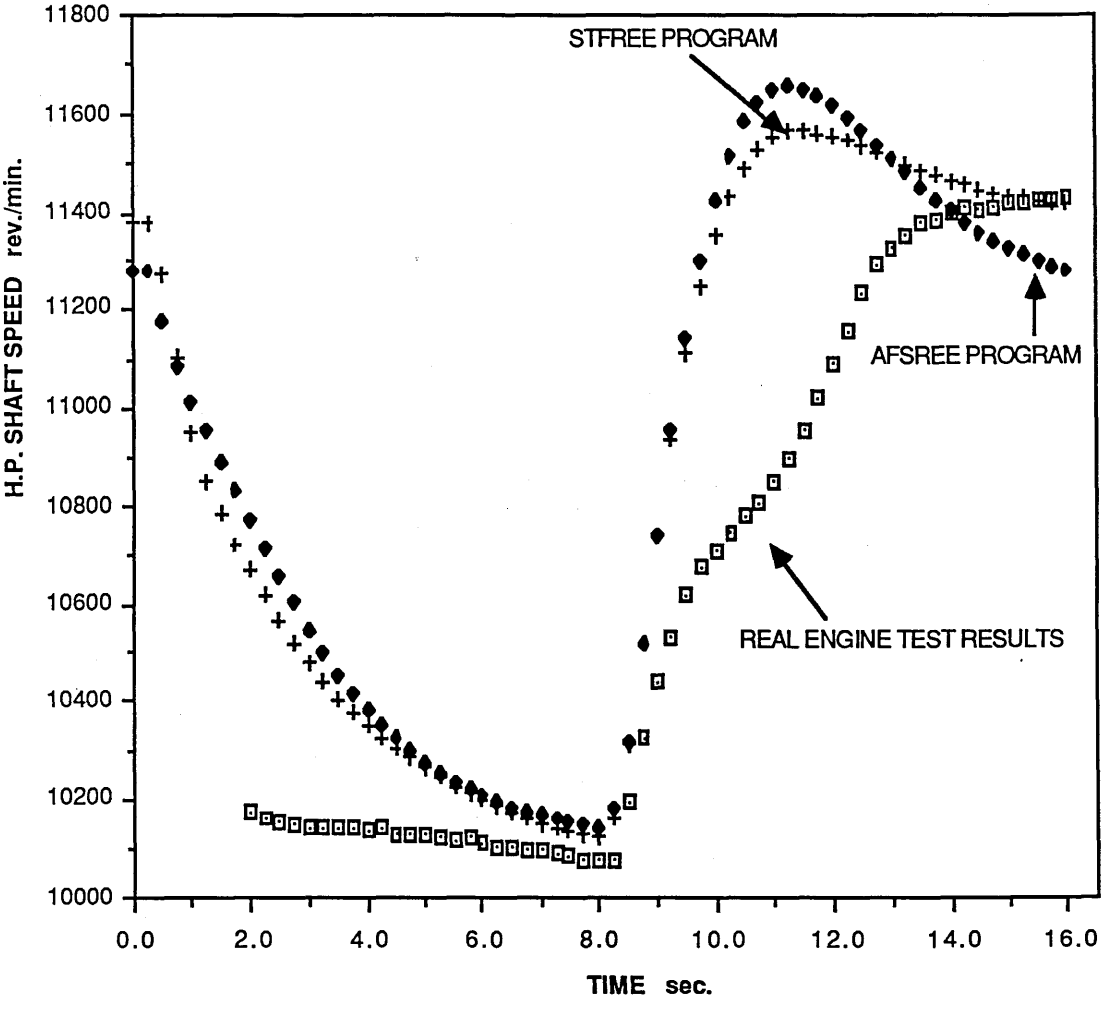

□ = TYPICAL TURBOFAN ENGINE TEST RESULTS

◆ = AFSREE PROGRAM PREDICTION

\+ = STFREE PROGRAM PREDICTION

FIGURE 108

COMPARISON OF OUTER FAN PERFORMANCE

BETWEEN PREDICTED AND ACTUAL TEST RESULTS

DURING A "BODIE" AT 43,000ft.

MACH=0.8

Data from "TABLE 27"

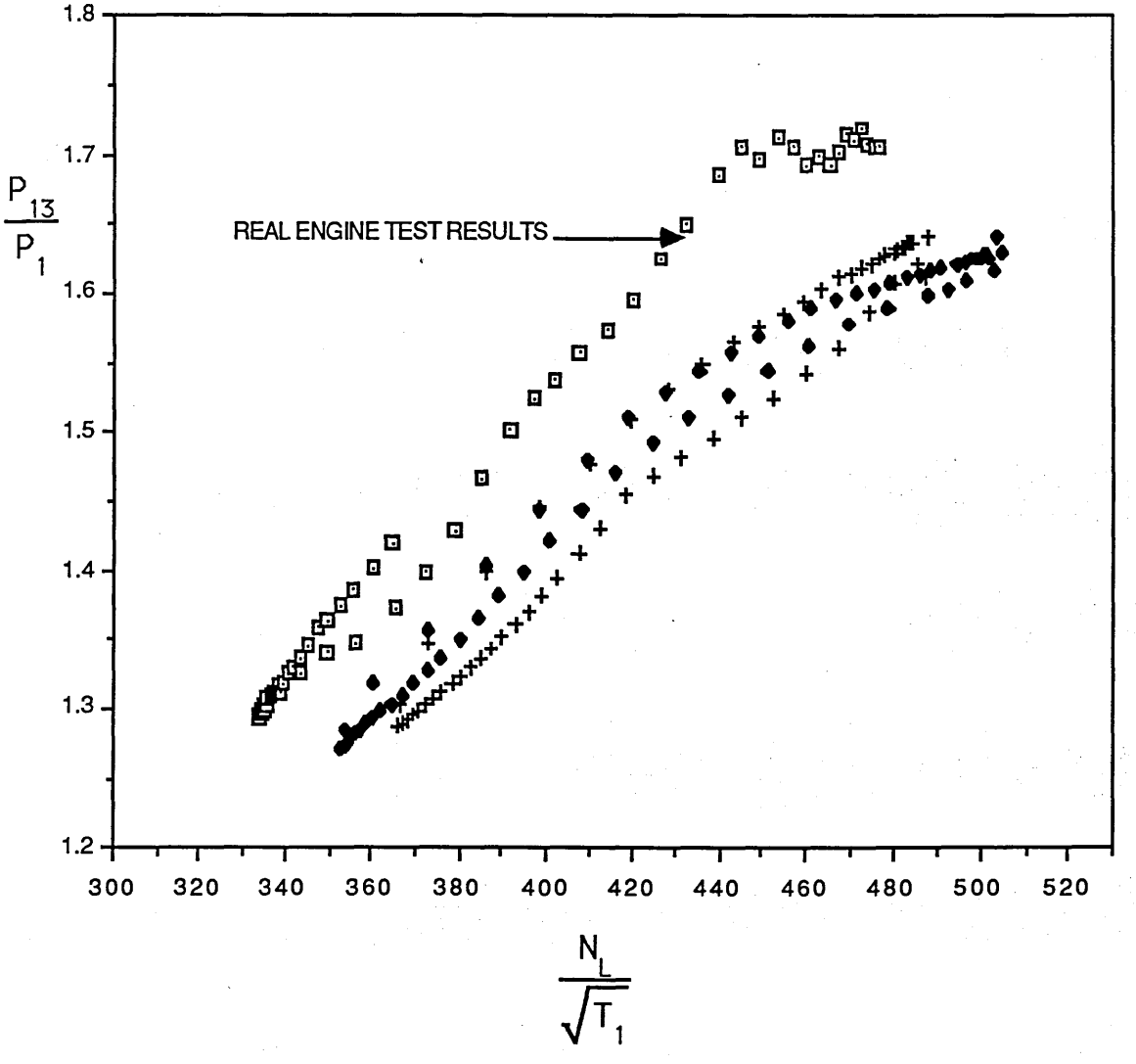

□ = TYPICAL TURBOFAN ENGINE TEST RESULTS

◆ = AFSREE PROGRAM PREDICTION

\+ = STFREE PROGRAM PREDICTION

FIGURE 108A

COMPARISON OF OUTER FAN PERFORMANCE

BETWEEN PREDICTED AND ACTUAL TEST RESULTS

DURING A "BODIE" AT 43,000ft.

MACH=0.8

Data from "TABLE 27"

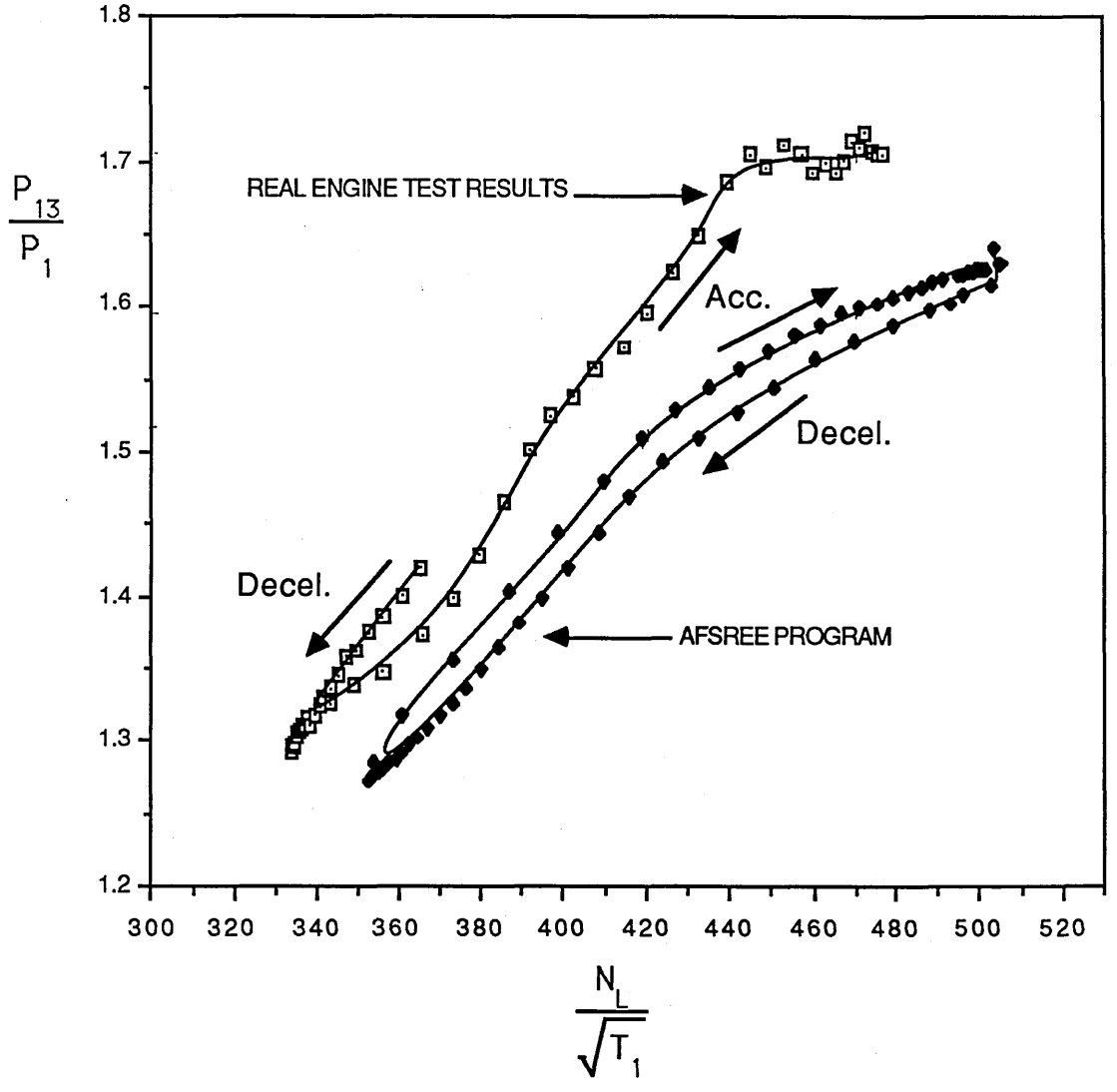

□ = TYPICAL TURBOFAN ENGINE TEST RESULTS

◆ = AFSREE PROGRAM PREDICTION

FIGURE 108B

COMPARISON OF OUTER FAN PERFORMANCE

BETWEEN PREDICTED AND ACTUAL TEST RESULTS

DURING A "BODIE" AT 43,000ft.

MACH=0.8

Data from "TABLE 27"

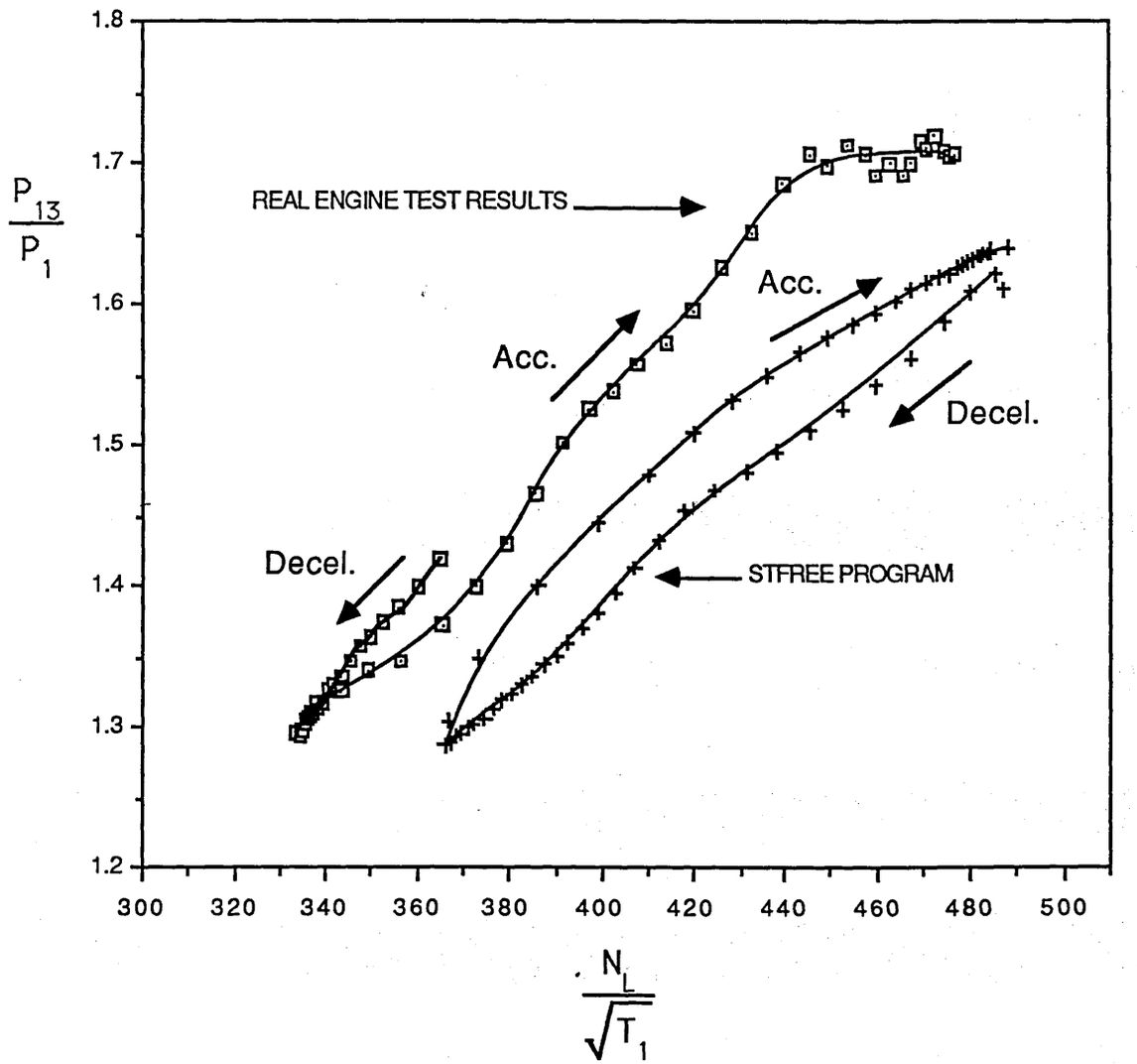

▫ = TYPICAL TURBOFAN ENGINE TEST RESULTS

\+ = STFREE PROGRAM PREDICTION

FIGURE 109

COMPARISON OF COMBINED INNER FAN AND I.P. COMPRESSOR PERFORMANCE

BETWEEN PREDICTED AND ACTUAL TEST RESULTS

DURING A "BODIE" AT 43,000ft.

MACH=0.8

Data from "TABLE 27"

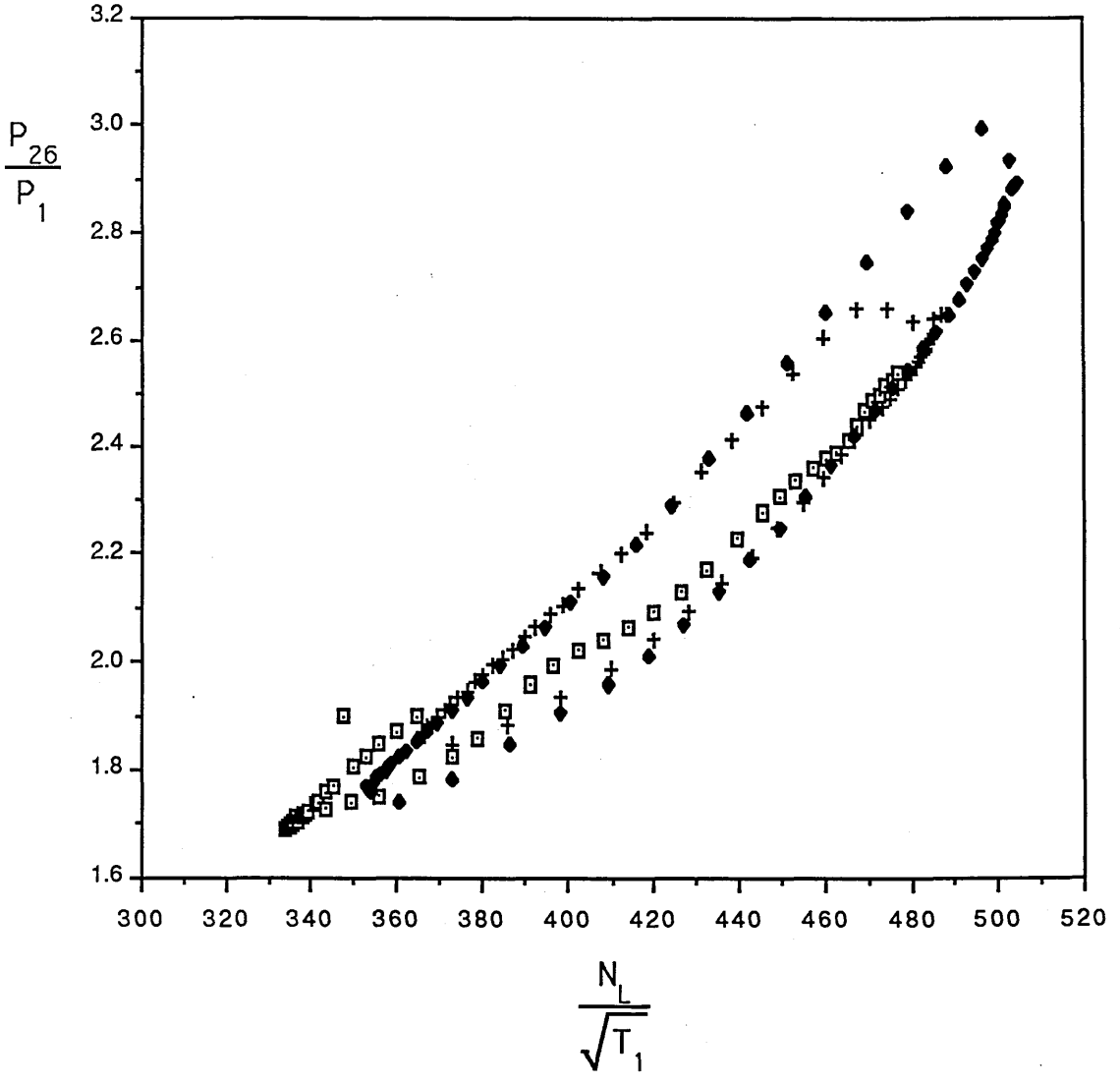

□ = TYPICAL TURBOFAN ENGINE TEST RESULTS

◆ = AFSREE PROGRAM PREDICTION

\+ = STFREE PROGRAM PREDICTION

FIGURE 109A

COMPARISON OF COMBINED INNER FAN AND I.P. COMPRESSOR PERFORMANCE

BETWEEN PREDICTED AND ACTUAL TEST RESULTS

DURING A "BODIE" AT 43,000ft.

MACH=0.8

Data from "TABLE 27"

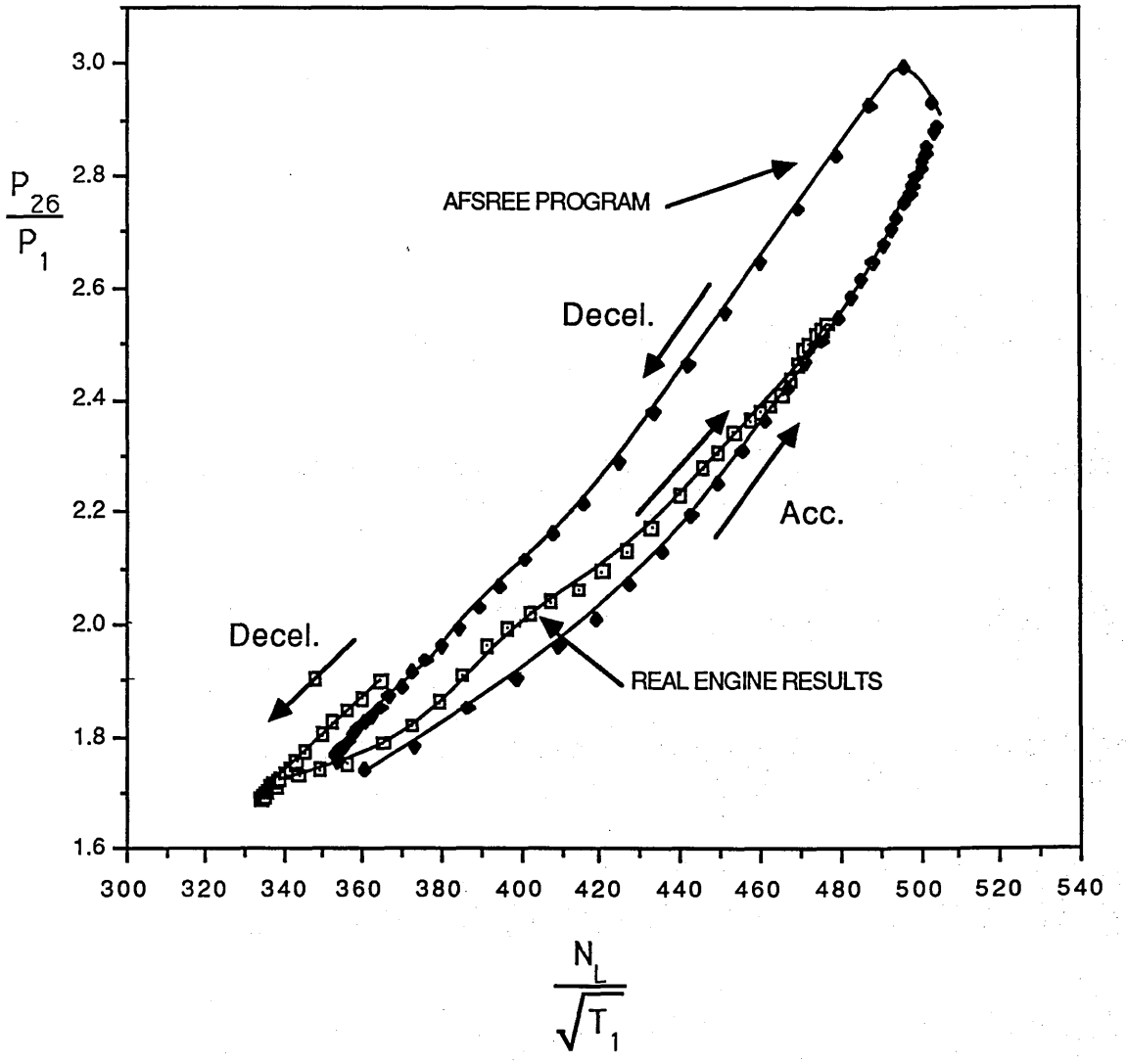

▫ = TYPICAL TURBOFAN ENGINE TEST RESULTS

◆ = AFSREE PROGRAM PREDICTION

FIGURE 109B

COMPARISON OF COMBINED INNER FAN AND I.P. COMPRESSOR PERFORMANCE

BETWEEN PREDICTED AND ACTUAL TEST RESULTS

DURING A "BODIE" AT 43,000ft.

MACH=0.8

Data from "TABLE 27"

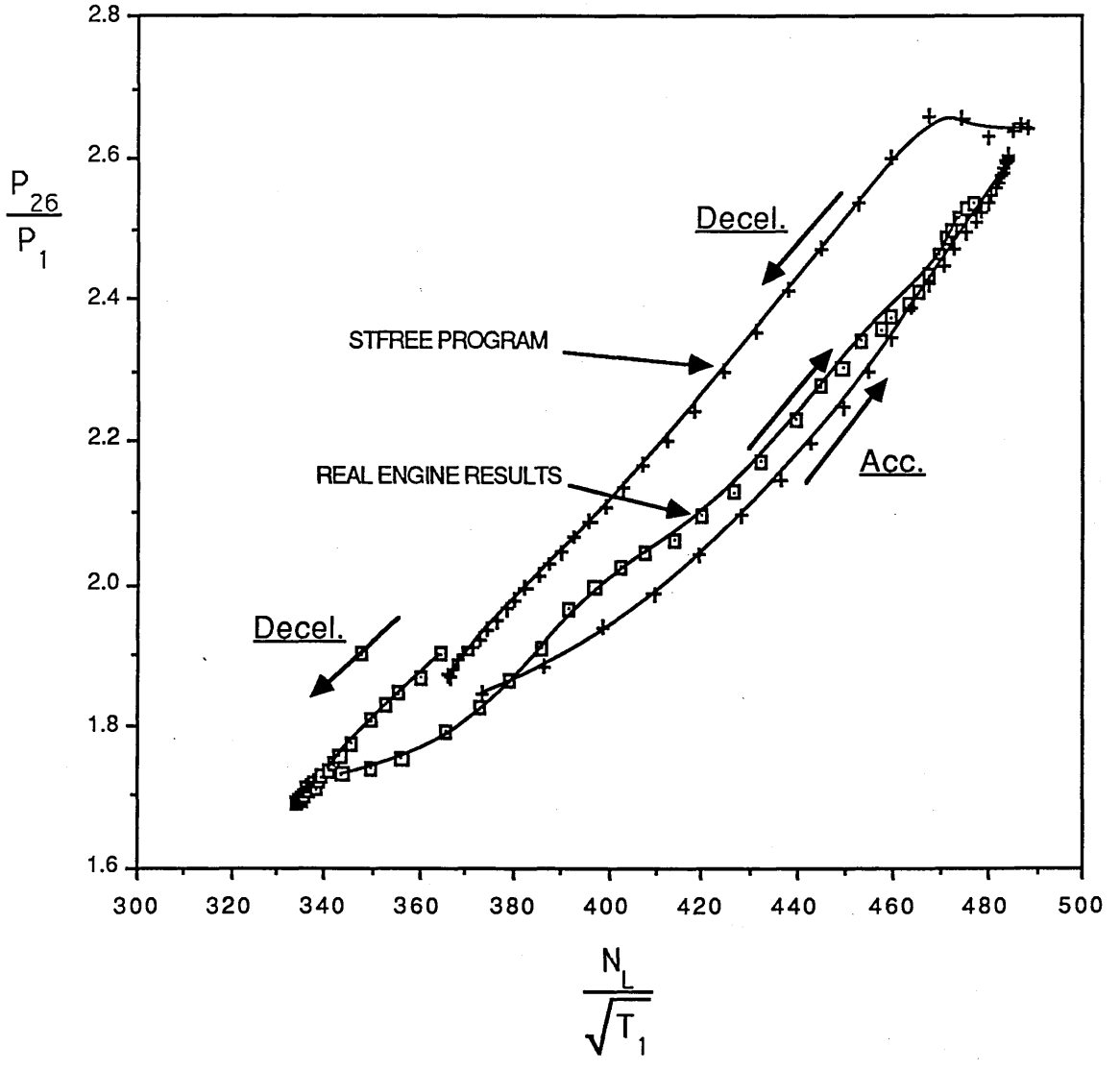

□ = TYPICAL TURBOFAN ENGINE TEST RESULTS

\+ = STFREE PROGRAM PREDICTION

FIGURE 110

COMPARISON OF H.P. COMPRESSOR PERFORMANCE

BETWEEN PREDICTED AND ACTUAL TEST RESULTS

DURING A "BODIE AT 43,000ft.

MACH=0.8

Data from "TABLE 27"

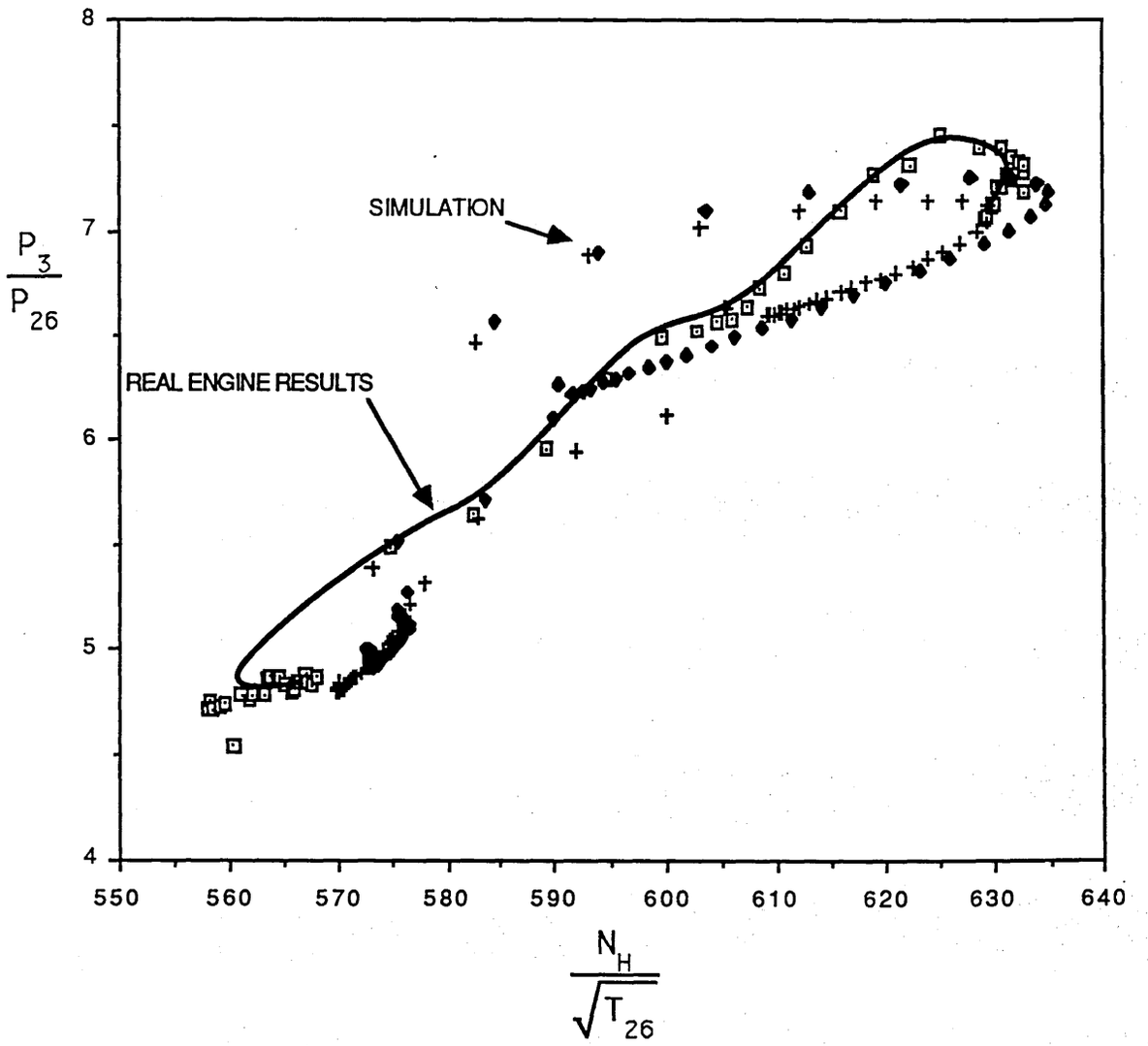

□ = TYPICAL TURBOFAN ENGINE TEST RESULTS

◆ = AFSREE PROGRAM PREDICTION

\+ = STFREE PROGRAM PREDICTION

FIGURE 110A

COMPARISON OF H.P. COMPRESSOR PERFORMANCE

BETWEEN PREDICTED AND ACTUAL TEST RESULTS

DURING A "BODIE" AT 43,000ft.

MACH=0.8

Data from "TABLE 27"

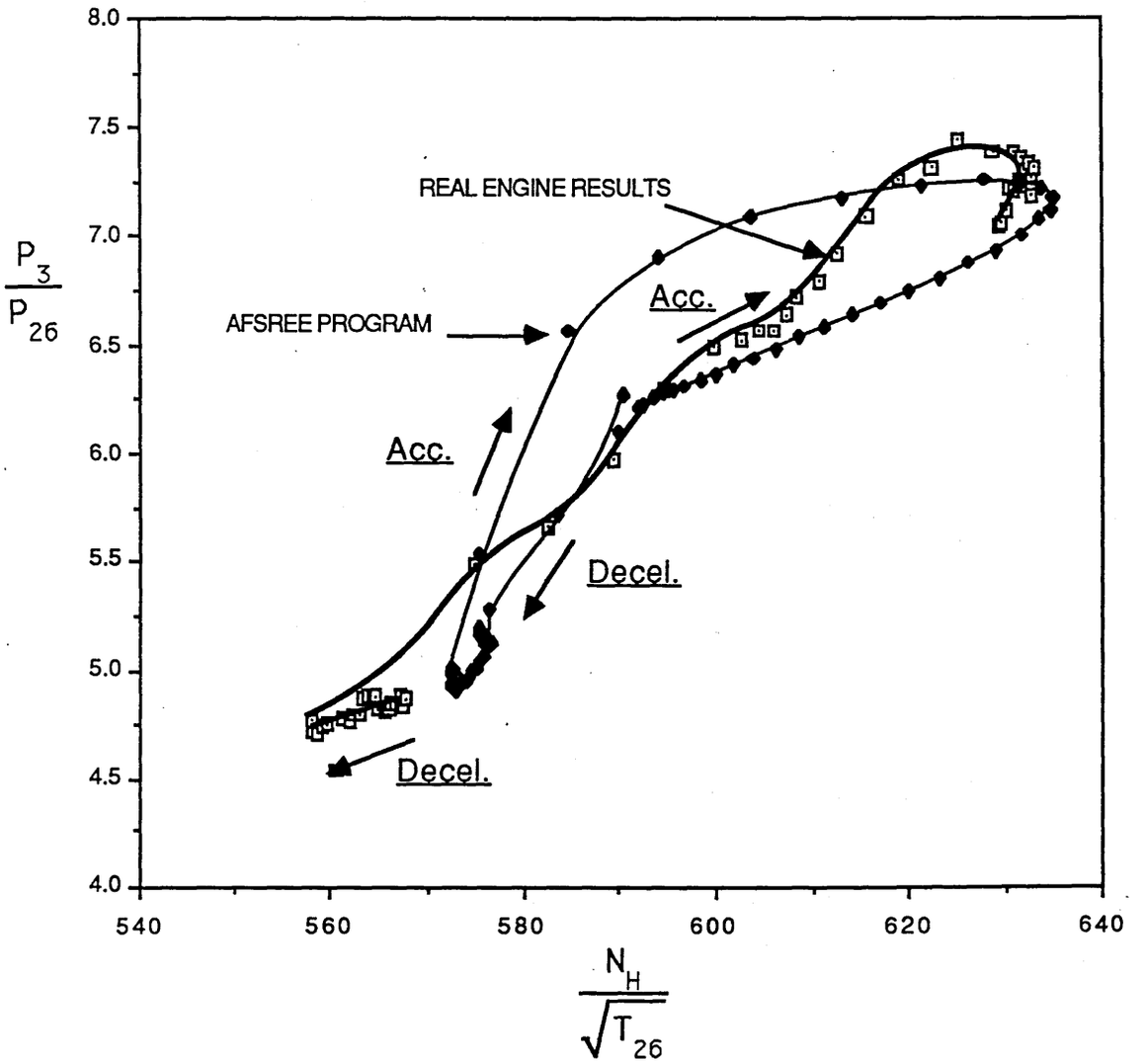

▫ = TYPICAL TURBOFAN ENGINE TEST RESULTS

◆ = AFSREE PROGRAM PREDICTION

FIGURE 110B

COMPARISON OF H.P. COMPRESSOR PERFORMANCE

BETWEEN PREDICTED AND ACTUAL TEST RESULTS

DURING A "BODIE" AT 43,000ft.

MACH=0.8

Data from "TABLE 27"

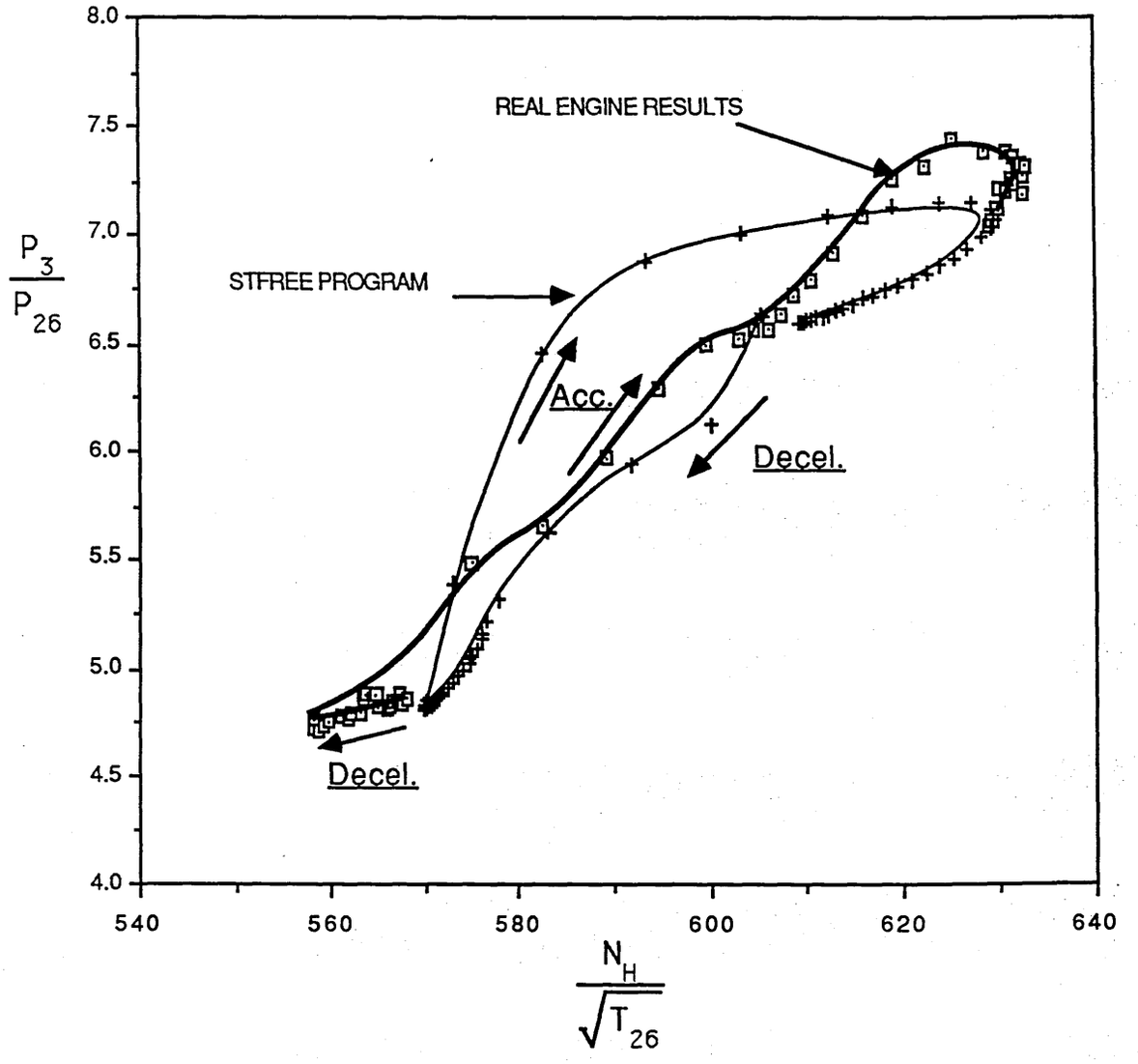

□ = TYPICAL TURBOFAN ENGINE TEST RESULTS

\+ = STFREE PROGRAM PREDICTION

FIGURE 83

COMPARISON OF H.P. COMPRESSOR PERFORMANCE

BETWEEN PREDICTED AND ACTUAL TEST RESULTS

DURING A "COLD" ACCELERATION AT 43,000ft.

MACH=0.8

Data from "TABLE 23"

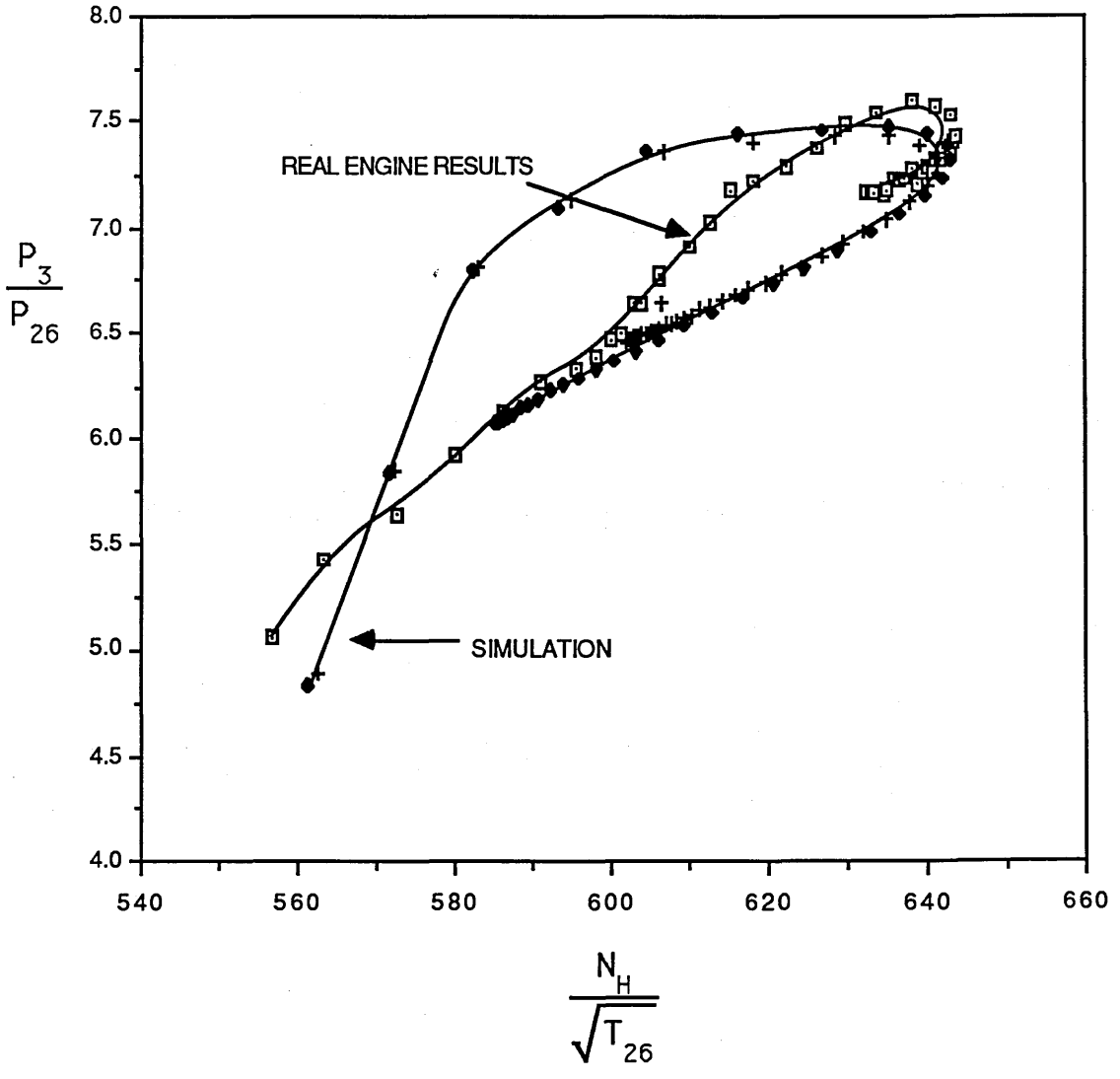

APPENDIX A

There are many cases where a compressor can no longer sustain the pressure ratio it has generated and is forced to a sudden change of its operating point. This generally means a reduction in flow and pressure ratio at a given speed. This is associated with aerodynamic stalling of some of the blades of the compressor. It is the transfer from unstalled to stalled operation that causes the sudden change mentioned above.

There are a variety of types of change from unstalled to stalled operation. Surge, which is one of the most important, is also associated with a sudden drop in delivery pressure and with a pulsation of the working fluid which is transmitted throughout the whole machine. This pulsation is due to the surging of the fluid backwards and forwards through the compressor. The pulsation of the working fluid causes extensive vibration of the blades and continuous operation under surge could lead to breakage of blades.

The phenomenon of surge can be explained as follows; If the compressor is forced for some reason to operate on the part of its characteristics of positive slope then a decrease in mass flow will be followed with a subsequent drop in pressure ratio. If the pressure downstream of the compressor does not fall quickly enough, then the working fluid is forced to reverse its direction of flow. Meanwhile the pressure downstream has fallen also and the working fluid is capable of reversing again its direction of flow. This is the cause of the surging of the fluid backwards and

forwards in the compressor.

Another important cause of instability in the compressor operation, is the rotating stall which can also exist in the stable operating range of the compressor. When the mass flow through the compressor is reduced, this causes the mass flow through the individual blade-to-blade passages of a row to reduce, and in general the incidence angle of the flow into these passages rises. Due to turbulence effects and the inevitable unevenness of the flow, one passage will reach the critical incidence angle at which the flow on the suction surface stalls ahead of its neighbouring passages. When the passage has stalled, that particular passage will then be accepting less air, so the air approaching that sector is deflected-some towards the passage which is forward(in a rotational direction) from the passage already stalled, and some towards the passage behind. For the forward passage, the deflected flow reduces the incidence angle and relieves the tendency to stall. However the passage behind suffers an increased incidence angle and this causes it to stall. This then relieves the stall in the passage where it had first occured. Thus, in the moving blade, the stall propagates in a counter rotating direction. This is the reason for naming this particular malfunction of the compressor as Rotating Stall. It has been observed that the above described rotating stall regions, or otherwise called Rotating Stall Cells-(RSC), rotate within the compressor at 20 to 70 per cent of the rotor's speed.

Sometimes a severe case of rotating stall is called Deep stall and in that case the circumferential width of the stall cells could vary from a small arc to a large sector.

Turning now to the phenomenon of surge again, it is worth mentioning the mechanics of onset of surge. Generally, the amount of air mass flow rate through the compressor is controlled by choking in the various stages. This could occur either in the early or in the late stages of the compressor.

When the compressor is operating at its design point then the flow at all stages has a correct angle of incidence. If at the design speed the operating point of the compressor is forced on to the surge line, then the delivery pressure will increase substantially accompanied by a relatively small reduction in air mass flow rate. This in turn will cause the density at the compressor's exit to increase. These effects have as a result the reduction of the axial velocity which in turn will force the angle of incidence at the last stages to increase and the rotor blades to stall. Research has shown that at high speeds surge is initialised by the stalling of the last stages.

At low speeds, the opposite is the case due to the more rapid reduction of mass flow in comparison with the decrease in speed. Hence the axial velocity at the inlet decreases and the incidence at the early stages increases. As a result it is thought that at low speeds surge occurs due to stalling of the early stages.

Investigation that has been carried out over the years has shown that if the last stages stall then the surging progresses upstream and could cause surge in the whole of the compressor.

APPENDIX B

1. Air Intake Calculations

The entry stagnation Temperature and Pressure are calculated using the Flight Mach number and the Ambient temperature and pressure according to the Altitude.

Using the following equations T_{STAGN} and P_{STAGN} are evaluated:

$$T_{STAGN}=T_{AMB}\times(1+0.2M^2)$$

$$P_{STAGN}=RECOVY\times P_{AMB}\times\left(\frac{T_1}{T_{AMB}}\right)^{3.5}$$

where RECOVY is the pressure Recovery factor of 0.995 used to account for non-isentropic diffusion losses.

2.The Inner,Outer Fan and I.P. Compressor calculations

The known parameters are : P_i, T_i, N, GEOM

The guessed parametrs are : $\frac{\dot{m}\sqrt{T}}{P}$ and FCSP

The Factor of Split is used to calculate the equivelant non-dimensional mass flow rate using:

$$\left(\frac{\dot{m}\sqrt{T}}{P}\right)_{CHICS}=\frac{1}{FCSP}\left(\frac{\dot{m}\sqrt{T}}{P}\right)_{ACT.}$$

It is also used to evaluate the non-dimensional mass flow rate

$$\left(\frac{\dot{m}\sqrt{T}}{P}\right)_{OUTER}=\left(\frac{1.0-GEOM\times FCSP}{GEOM\times FCSP}\right)\times\left(\frac{\dot{m}\sqrt{T}}{P}\right)_{INNER}$$

The non-dimensional speed can now be calculated and by interpolating in the characteristics together with the non-dimensional mass flow rate, then the Pressure ratio, Isentropic efficiency and exact Beta value are found.

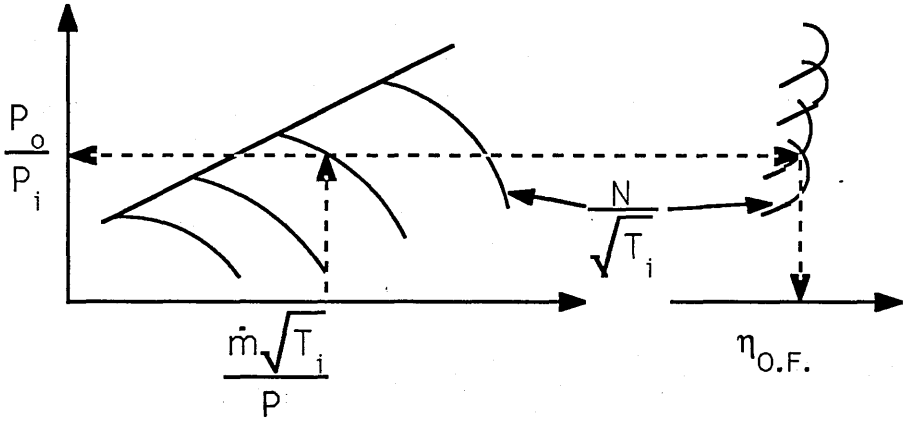

Knowing now the pressure ratio P_o/P_i then the P_o is found.

The outlet temperature T_o can be calculated using C_p= 1 initially. Then $\gamma = C_p/(C_p-R)$ and the isentopic outlet temperature is calculated using:

$$T'_o-T_i=T_i\left[\left(\frac{P_o}{P_i}\right)^{\frac{\gamma-1}{\gamma}}-1\right]$$

From the interpolation η was defined which is also equal to:

$$\eta=\frac{T'_o-T_i}{T_o-T_i}$$

hence T_o can be evaluated. Now a better value for Cp is calculated using the following equation:

$$C_p = 0.944 + 0.0019 \times \left(\frac{T_o + T_i}{2} \right)$$

The above mentioned process is repeated in order to find an actual value of T_o.

3. The H.P. Compressor calculation

Known parameters are : P_i, T_i, N_H

Guessed parameters are : P_o/P_i

Using the known parameters, the non-dimensional speed can be evaluated. Interpolating linearly on the characteristics the non-dimensional mass flow rate as well as the isentropic efficiency and exact Beta value can be evaluated.

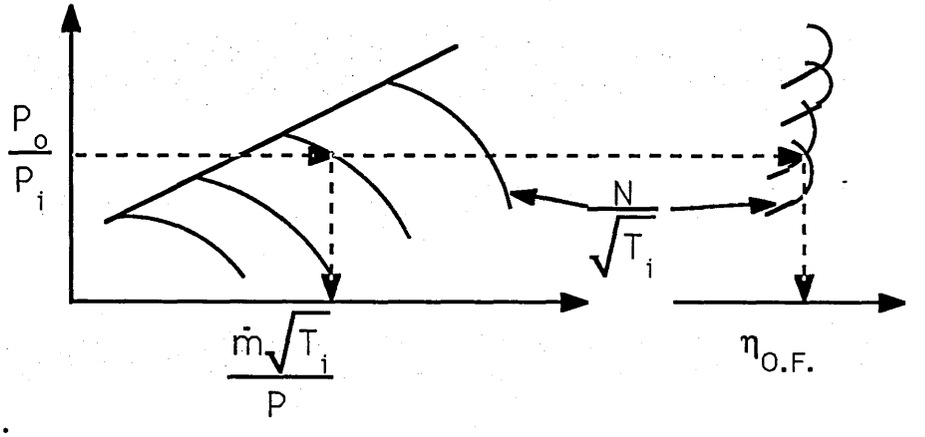

In order to calculate the outlet temperature T_o the same procedure is followed as in the Inner and Outer Fan calculations.

4. The Turbine Calculations

The known parameters are: T_i, Pi, N_H from the exit of the previous component.

$$C_p = 0.944 + 0.00019 \times \left(\frac{T_0 + T_i}{2} \right)$$

The above mentioned process is repeated in order to find an actual value of T_0.

3. The H.P. Compressor calculation

Known parameters are : P_i, T_i, N_H

Guessed parameters are : P_0/P_i

Using the known parameters, the non-dimensional speed can be evaluated. Interpolating linearly on the characteristics the non-dimensional mass flow rate as well as the isentropic efficiency and exact Beta value can be evaluated.

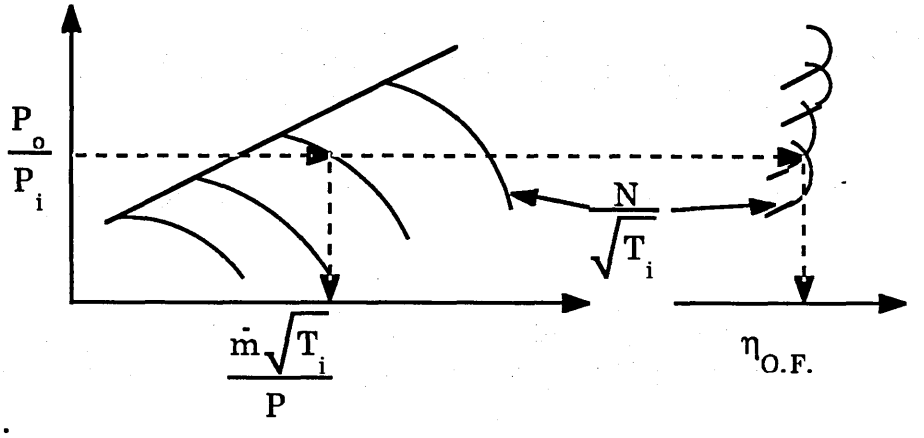

In order to calculate the outlet temperature T_0 the same procedure is followed as in the Inner and Outer Fan calculations.

4. The Turbine Calculations

The known parameters are: T_i, P_i, N_H from the exit of the previous component.

Guessed values are the : Work Factor

The mass flow rate and C_p values at the beginning of the calculations are taken as of the previous component. The non-dimensional speed can now be calculated from the known parameters. Linear interpolation is now used to evaluate the non-dimensional mass flow rate and isentropic efficiency, as it is shown in the figure below:

At this stage T_o can be calculated using the following expression:

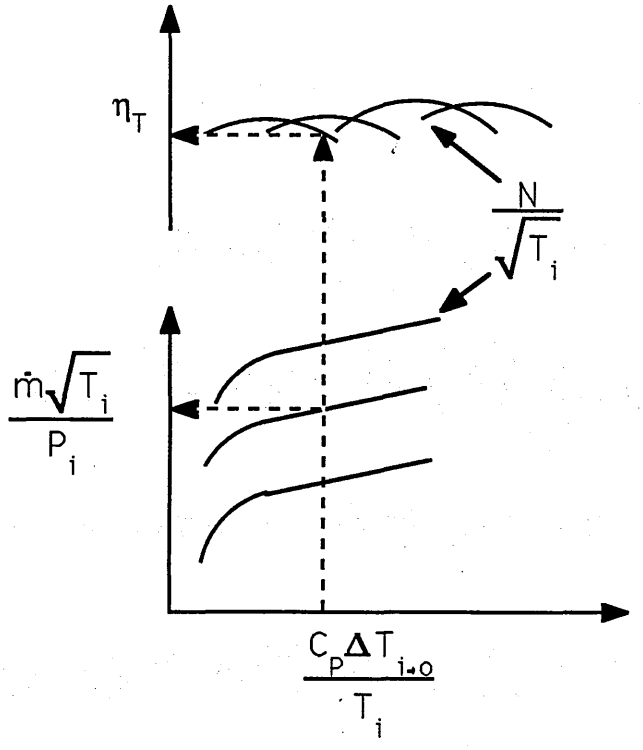

$$T_o = T_i \times \left(1.0 - \frac{\text{WORK FACTOR}}{C_p} \right)$$

A corrected C_p is calculated from:

$$C_p = 0.944 + 0.00019 \left(\frac{T_i + T_o}{2} \right)$$

The isentropic outlet temperature is calculated using :

$$T_i - T'_o = T_i \left[1 - \left(\frac{P_o}{P_i} \right)^{\frac{\gamma-1}{\gamma}} \right]$$

and T_O is calculated from:

$$T_i - T_o = \eta_T (T_i - T'_o)$$

The non-dimensional mass flow rate can now be calculated and the value obtained is compared to the one obtained from the interpolation in the characteristics. If the two values do not agree, the initial guessed value of the Work Factor into the turbine is revised.

5.The Final Nozzle Calculations

The mass flow rates entering the Final nozzle are equal to the core gas and by-pass air mass flow rates leaving the mixer. The two flows (core and by-pass) are assumed not to mix and both flows are assumed isentropic.

Firstly, it is determined whether or not the flow is chocked, using the following expression from Gas Dynamics :

$$\frac{P}{P_S} = \left(1 + \frac{\gamma-1}{2} M^2 \right)^{\frac{\gamma}{\gamma-1}}$$

If the flow is chocked then M=1 and the above expression reduces to :

$$\frac{P}{P_S} = \left(\frac{1+\gamma}{2} \right)^{\frac{\gamma}{\gamma-1}}$$

Hence if the LHS of the above equation is greater or equal to

the RHS then the flow is chocked.

The exit areas requires from each of the two flows can be calculated using the following equation which is derived from the theory of gas dynamics :

$$\frac{m\sqrt{T}}{PA} = M\sqrt{\frac{\gamma}{R}}\left(1+\frac{\gamma-1}{2}M^2\right)^{\frac{\gamma+1}{2(1-\gamma)}}$$

For chocked flow, M=1, and the above equation is reduced to:

$$\frac{m\sqrt{T}}{PA} = \sqrt{\frac{\gamma}{R}}\left(\frac{1+\gamma}{2}\right)^{\frac{\gamma+1}{2(1-\gamma)}}$$

The mass flow rates that are used in the above equation are the ones leaving the mixer. The required exit area is equal to the sum of the two calculated ones. A coefficient of discharge is then used to modify the required exit area. At the end of the programs a test is carried out between the required and the available area and the mass flow rate into the engine is revised accordingly.

APPENDIX C

Using T_{013}=295.94K and P_{013}=109.46, then the non-dimensional air mass flow rate into the by-pass duct is :

$$\frac{\dot{m}\sqrt{T}}{P}=\frac{m_{bp}\sqrt{T_{013}}}{P_{013}}=132.95\ \frac{lb/sec\ x\sqrt{K}}{lbf/in^2}$$

$$132.95\ \frac{lb/sec\ x\sqrt{K}}{lbf/in^2}=132.95\ x\ \frac{0.45359}{6894.8}\ \frac{Kg/sec\ x\sqrt{K}}{N/m^2}=$$
$$=8.74464x\ 10^{-3}\ \ \frac{Kg/sec\ x\sqrt{K}}{N/m^2}$$

Also A_{14}=0.566542 m^2 and it is also known that:

$$R=\frac{R_o}{M}\ \text{ hence }\ \sqrt{\frac{\gamma}{R}}=0.0698309$$

Substituting the above known values to the Continuity equation given in 2.2.5 we get the following expression:

$$8.74464\ x\ 10^{-3}=0.0698309\ x\ \frac{M_{14}}{(1+0.2M_{14}^2)^3}$$
$$\Rightarrow\ \frac{M_{14}}{(1+0.2M_{14}^2)^3}=0.2210355$$

By iterating M_{14} is found to be equal to 0.228, then substituting to:

$$U_{14}=M_{14}\sqrt{\gamma RT_{013}}\ \text{ it is found that}$$
$$U_{14}=0.228\ x\sqrt{1.4\ x\ 287.09\ x\ 295.94}\ \Rightarrow\ U_{14}=78.635\ m/sec$$

Similarly it can be found that U_{25}=69.924 m/sec. Now the shear force can be evaluated using the following equation:

$$\tau=\frac{1}{2} f \rho u^2$$

where u=78.635-69.924=8.711m^2

f=0.094 and

$$\rho=\frac{P}{RT}=\frac{\frac{(P_{025}+P_{014})}{2}}{\frac{R(T_{025}+T_{014})}{2}}=\frac{\frac{(P_{024}+P_{013})}{2}}{\frac{R(T_{024}+T_{013})}{2}}=\frac{110010}{287.099 \times 297.03} \Rightarrow$$

$$\Rightarrow \rho=1.2905 \ \frac{Kg}{m^3}$$

Hence $\tau=0.5x0.094x1.2905x8.711^2 \Rightarrow \tau=4.6024$

Substituting into equation **[IV]**:

$$A_{14}xP_{013}-A_{14}xP_{014}=\tau xA_{CON}$$

where $A_{CON}=0.0446m^2$

Hence $0.566542x109.46-0.566542xP_{014}=$

$=4.6024x0.0446 \Rightarrow$

$\Rightarrow 62013.687-0.566542xP_{014}=0.20527 \Rightarrow$

$\Rightarrow P_{014}=109.459$

Hence the value of P_{014} just found is the new pressure that is going to be used in the calculations of the next component while $P_{013}=109.460$ would be the one that it would be used if the shear force effects were not considered.

The predictions of the AFCSP program were used to evaluate the difference in the pressures that would occur under the following flight conditions:

Program AFCSP

Altitude=47,000ft.

Mach=0.92

f=0.094

FCSP=0.6329

A14 = 0.566542 m^2

and $A_{14} \times (P_{013}-P_{014}) = \tau \times A_{CON}$

T_{013}=303.13 K

P_{013}=30.43

$$\frac{m_{bp}\sqrt{T_{013}}}{P_{013}}=320.42\ \frac{lb/sec\sqrt{K}}{lbf/in^2}=320.42 \times \frac{0.45359\ Kg/sec\sqrt{K}}{6894.8\ N/m^2} \Rightarrow$$

$$\Rightarrow \frac{m_{bp}\sqrt{T_{013}}}{P_{013}}=0.021079\ \frac{Kg/sec\sqrt{K}}{N/m^2}$$

$$R=\frac{R_0}{M}=287.09945 \qquad \text{and} \qquad \sqrt{\frac{\gamma}{R}}=0.0698309$$

Then

$$\frac{m_{bp}\sqrt{T_{013}}}{P_{013}} = A_{14} \times \sqrt{\frac{\gamma}{R}} \times \frac{M_{14}}{\left(1+\frac{\gamma-1}{2}M_{14}^2\right)^{\frac{\gamma-1}{2(\gamma-1)}}}$$

Substituting the known values to the equation above we get:

$$0.021079=0.566542 \times 0.069831 \times \frac{M_{14}}{\left(1+0.2\ M_{14}^2\right)^3}$$

which can be reduced to:

$$\frac{M_{14}}{\left(1+0.2M_{14}^2\right)^2}=0.532807$$

Using the above expression and a number of iterations, an actual number for the M_{14} can be evaluated. In the actual

program a subroutine was used to execute the iterations needed to calculate a value for the M_{14}.

For M_{14} = 0.4 the LHS of the above equation is LHS=0.36

For M_{14}=0.6 the LHS of the above equation is: LHS=0.487

" M_{14}=0.7 " " " " " " ": LHS=0.528799

" M_{14}=0.71" " " " " " " LHS=0.532242

" M_{14}=0.711" " " " " " "LHS=0.532579

" M_{14}=0.712" " " " " " "LHS=0.532915

Now the already found value of M_{14} can be substituted to the following expression:

$$U_{14}=M_{14} \times \sqrt{\gamma RT_{013}}$$

By substituting all the known values to the above expression then U_{14} can be calculated.

$$U_{14}=0.712 \times \sqrt{1.4 \times 287.099 \times 303.13} \Rightarrow U_{14}=248.5274 \text{ m/sec}$$

For the core flow

$$\frac{m_c\sqrt{T_{024}}}{P_{024}} = A_{25} \times \sqrt{\frac{\gamma}{R}} \times \frac{M_{25}}{\left(1+\frac{\gamma-1}{2}M_{25}^2\right)^{\frac{\gamma+1}{2(\gamma-1)}}}$$

For the core flow the known parameters are:

A_{25}=0.363168 - 0.152053=0.211115 m^2

T_{024}=305.35k

P_{024}=31.19

Hence the non-dimensional mass flow rate for the core flow can now be evaluated by substituting the known values to the above written expression:

$$\frac{m_c\sqrt{T_{024}}}{P_{024}}=106.81\ \frac{lb/sec\ x\sqrt{K}}{lbf/in^2}\ \Rightarrow$$

$$\Rightarrow \frac{m_c\sqrt{T_{024}}}{P_{024}}=7.0267\times 10^{-3}\ \frac{Kg/sec\sqrt{K}}{N/m^2}$$

and $\sqrt{\frac{\gamma}{R}}=0.069831$

Then by substituting again we get:

$$7.0267\times 10^{-3}=0.211115\times 0.069831\times \frac{M_{25}}{\left(1+\frac{\gamma-1}{2}M_{25}^2\right)^3}\ \Rightarrow$$

$$\Rightarrow \frac{M_{25}}{(1+0.2M_{25}^2)^3}=0.476633$$

Iterating as in the by-pass flow a value for M_{25} can be found. It should be mentioned again that the iterations in the actual program are performed by the computer using a NAG subroutine.

M_{25} is found to be equal to: $M_{25}=0.579$

Now U_{25} can be evaluated by substituting the already found value of M_{25} to the following expression:

$$U_{25}=M_{25}\sqrt{\gamma\times R\times T_{024}}\ \Rightarrow$$

$$U_{25}=0.579\sqrt{1.4\times 287.099\times 305.35}$$

$U_{25}=202.84$m/sec

Now the shear force can be calculated using the following expression:

$$\tau = \frac{1}{2} f \rho u^2$$

U=248.5274-202.8418=45.685634 m/sec

$$\rho = \frac{P}{RT} = \frac{\frac{P_{025}+P_{014}}{2}}{R_x\left(\frac{T_{025}+T_{014}}{2}\right)} = \frac{\frac{P_{013}+P_{024}}{2}}{R_x\left(\frac{T_{013}+T_{024}}{2}\right)} =$$

$$= \frac{(31.19+30.43)/2}{0.287099_x\left(\frac{303.13+305.35}{2}\right)}$$

Hence ρ=0.352731 and τ=34.60197

Using again equation **[IV]** P_{014} can be evaluated, but first the Area of contact must be calculated using the following equation:

$A_{CON}=\pi(R+r)l$

$l=\sqrt{L_G^2+L_A^2}$

L_G=60mm and $L_A=L_{24}$ x (1-FCSP)

L_{24}=124mm and FCSP=0.6329

L_A=124 x(0.3671)=45.5204mm

Hence l=0.0753m and

A_{CON}=3.14159(0.120+0.078) x 0.0753=0.0469m^2

From equation [IV] :

$$P_{014} = \frac{P_{013} \times A_{14} - \tau A_{CON}}{A_{14}}$$

$$\Rightarrow P_{014} = \frac{1000 \times 30.43 \times 0.566542 - 34.60197 \times 0.0469}{0.566542} =$$

=30427.13 N/m^2

or P_{014}=30.427 KN/m^2 and

P_{013}=30.430 KN/m^2

P_{025}=31.19779 KN/m^2

P_{024}=31.190 KN/m^2

APPENDIX D

COMPUTATIONAL MODELS FOR SIMULATING A A TYPICAL TURBOFAN ENGINE ORIGINATING FROM DIFFERENT FAN TREATMENTS

P. Petrides, Research Student,
University of Glasgow
Glasgow, Scotland.

N.R.L. Maccallum, Reader,
University of Glasgow
Glasgow, Scotland.

11th. July 1986

ABSTRACT

This report describes an investigation of the best representation of the fan and also of the flow distribution into the fan of a typical Turbofan Engine. Based on the different Fan treatments, three computational models have been developed to simulate the engine.

All programs were based on the existing General program for the prediction of the performance of Gas Turbines, developed by Pilidis and Maccallum, Ref.(1).

A description of this general program is included in this report. The programs have been used to obtain the steady running performance of the Turbofan engine in two different flight conditions.

1.INTRODUCTION

A typical example of a Turbofan engine is the Tay engine which derives its pedigree from the Spey family of engines. The main factor in the concept of this engine was the reduction in noise.

In order to meet this major requirement, efforts were concentrated in increasing the bypass ratio and the Low Pressure compressor (L.P.) flow. This was fundamentally achieved by replacing the LP compressor of the Spey engine, with a wide chord fan and an Intermediate Pressure Compressor (IP compressor).

Efforts were also directed towards further improvement in fan efficiency which has resulted in the new technology of the wide chord snubberless fan.

Pilidis and Maccallum, Ref.(1),developed firstly a general program for the prediction of the performance of Gas Turbines, and later a computer model to simulate the Tay engine. Using this program as the basis, the different fan treatments were applied, and three more computer models were developed, each one representing a different fan treatment.

All four programs were used to predict the steady running conditions of the engine for two inlet conditions:

1. At sea level and Mach=0.2
2. At altitude of 47000 ft. and Mach=0.92

A brief description of the general program ,mentioned above, is also included, so that the reader can follow easily the

required changes for the application of the different fan treatments.

All the results are discussed and shown in graphs. The results of the programs are compared with actual test results of a typical Turbofan engine.

Predictions of the behaviour of the engine during transients are not included in this Report, but will follow in a subsequent Report.

2. DESCRIPTION OF THE GENERAL PROGRAM FOR THE PREDICTION OF THE TRANSIENT PERFORMANCE OF GAS TURBINES

When the representation of a gas turbine is desired a model is devised which in this case could either be physical or mathematical.

Pilidis and Maccallum developed a general mathematical model for the representation and prediction of the performance of gas turbines.

Because of the lengthy calculations required, the mathematical model involves computer programing, in particular for the more complex engines.

In the first instance the characteristics of the components of the engine, are predicted. These characteristics are then used by this general program for the calculation of the complete engine's performance.

It is necessary to update the component performance, using experimental observation of the performance of each component, in order to obtain more accurate and realistic results from the model of the engine.

The characteristics of these components at a particular instant during a transient differ from the characteristics observed in the steady state at the same non-dimensional speed. This difference is due to tip clearance changes, seal clearance changes and heat transfer effects, which have been incorporated

in the general program.

There are two commonly known alternative procedures, these being the method of "intercomponent volumes" and the method of "continuity of mass flow". Generally the method of "continuity of mass flow" requires less computing time and involves a number of iterations in order to achieve consistency of mass flows at each section.

Pilidis and Maccallum, in developing their general program, used the method of "continuity of mass flow".

In brief, the object of the calculation procedure is to determine the acceleration of the engine under different circumstances.

The acceleration is primarily a function of parameters such as shaft speed, fuel flow, inlet temperature and pressure, and secondary a functions of several other variables such as component efficiencies, pressure ratios, temperature ratios, etc..

Having evaluated the acceleration, the rotational speed for the next time interval is found, using Euler's simple assumption that the acceleration remains constant for a particular time interval.

The procedure of the method is illustrated in detail in Reference (1) .In brief, if the external parameters are defined and the rotational speed and fuel flow are fixed, the compressor's non-dimensional mass flow and isentropic efficiency are obtained. The delivery conditions of the compressor can then be found which are going to be the inlet conditions for the next component. This is repeated for each

component until it is necessary to calculate the required nozzle area to discharge the flow. If this is different from the actual nozzle available, then, if the turbine is choked, the compressor pressure ratio is modified until the required value of the turbine capacity is obtained. Once this has been achieved the variable to be adjusted to satisfy mass continuity at the final nozzle is the pressure ratio of the chocked turbine nearest to this nozzle.

The next step was to evaluate the torque imbalance between the shafts, which determines the instantaneous acceleration for a given time step. This acceleration over the time interval gives the rotational speed of the shaft at the next time step.

Also for by-pass engines with mixed exhaust the principle of momentum conservation must be satisfied by the fraction of core gas and the by-pass air to be mixed. No dissipation is assumed in the mixing process.

Before proceeding to a component all tests on the previous component must be satisfied, if not then the inlet parameters of the nearest upstream "free component" are modified until a satisfactory operating point is obtained. Free component is one at which the thermodynamic variables for the operation of the components downstream are generated.

This general computer model can also incorporate air bleed systems, reheat systems and also any form of fuel scheduling can be adopted for control of accelerations and decelerations.

3.DESCRIPTION OF THE DIFFERENT COMPUTER PROGRAMS

3.1 Representation of Fan and IP Characteristics

Initially, predicted characteristics for the Outer fan, the Inner fan and the I.P. Compressor, were provided for a typical Turbofan engine.

It is to be noted that the use of single, separate characteristics for the Outer fan and for the Inner fan, implies that changes in the core of the engine which affect the flow through the Inner fan do not alter the flow through the Outer fan.

When the first modelling of the Turbofan engine was carried out, Ref(2), this simplification was thought to be a weakness and an alternative treatment was adopted. The concept of an adjusting boundary between the Inner and the Outer Fan was introduced to the first computer model, resulting in the program labelled AFCSP and explained in Section 3.2.

In this research it is of interest to investigate and compare the treatment adopted in the program AFCSP with the original simplified concept mentioned earlier, which is used in the program FFCSP outlined in Section 3.3.

In practice it is not possible to measure the conditions between the Inner fan and the IP Compressor. For this reason another fan treatment was adopted, in which the pressure rises of the Inner Fan and I.P. Compressor are combined. This is explained in section 3.4. Section 3.5 of this chapter describes the fourth computer model developed in this research, which uses a combination of the fan and flow distribution treatments

adopted in the previous programs.

3.2. The AFCSP Program

Maccallum, Ref.(2), used the method of continuity of mass flow for modelling the performance of the RB 183-03 TAY Engine.

In this method the calculation procedure at each time step is iterative until continuity of mass flow is achieved at each section. This method requires a number of iteration loops and this number depends on the geometric complexity of the engine.

The Fan of the engine was treated as two separate sections, the Inner and the Outer. Separate characteristics were thus used for the two sections of the fan.

Although this is a satisfactory way of treating the fan under steady running conditions, some allowance is made for interchange of flow between the two sections of the Fan, in order to give what were thought would be more realistic results for the transient performance of the engine. The characteristics provided were based on a frontal area split ratio of 1 to 3, similar to the by-pass ratio of TAY engine. In the actual program, Ref (2), the parameter GEOM was used to represent the fraction of the total frontal area allocated to the Inner section. GEOM had initially the value of 0.25.

The interchange of flow between the two sections of the fan was allowed by introducing another factor named Factor of Split, labelled FCSP. It was assumed that the axial velocity of the air into the Fan is constant over the whole inlet area of the

Fan and a fraction of this area feeds the Inner Fan which is not necessarily equal to GEOM but some fraction of it. This fraction is the factor named above FCSP

The final step of the program consists of a test between the final nozzle area required and the final nozzle area available. This test revises the value of the Factor of Split until equality between the two areas is achieved. The logic of the program is outlined in Fig.A-see Figure(4) of the Thesis.

This computational model, labelled AFCSP, was the basic model used in this research. The other three models were derived from the program AFCSP.

The AFCSP program was used to predict the performance of the engine under the following inlet conditions:

1.Steady Running, Sea Level, Mach=0.2

2.Steady Running, 47000 ft., Mach=0.92.

3.3. Program FFCSP

As it was explained in the description of the program AFCSP, the Factor of Split is revised after the test for the required and available nozzle area which takes place at the end of the program.

In program FFCSP (Fixed Factor of Split) the treatment of flow distribution into the Fan is different. In this case the Factor of Split is kept constant and equal to 1.0. In order to keep the equality between the required and available nozzle area, the test that is carried out at the end of the program revises the amount of air flow into the entire engine. To achieve that, the link which had existed existed between the Inner and the Outer

fan was removed.

The program was run for the two flight conditions mentioned in program AFCSP.

The new program is labelled on the graphs: FFCSP.

3.4. Program FFCSP INFCIPC

Since in practice it is not possible to measure the conditions in between the Inner Fan and the I.P. Compressor, it was considered that the Inner fan and the I.P. compressor could be combined and represented as one section.

The programs AFCSP & FFCSP at a certain stage read the values of the characteristics of the Inner Fan, I.P. Compressor, Outer Fan, in the sequence just mentioned. The new program developed, by-passes the characteristics of the I.P. Compressor and instead of reading the Inner Fan's characteristics, these are replaced with the characteristics of the combined Inner Fan & I.P. Compressor, produced from the program CH INFCIPC.

This program (CH INFCIPC) has been developed to produce the characteristics of the new section which consisted of the combined Inner Fan & IP Compressor. It used the separate characteristics of the Inner fan & IP Compressor and with certain interpolations produced the new combined characteristics are shown in Figure B.

The program gives the combined:

Pressure Ratio = RCMPC

Air Mass Flow(Non-Dim.)=AI1ERR

Beta Values = BETAC

In order to bypass the characteristics of the IP compressor a new parameter was introduced in the program, labelled NDELI. If this parameter is given the value of 1, then the program uses the combined characteristics instead of the Inner Fan's, bypasses the I.P. Compressor's characteristics and then reads the Outer Fan's.

This program, like the FFCSP, keeps the Factor of Split fixed and revises the air mass flow into the engine until equality between the available and required nozzle area is achieved.

This new program is labelled on the graphs as FFCSP INFCIPC (Inner Fan Combined with I.P. Compressor).

This program should give virtually the same predictions as those from program FFCSP. This is confirmed from the results presented in this report.

3.5. The TAYN1 Program

This last program uses the same fan treatment as the FFCSP INFCIPC Program, i.e. the Inner Fan is considered combined with the I.P. Compressor. The new development in this program is that a variable Factor of Split is once again used, but applied only to the Outer Fan. The final nozzle test was used to revise the Factor of Split.

This new program was derived from the FFCSP INFCIPC program, after making the necessary changes in the logic of the previous program.

This new program was also run for the same flight conditions.

4. DISCUSSION OF RESULTS

4.1. Results For Flight Conditions : Sea Level, Mach=0.2

4.1.1. H.P.-L.P. Shaft speed relationship

In Figures 1,2,3&4 the HP-LP shaft speed relationship is illustrated for the four programs. The programs AFCSP, FFCSP and FFCSP INFCIPC appear to produce the same results. The fourth program TAYN1 has results that coincide with the results of the other programs at the middle range of shaft speed values, but appears to have discrepancies at the lower and upper range of values.

At the lower end the discrepancies are of the order of 7.9%.

At the upper values the discrepancy is of the order of 4.3%.

4.1.2. In the next set of graphs the Inner Fan plus I.P. Compressor pressure ratio is plotted against the non-dimensional speed.

The results are shown in the Figures 5,6,7&8.

Since in practice the value of P_{24} cannot be measured it was decided, for the two programs AFCSP&FFCSP that do not consider the Inner Fan & I.P. Compressor combined, to plot P_{26}/P_1 versus the non-dimensional speed.

It is seen from the graphs that the results of all the programs almost coincide.

4.1.3. H.P.- Fan & I.P. Pressure Ratio Relationship

In Figures 9,10,11,&12 the HP to Fan & IP compressor pressure ratio is plotted

The results of all the programs are quite close to each other although they show a maximum discrepancy of about 6%.

4.1.4. In order to further examine the results mentioned above,(4.1.3), the HP compressor pressure ratio was plotted against the non-dimensional speed. The results are shown in Figures 13,14,15&16.

It appears that the results of all the programs show again a discrepancy of the order of 5.2%.

The deviation of these results is very similar to the deviation which appeared in the HP-IP Pressure Ratio relationship (3), confirming that the results of the programs shown in the figures 9 to 16 are consistent.

4.1.5.Inner Fan Working Lines

Figures 17 & 18 show the Inner Fan working lines for the programs AFCSP and FFCSP, while Figures 19 & 20 show the working lines of the combined Inner Fan + IP compressor.

The results of the two programs AFCSP & FFCSP deviate quite substantially, by about 10%, while the working lines predicted by the programs FFCSP INFCIPC & TAYN1 show only a slight discrepancy of about 2.5%.

The deviations in the predicted Inner Fan working lines between the programs are due to the different fan treatments and to the different air flow distributions into the engine that are used in each program.

4.1.6. Outer Fan Working Lines

The Outer fan's working lines are also represented for each program in the Figures 21,22,23&24. The three programs AFCSP, FFCSP & FFCSP INFCIPC show very similar results, while the other program, TAYN1, shows a slight discrepancy of about 3% at the higher mass flow rates. This is due to the different logic approach to the flow distribution into the engine of the program TAYN1 compared with the FFCSP INFCIPC and the other programs.

4.2. Results for Flight Conditions : 47000ft., Mach=0.92

The four programs were used to predict the steady state results at the flight conditions mentioned above. The predictions of the programs are compared, for each program separately, with the actual test results.

4.2.1. Fan & I.P. Compressor Working Lines

In Figures 25,26,27&28 the IP compressor working lines at 47000ft. & Mach=0.92 are shown together with the actual test results of the engine. In each graph the Rig surge line is also shown.

Program AFCSP appears to have a very substantial deviation from the engine test results. The predictions of the program deviate from the actual results apart from the highest air mass flow rates, where they appear to coincide.

The results of the programs FFCSP and FFCSP INFCIPC are identical and in comparison with those from the AFCSP program are much closer to the test results.

At the low air mass flow range the predictions of the two programs (FFCSP&FFCSP INFCIPC) are very close to the surge line, while at the middle and higher air mass flow rates appear to lie between the surge and the test results of the IP compressor working line.

Although the results of the program TAYN1 did not reach the high air mass flow values that the engine reached during the handling tests, the predicted working line is very close to the actual Fan & IP compressor working line. The deviation of the prediction from the actual working line does not exceed 1.5%.

4.2.2. H.P. Compressor Working Lines

These results are shown in the Figures 29,30,31&32, together with the engine's actual test results and the Rig surge line.

All the programs produced predictions that are very close to the actual test results of the engine.

The program TAYN1 appears to have the smallest deviation from the engine's test results. In particular at the highest air mass flow values the predicted and the actual working lines coincide.

5. OVERALL COMPARISON OF RESULTS

5.1. Inner Fan Working Lines

At this stage it was thought helpful to compare the results for both the flight conditions

These results are shown in figures 33,34,35&36.

The predictions of the program AFCSP deviate very much from the reality. As it is shown in Figure 33, the predicted steady running working line for the Sea level appears to be higher than that predicted for the altitude of 47000 ft. When the altitude is increased the working lines of the components are expected to lift towards the surge line, something that does not happen with the predictions of the AFCSP program.

Only at the highest air mass flow values the predictions come very close to the actual results.

For the programs FFCSP & FFCSP INFCIPC the predicted working lines are more realistic, as the results for the 47000ft. altitude appear to be lifted from the sea level predictions. It is clearly shown in the graphs that both predictions for the inlet conditions appear to be lifted towards the surge line. The Sea level predicted working line is close to the 47000ft. actual test line and the 47000ft. predicted working line, closer to the surge line.

The most realistic results appear to have been produced from the TAYN1 program. Figure 36 shows clearly the predicted 47000ft. working line very close to the actual one obtained from the engine's actual test results, and the predicted working line

for the Sea level to be lower than that predicted for the higher altitude and also from the actual test working line.

5.2. H.P. Compressor Working Lines

The predictions of all the programs for the HP compressor are very close to the working line obtained from the actual test results. The only program that appears to produce slightly better predictions is the TAYN1 program, which shows that the predicted high altitude results and the actual ones almost coincide at the higher pressure ratio values.

6. CONCLUSIONS AND FURTHER INVESTIGATION

The four programs were run successfuly and the results were used to compare the predictions of the programs between them as well as with the actual handling tests of the engine.

The object of this research is to find the best way of representing the Fan and also the air flow distribution into the Fan of a typical Turbofan Engine, in order to develop the most accurate and realistic computer model to represent this type of engine.

Although the predictions of the four programs do not show large discrepancies between them-average discrepancy was about 5%- the differences are sufficient to indicate that, using the component characteristics for the original simulation (Ref.2), the program which best fits the test results is Program TAYN1.

In order to have a better test of the programs it is desirable to have the most up-to-date characteristics for the components.

There is evidence that the actual engine characteristics differ from those originally used (Ref.2). An example of this is illustrated in Figure C where the original characteristics of the H.P. Compressor are plotted together with actual points obtained from the handling test results of the engine. The differences between them are substantial. Such differences in the characteristics could exist in other components of the engine.

It is thus important for the continuation of this research to update the component characteristics.

Once this is done, then it will be possible to decide which

program gives the most realistic and accurate predictions.

That program will be used to continue the investigation into the prediction of the Transient Performance of the engine incorporating Heat Transfer Effects.

REFERENCES

1. P. Pilidis and N.R.L. Maccallum,

   " General Program for the Prediction of the Steady Running and Transient Performance of Gas Turbines."
   ASME Paper No. 85-GT-209. March 1985

2. N.R.L. Maccallum,

   "Computational Models for the Transient Performance of the RB 183-02 (Spey) and the RB 183-03 (Tay) engine."
   13th. August1984. G.U. Report RR/1.

3. P.J. Ashmole,

   "Introducing the Rolls-Royce Tay."
   Paper AIAA-83-1377. 19th. Joint Propulsion Conference June 1983.

4. R.A. Bower

   "RB 183-03 Engine 4/2 Handling Tests at RAE (Pyestock). Performance technical Report."
   Rolls-Royce Limited RTR 19522. 29th. July 1985.

5. P. Petrides,

   "Departmental Progress Report" University of Glasgow, Department of Mechanical Engineering, June 1985.

FIG 8

COMBINED CHARACTERISTICS
OF
INNER FAN & I.P. COMPRESSOR

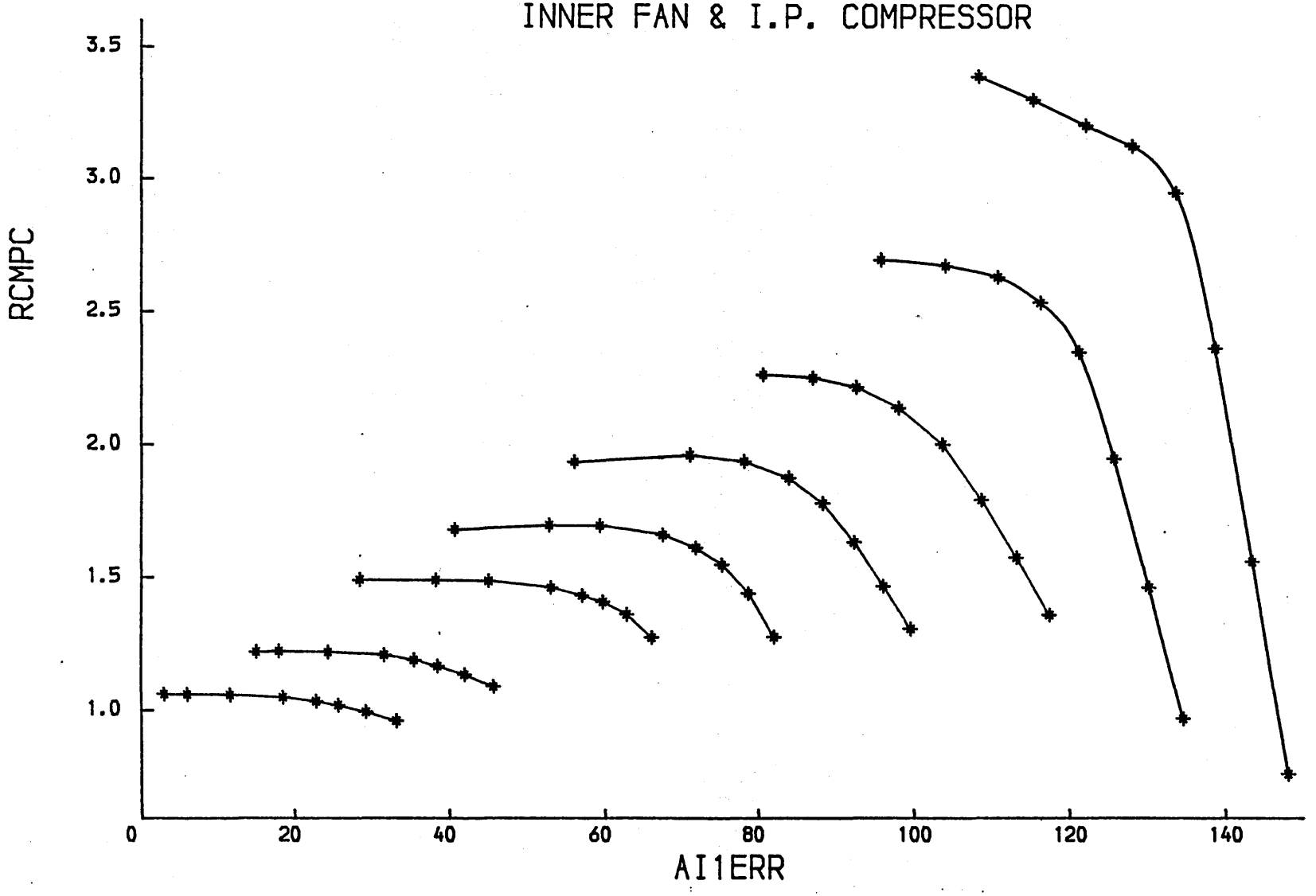

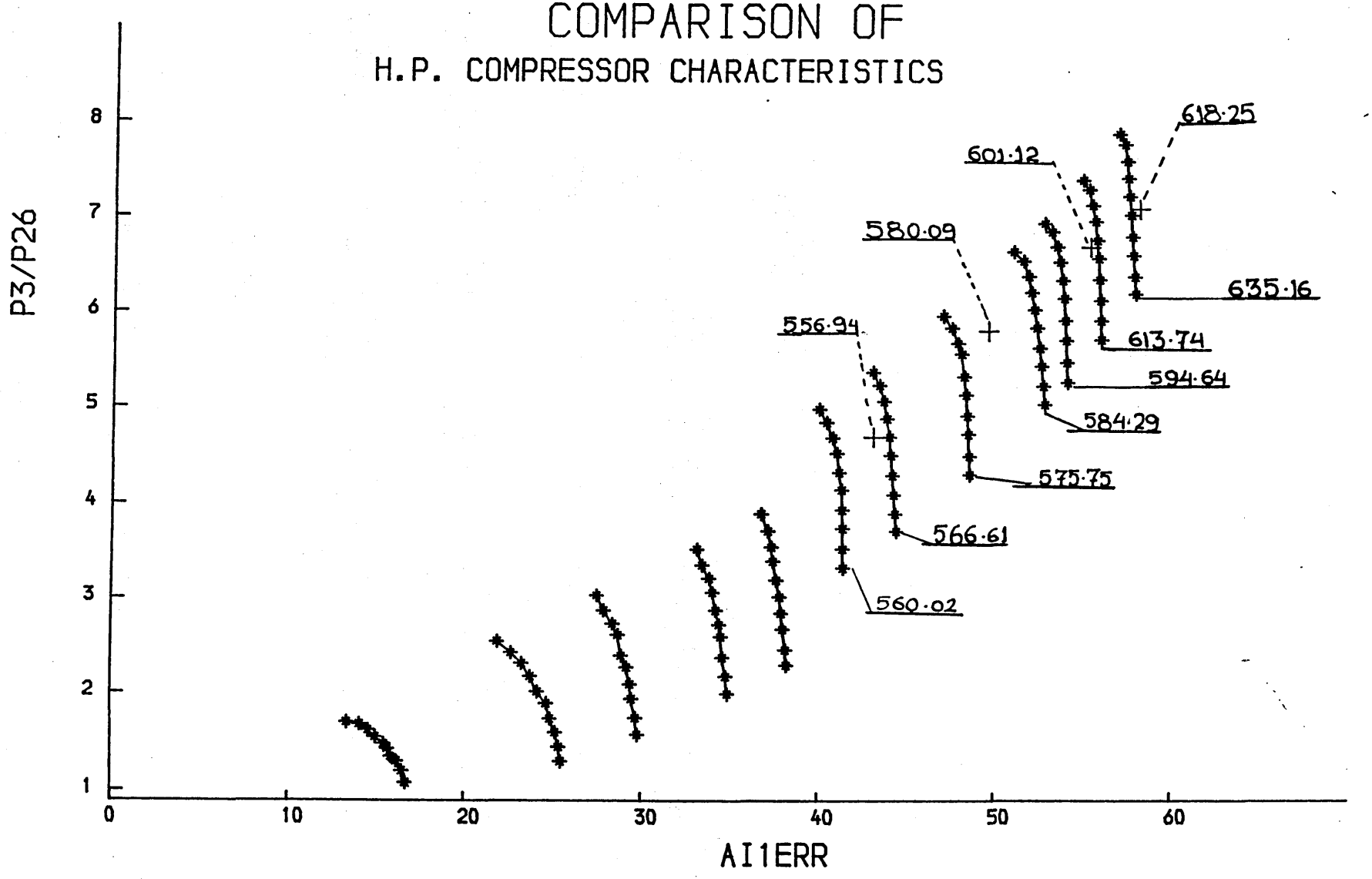
COMPARISON OF
H.P. COMPRESSOR CHARACTERISTICS
P3/P26
AI1ERR
618·25
601·12
580·09
635·16
556·94
613·74
594·64
584·29
575·75
566·61
560·02
1
2
3
4
5
6
7
8
0
10
20
30
40
50
60

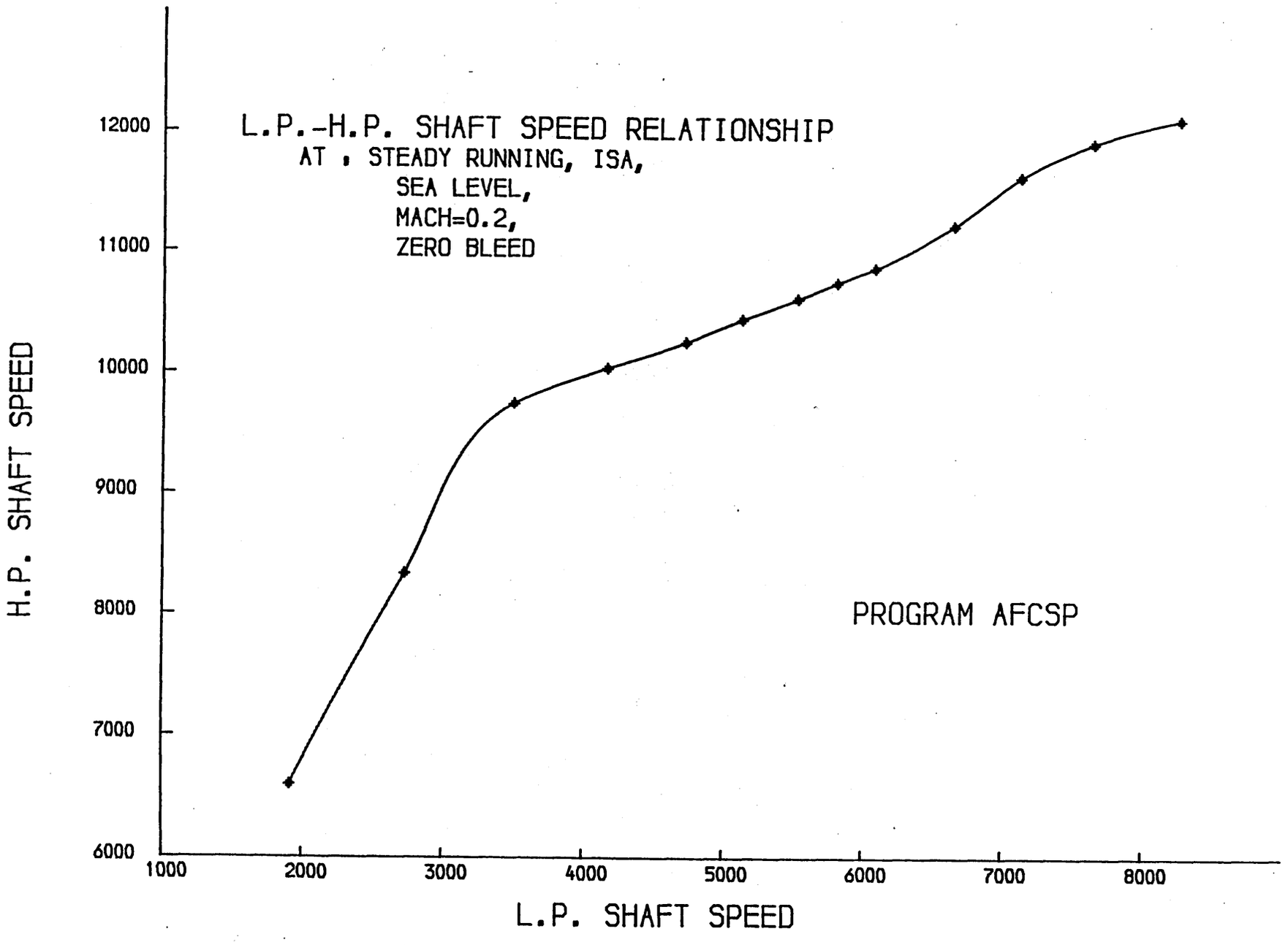
L.P.-H.P. SHAFT SPEED RELATIONSHIP
AT : STEADY RUNNING, ISA,
SEA LEVEL,
MACH=0.2,
ZERO BLEED
PROGRAM AFCSP
H.P. SHAFT SPEED
12000
11000
10000
9000
8000
7000
6000
1000
2000
3000
4000
5000
6000
7000
8000
L.P. SHAFT SPEED

FIG. 1

FIG. 6

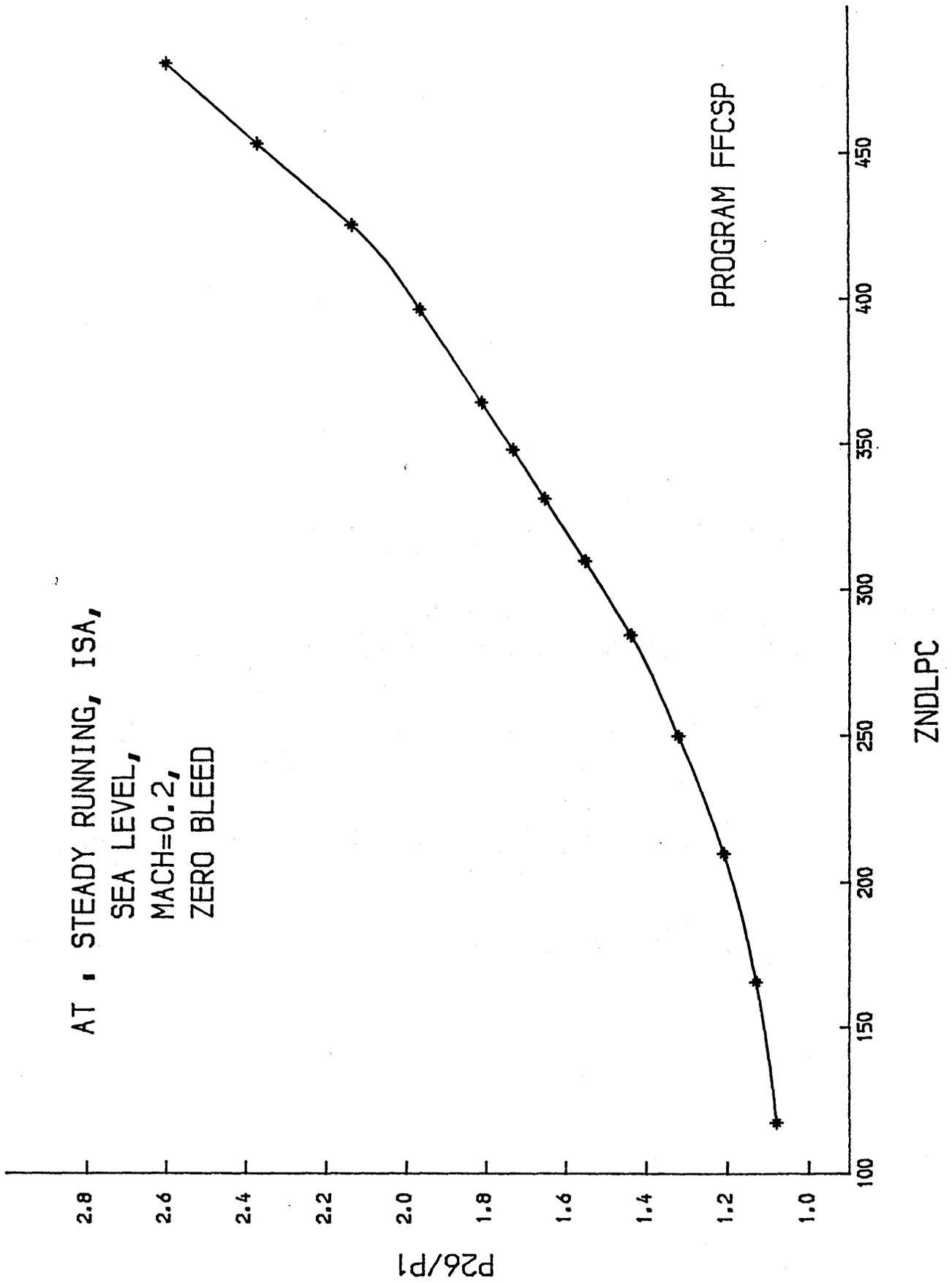
AT • STEADY RUNNING, ISA,
SEA LEVEL,
MACH=0.2,
ZERO BLEED
PROGRAM FFCSP
P26/P1
ZNDLPC
2.8
2.6
2.4
2.2
2.0
1.8
1.6
1.4
1.2
1.0
100
150
200
250
300
350
400
450

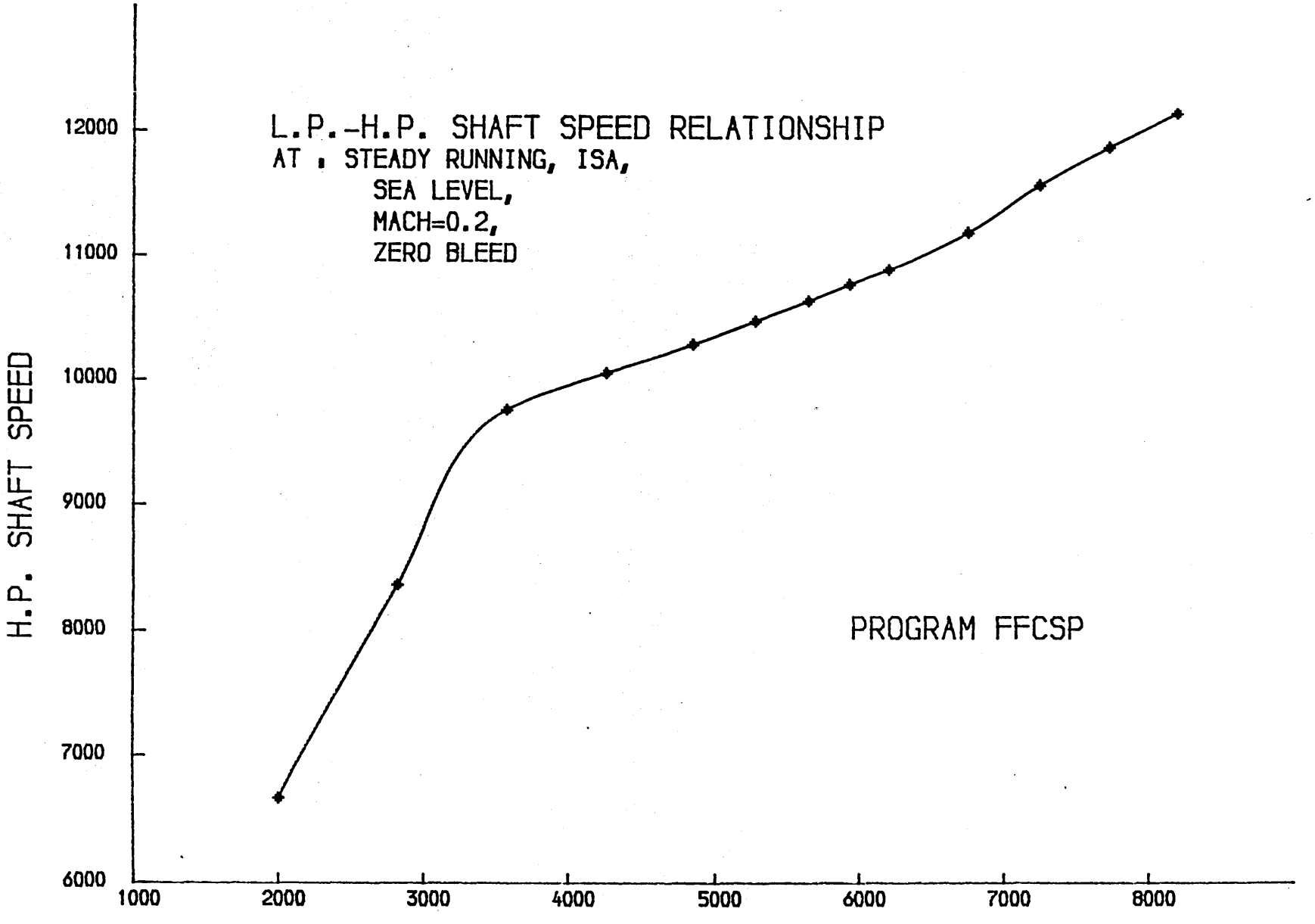
L.P.-H.P. SHAFT SPEED RELATIONSHIP
AT : STEADY RUNNING, ISA,
SEA LEVEL,
MACH=0.2,
ZERO BLEED
PROGRAM FFCSP
H.P. SHAFT SPEED
12000
11000
10000
9000
8000
7000
6000
1000
2000
3000
4000
5000
6000
7000
8000

FIG. 2

FIG. 3

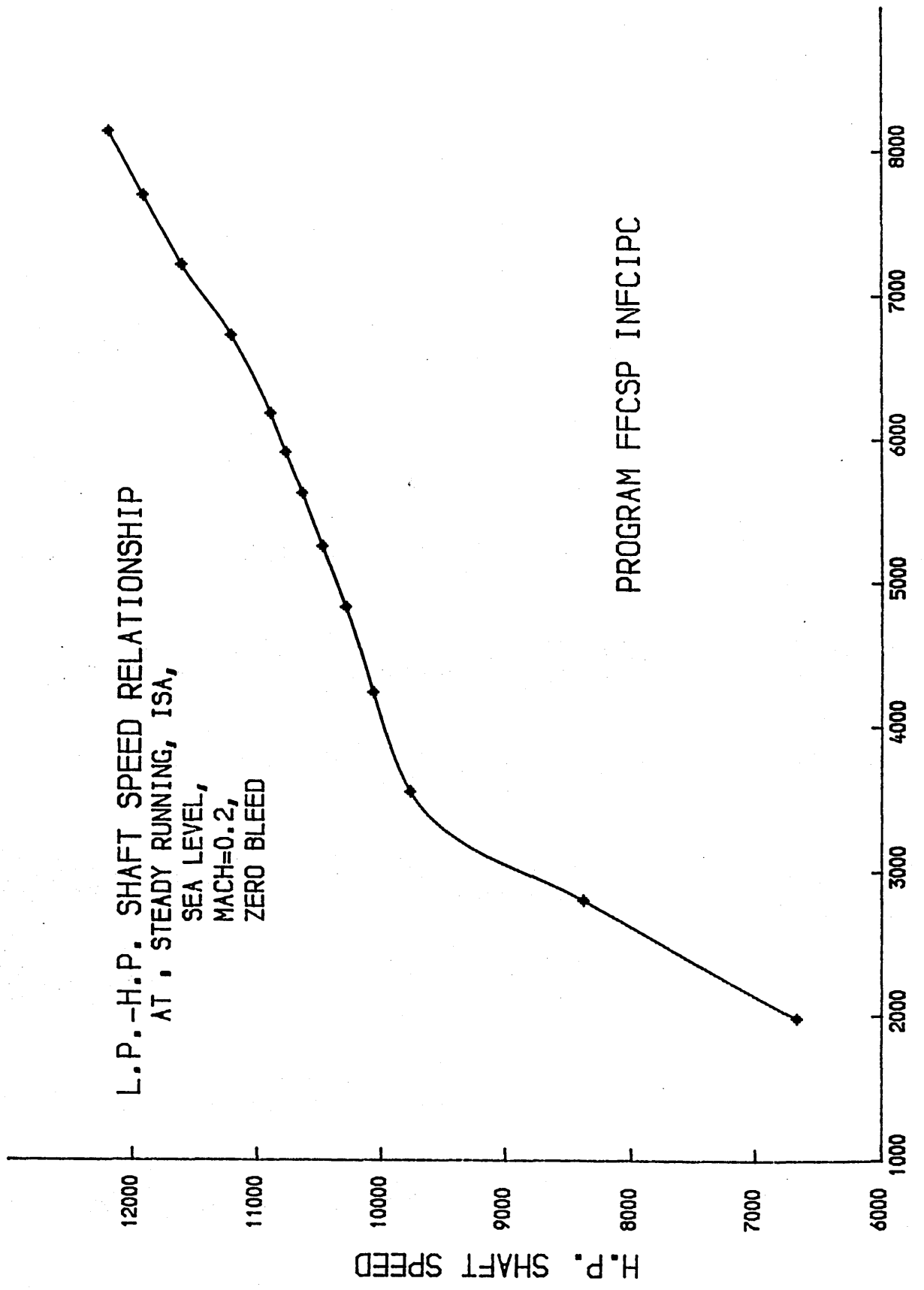
L.P.-H.P. SHAFT SPEED RELATIONSHIP
AT , STEADY RUNNING, ISA,
SEA LEVEL,
MACH=0.2,
ZERO BLEED
PROGRAM FFCSP INFCIPC
H.P. SHAFT SPEED
12000
11000
10000
9000
8000
7000
6000
1000
2000
3000
4000
5000
6000
7000
8000

FIG. 4

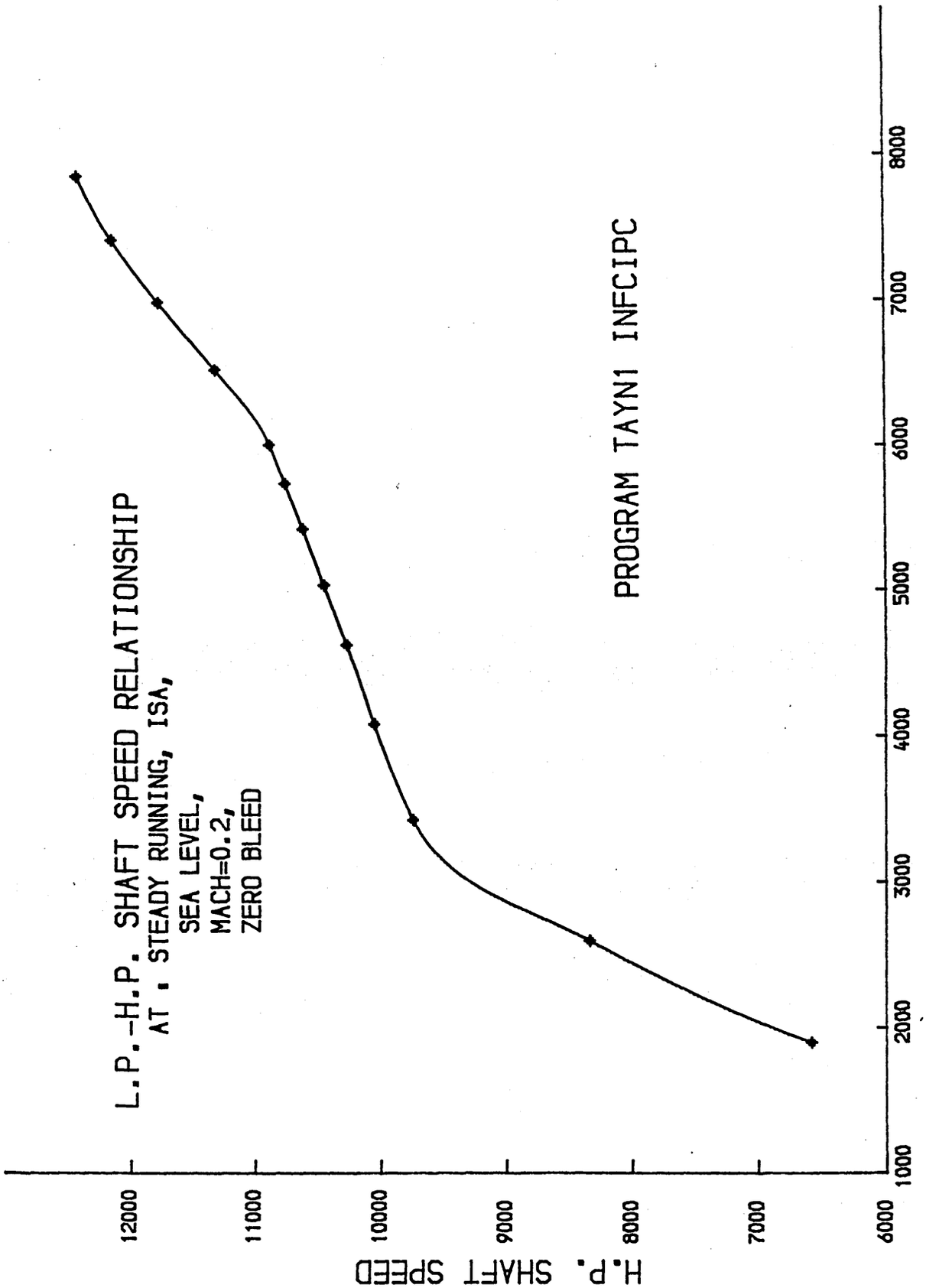
L.P.-H.P. SHAFT SPEED RELATIONSHIP
AT . STEADY RUNNING, ISA,
SEA LEVEL,
MACH=0.2,
ZERO BLEED
PROGRAM TAYN1 INFCIPC
H.P. SHAFT SPEED
12000
11000
10000
9000
8000
7000
6000
1000
2000
3000
4000
5000
6000
7000
8000

FIG. 5

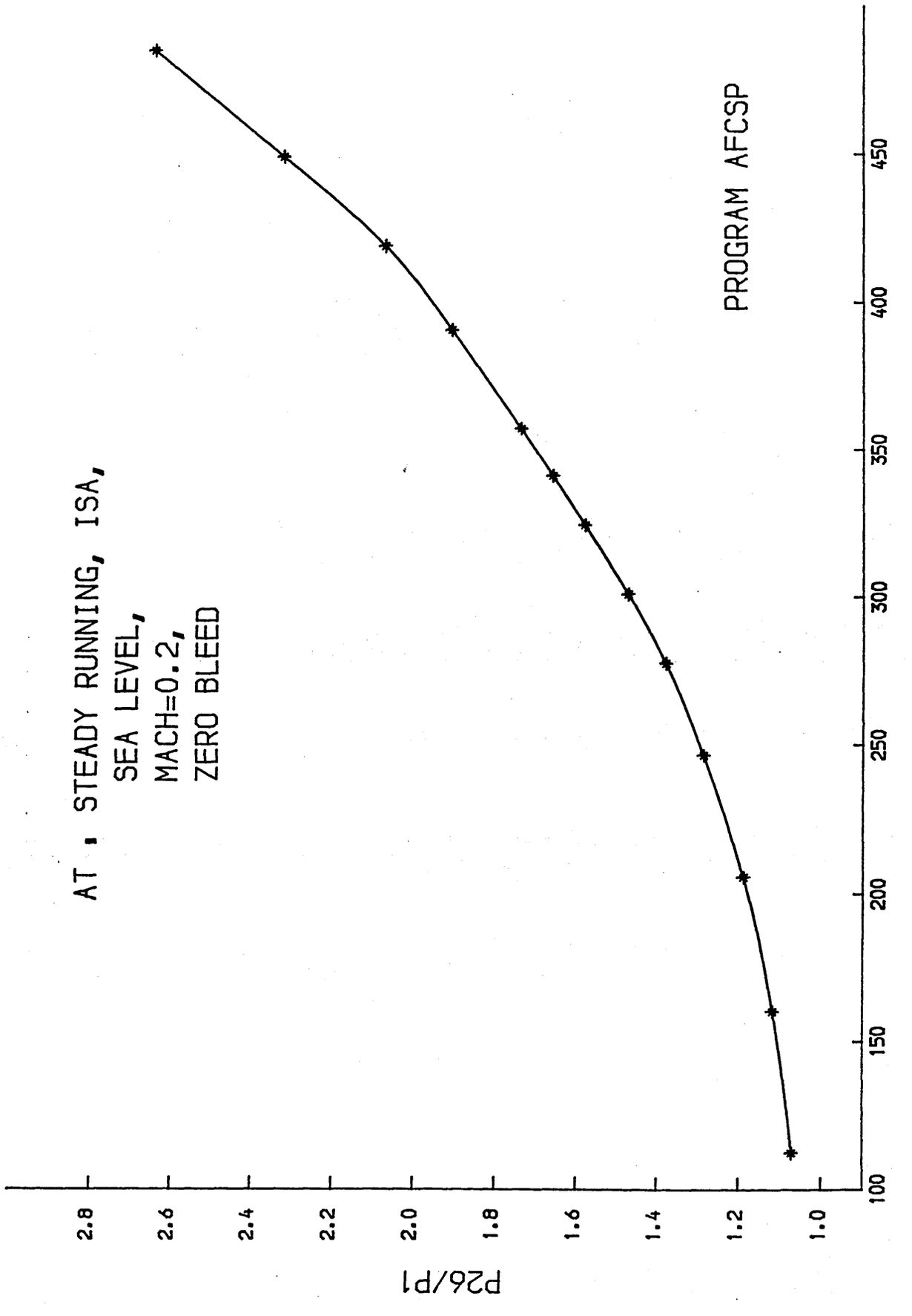
AT • STEADY RUNNING, ISA,
SEA LEVEL,
MACH=0.2,
ZERO BLEED
PROGRAM AFCSP
P26/P1
ZNDLPC
2.8
2.6
2.4
2.2
2.0
1.8
1.6
1.4
1.2
1.0
100
150
200
250
300
350
400
450

FIG. 7

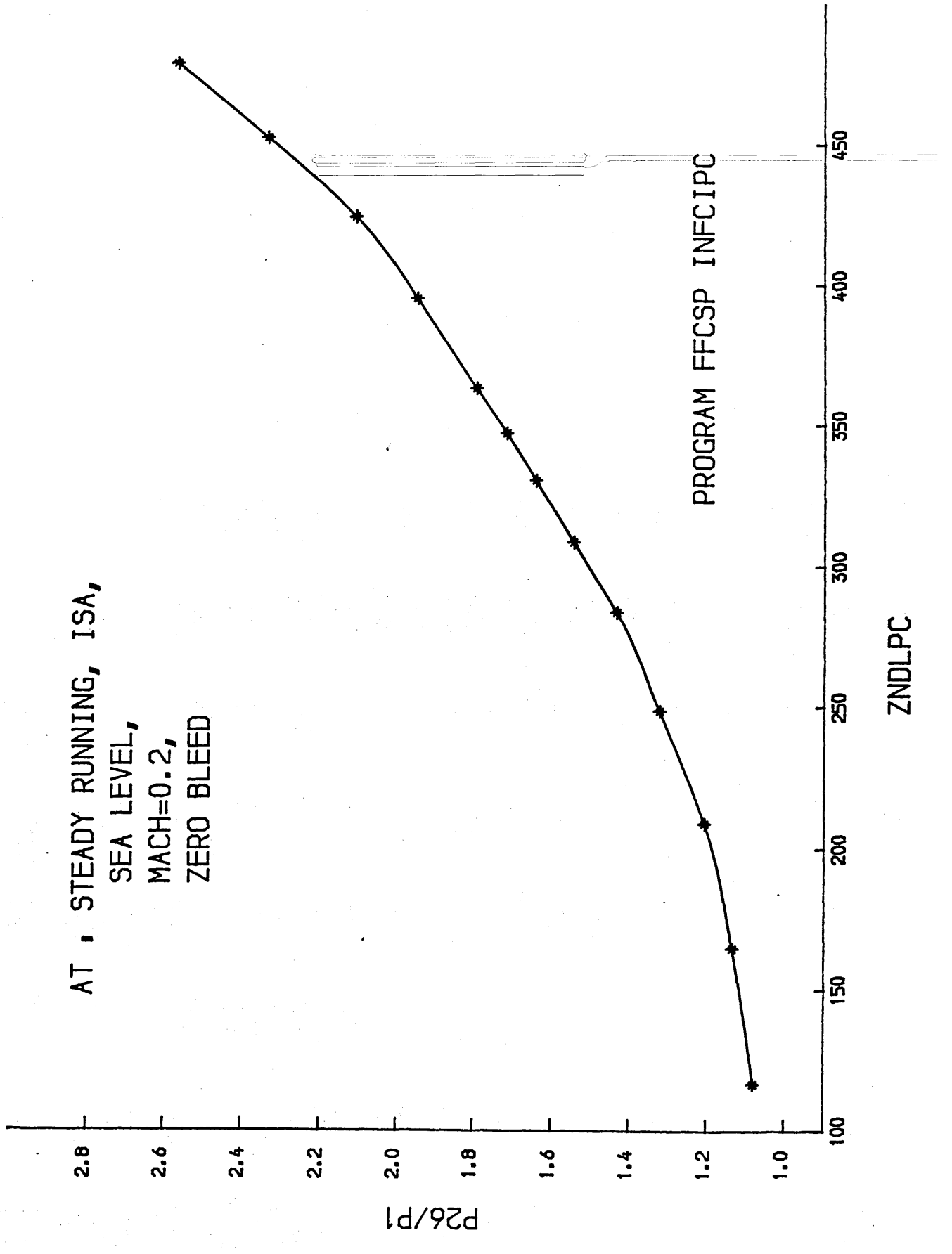
AT , STEADY RUNNING, ISA,
SEA LEVEL,
MACH=0.2,
ZERO BLEED
PROGRAM FFCSP INFCIPC
P26/P1
ZNDLPC
2.8
2.6
2.4
2.2
2.0
1.8
1.6
1.4
1.2
1.0
100
150
200
250
300
350
400
450

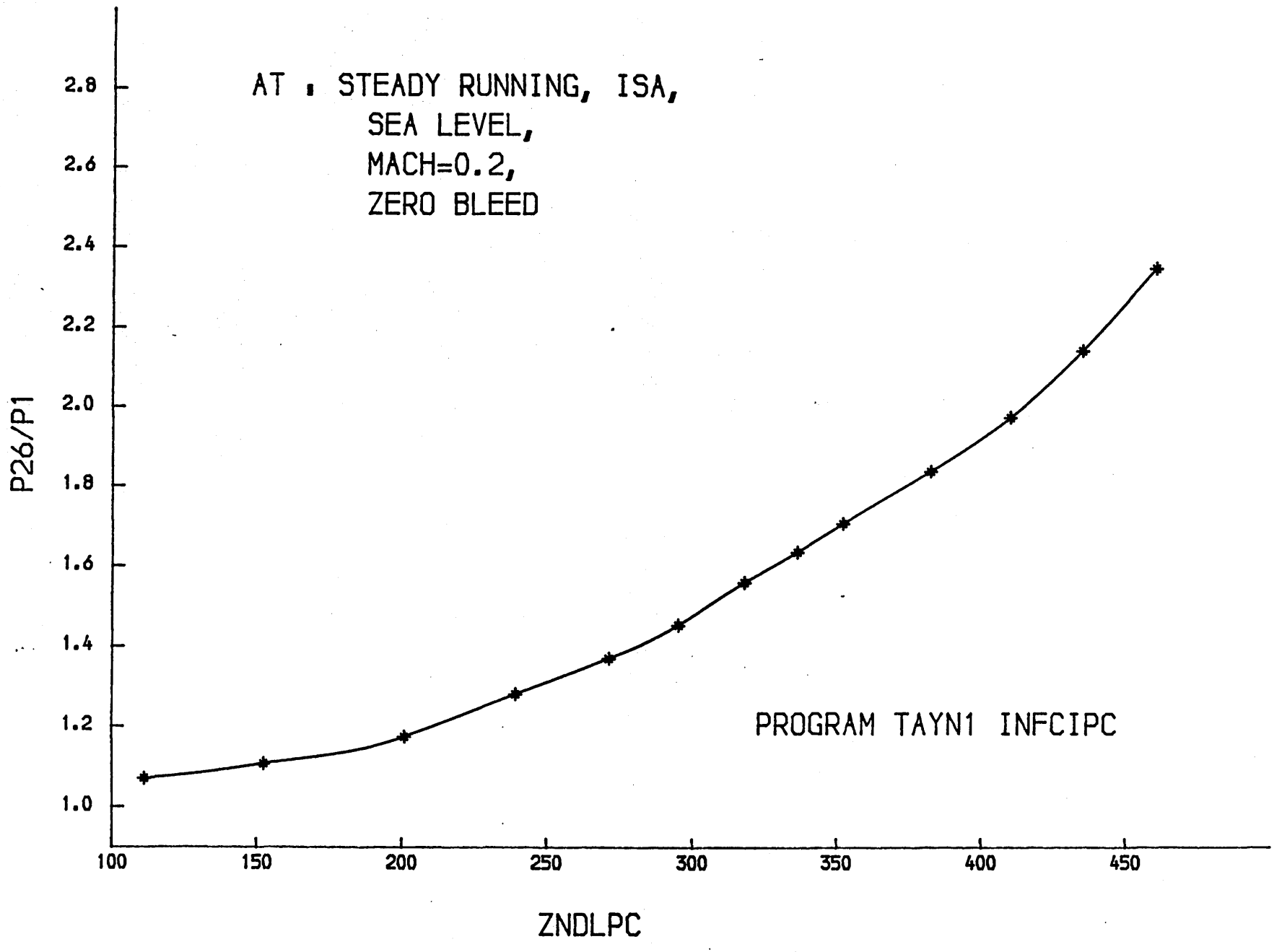
AT : STEADY RUNNING, ISA,
SEA LEVEL,
MACH=0.2,
ZERO BLEED
PROGRAM TAYN1 INFCIPC
P26/P1
ZNDLPC
2.8
2.6
2.4
2.2
2.0
1.8
1.6
1.4
1.2
1.0
100
150
200
250
300
350
400
450

FIG. 8

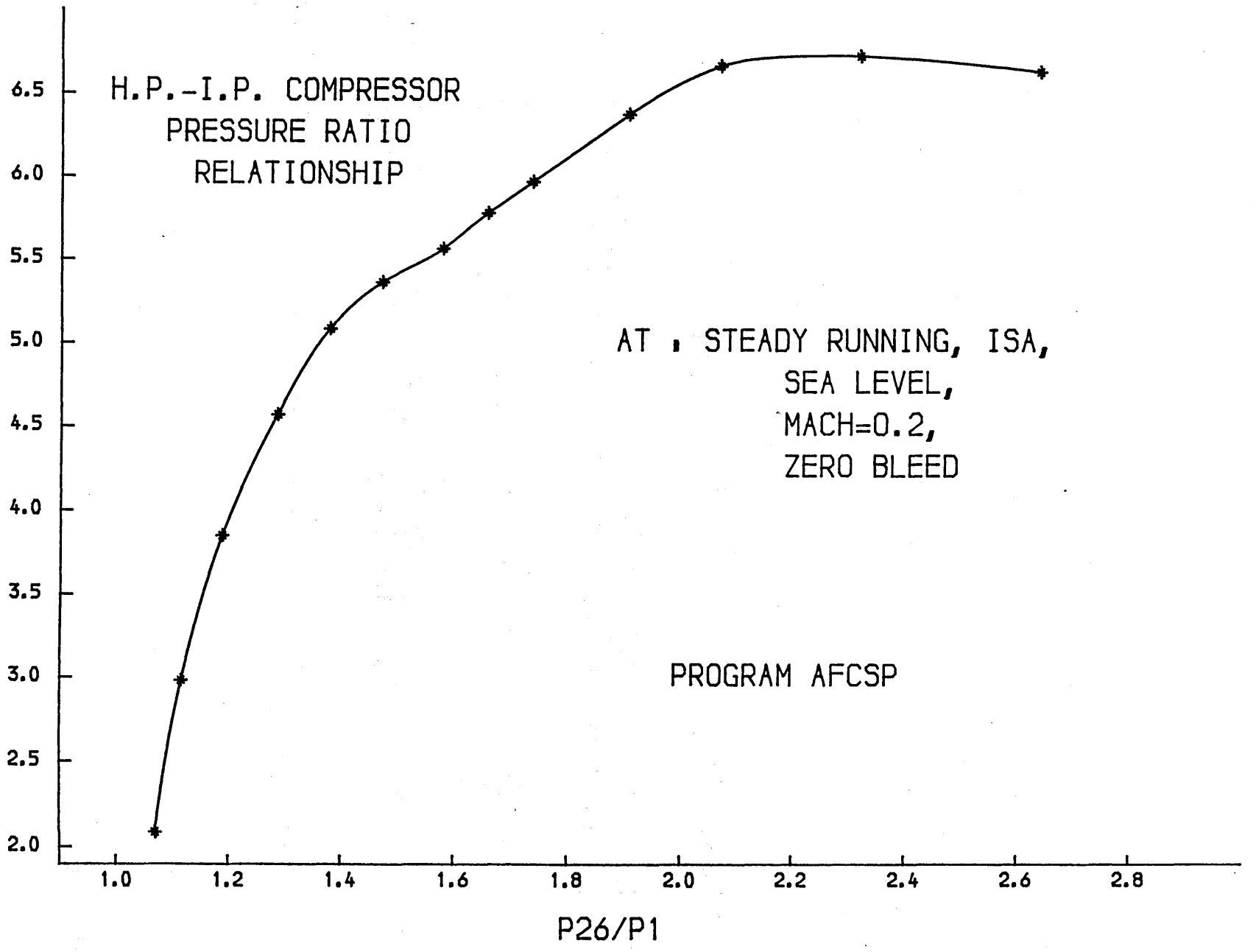
H.P.-I.P. COMPRESSOR
PRESSURE RATIO
RELATIONSHIP
AT : STEADY RUNNING, ISA,
SEA LEVEL,
MACH=0.2,
ZERO BLEED
PROGRAM AFCSP
6.5
6.0
5.5
5.0
4.5
4.0
3.5
3.0
2.5
2.0
1.0
1.2
1.4
1.6
1.8
2.0
2.2
2.4
2.6
2.8
P26/P1

FIG 9.

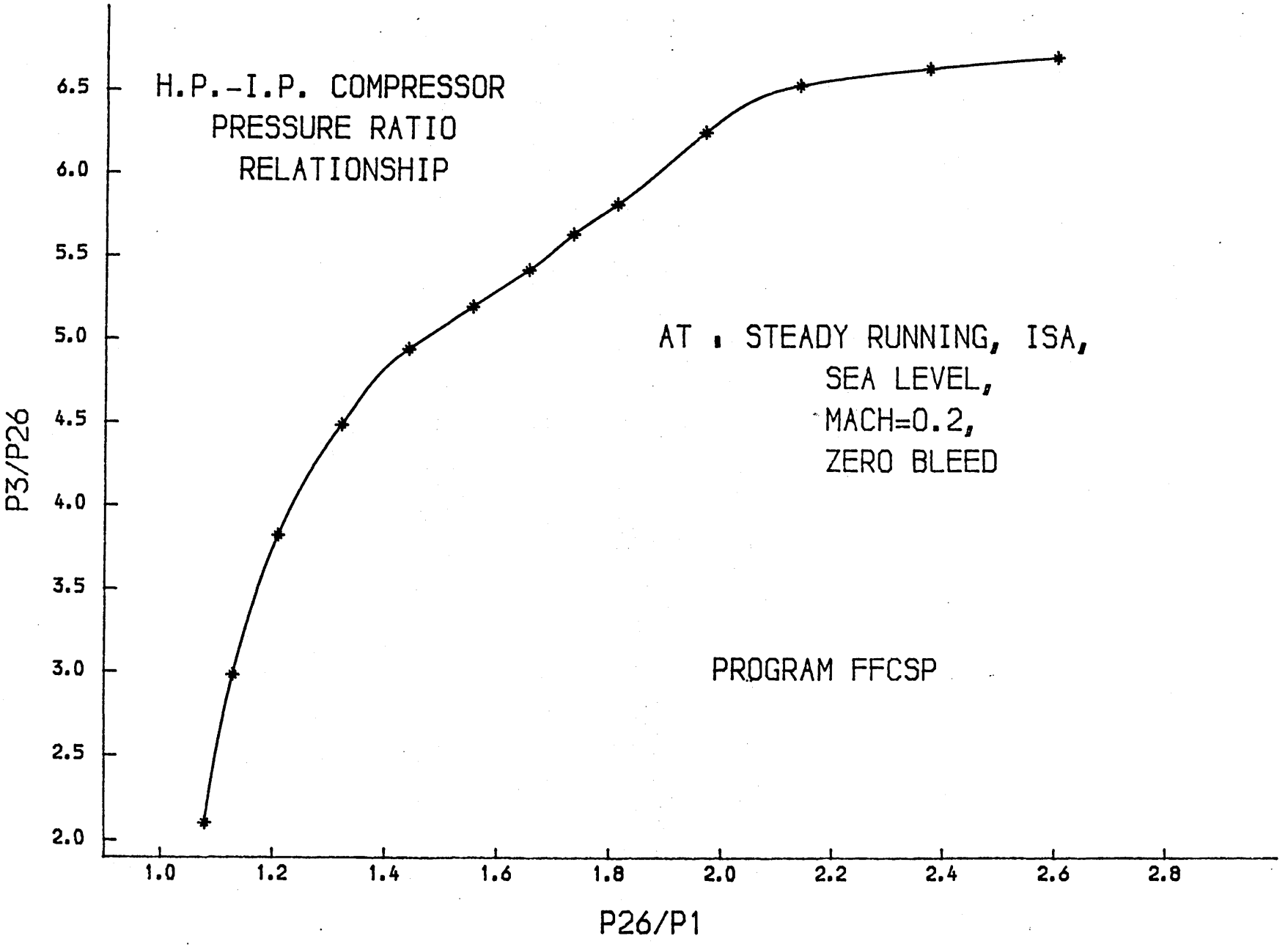
H.P.-I.P. COMPRESSOR
PRESSURE RATIO
RELATIONSHIP
AT : STEADY RUNNING, ISA,
SEA LEVEL,
MACH=0.2,
ZERO BLEED
PROGRAM FFCSP
P3/P26
P26/P1
6.5
6.0
5.5
5.0
4.5
4.0
3.5
3.0
2.5
2.0
1.0
1.2
1.4
1.6
1.8
2.0
2.2
2.4
2.6
2.8

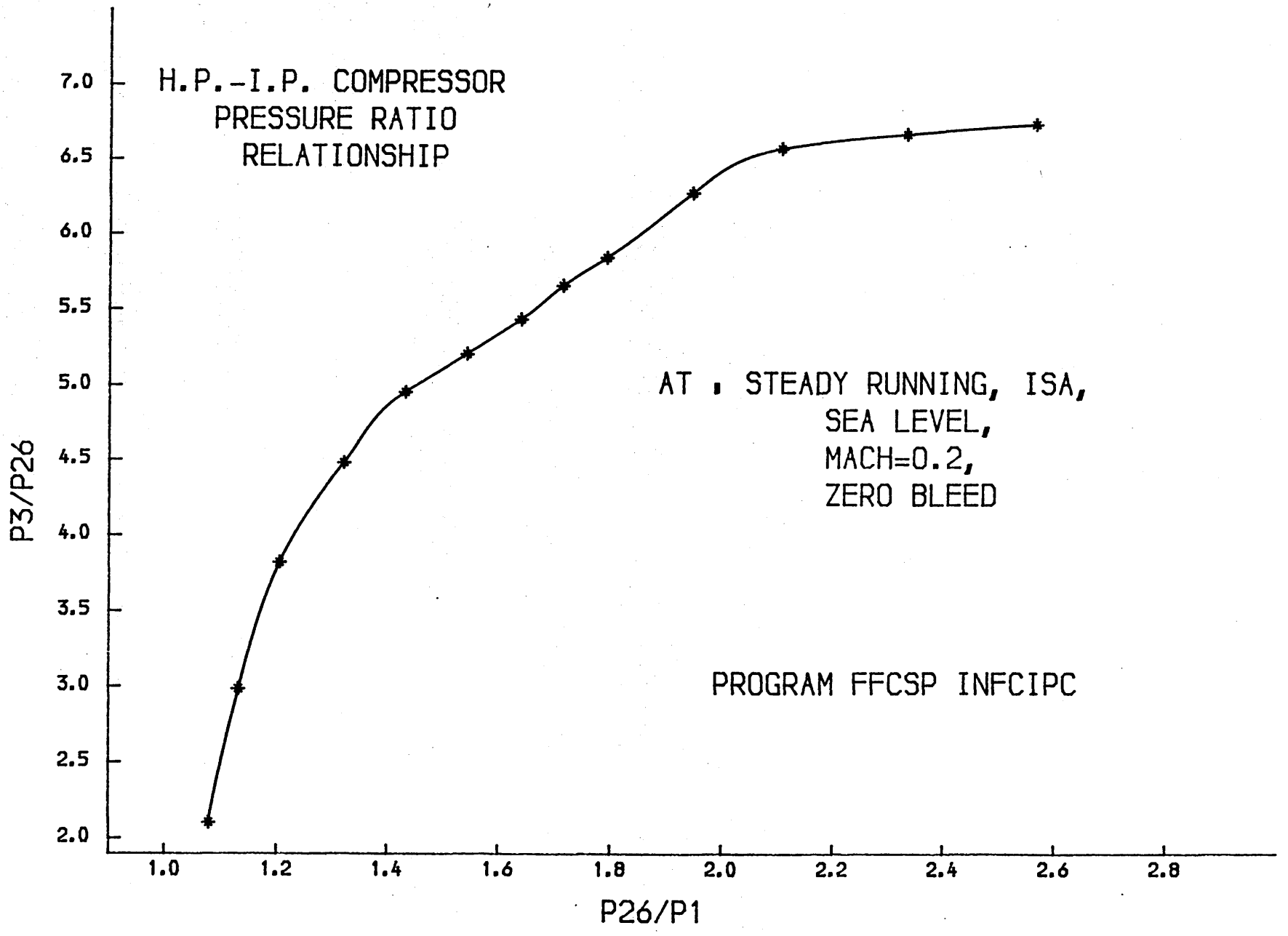
H.P.-I.P. COMPRESSOR
PRESSURE RATIO
RELATIONSHIP
AT : STEADY RUNNING, ISA,
SEA LEVEL,
MACH=0.2,
ZERO BLEED
PROGRAM FFCSP INFCIPC
P3/P26
P26/P1
7.0
6.5
6.0
5.5
5.0
4.5
4.0
3.5
3.0
2.5
2.0
1.0
1.2
1.4
1.6
1.8
2.0
2.2
2.4
2.6
2.8

FIG 1

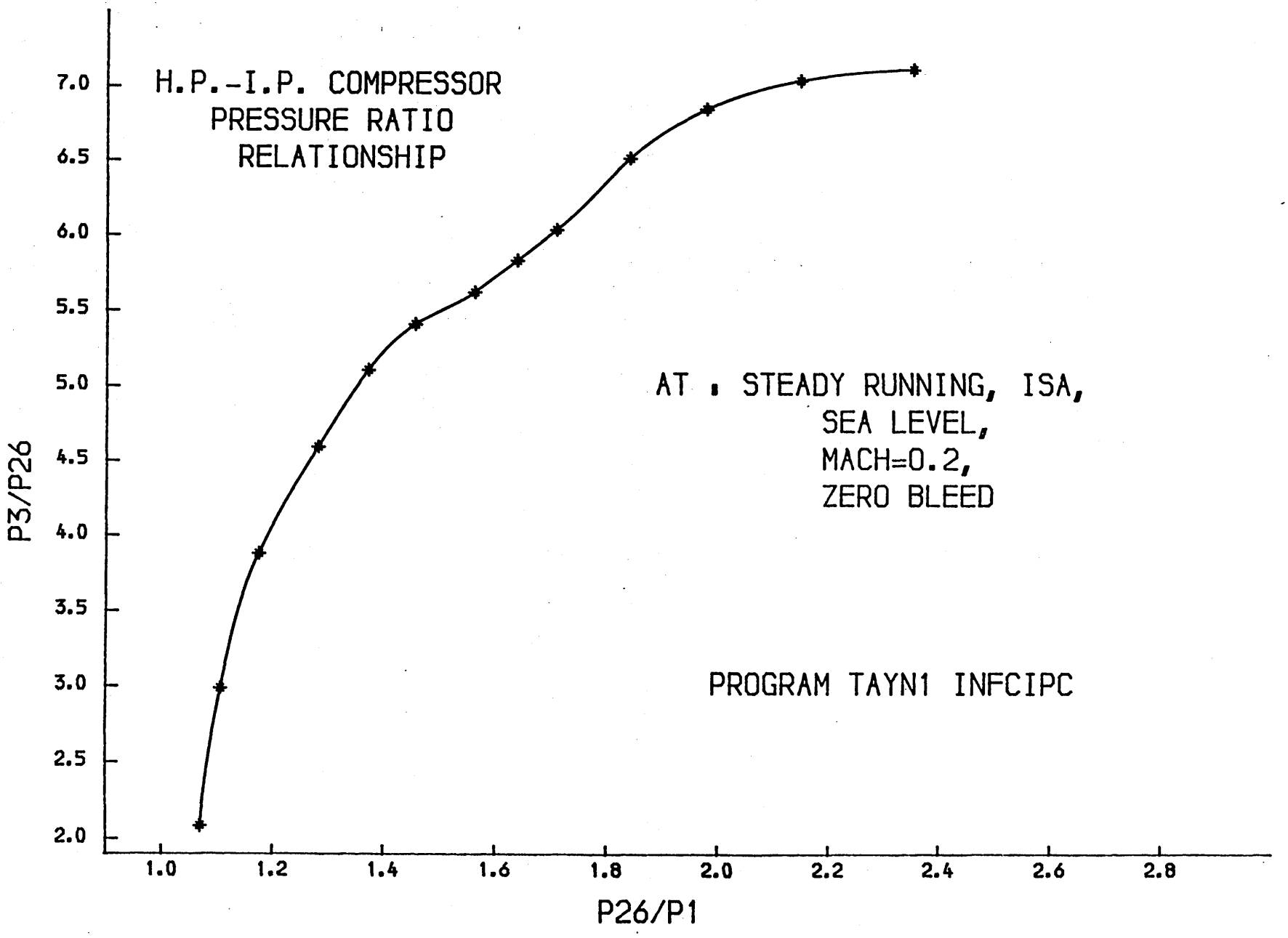
H.P.-I.P. COMPRESSOR
PRESSURE RATIO
RELATIONSHIP
AT : STEADY RUNNING, ISA,
SEA LEVEL,
MACH=0.2,
ZERO BLEED
PROGRAM TAYN1 INFCIPC
P3/P26
P26/P1
7.0
6.5
6.0
5.5
5.0
4.5
4.0
3.5
3.0
2.5
2.0
1.0
1.2
1.4
1.6
1.8
2.0
2.2
2.4
2.6
2.8

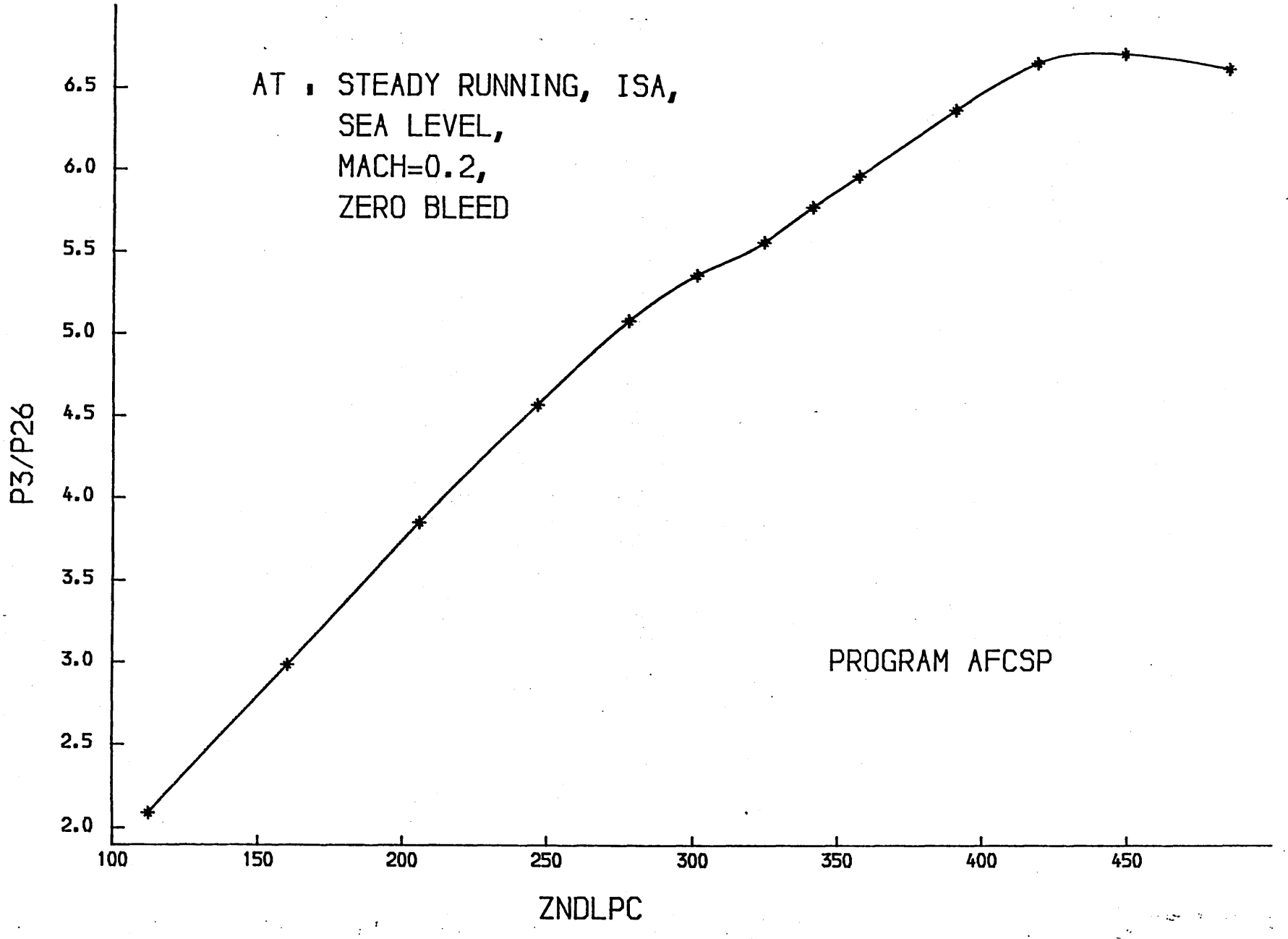
AT : STEADY RUNNING, ISA,
SEA LEVEL,
MACH=0.2,
ZERO BLEED
PROGRAM AFCSP
P3/P26
ZNDLPC
6.5
6.0
5.5
5.0
4.5
4.0
3.5
3.0
2.5
2.0
100
150
200
250
300
350
400
450

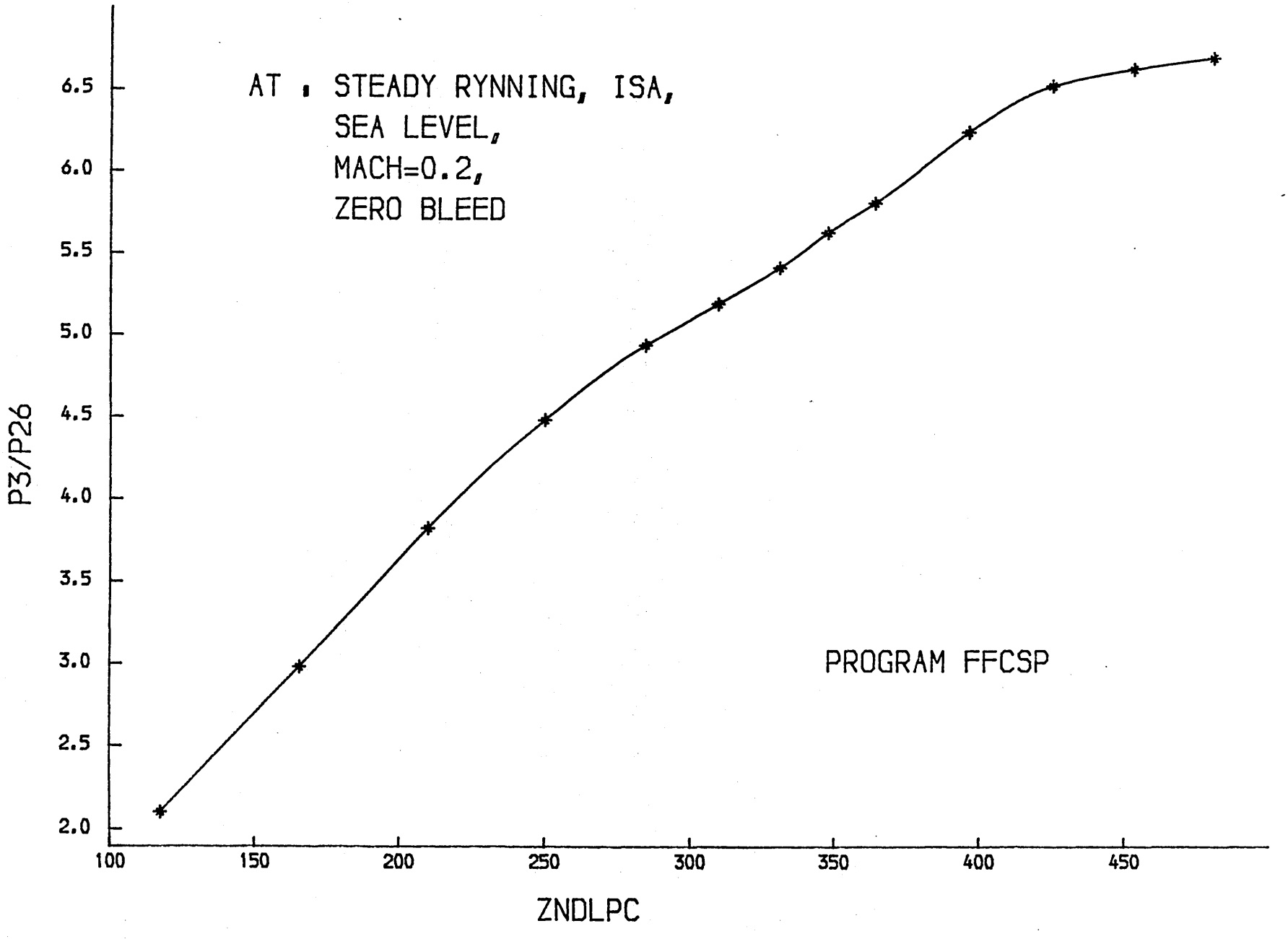
AT : STEADY RYNNING, ISA,
SEA LEVEL,
MACH=0.2,
ZERO BLEED
PROGRAM FFCSP
P3/P26
ZNDLPC
6.5
6.0
5.5
5.0
4.5
4.0
3.5
3.0
2.5
2.0
100
150
200
250
300
350
400
450

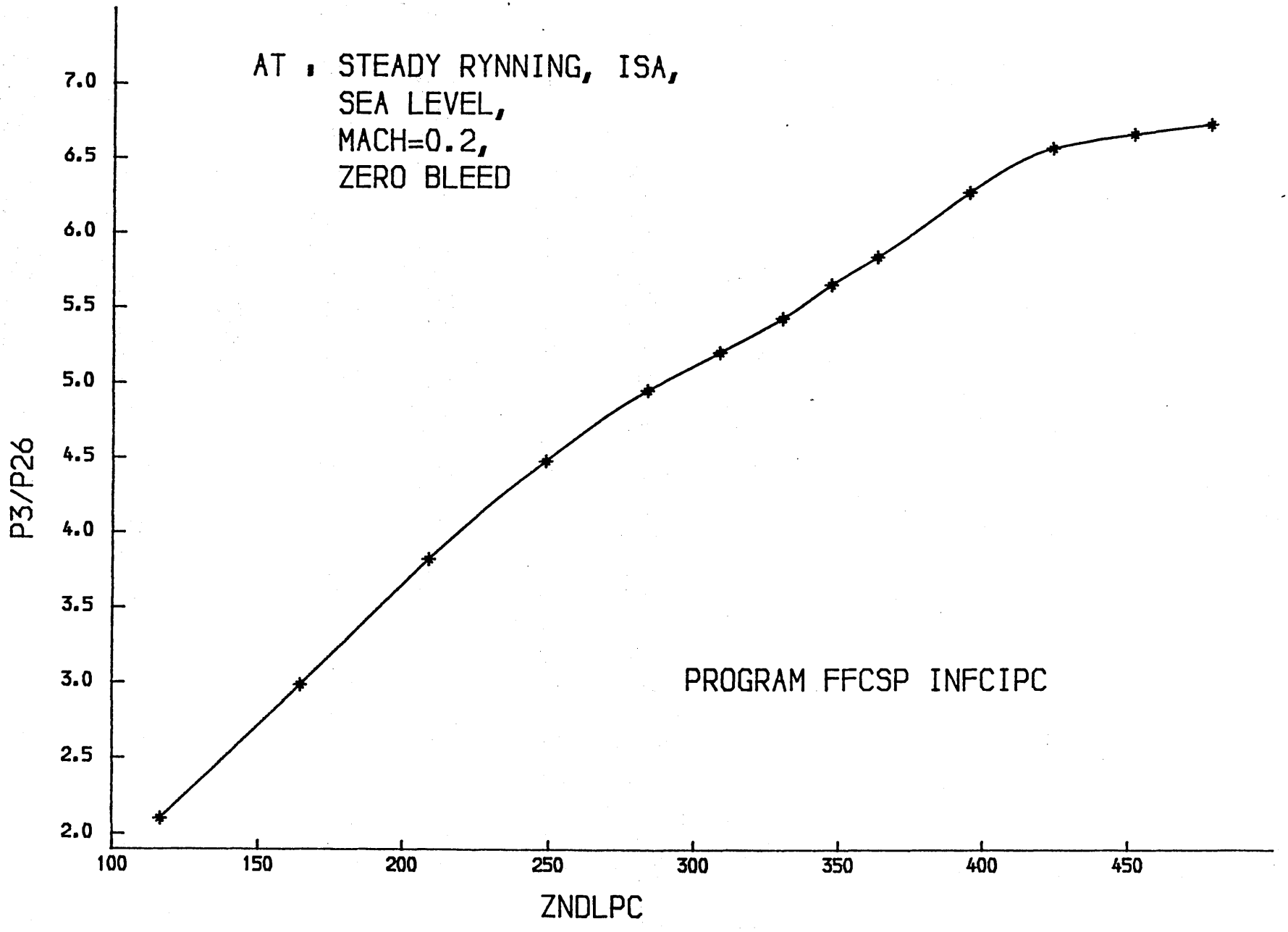
AT : STEADY RYNNING, ISA,
SEA LEVEL,
MACH=0.2,
ZERO BLEED
PROGRAM FFCSP INFCIPC
P3/P26
ZNDLPC
7.0
6.5
6.0
5.5
5.0
4.5
4.0
3.5
3.0
2.5
2.0
100
150
200
250
300
350
400
450

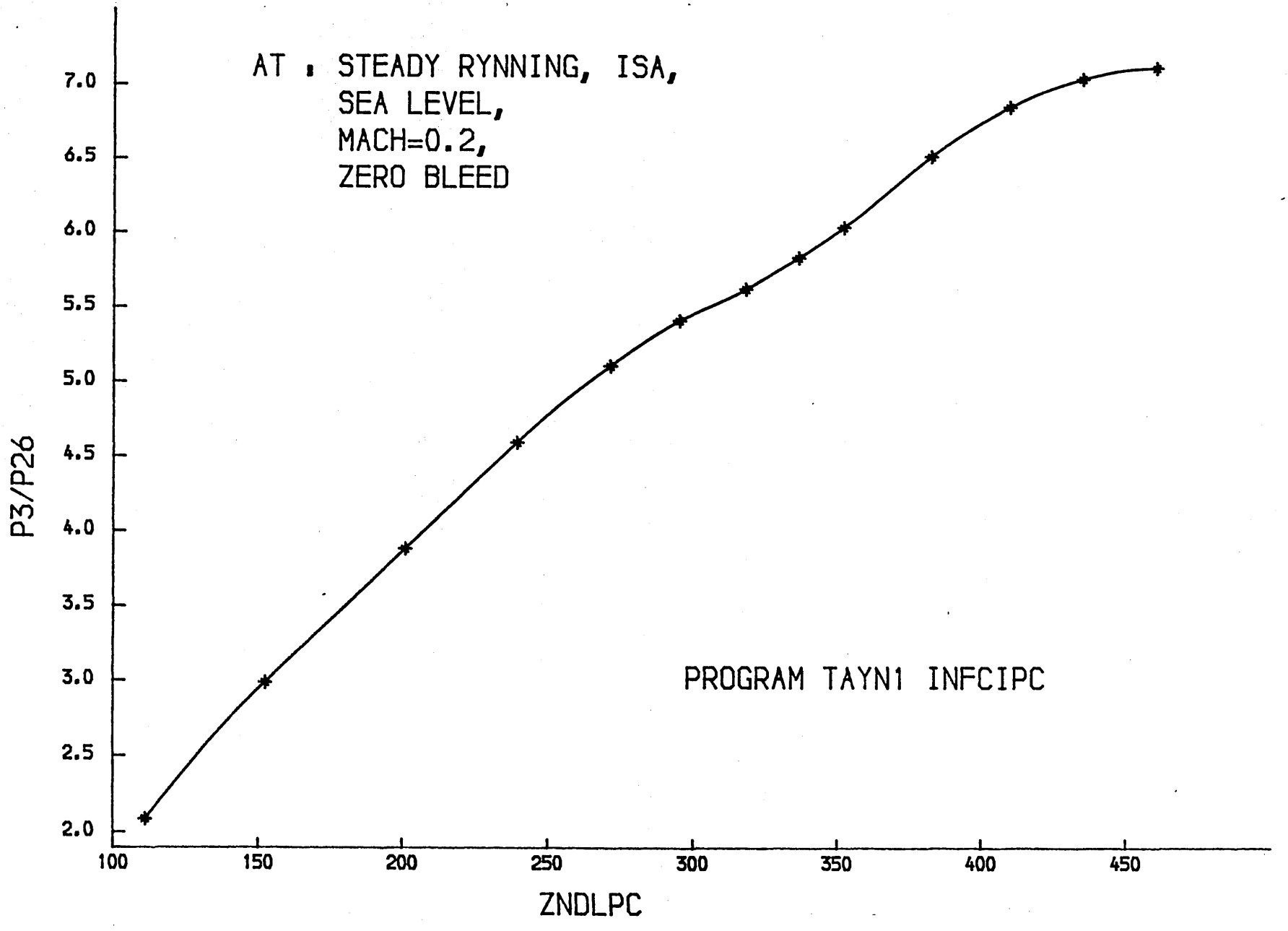
AT : STEADY RYNNING, ISA,
SEA LEVEL,
MACH=0.2,
ZERO BLEED
PROGRAM TAYN1 INFCIPC
P3/P26
ZNDLPC
7.0
6.5
6.0
5.5
5.0
4.5
4.0
3.5
3.0
2.5
2.0
100
150
200
250
300
350
400
450

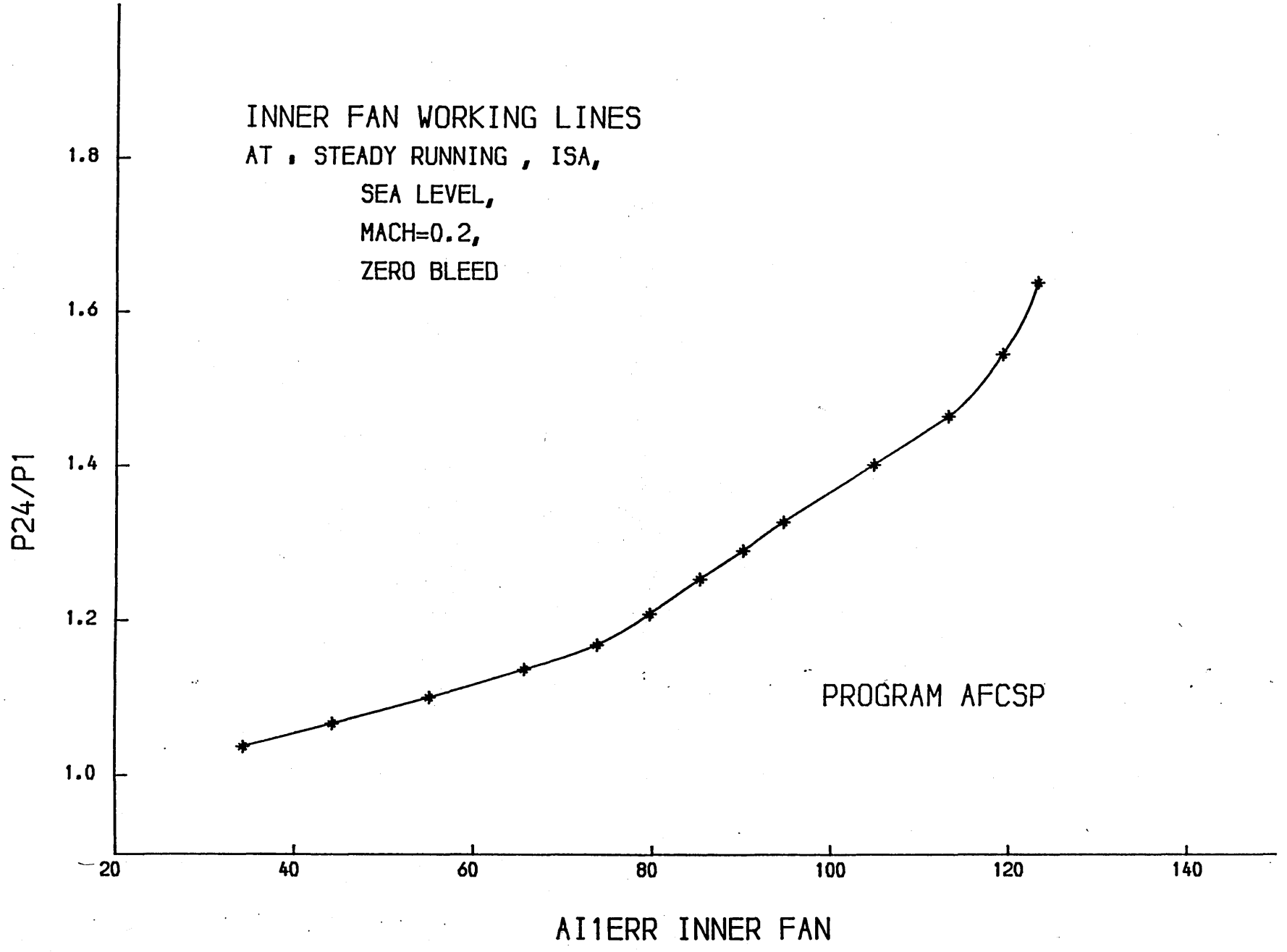
INNER FAN WORKING LINES
AT , STEADY RUNNING , ISA,
SEA LEVEL,
MACH=0.2,
ZERO BLEED
PROGRAM AFCSP
P24/P1
1.8
1.6
1.4
1.2
1.0
20
40
60
80
100
120
140
AI1ERR INNER FAN

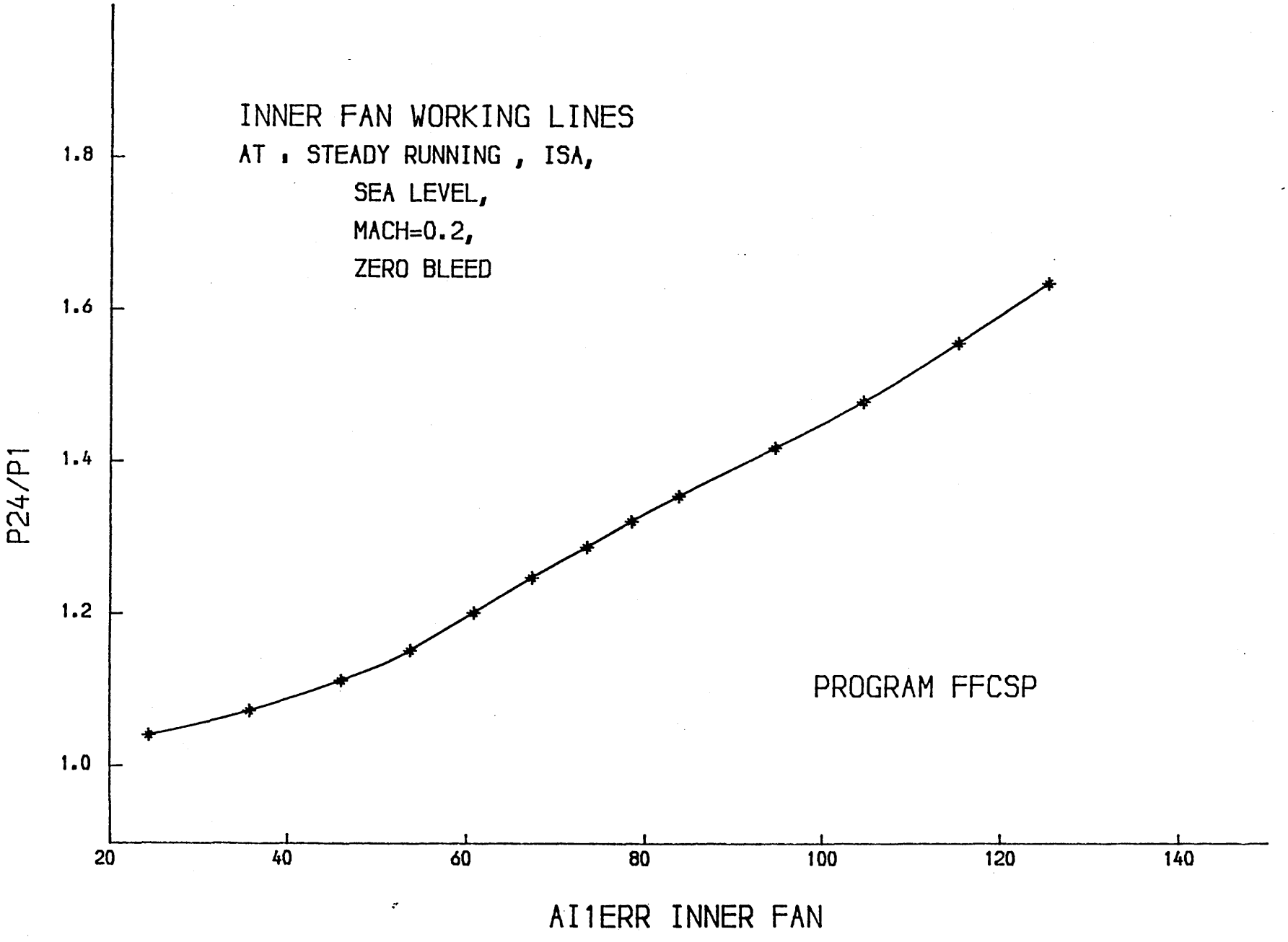
INNER FAN WORKING LINES
AT : STEADY RUNNING , ISA,
SEA LEVEL,
MACH=0.2,
ZERO BLEED
PROGRAM FFCSP
P24/P1
1.8
1.6
1.4
1.2
1.0
20
40
60
80
100
120
140
AI1ERR INNER FAN

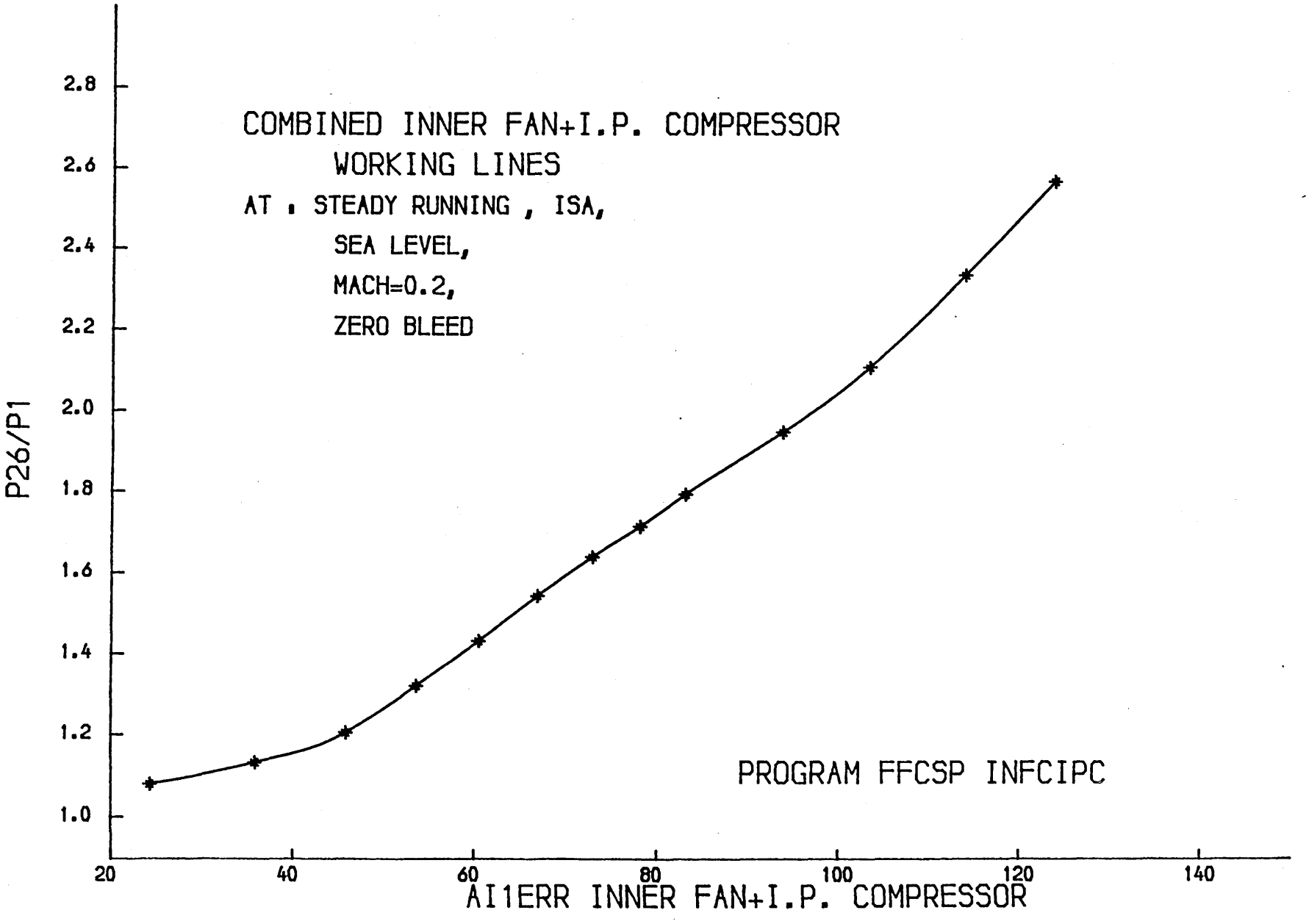
COMBINED INNER FAN+I.P. COMPRESSOR
WORKING LINES
AT : STEADY RUNNING , ISA,
SEA LEVEL,
MACH=0.2,
ZERO BLEED
PROGRAM FFCSP INFCIPC
P26/P1
2.8
2.6
2.4
2.2
2.0
1.8
1.6
1.4
1.2
1.0
20
40
60
80
100
120
140
AI1ERR INNER FAN+I.P. COMPRESSOR

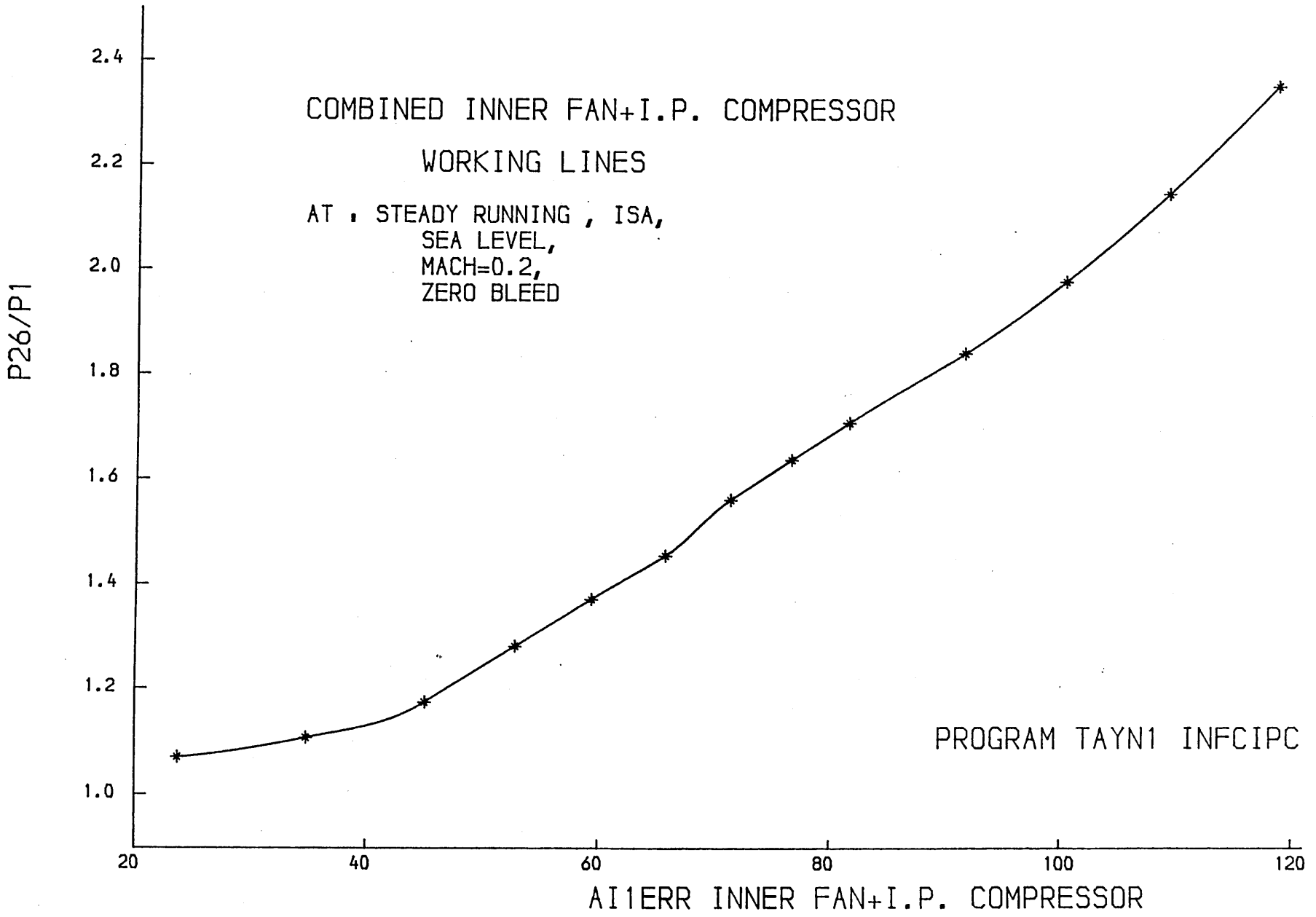
COMBINED INNER FAN+I.P. COMPRESSOR
WORKING LINES
AT . STEADY RUNNING , ISA,
SEA LEVEL,
MACH=0.2,
ZERO BLEED
PROGRAM TAYN1 INFCIPC
P26/P1
2.4
2.2
2.0
1.8
1.6
1.4
1.2
1.0
20
40
60
80
100
120
AI1ERR INNER FAN+I.P. COMPRESSOR

FIG 20

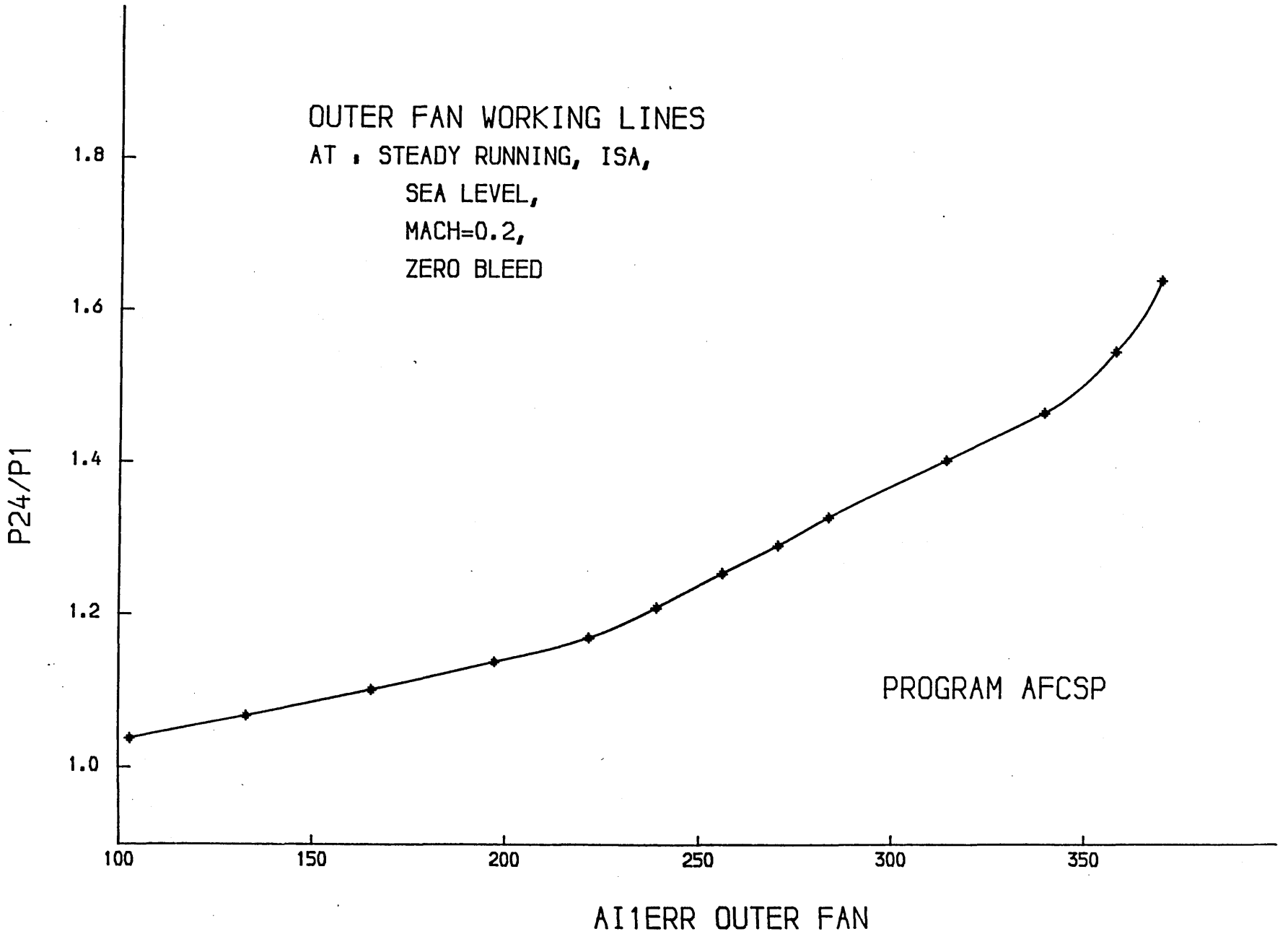
OUTER FAN WORKING LINES
AT : STEADY RUNNING, ISA,
SEA LEVEL,
MACH=0.2,
ZERO BLEED
PROGRAM AFCSP
P24/P1
1.8
1.6
1.4
1.2
1.0
100
150
200
250
300
350
AI1ERR OUTER FAN

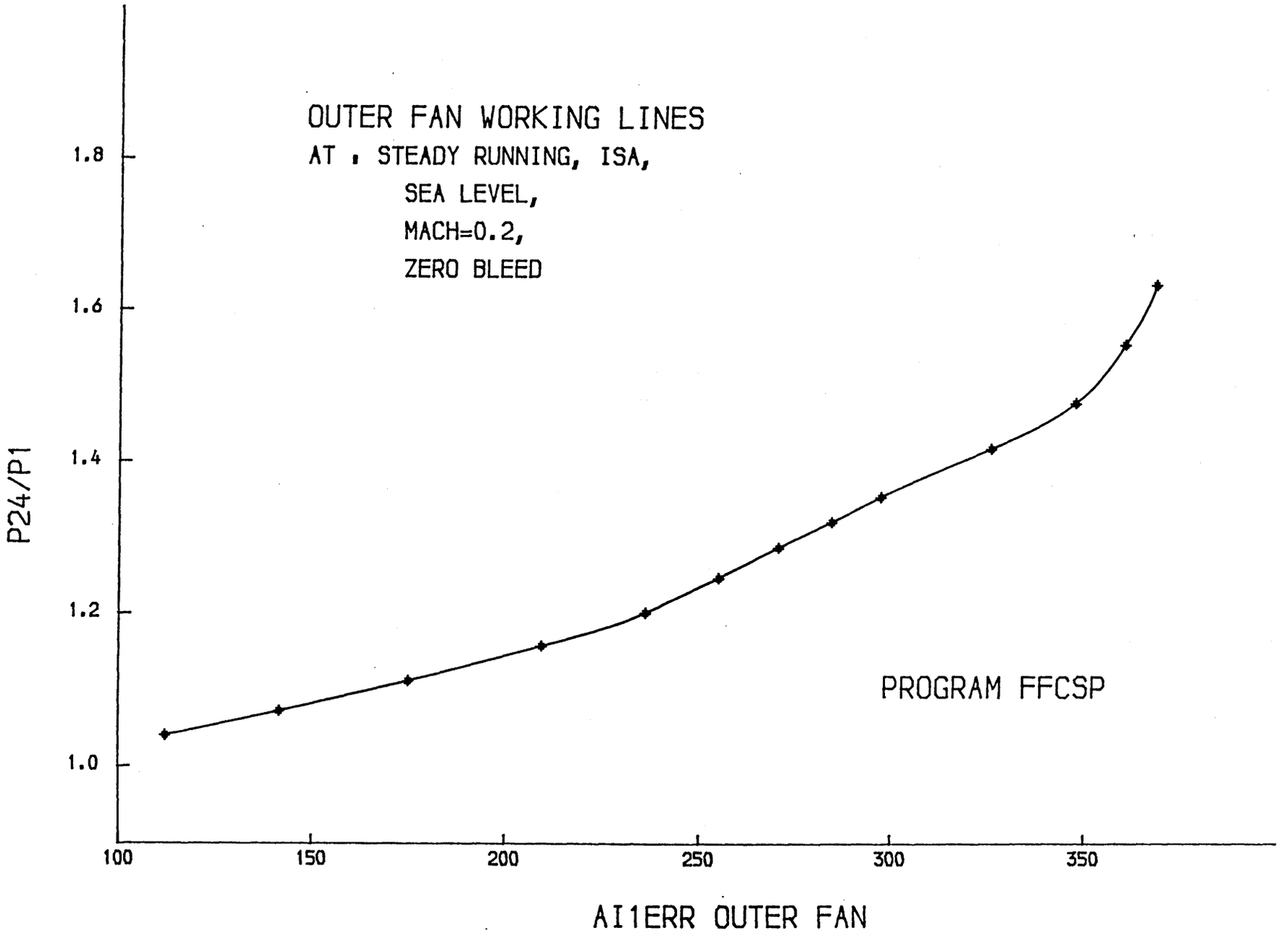
OUTER FAN WORKING LINES
AT : STEADY RUNNING, ISA,
SEA LEVEL,
MACH=0.2,
ZERO BLEED
PROGRAM FFCSP
P24/P1
1.8
1.6
1.4
1.2
1.0
100
150
200
250
300
350
AI1ERR OUTER FAN

FIG 4.7

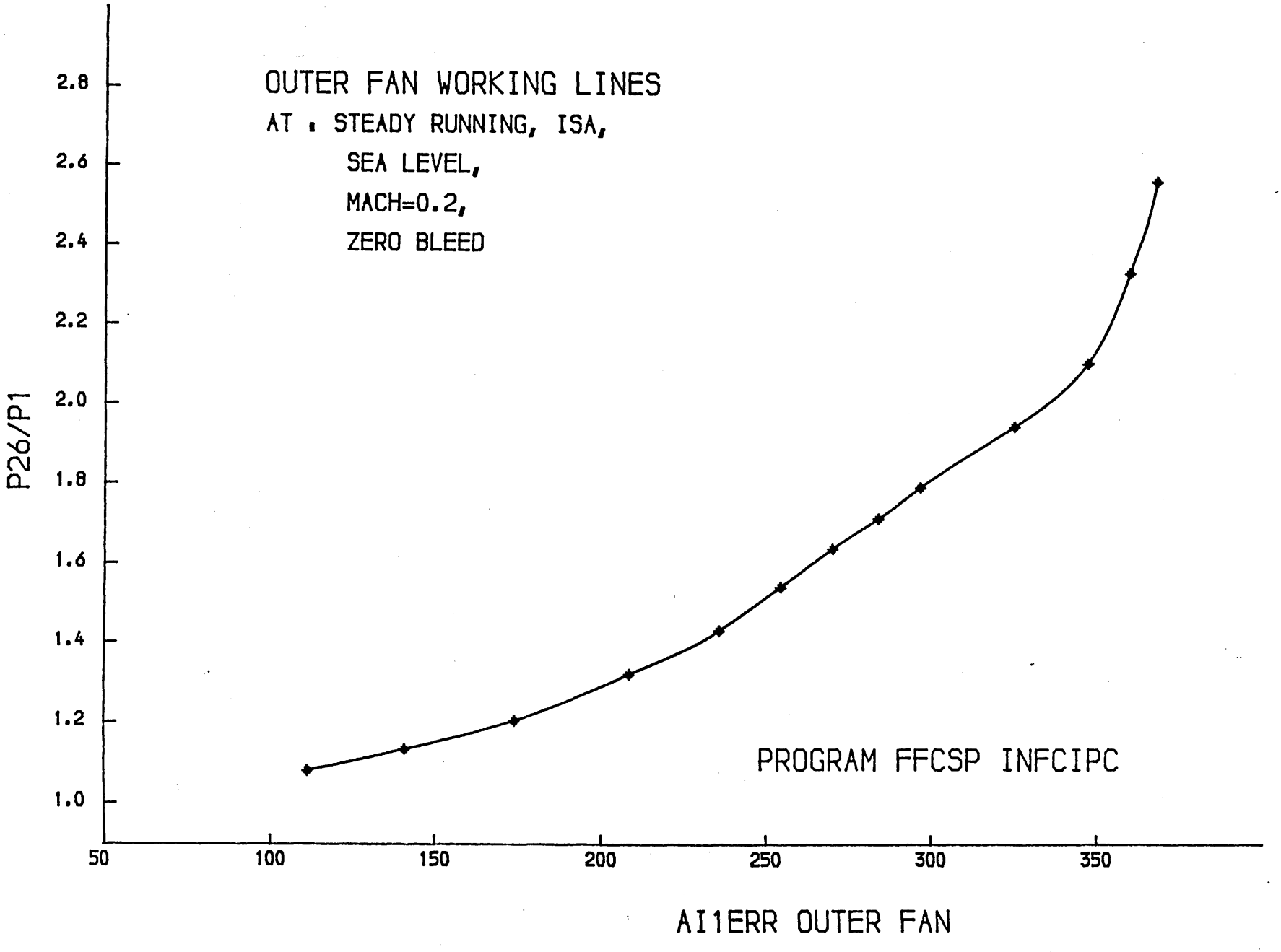
OUTER FAN WORKING LINES
AT : STEADY RUNNING, ISA,
SEA LEVEL,
MACH=0.2,
ZERO BLEED
P26/P1
2.8
2.6
2.4
2.2
2.0
1.8
1.6
1.4
1.2
1.0
50
100
150
200
250
300
350
PROGRAM FFCSP INFCIPC
AI1ERR OUTER FAN

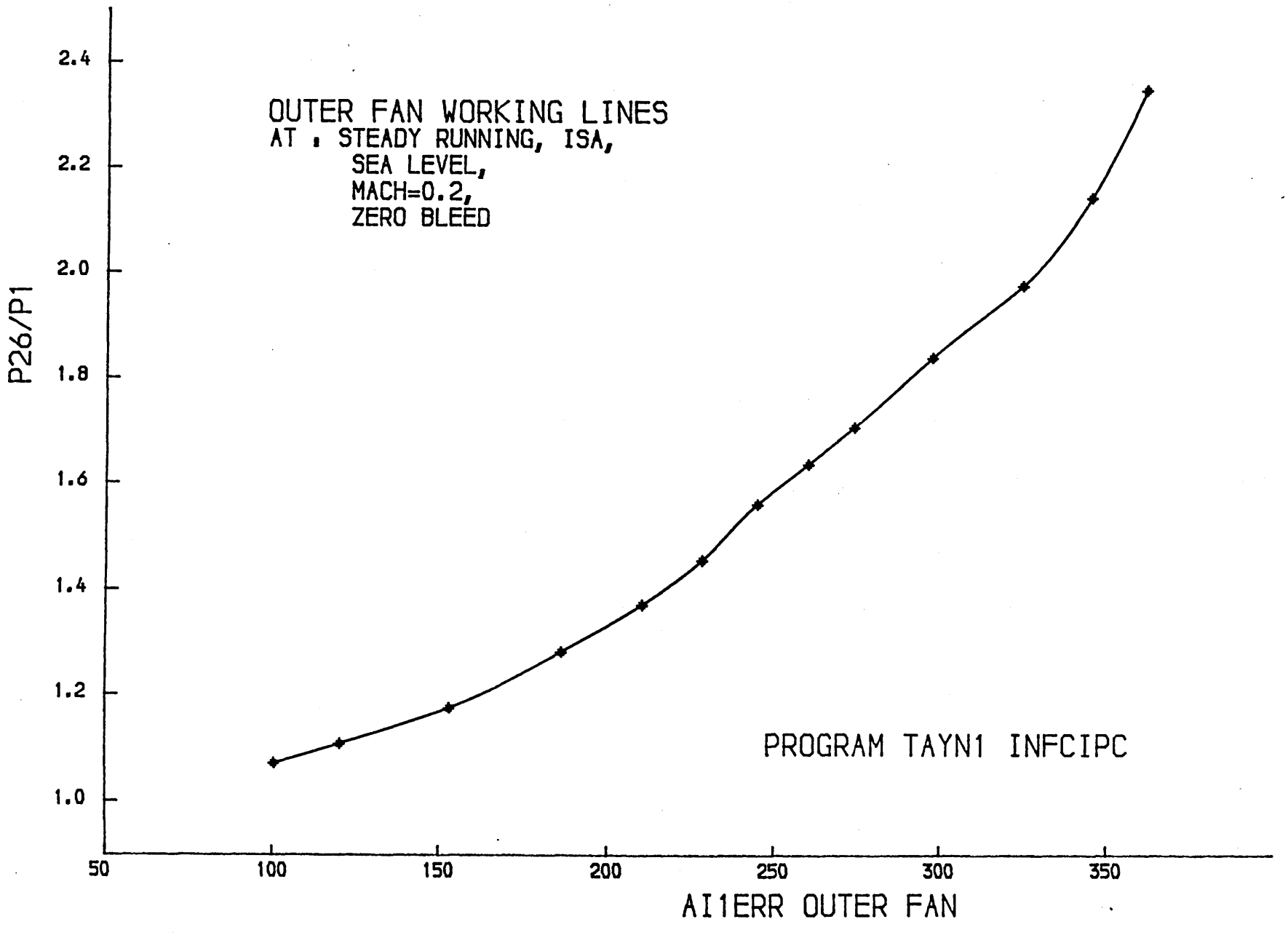
OUTER FAN WORKING LINES
AT : STEADY RUNNING, ISA,
SEA LEVEL,
MACH=0.2,
ZERO BLEED
PROGRAM TAYN1 INFCIPC
P26/P1
2.4
2.2
2.0
1.8
1.6
1.4
1.2
1.0
50
100
150
200
250
300
350
AI1ERR OUTER FAN

FIGURES : 25. 26. 27.

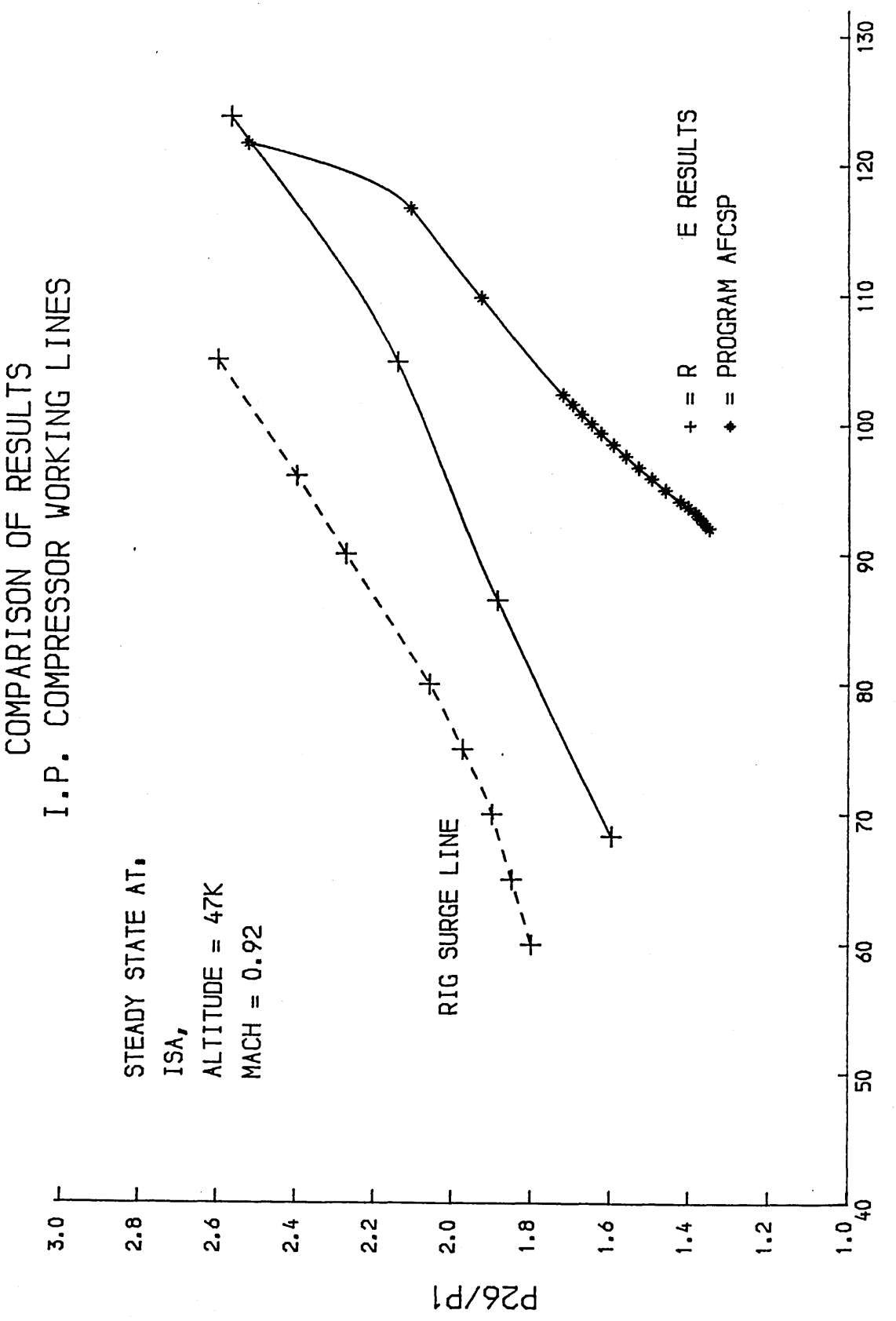

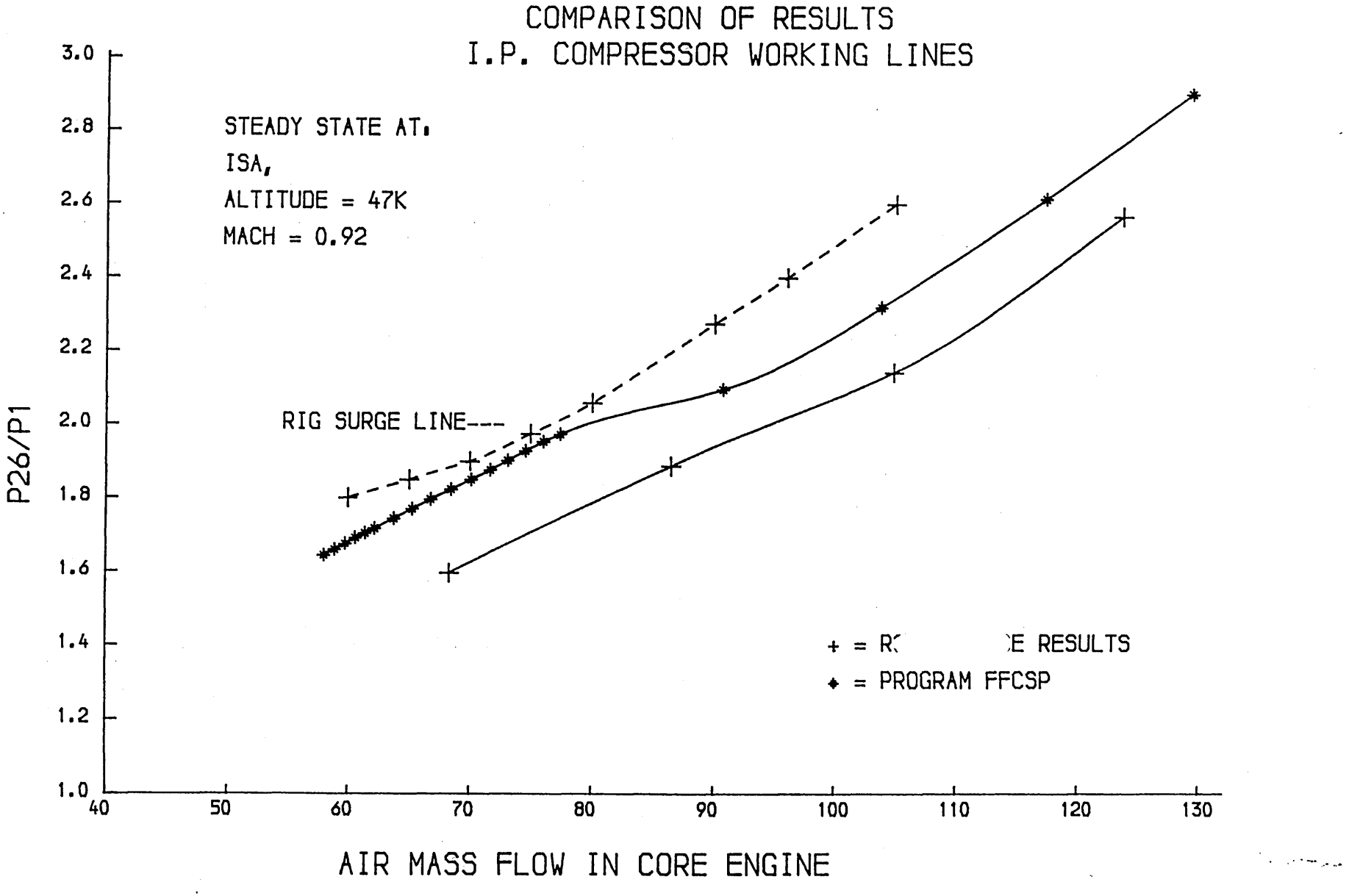
COMPARISON OF RESULTS
I.P. COMPRESSOR WORKING LINES
STEADY STATE AT,
ISA,
ALTITUDE = 47K
MACH = 0.92
RIG SURGE LINE---
+ = R E RESULTS
* = PROGRAM FFCSP
P26/P1
3.0
2.8
2.6
2.4
2.2
2.0
1.8
1.6
1.4
1.2
1.0
40
50
60
70
80
90
100
110
120
130
AIR MASS FLOW IN CORE ENGINE

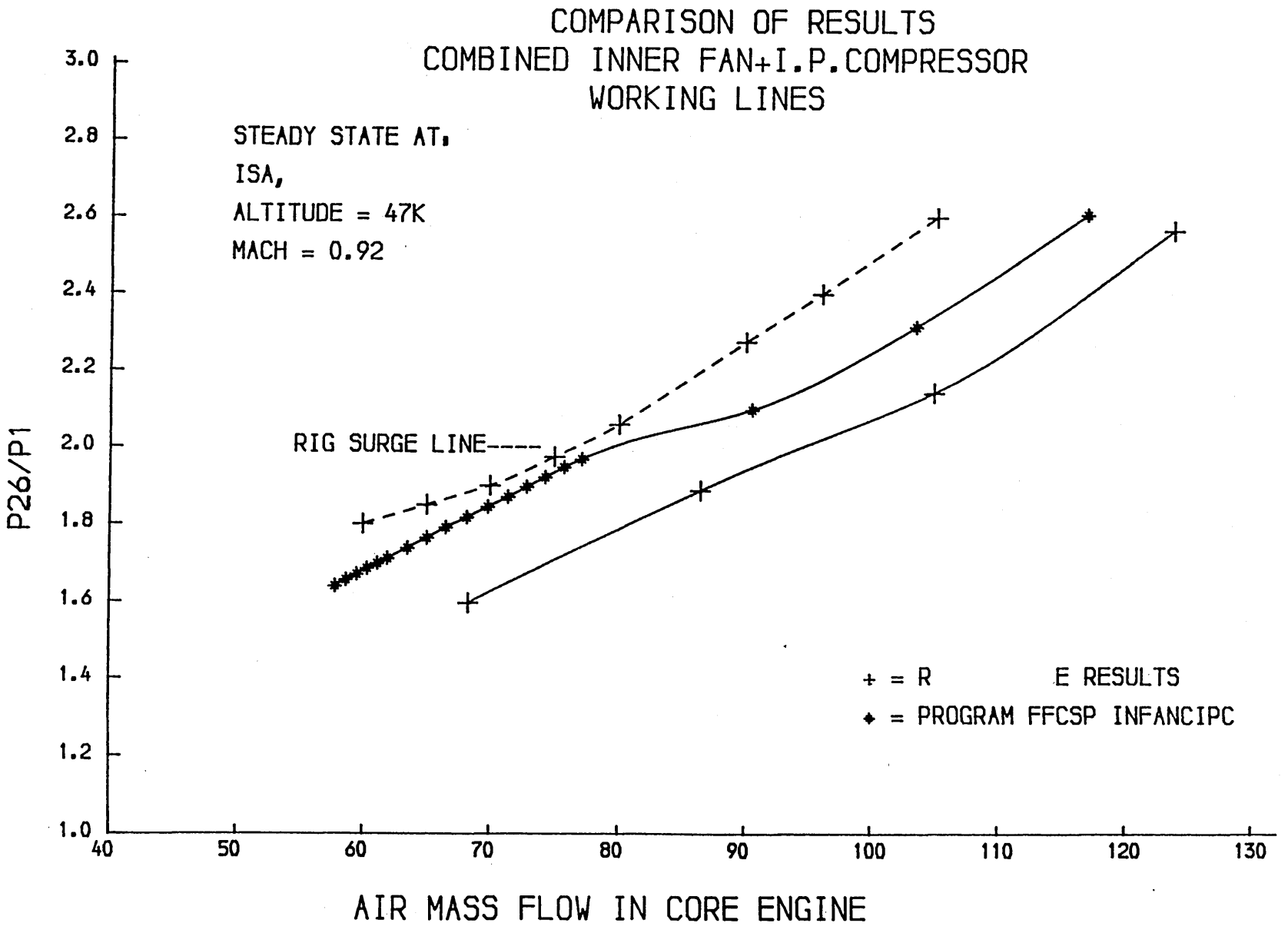
COMPARISON OF RESULTS
COMBINED INNER FAN+I.P.COMPRESSOR
WORKING LINES
STEADY STATE AT,
ISA,
ALTITUDE = 47K
MACH = 0.92
RIG SURGE LINE----
+ = R E RESULTS
* = PROGRAM FFCSP INFANCIPC
P26/P1
3.0
2.8
2.6
2.4
2.2
2.0
1.8
1.6
1.4
1.2
1.0
40
50
60
70
80
90
100
110
120
130
AIR MASS FLOW IN CORE ENGINE

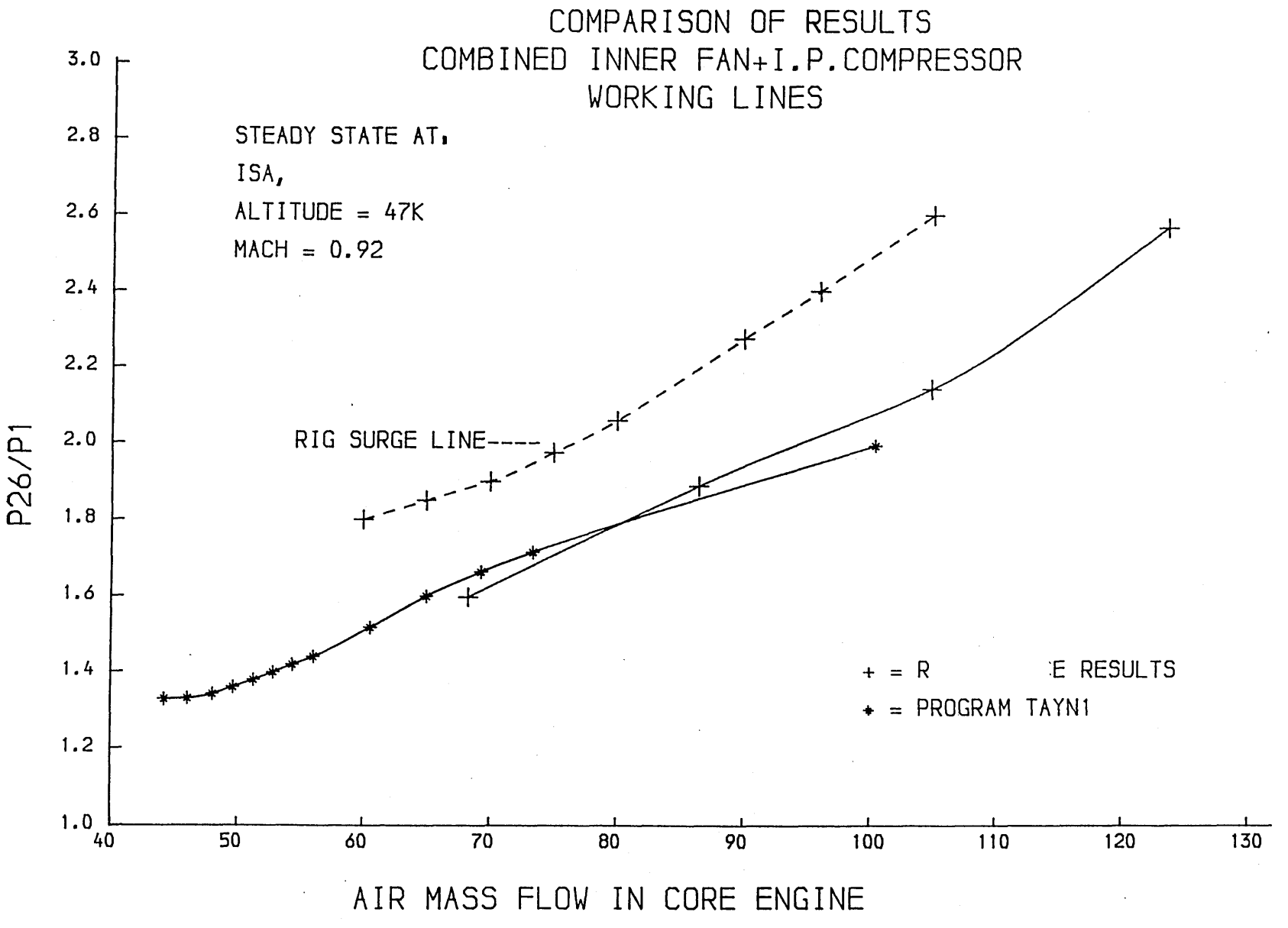
COMPARISON OF RESULTS
COMBINED INNER FAN+I.P.COMPRESSOR
WORKING LINES
STEADY STATE AT,
ISA,
ALTITUDE = 47K
MACH = 0.92
RIG SURGE LINE----
+ = R E RESULTS
* = PROGRAM TAYN1
P26/P1
3.0
2.8
2.6
2.4
2.2
2.0
1.8
1.6
1.4
1.2
1.0
40
50
60
70
80
90
100
110
120
130
AIR MASS FLOW IN CORE ENGINE

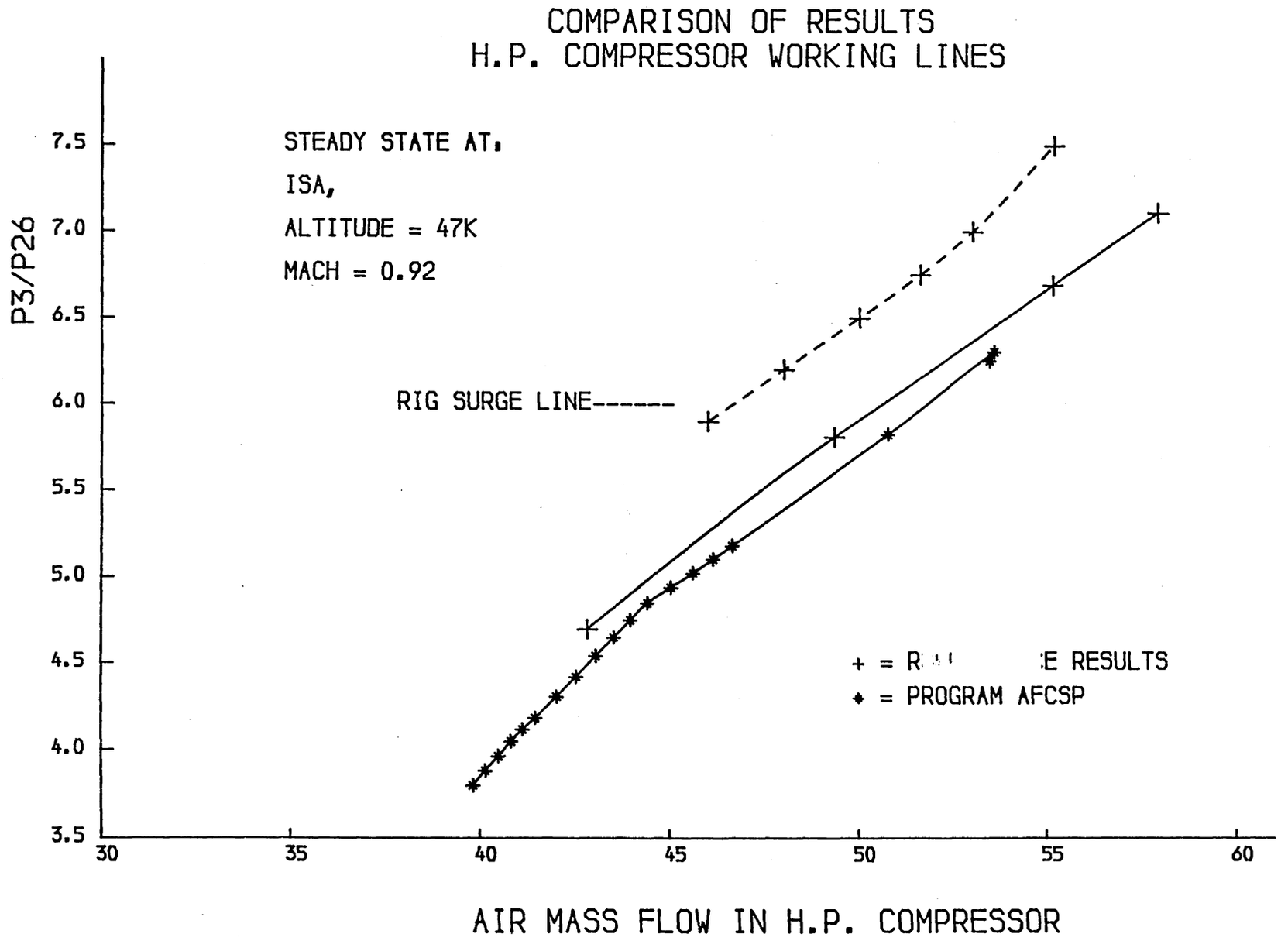
COMPARISON OF RESULTS
H.P. COMPRESSOR WORKING LINES
STEADY STATE AT,
ISA,
ALTITUDE = 47K
MACH = 0.92
RIG SURGE LINE------
+ = R E RESULTS
* = PROGRAM AFCSP
P3/P26
7.5
7.0
6.5
6.0
5.5
5.0
4.5
4.0
3.5
30
35
40
45
50
55
60
AIR MASS FLOW IN H.P. COMPRESSOR

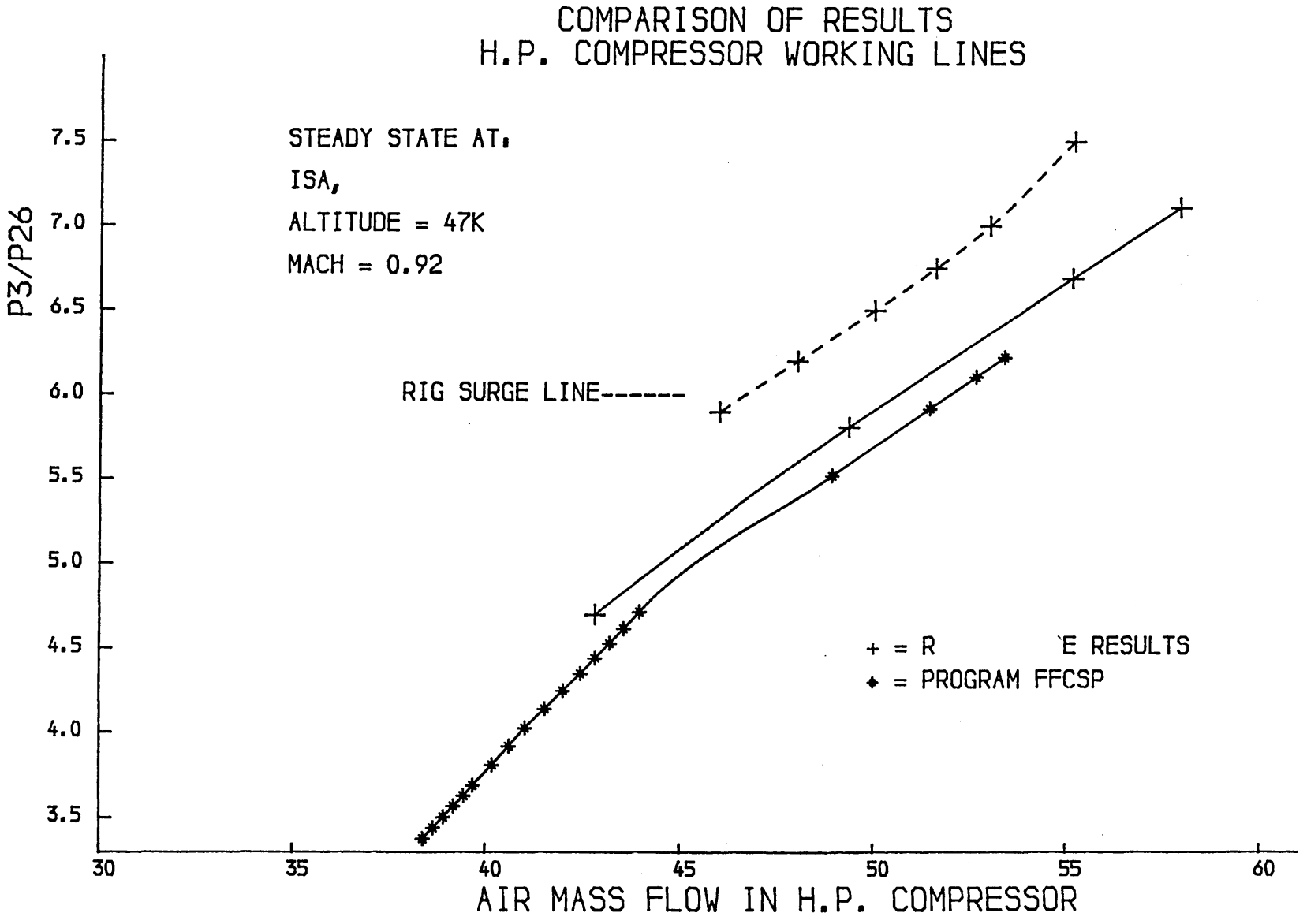
COMPARISON OF RESULTS
H.P. COMPRESSOR WORKING LINES
STEADY STATE AT:
ISA,
ALTITUDE = 47K
MACH = 0.92
RIG SURGE LINE------
+ = R E RESULTS
* = PROGRAM FFCSP
P3/P26
7.5
7.0
6.5
6.0
5.5
5.0
4.5
4.0
3.5
30
35
40
45
50
55
60
AIR MASS FLOW IN H.P. COMPRESSOR

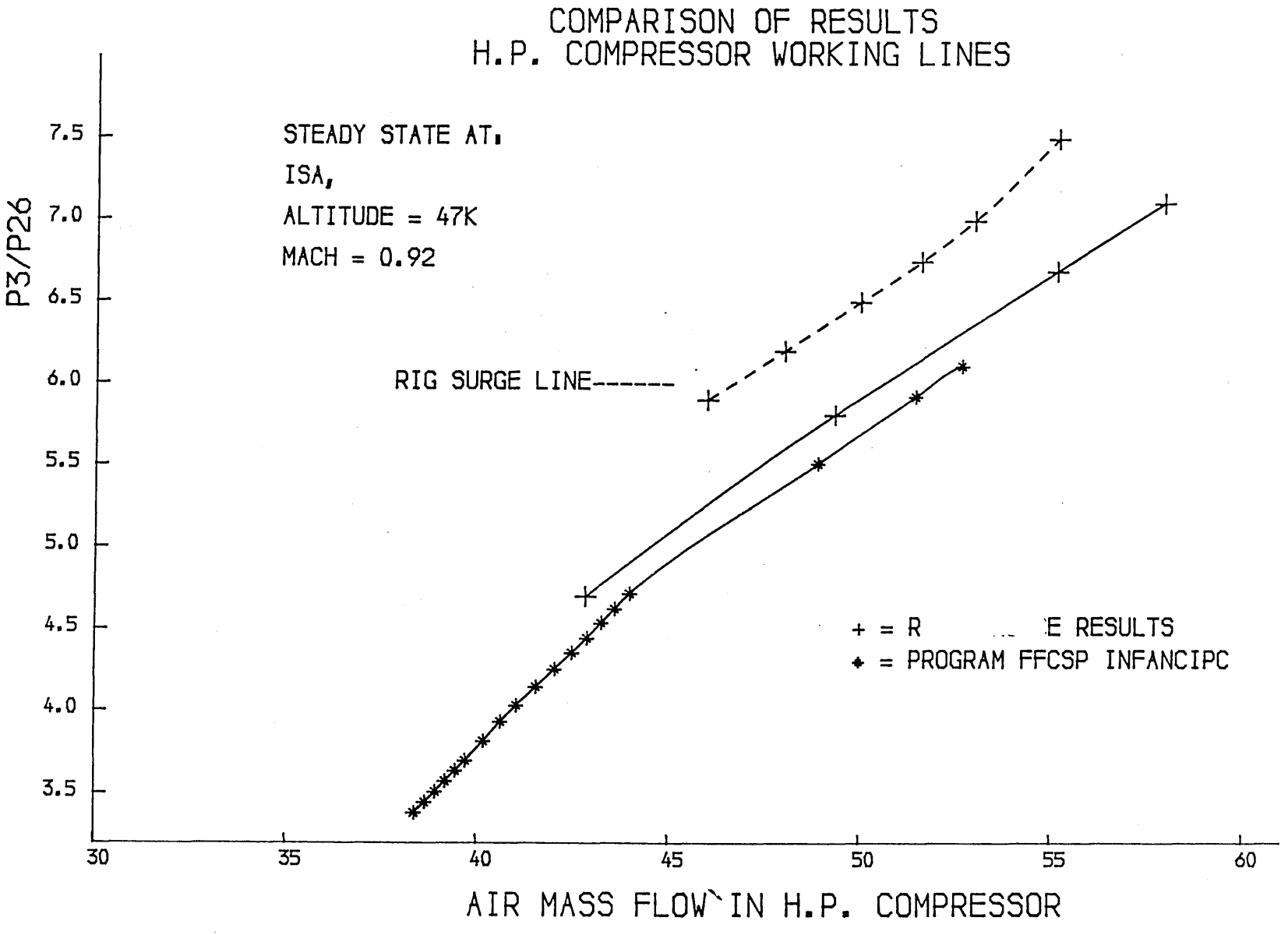
COMPARISON OF RESULTS
H.P. COMPRESSOR WORKING LINES
STEADY STATE AT,
ISA,
ALTITUDE = 47K
MACH = 0.92
RIG SURGE LINE------
+ = R ... E RESULTS
* = PROGRAM FFCSP INFANCIPC
P3/P26
7.5
7.0
6.5
6.0
5.5
5.0
4.5
4.0
3.5
30
35
40
45
50
55
60
AIR MASS FLOW IN H.P. COMPRESSOR

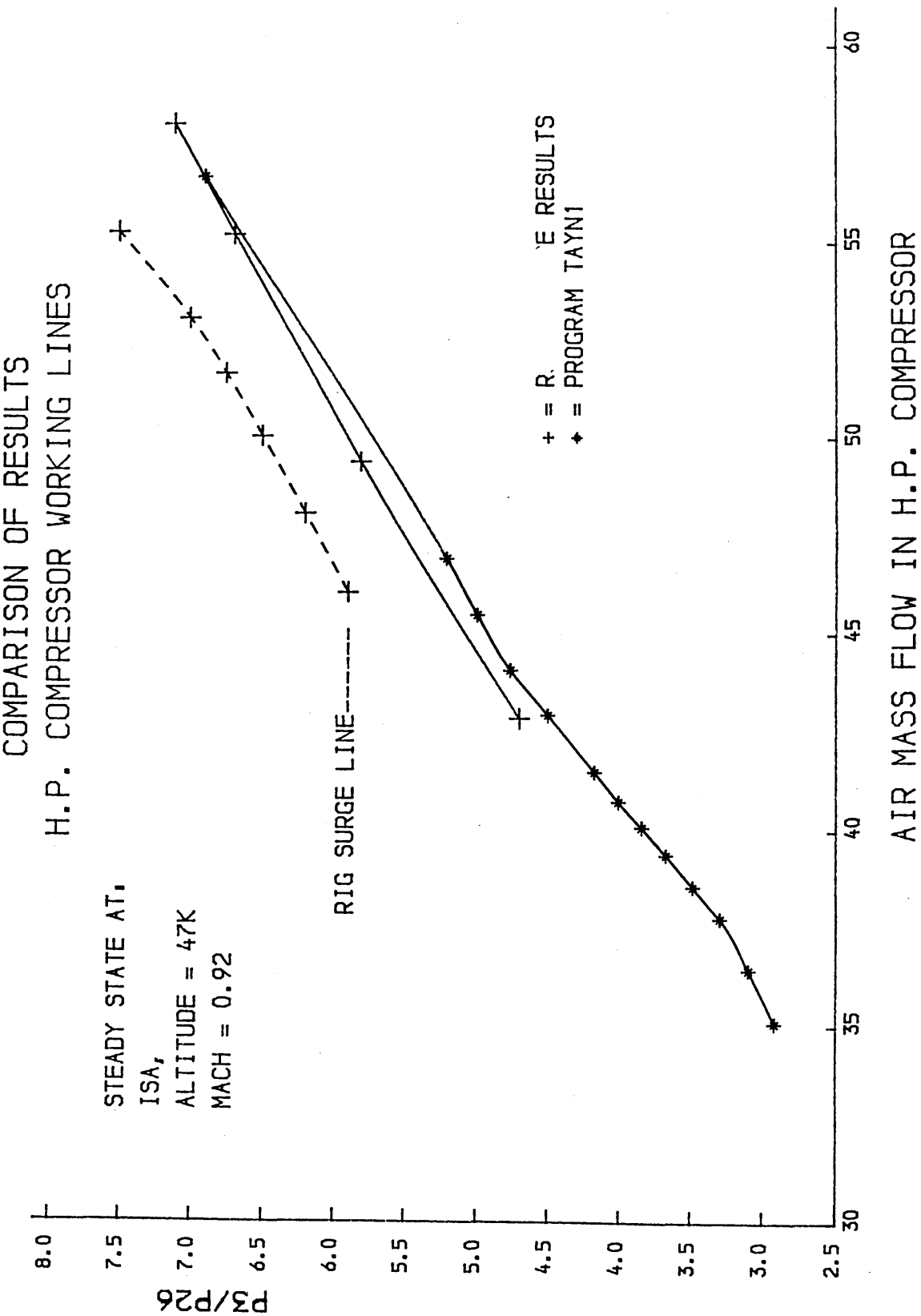
COMPARISON OF RESULTS
H.P. COMPRESSOR WORKING LINES
STEADY STATE AT,
ISA,
ALTITUDE = 47K
MACH = 0.92
RIG SURGE LINE------
+ = R E RESULTS
* = PROGRAM TAYN1
P3/P26
AIR MASS FLOW IN H.P. COMPRESSOR
8.0
7.5
7.0
6.5
6.0
5.5
5.0
4.5
4.0
3.5
3.0
2.5
30
35
40
45
50
55
60

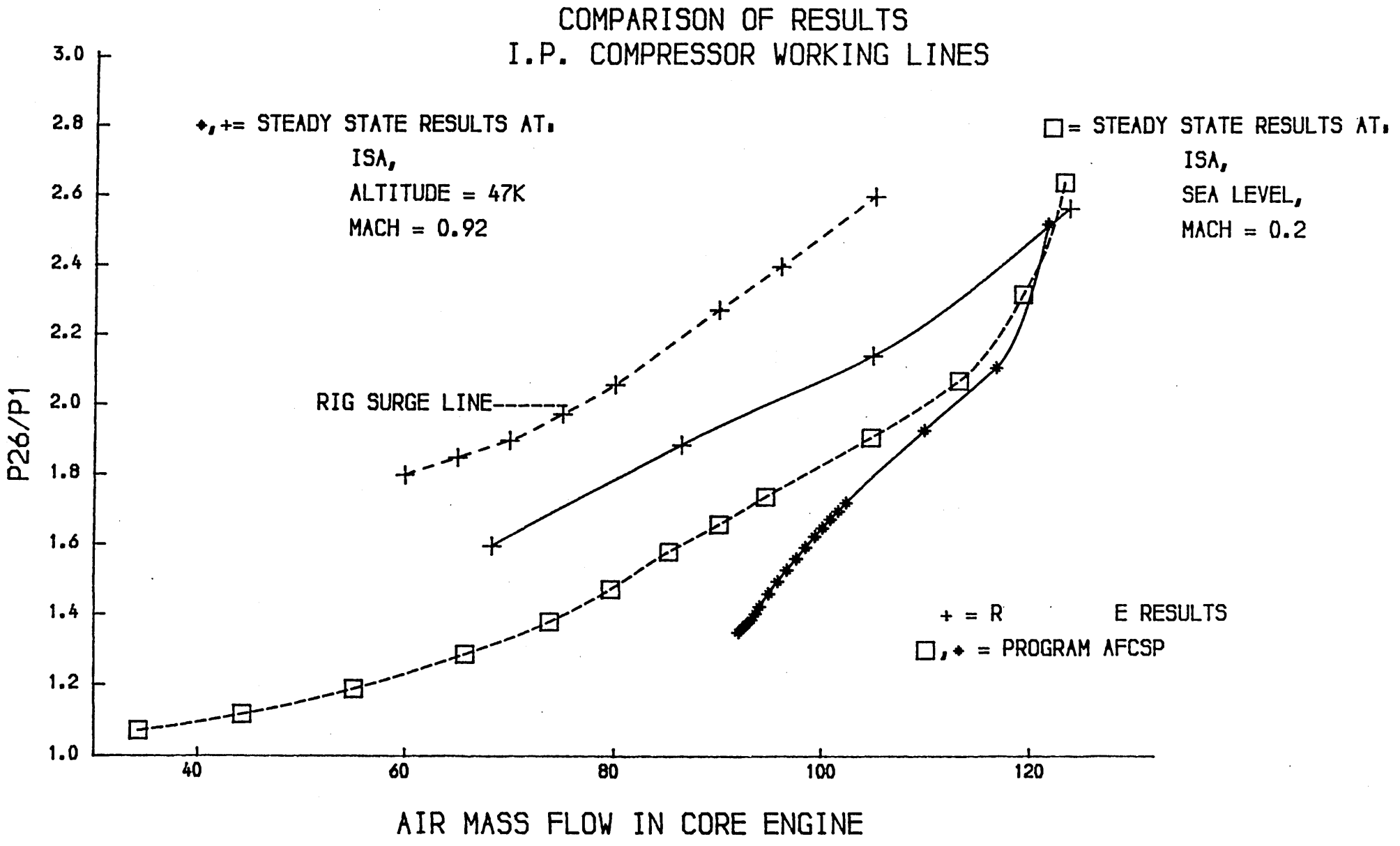
COMPARISON OF RESULTS
I.P. COMPRESSOR WORKING LINES
+,+= STEADY STATE RESULTS AT,
ISA,
ALTITUDE = 47K
MACH = 0.92
□= STEADY STATE RESULTS AT,
ISA,
SEA LEVEL,
MACH = 0.2
RIG SURGE LINE
+ = R E RESULTS
□,* = PROGRAM AFCSP
P26/P1
3.0
2.8
2.6
2.4
2.2
2.0
1.8
1.6
1.4
1.2
1.0
40
60
80
100
120
AIR MASS FLOW IN CORE ENGINE

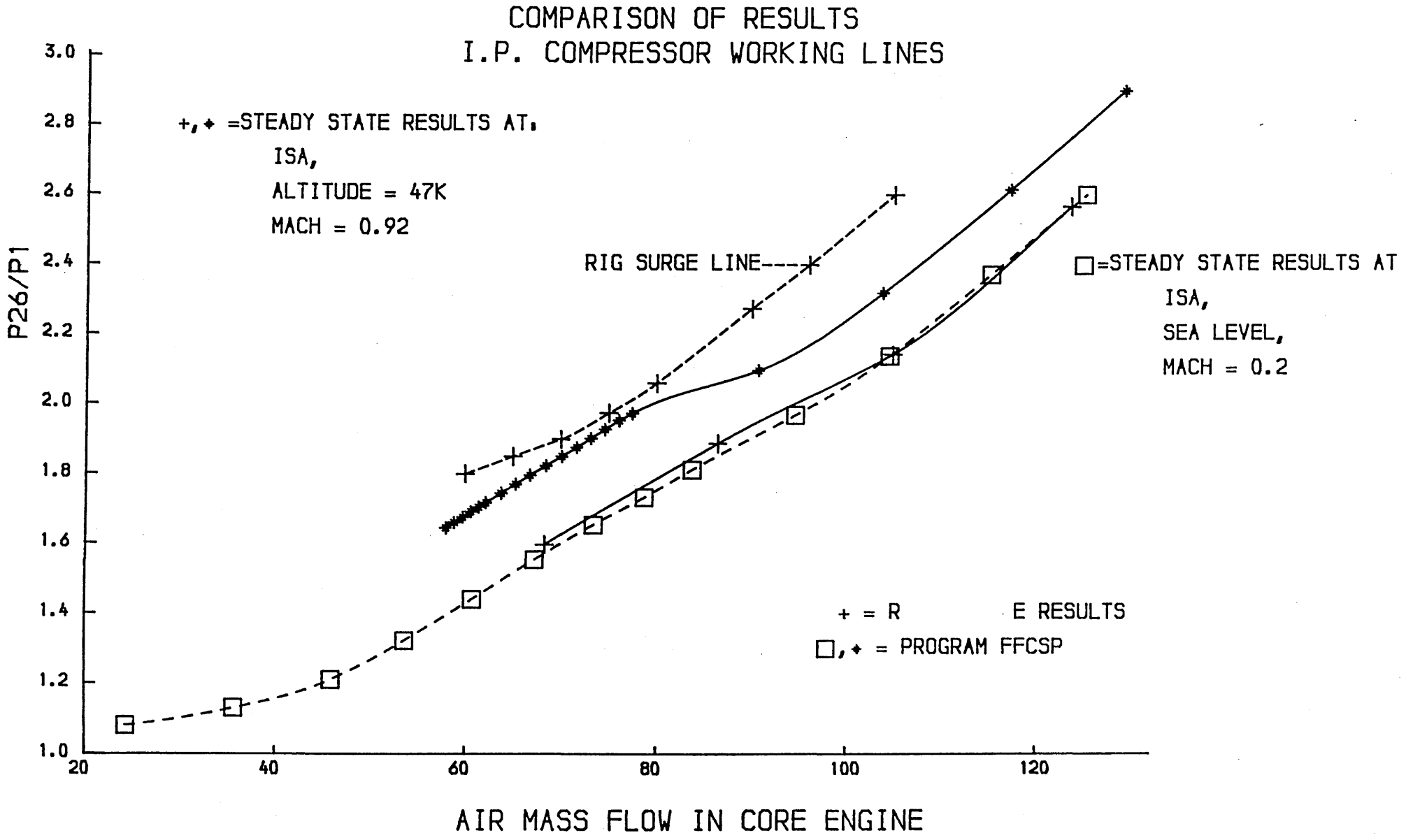
COMPARISON OF RESULTS
I.P. COMPRESSOR WORKING LINES
+,✦ =STEADY STATE RESULTS AT:
ISA,
ALTITUDE = 47K
MACH = 0.92
RIG SURGE LINE---
□=STEADY STATE RESULTS AT
ISA,
SEA LEVEL,
MACH = 0.2
+ = R E RESULTS
□,✦ = PROGRAM FFCSP
P26/P1
3.0
2.8
2.6
2.4
2.2
2.0
1.8
1.6
1.4
1.2
1.0
20
40
60
80
100
120
AIR MASS FLOW IN CORE ENGINE

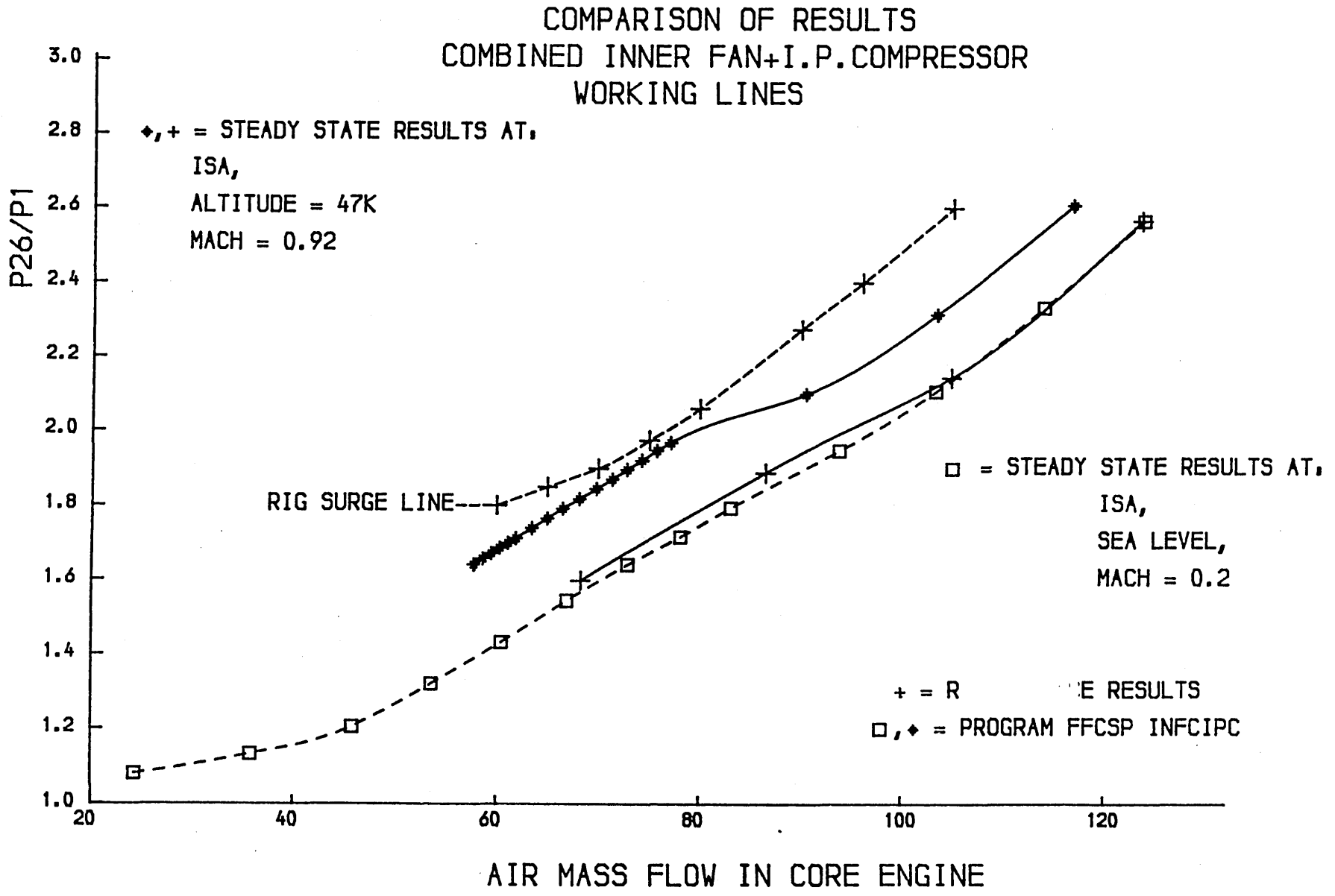
COMPARISON OF RESULTS
COMBINED INNER FAN+I.P.COMPRESSOR
WORKING LINES
P26/P1
3.0
2.8
2.6
2.4
2.2
2.0
1.8
1.6
1.4
1.2
1.0
20
40
60
80
100
120
AIR MASS FLOW IN CORE ENGINE
♦,+ = STEADY STATE RESULTS AT:
ISA,
ALTITUDE = 47K
MACH = 0.92
RIG SURGE LINE
□ = STEADY STATE RESULTS AT:
ISA,
SEA LEVEL,
MACH = 0.2
+ = R E RESULTS
□,♦ = PROGRAM FFCSP INFCIPC

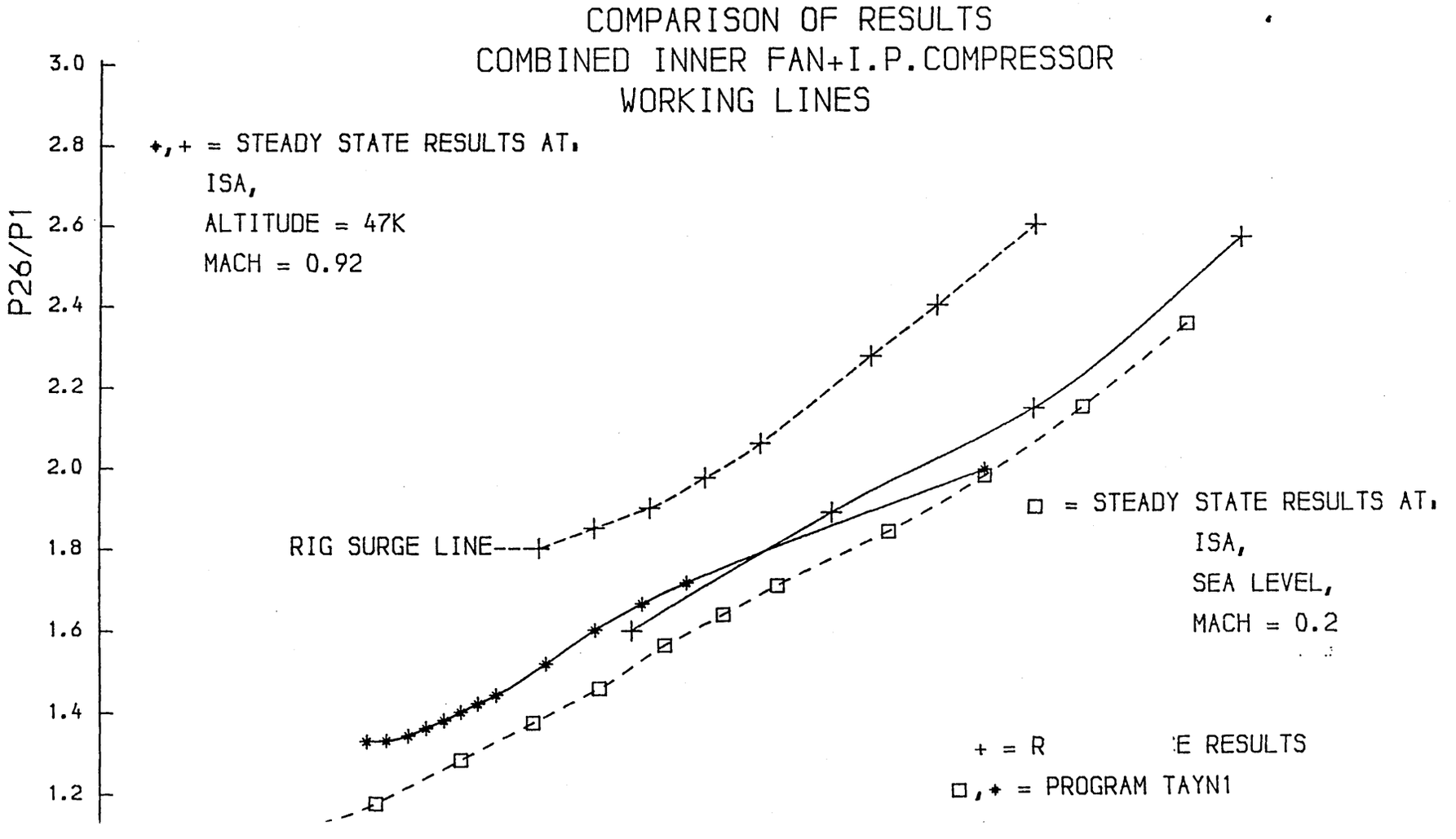
COMPARISON OF RESULTS
COMBINED INNER FAN+I.P.COMPRESSOR
WORKING LINES
P26/P1
3.0
2.8
2.6
2.4
2.2
2.0
1.8
1.6
1.4
1.2
+,+ = STEADY STATE RESULTS AT,
ISA,
ALTITUDE = 47K
MACH = 0.92
RIG SURGE LINE
□ = STEADY STATE RESULTS AT,
ISA,
SEA LEVEL,
MACH = 0.2
+ = R E RESULTS
□,* = PROGRAM TAYN1

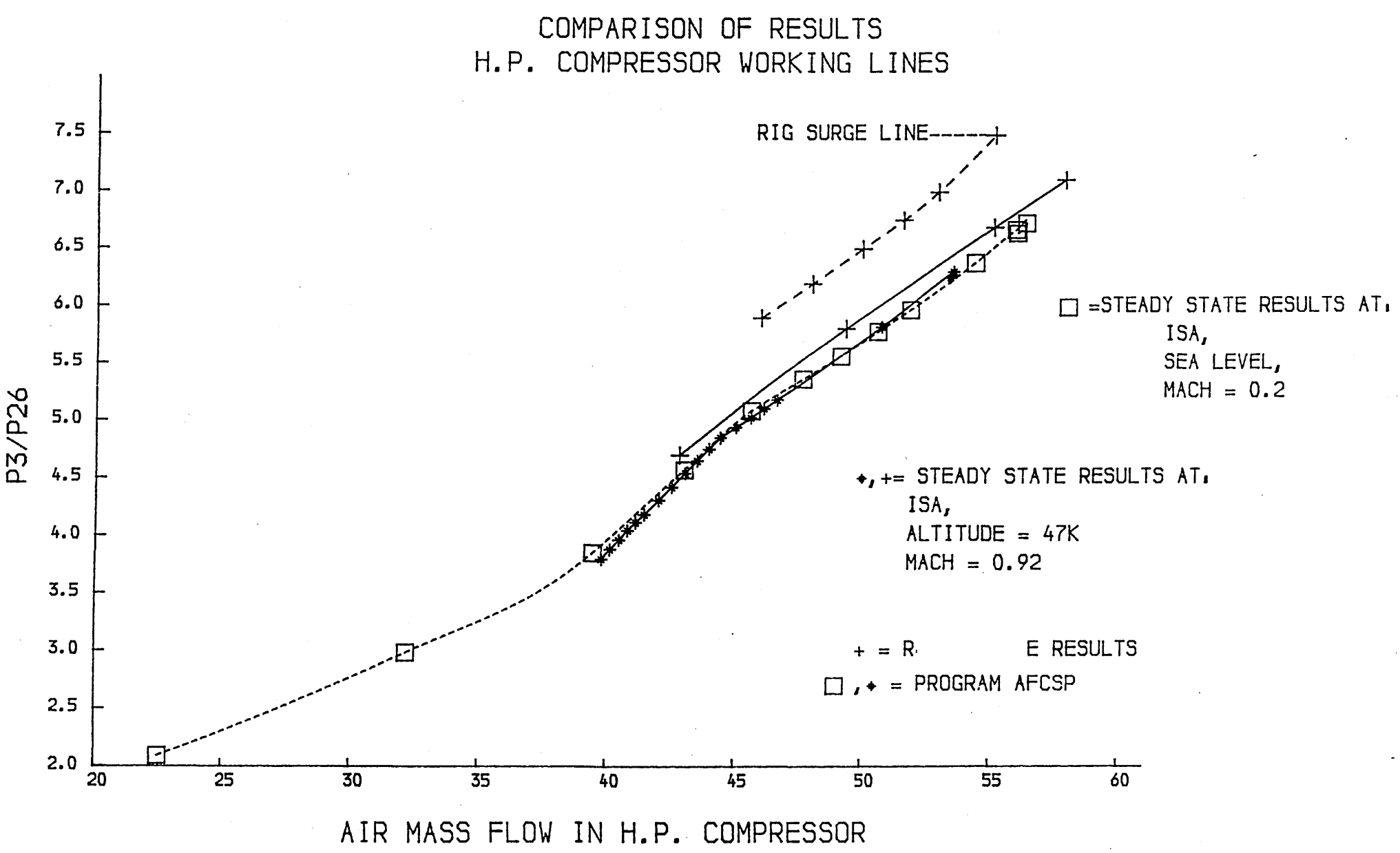
COMPARISON OF RESULTS
H.P. COMPRESSOR WORKING LINES
RIG SURGE LINE
□ =STEADY STATE RESULTS AT:
ISA,
SEA LEVEL,
MACH = 0.2
•,+= STEADY STATE RESULTS AT:
ISA,
ALTITUDE = 47K
MACH = 0.92
+ = R E RESULTS
□ ,• = PROGRAM AFCSP
P3/P26
7.5
7.0
6.5
6.0
5.5
5.0
4.5
4.0
3.5
3.0
2.5
2.0
20
25
30
35
40
45
50
55
60
AIR MASS FLOW IN H.P. COMPRESSOR

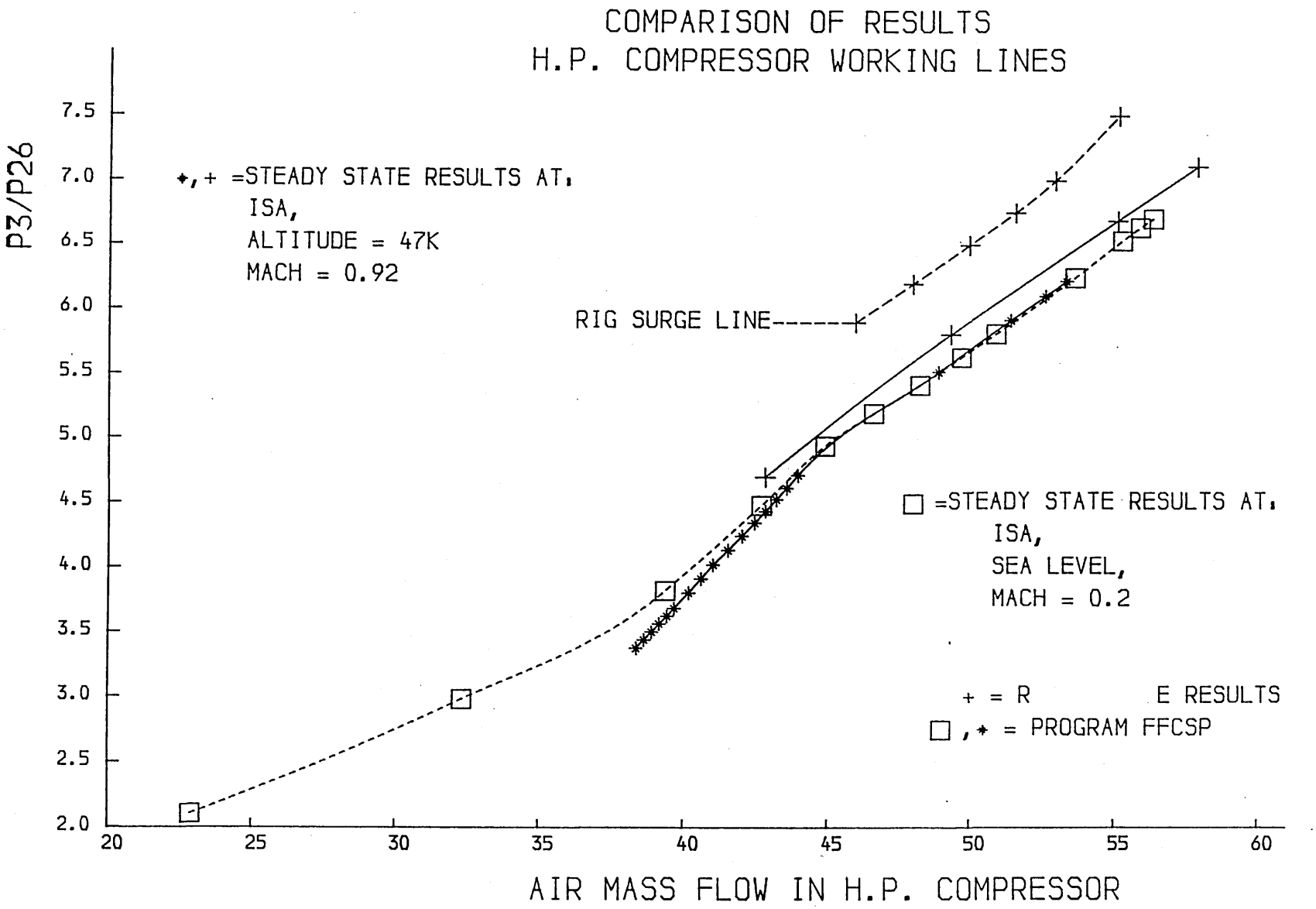
COMPARISON OF RESULTS
H.P. COMPRESSOR WORKING LINES
P3/P26
7.5
7.0
6.5
6.0
5.5
5.0
4.5
4.0
3.5
3.0
2.5
2.0
*,+ =STEADY STATE RESULTS AT:
ISA,
ALTITUDE = 47K
MACH = 0.92
RIG SURGE LINE------
□ =STEADY STATE RESULTS AT:
ISA,
SEA LEVEL,
MACH = 0.2
+ = R E RESULTS
□ ,* = PROGRAM FFCSP
20
25
30
35
40
45
50
55
60
AIR MASS FLOW IN H.P. COMPRESSOR

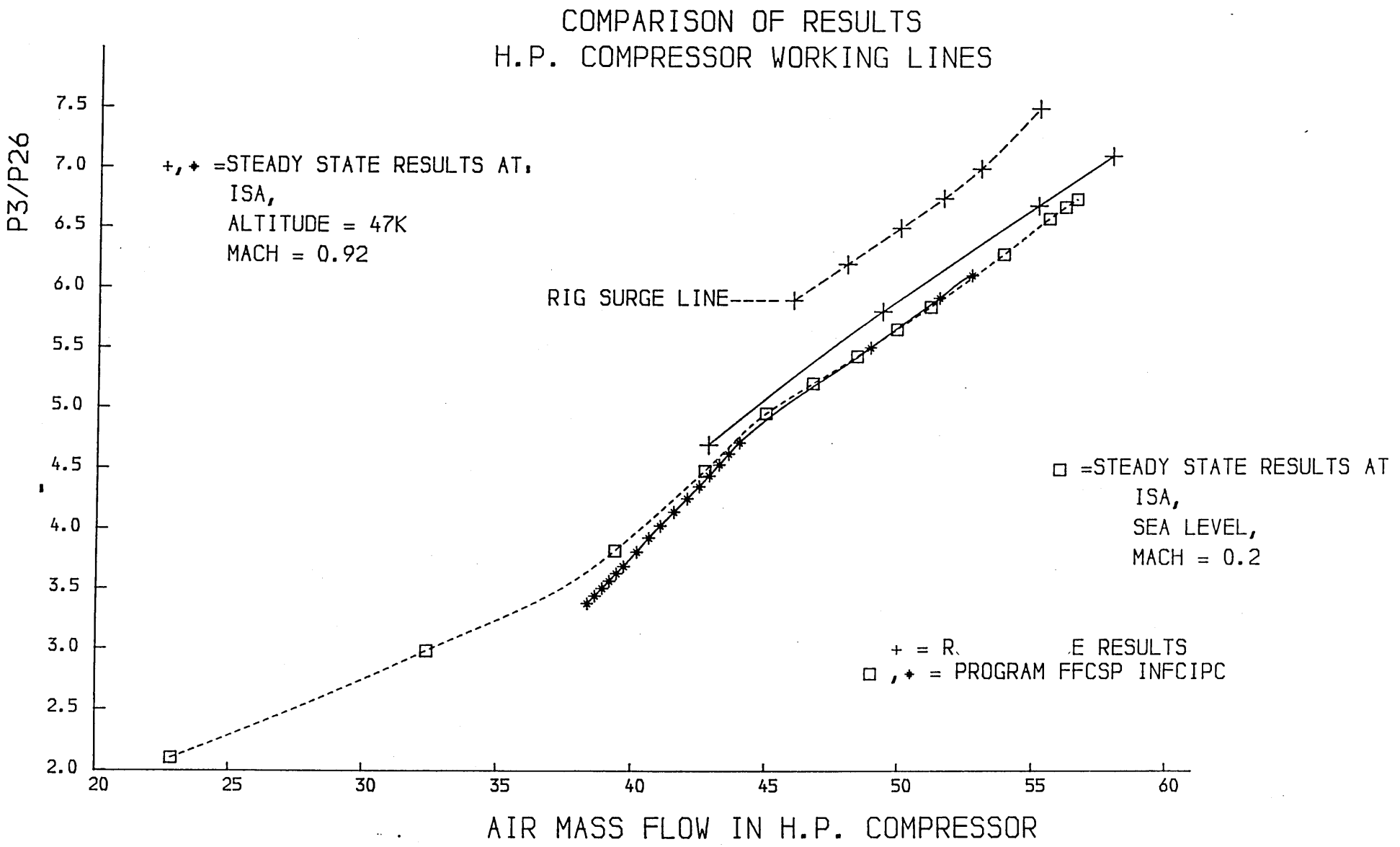
COMPARISON OF RESULTS
H.P. COMPRESSOR WORKING LINES
P3/P26
7.5
7.0
6.5
6.0
5.5
5.0
4.5
4.0
3.5
3.0
2.5
2.0
20
25
30
35
40
45
50
55
60
+,* =STEADY STATE RESULTS AT:
ISA,
ALTITUDE = 47K
MACH = 0.92
RIG SURGE LINE----
□ =STEADY STATE RESULTS AT
ISA,
SEA LEVEL,
MACH = 0.2
+ = R E RESULTS
□ ,* = PROGRAM FFCSP INFCIPC
AIR MASS FLOW IN H.P. COMPRESSOR

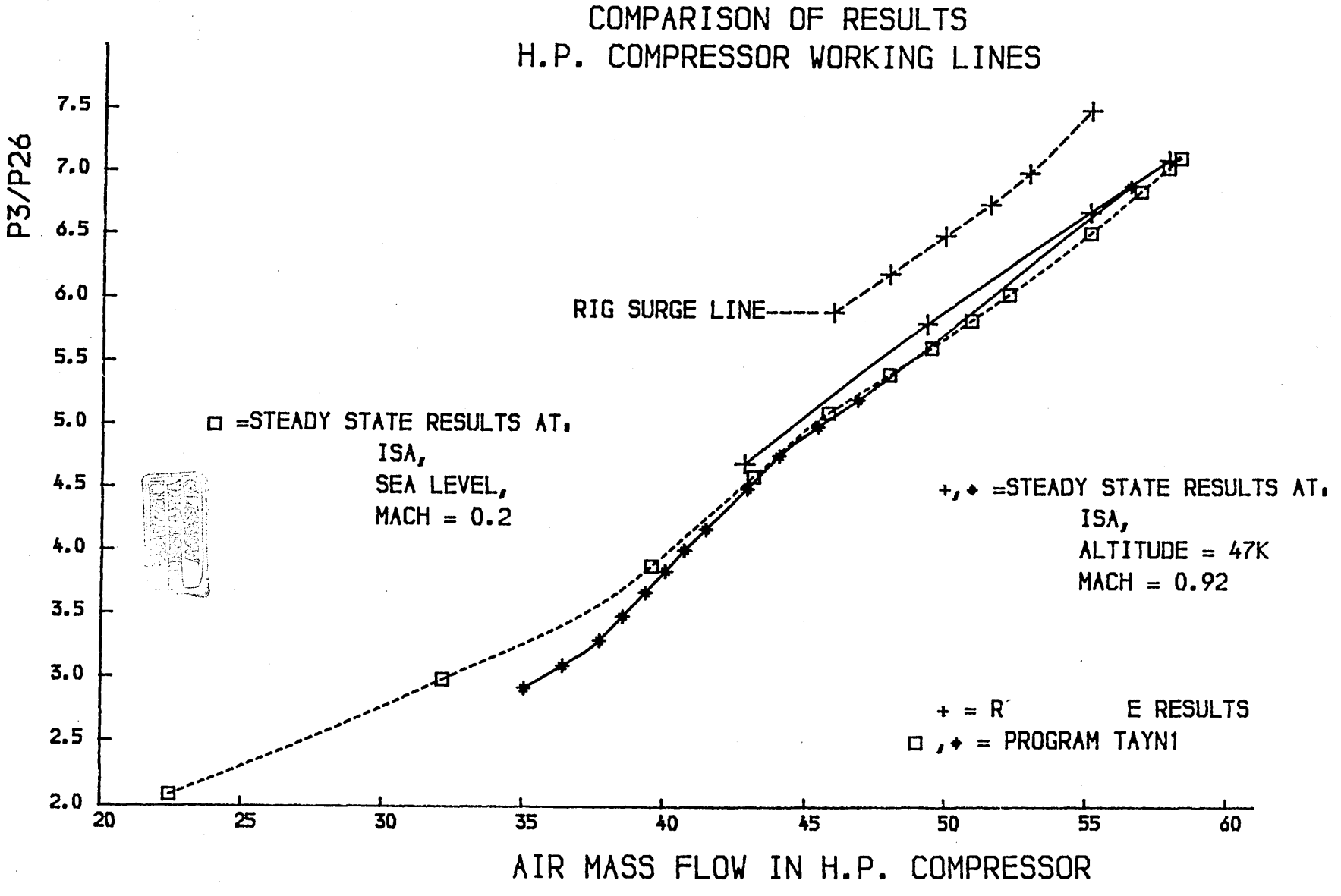
COMPARISON OF RESULTS
H.P. COMPRESSOR WORKING LINES
P3/P26
7.5
7.0
6.5
6.0
5.5
5.0
4.5
4.0
3.5
3.0
2.5
2.0
RIG SURGE LINE-----
□ =STEADY STATE RESULTS AT,
ISA,
SEA LEVEL,
MACH = 0.2
+,◆ =STEADY STATE RESULTS AT,
ISA,
ALTITUDE = 47K
MACH = 0.92
+ = R E RESULTS
□ ,◆ = PROGRAM TAYN1
20
25
30
35
40
45
50
55
60
AIR MASS FLOW IN H.P. COMPRESSOR

TABLES NOMENCLATURE

AC	Acceleration
ACC	Acceleration
AD	Adiabatic
AF	AFSREE program results
AIOEQV	Outer Fan non-dimensional air mass flow rate
AI1EQV	Inner Fan non-dimensional air mass flow rate
CAP	Capacity (non-dimensional air mass flow rate)
DC	Deceleration
DEC	Deceleration
FCSP	Factor of Split value
H.P.C.m	H.P. Compressor non-dimensional air mass flow rate
HPSHSP	H.P. Compressor shaft speed
HT	Heat Transfer
IC	Successive approximations method of evaluating the C_p
INEQm	Equivalent Inner Fan non-dimensional air mass flow rate
INNERm	Inner Fan non-dimensional air mass flow rate
LPSHSP	L.P. Compressor shaft speed
m	Non-dimensional mass flow rate

mfl	Mass flow rate(non-dimensional)
mSL	Non-dimensional mass flow rate at the Surge Line
NC	No variation of C_p
NDSLP	Non-dimensional speed of the L.P.shaft
NDSP	Non-dimensional speed
NDSHP	Non-dimensional speed of the H.P.shaft
NH(1,2..)	H.P. shaft speed
NHssp	H.P. shaft speed
NH/RT	Non-dimensional speed(H.P. shaft)
NLDSP	Non-dimensional speed of the L.P.shaft
NL(1,2,..)	L.P. shaft speed
NLssp	L.P. shaft speed
NL/RT	Non-dimensional speed(L.P. shaft)
OUTEQm	EquivelantOuter Fan non-dimensional air mass flow rate
OUTERm	Outer Fan non-dimensional air mass flow rate
PR	Pressure ratio
PRSL	Pressure ratio value at the Surge Line
R	Once through calculation method of C_p
RCMPL(1,2..)	Inner Fan pressure ratio
RE or RR	Real Engine Results
SF	STFREE program results
SL	Surge Line values
SR	Steady Running
T	Time
THR or TH	Thrust

ZNDLPC(1,2..) Non-dimensional speed of the L.P.shaft

TABLE 1 Mon, Jul 18, 1988 3:55 pm

	FUEL FLOW	LPSHSP1	LPSHSP2	HPSHSP1	HPSHSP2	THRUST1	THRUST2	AIOEQV1	P13/P1	AIOEQV2
1	0.08	1915.61	1915.64	6596.83	6596.65	200.69	200.68	102.93	1.023736	102.92
2	0.12	2730.45	2730.36	8339.52	8339.32	677.34	677.40	132.91	1.056156	132.91
3	0.16	3507.68	3507.34	9751.09	9750.99	1388.80	1388.70	165.36	1.101312	165.32
4	0.20	4168.49	4168.95	10043.45	10043.69	2282.60	2282.70	197.31	1.155152	197.32
5	0.24	4729.98	4729.97	10258.77	10258.64	3115.90	3115.60	221.46	1.203975	221.45
6	0.28	5129.04	5129.54	10446.73	10446.86	3834.80	3834.50	239.05	1.244789	239.04
7	0.32	5527.45	5527.31	10617.70	10617.33	4583.50	4583.20	255.87	1.286665	255.81
8	0.36	5811.00	5811.01	10751.88	10751.92	5294.20	5293.50	270.30	1.326225	270.28
9	0.40	6084.01	6083.97	10873.11	10872.87	6007.90	6007.30	283.85	1.365592	283.81
10	0.50	6651.23	6651.22	11231.21	11231.27	7769.30	7769.30	314.09	1.462369	314.09
11	0.60	7132.27	7132.51	11636.24	11635.75	9428.10	9428.20	339.19	1.552682	339.18
12	0.70	7647.30	7658.64	11923.02	11921.63	10865.00	10865.00	357.62	1.625145	369.51
13	0.80	8266.78	8267.46	12123.75	12123.66	12040.00	12037.00	369.50	1.678502	

TABLE 1 Mon, Jul 18, 1988 3:55 pm

	P14/P1	AI1EQV1	P24/P1	AI1EQV2	P25/P1
1	1.022898	34.31	1.037244	34.31	1.037288
2	1.056116	44.30	1.066769	44.30	1.066720
3	1.101310	55.12	1.101602	55.11	1.101614
4	1.155177	65.77	1.138749	65.77	1.138802
5	1.203998	73.82	1.170011	73.82	1.169989
6	1.244855	79.68	1.210729	79.68	1.210850
7	1.286738	85.29	1.254921	85.27	1.254951
8	1.326269	90.10	1.292551	90.09	1.292561
9	1.365668	94.62	1.329216	94.60	1.329287
10	1.462372	104.70	1.403898	104.70	1.403936
11	1.548088	113.06	1.467194	113.06	1.464578
12	1.729672	119.21	1.548726		
13		123.17	1.641451		

TABLE 2 Mon, Jul 18, 1988 3:57 pm

	FUEL FLOW	NL1	NH1	THRUST1	P13/P1	AIOEQV1	P24/P1	AI1EQV1	NL2	NH2
1	0.050	5204.6	10140.6	343.50	1.153145	291.14	1.206074	97.04	5204.68	10140.54
2	0.052	5285.8	10181.4	369.71	1.164859	293.05	1.215618	97.67	5284.68	10180.25
3	0.054	5365.0	10219.3	395.99	1.174837	295.05	1.225163	98.35	5366.17	10220.04
4	0.056	5438.2	10256.8	422.17	1.185683	296.92	1.235141	98.98	5438.39	10257.09
5	0.058	5494.1	10292.4	446.18	1.195228	298.53	1.244252	99.50	5494.34	10292.30
6	0.060	5548.8	10326.2	470.49	1.204338	300.13	1.253362	100.04	5547.72	10325.96
7	0.064	5659.0	10393.0	519.83	1.223427	303.47	1.271149	101.15	5658.70	10393.00
8	0.068	5767.2	10455.1	569.60	1.243384	306.81	1.288503	102.30	5767.40	10455.23
9	0.072	5872.3	10513.5	620.04	1.262473	310.22	1.304989	103.40	5873.71	10513.88
10	0.076	5978.4	10567.5	669.79	1.281996	313.64	1.321475	104.54	5997.98	10567.74
11	0.080	6084.8	10567.8	720.16	1.300651	317.03	1.337527	105.68	6084.90	10619.16
12	0.084	6189.6	10619.1	770.58	1.320173	320.41	1.353145	106.81	6190.02	10669.61
13	0.088	6271.9	10669.2	818.84	1.337961	323.55	1.365727	107.84	6272.15	10712.74
14	0.092	6355.1	10712.9	867.52	1.357049	326.62	1.377874	108.88	6353.64	10755.05
15	0.096	6438.2	10755.5	916.23	1.374837	329.77	1.390022	109.93	6437.58	10797.04
16	0.100	6521.4	10838.3	964.87	1.393058	332.96	1.402169	110.99	6521.45	10838.29
17	0.120	6921.1	11162.9	1200.10	1.479393	348.19	1.459870	116.06	6921.02	11162.71
18	0.140	7465.0	11416.3	1412.60	1.527115	359.83	1.550976	119.94	7463.27	11392.71
19	0.160	8048.3	11598.6	1603.50	1.597397	368.40	1.641215	122.80	8048.46	11598.37

TABLE 2 Mon, Jul 18, 1988 3:57 pm

	THRUST2	P14/P1	AIOEQV2	P25/P1	AI1EQV2
1	343.53	1.153280	291.12	1.206269	97.04
2	369.83	1.163826	293.11	1.215557	97.70
3	396.00	1.175370	295.00	1.225228	98.33
4	422.16	1.185913	296.92	1.235058	98.97
5	446.15	1.195314	298.53	1.244364	99.51
6	470.47	1.203944	300.14	1.253124	100.05
7	519.85	1.223579	303.45	1.271150	101.15
8	569.76	1.243406	306.79	1.288495	102.26
9	620.09	1.262291	310.24	1.305045	103.41
10	670.09	1.282108	313.59	1.321215	104.53
11	720.17	1.300750	317.01	1.337505	105.67
12	770.54	1.320221	320.43	1.353297	106.81
13	818.89	1.338490	323.51	1.365583	107.84
14	867.35	1.356616	326.62	1.377874	108.87
15	916.02	1.374403	329.79	1.390022	109.93
16	965.00	1.393492	332.94	1.405169	110.98
17	1200.30	1.479393	348.17	1.459870	116.06
18	1413.00			1.551410	119.93

TABLE 3 Mon, Jul 18, 1988 3:58 pm

	FUEL FLOW	P24/P1	RCMPL1	AI1ERR1	NH1	NL1	ZNDLPC1	RCMPL2	AI1ERR2	NL2
1	0.08	1.040	1.080	24.35	6666.22	2002.67	117.5	1.080	24.32	1987.34
2	0.12	1.072	1.130	35.73	8370.74	2822.86	165.7	1.133	35.86	2809.03
3	0.16	1.112	1.210	46.02	9767.17	3577.37	209.9	1.206	45.88	3562.34
4	0.20	1.158	1.322	53.76	10062.32	4260.00	250.0	1.322	53.69	4239.38
5	0.24	1.202	1.441	60.82	10290.38	4846.86	284.5	1.433	60.53	4834.87
6	0.28	1.248	1.555	67.32	10478.05	5279.14	309.8	1.544	66.99	5258.80
7	0.32	1.288	1.655	73.43	10640.39	5643.73	331.2	1.641	72.98	5628.47
8	0.36	1.322	1.734	78.73	10774.37	5928.56	347.9	1.716	78.13	5910.84
9	0.40	1.355	1.813	83.76	10893.83	6203.90	364.1	1.794	83.10	6182.86
10	0.50	1.419	1.969	94.61	11192.83	6753.33	396.4	1.948	93.81	6730.20
11	0.60	1.480	2.139	104.52	11573.79	7246.80	425.3	2.107	103.34	7219.70
12	0.70	1.558	2.373	115.24	11878.37	7727.53	453.5	2.334	113.93	7698.38
13	0.80	1.636	2.602	125.31	12153.41	8197.30	481.1	2.564	123.85	8149.79

TABLE 3 Mon, Jul 18, 1988 3:58 pm

	NH2	ZNDLPC2	THRUST2	THRUST1
1	6666.44	116.6	190.85	196.69
2	8385.72	164.9	674.89	680.83
3	9772.86	209.1	1383.00	1399.70
4	10075.51	248.8	2264.30	2288.10
5	10297.88	283.8	3138.40	3159.20
6	10487.07	308.6	3896.60	3928.20
7	10651.79	330.3	4631.60	4667.50
8	10786.18	346.9	5337.80	5381.80
9	10909.02	362.8	6038.90	6093.60
10	11227.03	395.0	7759.20	7828.60
11	11627.18	423.7	9354.60	9430.50
12	11935.53	451.8	10749.00	10835.00
13	12214.19	478.3	11999.00	12086.00

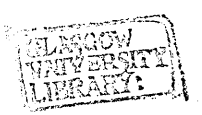

TABLE4

Mon, Jul 18, 1988 3:59 pm

	FUEL FLOW	P24/P1	RCMPL1	AI1ERR1	NL1	NH1	ZNDLPC1	THRUST1	RCMPL2	AI1ERR2
1	0.050	1.313	1.810	66.96	5766.2	10290.9	347.49	310.82	1.806	66.77
2	0.052	1.320	1.829	68.20	5826.8	10325.7	351.12	337.27	1.826	68.01
3	0.054	1.327	1.848	69.41	5886.2	10359.6	354.69	363.60	1.845	69.22
4	0.056	1.334	1.868	70.59	5947.0	10391.8	358.37	389.97	1.865	70.39
5	0.058	1.340	1.887	71.71	6004.4	10422.4	361.84	416.30	1.884	71.51
6	0.060	1.347	1.906	72.80	6062.3	10452.4	365.33	442.50	1.903	72.60
7	0.064	1.360	1.945	74.96	6173.3	10510.3	372.01	495.88	1.941	74.73
8	0.068	1.370	1.975	76.97	6265.7	10561.4	377.58	548.90	1.974	76.79
9	0.072	1.380	1.999	78.98	6346.6	10608.4	382.46	600.59	2.001	78.84
10	0.076	1.389	2.016	81.04	6410.7	10653.2	386.32	649.64	2.019	80.95
11	0.080	1.398	2.034	83.08	6477.7	10697.4	390.36	699.08	2.039	83.03
12	0.084	1.406	2.049	85.10	6544.3	10741.4	394.37	748.89	2.058	85.05
13	0.088	1.415	2.065	87.07	6612.7	10785.0	398.50	798.80	2.074	87.03
14	0.092	1.423	2.081	88.85	6681.5	10824.3	402.65	847.18	2.090	88.86
15	0.096	1.431	2.099	90.62	6750.3	10863.0	406.79	896.06	2.108	90.65
16	0.100	1.439	2.116	92.36	6819.7	10900.6	410.97	944.61	2.127	92.39
17	0.120	1.503	2.296	102.18	7241.6	11113.1	436.40	1177.70	2.299	102.04
18	0.140	1.575	2.516	112.30	7669.4	11338.7	462.17	1399.30	2.522	112.17
19	0.160	1.644	2.734	121.57	8088.8	11590.4	487.45	1600.00	2.748	121.62

TABLE4

Mon, Jul 18, 1988 3:59 pm

	NL2	ZNDLPC2	THRUST2	NH2
1	5751.4	346.59	308.24	10305.0
2	5812.6	350.28	334.23	10340.7
3	5870.1	353.75	360.42	10374.5
4	5930.6	357.39	386.70	10407.2
5	5988.1	360.86	412.79	10438.3
6	6044.2	364.24	439.01	10468.8
7	6157.7	371.08	491.85	10526.8
8	6250.3	376.66	545.06	10579.7
9	6330.5	381.49	596.50	10628.4
10	6392.9	385.25	645.79	10673.9
11	6457.9	389.17	695.34	10718.7
12	6524.9	393.21	744.68	10762.8
13	6592.1	397.26	794.42	10807.0
14	6660.0	401.35	843.31	10847.6
15	6728.4	405.47	891.99	10886.9
16	6797.1	409.61	940.61	10924.9
17	7205.2	434.20	1173.00	11134.0
18	7632.3	459.94	1394.60	

TABLE 5

Mon, Jul 18, 1988 4:01 pm

	FCSP,SR,0.2	NDSLP,SR,0.2	NDSHP,SR,0.2	FCSP,SR,0.8	NDSLP,SR,0.8	NDSHP,SR,0.8	FCSP,ACC,0.2	NDSLP,AC,0.2	NDSHP,AC,0.2	FCSP,DEC,0.2
1	0.6937	112.43	381.87	0.6020	277.86	560.58	0.6749	110.93	376.21	1.0247
2	0.7947	160.25	478.87	0.6302	294.70	563.30	0.6886	115.50	388.94	0.9649
3	0.8241	205.87	553.76	0.6564	310.67	565.70	0.7103	119.94	402.92	0.8325
4	0.8043	244.65	563.01	0.6802	324.98	567.72	0.7256	122.29	410.06	0.7781
5	0.8061	277.61	568.99	0.7367	349.09	573.10	0.7474	127.43	424.00	0.7628
6	0.8241	301.03	573.21	0.7835	372.27	577.21	0.7647	133.40	436.99	0.7474
7	0.8423	324.41	576.29	0.8194	389.74	581.27	0.7778	140.03	449.44	0.7373
8	0.8558	341.06	579.27	0.8509	406.66	585.40	0.7870	147.05	461.77	0.7253
9	0.8689	357.08	581.89	0.8622	413.23	588.80	0.7963	154.46	474.28	0.7162
10	0.8920	390.37	592.68	0.8837	424.27	591.58	0.8040	162.40	486.66	0.7089
11	0.9111	418.60	606.41	0.9031	433.42	591.43	0.8114	170.73	498.93	0.7319
12	0.9570	448.83	609.84	0.9223	442.48	591.38	0.8130	174.91	505.21	0.7540
13	1.0237	485.19	605.95	0.9414	451.25	591.45	0.8196	183.03	518.65	0.7738
14				0.9598	459.82	591.49	0.8217	190.95	534.27	0.7896
15				0.9797	469.14	590.79	0.8461	198.65	553.74	0.8013
16							0.8701	210.30	563.72	0.7958
17							0.9030	236.65	579.42	0.7899
18							0.9015	275.31	591.80	0.7845
19							0.9088	311.93	601.11	0.7799
20							0.9177	347.43	612.15	0.7724
21							0.9267	381.25	624.24	0.7637
22							0.9327	411.12	635.45	0.7527
23							0.9581	436.60	641.81	0.7418
24							0.9830	454.57	638.77	0.7301
25							1.0002	466.28	631.63	0.7207
26							1.0119	473.88	624.28	0.7121
27							1.0192	478.97	618.18	0.6929
28							1.0228	482.17	613.52	0.6734
29							1.0242	483.97	610.30	0.6534
30							1.0247	484.92	608.27	0.6353
31							1.0248	485.36	607.09	0.6188
32										0.6036

	NDSLP,DC,0.2	NDSHP,DC,0.2
1	485.19	606.27
2	465.24	585.58
3	437.47	569.84
4	406.41	566.48
5	377.97	563.79
6	353.44	561.53
7	331.47	559.49
8	311.84	557.00
9	293.49	554.32
10	261.64	548.92
11	236.42	543.05
12	217.81	535.70
13	204.11	527.09
14	193.79	517.84
15	185.75	508.31
16	178.93	498.59
17	172.58	489.02
18	166.52	480.08
19	160.80	471.87
20	150.50	457.19
21	141.73	443.28
22	134.20	430.28
23	127.64	418.24
24	121.97	407.19
25	117.34	397.50
26	113.74	388.89
27	108.74	373.86
28	104.72	358.54
29	102.93	350.71
30	101.03	341.72
31	99.52	334.11
32	98.32	327.62

TABLE 6

Mon, Jul 18, 1988 4:03 pm

	FCSP,SR,0.2	NDSLP,SR,0.2	NDSHP,SR,0.2	FCSP,SR,0.8	NDSLP,SR,0.8	NDSHP,SR,0.8	FCSP,AC,0.8	NDSLP,AC,0.8	NDSHP,AC,0.8	FCSP,DC,0.8
1	0.8374	335.07	580.57	0.6345	305.76	566.00	0.5424	296.01	546.95	0.9784
2	0.8400	340.87	581.61	0.6434	311.36	566.80	0.5643	296.72	553.07	0.9655
3	0.8453	346.75	582.60	0.6519	316.52	567.50	0.5939	298.32	558.87	0.9519
4	0.8501	352.55	583.54	0.6607	321.39	568.26	0.6213	301.00	564.17	0.9135
5	0.8548	358.33	584.73	0.6698	325.62	569.18	0.6472	304.85	569.08	0.8826
6	0.8672	374.28	590.85	0.6961	336.06	571.96	0.6744	309.49	573.67	0.8588
7	0.8702	382.55	596.15	0.7122	342.88	573.70	0.7005	314.66	577.94	0.8408
8	0.8751	390.96	601.88	0.7270	349.72	575.22	0.7262	320.40	582.18	0.8253
9	0.8790	398.99	607.15	0.7408	356.47	576.48	0.7439	326.64	585.61	0.8120
10	0.8844	407.26	611.60	0.7539	363.20	577.58	0.7671	339.41	590.74	0.7889
11	0.8903	415.47	615.80	0.7663	369.71	578.60	0.7904	352.42	596.39	0.7685
12	0.8988	423.56	618.48	0.7775	375.34	579.77	0.8118	365.67	602.55	0.7517
13	0.9117	432.44	619.49	0.7876	380.25	580.97	0.8301	377.93	608.15	0.7380
14	0.9247	440.98	620.21	0.7974	385.25	582.14	0.8436	388.83	613.30	0.7264
15	0.9388	449.82	620.38	0.8071	390.26	583.24	0.8549	398.19	618.06	0.7166
16	1.0352	503.35	613.46	0.8484	414.24	594.49	0.8643	406.30	622.37	0.7084
17				0.9091	444.24	596.71	0.8722	413.40	625.69	0.6928
18				0.9773	477.16	594.35	0.8914	425.22	628.69	0.6804
19							0.9119	435.26	628.79	0.6746
20							0.9208	439.74	628.12	0.6643
21							0.9289	443.88	627.07	0.6563
22							0.9362	447.63	625.74	0.6470
23							0.9423	451.08	624.14	0.6425
24							0.9527	457.00	620.58	0.6398
25							0.9610	461.81	616.84	0.6379
26							0.9671	465.59	613.23	0.6372
27							0.9711	468.55	609.80	0.6363
28							0.9754	472.60	604.40	
29							0.9777	475.11	600.55	
30							0.9786	476.49	597.92	
31										
32										
33										
34										
35										

	NDSLP,DC,0.8	NDSHP,DC,0.8	FCSP,AC,0.2	NDSLP,AC,0.2	NDSHP,AC,0.2	FCSP,DC,0.2	NDSLP,DC,0.2	NDSHP,DC,0.2
1	477.16	594.61	0.8253	313.13	577.27	1.0358	503.36	613.72
2	473.50	589.57	0.8450	315.98	580.77	1.0275	500.14	609.41
3	469.61	584.98	0.8627	319.22	584.25	1.0189	496.79	605.35
4	465.25	578.89	0.8680	322.72	586.50	1.0100	493.31	601.53
5	460.10	575.01	0.8706	326.34	588.77	1.0007	489.72	597.95
6	454.57	572.98	0.8778	333.81	593.04	0.9909	486.01	594.51
7	448.92	571.92	0.8828	341.62	597.34	0.9799	482.19	591.30
8	443.23	571.34	0.8874	349.73	601.75	0.9685	478.24	588.27
9	437.56	571.09	0.8934	358.18	606.34	0.9569	474.17	585.50
10	426.37	571.02	0.8999	367.01	611.01	0.9099	465.39	578.72
11	415.50	570.85	0.9044	376.25	615.59	0.8708	455.41	575.06
12	405.41	569.63	0.9060	385.41	620.58	0.8450	445.14	573.71
13	396.21	568.78	0.9066	393.88	625.59	0.8259	435.08	573.34
14	387.92	568.11	0.9103	401.72	630.38	0.8143	425.64	573.76
15	380.42	567.58	0.9126	408.85	635.01	0.8075	416.93	574.31
16	373.63	567.16	0.9184	415.32	639.41	0.8049	409.02	574.18
17	361.70	566.58	0.9236	421.22	643.01	0.8035	401.85	574.22
18	351.37	566.10	0.9305	426.68	645.76	0.8064	389.55	574.81
19	346.76	565.88	0.9365	431.73	647.91	0.8128	379.70	575.57
20	338.59	565.50	0.9420	436.42	649.55	0.8195	371.88	576.37
21	331.80	565.33	0.9477	440.82	650.72	0.8218	365.53	577.09
22	322.33	565.39	0.9531	444.92	651.51	0.8237	360.27	577.62
23	316.28	565.57	0.9638	448.77	651.97	0.8251	355.90	578.01
24	312.46	565.71	0.9688	455.82	651.99	0.8268	352.27	578.47
25	310.04	565.81	0.9737	459.05	651.59	0.8301	349.28	578.80
26	308.53	565.87	0.9839	462.06	650.94	0.8319	344.79	579.31
27	307.58	565.90	0.9888	467.53	648.97	0.8334	341.76	579.70
28			0.9921	470.08	647.76	0.8352	339.72	579.96
29			0.9993	472.49	646.50	0.8358	338.36	580.13
30			1.0054	477.00	643.67	0.8377	337.44	580.23
31			1.0106	481.02	640.70	0.8367	336.84	580.32
32			1.0152	484.51	637.82			
33			1.0191	487.57	635.08			
34			1.0224	490.22	632.48			
35				492.31	630.05			

TABLE 7 Mon, Jul 18, 1988 4:05 pm

	Column 1	2.(f.flow)	2.(P24/P1)	2.(P26/P1)	2.(P3/P26)	2.(P26/P24)	2.(P13/P1)	2.(INNERm)	2.(OUTERm)	2.(H.P.C.m)
1		0.08	1.040	1.080	2.104	1.0380	1.0226	24.35	112.29	22.88
2		0.12	1.072	1.130	2.984	1.0537	1.0562	35.73	141.79	32.36
3		0.16	0.112	1.210	3.826	1.0881	1.1019	46.02	175.13	39.39
4		0.20	1.158	1.322	4.486	1.1416	1.1553	53.76	209.57	42.71
5		0.24	1.202	1.441	4.943	1.1989	1.2063	60.82	236.28	44.93
6		0.28	1.248	1.555	5.197	1.2457	1.2502	67.32	255.09	46.64
7		0.32	1.288	1.655	5.419	1.2847	1.2913	73.43	270.76	48.35
8		0.36	1.322	1.734	5.636	1.3115	1.3309	78.73	284.66	49.72
9		0.40	1.355	1.813	5.817	1.3382	1.3700	83.76	297.45	50.93
10		0.50	1.419	1.969	6.250	1.3881	1.4651	94.61	325.93	53.67
11		0.60	1.480	2.139	6.535	1.4452	1.5509	104.52	347.70	55.31
12		0.70	1.558	2.373	6.638	1.5228	1.6218	115.24	360.61	55.93
13		0.80	1.636	2.602	6.707	1.5910	1.6826	125.31	368.69	56.38
14		0.82	1.652	2.650	6.712	1.6040	1.6931	127.23	369.64	56.43
15		0.84	1.668	2.695	6.722	1.6163	1.7035	129.11	370.57	56.48

TABLE 7 Mon, Jul 18, 1988 4:05 pm

	2.(NHssp)	2.(NLssp)	2.(THRUST)	3.(P26/P1)	3.(P3/P26)	3.(P13/P1)	3.(INNERm)	3.(OUTERm)	3.(H.P.C.m)	3.(NLssp)
1	6666.22	2002.67	196.69	1.0721	2.0899	1.0228	23.85	102.70	22.56	1913.12
2	8370.74	2822.86	680.83	1.1219	2.9868	1.0557	35.44	132.39	32.32	2719.60
3	9767.17	3577.77	1399.70	1.1924	3.8513	1.1006	45.52	164.88	39.49	3499.30
4	10062.32	4260.00	2288.10	1.2997	4.5463	1.1535	53.21	196.49	42.96	4150.20
5	10290.38	4846.86	3159.20	1.3970	5.0531	1.2025	59.86	220.85	45.46	4714.80
6	10478.05	5279.14	3928.20	1.4904	5.3336	1.2438	66.01	238.76	47.47	5121.30
7	10640.39	5643.73	4667.50	1.5982	5.5348	1.2860	72.22	255.54	48.96	5521.40
8	10774.37	5928.56	5381.80	1.6711	5.7613	1.3251	77.29	269.88	50.47	5803.80
9	10893.83	6203.90	6093.60	1.7418	5.9654	1.3638	82.16	283.12	51.81	6071.40
10	11192.83	6753.33	7828.60	1.8975	6.3965	1.4587	92.86	312.84	54.50	6631.30
11	11573.79	7246.80	9430.50	2.0350	6.7311	1.5462	101.67	337.17	56.29	7095.90
12	11878.37	7727.53	10835.00	2.2690	6.8073	1.6196	112.29	355.75	56.79	7594.60
13	12153.41	8197.30	12086.00	2.5906	6.7033	1.6751	124.32	368.47	56.38	8180.60
14	12203.80	8291.20	12311.00	2.6832	6.6424	1.6827	127.23	370.08	56.08	8330.10
15	12254.10	8381.10	12536.00	2.7667	6.5919	1.6900	129.88	371.52	55.84	8465.30

TABLE 7 Mon, Jul 18, 1988 4:05 pm

	3.(NIIssp)	3.(THRUST)	4.(P24/P1)	4.(P13/P1)	4.(P26/P24)	4.(P3/P26)	4.(P26/P1)	4.(INNERm)	4.(OUTERm)	4.(I.P.C.m)
1	6603.26	199.03	1.0369	1.0241	1.0476	2.1156	1.0863	24.76	114.61	23.12
2	8363.50	670.16	1.0734	1.0602	1.0627	2.9851	1.1408	36.23	145.50	32.46
3	9758.63	1378.90	1.1195	1.1072	1.1063	3.7838	1.2380	46.98	179.00	39.29
4	10061.40	2260.60	1.1686	1.1612	1.1588	4.4167	1.3540	54.71	212.75	42.44
5	10279.00	3098.10	1.2139	1.2149	1.2131	4.8674	1.4730	61.75	240.98	44.63
6	10460.80	3824.90	1.2530	1.2622	1.2534	5.1730	1.5700	67.91	261.86	46.49
7	10632.10	4574.20	1.2853	1.3038	1.2835	5.4398	1.6500	73.67	277.56	48.38
8	10764.70	5278.50	1.3143	1.3433	1.3103	5.6698	1.7220	78.82	291.06	49.91
9	10887.20	5979.70	1.3432	1.3847	1.3299	5.8851	1.7860	83.64	304.88	51.33
10	11258.40	7709.70	1.4085	1.4821	1.3744	6.3368	1.9360	94.44	333.83	54.15
11	11697.90	9316.90	1.4695	1.5643	1.4294	6.6299	2.1010	104.25	353.43	55.78
12	11997.80	10756.00	1.5391	1.6253	1.5071	6.7422	2.3200	114.49	362.45	56.46
13	12194.80	11965.00	1.6131	1.6729	1.5782	6.8038	2.5460	124.14	365.68	56.85
14	12216.50	12168.00	1.6248	1.6819	1.5893	6.8245	2.5820	125.78	366.34	56.96
15	12239.80	12360.00	1.6361	1.6911	1.6004	6.8433	2.6180	127.40	366.97	57.07

TABLE 7 Mon, Jul 18, 1988 4:05 pm

	4.(NLssp)	4.(NHssp)	4.(THRUST)	5.(P24/P1)	5.(P13/P1)	5.(P26/P24)	5.(P3/P26)	5.(P26/P1)	5.(INNERm)	5.(OUTERm)
1	2131.2	6703.3	217.46	1.0362	1.0242	1.0478	2.1154	1.086	24.74	114.63
2	2931.1	8371.6	734.17	1.0725	1.0603	1.0632	2.9846	1.140	36.20	145.63
3	3719.5	9766.9	1480.10	1.1188	1.1075	1.1072	3.7814	1.239	46.98	179.22
4	4389.6	10049.2	2377.40	1.1676	1.1612	1.1590	4.4180	1.353	54.68	213.04
5	4917.9	10277.2	3290.70	1.2133	1.2149	1.2132	4.8689	1.472	61.73	241.01
6	5305.9	10452.9	4116.20	1.2529	1.2622	1.2534	5.1737	1.570	67.91	261.85
7	5623.5	10606.0	4859.60	1.2867	1.3041	1.2841	5.4349	1.652	73.73	277.95
8	5908.9	10734.5	5569.90	1.3178	1.3438	1.3116	5.6585	1.728	78.97	291.11
9	6153.1	10846.2	6313.50	1.3466	1.3852	1.3311	5.8727	1.792	83.76	304.88
10	6685.0	11176.3	8083.70	1.4119	1.4824	1.3752	6.3249	1.942	94.57	333.74
11	7169.1	11574.0	9623.40	1.4718	1.5645	1.4292	6.6228	2.104	104.33	353.44
12	7659.6	11894.8	10871.00	1.5388	1.6261	1.5041	6.7529	2.314	114.39	362.82
13	8154.7	12192.3	11923.00	1.6170	1.6745	1.5755	6.8000	2.548	124.30	366.28
14	8246.5	12252.9	12125.00	1.6315	1.6839	1.5889	6.8114	2.592	126.17	366.74
15	8336.6	12312.6	12326.00	1.6454	1.6924	1.6021	6.8200	2.636	127.98	367.12

	5.(H.P.C.m)	5.(NLssp)	5.(NHssp)	5.(THRUST)
1	23.10	2133.1	6700.4	291.09
2	32.44	2935.3	8368.4	734.50
3	39.28	3727.1	9761.1	1484.10
4	42.44	4391.2	10048.5	2378.40
5	44.63	4918.0	10276.8	3291.00
6	46.49	5306.1	10453.0	4116.30
7	48.35	5626.1	10607.1	4861.30
8	49.84	5914.6	10737.5	5576.20
9	51.25	6156.9	10848.4	6318.80
10	54.08	6685.8	11172.5	8086.40
11	55.76	7166.9	11570.5	9627.30
12	56.51	7648.6	11898.6	10879.00
13	56.85	8136.0	12183.2	11950.00
14	56.91	8237.4	12239.4	12159.00
15	56.97	8333.9	12292.0	12356.00

TABLE 9

Mon, Jul 18, 1988 4:09 pm

	2.(P26/P1)SR	2.(INNERm)SR	3.(P26/P1)SR	3.(INEQm)SR	4.(P 1)SR	4.(I m)SR	5.(P26/P1)SR	5.(INNERm)SR	1.(P26/P1)SR	1.(INEQm)SR
1	1.080	24.35	1.0721	23.85			1.086	24.74	1.071	34.31
2	1.130	35.73	1.1219	35.44			1.140	36.20	1.117	44.32
3	1.210	46.02	1.1924	45.52			1.239	46.98	1.189	55.12
4	1.322	53.76	1.2997	53.21			1.353	54.68	1.287	65.77
5	1.441	60.82	1.3970	59.86			1.472	61.73	1.380	73.82
6	1.555	67.32	1.4904	66.01			1.570	67.91	1.474	79.68
7	1.655	73.43	1.5982	72.22			1.652	73.73	1.581	85.29
8	1.734	78.73	1.6711	77.29			1.728	78.97	1.660	90.10
9	1.813	83.76	1.7418	82.16			1.792	83.76	1.739	94.62
10	1.969	94.61	1.8975	92.86			1.942	94.57	1.909	104.69
11	2.139	104.52	2.0350	101.67			2.104	104.33	2.072	113.06
12	2.373	115.24	2.2690	112.29			2.314	114.39	2.321	119.21
13	2.602	125.31	2.5906	124.32			2.548	124.30	2.642	123.17
14	2.650	127.23	2.6832	127.23			2.592	126.17	2.715	123.67
15	2.695	129.11	2.7667	129.88			2.636	127.98	2.791	124.18
16										
17										
18										
19										
20										
21										
22										
23										
24										
25										
26										
27										
28										

TABLE 9

Mon, Jul 18, 1988 4:09 pm

	1.(P26/P1)Ac	1.(INEQm)Ac	1.(P26/P1)Dc	1.(INEQm)Dc	2.(P26/P1)Ac	2.(INNERm)Ac	2.(P26/P1)Dc	2.(INNERm)Dc	3.(P26/P1)Ac	3.(INEQm)Ac
1	1.073	33.50	2.632	123.27	1.072	22.63	2.685	129.32	1.074	22.62
2	1.081	35.62	2.547	122.04	1.087	25.49	2.588	120.35	1.083	25.35
3	1.090	38.53	2.447	118.11	1.097	29.04	2.507	100.76	1.090	28.81
4	1.099	40.65	2.192	111.17	1.112	32.35	2.263	88.46	1.105	32.06
5	1.114	43.60	1.995	102.01	1.130	35.72	2.085	80.15	1.122	35.29
6	1.133	46.70	1.834	94.72	1.156	39.04	1.812	68.29	1.140	38.30
7	1.164	50.14	1.697	88.13	1.191	42.78	1.606	59.48	1.166	41.59
8	1.167	52.45	1.588	83.01	1.194	50.08	1.368	49.26	1.185	51.88
9	1.172	55.95	1.501	78.34	1.207	59.26	1.252	44.54	1.223	61.32
10	1.188	62.82	1.377	70.24	1.335	67.81	1.156	38.65	1.349	69.12
11	1.276	72.10	1.298	64.01	1.511	77.43	1.127	34.19	1.518	78.09
12	1.434	81.04	1.243	59.06	1.696	87.74	1.107	30.72	1.688	87.53
13	1.605	90.58	1.204	55.10	1.887	98.13	1.093	27.82	1.862	97.05
14	1.786	100.52	1.155	49.57	2.091	107.87	1.082	25.54	2.014	105.52
15	1.957	110.00	1.133	47.10	2.273	117.52	1.072	22.69	2.198	114.54
16	2.143	116.69	1.120	44.80	2.427	123.42	1.070	20.76	2.353	120.74
17	2.324	120.88	1.109	42.73	2.530	126.35	1.068	19.38	2.482	124.64
18	2.462	122.48	1.091	39.33	2.602	128.06			2.583	127.13
19	2.565	123.13	1.079	36.65	2.647	128.87			2.654	128.63
20	2.645	123.57	1.070	34.72	2.672	129.21			2.705	129.53
21	2.701	123.86	1.063	32.66	2.687	129.31			2.739	129.96
22	2.742	124.00	1.061	31.61	2.694	129.30			2.757	130.10
23	2.780	124.16	1.060	30.94	2.698	129.22			2.766	130.10
24	2.789	124.18			2.698	129.14			2.771	130.00
25	2.790	124.18			2.698	129.14			2.770	129.96
26	2.790	124.18			2.697	129.13			2.769	129.92
27	2.790	124.18			2.696	129.10			2.768	129.90
28	2.790	124.18			2.697	129.10			2.768	129.89

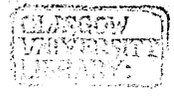

TABLE 9

Mon, Jul 18, 1988 4:09 pm

	3.(P26/P1)Dc	3.(INEQm)Dc	1.(INNERm)SR	1.(P24/P1)SR	1.(INNERm)Ac	1.(P24/P1)Ac	1.(INNERm)Dc	1.(P24/P1)Dc	2.(P24/P1)SR	2.(P24/P1)Ac
1	2.757	130.17	23.80	1.037	22.61	1.036	126.15	1.642	1.0400	1.036
2	2.642	120.30	35.22	1.067	25.30	1.042	117.76	1.593	1.0720	1.044
3	2.488	99.32	45.42	1.101	29.18	1.050	98.33	1.518	1.1120	1.052
4	2.206	87.68	52.89	1.138	31.78	1.056	86.50	1.432	1.1580	1.062
5	2.019	79.11	59.51	1.170	34.90	1.065	77.81	1.374	1.2020	1.072
6	1.868	72.37	65.66	1.210	37.97	1.076	72.25	1.319	1.2480	1.084
7	1.737	66.52	71.84	1.255	41.20	1.087	64.98	1.269	1.2880	1.100
8	1.633	61.76	77.11	1.292	44.38	1.095	60.21	1.230	1.3220	1.118
9	1.545	57.67	82.21	1.329	48.68	1.106	56.11	1.196	1.3550	1.147
10	1.416	51.04	93.37	1.404	56.73	1.132	49.79	1.154	1.4190	1.197
11	1.327	47.85	103.00	1.467	65.00	1.169	46.85	1.131	1.4800	1.271
12	1.261	45.28	114.08	1.548	73.65	1.233	44.53	1.113	1.5580	1.351
13	1.215	43.23	126.09	1.641	83.13	1.309	42.64	1.099	1.6360	1.423
14	1.157	40.05	128.53	1.659	93.15	1.385	39.72	1.082	1.6519	1.488
15	1.140	37.68	131.06	1.675	102.56	1.451	37.20	1.074	1.6676	1.559
16	1.114	33.51			112.13	1.519	34.94	1.067		1.605
17	1.096	30.07			120.04	1.577	33.00	1.061		1.635
18	1.082	27.16			124.63	1.615	29.60	1.051		1.652
19	1.072	24.98			127.33	1.640	26.76	1.043		1.661
20	1.064	22.16			129.10	1.656	24.72	1.038		1.666
21	1.061	20.19			130.14	1.665	21.99	1.033		1.668
22	1.059	18.73			130.67	1.671	20.08	1.030		1.669
23					131.09	1.675	18.67	1.028		1.669
24					131.10	1.675				1.668
25					131.05	1.675				1.668
26					131.03	1.675				1.668
27					131.05	1.675				1.668
28					131.05	1.675				1.668

TABLE 9

Mon, Jul 18, 1988 4:09 pm

	2.(P24/P1)Dc	5.(INNERm)Ac	5.(P26/P1)Ac	5.(INNERm)Dc	5.(P26/P1)Dc	3.(INNERm)SR	3.(INNERm)Ac	3.(INNERm)Dc
1	1.668	22.60	1.063	127.28	2.606	16.60	15.23	136.73
2	1.608	25.54	1.086	119.44	2.525	28.45	18.04	117.98
3	1.521	29.23	1.103	105.04	2.457	37.69	21.92	82.59
4	1.444	32.76	1.123	90.59	2.281	43.22	25.25	67.89
5	1.394	36.36	1.144	81.22	2.090	48.67	28.46	60.18
6	1.313	40.03	1.177	74.04	1.925	54.75	31.38	54.46
7	1.246	44.50	1.211	68.11	1.792	61.21	35.59	49.42
8	1.163	49.33	1.211	63.30	1.682	66.39	45.86	45.42
9	1.121	57.32	1.250	59.10	1.592	71.51	55.88	41.95
10	1.083	68.28	1.362	52.64	1.457	82.72	62.44	36.69
11	1.069	78.55	1.539	49.35	1.367	92.01	71.58	35.46
12	1.058	88.85	1.717	46.89	1.306	106.33	80.68	34.48
13	1.049	99.00	1.897	44.94	1.264	125.83	89.71	33.71
14	1.043	108.20	2.062	41.79	1.207	131.21	98.58	32.24
15	1.036	116.66	2.234	39.10	1.171	136.22	110.89	30.08
16	1.033	125.44	2.450	34.50	1.135		119.93	26.19
17	1.031	127.80	2.576	31.02	1.115		126.77	22.87
18		128.13	2.629	28.13	1.101		131.31	20.04
19		128.10	2.637	25.85	1.090		134.04	17.90
20		128.00	2.637	22.99	1.078		135.69	14.97
21		128.00	2.637	21.04	1.073		136.46	12.83
22		128.00	2.637	19.67	1.070		136.68	11.31
23		128.00	2.637				136.67	
24		128.00	2.636				136.47	
25		128.00	2.636				136.35	
26							136.28	
27							136.25	
28							136.23	

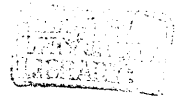

TABLE 9A

Mon, Jul 18, 1988 4:11 pm

	2.(p26/p1)Dc	2.(Innerm)Dc	3.(p26/p1)Dc	3.(Innerm)Dc	4.(p26/p2)Dc	4.(Innerm)Dc	5.(p26/p1)Dc	5.(Innerm)Dc	2.(P26/P1)sr	2.(INNERm)sr
1	2.685	129.32	2.757	130.17	2.608	127.59	2.606	127.28	1.969	94.61
2	2.588	120.35	2.642	120.30	2.530	119.91	2.525	119.44	2.139	104.52
3	2.507	100.76	2.488	99.32	2.486	105.79	2.457	105.04	2.373	115.24
4	2.263	88.46	2.206	87.68	2.311	91.28	2.281	90.59		
5	2.085	80.15			2.115	81.93	2.090	81.22		

TABLE 9A

Mon, Jul 18, 1988 4:11 pm

	1.(P26/P1)sr	1.(INNERm)sr	3.(P26/P1)sr	3.(INNERm)sr	5.(P26/P1)sr	5.(INNERm)sr	4.(P26/P1)sr	4.(INNERm)sr
1	1.909	93.37	1.8975	92.86	1.942	94.57	1.936	94.44
2	2.072	103.00	2.0350	101.67	2.104	104.33	2.101	104.25
3	2.321	114.08	2.2690	112.29	2.314	114.39	2.320	114.49

TABLE 9A

Mon, Jul 18, 1988 4:11 pm

	4.(P26/P1)SR	4.(INNERm)SR	4.(P26/P1)Ac	4.(INNERm)Ac	4.(P26/P1)Dc	4.(INNERm)Dc	1.(p26/p1)SR	1.(Innerm)SR	1.(p26/p1)Dc	1.(Innerm)Dc
1	1.0863	24.76	1.063	22.60	2.608	127.59	1.739	82.21	2.632	126.15
2	1.1408	36.23	1.087	25.55	2.530	119.91	1.909	93.37	2.547	117.76
3	1.2380	46.98	1.103	29.25	2.486	105.79	2.072	103.00	2.447	98.33
4	1.3540	54.71	1.123	32.79	2.311	91.28	2.321	114.08	2.192	86.50
5	1.4730	61.75	1.144	36.40	2.115	81.93	2.642	126.09		
6	1.5700	67.91	1.178	40.07	1.946	74.73	2.715	128.53		
7	1.6500	73.67	1.210	44.73	1.809	68.71	2.791	131.06		
8	1.7220	78.82	1.211	49.57	1.700	63.90				
9	1.7860	83.64	1.249	57.81	1.608	59.68				
10	1.9360	94.44	1.363	68.52	1.469	53.14				
11	2.1010	104.25	1.534	78.46	1.377	49.68				
12	2.3200	114.49	1.700	88.24	1.314	47.19				
13	2.5460	124.14	1.873	98.01	1.271	45.20				
14	2.5820	125.78	2.033	107.00	1.212	42.00				
15	2.6180	127.40	2.201	115.44	1.174	39.30				
16			2.460	124.50	1.136	34.64				
17			2.567	126.96	1.115	31.15				
18			2.594	127.49	1.091	25.93				
19			2.617	127.49	1.078	23.05				
20			2.619	127.42	1.073	21.09				
21			2.619	127.42	1.070	19.71				

TABLE 10 Mon, Jul 18, 1988 4:13 pm

	6.m11	6.PR11	6.m12	6.PR12	6.m13	6.PR13	6.mSL	6.PRSL	5.(INNERm)SR	5.(P24/P1)SR
1	122.55	1.671	127.25	1.695	127.35	1.697	10.60	1.0138	24.74	1.0362
2	126.45	1.671	127.91	1.695	128.01	1.697	21.30	1.0470	36.20	1.0725
3	127.30	1.671	128.57	1.695	128.67	1.697	31.60	1.0860	46.98	1.1188
4	127.95	1.671	129.15	1.695	129.25	1.697	41.20	1.1368	54.68	1.1676
5	128.55	1.671	129.65	1.695	129.75	1.697	51.60	1.2002	61.73	1.2133
6	129.25	1.671	130.15	1.695	130.25	1.697	68.90	1.3236	67.91	1.2529
7	129.79	1.671	130.67	1.695	130.77	1.697	86.90	1.4300	73.73	1.2867
8	130.33	1.671	131.19	1.695	131.29	1.697	96.30	1.4840	78.97	1.3178
9	130.87	1.671	131.71	1.695	131.81	1.697	106.30	1.5410	83.76	1.3466
10	131.41	1.671	132.23	1.695	132.33	1.697	114.90	1.5940	94.57	1.4119
11	131.95	1.671	132.75	1.695	132.85	1.697	122.55	1.6710	104.33	1.4718
12	132.49	1.671	133.27	1.695	133.37	1.697	127.25	1.6950	114.39	1.5388
13	133.03	1.671	133.79	1.695	133.89	1.697	127.35	1.6970	124.30	1.6170
14	133.57	1.671	134.31	1.695	134.41	1.697			126.17	1.6315

TABLE 10 Mon, Jul 18, 1988 4:13 pm

	6.m6	6.PR6	6.m7	6.PR7	6. m8	6.PR8	6.m9	6.PR9	6.m10	6.PR10
1	68.9	1.3236	86.9	1.43	96.3	1.484	106.30	1.541	114.90	1.5940
2	71.0	1.3248	89.0	1.43	98.2	1.484	107.90	1.541	116.65	1.5970
3	73.1	1.3260	91.0	1.43	100.2	1.484	109.50	1.541	118.55	1.5995
4	75.7	1.3270	93.1	1.43	101.9	1.484	111.10	1.541	120.25	1.6020
5	78.0	1.3280	95.3	1.43	103.8	1.484	112.60	1.541	121.85	1.6050
6	80.2	1.3290	97.3	1.43	105.7	1.484	114.30	1.541	123.40	1.6070
7	83.1	1.3300	99.2	1.43	107.1	1.484	115.40	1.541	124.25	1.6085
8	85.6	1.3310	100.8	1.43	108.5	1.484	116.50	1.541	125.10	1.6095
9	88.0	1.3318	102.6	1.43	109.9	1.484	117.60	1.541	126.00	1.6110
10	90.4	1.3325	104.3	1.43	111.3	1.484	118.65	1.541	126.90	1.6125
11	92.7	1.3331	105.9	1.43	112.7	1.484	119.70	1.541	127.80	1.6140
12	95.0	1.3336	107.5	1.43	114.1	1.484	120.75	1.541	128.70	1.6150
13	97.3	1.3342	109.1	1.43	115.5	1.484	121.80	1.541	129.60	1.6150
14	99.6	1.3347	110.7	1.43	116.9	1.484	122.85	1.541	130.50	1.6150

TABLE 10

Mon, Jul 18, 1988 4:13 pm

	6.m1	6.PR2	6.m2	6.PR2	6.m3	6.PR3	6.m4	6.PR4	6.m5	6.PR5
1	10.6	1.0138	21.3	1.0470	31.6	1.0860	41.2	1.1368	51.60	1.2002
2	12.3	1.0148	23.0	1.0475	33.3	1.0865	42.9	1.1376	53.55	1.2018
3	14.0	1.0156	24.7	1.0480	34.8	1.0870	44.6	1.1382	55.50	1.2028
4	15.7	1.0162	26.4	1.0485	36.7	1.0875	46.5	1.1388	57.50	1.2038
5	17.4	1.0166	28.1	1.0490	38.4	1.0880	48.4	1.1394	59.60	1.2050
6	19.1	1.0168	29.8	1.0495	40.3	1.0885	50.4	1.1400	61.70	1.2058
7	21.1	1.0168	31.8	1.0498	42.6	1.0890	52.9	1.1405	64.50	1.2068
8	23.1	1.0168	33.8	1.0500	44.9	1.0895	55.7	1.1410	67.50	1.2075
9	25.1	1.0168	35.8	1.0500	47.2	1.0900	58.6	1.1415	70.40	1.2080
10	27.1	1.0168	37.8	1.0500	49.5	1.0900	61.5	1.1420	73.40	1.2085
11	29.1	1.0168	39.8	1.0500	51.8	1.0900	64.5	1.1420	76.10	1.2090
12	31.1	1.0168	41.8	1.0500	54.1	1.0900	67.5	1.1420	78.80	1.2093
13	33.1	1.0168	43.8	1.0500	56.4	1.0900	70.5	1.1420	81.50	1.2093
14	35.1	1.0168	45.8	1.0500	58.7	1.0900	73.5	1.1420	84.20	1.2093
15										
16										
17										
18										
19										
20										
21										
22										
23										
24										
25										

	5.(INNERm)Ac	5.(P24/P1)Ac	5.(INNERm)Dc	5.(P24/P1)Dc
1	22.60	1.0267	127.28	1.633
2	25.54	1.0376	119.44	1.587
3	29.23	1.0480	105.04	1.519
4	32.76	1.0610	90.59	1.456
5	36.36	1.0740	81.22	1.399
6	40.03	1.0880	74.04	1.347
7	44.50	1.1070	68.11	1.303
8	49.33	1.1180	63.30	1.269
9	57.32	1.1510	59.10	1.238
10	68.28	1.2120	52.64	1.189
11	78.55	1.2850	49.35	1.159
12	88.85	1.3580	46.89	1.136
13	99.00	1.4270	44.94	1.121
14	108.20	1.4850	41.79	1.099
15	116.66	1.5430	39.10	1.084
16	125.44	1.6190	34.50	1.067
17	127.80	1.6400	31.02	1.055
18	128.13	1.6450	28.13	1.045
19	128.10	1.6460	25.85	1.039
20	128.00	1.6460	22.99	1.031
21	128.00	1.6450	21.04	1.027
22	128.00	1.6450	19.67	1.025
23	128.00	1.6450		
24	128.00	1.6450		
25	128.00	1.6450		

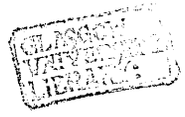

TABLE 10A

Mon, Jul 18, 1988 4:15 pm

	13.m1	13.PR1	13.m2	13.PR2	13.m3	13.PR3	13.m4	13.PR4	13.m5	13.PR5
1	8.24	1.0057	18.94	1.0385	30.55	1.0705	39.65	1.1178	48.20	1.1693
2	9.94	1.0063	20.64	1.0390	32.26	1.0710	41.35	1.1186	50.15	1.1709
3	11.64	1.0071	22.34	1.0395	33.76	1.0715	43.05	1.1192	52.10	1.1719
4	13.34	1.0077	24.04	1.0400	35.66	1.0720	44.95	1.1198	54.10	1.1729
5	15.04	1.0081	25.74	1.0405	37.36	1.0725	46.85	1.1204	56.20	1.1741
6	16.74	1.0083	27.44	1.0410	39.26	1.0730	48.85	1.1210	58.30	1.1749
7	18.74	1.0083	29.44	1.0413	41.56	1.0735	51.35	1.1215	61.10	1.1759
8	20.74	1.0083	21.44	1.0415	43.86	1.0740	54.15	1.1220	64.10	1.1766
9	22.74	1.0083	33.44	1.0415	46.16	1.0745	57.05	1.1225	67.00	1.1771
10	24.74	1.0083	35.44	1.0415	48.46	1.0745	59.95	1.1230	70.00	1.1776
11	26.74	1.0083	37.44	1.0415	50.76	1.0745	62.95	1.1230	72.70	1.1781
12	28.74	1.0083	39.44	1.0415	53.06	1.0745	65.95	1.1230	75.40	1.1784
13	30.74	1.0083	41.44	1.0415	55.36	1.0745	68.95	1.1230	78.10	1.1786
14	32.74	1.0083	43.44	1.0415	57.66	1.0745	71.95	1.1230	80.80	1.1786

TABLE 10A

Mon, Jul 18, 1988 4:15 pm

	13.m6	13.PR6	13.m7	13.PR7	13.m8	13.PR.8	13.m9	13.PR9	13.m10	13.PR10
1	66.85	1.2916	84.8	1.395	94.0	1.44	103.60	1.495	112.00	1.5520
2	68.95	1.2928	86.9	1.395	95.9	1.44	105.20	1.495	113.75	1.5550
3	71.05	1.2940	88.9	1.395	97.9	1.44	106.80	1.495	115.65	1.5575
4	73.65	1.2950	91.0	1.395	99.6	1.44	108.40	1.495	117.35	1.5600
5	75.95	1.2960	93.2	1.395	101.5	1.44	109.90	1.495	118.95	1.5630
6	78.15	1.2970	95.2	1.395	103.4	1.44	111.60	1.495	120.50	1.5650
7	81.05	1.2980	97.1	1.395	104.8	1.44	112.70	1.495	121.35	1.5665
8	83.55	1.2990	98.7	1.395	106.2	1.44	113.80	1.495	122.20	1.5675
9	85.95	1.2998	100.5	1.395	107.6	1.44	114.90	1.495	123.10	1.5690
10	88.35	1.3005	102.2	1.395	109.0	1.44	115.95	1.495	124.00	1.5705
11	90.65	1.3011	103.8	1.395	110.4	1.44	117.00	1.495	124.90	1.5720
12	92.95	1.3016	105.4	1.395	111.8	1.44	118.05	1.495	125.80	1.5730
13	95.25	1.3020	107.0	1.395	113.2	1.44	119.10	1.495	126.70	1.5740
14	97.55	1.3023	108.6	1.395	114.6	1.44	120.15	1.495	127.60	1.5750

TABLE 10A

Mon, Jul 18, 1988 4:15 pm

	13.m11	13.PR11	13.m12	13.PR12	13.m13	13.PR13	13SLm	13SLPR
1	120.00	1.58	122.90	1.62	123.00	1.622	8.24	1.0057
2	120.90	1.58	123.56	1.62	123.66	1.622	18.94	1.0385
3	121.75	1.58	124.22	1.62	124.32	1.622	30.55	1.0705
4	122.40	1.58	124.80	1.62	124.90	1.622	39.65	1.1178
5	123.00	1.58	125.30	1.62	125.40	1.622	48.20	1.1693
6	123.70	1.58	125.80	1.62	125.90	1.622	66.85	1.2916
7	124.24	1.58	126.32	1.62	126.42	1.622	84.80	1.3950
8	124.84	1.58	126.84	1.62	126.94	1.622	94.00	1.4400
9	125.32	1.58	127.36	1.62	127.46	1.622	103.60	1.4950
10	125.86	1.58	127.88	1.62	127.98	1.622	112.00	1.5520
11	126.40	1.58	128.40	1.62	128.50	1.622	120.00	1.5800
12	126.94	1.58	128.92	1.62	129 02	1.622	122.90	1.6200
13	127.48	1.58	129.44	1.62	129.54	1.622	123.00	1.6220
14	128.02	1.58	129.96	1.62	130.06	1.622		

Cricket Graph Data

TABLE 10B

Wed, Aug 24, 1988 15:18

	14.m1	14.PR1	14.m2	14.PR2	14.m3	14.PR3	14.m4	14.PR4	14.m5	14.PR5
1	49.9819	1.023	76.6161	1.056	107.1252	1.0979	142.2450	1.1579	182.8584	1.2388
2	54.4946	1.0215	80.0496	1.055	109.8720	1.0969	145.0899	1.1559	186.1938	1.2358
3	57.1432	1.0198	82.6983	1.054	112.6188	1.0959	148.1310	1.1534	190.8045	1.2318
4	59.4486	1.0178	86.6223	1.052	117.8181	1.0934	153.9189	1.1494	197.8677	1.2258
5	64.2555	1.0164	91.9197	1.050	123.7041	1.0904	160.5897	1.1449	205.4214	1.2188
6	66.4137	1.0155	94.4703	1.049	126.5490	1.0889	163.5327	1.1419	209.1492	1.2158
7	72.1035	1.0143	100.2582	1.0465	132.2388	1.0854	168.7320	1.1379	214.0542	1.2128
8	81.8154	1.008220	111.1473	1.03999	143.8146	1.077953	180.0135	1.127904	224.3547	1.198835
9	93.5874	1.000026	122.1345	1.030998	154.9980	1.067963	191.5893	1.116915	234.9495	1.183850
10	105.6537	0.988041	135.3780	1.017012	169.4187	1.052977	205.0290	1.098932	246.5253	1.164868
11	119.1915	0.970058	150.0930	0.996033	184.0356	1.031998	217.0953	1.076953	255.8448	1.145886
12	131.9445	0.947080	163.1403	0.971057	195.8076	1.008020	227.4939	1.053975	264.2812	1.124907
13	143.6184	0.920107	173.9313	0.945082	206.5005	0.983046	236.1267	1.028001	271.8350	1.104927

Cricket Graph Data

TABLE 10B

Wed, Aug 24, 1988 15:18

	14.m6	14.PR6	14.m7	14.PR7	14.m8	14.PR8	14.m9	14.PR9	14.m10	14.PR10
1	236.0286	1.4116	283.0183	1.5739	303.2271	1.6844	326.1824	1.8302	342.5649	1.9428
2	246.5253	1.4016	294.8887	1.5623	314.999	1.6730	334.7170	1.8076	348.7454	1.8912
3	258.6895	1.3887	306.3674	1.5473	325.5937	1.6574	340.7012	1.7691	351.4922	1.8308
4	266.6357	1.3787	313.7234	1.5341	333.0493	1.6346	344.4290	1.7317	353.2581	1.7783
5	274.4836	1.3677	321.0813	1.5175	337.9543	1.6070	346.8816	1.6906	354.4353	1.7275
6	278.2117	1.3627	324.7109	1.5065	340.0146	1.5889	347.7644	1.6702	355.0237	1.6995
7	282.9202	1.3547	326.8691	1.4975	341.7803	1.5715	348.1567	1.6394	355.5142	1.6692
8	291.8474	1.336702	331.6760	1.472569	344.9197	1.525318	348.8435	1.578067	356.1028	1.604841
9	299.8916	1.318719	335.6980	1.433407	346.0967	1.473768	349.8245	1.514529	355.9067	1.544299
10	307.9358	1.297739	337.0715	1.401038	346.1946	1.428612	350.6091	1.458182	355.6123	1.478963
11	313.6255	1.279757	338.0525	1.368470	346.3911	1.395644	351.0996	1.424215	355.5142	1.446195
12	317.9421	1.263772	338.4448	1.344094	346.5872	1.370468	351.3940	1.404835	355.4163	1.414625
13	321.1792	1.247787	338.8372	1.323514	346.7834	1.360079	351.4922	1.396842	355.4163	1.413426

	14.m11	14.PR11	14.m12	14.PR12	14.m13	14.PR13	14.SLm	14.SLPR
1	350.7073	1.9753	356.3972	2.0071	357.8687	2.0169	49.9819	1.023
2	355.5142	1.9313	361.4001	1.9721	363.0681	1.9851	76.6161	1.056
3	358.0649	1.8870	364.3433	1.9241	366.3052	1.9448	107.1252	1.0979
4	359.0459	1.8190	366.2073	1.8772	368.4636	1.8985	142.2450	1.1579
5	360.4192	1.7651	367.6787	1.8292	370.2292	1.8510	182.8584	1.2388
6	360.9097	1.7365	368.2671	1.8042	371.0139	1.8306	236.0286	1.4116
7	361.4001	1.7055	369.0520	1.7743	371.7007	1.8012	283.0183	1.5739
8	362.3811	1.643603	369.8369	1.710538	372.5837	1.736314	303.2271	1.6844
9	363.3623	1.581664	370.9160	1.648798	373.2703	1.374872	326.1824	1.8302
10	364.3433	1.521721	371.7988	1.588857	373.9570	1.614732	342.5649	1.9428
11	364.8337	1.487755	372.2893	1.555888	374.3496	1.581763	350.7073	1.9753
12	365.1279	1.468773	372.5837	1.537906	374.7419	1.561982	356.3972	2.0071
13	365.2263	1.461780	372.7798	1.529914	374.8401	1.554689	357.8687	2.0169

	2.(P13/P1)SR	2.(OUTERm)SR	3.(P13/P1)SR	3.(OUTEQm)SR	5.(P13/P1)Ac	5.(OUTERm)Ac	5.(P13/P1)SR	5.(OUTERm)SR	1.(P13/P1)SR	1.(OUTEQm)SR
1	1.0226	112.29	1.0228	102.70	1.0167	102.71	1.0242	114.63	1.023	102.93
2	1.0562	141.79	1.0557	132.39	1.0264	114.16	1.0603	145.63	1.056	132.95
3	1.1019	175.13	1.1006	164.88	1.0364	123.38	1.1075	179.22	1.101	165.37
4	1.1553	209.57	1.1535	196.49	1.049	134.62	1.1612	213.04	1.155	197.31
5	1.2063	236.28	1.2025	220.85	1.063	145.6	1.2149	241.01	1.204	221.76
6	1.2502	255.09	1.2438	238.76	1.078	156.70	1.2622	261.85	1.245	239.05
7	1.2913	270.76	1.2860	255.54	1.096	168.70	1.3041	277.95	1.287	255.87
8	1.3309	284.66	1.3251	269.88	1.108	175.2	1.3438	291.11	1.326	270.30
9	1.3700	297.45	1.3638	283.12	1.145	194.1	1.3852	304.88	1.366	283.35
10	1.4651	325.93	1.4587	312.84	1.218	229.2	1.4824	333.74	1.462	314.07
11	1.5509	347.7	1.5462	337.17	1.307	266.22	1.5645	353.44	1.552	339.19
12	1.6218	360.61	1.6196	355.75	1.406	300.83	1.6261	362.82	1.625	357.62
13	1.6826	368.69	1.6751	368.47	1.512	333.24	1.6745	366.28	1.678	369.50
14	1.6931	369.64	1.6827	370.08	1.592	352.6	1.6839	366.74	1.686	371.01
15	1.7035	370.57	1.6900	371.52	1.642	361.09	1.6924	367.12	1.693	372.54
16					1.678	364.99				
17					1.689	366.4				
18					1.692	366.94				
19					1.693	367.10				
20					1.693	367.03				
21					1.693	367.13				
22					1.693	367.13				
23					1.693	367.13				
24					1.693	367.13				
25					1.693	367.13				
26										
27										
28										
29										
30										
31										
32										
33										
34										
35										
36										
37										
38										
39										
40										
41										
42										

Cricket Graph Data

TABLE 11A

Wed, Aug 24, 1988 16:17

	1.(P13/P1)Ac	1.(OUTEQm)Ac	1.(P13/P1)Dc	1.(OUTEQm)Dc	2.(P13/P1)Ac	2.(OUTERm)Ac	2.(P13/P1)Dc	2.(OUTERm)Dc	3.(P13/P1)Ac	3.(OUTEQm)Ac
1	1.023	100.51	1.652	372.76	1.019	106.77	1.660	370.88	1.022	100.79
2	1.028	106.8	1.630	369.14	1.027	114.85	1.618	367.53	1.028	106.86
3	1.037	115.6	1.592	359.91	1.035	122.0	1.544	360.73	1.035	113.59
4	1.045	121.9	1.529	342.54	1.045	130.76	1.488	351.17	1.045	122.09
5	1.055	130.8	1.441	315.08	1.057	140.43	1.421	330.46	1.056	131.28
6	1.068	140.11	1.370	290.73	1.070	150.12	1.314	291.23	1.068	140.20
7	1.082	150.42	1.316	270.72	1.089	163.67	1.241	260.53	1.083	151.09
8	1.093	157.35	1.273	253.57	1.113	178.05	1.155	215.29	1.122	176.07
9	1.108	167.84	1.240	239.56	1.156	199.41	1.108	184.88	1.172	201.89
10	1.146	188.45	1.186	214.43	1.218	229.0	1.067	152.82	1.234	229.52
11	1.203	216.3	1.148	194.67	1.287	256.6	1.051	139.91	1.301	255.56
12	1.268	243.11	1.120	179.20	1.378	288.7	1.039	129.32	1.387	284.9
13	1.347	271.74	1.100	167.0	1.483	321.47	1.030	121.43	1.485	314.99
14	1.439	301.55	1.075	149.55	1.574	345.2	1.024	114.84	1.570	338.8
15	1.537	330.0	1.065	141.91	1.639	359.5	1.018	108.23	1.630	354.99
16	1.612	350.1	1.049	128.67	1.674	366.54	1.015	105.5	1.665	364.67
17	1.657	362.63	1.037	118.33	1.688	368.4	1.013	103.53	1.675	367.63
18	1.674	367.44	1.024	104.36	1.696	369.5			1.681	369.23
19	1.681	369.38	1.018	98.29	1.701	370.13			1.685	370.27
20	1.686	370.72	1.015	94.86	1.702	370.44			1.687	370.9
21	1.689	371.58	1.014	92.86	1.703	370.58			1.689	371.3
22	1.692	372.1			1.703	370.63			1.689	371.5
23	1.693	372.5			1.703	370.63			1.690	371.6
24	1.694	372.54			1.703	370.6			1.690	371.6
25	1.694	372.53			1.703	370.6			1.690	371.6
26	1.693	372.53			1.702	370.6			1.690	371.5
27	1.694	372.53			1.702	370.6			1.690	371.5
28	1.694	372.53			1.702	370.6			1.690	371.5
29										
30										
31										
32										
33										
34										
35										
36										
37										
38										
39										
40										
41										
42										

Cricket Graph Data

TABLE 11A

Wed, Aug 24, 1988 16:17

	3.(P13/P1)Dc	3.(OUTEQm)Dc	1.(OUTERm)SR	1.(OUTERm)Ac	1.(OUTERm)Dc	3.(OUTERm)SR	3.(OUTERm)Ac	3.(OUTERm)Dc	4.(P13/P1)SR	4.(OUTERm)SR
1	1.648	371.17	113.44	111.40	365.76	113.07	111.77	365.52	1.0241	114.61
2	1.628	368.1	142.05	117.11	372.83	141.09	117.13	370.48	1.0602	145.5
3	1.587	358.31	175.07	124.95	378.66	174.33	122.64	378.42	1.1072	179.0
4	1.520	339.7	210.18	130.76	366.88	208.78	130.73	365.24	1.1612	212.95
5	1.432	311.98	236.10	139.50	339.77	234.61	139.75	336.86	1.2149	240.98
6	1.364	288.5	253.06	148.84	314.74	252.33	148.63	312.30	1.2622	261.86
7	1.311	268.6	269.32	159.36	294.26	268.52	158.35	291.62	1.3038	277.56
8	1.269	251.9	283.29	165.42	276.42	282.57	182.88	274.11	1.3433	291.06
9	1.237	237.8	295.73	175.11	262.05	295.35	207.86	259.4	1.3847	304.88
10	1.184	212.98	325.38	194.54	235.41	324.23	236.91	232.94	1.4821	333.83
11	1.145	193.67	349.24	223.4	212.29	347.85	255.56	210.38	1.5643	353.43
12	1.118	178.38	362.74	250.5	194.07	361.71	292.33	192.55	1.6253	362.45
13	1.099	166.34	366.6	279.19	179.75	366.97	322.93	178.55	1.6729	365.68
14	1.078	149.25	366.15	308.92	159.48	366.22	346.23	158.95	1.6819	366.34
15	1.065	141.62	365.66	337.4	151.81	365.48	358.76	151.15	1.6911	366.97
16	1.049	128.65		354.65	138.40		365.48	138.02		
17	1.038	118.6		363.46	128.04		365.53	128.06		
18	1.029	110.4		365.28	114.35		365.18	120.04		
19	1.024	104.56		365.18	109.02		365.07	114.43		
20	1.018	98.38		365.18	106.37		365.01	109.01		
21	1.016	95.30		365.3	105.11		365.11	106.88		
22	1.014	93.03		365.43			365.23	105.31		
23				365.57			365.34			
24				365.6			365.43			
25				365.66			365.50			
26				365.67			365.43			
27				365.66			365.44			
28				365.66			365.45			
29										
30										
31										
32										
33										
34										
35										
36										
37										
38										
39										
40										
41										
42										

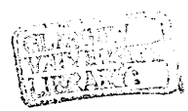

	4.(P13/P1)Ac	4.(OUTERm)Ac	4.(P13/P1)Dc	4.(OUTERm)Dc	5.(P13/P1)Dc	5.(OUTERm)Dc
1	1.016	103.3	1.650	367.63	1.649	367.71
2	1.026	114.16	1.613	364.9	1.617	367.35
3	1.036	123.36	1.563	363.1	1.570	367.25
4	1.049	134.57	1.506	356.4	1.516	361.76
5	1.063	145.51	1.447	341.10	1.444	340.8
6	1.078	156.62	1.382	319.27	1.379	318.36
7	1.097	168.72	1.327	298.31	1.323	297.00
8	1.109	175.71	1.285	281.1	1.281	279.5
9	1.147	195.34	1.248	264.82	1.244	262.9
10	1.222	230.96	1.190	235.3	1.187	233.7
11	1.309	267.20	1.153	214.26	1.150	212.6
12	1.405	300.74	1.127	197.11	1.124	195.6
13	1.507	332.18	1.110	185.71	1.108	184.7
14	1.588	352.6	1.089	169.58	1.087	168.7
15	1.640	361.79	1.073	157.78	1.072	157.16
16	1.676	365.2	1.054	143.26	1.054	142.9
17	1.688	366.5	1.042	131.96	1.041	132.02
18	1.691	366.93	1.027	117.76	1.033	123.5
19	1.691	367.03	1.020	110.26	1.027	117.68
20	1.691	367.0	1.016	106.82	1.019	110.29
21	1.691	367.0	1.014	104.45	1.016	106.9
22					1.014	104.48
23						
24						
25						
26						
27						
28						
29						
30						
31						
32						
33						
34						
35						
36						
37						
38						
39						
40						
41						
42						

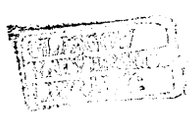

Cricket Graph Data

TABLE 11B

Wed, Aug 24, 1988 16:21

	1.(NDSP)SR	1.(P13/P1)SR	1.(NDSP)Ac	1.(P13/P1)Ac	1.(NDSP)Dc	1.(P13/P1)Dc	2.(NDSP)SR	2.(P13/P1)SR	2.(NDSP)Ac	2.(P13/P1)Ac
1	112.4	1.023	110.9	1.023	501.91	1.652	117.5	1.0226	110.93	1.019
2	160.3	1.056	119.9	1.028	481.31	1.630	165.7	1.0562	122.90	1.027
3	205.8	1.101	130.3	1.037	449.81	1.592	209.9	1.1019	134.82	1.035
4	246.6	1.155	143.5	1.045	416.7	1.529	250.0	1.1553	149.91	1.045
5	277.6	1.204	158.3	1.055	386.81	1.441	284.5	1.2063	165.56	1.057
6	301.8	1.245	174.9	1.068	361.11	1.370	309.8	1.2502	183.11	1.070
7	324.4	1.287	190.9	1.082	338.31	1.316	331.2	1.2913	199.14	1.089
8	341.0	1.326	198.6	1.093	318.04	1.273	347.9	1.3309	216.69	1.113
9	357.1	1.366	210.3	1.108	299.27	1.240	364.1	1.3700	246.04	1.156
10	390.4	1.462	236.6	1.146	266.34	1.186	396.4	1.4651	286.29	1.218
11	418.6	1.552	275.3	1.203	239.96	1.148	425.3	1.5509	324.94	1.287
12	448.8	1.625	311.9	1.268	220.42	1.120	453.5	1.6218	362.48	1.378
13	485.2	1.678	347.4	1.347	206.04	1.100	481.1	1.6826	397.33	1.483
14	493.4	1.686	381.2	1.439	186.91	1.075	486.62	1.6931	427.10	1.574
15	501.9	1.693	411.1	1.537	173.58	1.065	491.9	1.7035	452.97	1.639
16			437.7	1.612	151.27	1.049			469.69	1.674
17			459.4	1.657	134.28	1.037			480.05	1.688
18			474.2	1.674	114.0	1.024			486.21	1.696
19			484.7	1.681	105.52	1.018			489.52	1.701
20			491.9	1.686	101.1	1.015			491.20	1.702
21			496.6	1.689	98.36	1.014			491.95	1.703
22			499.4	1.692					492.22	1.703
23			501.6	1.693					492.22	1.703
24			501.9	1.694					492.04	1.703
25			501.8	1.694					492.03	1.703
26			501.8	1.693					491.98	1.702
27			501.8	1.694					491.88	1.702
28			501.8	1.694					491.96	1.702
29										

	2.(NDSP)Dc	2.(P13/P1)Dc	3.(NDSP)SR	3.(P13/P1)SR	3.(NDSP)Ac	3.(P13/P1)Ac	3.(NDSP)Dc	3.(P13/P1)Dc	4.(NDSP)SR	4.(P13/P1)SR
1	491.9	1.660	112.28	1.0228	110.9	1.022	496.84	1.648	125.08	1.0241
2	472.04	1.618	159.61	1.0557	119.8	1.028	476.05	1.628	172.03	1.0602
3	447.94	1.544	205.38	1.1006	130.12	1.035	446.38	1.587	218.30	1.1072
4	419.55	1.488	243.58	1.1535	142.82	1.045	413.57	1.520	257.63	1.1612
5	392.37	1.421	276.72	1.2025	159.28	1.056	383.83	1.432	288.64	1.2149
6	346.59	1.314	300.58	1.2438	175.18	1.068	358.61	1.364	311.41	1.2622
7	309.32	1.241	324.06	1.2860	191.66	1.083	336.17	1.311	330.05	1.3038
8	252.36	1.155	340.63	1.3251	220.36	1.122	316.11	1.269	346.80	1.3433
9	217.05	1.108	356.34	1.3638	254.78	1.172	297.32	1.237	361.13	1.3847
10	182.11	1.067	389.2	1.4587	293.12	1.234	264.72	1.184	392.35	1.4821
11	160.08	1.051	416.47	1.5462	328.98	1.301	238.60	1.145	420.77	1.5643
12	142.94	1.039	445.47	1.6196	363.29	1.387	219.36	1.118	449.55	1.6253
13	130.11	1.030	480.13	1.6751	394.93	1.485	205.25	1.099	478.61	1.6729
14	120.66	1.024	488.91	1.6827	421.66	1.570	186.58	1.078	484.0	1.6819
15	110.98	1.018	496.84	1.6900	445.78	1.630	173.10	1.065	489.29	1.6911
16	106.59	1.015			463.67	1.665	151.18	1.049		
17	103.97	1.013			475.73	1.675	135.21	1.038		
18					484.4	1.681	122.75	1.029		
19					490.01	1.685	114.10	1.024		
20					493.57	1.687	105.68	1.018		
21					495.66	1.689	101.39	1.016		
22					496.70	1.689	98.70	1.014		
23					497.15	1.690				
24					497.27	1.690				
25					497.11	1.690				
26					496.99	1.690				
27					496.93	1.690				
28					496.90	1.690				
29										

	4.(NDSP)Ac	4.P13/P1)Ac	4.(NDSP)Dc	4.(P13/P1)Dc	5.(NDSP)SR	5.(P13/P1)SR	5.(NDSP)Ac	5.(P13/P1)Ac	5.(NDSP)Dc	5.(P13/P1)Dc
1	110.93	1.016	489.29	1.650	125.20	1.0242	110.93	1.0167	489.13	1.649
2	126.75	1.026	469.32	1.613	172.28	1.0603	126.84	1.0264	468.71	1.617
3	141.22	1.036	447.48	1.563	218.75	1.1075	141.37	1.0364	446.06	1.570
4	157.16	1.049	420.28	1.506	257.73	1.1612	157.33	1.049	418.38	1.516
5	173.71	1.063	393.00	1.447	288.64	1.2149	173.85	1.063	390.49	1.444
6	190.51	1.078	368.18	1.382	311.42	1.2622	190.58	1.078	365.54	1.379
7	207.18	1.097	346.36	1.327	330.2	1.3041	207.23	1.096	343.59	1.323
8	217.82	1.109	326.76	1.285	347.14	1.3438	217.43	1.108	323.93	1.281
9	244.73	1.147	308.95	1.248	361.36	1.3852	243.66	1.145	306.19	1.244
10	286.37	1.222	278.62	1.190	392.4	1.4824	285.29	1.218	276.19	1.187
11	326.6	1.309	255.09	1.153	420.64	1.5645	326.44	1.307	252.97	1.150
12	363.20	1.405	237.13	1.127	448.91	1.6261	364.15	1.406	235.34	1.124
13	395.15	1.507	223.21	1.110	477.5	1.6745	397.08	1.512	221.69	1.108
14	422.21	1.588	202.66	1.089	483.47	1.6839	424.86	1.592	201.63	1.087
15	446.19	1.640	188.11	1.073	489.13	1.6924	449.01	1.642	187.39	1.072
16	475.47	1.676	166.42	1.054			477.22	1.678	165.99	1.054
17	486.08	1.688	150.40	1.042			486.90	1.689	150.18	1.041
18	488.98	1.691	129.47	1.027			489.18	1.692	138.44	1.033
19	489.49	1.691	118.45	1.020			489.44	1.693	129.42	1.027
20	489.37	1.691	112.97	1.016			489.30	1.693	118.49	1.019
21	489.37	1.691	109.78	1.014			489.19	1.693	112.98	1.016
22							489.16	1.693	109.73	1.014
23							489.14	1.693		
24							489.15	1.693		
25							489.15	1.693		
26										
27										
28										
29										

Cricket Graph Data — TABLE 11C — Wed, Aug 24, 1988 16:24

	1.(NDSP)SR	1.(P13/P1)SR	1.(NDSP)Dc	1.(P13/P1)Dc	2.(NDSP)Dc	2.(P13/P1)Dc	3.(NDSP)Dc	3.(P13/P1)Dc	4.(NDSP)Dc	4.(P13/P1)Dc
1	390.4	1.462	501.91	1.652	491.9	1.660	496.84	1.648	489.29	1.650
2	418.6	1.552	481.31	1.630	472.04	1.618	476.05	1.628	469.32	1.613
3	448.8	1.625	449.81	1.592	447.94	1.544	446.38	1.587	447.48	1.563
4	485.2	1.678	416.7	1.529	419.55	1.488	413.57	1.520	420.28	1.506
5	493.4	1.686	386.81	1.441	392.37	1.421	383.83	1.432	393.00	1.447
6	501.9	1.693								

Cricket Graph Data — TABLE 11C — Wed, Aug 24, 1988 16:24

	5.(NDSP)Dc	5.(P13/P1)Dc	1.(NDSP)Ac	1.(P13/P1)Ac	2.(NDSP)Ac	2.(P13/P1)Ac	3.(NDSP)Ac	3.(P13/P1)Ac	4.(NDSP)Ac	4.P13/P1)Ac
1	489.13	1.649	437.7	1.612	427.10	1.574	421.66	1.570	422.21	1.588
2	468.71	1.617	459.4	1.657	452.97	1.639	445.78	1.630	446.19	1.640
3	446.06	1.570	474.2	1.674	469.69	1.674	463.67	1.665	475.47	1.676
4	418.38	1.516	484.7	1.681	480.05	1.688	475.73	1.675	486.08	1.688
5	390.49	1.444	491.9	1.686	486.21	1.696	484.4	1.681	488.98	1.691
6			496.6	1.689	489.52	1.701	490.01	1.685	489.49	1.691
7			499.4	1.692	491.20	1.702	493.57	1.687	489.37	1.691
8			501.6	1.693	491.95	1.703	495.66	1.689	489.37	1.691
9			501.9	1.694	492.22	1.703	496.70	1.689		
10			501.8	1.694	492.22	1.703	497.15	1.690		
11			501.8	1.693	492.04	1.703	497.27	1.690		
12			501.8	1.694	492.03	1.703	497.11	1.690		
13			501.8	1.694	491.98	1.702	496.99	1.690		
14					491.88	1.702	496.93	1.690		
15					491.96	1.702	496.90	1.690		

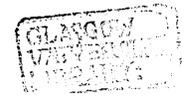

Cricket Graph Data

TABLE 11C

Wed, Aug 24, 1988 16:24

	5.(NDSP)Ac	5.(P13/P1)Ac	1.(NDSP)Sac	1.(P13/P1)Sac	2.(NDSP)SR	2.(P13/P1)SR	3.(NDSP)SR	3.(P13/P1)SR	4.(NDSP)SR	4.(P13/P1)SR
1	424.86	1.592	418.6	1.552	396.4	1.4651	389.2	1.4587	392.35	1.4821
2	449.01	1.642	448.8	1.625	425.3	1.5509	416.47	1.5462	420.77	1.5643
3	477.22	1.678	485.2	1.678	453.5	1.6218	445.47	1.6196	449.55	1.6253
4	486.90	1.689	493.4	1.686	481.1	1.6826	480.13	1.6751	478.61	1.6729
5	489.18	1.692	501.9	1.693	486.62	1.6931	488.91	1.6827	484.0	1.6819
6	489.44	1.693			491.9	1.7035	496.84	1.6900	489.29	1.6911
7	489.30	1.693								
8	489.19	1.693								
9	489.16	1.693								
10	489.14	1.693								
11	489.15	1.693								
12	489.15	1.693								

Cricket Graph Data

TABLE 11C

Wed, Aug 24, 1988 16:24

	5.(NDSP)SR	5.(P13/P1)SR
1	392.4	1.4824
2	420.64	1.5645
3	448.91	1.6261
4	477.5	1.6745
5	483.47	1.6839
6	489.13	1.6924

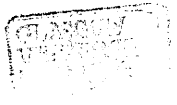

Cricket Graph Data TABLE 11D Wed, Aug 24, 1988 16:26

	2.(P13/P1)SR	2.(OUTERm)SR	1.(P13/P1)Dc	1.(OUTERm)Dc	2.(P13/P1)Dc	2.(OUTERm)Dc	3.(P13/P1)Dc	3.(OUTERm)Dc	4.(P13/P1)Dc	4.(OUTERm)Dc
1	1.5509	347.7	1.652	365.76	1.660	370.88	1.648	365.52	1.650	367.63
2	1.6218	360.61	1.630	372.83	1.618	367.53	1.628	370.48	1.613	364.9
3	1.6826	368.69	1.592	378.66	1.544	360.73	1.587	378.42	1.563	363.1
4	1.6931	369.64	1.529	366.88	1.488	351.17	1.520	365.24	1.506	356.4
5	1.7035	370.57								

Cricket Graph Data TABLE 11D Wed, Aug 24, 1988 16:26

	5.(P13/P1)Dc	5.(OUTERm)Dc
1	1.649	367.71
2	1.617	367.35
3	1.570	367.25
4	1.516	361.76

	2.(P3/P26)SR	2.(H.P.C.m)SR	3.(P3/P26)SR	3.(H.P.C.m)SR	4.(P3/P26)SR	4.(H.P.C.m)SR	5.(P3/P26)SR	5.(H.P.C.m)SR	1.(P3/P26)SR	1.(H.P.C.m)SR
1	2.104	22.88	2.0899	22.56	2.1156	23.12	2.1154	23.10	2.088	22.53
2	2.984	32.36	2.9868	32.32	2.9851	32.46	2.9846	32.44	2.985	32.22
3	3.826	39.39	3.8513	39.49	3.7838	39.29	3.7814	39.28	3.855	39.49
4	4.486	42.71	4.5463	42.96	4.4167	42.44	4.4180	42.44	4.574	43.04
5	4.943	44.93	5.0531	45.46	4.8674	44.63	4.8689	44.63	5.087	45.64
6	5.197	46.64	5.3336	47.47	5.1730	46.49	5.1737	46.49	5.366	47.65
7	5.419	48.35	5.5348	48.96	5.4398	48.38	5.4349	48.35	5.569	49.14
8	5.636	49.72	5.7613	50.47	5.6698	49.91	5.6585	49.84	5.785	50.59
9	5.817	50.93	5.9654	51.81	5.8851	51.33	5.8727	51.25	5.974	51.87
10	6.250	53.67	6.3965	54.50	6.3368	54.15	6.3249	54.08	6.380	54.40
11	6.535	55.31	6.7311	56.29	6.6299	55.78	6.6228	55.76	6.670	55.99
12	6.638	55.93	6.8073	56.79	6.7422	56.46	6.7529	56.51	6.730	56.40
13	6.707	56.38	6.7033	56.38	6.8038	56.85	6.800	56.85	6.639	56.05
14	6.712	56.43	6.6424	56.08	6.8245	56.96	6.8114	56.91	6.603	55.88
15	6.722	56.48	6.5919	55.84	6.8433	57.07	6.820	56.97	6.571	55.72
16										
17										
18										
19										
20										
21										
22										
23										
24										
25										
26										
27										
28										

	1.(P3/P26)Ac	1.(H.P.C.m)Ac	1.(P3/P26)Dc	1.(H.P.C.m)Dc	2.(P3/P26)Ac	2.(H.P.C.m)Ac	2.(P3/P26)Dc	2.(H.P.C.m)Dc	3.(P3/P26)Ac	3.(H.P.C.m)Ac
1	2.199	21.37	5.919	56.33	2.200	21.38	5.976	56.76	2.198	21.37
2	2.399	23.77	5.563	53.83	2.404	23.82	5.629	54.32	2.400	23.78
3	2.728	27.50	4.650	46.52	2.674	26.95	4.680	46.80	2.667	26.87
4	2.919	29.45	4.409	44.91	2.942	29.69	4.391	44.81	2.931	29.58
5	3.169	31.99	4.190	43.73	3.203	32.35	4.142	43.48	3.186	32.17
6	3.415	34.33	4.005	42.73	3.454	34.69	3.784	41.63	3.433	34.49
7	3.664	36.43	3.842	41.87	3.748	37.10	3.486	40.10	3.702	36.74
8	4.111	39.16	3.662	41.02	5.172	43.38	3.176	38.00	5.651	45.25
9	5.015	42.84	3.487	40.07	6.540	50.90	3.082	37.02	6.709	52.13
10	6.302	49.39	3.197	38.23	6.873	53.54	2.842	34.35	6.942	54.11
11	6.847	53.30	3.158	37.80	7.045	55.02	2.568	31.03	7.088	55.38
12	7.019	54.76	3.108	37.28	7.222	56.51	2.349	28.31	7.258	56.77
13	7.182	56.16	3.050	36.67	7.378	57.75	2.173	25.90	7.401	57.94
14	7.345	57.45	2.930	35.35	7.503	58.73	2.049	23.96	7.544	58.98
15	7.485	58.56	2.785	33.65	7.392	59.21	1.903	21.45	7.499	59.53
16	7.542	59.33	2.640	31.90	7.203	58.85	1.803	19.65	7.308	59.28
17	7.355	59.36	2.516	30.39	7.043	58.24	1.734	18.37	7.117	58.60
18	7.161	58.76	2.300	27.61	6.921	57.68			6.948	57.86
19	6.994	58.06	2.129	25.19	6.839	57.23			6.825	57.24
20	6.853	57.40	2.024	23.42	6.787	56.93			6.732	56.75
21	6.751	56.87	1.882	20.94	6.753	56.72			6.667	56.35
22	6.674	56.41	1.782	19.14	6.728	56.59			6.628	56.11
23	6.600	55.92	1.714	17.83	6.713	56.47			6.605	55.96
24	6.575	55.77			6.712	56.45			6.585	55.84
25	6.571	55.73			6.714	56.45			6.583	55.82
26	6.572	55.72			6.718	56.46			6.585	55.82
27	6.570	55.72			6.720	56.47			6.585	55.83
28	6.569	55.72			6.719	56.47			6.586	55.83

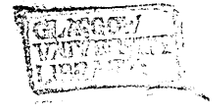

	3.(P3/P26)Dc	3.(H.P.C.m)Dc	5.(P3/P26)Dc	5.(H.P.C.m)Dc	5.(P3/P26)Ac	5.(H.P.C.m)Ac	4.(H.P.C.m)Ac	4.(P3/P26)Ac	4.(H.P.C.m)Dc	4.(P3/P26)Dc
1	5.873	56.12	6.059	57.25	2.209	21.48	21.47	2.21	57.35	6.074
2	5.525	53.60	5.729	54.99	2.405	23.84	23.85	2.40	55.10	5.745
3	4.655	46.60	4.987	49.32	2.674	26.95	26.96	2.675	49.20	4.969
4	4.523	45.48	4.482	45.30	2.947	29.74	29.75	2.948	45.15	4.454
5	4.275	44.17	4.189	43.73	3.219	32.50	32.52	3.221	43.67	4.177
6	4.072	43.08	3.997	42.72	3.481	34.92	34.94	3.483	42.72	3.999
7	3.887	42.08	3.806	41.73	3.877	37.93	38.15	3.918	41.76	3.814
8	3.687	41.14	3.633	40.89	4.795	42.06	42.26	4.848	40.91	3.636
9	3.512	40.23	3.470	39.99	6.016	47.63	48.07	6.088	40.05	3.479
10	3.203	38.29	3.219	38.40	6.785	52.82	52.94	6.800	38.49	3.234
11	3.169	37.92	3.172	37.96	7.005	54.77	54.86	7.022	37.99	3.175
12	3.124	37.45	3.127	37.48	7.212	56.44	56.52	7.226	37.53	3.131
13	3.070	36.39	3.073	36.93	7.382	57.79	57.84	7.396	36.98	3.078
14	2.953	35.61	2.959	35.7	7.526	58.87	58.91	7.528	35.77	2.965
15	2.808	33.93	2.835	34.26	7.462	59.44	59.54	7.512	34.37	2.843
16	2.542	30.71	2.568	31.04	7.112	58.52	58.71	7.158	31.13	2.576
17	2.323	27.93	2.350	28.34	6.923	57.61	57.81	6.965	28.43	2.357
18	2.145	25.49	2.176	25.97	6.876	57.16	57.32	6.882	24.12	2.053
19	2.036	23.63	2.050	24.06	6.819	57.01	57.14	6.848	21.65	1.909
20	1.891	21.09	1.907	21.61	6.815	56.96	57.06	6.838	19.89	1.814
21	1.789	19.25	1.813	19.85	6.815	56.96	57.07	6.844	18.63	1.745
22	1.718	17.89	1.744	18.60	6.815	56.95				
23					6.818	56.95				
24					6.821	56.95				
25					6.820	56.95				
26										
27										
28										

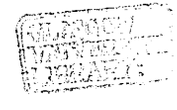

	1.(TIME)Ac	1.(THRUST)Ac	1.(TIME)Dc	1.(THRUST)Dc	2.(TIME)Ac	2.(THRUST)Ac	2.(TIME)Dc	2.(THRUST)Dc	3.(TIME)Ac	3.(THRUST)Ac
1	0.0	215.4	0.0	11281.0	0.0	175.8	0.0	11379.0	0.0	216.7
2	1.0	298.3	0.12	10639.0	1.0	279.82	0.12	10494.0	1.0	298.3
3	2.0	429.9	0.25	9709.5	2.0	396.66	0.25	8934.3	2.0	399.2
4	3.0	533.5	0.37	8511.2	3.0	543.5	0.37	7846.1	3.0	537.6
5	4.0	692.3	0.50	6974.6	4.0	720.9	0.50	6633.8	4.0	790.6
6	5.0	881.2	0.62	5740.0	5.0	924.7	0.75	4770.0	5.0	887.6
7	6.0	1117.1	0.75	4806.6	6.0	1226.9	1.0	3539.8	6.0	1135.4
8	6.5	1293.2	0.87	4070.7	6.5	1721.7	1.50	2137.8	6.75	1918.4
9	6.75	1614.5	1.00	3511.4	6.75	2569.7	2.0	1256.8	7.0	2848.4
10	7.0	2357.5	1.25	2632.1	7.0	3644.9	3.0	797.4	7.25	3919.6
11	7.25	3372.7	1.50	2022.8	7.25	4903.2	4.0	562.2	7.50	5135.8
12	7.50	4529.0	1.75	1596.9	7.50	6530.2	5.0	397.03	7.75	6668.2
13	7.75	5942.0	2.0	1295.5	7.75	8412.8	6.0	281.8	8.0	8426.5
14	8.0	7612.4	2.5	915.4	8.0	10104.0	7.0	203.1	8.25	9983.9
15	8.25	9379.7	3.0	762.7	8.25	11311.0	9.0	127.6	8.5	11134.0
16	8.50	10810.0	4.0	529.36	8.50	11971.0	11.0	93.61	8.75	11788.0
17	8.75	11641.0	5.0	371.0	8.75	12249.0	13.0	73.15	9.0	12026.0
18	9.0	11999.0	7.0	193.6	9.0	12404.0			9.25	12170.0
19	9.25	12161.0	9.0	129.6	9.25	12494.0			9.50	12259.0
20	9.50	12277.0	11.0	97.73	9.50	12529.0			9.75	12314.0
21	9.75	12348.0	13.0	78.92	9.75	12542.0			10.0	12345.0
22	10.0	12394.0			10.0	12544.0			10.25	12360.0
23	10.5	12419.0			10.50	12539.0			10.50	12367.0
24	11.0	12426.0			11.0	12533.0			11.0	12367.0
25	11.5	12427.0			11.50	12532.0			11.50	12364.0
26	12.0	12424.0			12.0	12525.0			12.0	12362.0
27	12.5	12428.0			12.50	12527.0			12.5	12361.0
28	13.0	12427.0			13.0	12523.0			13.0	12361.0
29										

Cricket Graph Data

TABLE 13

Wed, Aug 24, 1988 16:30

	3.(TIME)Dc	3.(THRUST)Dc	4.(TIME)Ac	4.(THRUST)Ac	4.(TIME)Dc	4.(THRUST)Dc	5.(TIME)Ac	5.(THRUST)Dc	5.(TIME)Dc	5 (THRUST)Dc
1	0.0	11217.0	0.0	147.29	0.0	11196.0	0.0	145.7	0.0	11179.0
2	0.12	10653.0	1.0	273.63	0.12	10395.0	1.0	273.4	0.12	10467.0
3	0.25	9608.1	2.0	412.4	0.25	9302.0	2.0	412.5	0.25	9414.0
4	0.37	8352.2	3.0	594.2	0.37	8148.4	3.0	594.0	0.37	8315.4
5	0.50	6814.8	4.0	799.28	0.50	7064.6	4.0	799.4	0.50	7018.5
6	0.62	5638.9	5.0	1039.7	0.62	5930.7	5.0	1040.2	0.62	5874.7
7	0.75	4721.5	6.0	1354.7	0.75	4977.1	6.0	1349.5	0.75	4917.9
8	0.87	4013.0	6.25	1632.2	0.87	4255.2	6.25	1612.4	0.87	4188.9
9	1.00	3456.8	6.50	2392.9	1.0	3643.8	6.50	2344.4	1.00	3576.0
10	1.25	2594.8	6.75	3716.4	1.25	2963.6	6.75	3659.6	1.25	2643.1
11	1.50	1997.5	7.0	5254.7	1.50	2118.3	7.0	5225.4	1.50	2074.3
12	1.75	1578.4	7.25	6938.8	1.75	1704.5	7.25	6977.9	1.75	1668.2
13	2.0	1282.4	7.50	8767.2	2.0	1444.7	7.50	8879.6	2.00	1421.0
14	2.5	909.82	7.75	10287.0	2.5	1104.4	7.75	10386.0	2.50	1086.9
15	3.0	758.6	8.0	11296.0	3.0	875.6	8.0	11344.0	3.0	863.33
16	4.0	528.9	8.50	12035.0	4.0	606.9	8.50	12085.0	4.0	600.4
17	5.0	375.4	9.0	12274.0	5.0	429.4	9.0	12301.0	5.0	426.4
18	6.0	263.6	9.50	12329.0	7.0	231.4	9.50	12360.0	6.0	305.82
19	7.0	194.66	10.0	12334.0	9.0	146.6	10.0	12369.0	7.0	229.84
20	9.0	130.3	11.0	12328.0	11.0	105.52	10.5	12363.0	9.0	146.34
21	11.0	99.93	13.0	12328.0	13.0	81.86	11.0	12360.0	11.0	105.6
22	13.0	81.03					11.5	12359.0	13.0	82.08
23							12.0	12358.0		
24							12.5	12358.0		
25							13.0	12359.0		
26										
27										
28										
29										

	1.(P13/P1)Dc	2.(P13/P1)Dc	3.(P13/P1)Dc	4.(P13/P1)Dc	5.(P13/P1)Dc
1	1.652	1.660	1.648	1.650	1.649
2	1.630	1.618	1.628	1.613	1.617
3	1.592	1.544	1.587	1.563	1.570
4	1.529	1.488	1.520	1.506	1.516
5	1.441	1.421	1.432	1.447	1.444
6	1.370	1.314	1.364	1.382	1.379
7	1.316	1.241	1.311	1.327	1.323
8	1.273	1.155	1.269	1.285	1.281
9	1.240	1.108	1.237	1.248	1.244
10	1.186	1.067	1.184	1.190	1.187
11	1.148	1.051	1.145	1.153	1.150
12	1.120	1.039	1.118	1.127	1.124
13	1.100	1.030	1.099	1.110	1.108
14	1.075	1.024	1.078	1.089	1.087
15	1.065	1.018	1.065	1.073	1.072
16	1.049	1.015	1.049	1.054	1.054
17	1.037	1.013	1.038	1.042	1.041
18	1.024		1.029	1.027	1.033
19	1.018		1.024	1.020	1.027
20	1.015		1.018	1.016	1.019
21	1.014		1.016	1.014	1.016
22			1.014		1.014
23					
24					
25					
26					
27					
28					
29					

Cricket Graph Data — Table 13A — Wed, Aug 24, 1988 16:33

	1.(TIME)Dc	2.(TIME)Dc	3.(TIME)Dc	4.(TIME)Dc	5.(TIME)Dc	1.(P13/P1)Dc	2.(P13/P1)Dc	3.(P13/P1)Dc	4.(P13/P1)Dc	5.(P13/P1)Dc
1	0.0	0.0	0.0	0.0	0.0	1.652	1.660	1.648	1.650	1.649
2	0.12	0.12	0.12	0.12	0.12	1.630	1.618	1.628	1.613	1.617
3	0.25	0.25	0.25	0.25	0.25	1.592	1.544	1.587	1.563	1.570
4	0.37	0.37	0.37	0.37	0.37	1.529	1.488	1.520	1.506	1.516
5	0.50	0.50	0.50	0.50	0.50	1.441	1.421	1.432	1.447	1.444
6	0.62	0.75	0.62	0.62	0.62	1.370	1.314	1.364	1.382	1.379
7	0.75	1.0	0.75	0.75	0.75	1.316	1.241	1.311	1.327	1.323
8	0.87		0.87	0.87	0.87	1.273		1.269	1.285	1.281
9	1.00		1.00	1.0	1.00	1.240		1.237	1.248	1.244

Cricket Graph Data — Table 13A — Wed, Aug 24, 1988 16:33

	1.(TIME)Ac	1.(THRUST)Ac	2.(TIME)Ac	2.(THRUST)Ac	3.(TIME)Ac	3.(THRUST)Ac	4.(TIME)Ac	4.(THRUST)Ac	5.(TIME)Ac	5.(THRUST)Ac
1	6.0	1117.1	6.0	1226.9	6.0	1135.4	6.0	1354.7	6.0	1349.5
2	6.5	1293.2	6.5	1721.7	6.75	1918.4	6.25	1632.2	6.25	1612.4
3	6.75	1614.5	6.75	2569.7	7.0	2848.4	6.50	2392.9	6.50	2344.4
4	7.0	2357.5	7.0	3644.9	7.25	3919.6	6.75	3716.4	6.75	3659.6
5	7.25	3372.7	7.25	4903.2	7.50	5135.8	7.0	5254.7	7.0	5225.4
6	7.50	4529.0	7.50	6530.2	7.75	6668.2	7.25	6938.8	7.25	6977.9
7	7.75	5942.0	7.75	8412.8	8.0	8426.5	7.50	8767.2	7.50	8879.6
8	8.0	7612.4	8.0	10104.0			7.75	10287.0	7.75	10386.0
9							8.0	11296.0	8.0	11344.0

Cricket Graph Data — Table 13A — Wed, Aug 24, 1988 16:33

	1.(FCSP)Ac
1	0.8217
2	0.8461
3	0.8701
4	0.9030
5	0.9015
6	0.9088
7	0.9177
8	0.9267

Cricket Graph Data

TABLE 14

Wed, Aug 24, 1988 16:36

	1.(P13/P1)SR	1.(NLDSP)SR	1.(OUTERm)SR	1.(FuelFlow)SR	1.(P13/P1)Ac	1.(NLDSP)Ac	1.(TIME)Ac	1.(THRUST)Ac	1.(TIME)Dc	1.(P13/P1)Dc
1	1.198	327.1	327.06	0.058	1.199	315.51	0.0	548.70	0.0	1.559
2	1.217	334.11	329.32	0.062	1.208	318.32	0.25	592.12	0.12	1.555
3	1.237	341.05	331.71	0.066	1.216	321.61	0.37	629.12	0.25	1.550
4	1.256	348.0	334.20	0.070	1.226	325.80	0.50	667.63	0.37	1.546
5	1.274	354.85	336.80	0.074	1.24	330.59	0.62	716.90	0.50	1.539
6	1.294	361.67	339.41	0.078	1.256	335.98	0.75	772.28	0.62	1.530
7	1.313	368.23	341.96	0.082	1.272	341.80	0.87	825.65	0.75	1.521
8	1.332	374.24	344.56	0.086	1.289	347.73	1.00	876.98	0.87	1.511
9	1.350	379.37	346.90	0.090	1.327	359.91	1.25	989.78	1.00	1.500
10	1.368	384.39	349.25	0.094	1.362	372.35	1.50	1084.5	1.25	1.481
11	1.387	389.47	351.59	0.098	1.399	383.77	1.75	1173.4	1.50	1.461
12	1.482	416.06	364.30	0.12	1.431	393.83	2.00	1254.4	1.75	1.430
13	1.551	447.39	368.93	0.14	1.459	402.53	2.25	1326.0	2.00	1.400
14	1.606	481.29	369.58	0.16	1.483	410.07	2.50	1388.2	2.25	1.373
15					1.505	416.74	2.75	1445.0	2.50	1.349
16					1.520	422.64	3.00	1484.8	2.75	1.327
17					1.539	433.17	3.50	1541.2	3.00	1.308
18					1.554	442.34	4.00	1588.3	3.50	1.282
19					1.567	450.12	4.50	1627.8	4.00	1.261
20					1.578	456.63	5.00	1660.1	4.50	1.246
21					1.586	462.0	5.50	1686.2	5.00	1.234
22					1.593	466.28	6.00	1707.6	6.00	1.219
23					1.598	472.62	7.00	1724.3	7.00	1.211
24					1.604	478.98	9.00	1742.2	9.00	1.203
25					1.606	481.12	11.0	1749.2	11.0	1.201
26					1.607	481.61	13.0	1749.5	13.0	1.200
27										
28										

Cricket Graph Data

TABLE 14

Wed, Aug 24, 1988 16:36

	1.(NLDSP)Dc	1.(OUTERm)Dc	2.(P13/P1)SR	2.(NLDSP)SR	2.(OUTERm)SR	2.(P13/P1)Ac	2.(NLDSP)Ac	2.(TIME)Ac	2.(THRUST)Ac	2.(TIME)Dc
1	481.28	369.67	1.18	354.52	315.09	1.120	315.51	0.0	382.32	0.0
2	477.69	370.62	1.20	362.46	318.81	1.131	318.43	0.12	422.77	0.12
3	473.85	371.60	1.221	370.10	322.52	1.144	322.31	0.25	469.54	0.25
4	469.52	375.45	1.242	376.34	325.96	1.161	327.22	0.37	528.90	0.37
5	464.44	378.18	1.262	380.65	328.47	1.182	333.05	0.50	595.36	0.50
6	458.99	379.31	1.279	385.08	331.09	1.206	339.29	0.62	666.49	0.62
7	453.41	379.67	1.299	389.53	333.71	1.230	345.94	0.75	745.45	0.75
8	447.8	379.62	1.318	393.9	336.28	1.257	353.02	0.87	823.46	0.87
9	442.2	379.40	1.335	398.24	338.87	1.280	360.23	1.00	891.50	1.00
10	431.14	378.47	1.355	402.49	341.38	1.325	374.57	1.25	1008.2	1.25
11	420.36	377.37	1.372	406.78	343.95	1.368	387.62	1.50	1111.6	1.50
12	410.08	372.79	1 165	433.75	355.64	1.404	398.85	1.75	1203.5	1.75
13	400.66	368.05	1.540	459.18	363.22	1.436	408.44	2.00	1281.7	2.00
14	392.12	363.54	1.602	483.97	368.22	1.464	416.74	2.25	1350.4	2.25
15	384.39	359.33				1.482	424.04	2.50	1401.8	2.50
16	377.38	355.21				1.498	430.71	2.75	1444.7	2.75
17	371.09	351.52				1.512	436.81	3.00	1483.4	3.00
18	360.58	345.80				1.536	447.74	3.50	1550.5	3.25
19	352.43	341.27				1.555	455.99	4.00	1605.6	3.50
20	346.29	337.63				1.570	462.77	4.50	1649.5	3.75
21	341.63	335.12				1.580	467.95	5.00	1678.8	4.00
22	335.41	331.47				1.591	475.13	6.00	1711.0	4.50
23	331.83	329.42				1.597	479.43	7.00	1729.5	5.00
24	328.62	327.63				1.602	483.15	9.00	1743.9	6.00
25	327.58	326.91				1.603	483.99	11.0	1745.2	7.00
26	327.25	326.71				1.603	484.05	13.0	1744.5	9.00
27										11.0
28										13.0

Cricket Graph Data

TABLE 14

Wed, Aug 24, 1988 16:36

	2.(P13/P1)Dc	2.(NLDSP)Dc	2.(OUTERm)Dc	3.(P13/P1)SR	3.(NLDSP)SR	3.(OUTERm)SR	3.(P13/P1)Ac	3.(TIME)Ac	3.(THRUST)Ac	3.(TIME)Dc
1	1.558	483.97	368.42	1.199	327.17	325.41	1.201	0.0	554.43	0.0
2	1.548	480.46	367.85	1.217	334.19	327.93	1.225	0.50	678.51	0.12
3	1.533	476.84	367.28	1.236	341.06	330.49	1.240	0.62	731.17	0.25
4	1.510	472.85	366.66	1.255	347.85	333.11	1.257	0.75	789.96	0.37
5	1.493	468.58	365.97	1.274	354.81	335.59	1.276	0.87	847.66	0.50
6	1.478	464.29	365.04	1.294	361.66	338.20	1.294	1.00	903.08	0.62
7	1.464	460.03	363.78	1.313	368.12	340.87	1.332	1.25	1018.8	0.75
8	1.450	455.82	362.53	1.331	374.05	343.47	1.368	1.50	1103.2	0.87
9	1.439	451.68	361.29	1.350	379.09	345.69	1.404	1.75	1192.9	1.00
10	1.419	443.60	358.88	1.368	384.02	348.01	1.436	2.00	1271.2	1.25
11	1.400	435.88	356.58	1.386	388.98	350.33	1.463	2.25	1339.0	1.50
12	1.383	428.48	354.38	1.480	415.02	363.24	1.486	2.50	1401.6	1.75
13	1.365	421.38	352.27	1.547	445.45	368.27	1.507	2.75	1452.9	2.00
14	1.346	414.65	348.91	1.602	478.15	369.00	1.521	3.00	1490.4	2.25
15	1.325	408.51	345.32				1.530	3.25	1518.4	2.50
16	1.309	402.9	342.00				1.539	3.50	1545.2	2.75
17	1.293	397.85	339.02				1.547	3.75	1569.1	3.00
18	1.281	393.31	336.22				1.554	4.00	1589.3	3.50
19	1.269	389.24	333.89				1.566	4.50	1627.5	4.00
20	1.258	385.61	331.73				1.576	5.00	1656.6	4.50
21	1.248	382.37	329.79				1.584	5.50	1682.6	5.00
22	1.233	376.93	326.50				1.590	6.00	1701.8	6.00
23	1.220	372.60	323.91				1.595	7.00	1720.2	7.00
24	1.205	365.95	320.60				1.601	9.00	1737.3	9.00
25	1.194	361.55	318.49				1.602	11.0	1741.3	11.0
26	1.185	357.19	316.38				1.602	13.0	1742.0	13.0
27	1.183	355.58	315.56							
28	1.180	354.96	315.31							

	3.(P13/P1)Dc	3.(OUTERm)Dc	3.(NLDSP)Ac	3.(NLDSP)Dc
1	1.557	369.09	315.51	478.16
2	1.552	370.10	325.57	474.54
3	1.547	371.50	330.70	470.68
4	1.542	375.48	336.45	466.37
5	1.534	378.69	342.72	461.25
6	1.524	379.79	349.09	455.67
7	1.515	380.23	362.02	449.95
8	1.504	380.14	374.58	444.18
9	1.494	379.78	385.84	438.44
10	1.466	376.63	395.60	427.20
11	1.450	376.44	403.98	416.31
12	1.418	371.02	411.25	406.07
13	1.389	365.85	417.63	396.84
14	1.363	361.15	423.27	388.58
15	1.338	356.93	428.52	381.22
16	1.317	352.75	433.41	374.62
17	1.303	349.29	437.97	368.71
18	1.281	344.56	442.18	358.66
19	1.257	339.16	449.58	350.83
20	1.244	335.98	455.7	344.91
21	1.231	333.08	460.74	340.44
22	1.217	329.67	464.76	334.65
23	1.208	327.97	470.54	331.37
24	1.202	326.21	476.33	328.53
25	1.200	325.65	478.16	327.61
26	1.199	325.47	478.47	317.31
27				
28				

	4.(P13/P1)SR	4.(NLDSP)SR	4.(OUTERm)SR	4.(P13/P1)Ac	4.(NLDSP)Ac	4.(TIME)Ac	4.(THRUST)Ac	4.(TIME)Dc	4.(P13/P1)Dc	4.(NLDSP)Dc
1	1.198	336.95	323.48	1.156	315.52	0.0	463.36	0.0	1.551	483.32
2	1.219	344.24	327.22	1.168	318.16	0.12	504.13	.012	1.542	479.73
3	1.240	351.17	330.29	1.183	321.78	0.25	554.87	0.25	1.530	476.08
4	1.262	360.99	333.69	1.199	326.50	0.37	615.49	0.37	1.510	472.23
5	1.283	370.05	336.94	1.220	331.91	0.50	678.94	0.50	1.492	468.03
6	1.304	378.06	339.92	1.243	337.77	0.62	748.89	0.62	1.480	463.78
7	1.325	385.28	342.70	1.266	344.14	0.75	821.30	0.75	1.471	459.53
8	1.345	391.71	345.49	1.286	350.84	0.87	880.79	0.87	1.463	455.26
9	1.364	397.14	347.93	1.306	357.62	1.00	940.83	1.00	1.455	451.00
10	1.380	401.78	349.84	1.349	371.36	1.25	1055.6	1.25	1.441	442.49
11	1.398	406.43	351.74	1.388	384.13	1.50	1149.7	1.50	1.421	434.29
12	1.479	431.93	359.49	1.425	395.43	1.75	1240.1	1.75	1.405	426.78
13	1.540	459.39	362.77	1.451	405.25	2.00	1309.0	2.00	1.389	419.91
14	1.594	483.32	365.85	1.474	413.96	2.25	1369.4	2.25	1.371	413.57
15				1.494	421.73	2.50	1423.9	2.50	1.355	407.74
16				1.509	428.66	2.75	1467.0	2.75	1.340	402.35
17				1.523	434.83	3.00	1506.2	3.00	1.327	397.40
18				1.543	445.24	3.50	1566.3	3.25	1.316	392.85
19				1.555	453.89	4.00	1604.1	3.50	1.307	388.51
20				1.565	461.13	4.50	1635.8	3.75	1.297	384.36
21				1.573	467.03	5.00	1661.4	4.00	1.288	380.37
22				1.583	474.99	6.00	1696.6	4.50	1.273	372.79
23				1.591	479.35	7.00	1715.8	5.00	1.259	365.81
24				1.596	482.75	9.00	1729.5	6.00	1.239	354.68
25				1.597	483.42	11.0	1730.9	7.00	1.223	346.90
26				1.595	483.43	13.0	1729.7	9.00	1.206	339.99
27								11.0	1.200	337.94
28								13.0	1.199	337.32

Cricket Graph Data

TABLE 14A

Wed, Aug 24, 1988 16:38

	4.(OUTERm)Dc	5.(P13/P1)SR	5.(NLDSP)SR	5.(OUTERm)SR	5.(P13/P1)Ac	5.(NLDSP)Ac	5.(TIME)Ac	5.(THRUST)Ac	5.(TIME)Dc	5.(P13/P1)Dc
1	366.42	1.198	336.81	324.50	1.160	315.51	0.0	469.44	0.0	1.553
2	365.83	1.219	343.73	327.81	1.171	318.09	0.12	508.12	0.12	1.547
3	365.24	1.240	350.59	330.81	1.184	321.70	0.25	556.05	0.25	1.536
4	364.68	1.262	360.01	334.20	1.200	326.39	0.37	612.66	0.37	1.529
5	363.99	1.283	368.61	337.50	1.219	331.69	0.50	672.51	0.50	1.511
6	363.52	1.304	376.27	340.46	1.241	337.45	0.62	739.76	0.62	1.494
7	363.35	1.325	383.21	343.27	1.262	343.74	0.75	808.62	0.75	1.480
8	363.17	1.345	389.36	346.00	1.283	350.38	0.87	866.57	0.87	1.470
9	363.04	1.364	394.96	348.62	1.303	357.09	1.00	926.76	1.00	1.462
10	362.75	1.381	399.30	350.94	1.346	370.77	1.25	1047.2	1.25	1.445
11	361.31	1.399	403.40	353.11	1.385	383.60	1.50	1142.8	1.50	1.431
12	360.00	1.486	428.64	362.57	1.423	394.97	1.75	1234.6	1.75	1.418
13	358.84	1.549	455.59	366.31	1.451	404.82	2.00	1305.8	2.00	1.393
14	356.21	1.601	479.04	369.22	1.475	413.50	2.25	1367.6	2.25	1.367
15	353.63				1.497	421.19	2.50	1424.6	2.50	1.345
16	351.26				1.511	428.04	2.75	1467.8	2.75	1.328
17	349.09				1.524	434.15	3.00	1506.2	3.00	1.316
18	347.24				1.544	444.57	3.50	1567.2	3.25	1.305
19	345.55				1.558	453.06	4.00	1609.4	3.50	1.294
20	344.01				1.569	459.94	4.50	1644.1	3.75	1.285
21	342.55				1.581	465.29	5.00	1674.2	4.00	1.277
22	339.77				1.591	472.30	6.00	1707.7	4.50	1.262
23	337.22				1.597	476.02	7.00	1724.8	5.00	1.250
24	333.00				1.600	478.74	9.00	1736.0	6.00	1.231
25	329.39				1.601	479.17	11.0	1738.0	7.00	1.216
26	325.31				1.602	479.12	13.0	1738.0	9.00	1.204
27	324.11								11.0	1.200
28	323.68								13.0	1.200

	5.(NLDSP)Dc	5.(OUTERm)Dc
1	479.04	369.54
2	475.38	369.24
3	471.66	369.04
4	467.89	368.71
5	464.00	368.33
6	459.76	367.95
7	455.36	367.62
8	450.95	367.32
9	446.55	367.09
10	437.82	366.94
11	429.28	367.06
12	421.04	367.27
13	413.29	363.20
14	406.52	358.57
15	400.47	354.35
16	395.14	350.89
17	390.20	348.90
18	385.46	347.01
19	380.91	345.27
20	376.54	343.58
21	372.36	341.93
22	364.90	338.92
23	358.66	336.18
24	349.27	332.01
25	343.59	328.48
26	338.90	325.58
27	337.54	324.83
28	337.13	324.54

Cricket Graph Data — TABLE 14B — Wed, Aug 24, 1988 16:40

	1.(P13/P1)SR	1.(OUTERm)SR	2.(P13/P1)SR	2.(OUTERm)SR	3.(P13/P1)SR	3.(OUTERm)SR	4.(P13/P1)SR	4.(OUTERm)SR	5.(P13/P1)SR	5.(OUTERm)SR
1	1.350	346.90	1.465	355.64	1.350	345.69	1.345	345.49	1.345	346.00
2	1.368	349.25	1.540	363.22	1.368	348.01	1.364	347.93	1.364	348.62
3	1.387	351.59	1.602	368.22	1.386	350.33	1.380	349.84	1.381	350.94
4	1.482	364.30			1.480	363.24	1.398	351.74	1.399	353.11
5	1.551	368.93			1.547	368.27	1.479	359.49	1.486	362.57
6	1.606	369.58			1.602	369.00	1.540	362.77	1.549	366.31
7							1.594	365.85	1.601	369.22

Cricket Graph Data — TABLE 14B — Wed, Aug 24, 1988 16:40

	1.(P13/P1)Ac	1.(NLDSP)Ac	2.(P13/P1)Ac	2.(NLDSP)Ac	3.(P13/P1)Ac	3.(NLDSP)Ac	4.(P13/P1)Ac	4.(NLDSP)Ac	5.(P13/P1)Ac	5.(NLDSP)Ac
1	1.554	442.34	1.536	447.74	1.554	442.18	1.543	445.24	1.544	444.57
2	1.567	450.12	1.555	455.99	1.566	449.58	1.555	453.89	1.558	453.06
3	1.578	456.63	1.570	462.77	1.576	455.7	1.565	461.13	1.569	459.94
4	1.586	462.0	1.580	467.95	1.584	460.74	1.573	467.03	1.581	465.29
5	1.593	466.28	1.591	475.13	1.590	464.76	1.583	474.99	1.591	472.30
6	1.598	472.62	1.597	479.43	1.595	470.54	1.591	479.35	1.597	476.02
7	1.604	478.98	1.602	483.15	1.601	476.33	1.596	482.75	1.600	478.74
8	1.606	481.12	1.603	483.99	1.602	478.16	1.597	483.42	1.601	479.17
9	1.607	481.61	1.603	484.05	1.602	478.47	1.595	483.43	1.602	479.12

Cricket Graph Data TABLE 15 Wed, Aug 24, 1988 16:43

	FUEL FLOW.NC	NL.NC	NH.NC	THRUST.NC	SFC.NC	NL.R	NH.R	THRUST.R	SFC.R	NL.IC
1	0.20	4139.6	10030.0	2235.2	0.710	4156.5	10035.0	2261.9	0.702	4167.0
2	0.24	4708.3	10247.6	3071.2	0.620	4727.6	10252.5	3104.9	0.613	4737.2
3	0.28	5103.8	10433.4	3776.2	0.589	5126.7	10440.2	3821.5	0.581	5138.1
4	0.32	5498.0	10603.7	4514.0	0.563	5524.8	10611.8	4569.5	0.556	5538.0
5	0.36	5784.6	10738.9	5212.0	0.548	5807.4	10746.0	5277.9	0.541	5819.8
6	0.40	6053.3	10859.6	5911.9	0.537	6079.6	10867.0	5987.9	0.530	6092.8
7	0.50	6619.0	11193.2	7640.0	0.519	6646.5	11195.9	7745.5	0.512	6661.2
8	0.60	7092.6	11591.3	9270.9	0.514	7127.3	11589.0	9403.7	0.506	7145.9
9	0.70	7591.9	11888.5	10689.0	0.520	7638.9	11875.1	10839.0	0.512	7666.6
10	0.80	8176.7	12100.9	11873.0	0.535	8253.4	12081.6	12014.0	0.528	8298.8
11						8397.3	12110.0	12216.0	0.533	8443.2

Cricket Graph Data TABLE 15 Wed, Aug 24, 1988 16:43

	NH.IC	THRUST.IC	SFC.IC	FUEL FLOW
1	10039.0	2275.8	0.697	0.20
2	10256.4	3120.0	0.610	0.24
3	10445.1	3843.3	0.578	0.28
4	10617.7	4596.0	0.553	0.32
5	10751.7	5309.0	0.538	0.36
6	10872.1	6024.4	0.527	0.40
7	11206.5	7796.7	0.509	0.50
8	11602.6	9467.4	0.503	0.60
9	11884.9	10910.0	0.509	0.70
10	12088.1	12074.0	0.526	0.80
11	12118.9	12272.0	0.530	0.82

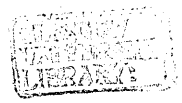

Cricket Graph Data TABLE 16 Thu, Aug 25, 1988 10:21

	CAP.93	PR.93	CAP.186	PR.186	CAP.279	PR.279	CAP.326	PR.326	CAP.372	PR.372
1	3.0282	1.0188	15.141	1.0749	28.7679	1.1639	41.0826	1.235	56.5264	1.3191
2	6.0564	1.0198	18.1692	1.0789	38.5591	1.1809	53.2963	1.263	71.6674	1.3551
3	11.6081	1.0228	24.6293	1.0839	45.4230	1.191	59.8574	1.272	78.7332	1.3681
4	18.6739	1.0248	31.998	1.0859	53.4982	1.196	68.1345	1.279	84.5878	1.3731
5	23.0143	1.0258	35.8337	1.0869	57.5358	1.195	72.4749	1.278	89.0291	1.3741
6	25.9416	1.0258	38.8619	1.0869	60.2612	1.193	75.6069	1.277	93.1676	1.3721
7	29.5754	1.0258	42.3948	1.0859	63.3902	1.1889	79.3389	1.272	96.9024	1.3681
8	33.5620	1.0258	46.1801	1.0844	66.7214	1.1839	82.7708	1.265	100.4353	1.3631

Cricket Graph Data TABLE 16 Thu, Aug 25, 1988 10:21

	CAP.419	PR.419	CAP.465	PR.465	CAP.512	PR.512	CAP.SURGE	PR.SURGE
1	81.2567	1.4281	96.4987	1.5312	109.0152	1.6463	3.028	1.0188
2	87.8178	1.4432	104.7758	1.5592	116.0810	1.6673	15.141	1.0749
3	93.3695	1.4532	111.5387	1.5813	122.9450	1.6894	28.7679	1.1639
4	98.9212	1.4602	117.0904	1.5913	128.9004	1.7094	41.0826	1.2350
5	104.4729	1.4682	122.1374	1.5953	134.5531	1.7264	56.5264	1.3191
6	109.5199	1.4712	126.6797	1.5953	139.7010	1.7384	81.2567	1.4281
7	114.0622	1.4692	131.222	1.5933	144.6771	1.7464	96.4987	1.5312
8	118.3522	1.4647	135.7643	1.5903	149.4922	1.7524	109.0152	1.6463

Cricket Graph Data TABLE 17 Thu, Aug 25, 1988 10:22

	CAP.86	PR.86	CAP.173	PR.173	CAP.259	PR.259	CAP.303	PR.303	CAP.346	PR.346
1	11.473	1.0363	23.1557	1.119	35.9522	1.241	42.9599	1.3307	50.5769	1.4436
2	15.0309	1.0333	26.9134	1.115	38.8975	1.2339	46.3114	1.3236	54.4362	1.4396
3	17.5699	1.0262	29.2493	1.1069	40.9287	1.2269	48.5457	1.3156	56.8736	1.4285
4	20.6167	1.0162	32.1945	1.0898	44.6864	1.2097	52.4050	1.2984	60.1235	1.4043
5	23.5619	1.0051	34.8351	1.0706	47.7332	1.1875	55.2486	1.2773	62.7641	1.3781
6	26.1009	0.99	37.2725	1.0514	50.7800	1.1664	58.1939	1.2460	65.2015	1.3388
7	28.2337	0.9748	39.6084	1.0262	53.5224	1.1331	60.2251	1.2117	66.8625	1.3025
8	30.5696	0.9567	41.5380	1.0051	55.3502	1.0988	62.1547	1.1744	68.4514	1.2601
9	33.3117	0.9335	43.4677	0.9748	56.8736	1.0565	63.5766	1.1311	69.8733	1.2127
10	36.2569	0.9078	45.3979	0.9401	58.2447	1.0101	64.7445	1.0847	71.1336	1.1628

Cricket Graph Data TABLE 17 Thu, Aug 25, 1988 10:22

	CAP.389	PR.389	CAP.432	PR.432	CAP.476	PR.476	CAP.SURGE	PR.SURGE
1	58.9048	1.5847	70.8889	1.747	83.4823	1.9073	11.4763	1.0363
2	62.7641	1.5656	73.8341	1.7198	85.3104	1.8660	23.1557	1.119
3	65.6078	1.5454	76.0684	1.6886	86.3260	1.8277	35.9522	1.2410
4	68.3499	1.5152	78.2012	1.6513	87.3416	1.7712	42.9599	1.3307
5	70.4826	1.4819	79.8262	1.6099	87.8494	1.7158	50.5769	1.4436
6	72.7170	1.4396	81.5527	1.5565	88.3572	1.6472	58.9048	1.5847
7	74.1388	1.3992	82.5683	1.5121	88.5603	1.5928	70.8889	1.747
8	75.5606	1.3549	83.5839	1.4597	88.865	1.5302	83.4823	1.9073
9	76.8809	1.3055	84.2948	1.4063	89.1697	1.4688		
10	78.1504	1.2536	84.8534	1.3524	89.4744	1.4078		

Cricket Graph Data

TABLE 18

Thu, Aug 25, 1988 10:24

	CAP.93	PR.93	CAP.186	PR.186	CAP.279	PR.279	CAP.326	PR.326	CAP.372	PR.372
1	3.0	1.0607	15.0	1.2208	28.5002	1.4923	40.6993	1.6838	55.9999	1.9385
2	6.0	1.0591	18.0	1.2218	38.2002	1.4918	52.7991	1.7007	70.9999	1.9643
3	11.5001	1.0574	24.4	1.2198	45.0002	1.4886	59.2992	1.6986	77.9999	1.9390
4	18.5001	1.0482	31.7	1.2087	53.0002	1.4638	67.4992	1.6621	83.7999	1.8771
5	22.8001	1.0335	35.5	1.1891	57.0002	1.4329	71.7991	1.6135	88.1999	1.7819
6	25.7001	1.0191	38.5	1.1666	59.7002	1.4078	75.1991	1.5493	92.2999	1.6353
7	29.3001	0.9938	42.0	1.1339	62.8002	1.3612	78.5991	1.4404	95.9999	1.4699
8	33.2501	0.9603	45.75	1.0854	66.1003	1.2742	81.9991	1.2776	99.4999	1.3085

Cricket Graph Data

TABLE 18

Thu, Aug 25, 1988 10:24

	CAP.419	PR.419	CAP.465	PR.465	CAP.512	PR.512	CAP.SURGE	PR.SURGE
1	80.4999	2.2645	95.6002	2.6962	107.9999	3.3905	3.0	1.0607
2	86.9992	2.2519	103.8	2.6744	114.9999	3.3028	15.0	1.2208
3	92.4993	2.2163	110.5	2.6325	121.7999	3.2076	28.5002	1.4923
4	97.9993	2.1383	116.0	2.5358	127.6999	3.1288	40.6993	1.6838
5	103.4999	2.0031	121.0	2.35	133.3999	2.9516	55.9999	1.9385
6	108.4999	1.795	125.5	1.9517	138.3999	2.3668	80.4999	2.2645
7	112.9999	1.5771	130.0	1.4653	143.2999	1.5633	95.6002	2.6962
8	117.2499	1.36	134.5	0.9724	148.0999	0.7661	107.9999	3.3905

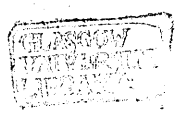

Cricket Graph Data TABLE 19 Thu, Aug 25, 1988 10:26

	CAP.93	PR.93	CAP.186	PR.186	CAP.279	PR.279	CAP.326	PR.326	CAP.372	PR.372
1	44.8708	1.019	111.18	1.0939	184.469	1.2268	213.3858	1.3287	242.3026	1.4386
2	50.8536	1.019	115.6671	1.0919	194.4403	1.2248	225.3514	1.3167	258.2566	1.4366
3	56.8364	1.019	120.1542	1.0899	201.4202	1.2218	233.3284	1.3117	268.2278	1.4356
4	65.3120	1.017	129.1283	1.0849	211.3915	1.2158	243.7983	1.3037	280.6604	1.4286
5	74.2862	1.015	139.0996	1.080	221.8614	1.2068	255.2653	1.2907	291.6604	1.4116
6	83.2603	1.013	148.5724	1.074	231.8327	1.1978	264.7378	1.2808	300.0361	1.3976
7	93.7302	1.007	160.0394	1.066	240.8069	1.1868	273.7122	1.2678	308.6116	1.3817
8	103.2029	1.001	170.5092	1.059	249.2825	1.1739	281.6892	1.2518	314.7937	1.3647
9	111.6785	0.994	179.4834	1.052	258.2566	1.1579	288.1704	1.2318	319.4802	1.3387
10	120.1542	0.986	188.4576	1.044	265.7351	1.1339	294.1533	1.2058	322.8706	1.3067
11	128.6928	0.9761	198.9274	1.034	272.7148	1.1189	298.6404	1.1719	324.6655	1.2588
12	137.1054	0.9651	210.1451	1.023	279.4456	1.0964	302.3796	1.1339	325.6626	1.2028

Cricket Graph Data TABLE 19 Thu, Aug 25, 1988 10:26

	CAP.419	PR.419	CAP.465	PR.465	CAP.512	PR.512	CAP.SURGE	PR.SURGE
1	284.1819	1.6104	336.5312	1.8312	373.2256	2.0061	44.8708	1.019
2	297.6431	1.6104	343.0127	1.8222	373.3252	1.9851	111.18	1.0939
3	311.3097	1.6084	349.9924	1.8242	373.4250	1.9641	184.469	1.2268
4	319.6799	1.6014	356.3740	1.8132	373.6245	1.9161	213.3858	1.3287
5	326.8591	1.5914	361.26	1.7943	373.9236	1.8702	242.3026	1.4386
6	333.0413	1.5755	363.7529	1.7563	374.1230	1.8202	284.1819	1.6104
7	339.3232	1.5555	365.1489	1.7083	374.2229	1.7643	336.5312	1.8312
8	344.7078	1.5355	365.9465	1.6634	374.4221	1.7143	373.2256	2.0061
9	349.2947	1.5105	366.4451	1.6134	374.6216	1.6614		
10	351.9868	1.4756	366.8440	1.5655	374.7214	1.6134		
11	352.9839	1.4266	367.0435	1.5105	374.9207	1.5585		
12	353.1333	1.3707	367.1431	1.4521	375.1699	1.5		

Cricket Graph Data — TABLE 20 — Thu, Aug 25, 1988 10:28

	CAP.300	PR.300	CAP.400	PR.400	CAP.447	PR.447	CAP.500	PR.500	CAP.549	PR.549
1	13.5478	1.7102	22.2475	2.5653	27.8608	3.0582	33.54	3.5512	37.2224	3.9234
2	14.2968	1.6901	23.03	2.4446	28.3646	2.8973	33.8887	3.3802	37.5721	3.7423
3	14.8209	1.6297	23.5976	2.3339	28.765	2.7564	34.2465	3.2393	37.8032	3.5713
4	15.2456	1.5593	24.1551	2.1931	29.0538	2.6357	34.4786	3.0884	37.9228	3.4204
5	15.6692	1.4889	24.4977	2.0321	29.3427	2.4144	34.7107	2.8973	38.1631	3.2192
6	15.9855	1.4386	25.0552	1.9114	29.5657	2.2937	34.8273	2.7664	38.2337	3.0381
7	16.2024	1.3581	25.2802	1.7504	29.7988	2.1126	35.0016	2.6156	38.3932	2.8671
8	16.4102	1.3078	25.5052	1.6096	29.9113	1.9617	35.1172	2.3943	38.5138	2.6961
9	16.7264	1.2072	25.7302	1.4587	30.1334	1.7605	35.2337	2.1931	38.6942	2.4748
10	16.9433	1.0865	25.8387	1.3078	30.2560	1.5895	35.3493	2.012	38.7540	2.3138

Cricket Graph Data — TABLE 20 — Thu, Aug 25, 1988 10:28

	CAP.560	PR.560	CAP.566	PR.566	CAP.575	PR.575	CAP.584	PR.584	CAP.594	PR.594
1	40.5389	5.0199	43.5706	5.4123	47.6189	6.0058	51.6429	6.6798	53.4167	6.9816
2	40.9424	4.8791	43.9548	5.2714	48.1055	5.875	52.2105	6.5792	53.8424	6.8911
3	41.2951	4.7181	44.2183	5.1004	48.4602	5.7141	52.5248	6.4183	54.1465	6.7301
4	41.5475	4.5572	44.4109	4.9193	48.6731	5.6034	52.7072	6.2473	54.3290	6.5692
5	41.6985	4.3560	44.5629	4.7282	48.8353	5.362	52.8795	6.0662	54.4810	6.378
6	41.8293	4.1749	44.6440	4.5371	48.9569	5.1708	53.0316	5.875	54.5824	6.1869
7	41.8998	3.9636	44.7352	4.3258	49.038	4.9495	53.1937	5.6638	54.6533	5.9555
8	41.9002	3.7725	44.8163	4.1246	49.1089	4.7584	53.5052	5.4726	54.7141	5.7443
9	41.9103	3.5512	44.9167	3.9234	49.1495	4.5270	53.4167	5.2614	54.7648	5.5129
10	41.9509	3.35	44.9876	3.7423	49.1799	4.3359	53.5181	5.0702	54.8155	5.3016

Cricket Graph Data — TABLE 20 — Thu, Aug 25, 1988 10:28

	CAP.613	PR.613	CAP.635	PR.635	CAP.644	PR.644	CAP.649	PR.649	CAP.663	PR.663
1	55.6467	7.4444	57.7245	7.9373	58.6773	8.1788	59.0827	8.2894	59.8531	8.5108
2	56.0014	7.3438	58.0489	7.8267	58.9814	8.0681	59.3767	8.1788	60.1369	8.4001
3	56.1839	7.1728	58.1806	7.6456	59.0827	7.8870	59.4679	7.9876	60.1876	8.1989
4	56.3562	7.0018	58.2415	7.4645	59.1132	7.6959	59.4882	7.7965	60.1977	7.9977
5	56.4575	6.8006	58.3327	7.2734	59.1740	7.5048	59.5287	7.6054	60.1977	7.7965
6	56.5589	6.6094	58.4036	7.0722	59.2247	7.2935	59.5693	7.3840	60.2078	7.5752
7	56.6096	6.3881	58.4847	6.8408	59.2855	7.0521	59.6098	7.1426	60.2078	7.3237
8	56.6805	6.1668	58.5455	6.6396	59.3260	6.8509	59.6402	6.9313	60.2078	
9	56.7211	5.9555	58.6368	6.4183						

	CAP.685	PR.685	CAP.SURGE	PR.SURGE
1	60.664	8.712	13.5478	1.7102
2	60.9174	8.6013	22.2475	2.5653
3	60.968	8.4001	27.8608	3.0582
4	60.9782	8.1989	33.54	3.5512
5	60.9822	7.9977	37.2224	3.9234
6	60.9863	7.7764	40.5389	5.0199
7	60.9883	7.5048	43.5706	5.4123
8	60.9904	7.2533	47.6189	6.0058
9	60.9924	7.0018	51.6429	6.6798
10	60.9944	6.7402	53.4167	6.9816
11			55.6467	7.4444
12			57.7245	7.9373
13			58.6773	8.1788
14			59.0827	8.2894
15			59.8531	8.5108
16			60.664	8.712

Cricket Graph Data

TABLE 21

Thu, Aug 25, 1988 10:30

	fuel flow	SR.mfl-AD	SR.PR-AD	SR.mfl-HT	SR.PR-HT	AC.mfl-HT	AC.PR-HT	AC.mfl-AD	AC.PR-AD	DC.mfl-AD
1	0.08	23.81	1.0714	23.50	1.0715	23.32	1.0707	23.23	1.0703	131.30
2	0.12	35.43	1.1182	34.51	1.1197	25.54	1.0789	25.15	1.0809	130.53
3	0.16	45.38	1.1911	45.01	1.1886	29.94	1.0876	29.40	1.0902	127.27
4	0.20	52.87	1.29	52.69	1.2892	33.97	1.1045	33.36	1.1080	118.25
5	0.24	59.47	1.3848	59.34	1.3854	37.93	1.1265	37.44	1.1296	103.08
6	0.28	65.65	1.4814	65.51	1.4821	39.82	1.1432	39.31	1.1479	86.77
7	0.32	71.82	1.5891	71.69	1.5906	42.15	1.162	41.54	1.1681	75.91
8	0.36	77.07	1.6698	76.95	1.6713	46.40	1.1461	42.79	1.1769	67.56
9	0.40	82.16	1.75	82.04	1.7515	55.07	1.1275	48.42	1.1718	51.32
10	0.50	93.31	1.9220	93.23	1.9240	64.84	1.2334	59.48	1.1862	46.86
11	0.60	103.0	2.0872	102.97	2.0894	74.90	1.4018	69.76	1.3643	43.95
12	0.70	114.12	2.3436	114.16	2.3467	85.83	1.5919	81.86	1.5867	41.71
13	0.80	126.27	2.6741	126.36	2.6793	96.91	1.7854	94.97	1.8285	38.82
14	0.82	128.33	2.7527	128.88	2.7588	106.31	1.9635	107.21	2.0598	35.24
15	0.84	131.29	2.8286	131.37	2.8324	116.10	2.1601	118.87	2.3116	32.75
16						123.25	2.3243	125.18	2.5011	30.53
17						126.84	2.4354	128.44	2.6335	28.55
18						128.88	2.5451	130.12	2.7242	26.78
19						129.87	2.6259	130.94	2.7804	24.27
20						130.0	2.7039	131.36	2.8229	22.50
21						129.48	2.7255	131.33	2.8286	21.10
22						129.02	2.7345	131.25	2.8263	19.97
23						128.63	2.7417	131.24	2.8261	19.04
24						127.87	2.7527	131.30	2.8282	18.27
25						127.17	2.7568	131.30	2.8281	17.64
26						126.64	2.7606			17.13
27										
28										
29										

	DC.PR-AD	DC.mfl-HT	DC.PR-HT	TIME-AC	THR.AC-HT	THR.AC-AD	TIME-DC	THR.DC-HT	THR.DC-AD	T.DC.U
1	2.8283	131.56	2.8378	0.0	191.0	187.8	0.0	12497.0	12465.0	0.0
2	2.8189	130.86	2.8360	1.0	286.35	292.78	0.12	12271.0	12189.0	0.12
3	2.7899	127.41	2.8291	2.0	423.92	427.48	0.25	11887.0	11754.0	0.25
4	2.7528	115.24	2.8110	3.0	610.33	611.26	0.37	11167.0	11041.0	0.37
5	2.5286	97.21	2.5574	4.0	840.24	845.4	0.50	9793.9	9673.1	0.50
6	2.2	80.51	2.2078	4.5	959.18	970.85	0.62	8051.8	8045.7	0.62
7	1.953	70.65	1.9648	5.0	1133.7	1151.11	0.75	6246.0	6177.5	0.75
8	1.7593	63.44	1.7847	5.25	1295.8	1253.0	0.87	5095.2	4939.6	0.87
9	1.4069	57.86	1.6427	5.50	1944.5	1590.7	1.00	4218.7	3996.3	1.00
10	1.2992	50.86	1.4516	5.75	3155.0	2607.1	1.25	3079.6	2736.5	1.25
11	1.2303	47.18	1.3488	6.00	4438.0	4010.2	1.50	2345.5	1948.7	1.50
12	1.1867	44.24	1.2771	6.25	6030.3	5756.0	1.75	1813.6	1449.8	1.75
13	1.1404	42.0	1.2301	6.50	7868.3	7993.5	2.0	1459.9	1130.0	2.0
14	1.1226	40.17	1.1977	6.75	9576.5	10185.0	2.25	1209.3	913.84	
15	1.1075	38.43	1.1763	7.0	10805.0	11554.0	2.50	1027.2	814.94	
16	1.0958	36.82	1.1621	7.25	11498.0	12050.0	2.75	910.18	724.52	
17	1.0866	35.42	1.1511	7.50	11771.0	12251.0	3.00	831.17	644.76	
18	1.0791	32.97	1.1362	7.75	11924.0	12372.0	3.5	688.64	510.82	
19	1.0689	30.71	1.1231	8.0	12014.0	12425.0	4.0	568.24	407.07	
20	1.0645	28.71	1.1114	8.5	12097.0	12462.0	4.5	467.77	324.72	
21	1.0626	26.97	1.0999	9.0	12121.0	12467.0	5.0	382.43	259.41	
22	1.0614	24.34	1.0834	9.5	12134.0	12465.0	6.0	264.3	179.15	
23	1.0605	22.45	1.0753	10.0	12146.0	12461.0	7.0	202.13	138.05	
24	1.0598	20.96	1.0712	11.0	12162.0	12459.0	8.0	163.77	113.53	
25	1.0593	19.74	1.0684	12.0	12172.0	12460.0	9.0	137.49	95.33	
26	1.0591	18.75	1.0663	13.0	12179.0	12466.0	10.0	117.88	82.61	
27		17.92	1.0648				11.0	102.65	72.91	
28		17.25	1.0637				12.0	91.12	65.58	
29		16.71	1.0629				13.0	82.22	59.82	

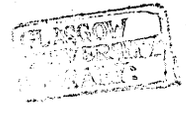

	TH.DC.HT	TH.DC.AD	TIME.DC.L	TH.DC.HT.L	TH.DC.AD.L
1	12497.0	12465.0	4.0	568.24	407.07
2	12271.0	12189.0	4.5	467.77	324.72
3	11887.0	11754.0	5.0	382.43	259.41
4	11167.0	11041.0	6.0	264.3	179.15
5	9793.9	9673.1	7.0	202.13	138.05
6	8051.8	8045.7	8.0	163.77	113.53
7	6246.0	6177.5	9.0	137.49	95.33
8	5095.2	4939.6	10.0	117.88	82.61
9	4218.7	3996.3	11.0	102.65	72.91
10	3079.6	2736.5	12.0	91.12	65.58
11	2345.5	1948.7	13.0	82.22	59.82
12	1813.6	1449.8			
13	1459.9	1130.0			
14					
15					
16					
17					
18					
19					
20					
21					
22					
23					
24					
25					
26					
27					
28					
29					

Cricket Graph Data TABLE 22 Thu, Aug 25, 1988 10:32

	FUEL FLOW	SR.mfl-HT	SR.PR-HT	SR.mfl-AD	SR.PR-AD	AC.mfl-HT	AC.PR-HT	AC.mfl-AD	AC.PR-AD	DC.mfl-HT
1	0.08	22.24	2.0594	22.54	2.093	22.08	2.051	22.00	2.060	55.18
2	0.12	31.51	2.9149	32.39	3.035	24.03	2.3933	23.63	2.3877	54.90
3	0.16	39.12	3.7881	39.39	3.8559	27.99	2.74	27.44	2.8081	53.22
4	0.20	42.80	4.5374	42.93	4.5755	31.36	3.0659	30.73	3.0479	48.62
5	0.24	45.35	5.0563	45.47	5.0743	34.43	3.3801	33.94	3.3752	44.46
6	0.28	47.32	5.3280	47.44	5.3562	37.30	3.7189	36.63	3.6941	41.74
7	0.32	48.78	5.5271	48.91	5.5571	41.56	4.6377	37.50	3.8094	40.44
8	0.36	50.21	5.74	50.32	5.7674	49.95	6.2232	42.63	4.9755	39.40
9	0.40	51.42	5.9225	51.54	5.9499	54.61	6.8562	51.84	6.6805	38.55
10	0.50	53.95	6.3204	54.05	6.3463	56.65	7.1090	54.10	6.9394	37.15
11	0.60	55.57	6.6114	55.64	6.6313	58.25	7.3155	57.42	7.3338	35.76
12	0.70	55.91	6.6616	55.96	6.6742	59.63	7.4927	59.04	7.3387	33.97
13	0.80	55.51	6.5635	55.56	6.5731	60.37	7.6047	57.29	6.8631	31.89
14	0.82	55.34	6.5628	55.38	6.5348	60.79	7.5838	55.85	6.6008	30.01
15	0.84	55.18	6.4916	55.21	6.5011	60.08	7.2288	55.22	6.5030	28.23
16						57.75	6.8094	55.23	6.5022	26.63
17						55.81	6.5277	55.23	6.5022	25.23
18						55.18	6.4448	55.22	6.5014	23.04
19						54.68	6.3810			21.40
20						54.33	6.3408			18.92
21						54.05	6.3092			17.22
22										16.08
23										
24										
25										

	DC.PR-HT	DC.mfl-AD	DC.PR-AD
1	6.4896	55.22	6.4959
2	6.3266	55.03	6.3433
3	6.0062	54.07	6.0794
4	5.2565	50.72	5.4939
5	4.4974	47.44	4.7889
6	4.2120	44.90	4.4458
7	4.048	43.45	4.1732
8	3.9048	42.24	3.9477
9	3.7901	41.21	3.7345
10	3.2615	38.70	3.2914
11	3.0983	37.80	3.1751
12	2.9321	37.11	3.1088
13	2.7456	36.30	3.0314
14	2.5803	34.47	2.8685
15	2.4294	32.11	2.6708
16	2.3032	30.18	2.5108
17	2.1939	28.38	2.3668
18	2.0405	26.71	2.2241
19	1.9376	25.20	2.1375
20	1.7916	23.97	2.0632
21	1.6987	23.02	2.0051
22	1.6368	21.41	1.9121
23		19.04	1.7791
24		17.44	1.6958
25		16.36	1.6399

	TIME	RE.NL	RE.NH	RE.NL/RT1	RE.NL/RTo1	RE.P13/P1	RE.P26/P1	RE.P3/P26	RE.P6/Po1	RE.NH/RT26I
1	0.0	5032.98	9559.48	315.429	335.018	1.230	1.597	5.057	1.456	556.690
2	0.25	5104.19	9675.72	319.912	339.758	1.248	1.618	5.433	1.498	563.361
3	0.50	5213.38	9839.80	326.755	347.027	1.260	1.636	5.635	1.536	572.614
4	0.75	5317.82	9973.13	333.322	353.979	1.272	1.650	5.929	1.565	580.069
5	1.00	5434.14	10082.52	340.656	361.721	1.285	1.671	6.136	1.593	585.989
6	1.25	5555.18	10174.85	348.309	369.778	1.304	1.694	6.274	1.620	590.874
7	1.50	5688.12	10267.07	356.644	378.627	1.337	1.737	6.331	1.655	595.434
8	1.75	5794.94	10328.65	363.342	385.738	1.365	1.772	6.388	1.684	598.207
9	2.00	5889.88	10373.07	369.271	392.058	1.391	1.809	6.475	1.713	599.877
10	2.25	5984.83	10414.09	375.177	398.378	1.419	1.848	6.501	1.746	601.275
11	2.50	6084.52	10458.51	381.403	405.014	1.443	1.880	6.648	1.782	602.831
12	2.75	6167.61	10492.75	386.636	410.544	1.467	1.908	6.640	1.814	604.004
13	3.00	6250.68	10540.55	391.843	416.074	1.474	1.931	6.755	1.843	605.988
14	3.25	6331.39	10585.07	396.952	421.446	1.493	1.954	6.791	1.872	606.212
15	3.50	6421.59	10639.77	402.608	427.451	1.516	1.984	6.906	1.908	609.974
16	3.75	6507.04	10701.25	407.965	433.139	1.538	2.018	7.029	1.950	612.445
17	4.00	6594.86	10766.23	413.471	438.984	1.571	2.053	7.185	1.996	615.213
18	4.25	6677.94	10834.60	418.680	444.514	1.594	2.090	7.229	2.040	618.060
19	4.50	6784.76	10930.32	425.377	451.625	1.623	2.133	7.300	2.096	622.208
20	4.75	6874.96	11015.76	431.032	457.629	1.656	2.175	7.385	2.138	626.002
21	5.00	6962.79	11097.80	436.539	463.475	1.668	2.202	7.488	2.175	629.627
22	5.25	7062.48	11190.13	442.789	470.111	1.663	2.241	7.541	2.214	633.643
23	5.50	7181.16	11292.63	450.229	478.011	1.665	2.281	7.601	2.254	638.110
24	5.75	7273.73	11367.89	456.033	484.173	1.670	2.327	7.579	2.274	641.058
25	6.00	7354.44	11422.59	461.093	489.545	1.686	2.361	7.540	2.286	642.947
26	6.25	7416.15	11460.21	464.962	493.653	1.705	2.403	7.433	2.296	643.579
27	6.50	7477.88	11480.68	468.833	497.762	1.708	2.435	7.404	2.306	643.356
28	6.75	7525.34	11494.36	471.808	500.921	1.696	2.465	7.345	2.319	642.969
29	7.00	7565.7	11508.03	474.339	503.608	1.715	2.481	7.388	2.329	642.835
30	7.25	7598.93	11511.42	476.422	505.820	1.691	2.499	7.378	2.326	642.020
31	7.50	7639.28	11521.70	478.952	508.506	1.680	2.515	7.316	2.336	641.591
32	7.75	7672.52	11525.09	481.036	510.718	1.692	2.534	7.315	2.339	640.852
33	8.00	7698.63	11531.98	482.673	512.456	1.692	2.545	7.260	2.341	640.630
34	8.25	7727.11	11535.38	484.458	514.352	1.689	2.552	7.299	2.346	639.859
35	8.50	7755.59	11542.26	486.244	516.248	1.705	2.571	7.268	2.354	639.390
36	8.75	7772.21	11545.66	487.286	517.354	1.711	2.594	7.211	2.361	638.799
37	9.00	7791.20	11545.66	488.476	518.618	1.703	2.601	7.278	2.373	638.199
38	9.5	7826.80	11549.05	490.708	520.988	1.722	2.624	7.243	2.386	636.978
39	10.0	7855.28	11559.33	492.494	522.884	1.725	2.640	7.227	2.398	636.492
40	10.5	7881.4	11562.73	494.132	524.622	1.727	2.642	7.235	2.391	635.664
41	11.0	7902.76	11566.12	495.471	526.044	1.720	2.647	7.187	2.391	634.978
42	11.5	7924.13	11573.00	496.811	527.467					

	TIME	RE.NL	RE.NH	RE.NL/RT1	RE.NL/RTo1	RE.P13/P1	RE.P26/P1	RE.P3/P26	RE.P6/Po1	RE.NH/RT26I
43	12.0	7933.61	11569.61	497.405	528.098	1.741	2.681	7.165	2.406	633.327
44	12.5	7947.86	11576.4	498.298	529.046	1.748	2.700	7.171	2.421	632.867
45	13.0	7959.73	11579.79	499.043	529.836	1.755	2.706	7.167	2.423	632.395
46										

	AF.NL	AF.NH	AF.NL/RT1	AF.P13/P1	AF.P26/P1	AF.P3/P26	AF.NH/RT26	AF.P6/Po1	AF.NL/RTo1	SF.NL
1	5032.56	9708.61	315.41	1.1939	1.5733	4.8297	561.43	1.470	334.990	5078.98
2	5134.00	9876.30	321.76	1.2111	1.5634	5.8334	571.74	1.540	341.743	5219.06
3	5337.47	10074.81	334.51	1.2518	1.5800	6.7935	582.32	1.635	355.287	5447.68
4	5599.55	10326.33	350.94	1.2990	1.6512	7.1012	593.29	1.713	372.732	5732.12
5	5870.21	10592.83	367.90	1.3507	1.7309	7.3574	604.65	1.792	390.748	6018.73
6	6136.84	10864.75	384.61	1.4039	1.8113	7.4489	616.20	1.866	408.496	6279.14
7	6367.82	11111.96	399.09	1.4516	1.8854	7.4627	626.70	1.932	423.871	6496.90
8	6563.38	11316.25	411.35	1.4925	1.9497	7.4813	635.25	1.986	436.889	6685.22
9	6730.88	11466.85	421.84	1.5224	2.0192	7.4523	640.12	2.029	448.038	6846.71
10	6879.87	11574.66	431.18	1.5395	2.0911	7.3903	642.46	2.062	457.956	6984.59
11	7016.44	11645.21	439.74	1.5549	2.1614	7.3173	642.97	2.089	467.047	7102.57
12	7140.91	11682.98	447.54	1.5682	2.2297	7.2379	641.94	2.114	475.332	7206.13
13	7252.73	11694.05	454.55	1.5801	2.2939	7.1563	639.69	2.135	482.775	7296.37
14	7352.95	11683.75	460.83	1.5896	2.3576	7.0667	636.48	2.156	489.446	7373.87
15	7441.45	11659.07	466.38	1.5969	2.4144	6.9779	632.79	2.171	495.337	7438.52
16	7519.72	11626.20	471.28	1.6005	2.4633	6.8934	628.75	2.180	500.547	7491.33
17	7589.20	11588.43	475.64	1.6043	2.5096	6.8119	624.67	2.189	505.172	7534.25
18	7650.45	11547.60	479.48	1.6073	2.5529	6.7353	620.64	2.198	509.249	7568.79
19	7703.77	11505.52	482.82	1.6106	2.5927	6.6644	616.75	2.200	512.798	7596.42
20	7750.21	11463.29	485.73	1.6135	2.6281	6.5992	613.02	2.203	515.890	7618.69
21	7790.38	11422.03	488.25	1.6150	2.6609	6.5385	609.49	2.212	518.564	7635.93
22	7824.20	11382.69	490.36	1.6168	2.6922	6.4775	606.18	2.215	520.815	7649.44
23	7852.48	11345.90	492.14	1.6183	2.7199	6.4232	603.17	2.218	522.697	7659.70
24	7875.96	11311.85	493.61	1.6198	2.7444	6.3755	600.45	2.217	524.260	7667.42
25	7895.49	11280.75	494.83	1.6208	2.7660	6.3324	598.01	2.219	525.560	7673.34
26	7910.94	11252.53	495.80	1.6209	2.7846	6.2953	595.83	2.222	526.589	7677.78
27	7923.50	11227.35	496.59	1.6226	2.8004	6.2621	593.91	2.222	527.425	7680.79
28	7933.20	11204.90	497.20	1.6224	2.8141	6.2319	592.21	2.225	528.070	7682.73
29	7940.29	11184.90	497.64	1.6227	2.8291	6.1961	590.63	2.224	528.542	7683.77
30	7944.66	11168.08	497.91	1.6230	2.8409	6.1671	589.33	2.224	528.833	7684.19
31	7946.79	11154.20	498.05	1.6230	2.8497	6.1431	588.29	2.228	528.975	7684.20
32	7947.05	11142.85	498.06	1.6236	2.8559	6.1254	587.48	2.227	528.992	7683.87
33	7946.05	11133.75	498.00	1.6241	2.8601	6.1109	586.85	2.222	528.926	7683.46
34	7944.33	11126.61	497.89	1.6241	2.8627	6.1011	586.38	2.225	528.811	7682.97
35	7942.12	11121.05	497.76	1.6236	2.8641	6.0935	586.03	2.222	528.664	7682.20
36	7939.87	11116.71	497.61	1.6236	2.8649	6.0877	585.77	2.225	528.514	7681.63
37	7937.32	11113.31	497.46	1.6242	2.8650	6.0831	585.58	2.224	528.345	7681.03
38	7932.22	11108.85	497.14	1.6235	2.8639	6.0786	585.36	2.221	528.005	7679.88
39	7927.48	11106.27	496.84	1.6236	2.8619	6.0763	585.27	2.221	527.690	7678.88
40	7923.43	11104.78	496.58	1.6234	2.8597	6.0756	585.23	2.222	527.420	7677.81
41	7919.94	11103.75	496.37	1.6230	2.8579	6.0756	585.21	2.222	527.188	7676.87
42	7916.82	11102.96	496.17	1.6230						

	AF.NL	AF.NH	AF.NL/RT1	AF.P13/P1	AF.P26/P1	AF.P3/P26	AF.NH/RT26	AF.P6/Po1	AF.NL/RTo1	SF.NL
43	7914.17	11102.32	496.00	1.6231	2.8544	6.0748	585.19	2.220	526.804	7675.73
44	7912.20	11101.75	495.88	1.6227	2.8533	6.0741	585.17	2.220	526.672	7675.25
45	7910.55	11101.09	495.78	1.6232	2.8525	6.0733	585.13	2.218	526.563	7674.87
46										

	SF.NH	SF.NL/RT1	SF.P13/P1	SF.P26/P1	SF.P3/P26	SF.NH/RT26	SF.P6/Po1	SF.NL/RTo1
1	9710.95	318.31	1.1738	1.6166	4.8974	562.51	1.471	338.080
2	9880.13	327.09	1.2089	1.6227	5.8479	572.13	1.555	347.405
3	10086.07	341.42	1.2656	1.6465	6.8118	582.88	1.665	362.623
4	10350.79	359.25	1.3214	1.7160	7.1413	594.86	1.754	381.556
5	10629.50	377.21	1.3823	1.7953	7.3633	606.75	1.841	400.634
6	10895.73	393.53	1.4398	1.8723	7.4114	618.09	1.918	417.968
7	11130.82	407.18	1.4799	1.9395	7.4344	628.24	1.972	432.464
8	11315.36	418.98	1.5126	2.0072	7.4303	635.19	2.022	444.999
9	11448.77	429.10	1.5380	2.0740	7.3926	639.15	2.057	455.749
10	11542.77	437.74	1.5591	2.1359	7.3383	641.24	2.088	464.926
11	11602.93	445.14	1.5724	2.1957	7.2719	641.41	2.113	472.780
12	11634.96	451.63	1.5827	2.2552	7.1947	639.94	2.136	479.673
13	11644.30	457.28	1.5945	2.3113	7.1188	637.61	2.148	485.680
14	11637.33	462.14	1.6010	2.3624	7.0444	634.77	2.169	490.839
15	11620.03	466.19	1.6077	2.4003	6.9800	631.99	2.178	495.142
16	11597.48	469.50	1.6129	2.4311	6.9232	629.28	2.186	498.657
17	11572.03	472.19	1.6191	2.4587	6.8691	626.64	2.188	501.514
18	11545.00	474.36	1.6218	2.4825	6.8174	624.11	2.196	503.813
19	11517.59	476.09	1.6227	2.5027	6.7776	621.72	2.202	505.653
20	11490.87	477.49	1.6279	2.5214	6.7373	619.52	2.200	507.135
21	11465.36	478.57	1.6292	2.5369	6.7075	617.51	2.205	508.283
22	11441.49	479.41	1.6307	2.5491	6.6801	615.69	2.207	509.182
23	11419.63	480.06	1.6317	2.5591	6.6560	614.09	2.208	509.865
24	11399.79	480.54	1.6322	2.5673	6.6348	612.67	2.210	510.379
25	11381.89	480.91	1.6321	2.5739	6.6150	611.42	2.210	510.773
26	11365.99	481.19	1.6328	2.5810	6.5930	610.28	2.210	511.068
27	11351.91	481.38	1.6331	2.5862	6.5759	609.31	2.210	511.269
28	11339.39	481.50	1.6336	2.5909	6.5631	608.46	2.209	511.398
29	11328.60	481.56	1.6340	2.5944	6.5510	607.74	2.208	511.467
30	11319.20	481.59	1.6342	2.5971	6.5421	607.12	2.208	511.495
31	11310.98	481.59	1.6343	2.5994	6.6380	606.59	2.208	511.496
32	11303.88	481.57	1.6346	2.6011	6.5279	606.14	2.207	511.474
33	11297.42	481.54	1.6348	2.6026	6.5188	605.73	2.207	511.446
34	11291.54	481.51	1.6327	2.6030	6.5141	605.37	2.212	511.414
35	11286.20	481.47	1.6338	2.6046	6.5114	605.03	2.208	511.363
36	11281.49	481.43	1.6341	2.6055	6.5063	604.74	2.207	511.325
37	11277.18	481.39	1.6340	2.6063	6.5029	604.47	2.207	511.285
38	11269.64	481.32	1.6341	2.6076	6.4960	604.00	2.206	511.208
39	11263.14	481.26	1.6344	2.6087	6.4861	603.59	2.205	511.142
40	11257.27	481.19	1.6323	2.6086	6.4845	603.24	2.210	511.070
41	11252.10	481.13	1.6323	2.6093	6.4811	602.92	2.209	511.008
42	11247.43	481.09	1.6331	2.6103	[illegible]	[illegible]		

	SF.NH	SF.NL/RT1	SF.P13/P1	SF.P26/P1	SF.P3/P26	SF.NH/RT26	SF.P6/Po1	SF.NL/RTo1
43	11242.87	481.06	1.6332	2.6112	6.4719	602.31	2.208	510.932
44	11238.87	481.03	1.6323	2.6118	6.4660	602.05	2.207	510.900
45	11234.91	481.01	1.6330	2.6126	6.4625	601.79	2.207	510.875
46								

	TIME	RR.NL	RR.NH	RR.NL/RT1	RR.NL/RTo1	RR.P13/P1	RR.P26/P1	RR.P3/P26	RR.NH/RT26	RR.P6/Po1
1	0.0	7893.27	11508.03	495.062	525.412	1.770	2.720	7.021	618.213	2.446
2	0.25	7871.90	11470.50	493.722	523.990	1.729	2.684	6.439	616.296	2.408
3	0.50	7736.6	11282.45	485.236	514.984	1.717	2.633	6.186	606.486	2.321
4	0.75	7549.08	11053.39	473.475	502.501	1.727	2.564	6.038	594.748	2.252
5	1.00	7378.18	10879.02	462.756	491.126	1.743	2.518	5.888	585.933	2.207
6	1.25	7204.90	10738.88	451.888	479.591	1.762	2.472	5.588	579.009	2.160
7	1.50	7005.51	10612.42	439.382	466.319	1.734	2.405	5.338	572.747	2.099
8	1.75	6772.88	10485.86	424.792	450.834	1.674	2.313	5.161	566.895	2.015
9	2.00	6601.98	10400.42	414.073	439.458	1.634	2.244	5.103	562.946	1.957
10	2.25	6447.69	10332.05	404.396	429.188	1.644	2.179	5.047	560.185	1.901
11	2.50	6310.02	10277.35	395.761	420.024	1.559	2.122	4.964	557.975	1.850
12	2.75	6169.98	10232.93	386.978	410.702	1.521	2.064	4.893	556.682	1.799
13	3.00	6060.79	10205.59	380.130	403.434	1.490	2.011	4.817	555.981	1.758
14	3.25	5963.46	10181.63	374.025	396.955	1.460	1.965	4.873	555.735	1.720
15	3.50	5885.14	10164.57	369.113	391.742	1.440	1.933	4.770	555.654	1.696
16	3.75	5802.05	10150.89	363.902	386.211	1.419	1.896	4.763	555.939	1.667
17	4.00	5737.96	10140.61	359.882	381.945	1.401	1.871	4.728	556.259	1.646
18	4.5	5633.52	10133.82	353.332	374.993	1.379	1.834	4.792	557.661	1.620
19	5.0	5543.32	10126.94	347.674	368.989	1.356	1.795	4.771	559.314	1.593
20	5.5	5483.98	10116.66	343.953	365.039	1.340	1.767	4.803	560.759	1.574
21	6.0	5441.25	10120.15	341.273	362.195	1.330	1.749	4.789	562.825	1.560
22	6.5	5410.39	10116.66	339.337	360.140	1.318	1.728	4.803	564.231	1.546
23	7.0	5389.04	10109.87	337.998	358.719	1.314	1.719	4.895	565.492	1.534
24	8.0	5362.92	10096.20	336.360	356.981	1.311	1.712	4.783	566.502	1.520
25	9.0	5343.94	10075.63	335.169	355.717	1.302	1.701	4.871	566.142	1.513
26	11.0	5298.84	10020.3	332.341	352.715	1.293	1.687	4.777	564.747	1.506
27	13.0	5246.61	9973.13	329.065	349.239	1.285	1.668	4.740	565.948	1.517

	AF.NL	AF.NH	AF.NL/RT1	AF.P13/P1	AF.P26/P1	AF.P3/P26	AF.NH/RT26	AF.P6/Po1	AF.NL/RTo1	SF.NL
1	7800.86	11377.57	488.90	1.6277	2.6922	6.5597	603.06	2.232	519.261	7771.70
2	7847.25	11366.60	491.81	1.6175	2.7209	6.6141	601.33	2.207	522.349	7779.80
3	7827.11	11229.65	490.55	1.5976	2.7447	5.9025	593.41	2.157	521.008	7725.70
4	7741.63	11025.12	485.19	1.5907	2.8350	5.3692	579.86	2.109	515.319	7621.72
5	7582.95	10900.79	475.25	1.5783	2.8203	4.9704	573.50	2.054	504.756	7493.30
6	7396.29	10807.84	463.55	1.5640	2.7147	4.8804	572.29	2.006	492.331	7342.07
7	7203.68	10729.36	451.48	1.5414	2.5952	4.8436	572.12	1.960	479.510	7189.29
8	7014.41	10655.87	439.61	1.5188	2.4761	4.8310	572.40	1.916	466.911	7040.50
9	6830.92	10584.36	428.11	1.4968	2.3604	4.8297	572.86	1.878	454.697	6896.42
10	6654.63	10513.75	417.06	1.4713	2.2553	4.8222	573.15	1.832	442.963	6758.39
11	6493.00	10450.23	406.93	1.4375	2.1813	4.7696	572.37	1.787	432.204	6628.50
12	6349.24	10396.24	397.93	1.4081	2.1151	4.7501	571.93	1.746	422.635	6516.26
13	6226.43	10353.25	390.23	1.3830	2.0575	4.7635	571.88	1.714	414.460	6420.16
14	6124.24	10319.81	383.82	1.3626	2.0072	4.7911	572.08	1.689	407.658	6339.29
15	6040.22	10292.82	378.56	1.3460	1.9658	4.8213	572.13	1.666	402.065	6271.21
16	5971.98	10270.26	374.28	1.3318	1.9322	4.8497	572.51	1.652	397.522	6210.59
17	5915.67	10250.84	370.75	1.3213	1.9049	4.8736	572.63	1.641	393.774	6156.66
18	5826.01	10218.89	365.13	1.3064	1.8621	4.9141	572.79	1.620	387.806	6066.12
19	5759.98	10193.92	360.99	1.2950	1.8317	4.9434	572.81	1.606	383.411	5994.19
20	5711.28	10174.24	357.94	1.2862	1.8091	4.9649	572.77	1.598	380.169	5936.77
21	5674.69	10158.36	355.65	1.2801	1.7918	4.9832	572.70	1.591	377.733	5890.79
22	5646.68	10145.37	353.89	1.2757	1.7786	4.9967	572.60	1.584	375.869	5853.47
23	5625.20	10134.76	352.55	1.2718	1.7685	5.0066	572.49	1.581	374.439	5823.42
24	5595.02	10118.59	350.66	1.2666	1.7543	5.0205	572.29	1.574	372.430	5779.39
25	5575.42	10107.21	349.43	1.2641	1.7452	5.0298	572.13	1.567	371.126	5748.96
26	5551.27	10092.57	347.91	1.2591	1.7337	5.0429	571.95	1.561	369.518	5711.29
27	5535.88	10083.73	346.95	1.2558	1.7262	5.0548	571.90	1.560	368.494	5687.68

	SF.NH	SF.NL/TR1	SF.P13/P1	SF.P26/P1	SF.P3/P26	SF.NH/RT26	SF.P6/Po1	SF.NL/RTo1
1	11379.39	487.07	1.6533	2.6471	6.6212	605.43	2.247	517.320
2	11373.71	487.58	1.6391	2.6439	6.4015	605.01	2.219	517.859
3	11242.95	484.19	1.6123	2.6327	6.0097	598.58	2.154	514.258
4	11034.90	477.68	1.5967	2.6232	5.7786	588.28	2.107	507.337
5	10866.73	469.63	1.5584	2.6835	5.1826	577.51	2.026	498.789
6	10758.85	460.15	1.5293	2.6313	4.9467	573.65	1.964	488.722
7	10677.73	450.57	1.5070	2.5508	4.8666	572.53	1.921	478.552
8	10606.87	441.25	1.4865	2.4690	4.8250	572.15	1.889	468.648
9	10544.29	432.22	1.4704	2.3895	4.7872	571.70	1.853	459.057
10	10486.84	423.57	1.4553	2.3121	4.7679	571.58	1.823	449.870
11	10432.58	415.43	1.4312	2.2413	4.7470	571.41	1.787	441.223
12	10383.97	408.39	1.4048	2.1903	4.7084	570.68	1.751	433.752
13	10342.52	402.37	1.3818	2.1487	4.6760	570.00	1.720	427.355
14	10308.43	397.30	1.3641	2.1137	4.6677	569.52	1.695	421.972
15	10281.50	393.04	1.3519	2.0814	4.6725	569.39	1.681	417.441
16	10258.97	389.24	1.3424	2.0525	4.6880	569.41	1.668	413.405
17	10239.66	385.86	1.3339	2.0267	4.7067	569.49	1.657	409.816
18	10207.94	380.18	1.3206	1.9838	4.7387	569.68	1.640	403.789
19	10182.85	375.67	1.3098	1.9485	4.7722	569.87	1.628	399.001
20	10162.59	372.07	1.3014	1.9205	4.8004	570.03	1.618	395.179
21	10146.10	369.19	1.2953	1.8988	4.8234	570.13	1.611	392.118
22	10132.46	366.85	1.2895	1.8808	4.8452	570.22	1.605	389.634
23	10120.58	364.97	1.2851	1.8666	4.8609	570.23	1.599	387.634
24	10102.04	362.21	1.2795	1.8471	4.8816	570.16	1.589	384.703
25	10088.79	360.30	1.2750	1.8335	4.8965	570.10	1.583	382.677
26	10071.81	357.94	1.2686	1.8166	4.9179	570.04	1.579	380.170
27	10061.55	356.46	1.2654	1.8063	4.9323	570.04	1.572	378.598

Cricket Graph Data

TABLE 24

Thu, Aug 25, 1988 10:54

	TIME	RE.NL	RE.NH	RE.NL/RT1	RR.NL/RTo1	RE.P13/P1	RE.P26/P1	RE.P3/P26	RE.NH/RT26	RE.P6/Po1	AF.NL
1	0.0	7893.27	11508.03	495.062	525.412	1.770	2.720	7.021	618.213	2.446	7800.86
2	0.25	7871.90	11470.50	493.722	523.990	1.729	2.684	6.439	616.296	2.408	7847.25
3	0.50	7736.6	11282.45	485.236	514.984	1.717	2.633	6.186	606.486	2.321	7827.11
4	0.75	7549.08	11053.39	473.475	502.501	1.727	2.564	6.038	594.748	2.252	7741.63
5	1.00	7378.18	10879.02	462.756	491.126	1.743	2.518	5.888	585.933	2.207	7582.95
6	1.25	7204.90	10738.88	451.888	479.591	1.762	2.472	5.588	579.009	2.160	7396.29
7	1.50	7005.51	10612.42	439.382	466.319	1.734	2.405	5.338	572.747	2.099	7203.68
8	1.75	6772.88	10485.86	424.792	450.834	1.674	2.313	5.161	566.895	2.015	7014.41
9	2.00	6601.98	10400.42	414.073	439.458	1.634	2.244	5.103	562.946	1.957	6830.92
10	2.25	6447.69	10332.05	404.396	429.188	1.644	2.179	5.047	560.185	1.901	6654.63
11	2.50	6310.02	10277.35	395.761	420.024	1.559	2.122	4.964	557.975	1.850	6493.00
12	2.75	6169.98	10232.93	386.978	410.702	1.521	2.064	4.893	556.682	1.799	6349.24
13	3.00	6060.79	10205.59	380.130	403.434	1.490	2.011	4.817	555.981	1.758	6226.43
14	3.25	5963.46	10181.63	374.025	396.955	1.460	1.965	4.873	555.735	1.720	6124.24
15	3.50	5885.14	10164.57	369.113	391.742	1.440	1.933	4.770	555.654	1.696	6040.22
16	3.75	5802.05	10150.89	363.902	386.211	1.419	1.896	4.763	555.939	1.667	5971.98
17	4.00	5737.96	10140.61	359.882	381.945	1.401	1.871	4.728	556.259	1.646	5915.67
18	4.5	5633.52	10133.82	353.332	374.993	1.379	1.834	4.792	557.661	1.620	5826.01
19	5.0	5543.32	10126.94	347.674	368.989	1.356	1.795	4.771	559.314	1.593	5759.98
20	5.5	5483.98	10116.66	343.953	365.039	1.340	1.767	4.803	560.759	1.574	5711.28
21	6.0	5441.25	10120.15	341.273	362.195	1.330	1.749	4.789	562.825	1.560	5674.69
22	6.5	5410.39	10116.66	339.337	360.140	1.318	1.728	4.803	564.231	1.546	5646.68
23	7.0	5389.04	10109.87	337.998	358.719	1.314	1.719	4.895	565.492	1.534	5625.20
24	8.0	5362.92	10096.20	336.360	356.981	1.311	1.712	4.783	566.502	1.520	5595.02
25	9.0	5343.94	10075.63	335.169	355.717	1.302	1.701	4.871	566.142	1.513	5575.42
26	11.0	5298.84	10020.3	332.341	352.715	1.293	1.687	4.777	564.747	1.506	5551.27
27	13.0	5246.61	9973.13	329.065	349.239	1.285	1.668	4.740	565.948	1.517	5535.88

Cricket Graph Data

TABLE 24

Thu, Aug 25, 1988 10:54

	AF.NH	AF.NL/RT1	AF.P13/P1	AF.P26/P1	AF.P3/P26	AF.NH/RT26	AF.P6/Po1	AF.NL/RTo1	SF.NL	SF.NH	SF.NL/TR1
1	11377.57	488.90	1.6277	2.6922	6.5597	603.06	2.232	519.261	7771.70	11379.39	487.07
2	11366.60	491.81	1.6175	2.7209	6.6141	601.33	2.207	522.349	7779.80	11373.71	487.58
3	11229.65	490.55	1.5976	2.7447	5.9025	593.41	2.157	521.008	7725.70	11242.95	484.19
4	11025.12	485.19	1.5907	2.8350	5.3692	579.86	2.109	515.319	7621.72	11034.90	477.68
5	10900.79	475.25	1.5783	2.8203	4.9704	573.50	2.054	504.756	7493.30	10866.73	469.63
6	10807.84	463.55	1.5640	2.7147	4.8804	572.29	2.006	492.331	7342.07	10758.85	460.15
7	10729.36	451.48	1.5414	2.5952	4.8436	572.12	1.960	479.510	7189.29	10677.73	450.57
8	10655.87	439.61	1.5188	2.4761	4.8310	572.40	1.916	466.911	7040.50	10606.87	441.25
9	10584.36	428.11	1.4968	2.3604	4.8297	572.86	1.878	454.697	6896.42	10544.29	432.22
10	10513.75	417.06	1.4713	2.2553	4.8222	573.15	1.832	442.963	6758.39	10486.84	423.57
11	10450.23	406.93	1.4375	2.1813	4.7696	572.37	1.787	432.204	6628.50	10432.58	415.43
12	10396.24	397.93	1.4081	2.1151	4.7501	571.93	1.746	422.635	6516.26	10383.97	408.39
13	10353.25	390.23	1.3830	2.0575	4.7635	571.88	1.714	414.460	6420.16	10342.52	402.37
14	10319.81	383.82	1.3626	2.0072	4.7911	572.08	1.689	407.658	6339.29	10308.43	397.30
15	10292.82	378.56	1.3460	1.9658	4.8213	572.13	1.666	402.065	6271.21	10281.50	393.04
16	10270.26	374.28	1.3318	1.9322	4.8497	572.51	1.652	397.522	6210.59	10258.97	389.24
17	10250.84	370.75	1.3213	1.9049	4.8736	572.63	1.641	393.774	6156.66	10239.66	385.86
18	10218.89	365.13	1.3064	1.8621	4.9141	572.79	1.620	387.806	6066.12	10207.94	380.18
19	10193.92	360.99	1.2950	1.8317	4.9434	572.81	1.606	383.411	5994.19	10182.85	375.67
20	10174.24	357.94	1.2862	1.8091	4.9649	572.77	1.598	380.169	5936.77	10162.59	372.07
21	10158.36	355.65	1.2801	1.7918	4.9832	572.70	1.591	377.733	5890.79	10146.10	369.19
22	10145.37	353.89	1.2757	1.7786	4.9967	572.60	1.584	375.869	5853.47	10132.46	366.85
23	10134.76	352.55	1.2718	1.7685	5.0066	572.49	1.581	374.439	5823.42	10120.58	364.97
24	10118.59	350.66	1.2666	1.7543	5.0205	572.29	1.574	372.430	5779.39	10102.04	362.21
25	10107.21	349.43	1.2641	1.7452	5.0298	572.13	1.567	371.126	5748.96	10088.79	360.30
26	10092.57	347.91	1.2591	1.7337	5.0429	571.95	1.561	369.518	5711.29	10071.81	357.94
27	10083.73	346.95	1.2558	1.7262	5.0548	571.90	1.560	368.494	5687.68	10061.55	356.46

	SF.P13/P1	SF.P26/P1	SF.P3/P26	SF.NH/RT26	SF.P6/Po1	SF.NL/RTo1
1	1.6533	2.6471	6.6212	605.43	2.247	517.320
2	1.6391	2.6439	6.4015	605.01	2.219	517.859
3	1.6123	2.6327	6.0097	598.58	2.154	514.258
4	1.5967	2.6232	5.7786	588.28	2.107	507.337
5	1.5584	2.6835	5.1826	577.51	2.026	498.789
6	1.5293	2.6313	4.9467	573.65	1.964	488.722
7	1.5070	2.5508	4.8666	572.53	1.921	478.552
8	1.4865	2.4690	4.8250	572.15	1.889	468.648
9	1.4704	2.3895	4.7872	571.70	1.853	459.057
10	1.4553	2.3121	4.7679	571.58	1.823	449.870
11	1.4312	2.2413	4.7470	571.41	1.787	441.223
12	1.4048	2.1903	4.7084	570.68	1.751	433.752
13	1.3818	2.1487	4.6760	570.00	1.720	427.355
14	1.3641	2.1137	4.6677	569.52	1.695	421.972
15	1.3519	2.0814	4.6725	569.39	1.681	417.441
16	1.3424	2.0525	4.6880	569.41	1.668	413.405
17	1.3339	2.0267	4.7067	569.49	1.657	409.816
18	1.3206	1.9838	4.7387	569.68	1.640	403.789
19	1.3098	1.9485	4.7722	569.87	1.628	399.001
20	1.3014	1.9205	4.8004	570.03	1.618	395.179
21	1.2953	1.8988	4.8234	570.13	1.611	392.118
22	1.2895	1.8808	4.8452	570.22	1.605	389.634
23	1.2851	1.8666	4.8609	570.23	1.599	387.634
24	1.2795	1.8471	4.8816	570.16	1.589	384.703
25	1.2750	1.8335	4.8965	570.10	1.583	382.677
26	1.2686	1.8166	4.9179	570.04	1.579	380.170
27	1.2654	1.8063	4.9323	570.04	1.572	378.598

	TIME	RE.NL	RE.NH	RE.NL/RT1	RR.NL/RTo1	RE.P13/P1	RE.P26/P1	RE.P3/P26	RE.P6/Po1	RE.NH/RT26	AF.NL
1	0.0	5032.98	9559.48	315.429	335.018	1.230	1.597	5.057	1.456	556.690	5034.52
2	0.25	5104.19	9675.72	319.912	339.758	1.248	1.618	5.433	1.498	563.361	5136.73
3	0.50	5213.38	9839.80	326.755	347.027	1.260	1.636	5.635	1.536	572.614	5332.60
4	0.75	5317.82	9973.13	333.322	353.979	1.272	1.650	5.929	1.565	580.069	5576.54
5	1.00	5434.14	10082.52	340.656	361.721	1.285	1.671	6.136	1.593	585.989	5825.37
6	1.25	5555.18	10174.85	348.309	369.778	1.304	1.694	6.274	1.620	590.874	6075.84
7	1.50	5688.12	10267.07	356.644	378.627	1.337	1.737	6.331	1.655	595.434	6299.26
8	1.75	5794.94	10328.65	363.342	385.738	1.365	1.772	6.388	1.684	598.207	6487.35
9	2.00	5889.88	10373.07	369.271	392.058	1.391	1.809	6.475	1.713	599.877	6646.02
10	2.25	5984.83	10414.09	375.177	398.378	1.419	1.848	6.501	1.746	601.275	6781.30
11	2.50	6084.52	10458.51	381.403	405.014	1.443	1.880	6.648	1.782	602.831	6903.44
12	2.75	6167.61	10492.75	386.636	410.544	1.467	1.908	6.640	1.814	604.004	7014.86
13	3.00	6250.68	10540.55	391.843	416.074	1.474	1.931	6.755	1.843	605.988	7116.15
14	3.25	6331.39	10585.07	396.952	421.446	1.493	1.954	6.791	1.872	606.212	7208.12
15	3.50	6421.59	10639.77	402.608	427.451	1.516	1.984	6.906	1.908	609.974	7290.49
16	3.75	6507.04	10701.25	407.965	433.139	1.538	2.018	7.029	1.950	612.445	7364.45
17	4.00	6594.86	10766.23	413.471	438.984	1.571	2.053	7.185	1.996	615.213	7430.84
18	4.25	6677.94	10834.60	418.680	444.514	1.594	2.090	7.229	2.040	618.060	7490.93
19	4.50	6784.76	10930.32	425.377	451.625	1 623	2.133	7.300	2.096	622.208	7545.45
20	4.75	6874.96	11015.76	431.032	457.629	1.656	2.175	7.385	2.138	626.002	7594.77
21	5.00	6962.79	11097.80	436.539	463.475	1.668	2.202	7.488	2.175	629.627	7639.22
22	5.25	7062.48	11190.13	442.789	470.111	1.663	2.241	7.541	2.214	633.643	7678.13
23	5.50	7181.16	11292.63	450.229	478.011	1.665	2.281	7.601	2.254	638.110	7711.70
24	5.75	7273.73	11367.89	456.033	484.173	1.670	2.327	7.579	2.274	641.058	7740.66
25	6.00	7354.44	11422.59	461.093	489.545	1.686	2.361	7.540	2.286	642.947	7765.55
26	6.25	7416.15	11460.21	464.962	493.653	1.705	2.403	7.433	2.296	643.579	7786.39
27	6.50	7477.88	11480.68	468.833	497.762	1.708	2.435	7.404	2.306	643.356	7804.46
28	6.75	7525.34	11494.36	471.808	500.921	1.696	2.465	7.345	2.319	642.969	7819.85
29	7.00	7565.7	11508.03	474.339	503.608	1.715	2.481	7.388	2.329	642.835	7832.40
30	7.25	7598.93	11511.42	476.422	505.820	1.691	2.499	7.378	2.326	642.020	7842.72
31	7.50	7639.28	11521.70	478.952	508.506	1 680	2.515	7.316	2.336	641.591	7851.25
32	7.75	7672.52	11525.09	481.036	510.718	1.692	2.534	7.315	2.339	640.852	7858.01
33	8.00	7698.63	11531.98	482.673	512.456	1.692	2.545	7.260	2.341	640.630	7863.02
34	8.25	7727.11	11535.38	484.458	514.352	1.689	2.552	7.299	2.346	639.859	7866.30
35	8.50	7755.59	11542.26	486.244	516.248	1.705	2.571	7.268	2.354	639.390	7868.39
36	8.75	7772.21	11545.66	487.286	517.354	1.711	2.594	7.211	2.361	638.799	7869.80
37	9.00	7791.20	11545.66	488.476	518.618	1.703	2.601	7.278	2.373	638.199	7870.45
38	9.5	7826.80	11549.05	490.708	520.988	1.722	2.624	7.243	2.386	636.978	7870.54
39	10.0	7855.28	11559.33	492.494	522.884	1.725	2.640	7.227	2.398	636.492	7868.41
40	10.5	7881.4	11562.73	494.132	524.622	1.727	2.642	7.235	2.391	635.664	7865.39
41	11.0	7902.76	11566.12	495.471	526.044	1.720	2.647	7.187	2.391	634.978	7862.02
42	11.5	7924.13	11573.00	496.811	527.467	1.729	2.656	7.155	2.396	634.380	7858.69
43	12.0	7933.61	11569.61	497.405	528.098	1.741	2.681	7.165	2.406	633.327	7855.32
44	12.5	7947.86	11576.4	498.298	529.046	1.748	2.700	7.171	2.421	632.867	7852.18
45	13.0	7959.73	11579.79	499.043	529.836	1.755	2.706	7.167	2.423	632.395	7849.43
46											
47											

	AF.NH	AF.NL/RT1	AF.P13/P1	AF.P26/P1	AF.P3/P26	AF.NH/RT26	SF.NL	SF.NH	SF.NL/RT1	SF.P13/P1	SF.P26/P1
1	9707.30	315.53	1.1939	1.5515	4.9372	562.69	5077.81	9709.29	318.24	1.1773	1.5936
2	9870.07	321.93	1.2116	1.5252	5.9278	573.37	5215.43	9873.17	326.87	1.2122	1.5825
3	10059.46	334.21	1.2504	1.5314	6.8347	583.86	5434.02	10069.59	340.57	1.2653	1.5934
4	10302.06	349.50	1.2942	1.5906	7.1354	594.68	5697.92	10324.89	357.10	1.3169	1.6499
5	10557.71	365.09	1.3411	1.6541	7.3914	605.98	5962.80	10593.19	373.71	1.3729	1.7166
6	10827.52	380.79	1.3919	1.7233	7.5544	617.56	6212.66	10866.56	389.37	1.4291	1.7804
7	11086.58	394.79	1.4383	1.7879	7.5935	628.68	6421.67	11116.11	402.46	1.4694	1.8375
8	11314.98	406.58	1.4775	1.8433	7.6248	638.44	6599.72	11327.76	413.62	1.5014	1.8904
9	11494.72	416.53	1.5104	1.8985	7.6165	645.52	6752.23	11490.62	423.18	1.5273	1.9461
10	11635.46	425.00	1.5301	1.9555	7.5743	650.22	6880.97	11616.70	431.25	1.5471	1.9966
11	11742.34	432.66	1.5444	2.0099	7.5254	653.26	6989.71	11711.57	438.07	1.5646	2.0409
12	11817.66	439.64	1.5576	2.0619	7.4721	654.80	7081.64	11777.54	443.83	1.5761	2.0822
13	11865.73	445.99	1.5689	2.1115	7.4171	655.05	7163.12	11821.68	448.93	1.5850	2.1244
14	11890.93	451.75	1.5789	2.1575	7.3625	654.23	7234.77	11846.07	453.42	1.5938	2.1623
15	11897.23	456.92	1.5875	2.2010	7.3087	652.58	7297.47	11854.38	457.35	1.5990	2.1971
16	11887.63	461.55	1.5950	2.2423	7.2547	650.24	7352.09	11849.56	460.78	1.6053	2.2289
17	11864.28	465.71	1.6018	2.2778	7.2029	647.41	7399.40	11834.18	463.74	1.6102	2.2552
18	11831.18	469.48	1.6048	2.3084	7.1527	644.19	7439.19	11811.26	466.24	1.6155	2.2747
19	11792.21	472.90	1.6078	2.3391	7.0961	640.76	7472.51	11783.92	468.32	1.6178	2.2918
20	11750.52	475.99	1.6108	2.3704	7.0321	637.26	7500.70	11754.93	470.09	1.6200	2.3080
21	11708.87	478.77	1.6131	2.3998	6.9716	633.88	7523.68	11725.79	471.53	1.6243	2.3242
22	11668.21	481.21	1.6146	2.4271	6.9143	630.51	7542.54	11698.17	472.71	1.6255	2.3376
23	11629.04	483.31	1.6161	2.4520	6.8609	627.37	7558.03	11672.36	473.68	1.6254	2.3492
24	11591.64	485.13	1.6177	2.4745	6.8122	624.45	7571.02	11648.57	474.50	1.6263	2.3595
25	11556.34	486.69	1.6193	2.4947	6.7683	621.75	7581.20	11626.78	475.14	1.6300	2.3694
26	11523.24	488.00	1.6207	2.5126	6.7292	619.29	7588.83	11606.72	475.61	1.6307	2.3770
27	11492.54	489.13	1.6220	2.5286	6.6945	617.03	7594.68	11588.25	475.98	1.6307	2.3836
28	11464.17	490.09	1.6225	2.5429	6.6626	614.98	7599.21	11571.37	476.26	1.6317	2.3891
29	11437.97	490.88	1.6235	2.5553	6.6343	613.13	7602.45	11556.36	476.47	1.6315	2.3940
30	11414.02	491.53	1.6241	2.5665	6.6086	611.43	7604.84	11542.82	476.62	1.6328	2.3979
31	11392.28	492.06	1.6244	2.5775	6.5814	609.85	7606.45	11530.73	476.72	1.6329	2.4008
32	11372.83	492.48	1.6247	2.5870	6.5586	608.45	7607.41	11520.08	476.78	1.6325	2.4034
33	11355.35	492.80	1.6249	2.5950	6.5379	607.23	7608.15	11510.20	476.82	1.6331	2.4058
34	11339.56	493.00	1.6259	2.6014	6.5206	606.15	7608.43	11501.35	476.84	1.6314	2.4074
35	11325.42	493.13	1.6252	2.6069	6.5056	605.20	7608.50	11493.39	476.85	1.6316	2.4088
36	11312.78	493.22	1.6247	2.6116	6.4919	604.36	7608.36	11486.24	476.84	1.6307	2.4105
37	11301.39	493.26	1.6251	2.6154	6.4797	603.62	7608.23	11479.68	476.83	1.6311	2.4119
38	11281.91	493.27	1.6251	2.6215	6.4596	602.36	7607.72	11467.99	476.80	1.6315	2.4141
39	11266.39	493.14	1.6254	2.6251	6.4448	601.41	7607.07	11458.11	476.76	1.6315	2.4158
40	11254.18	492.95	1.6253	2.6271	6.4340	600.69	7606.39	11449.69	476.71	1.6314	2.4173
41	11244.57	492.74	1.6253	2.6282	6.4259	600.13	7605.86	11442.33	476.68	1.6314	2.4182
42	11236.97	492.53	1.6252	2.6286	6.4203	599.71	7605.39	11435.67	476.65	1.6326	2.4193
43	11230.90	492.32	1.6250	2.6286	6.4154	599.37	7604.92	11429.60	476.62	1.6326	2.4204
44	11226.04	492.12	1.6251	2.6281	6.4122	599.12	7604.59	11423.93	476.60	1.6325	2.4217
45	11221.99	491.95	1.6248	2.6278	6.4090	598.90	7604.44	11418.55	476.59	1.6325	2.4227
46											
47											

	SF.P3/P26	SF.NH/RT26	AF.NL/RTo1	AF.P6/Po1	SF.NL/RTo1	SF.P6/Po1
1	5.0050	563.76	335.121	1.472	338.002	1.538
2	5.9427	57[illegible]75	341.924	1.536	347.163	1.554
3	6.8536	584.46	354.962	1.624	361.713	1.652
4	7.1752	596.25	371.200	1.693	379.280	1.730
5	7.4408	607.96	387.763	1.765	396.911	1.818
6	7.5313	619.87	404.436	1.838	413.543	1.886
7	7.5745	630.77	419.308	1.901	427.456	1.944
8	7.5939	639.69	431.828	1.952	439.308	1.987
9	7.5746	645.68	442.390	1.996	449.459	2.022
10	7.5379	649.93	451.395	2.028	458.029	2.051
11	7.4969	652.81	459.525	2.052	465.267	2.077
12	7.4543	654.15	466.941	2.076	471.387	2.096
13	7.3963	654.10	473.684	2.094	476.810	2.111
14	7.3538	653.28	479.806	2.112	481.580	2.123
15	7.3076	651.84	485.289	2.129	485.753	2.138
16	7.2640	649.92	490.212	2.146	489.389	2.147
17	7.2244	647.73	494.631	2.156	492.538	2.158
18	7.1921	645.54	498.631	2.164	495.187	2.163
19	7.1533	643.26	502.260	2.170	497.405	2.169
20	7.1155	641.00	505.543	2.173	499.281	2.175
21	7.0779	638.81	508.502	2.178	500.811	2.176
22	7.0520	636.81	511.092	2.184	502.066	2.179
23	7.0170	634.98	513.326	2.187	503.097	2.183
24	6.9952	633.27	515.254	2.190	503.962	2.185
25	6.9696	631.70	516.911	2.192	504.640	2.183
26	6.9481	630.30	518.298	2.196	505.147	2.183
27	6.9279	629.03	519.501	2.195	505.537	2.185
28	6.9134	627.90	520.525	2.197	505.838	2.185
29	6.8978	626.90	521.361	2.201	506.054	2.185
30	6.8820	626.01	522.048	2.202	506.213	2.185
31	6.8761	625.24	522.615	2.200	506.320	2.185
32	6.8613	624.57	523.065	2.200	506.384	2.185
33	6.8579	623.94	523.399	2.202	506.433	2.185
34	6.8437	623.39	523.617	2.203	506.452	2.190
35	6.8422	622.90	523.756	2.203	506.457	2.189
36	6.8353	622.45	523.850	2.206	506.447	2.189
37	6.8305	622.05	523.893	2.203	506.439	2.189
38	6.8209	621.33	523.899	2.205	506.405	2.188
39	6.8119	620.72	523.758	2.204	506.362	2.188
40	6.8069	620.21	523.557	2.203	506.316	2.187
41	6.8007	619.76	523.332	2.203	506.281	2.186
42	6.7933	619.35	523.111	2.202	506.250	2.186
43	6.7880	618.97	522.886	2.202	506.218	2.186
44	6.7860	618.61	522.677	2.201	506.196	2.186
45	6.7774	618.27	522.494	2.201	506.187	2.186
46						
47						

	TIME	RE.NL	RE.NH	RE.NL/RT1	RE.NL/RTo1	RE.P13/P1	RE.P26/P1	RR.P3/P26	RE.NH/RT26	RE.P6/Po1
1	0.0	7893.27	11508.03	495.062	525.412	1.770	2.720	7.021	618.213	2.446
2	0.25	7871.90	11470.50	493.722	523.990	1.729	2.684	6.439	616.296	2.408
3	0.50	7736.6	11282.45	485.236	514.984	1.717	2.633	6.186	606.486	2.321
4	0.75	7549.08	11053.39	473.475	502.501	1.727	2.564	6.038	594.748	2.252
5	1.00	7378.18	10879.02	462.756	491.126	1.743	2.518	5.888	585.933	2.207
6	1.25	7204.90	10738.88	451.888	479.591	1.762	2.472	5.588	579.009	2.160
7	1.50	7005.51	10612.42	439.382	466.319	1.734	2.405	5.338	572.747	2.099
8	1.75	6772.88	10485.86	424.792	450.834	1.674	2.313	5.161	566.895	2.015
9	2.00	6601.98	10400.42	414.073	439.458	1.634	2.244	5.103	562.946	1.957
10	2.25	6447.69	10332.05	404.396	429.188	1.644	2.179	5.047	560.185	1.901
11	2.50	6310.02	10277.35	395.761	420.024	1.559	2.122	4.964	557.975	1.850
12	2.75	6169.98	10232.93	386.978	410.702	1.521	2.064	4.893	556.682	1.799
13	3.00	6060.79	10205.59	380.130	403.434	1.490	2.011	4.817	555.981	1.758
14	3.25	5963.46	10181.63	374.025	396.955	1.460	1.965	4.873	555.735	1.720
15	3.50	5885.14	10164.57	369.113	391.742	1.440	1.933	4.770	555.654	1.696
16	3.75	5802.05	10150.89	363.902	386.211	1.419	1.896	4.763	555.939	1.667
17	4.00	5737.96	10140.61	359.882	381.945	1.401	1.871	4.728	556.259	1.646
18	4.5	5633.52	10133.82	353.332	374.993	1.379	1.834	4.792	557.661	1.620
19	5.0	5543.32	10126.94	347.674	368.989	1.356	1.795	4.771	559.314	1.593
20	5.5	5483.98	10116.66	343.953	365.039	1.340	1.767	4.803	560.759	1.574
21	6.0	5441.25	10120.15	341.273	362.195	1.330	1.749	4.789	562.825	1.560
22	6.5	5410.39	10116.66	339.337	360.140	1.318	1.728	4.803	564.231	1.546
23	7.0	5389.04	10109.87	337.998	358.719	1.314	1.719	4.895	565.492	1.534
24	8.0	5362.92	10096.20	336.360	356.981	1.311	1.712	4.783	566.502	1.520
25	9.0	5343.94	10075.63	335.169	355.717	1.302	1.701	4.871	566.142	1.513
26	11.0	5298.84	10020.3	332.341	352.715	1.293	1.687	4.777	564.747	1.506
27	13.0	5246.61	9973.13	329.065	349.239	1.285	1.668	4.740	565.948	1.517

	AF.NL	AF.NH	AF.NL/RT1	AF.P13/P1	AF.P26/P1	AF.P3/P26	AF.NH/RT26	SF.NL	SF.NH	SF.NL/RT1
1	7784.48	11389.06	487.88	1.6328	2.5562	6.7007	608.13	7753.03	11390.37	485.90
2	7811.57	11392.07	489.57	1.6192	2.5669	6.4676	607.78	7742.06	11398.10	485.22
3	7773.74	11263.73	487.20	1.5980	2.5785	6.0491	600.86	7671.68	11275.40	480.81
4	7678.96	11053.36	481.26	1.5884	2.5872	5.8116	589.98	7554.06	11068.66	473.44
5	7547.55	10872.12	473.03	1.5774	2.6838	5.2070	577.77	7427.51	10867.49	465.50
6	7364.49	10758.01	461.55	1.5610	2.6315	4.9501	573.61	7277.01	10719.12	456.07
7	7166.72	10672.06	449.16	1.5375	2.5245	4.8721	572.61	7113.27	10617.10	445.81
8	6970.92	10596.23	436.89	1.5140	2.4064	4.8474	572.66	6951.04	10536.40	435.64
9	6781.03	10523.68	424.99	1.4914	2.2911	4.8434	573.08	6794.42	10469.79	425.83
10	6600.34	10452.94	413.66	1.4606	2.1951	4.8117	572.90	6646.24	10409.55	416.54
11	6436.98	10392.11	403.42	1.4262	2.1235	4.7726	572.19	6516.15	10356.14	408.39
12	6296.11	10344.66	394.60	1.3977	2.0580	4.7839	572.13	6405.09	10312.20	401.43
13	6178.54	10308.07	387.23	1.3745	2.0018	4.8146	572.39	6313.86	10278.46	395.71
14	6082.02	10278.53	381.18	1.3550	1.9542	4.8508	572.72	6235.97	10251.14	390.83
15	6003.42	10253.82	376.25	1.3388	1.9156	4.8829	572.96	6167.67	10228.31	386.55
16	5939.42	10232.88	372.24	1.3265	1.8846	4.9099	573.13	6107.87	10208.66	382.80
17	5885.29	10214.84	368.85	1.3180	1.8587	4.9348	573.28	6055.81	10191.58	379.53
18	5799.19	10185.09	363.45	1.3028	1.8182	4.9748	573.44	5971.54	10163.32	374.25
19	5735.77	10161.85	359.48	1.2918	1.7888	5.0039	573.49	5907.84	10140.42	370.26
20	5688.90	10143.36	356.54	1.2838	1.7665	5.0287	573.49	5858.82	10121.66	367.19
21	5653.78	10128.18	354.34	1.2781	1.7493	5.0472	573.44	5820.61	10106.31	364.79
22	5626.84	10115.72	352.65	1.2733	1.7363	5.0612	573.36	5790.32	10093.76	362.90
23	5606.09	10105.55	351.35	1.2700	1.7263	5.0717	573.27	5765.89	10083.41	361.37
24	5577.04	10090.07	349.53	1.2650	1.7122	5.0866	573.10	5728.84	10067.49	359.04
25	5558.00	10079.16	348.34	1.2615	1.7029	5.0977	572.96	5702.88	10055.95	357.42
26	5534.57	10065.28	346.87	1.2574	1.6911	5.1128	572.82	5668.77	10040.69	355.28
27	5520.01	10057.07	345.96	1.2545	1.6834	5.1260	572.81	5647.26	10031.63	353.93

	SF.P13/P1	SF.P26/P1	SF.P3/P26	SF.NH/RT26	AF.NL/RTo1	AF.P6/Po1	SF.NL/RTo1	SF.P6/Po1	AFN.NL	AFN.NH
1	1.6586	2.5161	6.7621	610.52	518.171	2.213	516.077	2.232	8025.09	11275.39
2	1.6415	2.4987	6.5541	611.41	519.974	2.188	515.347	2.198	8022.77	11278.73
3	1.6156	2.4843	6.1460	605.65	517.456	2.132	510.662	2.128	7958.23	11152.48
4	1.5973	2.4720	5.9410	595.81	511.147	2.102	502.833	2.090	7821.11	10981.50
5	1.5774	2.4737	5.6757	585.76	502.400	2.051	494.409	2.051	7630.15	10876.30
6	1.5428	2.4602	5.1387	577.18	490.214	1.999	484.391	1.975	7427.81	10787.36
7	1.5141	2.4482	4.9615	574.51	477.050	1.949	473.492	1.924	7223.82	10706.89
8	1.4914	2.3747	4.8642	572.97	464.017	1.904	462.693	1.880	7024.72	10631.42
9	1.4722	2.2941	4.8185	572.40	451.377	1.862	452.268	1.842	6832.26	10558.33
10	1.4475	2.2170	4.7894	572.12	439.349	1.814	442.404	1.804	6648.13	10486.34
11	1.4177	2.1598	4.7435	571.36	428.475	1.767	433.745	1.757	6479.84	10422.21
12	1.3923	2.1126	4.7265	570.75	419.098	1.731	426.352	1.725	6332.47	10370.65
13	1.3726	2.0718	4.7296	570.53	411.272	1.700	420.280	1.703	6209.08	10331.24
14	1.3589	2.0350	4.7455	570.56	404.847	1.677	415.095	1.685	6107.56	10299.77
15	1.3479	2.0025	4.7663	570.69	399.615	1.659	410.548	1.670	6024.81	10273.68
16	1.3386	1.9743	4.7880	570.84	395.355	1.643	406.568	1.657	5957.58	10251.63
17	1.3295	1.9496	4.8088	570.99	391.752	1.629	403.103	1.647	5901.41	10232.66
18	1.3154	1.9091	4.8450	571.22	386.021	1.612	397.493	1.632	5812.01	10201.47
19	1.3055	1.8787	4.8757	571.32	381.799	1.600	393.253	1.618	5746.23	10177.20
20	1.2973	1.8557	4.8987	571.32	378.679	1.590	389.990	1.610	5697.68	10157.89
21	1.2916	1.8382	4.9154	571.28	376.342	1.584	387.447	1.601	5661.43	10142.04
22	1.2870	1.8247	4.9282	571.21	374.548	1.578	385.430	1.595	5633.60	10128.97
23	1.2831	1.8137	4.9394	571.16	373.167	1.573	383.804	1.591	5612.68	10118.30
24	1.2770	1.7970	4.9587	571.08	371.233	1.566	381.338	1.587	5582.16	10102.03
25	1.2734	1.7855	4.9718	571.00	369.966	1.562	379.610	1.582	5562.52	10090.60
26	1.2679	1.7699	4.9916	570.96	368.406	1.555	377.339	1.575	5538.55	10075.87
27	1.2653	1.7596	5.0085	571.02	367.437	1.552	375.908	1.567	5523.72	10067.12

	AFN.NL/RT1	AFN.P13/P1	AFN.P26/P1	AFN.P3/P26	AFN.NH/RT26
1	502.96	1.6463	2.7239	6.4327	595.15
2	502.81	1.6308	2.7179	6.2322	595.52
3	498.77	1.6084	2.7282	5.8158	588.90
4	490.17	1.5969	2.8660	5.1393	576.10
5	478.20	1.5836	2.7994	4.9395	573.10
6	465.52	1.5681	2.6812	4.8994	572.92
7	452.74	1.5443	2.5587	4.8623	572.77
8	440.26	1.5205	2.4369	4.8486	573.02
9	428.20	1.4971	2.3191	4.8467	573.44
10	416.66	1.4701	2.2127	4.8357	573.67
11	406.11	1.4346	2.1399	4.7810	572.80
12	396.87	1.4048	2.0726	4.7831	572.54
13	389.14	1.3798	2.0139	4.8121	572.73
14	382.78	1.3599	1.9643	4.8483	573.04
15	377.59	1.3433	1.9235	4.8824	573.30
16	373.38	1.3296	1.8908	4.9099	573.47
17	369.86	1.3200	1.8639	4.9353	573.60
18	364.26	1.3045	1.8218	4.9772	573.76
19	360.13	1.2934	1.7913	5.0086	573.80
20	357.09	1.2849	1.7683	5.0342	573.79
21	354.82	1.2794	1.7507	5.0524	573.73
22	353.07	1.2748	1.7373	5.0663	573.63
23	351.73	1.2709	1.7269	5.0776	573.53
24	349.85	1.2658	1.7126	5.0924	573.33
25	348.62	1.2622	1.7029	5.1030	573.19
26	347.12	1.2578	1.6910	5.1185	573.02
27	346.19	1.2552	1.6833	5.1313	572.99

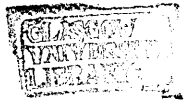

	RE.TIME	RE.NL	RE.NH	RE.NL/RT1	RE.P13/P1	RE.P26/P1	RE.P3/P26	RE.NH/RT26	RE.NL/RTo1	RE.P6/Po1
1	2.00	5816.29	10174.8	364.521	1.420	1.901	4.722	557.982	387.159	1.674
2	2.25	5745.09	10161.2	360.081	1.401	1.869	4.764	558.154	382.420	1.651
3	2.50	5676.25	10154.3	355.766	1.386	1.846	4.711	558.573	377.837	1.634
4	2.75	5626.41	10150.9	352.665	1.375	1.827	4.738	559.278	374.520	1.622
5	3.00	5576.55	10144.0	349.583	1.363	1.806	4.751	559.700	371.201	1.608
6	3.25	5540.95	10144.0	347.417	1.358	1.903	4.541	560.442	368.831	1.598
7	3.50	5502.97	10140.6	345.035	1.346	1.774	4.785	561.060	366.303	1.589
8	3.75	5474.49	10140.6	343.250	1.337	1.758	4.764	561.806	364.407	1.577
9	4.00	5450.75	10133.8	341.740	1.330	1.744	4.791	562.083	362.827	1.567
10	4.25	5434.14	10140.6	340.656	1.325	1.737	4.789	563.116	361.721	1.562
11	4.50	5412.77	10130.3	339.295	1.318	1.726	4.864	563.295	360.299	1.551
12	4.75	5398.53	10126.9	338.423	1.312	1.721	4.877	563.702	359.351	1.546
13	5.00	5389.04	10130.3	337.828	1.316	1.717	4.869	564.425	358.719	1.541
14	5.25	5377.16	10123.5	337.126	1.311	1.714	4.875	564.612	357.929	1.536
15	5.50	5367.67	10120.1	336.531	1.311	1.708	4.829	564.990	357.297	1.529
16	5.75	5362.92	10123.5	336.233	1.309	1.710	4.811	565.717	356.981	1.527
17	6.00	5355.80	10113.3	335.787	1.307	1.705	4.824	565.684	356.507	1.522
18	6.25	5351.05	10106.5	335.489	1.302	1.701	4.804	565.810	356.191	1.517
19	6.50	5346.30	10106.5	335.191	1.304	1.701	4.849	566.286	355.874	1.515
20	6.75	5343.94	10099.6	335.043	1.302	1.698	4.844	566.407	355.717	1.513
21	7.00	5339.19	10099.6	334.745	1.298	1.694	4.846	566.916	355.401	1.508
22	7.25	5336.81	10092.8	334.596	1.297	1.694	4.824	566.089	355.243	1.508
23	7.50	5334.44	10085.9	334.448	1.298	1.694	4.846	567.101	355.085	1.506
24	7.75	5327.32	10075.6	334.001	1.293	1.689	4.882	567.001	354.611	1.503
25	8.00	5324.95	10075.6	333.853	1.297	1.691	4.831	567.384	354.453	1.503
26	8.25	5322.57	10075.6	333.703	1.295	1.691	4.872	567.799	354.295	1.503
27	8.50	5393.78	10191.9	338.168	1.312	1.712	5.484	574.774	359.035	1.551
28	8.75	5479.24	10325.3	343.526	1.326	1.731	5.653	582.495	364.723	1.589
29	9.00	5571.80	10441.4	349.329	1.340	1.742	5.970	589.277	370.885	1.622
30	9.25	5678.62	10530.4	356.026	1.347	1.754	6.295	594.602	377.995	1.658
31	9.50	5825.79	10619.2	365.253	1.373	1.790	6.490	599.616	387.791	1.708
32	9.75	5944.48	10677.3	372.695	1.400	1.823	6.519	602.863	395.692	1.744
33	10.00	6046.54	10711.5	379.093	1.429	1.862	6.563	604.452	402.486	1.778
34	10.25	6146.48	10745.7	385.359	1.466	1.910	6.574	606.040	409.138	1.819
35	10.50	6245.94	10779.9	391.595	1.502	1.963	6.645	607.353	415.759	1.867
36	10.75	6331.39	10807.3	396.952	1.525	1.993	6.723	608.519	421.446	1.908
37	11.00	6416.84	10851.7	402.310	1.538	2.023	6.791	610.572	427.134	1.947
38	11.25	6502.28	10896.1	407.666	1.558	2.044	6.924	612.691	432.822	1.986
39	11.50	6604.36	10957.7	414.066	1.573	2.064	7.090	615.739	439.617	2.025
40	11.75	6699.30	11022.6	420.019	1.596	2.094	7.266	618.865	445.936	2.064
41	12.00	6799.00	11094.4	426.270	1.625	2.131	7.317	622.232	452.573	2.109
42	12.25	6896.22	11155.9							

Cricket Graph Data

TABLE 27

Thu, Aug 25, 1988 11:20

	RE.TIME	RE.NL	RE.NH	RE.NL/RT1	RE.P13/P1	RE.P26/P1	RE.P3/P26	RE.NH/RT26	RE.NL/RTo1	RE.P6/Po1
43	12.50	7010.26	11237.9	439.515	1.686	2.230	7.395	628.553	466.635	2.210
44	12.75	7098.08	11292.6	445.021	1.706	2.278	7.395	630.695	472.481	2.247
45	13.00	7164.54	11323.5	449.187	1.698	2.306	7.355	631.610	476.905	2.266
46	13.25	7228.63	11350.8	453.206	1.713	2.340	7.327	632.357	481.171	2.284
47	13.50	7292.73	11374.7	457.224	1.706	2.361	7.318	632.771	485.438	2.296
48	13.75	7335.45	11385.0	459.903	1.692	2.377	7.316	632.746	488.281	2.296
49	14.00	7380.55	11395.2	462.730	1.699	2.391	7.281	632.610	491.283	2.299
50	14.25	7420.90	11408.9	465.260	1.692	2.412	7.187	632.633	493.969	2.304
51	14.50	7454.13	11405.5	467.344	1.701	2.437	7.236	631.604	496.181	2.314
52	14.75	7484.99	11412.3	469.278	1.715	2.465	7.269	631.176	498.235	2.326
53	15.00	7511.10	11415.7	470.915	1.710	2.488	7.209	630.632	499.973	2.339
54	15.25	7534.84	11419.2	472.404	1.720	2.499	7.213	630.233	501.554	2.349
55	15.50	7558.57	11422.6	473.892	1.708	2.515	7.125	629.830	503.133	2.354
56	15.75	7582.32	11426.0	475.381	1.705	2.527	7.063	629.289	504.714	2.361
57	16.00	7603.68	11429.4	476.720	1.706	2.536	7.052	629.060	506.136	2.361
58										
59										
60										
61										
62										
63										
64										
65										

	TIME	SF.NL	SF.NH	SF.NL/RT1	SF.P13/P1	SF.P26/P1	SF.P3/P26	SF.NH/RT26	AF.NL	AF.NH
1	0.00	7771.57	11379.39	487.07	1.6113	2.6462	6.6209	605.45	8032.62	11278.75
2	0.25	7782.32	11379.59	487.74	1.6409	2.6452	6.6439	605.28	8052.61	11278.27
3	0.50	7741.00	11273.77	485.15	1.6215	2.6376	6.1244	600.03	8022.34	11179.25
4	0.75	7660.39	11106.84	480.10	1.6083	2.6319	5.9472	591.78	7918.73	11082.14
5	1.00	7568.26	10950.49	474.32	1.5863	2.6566	5.6306	582.97	7783.80	11016.66
6	1.25	7455.16	10851.96	467.24	1.5610	2.6585	5.3144	577.86	7640.62	10954.32
7	1.50	7335.54	10784.01	459.74	1.5420	2.6013	5.2179	576.56	7493.87	10892.65
8	1.75	7217.80	10724.09	452.36	1.5247	2.5376	5.1682	576.02	7344.67	10831.23
9	2.00	7102.50	10668.16	445.13	1.5108	2.4737	5.1408	575.83	7195.19	10772.31
10	2.25	6989.57	10615.51	438.06	1.4952	2.4147	5.0954	575.27	7048.37	10714.72
11	2.50	6879.18	10567.34	431.14	1.4811	2.3555	5.0656	574.90	6905.33	10658.29
12	2.75	6772.61	10521.91	424.46	1.4690	2.2982	5.0437	574.67	6766.76	10602.61
13	3.00	6669.98	10478.79	418.03	1.4542	2.2444	5.0255	574.47	6633.14	10548.25
14	3.25	6578.07	10438.93	412.27	1.4315	2.2002	4.9954	574.01	6510.20	10499.82
15	3.50	6497.59	10404.49	407.22	1.4127	2.1662	4.9626	573.39	6399.66	10456.92
16	3.75	6427.74	10374.73	402.85	1.3957	2.1363	4.9366	572.90	6300.77	10418.22
17	4.00	6367.50	10348.41	399.07	1.3809	2.1105	4.9141	572.45	6212.66	10383.35
18	4.25	6315.11	10324.82	395.79	1.3693	2.0880	4.8954	572.04	6134.30	10351.66
19	4.50	6267.30	10303.35	392.79	1.3604	2.0667	4.8802	571.71	6064.77	10322.96
20	4.75	6222.54	10283.39	389.98	1.3517	2.0465	4.8685	571.44	6003.14	10296.79
21	5.00	6180.55	10264.70	387.35	1.3438	2.0277	4.8576	571.18	5948.48	10272.87
22	5.25	6141.09	10247.17	384.88	1.3364	2.0100	4.8473	570.95	5898.27	10251.07
23	5.50	6103.87	10230.68	382.55	1.3298	1.9934	4.8378	570.73	5853.17	10233.11
24	5.75	6068.65	10215.11	380.34	1.3238	1.9779	4.8292	570.53	5813.82	10218.29
25	6.00	6035.26	10200.34	378.25	1.3181	1.9631	4.8217	570.34	5779.70	10205.71
26	6.25	6003.49	10186.14	376.26	1.3126	1.9490	4.8149	570.16	5750.26	10194.66
27	6.50	5973.16	10172.52	374.35	1.3074	1.9357	4.8080	569.98	5724.88	10184.94
28	6.75	5944.61	10160.28	372.57	1.3029	1.9232	4.8080	569.85	5702.96	10176.25
29	7.00	5918.48	10150.15	370.93	1.2991	1.9113	4.8134	569.82	5684.00	10168.48
30	7.25	5894.78	10141.60	369.44	1.2957	1.9003	4.8221	569.85	5667.49	10161.52
31	7.50	5873.33	10134.33	368.10	1.2928	1.8908	4.8316	569.90	5652.99	10155.18
32	7.75	5853.97	10127.41	366.89	1.2898	1.8811	4.8423	569.96	5640.37	10149.43
33	8.00	5836.59	10121.27	365.80	1.2866	1.8727	4.8522	570.01	5629.32	10144.28
34	8.25	5846.62	10162.53	366.42	1.3039	1.8660	5.3901	572.97	5644.68	10182.68
35	8.50	5955.14	10310.24	373.23	1.3483	1.8473	6.4597	582.68	5754.28	10319.20
36	8.75	6159.83	10522.73	386.05	1.3992	1.8844	6.8838	593.12	5953.62	10520.11
37	9.00	6360.71	10741.59	398.64	1.4454	1.9388	7.0135	603.02	6165.86	10742.04
38	9.25	6537.15	10938.71	409.70	1.4787	1.9879	7.0964	611.97	6361.09	10955.70
39	9.50	6693.90	11109.03	419.53	1.5090	2.0414	7.1410	619.01	6531.09	11146.80
40	9.75	6832.85	11244.55	428.23	1.5313	2.0966	7.1439	623.83	6680.66	11302.86
41	10.00	6956.97	11349.82	436.01	1.5492	2.1479	7.1456	627.17	6814.77	11424.98
42	10.25	7067.00	11429.68	442.91	1.5660					

	TIME	SF.NL	SF.NH	SF.NL/RT1	SF.P13/P1	SF.P26/P1	SF.P3/P26	SF.NH/RT26	AF.NL	AF.NH
43	10.50	7165.30	11488.70	449.07	1.5760	2.2495	7.0815	629.67	7058.30	11583.96
44	10.75	7253.18	11528.68	454.58	1.5857	2.2993	7.0408	629.25	7168.23	11627.37
45	11.00	7330.81	11552.85	459.44	1.5939	2.3453	6.9926	628.25	7269.06	11651.02
46	11.25	7398.75	11564.25	463.70	1.6019	2.3877	6.9388	626.83	7360.73	11657.86
47	11.50	7456.69	11565.98	467.33	1.6112	2.4238	6.8982	625.26	7443.43	11651.37
48	11.75	7505.27	11561.84	470.38	1.6151	2.4492	6.8635	623.82	7518.15	11636.23
49	12.00	7546.09	11554.25	472.94	1.6190	2.4725	6.8238	622.33	7585.88	11615.45
50	12.25	7580.41	11544.08	475.09	1.6219	2.4926	6.7995	620.86	7647.07	11590.69
51	12.50	7609.07	11532.39	476.88	1.6258	2.5108	6.7696	619.44	7701.92	11563.65
52	12.75	7632.68	11520.05	478.36	1.6274	2.5259	6.7458	618.09	7750.43	11535.49
53	13.00	7652.47	11507.77	479.60	1.6296	2.5392	6.7236	616.85	7793.21	11506.98
54	13.25	7668.26	11495.60	480.59	1.6310	2.5502	6.7028	615.70	7830.37	11478.96
55	13.50	7681.41	11484.01	481.42	1.6339	2.5603	6.6848	614.66	7862.52	11451.87
56	13.75	7691.98	11473.07	482.08	1.6345	2.5685	6.6692	613.73	7890.67	11426.35
57	14.00	7700.40	11463.00	482.61	1.6352	2.5753	6.6510	612.90	7914.57	11402.39
58	14.25	7707.14	11453.80	483.03	1.6357	2.5815	6.6373	612.15	7935.23	11380.31
59	14.50	7712.47	11445.49	483.36	1.6362	2.5869	6.6250	611.49	7952.39	11360.39
60	14.75	7716.61	11438.30	483.62	1.6367	2.5910	6.6198	610.94	7966.31	11341.75
61	15.00	7719.81	11431.99	483.82	1.6370	2.5948	6.6069	610.45	7978.08	11325.36
62	15.25	7722.32	11426.36	483.98	1.6369	2.5978	6.6035	610.04	7988.05	11310.86
63	15.50	7724.16	11421.57	484.10	1.6372	2.6001	6.6000	609.69	7995.97	11298.14
64	15.75	7725.48	11417.55	484.18	1.6369	2.6019	6.5912	609.45	8001.72	11287.33
65	16.00	7726.68	11413.95	484.25	1.6374	2.6036	6.5912	609.20	8005.95	11278.09

	AF.NL/RT1	AF.P13/P1	AF.P26/P1	AF.P3/P26	AF.NH/RT26
1	503.43	1.6413	2.8797	6.2682	590.36
2	504.68	1.6297	2.8917	6.1016	589.89
3	502.78	1.6160	2.9329	5.7192	583.49
4	496.29	1.6092	2.9923	5.2774	576.42
5	487.83	1.5994	2.9243	5.1895	575.39
6	478.86	1.5889	2.8371	5.1661	575.42
7	469.66	1.5782	2.7438	5.1608	575.83
8	460.31	1.5636	2.6493	5.1392	575.84
9	450.94	1.5455	2.5557	5.1260	575.95
10	441.74	1.5274	2.4643	5.1183	576.10
11	432.78	1.5102	2.3773	5.1170	576.33
12	424.09	1.4931	2.2919	5.1164	576.59
13	415.72	1.4709	2.2181	5.0997	576.49
14	408.01	1.4444	2.1632	5.0612	575.85
15	401.08	1.4214	2.1133	5.0323	575.37
16	394.89	1.4002	2.0687	5.0087	574.95
17	389.37	1.3814	2.0293	4.9888	574.57
18	384.45	1.3650	1.9946	4.9698	574.20
19	380.10	1.3503	1.9640	4.9526	573.84
20	376.23	1.3376	1.9371	4.9360	573.49
21	372.81	1.3266	1.9135	4.9197	573.13
22	369.66	1.3180	1.8918	4.9115	572.85
23	366.84	1.3103	1.8716	4.9156	572.74
24	364.37	1.3038	1.8539	4.9279	572.72
25	362.23	1.2979	1.8384	4.9413	572.73
26	360.39	1.2932	1.8251	4.9533	572.74
27	358.79	1.2887	1.8134	4.9650	572.74
28	357.42	1.2849	1.8030	4.9749	572.74
29	356.23	1.2819	1.7941	4.9839	572.73
30	355.20	1.2795	1.7864	4.9921	572.71
31	354.29	1.2770	1.7795	4.9988	572.68
32	353.50	1.2747	1.7736	5.0049	572.65
33	352.81	1.2726	1.7685	5.0097	572.61
34	353.77	1.2847	1.7601	5.5262	575.38
35	360.64	1.3178	1.7396	6.5691	584.54
36	373.13	1.3563	1.7853	6.9025	593.99
37	386.43	1.4033	1.8500	7.0954	603.67
38	398.67	1.4438	1.9078	7.1793	613.06
39	409.32	1.4797	1.9615	7.2318	621.35
40	418.70	1.5112	2.0130	7.2614	627.75
41	427.10	1.5293	2.0725	7.2519	631.57
42	434.96